Examining the Molecular Mechanism of Antimicrobial Peptides using Neutron and X-ray Scattering Techniques

Thesis for the degree of Philosophiae Doctor

by

Josefine Eilsø Nielsen

Department of Chemistry

The Faculty of Mathematics and Natural Sciences

University of Oslo

Norway

2020

Preface

The present project was carried out at the Department of Chemistry at the University of Oslo under the supervision of Assoc. Prof. Reidar Lund, from April 2017 to September 2020. In addition, experiments were carried out at external large-scale facilities, Heinz Maier-Leibnitz Zentrum (MLZ) in Garching, Germany, ISIS Neutron and Muon Source in Didcot, United Kingdom, Institut Laue-Langevin (ILL) in Grenoble, France, Oak Ridge National Laboratory (ORNL) in Oak Ridge, USA, The European Synchrotron Radiation Facility (ESRF) in Grenoble, France and Deutsches Elektronen-Synchrotron (DESY) in Hamburg, Germany, and during shorter and longer research stays at Roskilde University, Malmö University, Lawrence-Berkeley National lab and Stanford University. The project was financed by Nordforsk (project number 82004) and the University of Oslo.

First and foremost, I would like to thank my main supervisor, Reidar Lund for proposing the initial ideas for the project, and for giving me the opportunity to do a PhD in this very interesting topic. You are truly a supporting and encouraging supervisor, and your contribution has been essential for the successful progress of the work presented in this thesis. I appreciate you always being open to a scientific discussion either in the office or at the pub. Thanks for teaching me so much, for all your patience, and for being such a nice travel partner (I will especially never forget our endless road trip from Nashville to Oak Ridge, oddly enough via Alabama and Georgia, or the jazz clubs in New Orleans).

A huge thank you to my co-supervisor, Prof. Håvard Jenssen for all the support and encouragement, and for inviting me to visit you, and your group at Roskilde University on several occasions. It has been really great to always have you to answer my endless questions on biology, AMPs and so much more. I would also like to thank my other co-supervisor, Dr. Kenneth Knudsen for his support and feedback on this thesis.

In addition, I would like to thank all of the collaborators and co-authors that have been involved in the project. Especially, Prof. Marité Cárdenas, and her group who have thought me just about everything I know about Neutron Reflectometry, AFM and QCM-D. Marité, thank you for being such a motivating and fun person to work with.

In addition, I would like to thank Assoc. Prof. Annelise Barron for hosting me at Lawrence-Berkeley National lab and Stanford University in California, USA for two and a half months during my PhD. You are such a great mentor, always encouraging me to dream big. I look forward to working together with you in the next stage after my PhD.

I would especially like to thank all past and present members of the Soft Matter research group and the BiO^3 section for good scientific and social discussions. You have all been essential in making PhD life enjoyable. I especially want to thank Victoria for being the best master student, now fellow PhD colleague I could hope for. We have spent so many days and nights at beamlines (hope we can do it again) and in front of QtiKWS together, our collaboration has been essential for the success of the project. I would also like to thank Nico for all your support and encouragement, especially on the project with the peptide nanofibers, and for feedback on the thesis.

Lastly, I would like to give a huge thanks to all of my friends and family, for all your love and support, first during my studies for a Master in Pharmacy and eventually PhD.

Oslo, September 2020

Josefine Eilsø Nielsen

Abstract

The overall aim of this thesis was to examine the molecular mechanism of action of antimicrobial peptides using neutron and X-ray scattering techniques. Antimicrobial peptides (AMPs) are found in nature as a part of the innate immune system in a wide range of species, including humans, other animals, plants and fungi. Because of the emerging concern of widespread antibiotic resistance, new antibiotics or alternative therapeutics are of great importance for clinical treatments. AMPs have attracted considerable interest as a potential new class of antibiotics and both the use of natural and synthetic analogues have been thoroughly investigated over the recent years. Even with this wide-spread interest, the exact molecular mechanism of these compounds is still an object of debate, but their interaction with the membrane seems to be a key feature. AMPs have been hypothesised to cause pore formation, membrane-solubilisation, changes in lipid movements or changes to the overall membrane structures. Here we combine state-of-the-art small angle X-ray/neutron scattering (SAXS/SANS) techniques, together with neutron reflectometry (NR) to systematically study the effect of a broad selection of AMPs on lipid membranes.

As a result of the significant contrast in electron density between the tail region in the core of the lipid membrane and the AMPs, we were able to determine the peptide position and distribution in the bilayer using SAXS. Meanwhile, time resolved SANS (TR-SANS) and contrast variation enabled us to probe the peptide effect on both the intra-vesicular flip-flop and inter-vesicular exchange of phospholipids in vesicles. Our results revealed that all the studied peptides, (indolicidin, aurein 1.2, magainin II, cecropin A, lacticin Q and LL-37) cause a general acceleration of essential lipid transport processes, without necessarily altering the overall structure of the lipid membranes or creating organised pore-like structures. Enhanced lipid transport can be linked with rapid scrambling of the lipid composition which may trigger lethal signalling processes and enhance ion transport, and the reported membrane effects provide a plausible canonical mechanism of AMP-membrane interaction and may reconcile previously observed effects of AMPs on bacterial membranes.

In the last part of the thesis we examined the peptide-membrane interaction of more complex peptide systems. Here we use contrast variation SANS and NR to determine the membrane interaction of self-assembled peptide nanofibers with and without PEGylation. From this work we show that the membrane interaction is enhanced by self-assembly, but decreased by addition of PEGylation. This knowledge of how self-assembly and PEGylation may affect the peptide-membrane interaction is important in further development of AMP based drug molecules.

Table of contents

Abbreviations

AFM	atomic force microscopy
AMP	antimicrobial peptide
ATP	adenosintrifosfat
ATR-FTIR	attenuated-total reflectance Infrared spectroscopy
B. subtilis	*Bacillus subtilis*
CAC	critical aggregation concentration
CD	circular dichroism
cryo-EM	cryogenic electron microscopy
D_2O	deuterium Oxide
DLS	dynamic light scattering
DMPC	1,2-dimyristoyl-sn-glycero-3-phosphocholine
DMPE	1,2-dimyristoyl-sn-glycero-3-phosphoethanolamine
DMPE-PEG	1,2-dimyristoyl-sn-glycero-3-phosphoethanolamine-N-[methoxy(polyethylene glycol)-2000] (ammonium salt)
DMPG	1,2-dimyristoyl-sn-glycero-3-phospho-(1'-rac-glycerol)(sodium salt)
DNA	deoxyribonucleic acid
DSC	differential scanning calorimetry
E. coli	*Escherichia coli*
ESR	electron spin resonance
GI-SAXS	grazing-incidence small angle x-ray scattering

H$_2$O	hydrogen dioxide
HDP	host defence peptide
HPTS	8-Hydroxypyrene-1,3,6-trisulfonic acid
KZAC	kinetic zero-average-contrast
LAXS	diffuse low angle X-ray scattering
LB	Langmuir-Blodgett
LPS	lipopolysaccharides
LS	Langmuir-Schaefer deposition
M. tuberculosis	*Mycobacterium tuberculosis*
MD	molecular dynamics
MDP	multidomain peptide
MIC	minimum inhibitory concentration
mRNA	messenger- ribonucleic acid
MW	molecular weight
NMR	nuclear magnetic resonance
NR	neutron reflectometry
P	critical packing parameter
P. aeruginosa	*Pseudomonas aeruginosa*
PC	phosphocholine
PDB	protein data bank
PE	phosphatidylethanolamine
PEG	polyethylene glycol

X

PG	Phosphatidylglycerol
POPC	1-palmitoyl-2-oleoyl-glycero-3-phosphocholine
$\vec{Q}, Q = \lvert\vec{Q}\rvert$	scattering vector, momentum transfer
QCM-D	quartz crystal microbalance with dissipation monitoring
QENS	quasielastic neutron scattering
R_g	radius of gyration
RNA	ribonucleic acid
rRNA	ribosomal- ribonucleic acid
S. aureus	*Staphylococcus aureus*
S. epidermis	*Staphylococcus epidermis*
SANS	small angle neutron scattering
SAS	small angle scattering
SAXS	small angle X-ray scattering
SDP	scattering density profile
SFF	separated form factor
SLB	supported lipid bilayers
SLD	scattering length density
T_m	melting temperature
TEM	transmission electron microscopy
TR-SANS	time resolved small angle neutron scattering
Tris	tris(hydroxymethyl)aminomethane
tRNA	transfer-ribonucleic acid
WAXS	wide-angle X-ray scattering

ZAC   zero-average contrast

Å   Ångström (10^{-10} m)

List of publications

The thesis is comprised by results included in the following papers (which will be referred to in the text by their Roman numerals).

Paper I: Resolving the Structural Interactions between Antimicrobial Peptides and Lipid Membranes using Small-angle Scattering Methods: the case of Indolicidin.
Josefine Eilsø Nielsen, Victoria Ariel Bjørnestad and Reidar Lund
Soft Matter 14(43): 8750-8763.
(2018)
https://doi.org/10.1039/C8SM01888J

Paper II: A biophysical study of the interactions between the antimicrobial peptide indolicidin and lipid model systems
Josefine Eilsø Nielsen, Tania Kjellerup Lind, Abdullah Lone, Yuri Gerelli, Paul Robert Hansen, Håvard Jenssen, Marité Cárdenas and Reidar Lund
Biochimica et Biophysica Acta – Biomembranes 1861(7): 1355-1364.
(2019)
https://doi.org/10.1016/j.bbamem.2019.04.003

Paper III: Beyond Structural Models for the Mode of Action: How Natural Antimicrobial Peptides Disrupts Lipid Membranes
Josefine Eilsø Nielsen, Victoria Ariel Bjørnestad, Vitaliy Pipich, Håvard Jenssen and Reidar Lund
Journal of Colloid & Interface Science 582(B): 793-802
(2021)
https://doi.org/10.1016/j.jcis.2020.08.094

Paper IV: Impact of Antimicrobial Peptides on *E. coli*-mimicking Lipid Model Membranes: correlating structural and dynamic effects using scattering methods

Josefine Eilsø Nielsen, Sylvain François Prévost, Håvard Jenssen and Reidar Lund

Faraday Discussions (accepted for publication)

(2020)

https://doi.org/10.1039/D0FD00046A

Paper V: Kinetics of Lipid Exchange and Flip-flop in Lipid Bilayers with added Peptides: Extracting the Leaflet Compositions using Time-resolved Small-angle Neutron Scattering

Josefine Eilsø Nielsen and Reidar Lund

Manuscript

(2020)

Paper VI: Lipid Membrane Interactions of Self-assembling antimicrobial nanofibers: effect of PEGylation

Josefine Eilsø Nielsen, Nico König, Su Yang, Maximilian WA Skoda, Armando Maestro, He Dong, Marité Cardenas, and Reidar Lund

RSC Advances 10(58): 35329-35340.

(2020)

https://doi.org/10.1039/D0RA07679A

The following papers were published in peer reviewed journals during the course of the PhD, but are not included in the thesis:

Paper SI: Structure-Activity Study of an All-d Antimicrobial Octapeptide D2D
Abdullah Lone, Thomas Thyge Thomsen, **Josefine Eilsø Nielsen**, Peter Waaben Thulstrup, Rasmus Nielsen Klitgaard, Anders, Løbner-Olesen, Reidar Lund, Håvard Jenssen and Paul Robert Hansen
Molecules 24(24): 4571.
(2019)
https://doi.org/10.3390/molecules24244571

Paper SII: Halogenation as a tool to improve antimicrobial activity of peptoids
Natalia Molchanova, **Josefine Eilsø Nielsen**, Kristian Sørensen, Bala Krishna Prabhala, Paul Robert Hansen, Reidar Lund, Annelise Barron and Håvard Jenssen
Scientific reports 10: 14805
(2020)
https://doi.org/10.1038/s41598-020-71771-8

Paper SIII: Helicity modulation improves selectivity of antimicrobial peptoids
Ho Yeon Nam, Jieun Choi, S. Dinesh Kumar, **Josefine Eilsø Nielsen**, Minkyu Kyeong, Sungrok Wang, Dahyun Kang, Yunjee Lee, Jiyoun Lee, Myung-Han Yoon, Sukwon Hong, Reidar Lund, Håvard Jenssen, Song Yub Shin and Jiwon Seo
ACS Infectious Diseases 6(10): 2732-2744.
(2020)
https://doi.org/10.1021/acsinfecdis.0c00356

Paper SIV: Exceptional physical stability of beta-sheet nanofibers formed by self-assembly of a de novo antimicrobial peptide

Nico König, **Josefine Eilsø Nielsen**, Lutz Willner, Su Yang, Ari Benjamin, Martha Dunbar, Aurel Radulescu, Najet Mahmoudi, Sinan Keten, He Dong, and Reidar Lund

Manuscript

(2020)

Paper SV: The role cholesterol plays in protecting mammalian cell towards antimicrobial peptides

Josefine Eilsø Nielsen, Marité Cárdenas, Yuri Gerelli, Sarah Waldie, Harald Pichler, Gernot A. Strohmeier, V. Trevor Forsyth, Michael Haertlein, Håvard Jenssen and Reidar Lund

Manuscript

(2020)

1. Introduction

1.1 The discovery of natural antimicrobial peptides

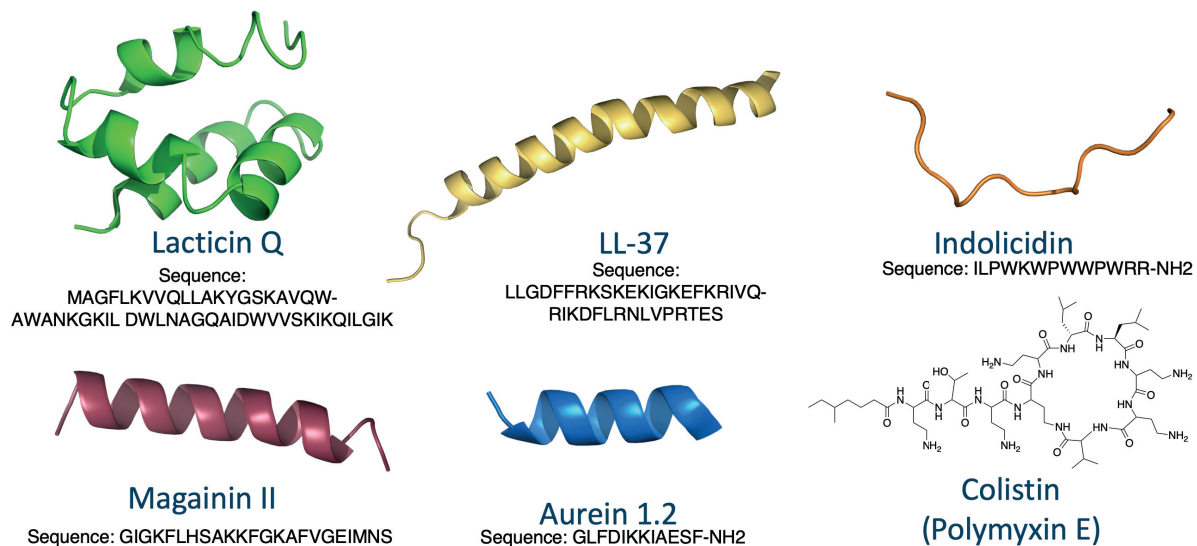*"I did not invent penicillin. Nature did that. I only discovered it by accident"*

– Alexander Flemming[1]

When Alexander Flemming discovered how all bacteria growing in proximity to colonies of the mould *Penicillium genum* on agar plates in his laboratory were dying, it paved the way for the first effective treatment of microbial infections. In the same way as Flemming was using something purely found in Nature to target bacteria, antimicrobial peptides are natural antimicrobial substances. These peptides are a part of the innate immune system of a wide range of species, including humans, animals, insects and fungi. Even some bacteria themselves are found to produce such peptides, also called bacteriocines,[2] as a defence against other microbial species. The first discovery of antimicrobial peptides from eukaryote cells traces back to as early as 1896 when it was discovered that wheat flour contained a substance that was lethal to bread yeast. This substance was later in 1942 isolated as the peptide purothionin produced by wheat endosperm. Discovery of prokaryote secreted peptides traces back to the 1939 when Gramicidines were isolated from Bacillus brevis.[3] Even though the discovery of AMPs traces back to the 19th century, the real start of research into using natural antimicrobial peptides in treatment of bacterial infections is considered to be the 1950s and 1960s.[3] This is related to the end of the "Golden era of antibiotics" with arising antibiotic resistance development and the resulting concerns in the 1960s.[3]

After the original discovery more than 1200 types of peptides with antibacterial activity have been isolated from various natural sources, including cells and tissues.[4] In humans it is found that antimicrobial peptides seem to be intricately involved in many parts of the immune system,[5] with pleiotropic functions not only to kill bacteria but also related to controlling host functions like inflammation, angiogenesis, and wound healing.[4] Recent research has further shown that a natural human AMP, LL-37, might even be an important factor in prevention of Alzheimer's disease,[6, 7] Parkinson's disease,[6] and

Type 2 diabetes.[8] Due to the peptides' roles in defending the host against various threats, including microbial infections, these peptides are classified as host defence peptides (HDP).

The peptides included in the group of AMPs are normally in the range 12-50 residues (number of amino acids), have an overall cationic charge and amphiphilic properties with about 50% hydrophobic residues.[9] Beyond these characteristics the group is diverse with regards to structure and number of charged residues. The most classical and well-described AMPs are the α-helical peptides (**Figure 1**). Some on the most well described peptides in this group is the human cathilicidin peptide LL-37, aureins and magainins found in frogs and cecropin from moths. Beyond the α-helical peptides, the group also includes unstructured peptides like indolicidin which is a cathilicidin from bovine origin, and β-sheet peptides including human β−defensines and protegrins. In addition to the long list of natural peptides, significant research efforts have resulted in a very large library of synthetic AMPs. Many of these synthetic molecules are closely based on peptides isolated from natural sources. Common synthetic strategies to improve the drugability of AMPs will be discussed further in Chapter 1.4.

Lacticin Q
Sequence:
MAGFLKVVQLLAKYGSKAVQW-
AWANKGKIL DWLNAGQAIDWVVSKIKQILGIK

LL-37
Sequence:
LLGDFFRKSKEKIGKEFKRIVQ-
RIKDFLRNLVPRTES

Indolicidin
Sequence: ILPWKWPWWPWRR-NH2

Magainin II
Sequence: GIGKFLHSAKKFGKAFVGEIMNS

Aurein 1.2
Sequence: GLFDIKKIAESF-NH2

Colistin
(Polymyxin E)

Figure 1. *PDB structure/chemical formula of the the AMPs probed in this thesis work: lacticin Q (2N8P),[10] LL-37 (2K6O),[11] magainin II (2MAG),[12] aurein 1.2 (1VM5),[13] indolicidin (1G89)[14] and Colistin. Cecropin A is not included due to PDB file not being available in the database.*

The next chapters will give an introduction into the scientific topics covered by the thesis and present the state of the science. After a general introduction to the bacterial cell and specifically the cytoplasmic membrane, particular focus will be given to antimicrobial peptides. Specifically, we will cover their proposed mechanisms of actions, their selectivity towards pathogens and antimicrobial resistance development. Furthermore, we will introduce different approaches that have been used to study AMPs and their mode of action. Specific focus will be on model systems, and small angle scattering and reflectivity methodologies that have been used in this thesis work. Finally, the last section of the chapter will discuss the problems related to using AMPs as treatment in the clinic, and molecular design strategies used to overcome these issues, and specific focus will be given to self-assembling $K_x(QL)_yK_z$ peptides which is the example treated in the thesis.

1.2 The cellular mechanism of antimicrobial peptides

1.2.1 The prokaryote cell

Cells are the fundamental units of life. The bacterial cell has the simplest structure of all types of cells, with no nucleus to hold its deoxyribonucleic acid (DNA), and almost no organelles. Bacteria are therefore classified as prokaryotes, while organisms whose cells have a nucleus are classified as eukaryotes. Bacteria are typically spherical (e.g. *Streptococcus pneumoniae*, *Staphylococcus aureus*), rod like (e.g. *Escherichia coli*, *Salmonella enterica*), or spiral shaped (e.g. *Treponema pallidum*, *Vibrio cholera*) cells that live as single-celled organisms. However, some are also known to cluster together.[15]
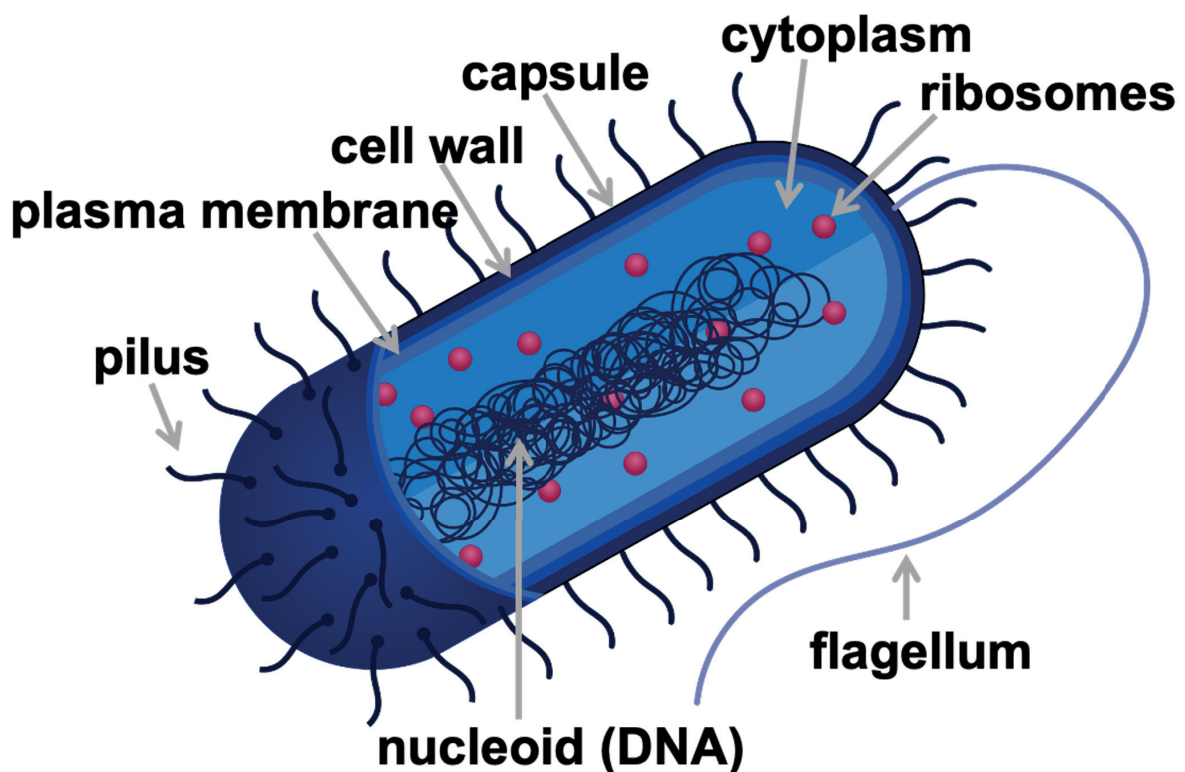
Figure 2. Illustration of a bacterial cell.

A sketch of the fundamental bacterial cell structure is shown in **Figure 2**. The internal structure of a bacterial cell consists of DNA, either floating freely as a continuous strand twisted together (chromosome) localised in the nucleoid region of the cell, or in a separate circular structure referred to as a plasmid. The chromosome has the genetic instructions for initiating and carrying out cell division, or binary fission, which is a process where a single bacterial cell makes a copy of its DNA and grows larger by doubling its cellular content. At some point the cell splits apart on the middle, resulting in the creation of two identical "daughter" cells. Plasmids are not involved in cell division, but appear to give bacteria a selective advantage, like transmitting properties important for antibiotic drug resistance, resistance to heavy metals, and virulence factors necessary for their ability to cause disease (pathogenicity).[16]
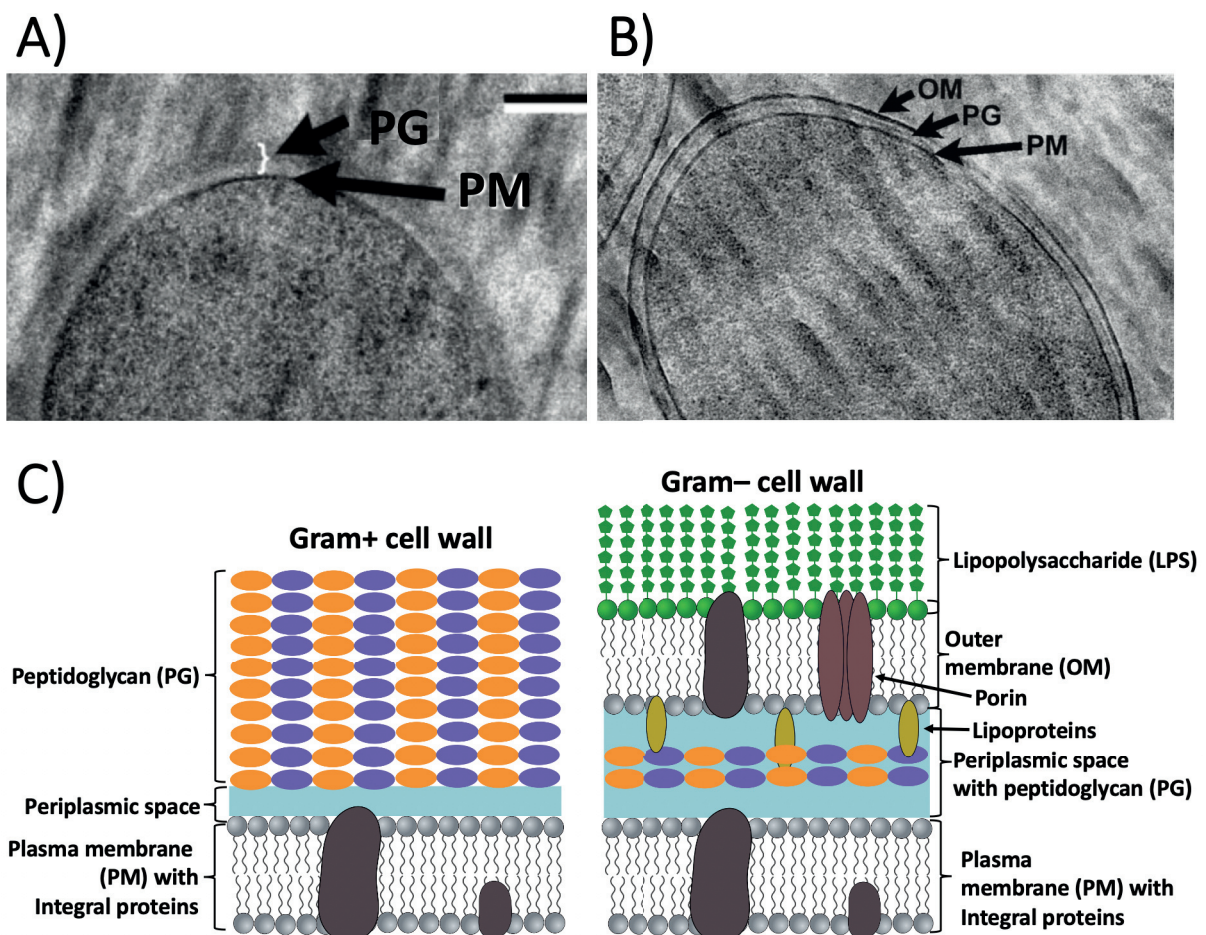
Figure 3. *Cryo-transmission electron microscopy images of frozen-hydrated sections showing the organisation of the cell envelope of the **A)** gram-positive bacteria Bacillus subtilis[17] and **B)** gram-negative bacteria E. coli.[18] Images have been reused with the permission from the journals. **C)** Schematic diagram of gram-positive and gram-negative cell wall including explanations on abbreviations used in A and B (the illustrations are not in size ratio to each other).*

Beyond DNA, the cytoplasm of the bacteria also contains ribonucleic acids (mRNA, tRNA and rRNA) and ribosomes. The inner structure of the bacteria is generally protected by the cytoplasmic membrane and the cell wall. However, certain bacteria like mycoplasmas do not have such a cell wall. We classify bacteria into two major groups according to the structure of the outer protective layer, called gram-positive and gram-negative bacteria (see **Figure 3**). The gram-negative cell wall is a multi-layered structure with an inner membrane (the cytoplasmic membrane) and an outer membrane (with embedded lipopolysaccharides (LPS) and membrane proteins) separated by the periplasm with a thin peptidoglycan layer. The gram-positive cell wall, on the other hand, consists of a thicker layer of peptidoglycan outside the cytoplasmic membrane without any outer membrane.[16] A comparison of gram-positive and negative cells as seen by cryo-transmission electron microscopy (TEM) images, and an illustration explaining the structure is shown in **Figure 3**.

1.2.2 The lipid cell membrane

Both the cytoplasmic membrane and the outer membrane (in gram-negative bacteria) are built up by a lipid bilayer, with embedded membrane proteins, glycolipids and LPS (only in the outer membrane). Phospholipids, the main lipid in the membrane, contain a hydrophilic (glycerol-phosphate) head group and a hydrophobic (typically two fatty acid chains) tail region (**Figure 4A**). Their amphipathic properties allow them to spontaneously assemble into lipid bilayers in solution, where the lipid tail region point inward towards each other forming a hydrophobic environment, while the hydrophilic lipid head groups are either exposed to the external environment of the cell or the internal cytoplasm.[16, 19] Lipid bilayers have been shown to undergo phase transitions with characteristic melting points associated with changes in their molecular packing. The most important of these transitions is the so-called main-chain-melting transition, in which the bilayer is transformed from a highly ordered quasi-two-dimensional crystalline solid (gel phase) to a quasi-two-dimensional liquid (liquid crystalline phase).[20] An illustration showing the two phase transitions states is included in **Figure 4B**.
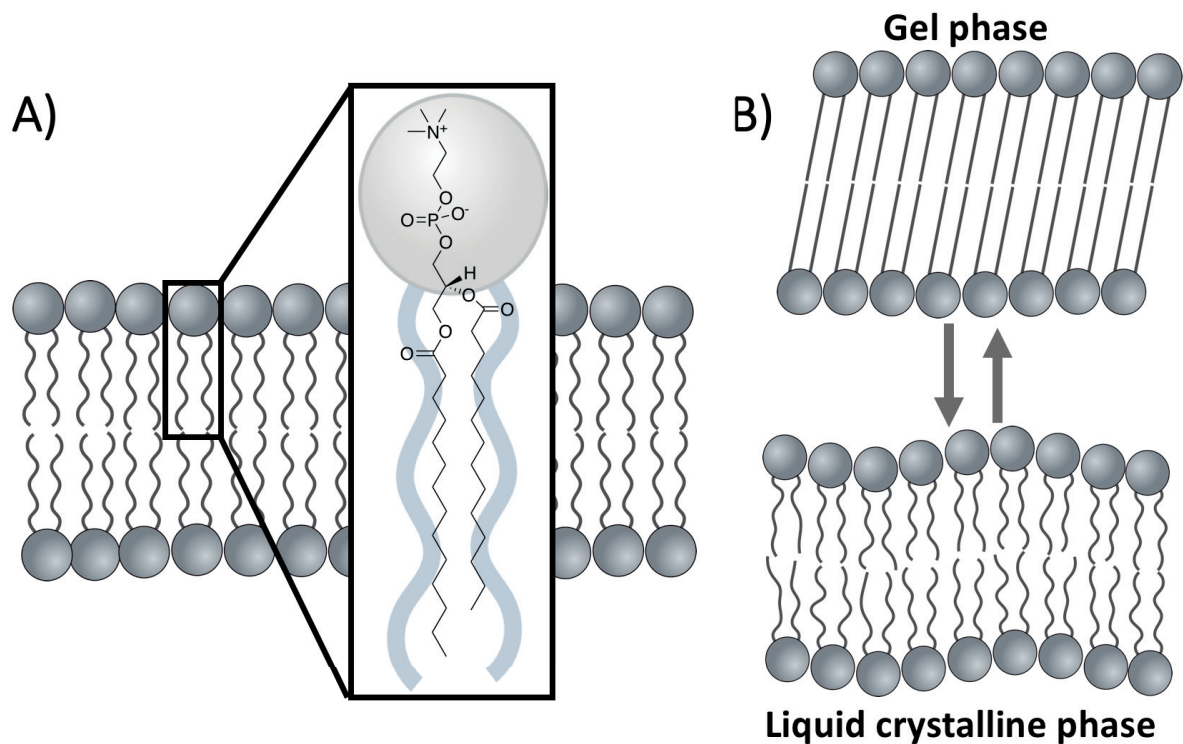
Figure 4. A) *Illustration of a phospholipid bilayer with highlighted structure of an example saturated phospholipid 1,2-dimyristoyl-sn-glycero-3-phosphocholine (DMPC).* ***B)*** *Scheme showing the different physical states adopted by a lipid bilayer in aqueous medium below and above the melting temperature (T_m).*

The first documented evidence pointing to a bilayer structure was presented in 1925 by Gorter and Grendel.[21] They compared the area of a "total" lipid extract from erythrocytes membranes (red blood cells) measured in a Langmuir trough, with the surface area of an erythrocyte. The results revealed that the area of the lipid extract monolayer was twice as large as the area of one erythrocyte, and they therefore concluded that the membrane of the cells had to be two lipids thick. The experimental method used for total extraction of lipids from the cells and the quantitative number for the area per erythrocytes used in this study have later been disputed. Despite the mistakes, however, their contribution to the discovery of the presence of a lipid bilayer is still seen as significant.[22] At the time Gorter and Grendel did their experiments the presence of membrane proteins was not yet known. Proteins were first presented as a part of the membrane in 1935 by Danielli and Davson. They based their model of a lipid bilayer coated with globular proteins on thermodynamics arguments focusing on the differences between the physical properties (for example the permeability of ions,

7

sugars and other hydrophilic solutes) observed in natural membranes and pure lipid membranes.[23]

The exact structure and properties of biological membranes were vastly discussed and several modified and alternative models to the *Danielli and Davson model* were presented in the following decades.[24-29] In 1972, Singer and Nicholson presented the *fluid mosaic model* which gave origin to the current view of the biological membrane. They described the membrane as a two-dimensional viscous solution of lipids and amphipathic membrane proteins in instantaneous thermodynamic equilibrium resembling a mosaic structure.[30] However, after the original proposal of the classical model in 1972, also this model has been thoroughly discussed and criticised for its limitations. The original fluid mosaic model entails a homogenous distribution of proteins which exhibit diffusion in both directions, while experimental data rather show a significant degree of heterogenicity.[28] The original model was therefore later modified to include factors like lipid rafts, heterogeneity, local curvature and lipid-protein interactions.[28, 31-34]

Mouritsen and Bloom presented in 1984 the *mattress model,* focusing on the effect of lipid-protein interactions in biological membranes. Their phenomenological theories are based directly on experimental data derived from mechanical and thermodynamic measurements of membrane properties (see **Figure 5**),[35] taking into account the observed effect that protein has on the phase transition temperature (T_m) of lipid matrixes from the gel phase to the liquid crystalline phase.[36] The *mattress model* suggests that the membrane-proteins and lipids display interaction with a positive free energy content, because of mismatch in the hydrophobic length of the molecules. If the hydrophobic core of a membrane protein is shorter or longer than the thickness of the lipid bilayer, either the lipid membrane has to be deformed to compensate for the unfavourable hydrophobic interactions or some part of the hydrophobic protein or lipid segment will be freely exposed to water. This effect gives rise to increased interfacial tension between lipids and proteins, which may lead to accumulation of specific lipid species around the proteins, as well as aggregation or clustering of proteins in the membrane due to attractive capillary forces.[35, 37]
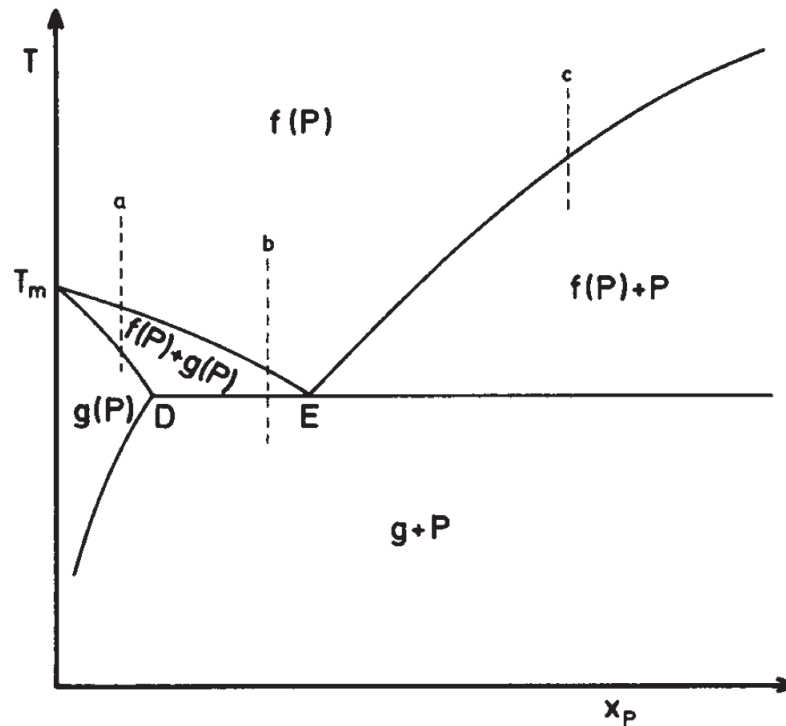
Figure 5. *General phase diagram of lipid protein mixture exhibiting eutectic behaviour in accordance with the mattress model. f(P) and g(P) denotes the lipid fluid (liquid crystalline) and gel phase with dispersed proteins respectively, while g indicate the pure lipid gel phase and P indicates the segregated protein phase. E denotes the eutectic point. Reprinted from Biophysical Journal, 46/2, Mouritsen and Bloom, Copyright (1984), with permission from Elsevier.[35]*

Biological membranes consist of hundreds of different lipid species with variable head group and chain compositions.[37, 38] Over many decades the gram-negative bacterium *E. coli* was used as a main model organism for the general study of bacterial lipid membranes. Information on lipid composition, the physiological function of specific lipid species and the fatty acid biosynthesis pathways in *E.coli* has been useful in understanding general concepts.[38] However, over recent years it has become clear that there is no such thing as a typical bacterial membrane lipid composition and lipid biosynthesis pathways, and using *E. coli* as a blueprint for all bacterial membranes is therefore not valid.[39] E. coli cells have an unusually simple phospholipid composition, generally reported to be Phosphatidylethanolamines (PE), phosphatidylglycerol (PG), and a smaller fraction of cardiolipins (CL).[38] Meanwhile for example the gram-positive bacterium *S. aureus* consist of PG, CL, lysyl-phosphatidylglycerols (LPG) and glycopeptidolipids (GPL)[40], while Mycobacterium tuberculosis consist of PG, CL, PE,

Phosphatidylinositol (PI), phosphatidylinositol mannosides (PIM) and ornithine-amide lipid (OL). This shows how different bacterial species display different membrane compositions, and it has further been shown that even within a single species the lipid composition is dependent on the environmental conditions to which the cells are exposed, and therefore not constant.

Lateral heterogenicity found in biological membranes does not only involve effects of embedded membrane proteins as described above, but also the lipids species can form different clusters or domains. Recent developments in the understanding of the eukaryote membrane have to some degree centred around the concept of clustering of cholesterol and sphingolipids, also referred to as lipid rafts.[41] In this scenario the sphingolipids interact with each other through weak interactions between the carbohydrate heads. These headgroups give rise to larger occupied volumes than their predominantly saturated hydrocarbon chain tails. In the raft model, the resulting voids are suggested to be filled by cholesterol molecules. The close-packed sphingolipid-cholesterol clusters behave as rafts in the membrane surrounded by fluid regions that are occupied by unsaturated phosphatidyl choline molecules.[41] This model for raft development is only relevant for eukaryote cells as it depends on the presence of cholesterol that is not found naturally in bacteria cell membranes. Even so, specific membrane microdomains have also been suggested for bacteria.[42-44] As an example, use of specific lipid dyes has demonstrated cardiolipin-enriched domains at the cell poles of *E. coli* and *B. subtilis* bacterial cells.[45-47] Other findings have revealed that also bacteria are able to organise many signal transduction cascades and protein transport into functional membrane microdomains constituted by specific lipids.[42, 43]
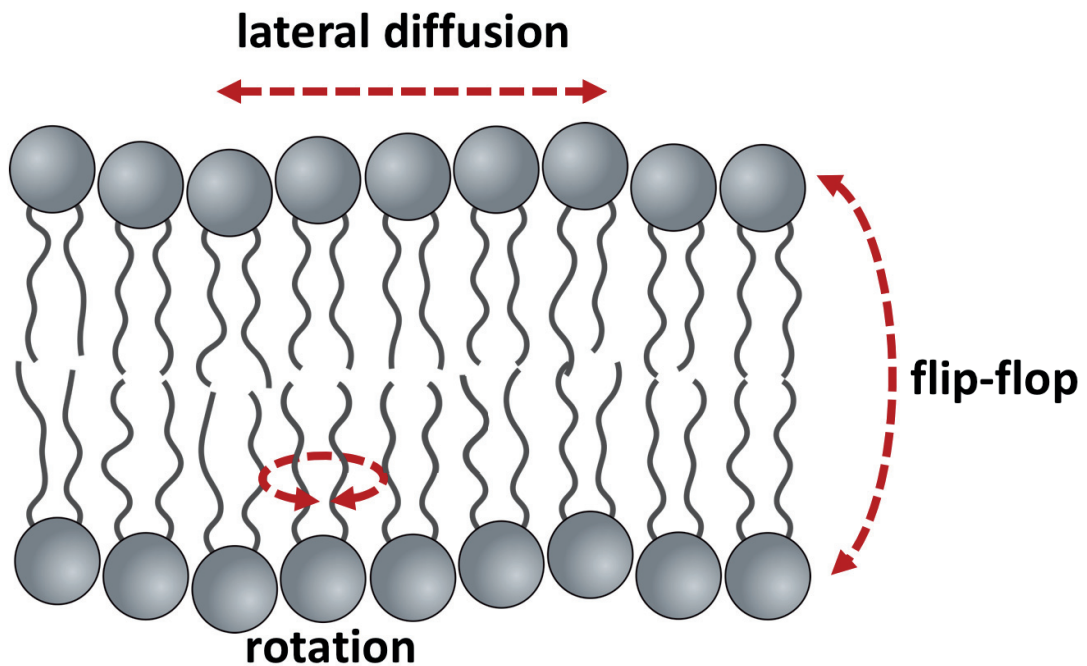
Figure 6. *Illustration of lipid transport processes in lipid bilayers*

Cell membranes are not static entities but are known to exhibit a wide range of dynamic behaviours, from larger scale shape fluctuations to local diffusion of individual molecules. Lipid molecules readily move laterally in the membrane by exchanging places with their neighbours within a leaflet (~10^7 times per second), which means that an average lipid molecule diffuses the length of a large bacterial cell (~2 µm) in about 1 second.[48] In addition to lateral movement of lipids in the biological membrane, the lipids are also able to move between the leaflets in the bilayer, but these processes are much slower as it requires the molecules to overcome substantial activation barrier (**Figure 6**). The events where lipids are transported across the membrane are commonly divided into two categories: lipid flip-flop (also referred to as transbilayer lipid movement) and lipid scrambling. While lipid flip-flop refers to diffusion of a single molecule, lipid scrambling involves a population of lipid molecules.[49] The former may happen spontaneously as a result of thermal motions where the frequency of the event depends highly on the molecular structure of the lipid,[50] or occur in the presence of proteins, e.g. enzyme catalysed by flippases, floppases or scramblases.[49] These proteins move lipids between both monolayers, thus modifying the membrane asymmetry. Flippases and floppases are ATP dependent membrane proteins which

11

move lipids to the inner monolayer and outer monolayer respectively, while scramblase is ATP independent and exchanges lipids between both monolayers.[51] Molecular dynamics (MD) simulations of transmembrane diffusion have revealed how membrane defects (caused for example by protein insertion, enzymes or ion gradient across the membrane) can facilitate diffusion of lipids through the hydrophobic membrane core due to the spontaneous formation of nanoscale water pores as shown in **Figure 7**.[52] Results from Electron Spin Resonance (ESR) spectroscopy have indicated that a phospholipid in a synthetic bilayer rarely flips from one leaflet to the other, and it has been estimated that it occurs less than once a month for an individual molecule.[48] However, the rate of spontaneous flip-flop highly depends on the acyl chain length of the lipid tails and the chemical composition of the head-group.[50]

Lipid scrambling is, on the other hand, somewhat of a precipitous action, where a collection of lipids is moved between leaflets in the membrane. For this event to occur there has to be a build-up of a certain amount of energy, by for example significant asymmetric insertion of proteins or certain surfactants.[49] The cytoplasmic membrane of eukaryotic and prokaryotic cells requires that an asymmetric lipid composition is maintained on both the inner and outer leaflet to function. In bacterial cells, disturbance of this balance has been linked to cell death, while in human cells it has been linked to disease development due to loss of function. One known example form humans is the rare bleeding disorder, Scott syndrome, where an abnormality in regulation of membrane phospholipid asymmetry causes a deficiency in platelet procoagulant activity.[51]
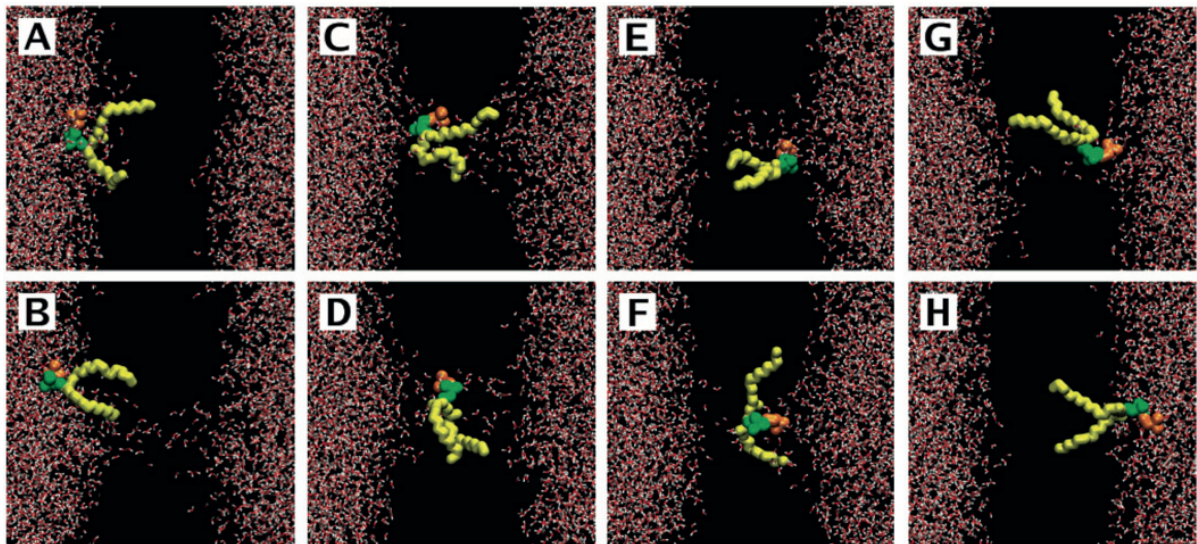
Figure 7. *Lipid flip-flop induced by spontaneous formation of nanoscale water pores as seen by atomic-scale MD simulations under physiological conditions. (A) 0 ns, (B) 43.85 ns, (C) 118.9 ns, (D) 122.4 ns, (E) 152.7 ns, (F) 204.65 ns, (G) 208.9 ns, and (H) 215 ns. Except for the flip-flopped lipid (shown in yellow (tail groups), green and red (the headgroup)) the lipids in the bilayer are not shown; water is shown in red and white. Reprinted with permission from Gurtovenko and Vattulaine (2007).[52] Copyright (2007) American Chemical Society.*

1.2.3 Effect of Bacteria invasion on the human host

Even though the structure of the bacterium cell is characterised as simple compared to eukaryotic cells, it is highly diverse and able to adapt to a range of different habitats, including the interior of other cells and organisms. Although bacteria often are associated with infections and disease, most species are non-pathogenic (not disease producing) in healthy individuals. The total number of bacteria in the human body is estimated to be of the same order as the number of human cells. For the 70 kg "reference man", the number of human cells are estimated to be $\sim 3.0 \cdot 10^{13}$ while the total number of bacteria has been found to be as high as $\sim 3.8 \cdot 10^{13}$.[53] Bacteria and other microorganisms in the body make up the human microbiota. The majority is located in the gastro-intestinal tract, but all surfaces exposed to the environment, like the skin, respiratory tract and genital tract, are colonised by bacteria. The microbiota are essential in helping us degrade food, neutralise toxins and salvage energy from nutrients, particularly carbohydrates that are otherwise indigestible by the host.[54, 55]

Even though most bacteria residing in the human body are commensal without causing disease, it is seen that under certain conditions or in people especially susceptible to

infections, these bacteria can become pathogenic. These bacteria are often referred to as opportunistic. The transition from commensal bacteria to pathogens can be related to the host having an impaired immune response due to for example having cancer, cystic fibrosis, HIV, or taking immunocompromising drugs. In these cases, the bacteria "take their opportunity" to rapidly multiply and cause infection.[56] One example of a known opportunistic gram-positive bacterium is *Staphylococcus epidermis,* which normally lives on the human skin without causing disease due to the competition with the human innate immune system and specifically secretion of antimicrobial peptides. In the case of a lowered immune barrier, for example related to skin wounds or due to contamination during a medical procedure, *S. epidermis* can cause dangerous wound infections and widespread biofilms.[56, 57] Another example is the gram-negative ubiquitous bacterium *Pseudomonas aeruginosa* found in soil and waterbodies. The bacterium is able to evade human defence and colonise in burn wounds causing severe infections. *P. aeruginosa* is also one of the biggest threats for patients with cystic fibrosis causing lung infection due to the lowered ciliated cell defence in the lungs caused by the disease.[58] The threat of pathogenic bacteria is the main motivation for use and development of antimicrobial agents in medicine.

1.2.4 How AMPs targets bacteria cells
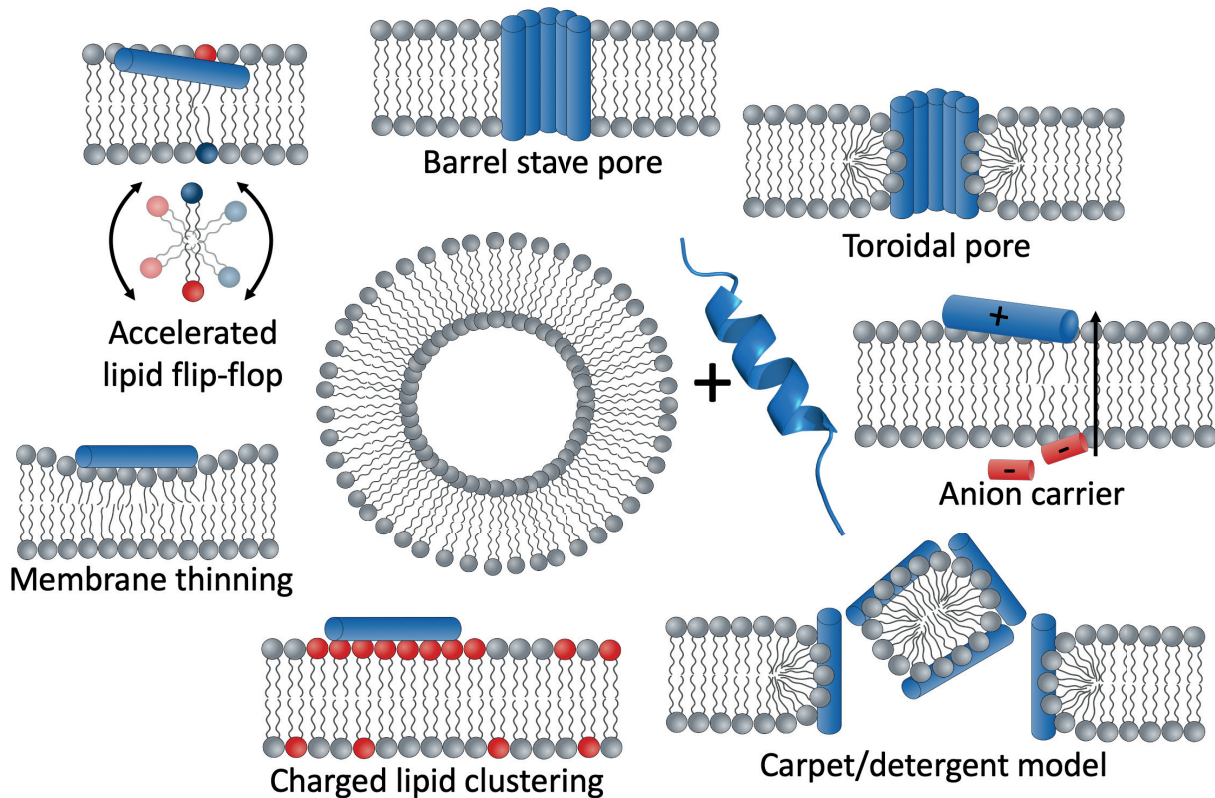
Figure 8. *Illustration showing some of the key proposed models for the mechanism of action of antimicrobial peptides.*

It has long been known that AMPs are effective in killing bacteria and other microorganisms as discussed above. However, the precise microscopic mechanism of how they attack their targets are still subject of much debate. Their interaction with the lipid membrane seems to be a key feature.[59] Some of the most commonly suggested models for the peptide effects on the lipid membrane is shown in **Figure 8**. The generally recognised theory involves formation of AMP induced pores in the cytoplasmic membrane as first presented in 1974 by Baumann and Mueller in their study of the fungi peptide Alamethicin.[60] Pore formation potentially leads to leakage of fluids, ions and other essential molecules over the membrane, and eventually results in cell death. Most textbooks describe the pores made by AMPs in the bacteria membrane as well defined channels either by the Barrel stave model which involves the formation of transmembrane pores, or the Toroidal pore model where the transmembrane channel is composed of both peptides and membrane lipids (both

models are illustrated in **Figure 8**). Formation of these channels involves α-helical peptides self-assembling in the membrane to form defined structures.[61, 62] This is proposed to happen because peptides with well-defined hydrophilic and hydrophobic domains can orient these facets toward corresponding domains in neighbouring peptides, and lipids constituents. The formation of these structures may allow the peptides to insert deeper into the membrane core than they would if their hydrophilic domains where freely exposed to the hydrophobic lipid tails.[63]

The existence of well-defined pores has been highly debated in the recent years, and amongst others Wimley and his group suggested a simpler interfacial activity model where the peptide inserts into the outer leaflet of the bilayer perturbating the packing of the lipids, and causing leakage of fluids over the membrane in that way.[64] It has also been suggested that AMP couple with small anions and thereby facilitate their transport over the membrane.[65]

Alternatively to pore formation, some peptides are suggested to disrupt the membrane by solubilising the lipids in a detergent like manner, often referred to as the carpet model (as illustrated in **Figure 8**). In this model a large number of peptides accumulate on the surface of the membrane. Membrane disruption happens due to the displacement of phospholipid, changes in the membrane fluidity and/or decreases in the barrier properties. Contrary to the pore formation mechanism, the detergent process entails the peptide interacting with the lipid headgroup through electrostatic interactions, carpeting the bilayer without having to penetrate into the membrane core.[63, 66, 67] The resulting disruption may lead to formation of non-lamellar lipid phases like mixed micelles or lipid discs. Sevcsik and co-workes found indication of LL-37 solubilising liposomes at higher concentrations, resulting in formation of disc-like structures. [68, 69]

Beyond the classical models involving pore-formation and solubilisation of the membrane, other models involving peptide-induced changes to the membrane have also been suggested. One example is peptide-induced membrane thinning[70, 71] and thickening[72] due to disordering of the lipid packing as well as peptide-induced changes in the membrane fluidity. Changes in the membrane thickness has both been reported as a mechanism for antimicrobial activity in itself and as the first step in other models.

In this case it is hypothesised that the induced membrane packing frustration causing the changes in membrane thickness that eventually results in membrane disruption. This may lead to membrane permeabilisation or solubilisation in order to relieve the strain stress and the acyl chain packing frustration.[73]

Alternatively to affecting the membrane structure, it has also been suggested that AMPs may affect the lipid transport both in the lateral direction as well as trans-bilayer movements. Epand and co-workers have suggested that AMPs are able to cluster negatively charged lipids in the cytoplasmic membrane due to their multiple positive charges. This effect would lead to in-plane lipid phase separation and sequential phase boundary defects that potentially will lower the permeability barrier between the cell and its surroundings. It would also affect stability of the membrane and cause changes in the existing heterogenicity (discussed in chapter 1.2.2) that may be important for the bacterial cell functionalities.[74-76] This model depends on the AMPs having multiple cationic groups enabling the interaction with several anionic lipids, a conformational flexibility allowing the peptide to adopt a conformation where the distance between positive charges matches the distance between anionic lipids in a cluster, and sufficient hydrophobicity to enable spontaneous partitioning of the peptide in the membrane. Jean-François *et al.* presented in 2008 nuclear magnetic resonance (NMR) data on the chromogranin A derived peptide cateslytin showing how the unstructured peptide adapts to a β-sheet structure when added to a lipid membrane, which causes the formation of rigid and thicker membrane domains enriched in negatively charged lipids.[77] However, a full picture of the effect of lipid composition, including the presence of large lipidic cardiolipins thought to be important in natural domain formation in bacteria, as well as stability and size of the domains formed, is still not elucidated in relation to this suggested effect of AMPs. This motivated our small-angle neutron scattering (SANS) experiments included in **Paper I**.

As described above researchers have discussed whether AMPs potentially also affect the transbilayer transport of single lipids, known as lipid flip-flop.[78-82] As described in section 1.2.2 the spontaneous lipid flip-flop is very slow, and thus effectively mostly regulated by membrane proteins. However, as seen by MD simulations, increased flip-flop rates could be facilitated by defects in the lipid membrane.[52] In addition, some AMPs are able to insert into lipid membranes causing large defects at high concentrations. However, one could imagine that even at low concentrations, below

what is necessary to form pores structures or complete solubilisation, local defects may affect lipid flip-flop.[83] This suggested mechanism is not as well-studied as the models for membrane destruction. This motivated the work in **Papers III-V**.

The proposed physical destruction of the membrane separates AMPs from most traditional antibiotics that act through blocking specific biochemical pathways in the bacteria cells by for example targeting the protein synthesis by inhibition of the small subunit (30S) or large subunit (50S) of the ribosome (70S) (tetracyclines, macrolides and aminoglycosides), the inhibition of the folate synthesis (sulfonamides and trimethroprimes) or cell wall synthesis (β-lactams).[84] Key evidence that points towards AMPs not targeting specific receptors is how their antimicrobial efficacy seem to be independent of the stereoisomerism, while receptor binding normally favours one enantiomer.[63, 85]

Even though membrane disruption has been observed and reported as a key mechanism of AMPs, there have also been results showing how some AMPs affect internal targets of the cells. In these cases, the peptide-membrane interaction may still be important as the peptide has to transport through the membrane to reach intracellular targets. In these cases, AMPs are proposed to cause cell death by translocating the membrane and targeting a variety of essential cellular processes, including inhibition of nucleic acid synthesis, protein synthesis, enzymatic activity, and cell wall synthesis (see **Figure 9**).[86, 87] Chongsiriwatana and co-workers have presented TEM images showing how a number of peptides and peptidomimetic compounds translocate into the cytoplasm of *E. coli* bacteria and cause intracellular biomass flocculation. They hypothesise that the cationic AMPs interact with intracellular polyanions like nucleic acids and ribosomes, causing them to aggregate or associate in non-native ways due to electrostatic interactions. This interaction causes the charge repulsion that usually exists between ribosomes/DNA strands to be reduced or neutralised resulting in flocculation of these entities. The authors argue that these effects can explain the antimicrobial activity of the peptides that could not be explained by neither membrane disruption nor changes in surface morphology.[88] This mechanism also adheres to the evidence pointing towards a non-receptor mediated effect.
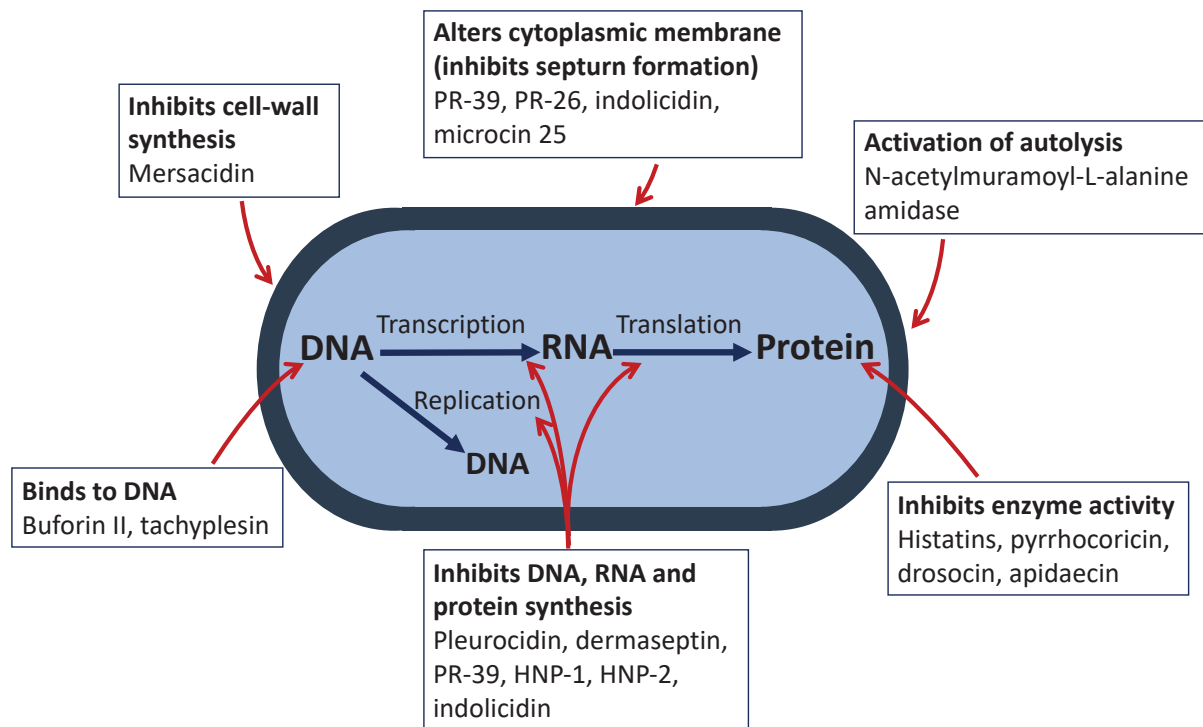
Figure 9. *Illustration showing potential intracellular AMP targets. In this figure E. coli is shown as the example. Adapted with permission from Brogden (2005).[86] Copyright (2005) Springer Nature.*

Beyond killing bacteria directly as antibiotics, AMPs have also been linked to having other host defence effects that potentially are important for their therapeutic activity towards infectious diseases in patients. AMPs have been shown to have a broad range of immunomodulatory effects in humans. These include modulation of expression of hundreds of genes in monocytes (a type of immune cell that can differentiate into macrophages or dendritic cells), epithelial cells and others, direct chemoattraction of immune cells, induction of chemokines (which play a vital role in chemotaxis and cell migration) and differentiation responses, promoting formation of new blood vessels, and wound-healing responses. Traditionally some of the properties listed would be considered proinflammatory, but AMPs have actually been found to have anti-inflammatory properties by amongst other suppressing Toll-like receptor signalling responses and the LPS-stimulated production of proinflammatory cytokines.[89]

As discussed in this section, a variety of different peptide effects have been observed and a variety of models for the antimicrobial mode of action has been presented. Stating a universal mode of action hypothesis is therefore difficult and probably unrealistic. The effect of AMPs seems to be highly complex where both membrane

disruption and intracellular targets may play important roles in the full picture. This uncertainty motivated us to systematically study the peptide-membrane interaction of a variety of peptides using high resolution scattering methodology, allowing us to focus both on the peptide effect on the membrane structure as well as the resulting effect on lipid transport. (**Paper I-V**).

1.2.5 Concentration threshold for membrane disruption

It has been established experimentally that an implicit concentration threshold is required for membrane disruption, independently of the perturbation models discussed above.[71, 90-93] This correlates with a two-step process where the initial step involves peptide binding to and integrating into the membrane, and secondly when enough peptide is bound to the membrane, they start to aggregate.[66] This second step requires a high local concentration of peptide and is essential in for example the pore models.

Melo and Castanho have over the last couple of decades published several papers where they argue that the observed membrane disruption events from biophysical studies require concentrations high enough that the vesicle membrane would be almost completely covered by the peptide.[90, 92, 94] In 2014 Roversi and co-workers published a study focusing on how the helical peptide PMAP-23 (a porcine cathelicidin similar to the human LL-37) only kills *E. coli* bacteria when the bound peptide completely saturated the bacterial membrane (10^6-10^7 bound peptides per cell). When taking into account that *E. coli* bacteria cell have a surface area of ~4.32 μm^2,[95] and an estimate of ~5×10^6 lipid molecules in a 1 μm^2 bilayer[48] a regular *E. coli* under continuous growth should on average contain 2.16×10^7 lipid molecules on the surface. The 10^6-10^7 bound peptides per cell would thereby equal to ratio of as high as ~1:2.2 – 1:22 peptides to lipid molecules.

The minimal inhibitory concentration (MIC) is a parameter used to detect susceptibilities of bacteria to drugs, for example AMPs, and to evaluate the activity of new antimicrobial agents. MIC is the lowest concentration of the assayed antimicrobial agent that, under defined test conditions, inhibits the visible growth of the bacterium being investigated.[96] The MIC values for antimicrobial peptides are typically in the low micromolar range.[92] How the need for high peptide concentrations to disrupt the bacterium membrane relates to the much lower MIC value for AMPs is suggested to be explained by the extent of peptide partitioning in the membrane calculated from the partitioning constant (K_p):[92]

$$K_p = \frac{[P]_L}{[P]_W} \tag{1.1}$$

where $[P]_L$ and $[P]_W$ are the concentrations of the peptide in the lipidic (corresponds to the membrane volume) and aqueous phase, respectively. Melo and Castanho have stated in their studies on a series of natural peptides that the local peptide concentration in a model bacterial membrane is approximately 10,000 times higher than its concentration in the aqueous phase. Therefore, they argue that local membrane-bound AMP concentrations close to or at bilayer saturation is possible even when adding physiologically relevant micromolar overall peptide concentrations (estimated based on MIC concentrations).[92]

The highly concentration dependent membrane disruption effects observed in the past inspired us to include concentration series in all of the membrane studies included in the thesis (**Papers I-VI**).

1.2.6 Selectivity of AMPs towards bacterial membranes

As discussed in chapter 1.1 AMPs have been isolated from various natural sources including cells and tissues in humans. An important question that researchers have tried to answer is why AMPs target microbial cells and not the cells of their host. The selectivity of AMPs towards microbial cells has been attributed to differences in the inherent structures or functions of microbial versus host cells. The fact that the bacterial membrane is composed of a relatively large proportion of anionic phospholipids while mammalian phospholipids are essentially neutral have been suggested as one of the key reasons for AMP selectivity. As the peptides generally has a positive net charge, the anionic and more fluid bacterial bilayers are more susceptible to peptide binding and therefore membrane disruption.[63, 92] Beyond electrostatic and hydrophobic interactions, some AMPs display specific structural affinity for anionic bacterial membrane constituents acting as pseudo-receptors, such as phospholipid head groups or membrane proteins.[63, 92, 97]

One of the main differences between mammalian and microbial cells is the presence of cholesterol in the membrane of mammalian cells. Several researchers have suggested that cholesterol may play a significant role in protecting mammalian cells from membrane destruction of AMPs.[98-105] Sharma *et al.* presented quasielastic neutron scattering (QENS) data on melittin (AMP from honeybee (*Apis mellifera*)

venom) interaction with lipid membranes with and without cholesterol. Their experiments showed that adding melittin to cholesterol-free membranes greatly influenced the phospholipid dynamics, and the peptide was found to act as a plasticiser in the solid gel phase and a stiffener in the fluid phase. When adding melittin to cholesterol loaded membranes, the dynamical properties were not affected in the same manner. The authors suggest that the difference is due to cholesterol preventing the embedding of melittin deep into the membrane.[103] For most AMPs, the detectable inhibitory effect of cholesterol is only noticeable at higher cholesterol concentrations. This has been explained by the formation of a liquid ordered lipid phase because cholesterol inclusion in the membrane increases the acyl chain order in the membrane core. This may suggest that the indirect effect cholesterol has on the membrane fluidity is more important than the direct interaction between the AMPs and cholesterol.[101] A definite conclusion on the role of cholesterol in selectivity of AMPs is yet to be drawn.

An alternative theory proposes that access of AMPs to potentially vulnerable host tissues may be limited by localisation and/or highly regulated expression. An example of this mechanism for selectivity is the presence of defensins in neutrophils, monocytes and macrophages (white blood cells important in the immune system) in various mammalian species. Defensins are amongst the most potent AMPs identified and have been found to be highly unselective and toxic also towards mammalian cells. An explanation of why these peptides still play a significant role in the immune response of mammalians without killing their host is the constrained localisation of these peptides in granules of mammalian phagocytes. The phagocytes normally internalise pathogens through phagocytosis and thereby expose the pathogens to lethal concentrations of defensins internally, rather than release these potentially toxic components into the extracellular environment where they could also attack host cells.[63]

The unanswered questions related to AMP selectivity towards bacterial membrane, especially the role of cholesterol inspired us to do small-angle X-ray scattering (SAXS) and neutron reflectometry (NR) experiments on membranes with different amount of cholesterol (**Paper SV** not included in the thesis but discussed in Chapter 3.3).

1.2.7 Mechanism of resistance of AMPs

Antimicrobial resistance occurs when microorganisms develop the ability to survive exposure to antimicrobial agents and therefore become significantly less susceptible to the drugs. The typical mechanisms for resistance development to antimicrobial agents are alteration of the drug target, reduced cellular uptake, inactivation of the drug and increased efflux of the drug from the cell interior.[84] Traditionally, antimicrobial peptides have been presented as less affected by development of antimicrobial resistance than convectional antibiotics. This has been related to their supposed mode of action involving a mechanical membrane disruption rather than a receptor interaction. It is therefore suggested to be less likely for the bacteria to adapt to withstand this physical attack as there is not a conventional target that can be altered to no longer bind to the drug. However, it is unrealistic to expect that no microbial pathogens are able to resist antimicrobial peptides due to the evolutionary development of a balanced pathogen-host relationship.[63, 106] Indeed prokaryotic pathogens have been found to devote a considerable part of their genome to express complex countermeasures designed to limit the effect of antimicrobial peptides.[63] Examples of suggested bacterial resistance mechanisms towards AMPs include release of extracellular proteases,[107] sequestration,[108] cell surface modifications[109, 110] and increased efflux activity.[111] A more thorough understanding of the balance between the opposing mechanisms of action and resistance among antimicrobial peptides is still being researched.

Beyond recognising that resistance towards AMPs actually does occur, researchers have recently shown that AMP-resistant pathogens (mutants) even display significant cross-resistance. This was found to include a broad range of AMPs even though the structure and modes of action varied. Unfortunately, this means that the widespread clinical use of AMPs to treat bacterial infections may select for resistant bacterial pathogens that are more capable of causing severe infections in humans because natural AMPs play a key role in the innate immune system. However, the actual outcome of exposure to therapeutic levels of AMPs on the development of AMP resistance and bacterial pathogenesis is not yet fully understood, and therefore needs to be further studied before widespread use in clinical settings.[112]

1.3 Approaches to study the membrane effects of AMPs

Traditionally, AMPs are characterised in regard to antimicrobial effect by their MIC values (defined above) against various different bacteria, and to selectivity by toxicity studies using human cell lines. While these results give valuable comparable information on the drug potential of the specific peptide, they do not provide insight into the molecular mode of action. Therefore, a series of different methods have been introduced as valuable tools in probing both the peptide effect on the cytoplasmic membrane and on internal targets. In this chapter some of the key biophysical and biochemical techniques used to study the peptide-membrane interaction are discussed. Focus will be given to the use of lipid model systems to mimic bacterial cell membranes and the main methods included in the thesis; neutron reflectometry (NR), small-angle X-ray (SAXS) and neutron scattering (SANS).

One of the most used approaches to visualise the membrane effect of AMPs is different types of microscopy. Confocal laser-scanning microscopy can be used to separate whether the peptide enters the bacterial cell and accumulates in the cytoplasm, or if it binds to the cell surface,[113] while scanning electron microscopy (SEM) and transmission electron microscopy (TEM) have been used to study the damaging effect of various antimicrobial peptides on the architecture of bacterial cells. These methods have been essential in revealing that there is no general effect of the peptides on microbial cells, leading to the understanding that different AMPs may have different modes of actions (as discussed in Chapter 1.2.4) and/or targets.[86] An advantage with these microscopy methods is that real microbial cells can be probed without having to resort to model systems. However, microscopy does not yield information on a molecular level with the required Ångström-nanometer (Å-nm) resolution. On the other hand, atomic force microscopy (AFM), which is based on imaging a three-dimensional shape of a sample surface, has been widely used to study peptide-membrane interactions using model systems.[114-117] Recently due to improvements in sample preparations, time resolution and image qualities, researchers have been able to observe real-time changes in living cells in time-scales relevant to dynamic cellular processes using high-speed AFM. Based on this types of experiments, the proposed two-stage mechanism discussed in Chapter 1.2.5 has been observed.[118]

Other surface sensitive techniques that have been used to study AMPs are quartz crystal microbalance with dissipation monitoring (QCM-D), which gives information on the mass and viscoelasticity of a supported lipid bilayer, ellipsometry, giving information on the absorbed mass of an interfacial film and in some cases its thickness, and attenuated-total reflectance Infrared spectroscopy (ATR-FTIR) which provides information on changes in the chemical composition at or close to the interface.[117] These techniques are often used in symbiosis with each other, and/or more comprehensive techniques like AFM and NR (which will be discussed in the next chapter). Examples of studies solely using QCM-D do exist though; Wang *et al.* reported a study where they try to pinpoint the mechanism of various AMPs by using only QCM-D by identifying signature patterns in the changes in frequency and dissipation, associated with either pore formation, peptide absorption on the membrane surface, or peptide insertion as single molecule or clusters in the membrane.[119]

Another very popular techniques used to study the effects of peptide on lipid membranes is fluorescence spectroscopy. One of the most frequently used methods to study the peptides ability to permeabilise the cell membrane is with the incorporation of fluorescent dyes (like for example calcein) in liposomes, followed by measuring the release upon peptide addition over time using fluorescence spectroscopy.[86, 120] Results from these membrane permeabilisation studies have often been used as evidence for the pore-formation model best representing the mode of action of the AMP. Permeabilisation of the membrane caused by peptides can also be probed by studying the occurrence of voltage-dependent ion channels in the membrane. This is done by measuring the conductivity across the membrane, where potential peptide-formed pores in the membrane enable an electrical current.[121, 122]

Circular dichroism (CD) is a popular method for determining the secondary structure of AMPs before and after being exposed to different lipid environments. CD is an absorption spectroscopy method that uses circularly polarised light to detect structural aspects of optically active chiral molecules.[123] This method has been essential in revealing that exposure to lipid membranes in many cases induces conformational changes in the peptides which have been linked the peptide's capability of inserting into the membrane.[86]

As discussed in Chapter 1.2.2, the lipid membrane undergoes an important phase transition upon heating or cooling of the system. Peptide-induced changes in the phase behaviour of lipid membranes have been meticulously studied using differential scanning calorimetry (DSC). Using this technique, one has been able to reveal that not only do different peptides have different effects, but also that the lipid composition of the bilayer will greatly influence the degree of changes in phase behaviour upon peptide exposure.[124]

NMR has been shown to be a very versatile tool for studying interactions between AMPs and lipid membranes. One of the major advantages is that contrary to other methods like fluorescence, NMR techniques often do not require any bulky chemical labelling, but rely on the nuclear spins of the elements that can be altered by isotope labels like ^{15}N,^{13}C, or ^{2}H which do not affect the chemical properties of the molecules.[125] Liquid state NMR can be used to determine the atomic resolution structure of the peptide particle.[126, 127] In these experiments, the peptides are often solubilised in "membrane-mimicking" solutions containing a certain amount of non-polar solvent like for example Tetrafluoroethylene/water mixtures. This is because the non-polar solvents have been found to promote helical conformations of the peptides which is often found when the peptide inserts in the membrane. However, as these solvents, contrary to the membrane, are isotropic, the peptide structure resulting from the NMR data may not necessarily represent the real situation in the membrane. Therefore, an alternative is to expose the peptides to lipid-like environments like micelles or bicelles that are still small enough to allow the use of liquid state NMR. Even though this is closer to the real membrane situation, the sizes of these aggregates are still quite small and the number of peptides per particle is difficult to adjust. A drawback in the use of bicelles is that the lipid composition cannot be varied much without disturbing the stability of the aggregates. Therefore, it has been deemed more favourable to study the peptides in genuine lipid bilayers, like in small unilamellar lipid vesicles (further discussed in Chapter 1.3.1). However, these structures are normally too large to be measured using traditional liquid state NMR, and therefore researchers have done these types of studies using solid state NMR instead. Using this method, a large number of papers has been published using different approaches, ranging from indirect studies of the peptides by probing the lipid structure (by labelling of lipids) to

direct measurements of the peptide structure in the bilayer by isotope labelling the peptides directly. [125]

Beyond these experimental methods, also computational methods have been vastly used to study AMPs and their mechanism of action. MD simulations have for example been used to reveal the thermodynamics, kinetics, and mechanism of pore formation and closures in lipid bilayers. These kinds of studies have shown how AMPs seem to increase the occurrence of pore formation in the membrane by decreasing the free energy cost, either by further reducing the enthalpy or decreasing the unfavourable entropic cost.[128] Furthermore, MD simulations have been able to separate whether the peptide-induced membrane pores can be classified as toroidal or pure cylindrical for specific peptides.[129]

An alternative approach to elucidating the antimicrobial peptide effect on both the structure of the membrane and on lipid transport processes using neutrons and X-rays will be thoroughly discussed below. However, first we will take a closer look at the use of lipid model systems as alternatives to live bacterial cells for peptide-membrane interaction experiments.

1.3.1 Lipid model systems

As described in Chapter 1.2.2, the cell membranes of real bacteria are highly intricate, consisting of a diverse group of membrane proteins, LPS (only in the outer membrane), and a vast number of different lipids, where phospholipids are the most abundant. The complexity of live bacteria will for many biochemical, biophysical, and theoretical methods obscure the results and complicate the interpretation with regard to the specific membrane-peptide interactions. Therefore, development of good model systems has been essential to enable detailed studies on peptide-lipid interactions. The model systems most used are phospholipid membranes either as flat model membranes (either supported or tethered lipid bilayers) used for surface sensitive techniques like NR[117, 130-135] and AFM[114-116, 136], hydrated multilamellar membrane stacks typically used for a small-angle scattering technique referred to as diffuse low angle scattering[137, 138] and free-floating lipid micelles, bicelles and vesicles frequently

used in amongst others NMR,[62, 127, 130, 139] SAXS/SANS,[69, 72, 82, 83, 135, 140-147], CD and fluorescence spectroscopy[148, 149].

The design of a model system is highly flexible depending on the aim of the study, ranging from a simple monolayer of only one type of phospholipid, to very complex lipid mixtures with embedded membrane proteins and LPS.[150] The composition of model systems is adjustable to mimicking specific cell types. This can, for example, involve incorporating cholesterol to a lipid bilayer made to mimic a mammalian cell, or anionic lipids to model membranes made to mimic bacterial cells. Beyond the simpler model systems, efforts have gone into developing systems more closely related to the real bacteria membrane. Clifton and co-workers recently presented a full NR characterisation of a floating lipid membrane closely mimicking the inner and outer membrane of *E. coli* including the LPS layer.[133]

In **Figure 11** an illustration of a supported lipid bilayer and an unilamellar lipid vesicles (the two model systems used for the work included in this thesis) is shown. Lipid vesicles are formed through spontaneous self-assembly of dry lipid films upon hydration in an aqueous solvent. A range of different combinations of lipids with different headgroup structure, tail length and degree of saturation can be used to form lipid vesicles.[151-156] However, to mimic bacterial cells, often a combination of zwitterionic and anionic lipids with or without cardiolipin is used.

Figure 11. Illustrations of unilamellar lipid vesicles and supported lipid bilayers used as model systems to probe membrane interactions. Chemical structure of three phospholipids often used in model membranes.

The self-assembly process of lipid bilayers is entropically driven by the hydrophobic effect bringing hydrophobic segments of the lipids together in order to reduce the overall contact with water thereby reducing the surface energy.[157, 158] The shapes that are formed are largely dependent on the geometrical shape of the lipid molecule as illustrated in **Figure 12**. The packing properties of lipids can be expressed in terms of the critical packing parameter, P:

$$P = \frac{v}{a_o \cdot l} \tag{1.2}$$

where v is the lipid chain volume, a is the optimal surface area and l is the maximum length of the hydrocarbon chain(s).[158]
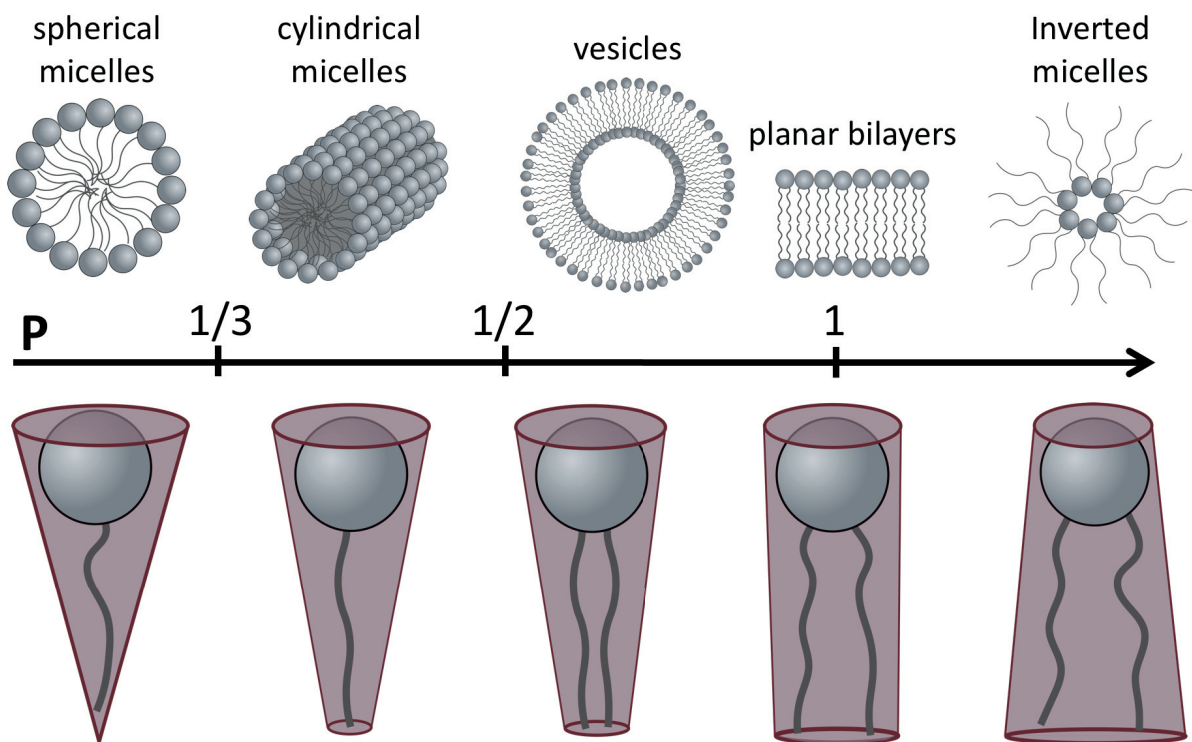
Figure 12. Sketch giving an overview of the critical packing parameter with the resulting morphology.

Bilayers are formed spontaneously by amphiphiles (lipid in the case of membranes) that have a small headgroup area (a_0) or too bulky hydrocarbon chains to fit into smaller aggregates like micelles while still maintaining the surface area at its optimal value. The P of bilayer forming lipids must lie close to 1, meaning that for the same headgroup area (a_0) and tail length (l) their lipid chain volume (v) must be twice that of a micelle-forming lipid (for these the P mostly range from 1/3 to 1/2). This is the reasoning behind why most phospholipids, which have two tails, are likely to form bilayer structures in aqueous solution. The closing of bilayers into vesicles eliminates the unfavourable edges of a finite bilayer, and therefore happens spontaneously under certain conditions as this structure is both entropically and energetically favoured.[158] However, the lipids need to have a truncated cone geometry, in other words $P < 1$, in order for the lipids to pack in the outer leaflet, enabling the bilayer to curve.[158] Based on simple geometrical considerations the radius of the smallest vesicle that can be formed without introducing unfavourable packing stress on the lipids, in other words the headgroup area, a not exceeding a_0 is:

$$R_c \approx l \left[\frac{3 + \sqrt{3(4v/a_o l - 1)}}{6\left(1 - \frac{v}{a_0 l}\right)} \right] \approx \frac{l}{\left(1 - \frac{v}{a_0 l}\right)} \qquad (1.3)$$

Note that the same unfavourable stresses do not arise for the inner leaflet lipids, because these can maintain their optimum area without requiring their chains to extend beyond l due to curving in the opposite direction.[157] Even though vesicle radii, $R < R_c$ are energetically unfavourable, the vesicles will not grow infinite because $R > R_c$ is entropically unfavourable. That being said, the radius of vesicles used as model membranes for experiments is usually determined by the preparation methods, which often includes sonication (either bath sonication or using a more aggressive tip sonicator) to break up bigger vesicles, leaving a polydisperse mixture of smaller unilamellar vesicles, and/or extrusion where the vesicles are forced through a polycarbonate filter with a defined pore size. Using the latter method also breaks apart multilamellar structures, resulting in a relative uniform sample of vesicles with radii reflecting the chosen pore size. The resulting vesicles will normally be stable throughout the experiment (not taking into account eventual addition of destabilising

substrates like AMPs) even though the radius is lower or higher than R_c due to the low solubility of the lipids and the consequently slow exchange and Ostwald ripening processes.[158]

Supported lipid bilayers (SLBs) can be formed by the vesicle fusion method or by Langmuir-Blodgett (LB) and Langmuir-Schaefer deposition (LS). The vesicle fusion method is beneficial because it can be done *in situ*; however, it does not give the same control over the deposition as for LB/LS and can therefore not be used for formation of asymmetric leaflet compositions.[159, 160] The vesicle fusion method entails deposition of small sonicated lipid vesicles to a substrate until a critical amount of vesicles have attached to the surface. At this point the vesicles become unstable and eventually break apart and fuse together to form a continuous bilayer.[159] The ideal conditions with regards to for example vesicle concentration, temperature, flow rate and duration of the vesicle injection is dependent on the lipid composition. Because QCM-D allows real-time observation of SLB formation, this method is well used to determine the ideal conditions for a given lipid mixture.[161] Lipids with a PC headgroup (zwitterionic) are the most commonly used in SLBs because the formation of these bilayer structures are well established.[116, 119, 130, 132, 162-167] To closer replicate the bacterial cell membrane, PG (anionic) or PE (zwitterionic) lipids are sometimes added to the composition (the structure of PC, PG and PE lipids with 14 carbon tails have been included in **Figure 12**),[168] while mimicking of mammalian cells is often achieved by adding cholesterol.[169] However, recently Lind *et al.* reported a new protocol to form high coverage SLBs consisting of only PE and PG, directly mimicking the phospholipid composition of the membrane of *E. coli* bacteria.[134]

1.3.2 Neutron Reflectometry – general theory

Reflectometry experiments can be done with different radiation sources (for example X-rays and neutrons). However, we will focus on neutrons in this part because it has been shown to be a powerful technique for the study of antimicrobial peptides on lipid bilayers. When comparing neutrons to X-rays there are some beneficial properties of neutrons that makes neutron reflectometry more ideal for the study of peptide-membrane interactions.

Firstly, because neutrons carry no net charge, they will interact with the atomic nucleus rather than with the electron cloud as for X-rays, and thus have a smaller scattering cross-section (i.e., interaction probability). This allows the neutrons to penetrate deeply into the samples and therefore probe interfaces buried in complex environments. One example is the possibility to carry out detailed studies on SLBs situated inside solid-liquid interface flow cells. Cold, thermal and epithermal neutrons that are normally used for these experiments have wavelengths in the Ångström regime making them very suitable to study molecular structures, like biological systems.[117] When comparing with X-rays, neutrons are non-damaging to biological samples because they do not cause radiation damage. Lastly, the relationship between scattering probability (known as scattering length, b) and the atomic number is different for X-rays and neutrons. Because X-rays interact with the electrons, a higher number of electrons equals more interaction and the scattering lengths are therefore proportional to the atomic number. Neutrons on the other hand, interact with the nucleus and the nuclear structure is therefore decisive of the interaction, resulting in the scattering lengths being isotope dependent and non-monotonic across the periodic table. In practice, however, the relevant quantity is the scattering length density (SLD), ρ, i.e., the scattering length per volume:

$$\rho(z) = \frac{\sum_{i=1}^{N} b_i}{V_m} \tag{1.4}$$

where b_i is the coherent neutron scattering length from the N atoms in a molecule and V_m is the is the molecular volume.[117, 170]
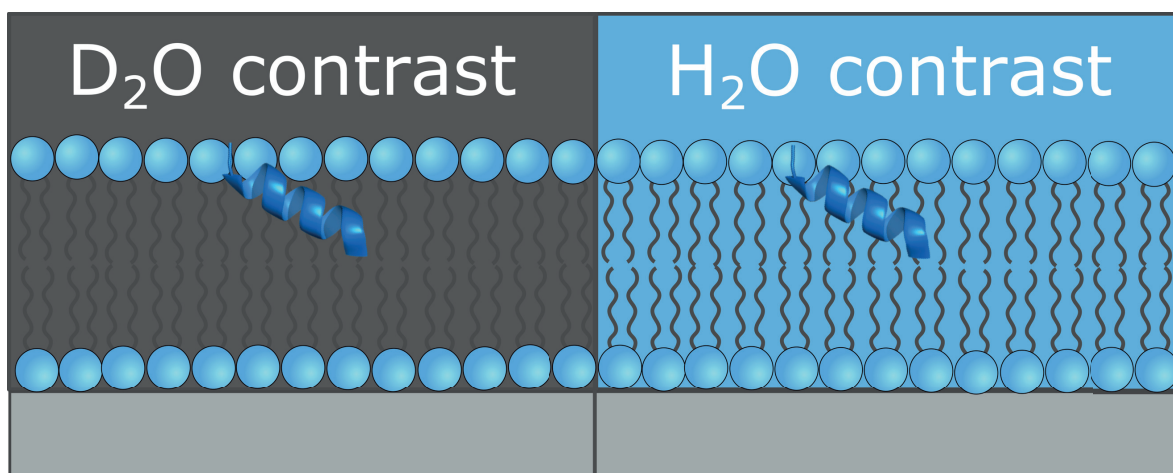
Figure 13. Schematics of contrast variation in studying the peptide insertion in a lipid membrane consisting of tail deuterated phospholipids using neutron reflectometry.

The isotope sensitivity of neutrons gives rise to an interesting effect: The neutron scattering lengths of hydrogen and its isotope deuterium are markedly different, while for X-rays these are identical. This means that we can probe a system in different "contrasts" between solute and solvent, which for a particle with SLD $\rho(z)$ in a solvent with SLD ρ_s, is defined as the excess scattering length density

$$\Delta\rho(z) = \rho(z) - \rho_s. \tag{1.5}$$

The contrast can be adjusted by altering the amount of D_2O and H_2O in the solvent, in other words altering the ρ_s. Because the SLDs of biological molecules in their native form are in-between those of D_2O and H_2O, this allows us to match the SLD of the solvent to individual components within a complex sample and thereby emphasising the scattering from another component. This technique is often referred to as contrast variation. Normally in a neutron reflectometry experiment, the sample will be measured in several different contrasts ranging from pure H_2O to pure D_2O, and it has been stated that at least two contrasts are necessary to obtain accurate structural information from the data.[159] Beyond only using the solvent to highlight different parts of the system we can further utilise this difference in scattering length between deuterium and hydrogen by labelling parts of the system using deuteration. This is for example often done in the study of lipid membranes. By using tail deuterated phospholipids there will be a significant contrast between the proteated lipid heads (which will be visible in D_2O but hidden in H_2O) and the deuterated tails (which will be visible in H_2O but hidden in D_2O). This allows for very precise determination of the exact thickness of both the head and tail region of the bilayer and is also convenient when studying interactions between for example peptides and membranes as it also increases the contrast between the substrate and the membrane core. A schematic showing the details of such a contrast variation experiments on a lipid bilayer with tail deuterated lipids have been included in **Figure 13**.

NR is a powerful technique for analysis of thin films providing information on structural features in the direction normal to the interface. When the beam is reflected on a flat surface, we refer to this as specular reflection. In specular reflection, the angle, θ_i, of

the incident wave vector ($\vec{k}_i$) with the surface, equals the angle, θ_r, of the reflected wave vector ($\vec{k}_r$). The lengths of the incident and the reflected wave vectors are assumed to be equal (elastic scattering) and given by:

$$\left|\vec{k}_i\right| = \left|\vec{k}_r\right| = \frac{2\pi}{\lambda} \tag{1.6}$$

where λ is the wavelength of the neutron beam. The data acquired in a neutron reflection experiment is normally presented as the relative intensity of the reflected beam as a function of the scattering vector, $\vec{Q}$. The changes in $\vec{k}$ on the reflection at the surface can be related to $\vec{Q}$ by:

$$\left|\vec{k}_r - \vec{k}_i\right| = 2\left|\vec{k}_{i\perp}\right| = \frac{4\pi}{\lambda}\sin(2\theta/2) = Q \tag{1.7}$$

where $\left|\vec{k}_{i\perp}\right|$ is the length of the component of $\vec{k}_i$ normal to the interface.[159] **Figure 14** illustrates the principles of specular neutron reflectometry (A) and gives an example of how the neutron beam is reflected from a silicon crystal often used as the solid substrate in a neutron reflectometry experiment.
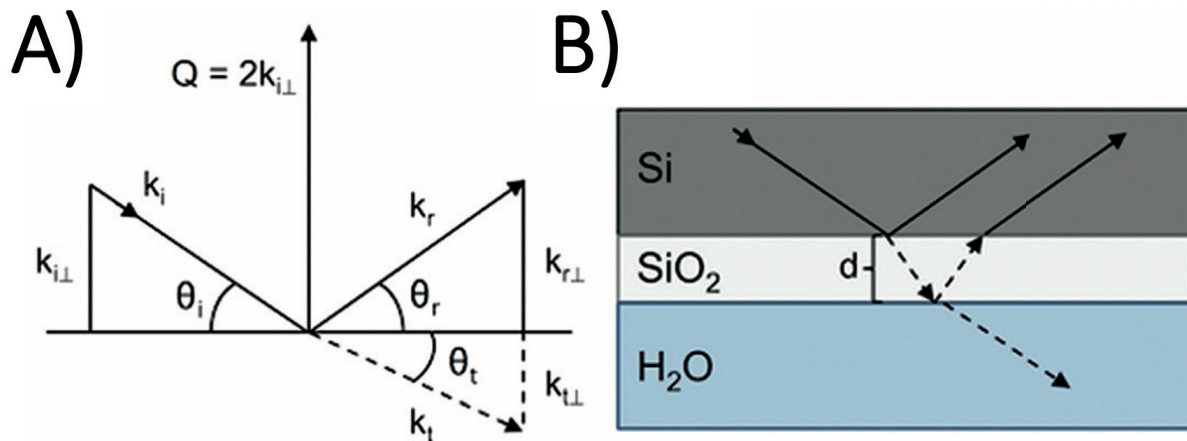
Figure 14. A) *Sketch of a neutron beam reflected on a surface in a specular neutron reflectometry experiment. The sketch includes definitions on the incoming, reflected, and transmitted wave vectors ($\vec{k}_i$, $\vec{k}_r$, and $\vec{k}_t$, respectively) their angles with the surface ($\theta_i = \theta_r$ and θ_t) and the scattering vector $\vec{Q}$. B) Illustration of neutron beam scattered from a thin layer of native oxide on silicon having a thickness, d, facing a H₂O bulk. Reprinted with permission from Lind and Cárdenas (2016).[159] Copyright (2016) American Vacuum Society.*

The reflectivity curve resulting from a successful neutron reflectivity experiment on a layered interface normally exhibits Kiessig fringes, due to interference occurring between the waves reflected within the interfacial film. The spacing and intensity of the interference fringes can be used to extract a SLD profile, $\rho(z)$, perpendicular to the surface, yielding information on both the SLD and the thickness of the different layers parallel to the surface. Extracting precise structural parameters from neutron reflectivity data can be done in several different ways. Model data fitting of the thickness, composition, solvation and roughness of a finite number of stratified layers parallel to the interface is by far the most common technique to evaluated NR data.[117]

1.3.3 Peptide-membrane interactions as seen by Neutron Reflectometry

The ability to extract detailed structural information about different layers deposited on a substrate makes NR a well-suited technique to study AMP effects on lipid membranes. The protocol for deposition and characterisation of supported lipid bilayers mimicking different membranes on silica crystals using NR has been well established.[117, 159, 171-174] Based on these principles researchers have used the same methodology to study the membrane effect of a series of different biomacromolecules,[130-132, 166, 175-178] including natural and synthetic antimicrobial peptides.

With regards to natural AMPs, Fernandez *et al.* have shown how aurein 1.2 disrupts DMPC/DMPG membranes following the carpet model (described in detail in Chapter 1.2.4). The neutron reflectivity data revealed how addition of aurein 1.2 led to a slight degree of membrane thinning, with peptide insertion into the tail region rather than translocation across the membrane.[130] The same authors later showed how another frog extracted peptide, maculatin 1.1, instead causes a slight thickening of the membrane. This peptide, contrary to aurein 1.2, seems to translocate the membrane through passive diffusion.[131]

Cárdenas and co-workers have extensively studied synthetic Poly(amidoamine) (PAMAM)[166] and BALY[132] dendrimeric AMPs using NR. They have found that when comparing these peptides with varying size, the smaller dendrimers are able to penetrate into the bilayer affecting the lipid phase and ordering[132], while larger sized

dendrimers rather situates on the surface of the membrane.[166] In this work, the authors also showed how by using AFM with continuous flow it was possible to image the dendrimer effect on the membrane in real time, giving highly complementary data to what they could determine by NR.[116]

It has further been shown by Nordström *et al.* that NR also can be used to study the membrane effect of AMP-containing drug carriers. In this case anionic poly(ethyl acrylate-*co*-methacrylic acid) (MAA) microgels were used as carriers for the natural AMP LL-37. By NR, they were able to establish that the effect of LL-37 loaded into MMA microgels qualitatively mirrored the effect of pure LL-37 when added to a supported lipid bilayer, and in both cases, they observed a concentration dependent insertion of the peptide. The peptide seems to preferentially insert in the outer leaflet at low concentrations, but when increasing the concentration LL-37 was found to penetrate both leaflets, resulting in a more pronounced membrane defect. From these results the authors concluded that the membrane interactions for microgel-loaded LL-37 are dominated by released peptide. However, the kinetic effects of the peptide-membrane interaction are substantially affected by the carrier due to the slow release of peptide from the microgel.[178]

The results discussed so far have all been based on supported lipid bilayers consisting solely of phospholipids (either a single lipid or a mixture of different lipid types), while Paracini *et al.* has recently showed that NR also can be used to study the peptide interaction of much more complex model systems. In this work, they studied the effect of polymyxin B on an asymmetric d62-DPPC/LPS outer membrane model bilayer deposited on a silicon substrate following a protocol prior developed by Clifton *et al.*[160] In this way, they could both probe the peptide effect on the phospholipid bilayer and on LPS present on the surface of the outer membrane of gram-negative bacteria. From the NR data they found that the physical state of the lipid matrix is critical in regulating the peptide interaction. When LPS goes from the gel to the crystalline state, the peptide is able to insert into the membrane causing large-scale disruption and loss of membrane asymmetry.[179]

The established proof that NR is a useful technique to study AMP-membrane interaction inspired some of the work presented in this thesis. However, the drawbacks of NR are that the experiments are highly time consuming and costly as it requires

deuterated components and access to a neutron source. In addition, the bilayer in this case is not free-floating in the same way as for a bacterial cell which potentially leads to confounding factors in the analysis of the results. This motivates using SAXS, which is much faster, more easily available, does not require isotope labelling and can be used on free-floating vesicles rather than supported lipid bilayers, as an alternative probe to study a larger series of peptides. A direct comparison of the two methods are presented in **Paper II**. Meanwhile, **Paper VI** focuses on a specific system of large peptide nanofibers where NR has large advantages over SAXS/SANS because it lacks 3D orientation averaging and therefore enables precise structural determination of complex nanofiber-membrane structures.

1.3.4 Small Angle Scattering – general theory
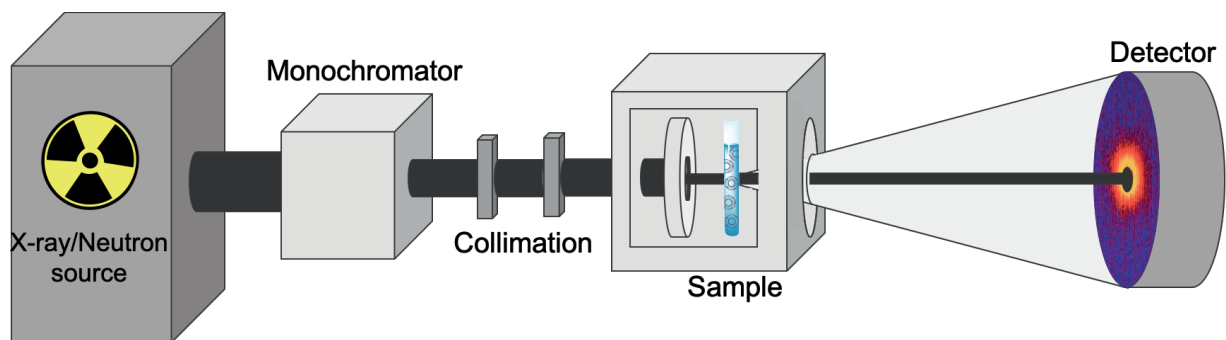
Figure 15. *Schematic showing the SAS instrument setup.*

Small angle scattering (SAS) experiments can, in the same way as reflectometry, in principle be performed by any kind of radiation but we will focus this section on X-rays (SAXS) and neutrons (SANS). In a SAS experiment a well collimated beam of radiation with a wavelength λ and energy E are incident on a sample (for example an antimicrobial peptide dissolved in a buffer). In the case of SAXS, X-ray photons interact with the atomic electron shell, whereas in SANS, neutrons interact with the nucleus as described in Chapter 1.3.2. While most of the radiation is transmitted through the sample, some of the beam will be scattered away from the incident direction. In a SAS experiment a 2D detector at a distance L away from the sample records the scattered

intensity I as a function of the scattering angle θ (see sketch of instrument setup in **Figure 15**). With sample particles tumbling freely in solution, the scattering pattern is usually isotropic and can thus be azimuthally integrated into an 1D $I(\theta)$ scattering curve. In a diluted system the scattering curve contains information on the structure of the individual particles, and the scattering length arrangement within them (the so-called form factor). For example, we can gain information about the bilayer thickness as well as the overall radius of a lipid vesicle from this scattering pattern. In a concentrated system, we additionally gain information about positional correlations and the average spatial arrangement of the particles in the sample (the so-called structure factor). When the instrument is calibrated to the absolute magnitude of the scattering intensity (achieved by using water as a primary standard in SAXS while Vanadium and Plexiglas are used as primary and secondary standards in SANS), we can also gain information on the mass or molecular weight of the scattering objects.

To be able to compare results obtained with different types of radiation or at different wavelengths, detector distances and scattering angles, a more convenient parameter is the scattering vector, $\vec{Q}$ (see Equation 1.7), defined as the difference between the wave vectors of the scattered and incident radiation, $\vec{k}_s$ and $\vec{k}_i$, respectively, as visualised in **Figure 16**.[170]
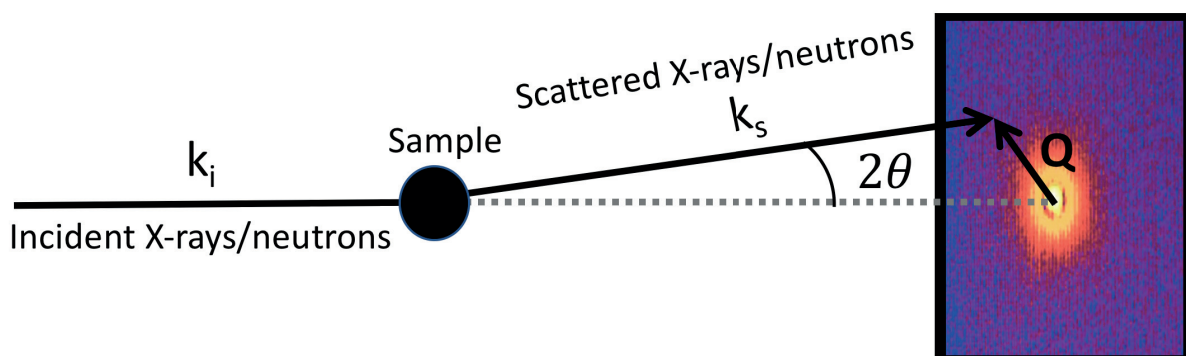
Figure 16. *Sketch of the scattering geometry, showing the definition of the scattering vector $\vec{Q}$. The modulus of the wave vectors (elastic scattering) is $|\vec{k}_s| = |\vec{k}_i| = 2\pi/\lambda$ | and $\vec{Q} = \vec{k}_s - \vec{k}_i$.*

For structural studies of soft matter systems, the elastic coherent scattering process with approximately zero energy transfer is of primary interest, while the inelastic scattering is much weaker and incoherent scattering is treated as an additional background (mainly relevant for neutrons).

In a SAS experiment with an assembly of N atoms at individual positions r_i with fixed orientation (example a peptide chain), the scattering pattern recorded arises from the incident plane waves interacting with the atoms in the sample. This interaction leads to emission of spherical symmetrical secondary waves from each atom i at position r_i with wave functions A_i. By applying the Born approximation,[180] the superpositioned amplitude of the scattered waves can be written as the sum of N wave functions A_i:

$$A(\vec{Q}) = \sum_N b_i \exp[-i\vec{Q}\vec{r}_i] \tag{1.8}$$

where b_i is the scattering length as defined above which depends on the radiation source. However, for SAS experiments the observed length scale is much larger than the distance between the atoms, therefore the sum over N can be replaced by an integral over the volume of the object:

$$A(\vec{Q}) = \int_V \rho(\vec{r}_i) \exp[-i\vec{Q}\vec{r}_i] d^3\vec{r} \tag{1.9}$$

where $\rho(\vec{r}_i)$ is the SLD defined as:

$$\rho(\vec{r}_i) = \sum \frac{b_i}{V} \tag{1.10}$$

$A(\vec{Q})$ is thus the 3-dimensional Fourier transformation of $\rho(\vec{r}_i)$.

For isotropic materials, for example a particle freely tumbling in solution, an average over all orientations $\langle \cdot \rangle$ is applied and the product with the complex conjugate of $A(Q)$ gives the differential scattering cross-section $\frac{d\sigma}{d\Omega}(Q)$:

$$\frac{d\sigma}{d\Omega}(Q) = \langle A(\vec{Q})A^*(\vec{Q}) \rangle = \langle \sum\sum b_i b_j^* \exp[-i\vec{Q}(\vec{r}_i - \vec{r}_j)] \rangle \tag{1.11}$$

$\frac{d\sigma}{d\Omega}$ represents the probability of a particle of the incident beam being scattered out from the unit sample volume into the solid angle $\Delta\Omega$, and contains all information on the structure of the sample.

As generally only the relative positions of every pair of scatterers are significant in the fundamental equation, the equation above can be rearranged in the following way:

$$\frac{d\sigma}{d\Omega}(Q) = \rho^2 \int_V P(\vec{r})\exp\left[-i\vec{Q}\vec{r}\right]d^3\vec{r} \tag{1.12}$$

where $P(\vec{r})$ is the spatial correlation function.

For a particle in solution the ρ is replaced by $\Delta\rho = \rho - \rho_o$ which is the contrast between the scatterer with SLD ρ (for example the peptide chain) and the solvent with SLD ρ_0. The $\Delta\rho$ is radiation specific. The scattering cross section is a combination of the form factor and the structure factor. These contain information on the conformation of the individual particles and the interaction between the particles, respectively. In dilute systems the interaction between particles are neglectable and therefore the structure factor is equal to 1. We then only focus of the form factor which for many geometrical shapes can be calculated analytically. This enables analysis of scattering patterns to determine the structure of the particles that are being probed.[170, 181] We will discuss different form factors for peptides and liposomes further in the next sections.

In a dilute system where the interactions between particles are negligible, the experimental scattering intensity, I as a function of Q is proportional to the so-called macroscopic scattering cross-section $d\Sigma/d\Omega$:

$$I(Q) = C'\frac{d\Sigma}{d\Omega}(Q) = C'\phi V\frac{d\sigma}{d\Omega}(Q) \tag{1.13}$$

Where ϕ is the particle volume fraction, V is the particle volume and C' is the calibration factor which is specific for the experimental configuration, dependent on sample parameters like sample transmission T and sample thickness d, and instrumental parameters like sample-to-detector distance L, incident beam intensity I_i and area of sample aperture area A. The scattering intensity is what the detector actually records and is the Fourier transform of real-space SLD. [170]

The size of antimicrobial peptides and lipid model systems are typically on a length scale 1–100 nm (for vesicles the size can be varied by extruding using filters with different pore sizes) and are therefore suited to be studied by SAS techniques. One of the main advantages with using the SAS technique to characterise AMPs and their membrane interactions is that in contrast to methods like TEM and cryo-EM/TEM, the samples for SAS can be measured in solution directly without having to dry or freeze the samples prior. Another advantage is that SAS can be used to do time-resolved studies with down to millisecond resolution in the case of synchrotrons SAXS, or ~50 ms resolution in the case of SANS by using a stopped flow apparatus, or minutes resolution with hand mixing (synchrotron SAXS or SANS). Thirdly, time-resolved SANS (TR-SANS) can be used to study both how lateral and transmembrane lipid movements are affected by addition of substrates like AMPs in real time by using the contrast between deuterated and proteated molecules, without having to add large labels to the lipids like fluorophores that may affect the movements.

1.3.5 Peptide structures in solution as seen by SAXS

As described in the introduction to this chapter, the focus in this part of the thesis will be on methods used to study the peptide-lipid membrane interaction. However, to be able to fully understand the membrane interaction for different antimicrobial peptides it is of high importance to gather as much information about the specific peptides as possible. This includes of course the chemical structure, charge density and specific volume in solution, which normally can be found in literature for most natural peptides, but also includes the structure of the peptide in solution, which we can study using SAXS. Traditionally, peptides and proteins structures are characterised in terms of α-helical and β-sheet contents that can be measured using CD (as described above) and by the structure in crystal form as seen by X-ray crystallography. However, to gain information on the structure of the peptide/proteins in solution, closer to the native environment, SAXS and/or NMR are considered the most powerful approaches.[182]

While NMR is limited with regards to the size of the probed molecule (used for moderately sized macromolecules < 50 kDa), SAXS lacks the same size limitation.[182] SAXS is a convenient method to gain information on the overall structure of peptides

in solution, as well as the interaction and flexibility of the particles. As a simple example, peptides with a random chain conformation can be analysed using an analytical model for free chains to determine their radius of gyration, R_g. The form factor $P_{chain}(Q)$, for the random, unstructured, peptide chains is given by the Debye expression for Gaussian chains:[183]

$$P_{chain}(Q) = \frac{2 \cdot exp\left[-(QR_g)^2\right] - 1 + (QR_g)^2}{(QR_g)^4} \qquad (1.14)$$

A peptide with an α-helical structure can be modelled as a simple solid cylinder given by:[184]

$$
\begin{aligned}
P(Q)_{cyl} &= \int_0^{\frac{\pi}{2}} \left|A(Q,\alpha)_{cyl}\right|^2 \sin\alpha \, d\alpha \, ; A(Q,\alpha)_{cyl} \\
&= \frac{2J_1(QR\sin\alpha)}{QR\sin\alpha} \frac{\sin(QL\cos\alpha/2)}{QL\cos\alpha/2}
\end{aligned}
\qquad (1.15)
$$

where L is the total length of the cylinder, R is the radius and α is the angle between the momentum transfer vector Q and the cylinder axis parallel to L. J_1 is the first order Bessel function.

SAXS is also able to determine much larger structures than that for a single peptide random chain or helix. It can therefore be used to elucidate potential supramolecular structures in self-assembling peptides.[184-190] This can range from "smaller" structures like bundles of α-helical peptides (modelled as bundles of parallel cylinders with the form factor described above) as shown by Lund *et al.*[184], to larger structures like peptide nanofibers[187, 189] or hollow nanotubes.[188, 191] The formation of supramolecular structures has been linked to changes in the antimicrobial effect and toxicity of antimicrobial peptides, as further discussed in Chapter 1.4 and may therefore be an important property to elucidate to fully understand the peptide effect.[192]

1.3.6 Peptide-membrane interactions as seen by SAXS

Recent efforts have explored the possibility of determining structural information of live bacterial cells from SAS data. Semeraro *et al.* determined the ultrastructure of live *E. coli* using ultra-SAXS and detailed modelling,[193] while Nickels and co-workers have used SANS and contrast variation to characterise the membrane heterogeneities of live *B. subtilis*.[44] Although these exciting findings reveal that it is be possible to determine structural parameters of live cells they still justify the need for simplified model systems due to the high complexity in differentiating the specific effects of an added substrate. Therefore, using lipid model systems as discussed in Chapter 1.3.1. is still the preferential method for investigating the effect of AMPs using SAS.

To be able to fully determine the effect of the peptide on the structure of the lipid membrane, the scattering from the pure vesicle sample needs to be analysed first. The interesting parameters are the overall thickness of the bilayer, the position and distribution of the head and tail components, as well as the overall size of the vesicles and the polydispersity. Extensive work has been put into developing scattering methods able to characterise symmetric and asymmetric lipid vesicles in terms of their SLD profiles.[152, 194-201]

The coherent scattering from symmetric large unilamellar vesicles can be described by the separated form factor (SFF) approximation as described by Kiselev *et al.* and Pencer *et al.*:[198, 202]

$$I(Q) \simeq S(Q) \cdot |F_{TS}(Q)|^2 \cdot |F_{FB}(Q)|^2 \qquad (1.16)$$

where S is the structure factor (gives information about the interaction between the vesicles), F_{TS} is the form factor of a thin spherical shell (gives information about the vesicle size and polydispersity), and F_{FB} is the form factor of a flat bilayer sheet (gives information about the distribution of the lipid components across the bilayer). However, this approximation is only valid when the length scales of the vesicle radius and the bilayer thickness are well separated.[198] Pencer et al. showed that the scattering curves generated from the SFF approximation and an exact analytical model, that the SFF model is correct up to values t/R $\simeq$ 0.5.[198] For example in the case of vesicles extruded through a 100 nm filter, made of DMPC/DMPG lipids which are known to

have a bilayer thickness is 36.7 Å at 30 °C[203], the t/R ratio $\simeq 0.07$, and the SFF approximation that is computational much less expensive, is therefore valid.

Brzustowicz & Brunger were the first to describe a smooth SLD model function to analyse SAXS data from asymmetric lipid vesicles in 2005. Here they demonstrated that the scattering from freely floating vesicles with transmembrane asymmetry can be described using a flat bilayer model:[197]

$$|F_{FB}| = \left| \int_{-D_i}^{D_o} \Delta\rho \exp(iQz)dz \right| = \sqrt{(F_{cos}^2 + F_{sin}^2)} \qquad (1.17)$$

where the integral extends from the innermost distance in the bilayer, D_i to the outermost distance in the bilayer D_o. $\Delta\rho$ is the difference in the SLDs of the membrane and the solvent, and $F_{cos} = \int_{-D_i}^{D_o} \Delta\rho \cos(Qz)dz$ and $F_{sin} = \int_{-D_i}^{D_o} \Delta\rho \sin(Qz)dz$ are the real and imaginary parts of the form factor of the flat bilayer sheet, F_{FB}.
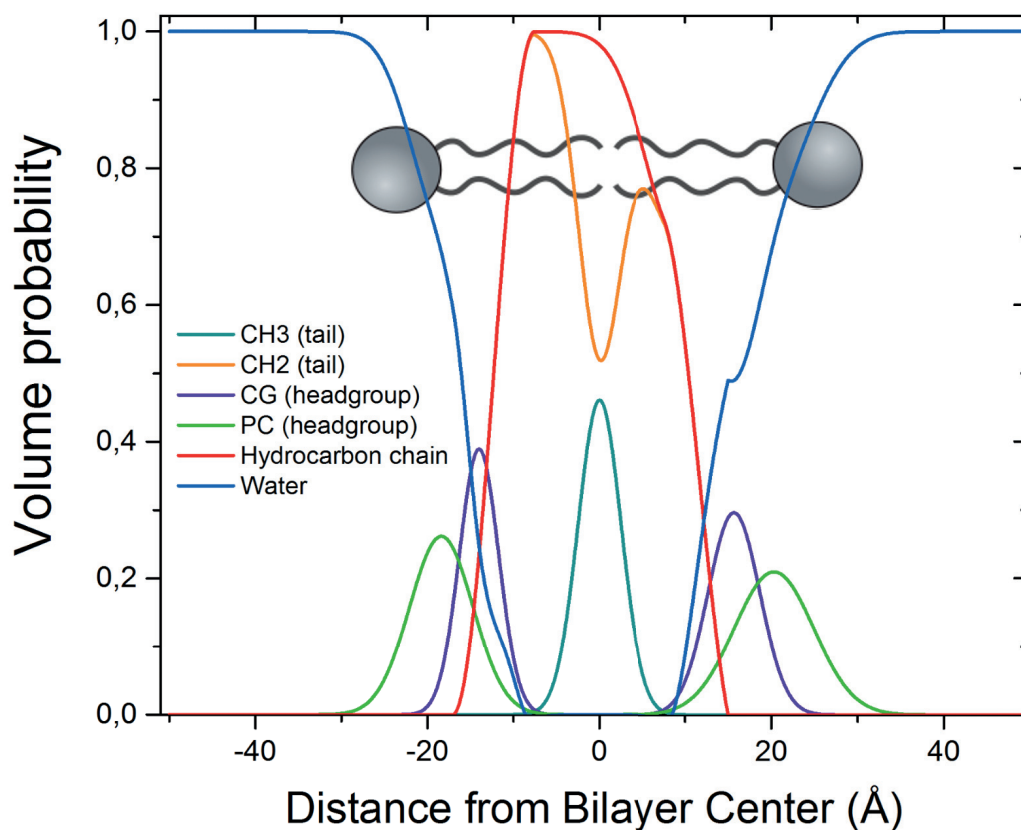
Figure 17. *Schematic illustration of how the resulting volume probability distribution of a slightly asymmetric lipid bilayer divided into an outer (PC) and inner headgroup (CG), CH2 region and CH3 groups.*

The scattering density profile (SDP) model presented by Kučerka and co-worker allow the bilayer structure to be described in terms of one-dimensional volume probability profiles of quasi-molecular lipid fragments. This model allows for joint SAXS and SANS data analysis of asymmetric membranes. The volume probabilities, as illustrated in **Figure 17**, are modelled as Gaussians, scaled either by the number of electrons (for SAXS) or by the total coherent neutron scattering length (for SANS):[152, 199, 204]

$$P_n(z) = \frac{c_n}{(2\pi)^{1/2}} \exp\left[-\frac{(z - z_n)^2}{2\sigma_n^2} \right] \tag{1.18}$$

where n represents the the specific quasi-molecular lipid fragment, as for example the outer or inner part of the headgroup, while σ_n is the width and z_n is the position of the distribution and $c_n = V_n/(A_L\sigma_n)$.

Taking into account potential differences in the inner and outer hydrocarbon tail region and to comply with spatial conservation considerations stating that no water is present in the tail region of the membrane, this part of the lipid bilayer can be described by a half-period squared sine/cosine function rather than by additional Gaussians:[201]

$$P_{HC}(z) = \begin{cases} \sin\left(\dfrac{z - z_{MN_i} + \sigma_{MN_i}}{2\sigma_{MN_i}}\dfrac{\pi}{2}\right)^2 \\ \quad for\ z_{MN_i} - \sigma_{MN_i} \leq z < z_{MN_i} + \sigma_{MN_i} \\ \\ 1\ for\ z_{MN_i} + \sigma_{MN_i} \leq z < z_{MN_o} - \sigma_{MN_o} \\ \\ \cos\left(\dfrac{z - z_{MN_o} + \sigma_{MN_o}}{2\sigma_{MN_o}}\dfrac{\pi}{2}\right)^2 \\ \quad for\ z_{MN_o} - \sigma_{MN_o} \leq z < z_{MN_o} + \sigma_{MN_o} \end{cases} \tag{1.19}$$

where $z_{MN_{i,o}}$ is the 0.5-probability value for the HC group and $2\sigma_{MN_{i,o}}$ is the width of the squared sine/cosine functions.

Lastly the solvent (example water) probability function, P_s is calculated as:[204]

$$P_s(z) = 1 - \sum_n P_n(z) \qquad (1.20)$$

The peptide effect on the structural integrity of the lipid membranes can be can be probed using SAXS by measuring samples where lipid vesicles are mixed with antimicrobial peptides.[68, 69, 72, 124, 142, 143, 145, 205-207]

Sevcsik *et al.* have presented SAXS data on how LL-37 affects the bilayer structure of DPPC/DPPS lipid vesicles. Model analysis of SAXS data measured at 35 °C revealed how the scattering pattern from the lipid vesicle- LL-37 mixtures could not be explained by the bilayer model in the same way as the pure vesicles. The authors explain this with LL-37 causing either formation of asymmetric bilayers, or solubilising the membrane resulting in a co-existence of two populations of structures (disks and extended bilayers).[68, 69]

On the other hand, Pabst *et al.* reported a less dramatic peptide effect when they mixed peptidyl-glycylleucine-carboxyamide (PGLa), a natural antimicrobial peptide isolated from South African clawed frogs, with lipid vesicles with altering tail lengths (DMPG. DPPG, DSPG). In their study they used a combination of SAXS and wide-angle X-ray scattering (WAXS) to fully determine both the structure and fluidity of the membrane at different temperatures. The scattering patterns were analysed using the global analysis program (GAP)[208] based on the SDP model described above. From the analysis they were able to determine the structure of the lipid vesicles prior to peptide addition and after peptide addition (only using a single bilayer phase). The results revealed a 1-2 Å increase in the thickness of the DMPG and DPPG vesicles when in the fluid phase.[72]

Castelletto and co-workes have used TEM and SAXS to study how several surfactant-like arginine-rich peptides interact with lipid vesicles with altering lipid composition .Their results have revealed how the membrane effect is highly dependent on the number of arginines in the peptide structure.[142, 143] For example they revealed how addition of the arginine-capped bolaamphiphile peptide RA3R (A: alanine, R: arginine)

to unilamellar POPG/POPE vesicles induced a strong correlation between the lipid bilayers seen qualitatively by the appearance of distinct Bragg peaks associated with the formation of multilamellar vesicles.[143]

Beyond traditional SAXS methodology, also other X-ray based techniques including grazing-incidence small angle x-ray scattering (GI-SAXS)[163, 164, 209, 210] and diffuse low angle X-ray scattering[137, 138] have been used to study peptide-membrane effects.

Diffuse low angle X-ray scattering (LAXS) on hydrated oriented stacks of lipid bilayers[151] mixed with peptides, was used by Pan *et al.* in combination with molecular dynamics (MD) simulations to reveal a transmembrane orientation of Alamethicin in DOPC membranes[137]. Furthermore, they could determine a slight membrane thinning as a result of the peptide insertion in the membrane in contrast to the membrane thickening Pabst *et al.* saw for PGLa.[137] The same method was used by Dupuy *et al.* to determine how colistin (polymyxin E) inserts deeper into a lipid membrane made to mimic gram-negative bacteria than in the membranes mimicking gram-positive bacteria.[138]

As seen from these examples, there is no clear trend in the observed effects of peptides addition to lipid vesicles as determined by X-ray based methodologies. The discrepancies in the results can be explained by the focus on different antimicrobial peptides and model systems, as well as differences in experimental protocols and instrumental setup. The latter makes it difficult to compare the membrane effects of different peptides, indicating that a systematic SAXS study on comparing different antimicrobial peptides on the same model system using the same experimental protocol might provide some necessary clarity. Furthermore, the analysis of the data presented above is done in a variety of ways, ranging from a qualitative approach to model analysis using the SDP model (without modifications with regards to peptide addition). The lack of systematic peptide studies and a modified model where the peptide has been modelled as a separate fragment in the volume probability plot inspired the work presented in the first part of the thesis work (**Papers I-IV**).

1.3.7 Peptide effect on lateral distribution of lipid as seen by SANS

It has previously been shown that changes in the lateral distribution of lipids in the membrane and formation of lipid domains/rafts can be studied using SANS.[44, 153, 211, 212] Pencer *et al.* has shown that vesicles with homogenously distributed lipids can be distinguished from vesicles with heterogeneously distributed lipids by using contrast variation SANS. In these experiments they looked at lipid domain formation in samples containing 1:1:1 DOPC:DPPC:cholesterol and 1:1:1 SOPC:DPPC:cholesterol mixtures. The samples were prepared under contrast matching conditions, meaning that the average SLD of the vesicles matches the solvent SLD ($D_2O:H_2O$ mixture), at a temperature where the lipids are known to be mixed homogeneously over the membrane (50 °C). When the lipids are homogenously mixed the scattering from the vesicles is minimised due to the contrast matching condition. However, when the temperature is decreased and the lipids in the membrane segregate, they observed an additional contribution to the scattered intensity. This additional scattering can be explained by internal variations in SLD due to the differences between the acyl chain and headgroup regions of the lipids. This methodology was further developed when Heberle *et al.* introduced a modified protocol where they include tail deuterated lipids in their lipid composition enabling a more significant change in the scattering signal upon lipid segregation (see **Figure 18** for details on the this method and the results).[153]

Using SANS and contrast variation to detect lipid segregation is interesting also for studies of AMPs. This is because induced changes in the lateral distribution of lipids in the cytoplasmic membrane of bacteria has been introduced as a potential mode of action of AMPs (as previously discussed in chapter 1.2.4). [76] This inspired us to look at lipid domain formation of anionic lipids in the presence of AMPs as presented in **Paper I**.
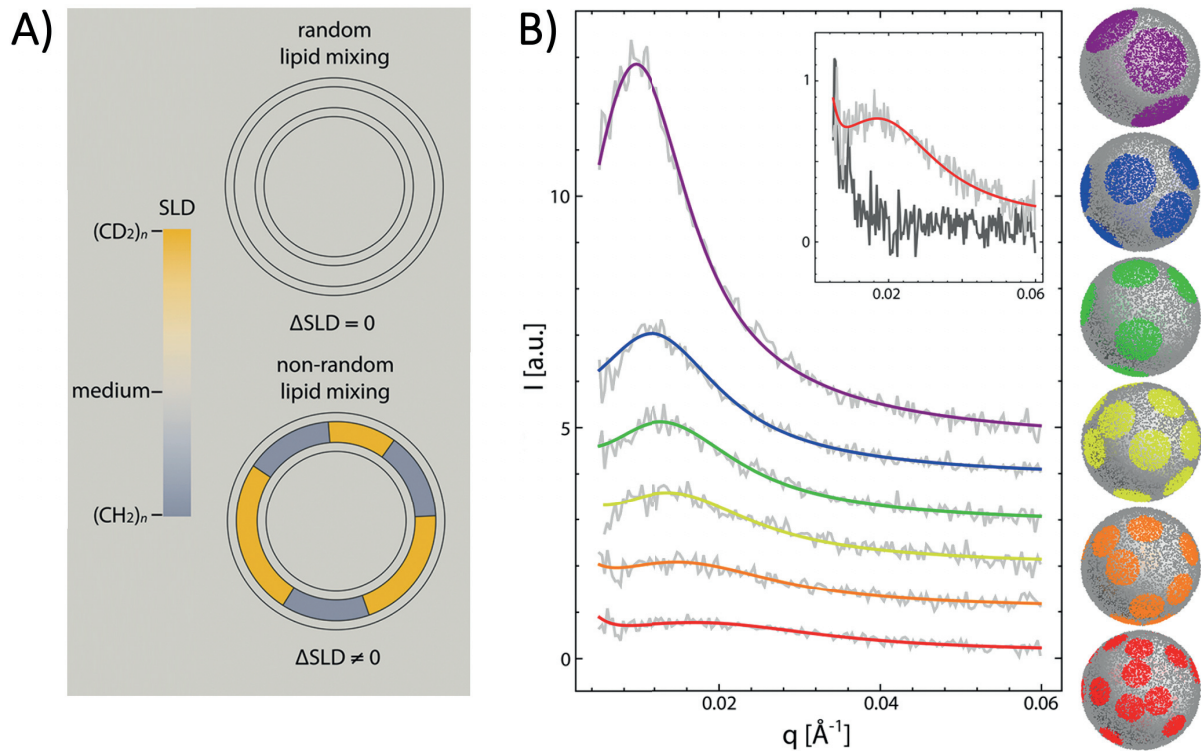
Figure 18. A) Schematic of the SANS contrast matching experiment design. Random mixing of lipids results in contrast matched vesicles giving no scattering signal, while SLD contrast between co-existing phases in vesicles with non-random lipid mixing result in an increased scattering signal. This SLD contrast is achieved by using partly chain-perdeuterated lipids (in this case DSPC), which has a significantly higher SLD than the surrounding proteated lipids (in this case POPC or DOPC). B) SANS data (light gray lines) and best-fit curves (colored lines) corresponding to different lipid compositions with different degrees of lipid segregation and domain sizes. Reprinted with permission from Heberle et al. (2013)[153]. Copyright (2013) American Chemical Society.

1.3.8 Peptide effect on lipid flip-flop as seen by TR-SANS

As described above SANS and contrast variation/ isotope labelling can be used to study the movements of lipids in the lateral direction of the membrane *in situ* without perturbation of the sample. The same principles allow us to also study the transmembrane movements of lipids. Qian and Heller have presented SANS data on tail-deuterated d54-DMPC:proteated-DMPG vesicles in the presence of melittin and alamethicin. Based on model analysis of the changes in contrast between the inner and outer leaflet they showed how the peptides induced an asymmetric distribution of the lipids between leaflets, enriching the outer leaflet with the anionic DMPG lipids.[140] The

same trend was see for aurein 1.2 by Rai and Qian on the same composition model system.[213]

Beyond probing the indirect peptide effect of lipid distribution between bilayers, several methods have been developed to elucidate transmembrane lipid transport (flip-flop) directly with and without addition of peptides. We will fist discuss different techniques used to elucidate lipid transport rates, and then focus on how these methods can be used to study the membrane effect of antimicrobial peptides.

Conboy and co-workers have successfully shown that Sum-Frequency Vibrational Spectroscopy sensitive to the asymmetry in a planar supported lipid bilayer can be used to follow the lipid flip-flop in a supported bilayer. This method requires deposition of a deuterated leaflet on a solid substrate. Upon flip-flop, the composition of the inner and outer leaflet is mixed, which can be followed by monitoring the amount of -CH_3 (as opposed to -CD_3) groups on the surface.[214, 215] The same idea has also been used in neutron reflectometry by Gerelli and co-workers who deposited a H:D labelled bilayer on silica. However, they found that the inter-bilayer exchange was rate limiting and lipid flip-flop was too fast to be resolved by the instrumental time resolution,[216] which is explained by enhanced fluctuations at the phase transition when heating the sample from the gel phase (asymmetric SLBs where prepare in the gel phase) to the liquid crystalline phase, as well as natural defects in supported lipid bilayers.[217]

To eliminate the potential influence of a solid substrate (mostly due to more frequent occurrence of membrane defects[218]) several techniques using free floating bilayers, also known as lipid vesicles or liposomes, have been developed. The Zero-Average Contrast (ZAC) TR-SANS scheme enables us to follow the net movement of single phospholipids between leaflets (lipid flip-flop) in the membrane of a lipid vesicle in real time. Additional to lipid flip-flop these experiments also determines the rate of exchange of lipids between vesicles. The protocol was first developed to study molecular exchange kinetics in polymeric micelles,[219-222] but later adapted to study lipid vesicles firstly by Nakano et co-workers in 2007.[223] The technique is based on mixing identical, but differently isotope-labelled vesicles with H-lipids and D-lipids, in a H_2O:D_2O buffer mixtures that matches the average SLD of the randomly mixed liposomes. As described above neutrons are scattered differently by different isotopes. Therefore, the initial state will have a maximum contrast giving a relatively good

scattering signal. Then over time random exchange and lipid flip-flop of D and H lipids will result in a decreased scattering intensity because the average scattering length density of the vesicles goes towards the same value as for the solvent. In other words, the liposomes become practically "invisible" for the neutrons over time (see **Figure 19** for illustration of the method and **Figure 20** for an example of lipid vesicle experiment showing a decreasing scattering curve intensity over time).[223-230] .
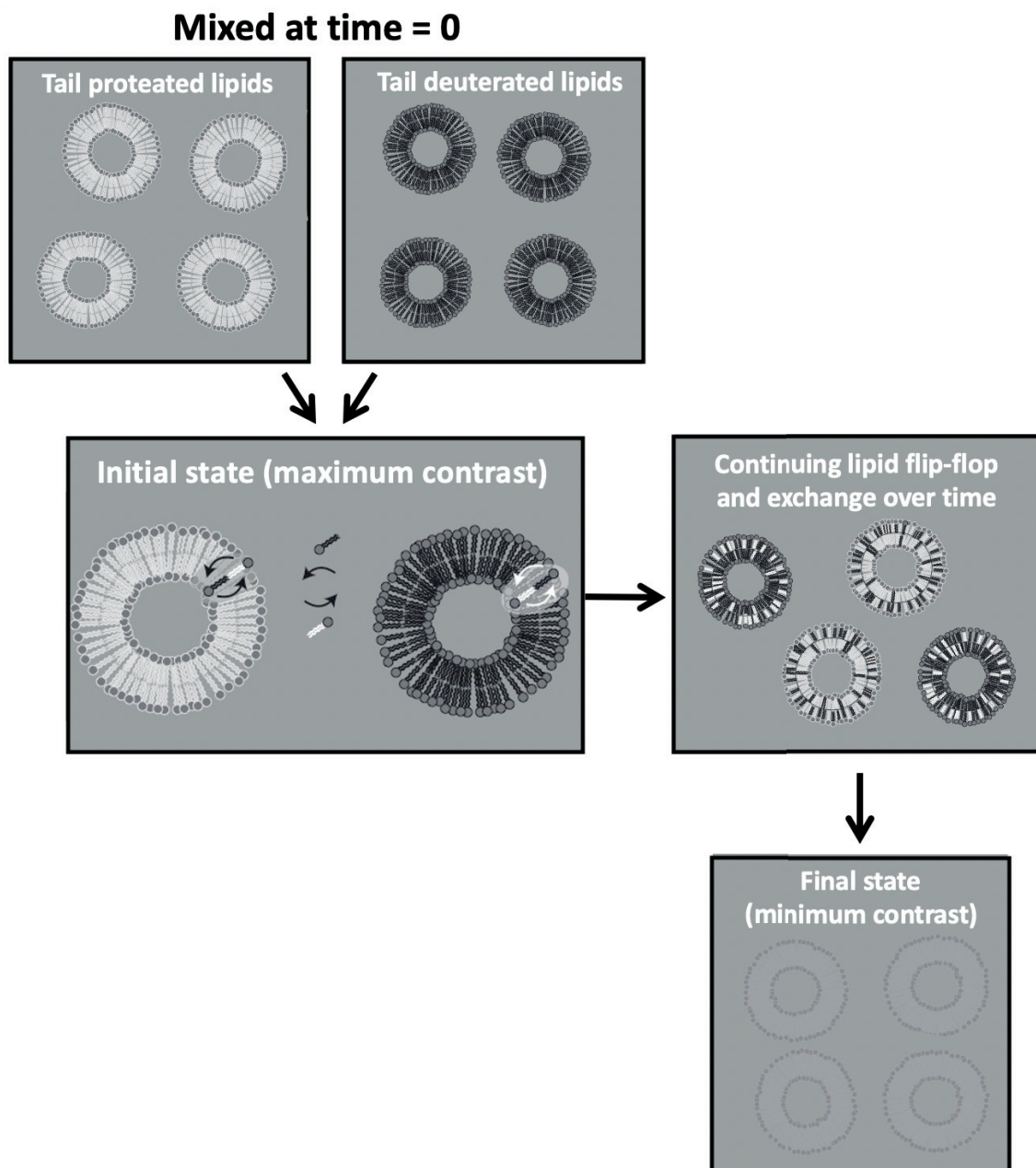
*Figure 19. Schematics of the KZAC TR-SANS method used to measure lipid flip-flop and exchange in vesicles. Figure adapted from **Paper V**.*
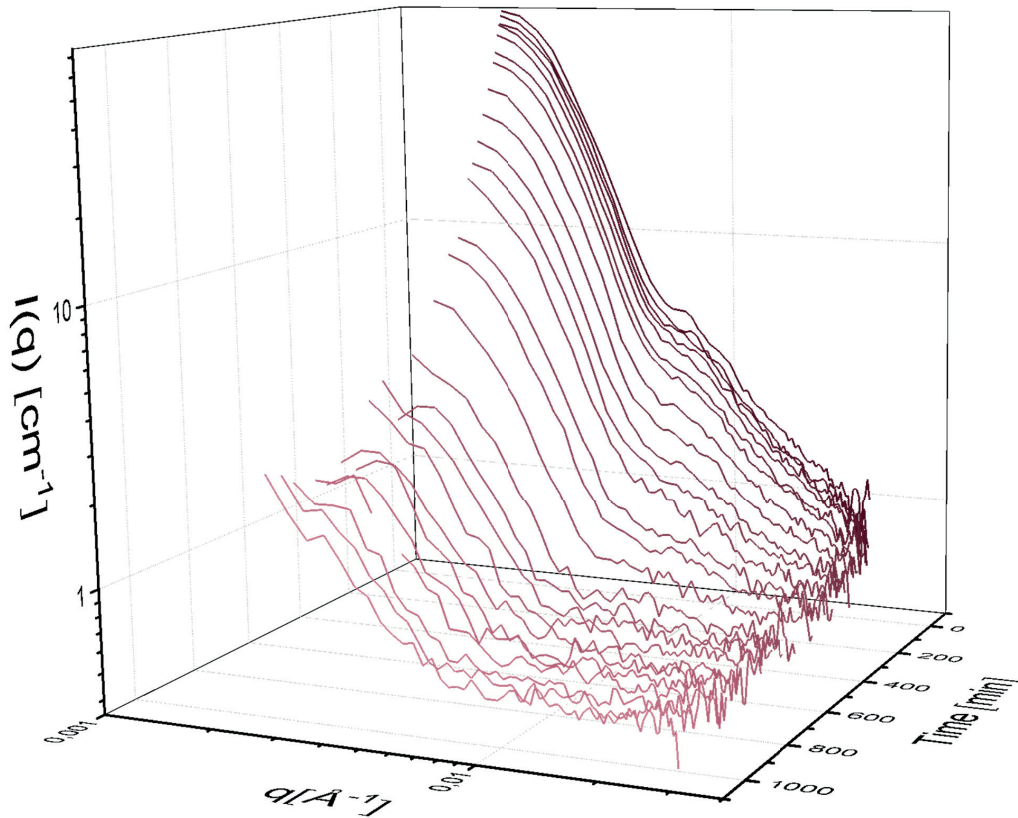
Figure 20. *Scattering curves from a KZAC experiment at KWS1 Heinz Maier-Leibnitz Zentrum (MLZ) following the exchange of DMPC/DMPG vesicles. Data from **Paper V**.*

Using a model-independent approach the lipid transport induced reduction in the scattering intensity can quantitatively be evaluated by determining the relaxation function $R(t)$ according to:

$$R(t) = \sqrt{\frac{I(t) - I_\infty}{I(0) - I_\infty}} \qquad (1.21)$$

where $I(t) = \int I(Q,t)dQ$ is the integral intensity at a given time, I_∞ is the intensity of the premixed blend representing the final state and $I(0)$ is the averaged intensity of the H-vesicles and D-vesicles measured separately representing the initial state.

The lipid transport processes, intervesicular exchange, (k_{ex}) and intra-vesicular flip-flop, (k_{flip}) can be described by:[223]

$$-\frac{d|\Delta\rho_{out}|}{dt} = k_{ex}(|\Delta\rho_{out}| - 0) + k_{flip}(|\Delta\rho_{out}| - |\Delta\rho_{in}|),$$

$$-\frac{d|\Delta\rho_{in}|}{dt} = -k_{flip}(|\Delta\rho_{out}| - |\Delta\rho_{in}|)$$

(1.22)

where $\Delta\rho_{out}$ is the contrast with the solvent of the outer leaflet and $\Delta\rho_{in}$ is the contrast of the inner bilayer leaflets of the vesicles. This expression is based on the assumption that the contrast of D and H-vesicles have identical absolute values (one positive and one negative) because of the zero-average contrast solvent conditions.

Based on these experiments Nakano *et al.* found the need of two independent rate constants to explain the relaxation function. Therefore, $R(t)$ is explained by a double-exponential decay function, taking into account the initial condition that $\Delta\rho_{out}(0) = \Delta\rho_{in}(0) = 1$ and taking an average of $|\Delta\rho_{out}|$ and $|\Delta\rho_{in}|$ the following equation yields the two rate constants:[223]

$$R(t) = \left(\frac{1}{2} - \frac{k_{flip}}{X}\right)\exp\left(\frac{-k_{ex} + 2k_{flip} + X}{2}t\right)$$
$$+ \left(\frac{1}{2} + \frac{k_{flip}}{X}\right)\exp\left(\frac{k_{ex} + 2k_{flip} - X}{2}t\right)$$

(1.23)

where $X = \sqrt{4k_{flip}^2 + k_{ex}^2}$

Earlier work by other researchers, including Homan and Pownalls work from 1999 using a label based kinetic fluorimetry method has revealed that the lipid flip-flop is a significantly slower process than lipid exchange.[50] The TR-SANS method confirmed the same trend without the uncertainty of the addition of labels on the lipids.[223, 224, 229] It has further revealed how the lipid transport rates are highly dependent both on the acyl chain length of the lipid tail and the fluidic state of the membrane. [155, 225] Similar methods using the same principles but changing the vesicles for lipid discs have proven successful in studying lipid transport in a bilayer under different conditions. [155, 227, 231]

Beyond only extracting the rate constants from these experiments also several other thermodynamical parameters can be elucidated by doing the same experiments at a series of different temperatures. Plotting $\ln k_{ex}$ and $\ln k_{flip}$ against the inverse temperature in Kelvin, $1/T$ gives an Arrhenius relationship. This analysis gives the activation energy E_a and the fundamental time constant, τ_0 according to:

$$\tau = \tau_0 \exp\left(\frac{E_a}{RT}\right) \qquad (1.24)$$

where $\tau = 1/k$, R is the universal gas constant and τ_0 is a system specific constant and is related to the time between each time the molecule "attempts" to overcome the energetic barrier.[232] Equation (1.24) can further be split into

$$\tau = \tau_{00} \exp(-\Delta S/R) exp\,(\Delta H/RT) \qquad (1.25)$$

where ΔS is the entropy change, ΔH is the enthalpy change and τ_{00} is the estimated fundamental time constant.

Beyond probing how the lipid transport is affected by changes in conditions like the lipid structure, morphology and temperature the KZAC TR-SANS techniques can also be used to study the effect of peptide or protein additions. Kaihara *et al.* showed how addition of a transmembrane peptide with a fully hydrophobic transmembrane region (TMP-L) did not affect the lipid flip-flop. Addition of two transmembrane peptides with lysine and glutamate groups in the centre of their transmembrane region (TMP-K and TMP-E), on the other hand, significantly accelerated the lipid flip-flop rates. The increase in flip-flop rate is explained by a lowered activation energy due to the presence of polar residues in the membrane spanning helices creating locally polar regions in the originally hydrophobic membrane core. The same trend has been seen for transmembrane proteins and peptides by fluorescence based methods,[79, 226, 233-235] Sum-Frequency Vibrational Spectroscopy[81] and MD simulations.[236]

Flip-flop can also be detected directly, without the confounding factor of lipid exchange, by TR-SANS using asymmetric vesicles[156] where one leaflet contains a deuterated lipid. Similar to the KZAC TR-SANS technique described above, flip-flop can be detected by following the loss in the overall intensity over time. Using this approach, Nguyen *et al.* have studied three different antimicrobial peptides (alamethicin, melittin

and gramicidin). They found that the rate for flip-flop was significantly accelerated by the addition of the peptides. From a slow spontaneous flip-flop half-life approaching 6 days in the pure vesicles, to complete elimination of bilayer asymmetry in 2 h by addition of melittin and alamethicin. Eventual peptide-induced effects on molecular exchange between vesicles could not be observed from these data due to the use of asymmetric vesicles rather than the KZAC method described in detail above.[82]

As it has been shown that lipid transport in cell membranes may be affected by addition of AMPs, this may potentially be a significant key in uncovering the complete picture of AMPs mechanism of action. However, some unanswered question with regards to the connection between structural effects on the membrane and the peptides ability to affect lipid transport is still unanswered. The difference between the effect of transmembrane peptides and peptides that only insert in the surface of the membrane potentially interesting factors. These unanswered questions inspired the work in **Papers III-IV**, while in **Paper V** we develop a time-dependent scattering function enabling us to independently determine the composition of the inner and outer directly from the scattering curve rather than using the model-independent approach introduced above.

1.4 Strategies to overcome issues related to drugability of AMPs

1.4.1 The pharmaceutical potential of natural antimicrobial peptides

As discussed in the previous chapters, AMPs have shown to be naturally effective in killing microbial cells making them obvious candidates for drug therapies against a range of different infections. Natural AMPs have been deemed good alternatives to existing commercial antibiotics due to a number of factors, including: I. natural compounds are assumed to be less toxic and more biocompatible, II. the development of antimicrobial resistance is thought to be lower (this statement is further discussed in Chapter 1.2.6), III. the cationic peptides naturally assist in intracellular delivery, and IV. natural AMPs exhibit antimicrobial activity against a broad range of bacteria, fungi and viruses, making them natural candidates to be used in patients with infections from multiple pathogens (for example in highly immunocompromised patients).[87, 237]

Even though they have been considered to have great potential, in reality very few peptides have actually reached the commercialisation stage due to various problems in drugability.[9, 237] Because the peptides are highly susceptible to proteolytic degradation in the blood stream, the pharmacokinetic *in vivo* life time of the molecules is reduced.[87] This has hindered the use of AMPs for systemic administration, while still leaving room for using them as topical drug treatment alternatives which has been extensively researched.[238-243] Secondly, even though it has been assumed that AMPs lack toxicity due to their natural origin, there is still a lack of systemic information of the potential toxicity of these large and cationic peptides that are known to be highly surface active and therefore are potentially able to interact with a series of internal targets other than microbial cells. Beyond these pharmaceutical obstacles, peptide-based drug development and manufacturing comes with high costs compared to traditional antibiotics consisting of small molecules.[87, 244-246]

This being said, an enormous amount of research has been carried out to design new drug molecules based on natural AMPs, in particular against difficult to treat infections. We will discuss some of the main design strategies in the next chapter.

1.4.2 New drug molecules

Different approaches have been used in the design of new peptides and peptidomimetics (small protein-like molecules designed to mimic peptides) for antimicrobial application. The common approach is to use the current knowledge regarding the relationship between peptide structure and function as well as the mechanism of action to (semi)rationally design drug variants with enhanced activity and tuneable target pathogen specificity. However, this approach has turned out to be rather slow, and approximately less than some hundred peptides have been evaluated for clinical potential based on the results.[87] This is a very low number when comparing to the antibiotic development programs used in modern drug industry. As an alternative to this approach, random screening methods have been developed. For example, Hilpert *et al.* presented a high-through method relaying on peptide arrays synthesised on cellulose sheets combined with a highly sensitive luminescence-based antimicrobial assay. This allowed them to synthesise hundreds of peptides which were all screened for activity.[247]

It is generally recognised that larger biomacromolecules like peptides have poor drugability due to factors like high production cost, and problems in bioavailability and *in vivo* stability. This has encouraged researchers to developed shorter synthetic peptides with antimicrobial properties.[9, 175, 190, 248-251] Many of these compounds are based on motifs found in natural AMPs. For example, Kim *et al.* made a library of short AMPs using only unmodified natural amino acids, keeping structural features known from natural AMPs to be important for the antimicrobial activity and selectivity. From their studies they identified two lead compounds. These peptides showed potent antimicrobial activity against bacteria (amongst others methicillin-resistant *S. aureus* and vancomycin-resistant *enterococci*) and fungi, low toxicity and were stabile upon exposure to trypsin, chymotrypsin and aureolysin for up to 12 h. Apart from their improved pharmaceutical properties these peptides would also be less costly to produce and shorter peptides therefore may have a greater potential for commercialisation.
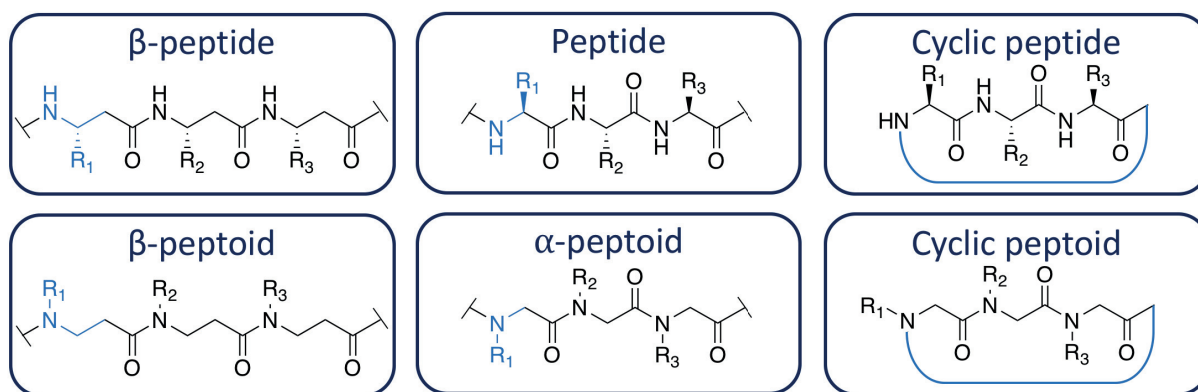
Figure 21. Schematic illustrating different backbone compositions of a variety of peptide and peptidomimetic structures that has been proven to possess antibacterial properties. Adapted with permission from Mojsoska and Jenssen (2015).[252]

An alternative approach to changing the length or amino acids sequence of the peptides to improve the pharmaceutical properties is the development of so called peptidomimetics. These are compounds that are able to imitate the structural properties and/or biological activities of peptides. Some of the most popular strategies to make peptidomimetics include incorporation of unnatural amino acids (e.g. D-amino acids), β-peptides, hybrid peptide-peptidomimetic structures, lipidation and peptoids (poly-N-substituted glycines) (see Figure 21).[252] The latter involves changing the backbone structure of the peptides by appending the side chains to the nitrogen atom rather than to the α-carbons (as for amino acids). This modification to the structure significantly improves the *in vivo* stability of the compounds because peptoids, contrary to traditional peptides, are protease-resistant.[85, 190, 250, 253-260] The modification also has important structural implications. The achiral backbone structure of peptoids precludes backbone hydrogen bonding, which is essential for α−helical secondary structures and also gives rise to a more flexible backbone. However, it has been shown that incorporation of bulky, α-chiral side chains can induce formation of stable polyproline type-I-like helices.[259] Barron and co-workers has developed a large library of such helical peptoids closely mimicking the structure, function and mechanism of natural α-helical AMPs like magainins.[85, 254] By using this strategy they have even been able to prove antimicrobial activity against the very resilient bacteria *M. tuberculosis,* which is the pathogen responsible for tuberculosis disease, one of the leading death causes world-wide.[255] Building upon Barron's library of peptoids we showed in

Molchanova *et al.* (publication not included in the thesis) that the toxicity of these compounds could be significantly lowered by shortening the chains from twelve to six residues, while maintaining the antimicrobial activity by halogen (in this case chlorine and bromine) substitution in position 4 of the phenyl rings in the peptoid structure.

Over recent years, development of peptides known to self-assemble into larger nanostructures has emerged as an interesting strategy to improve the pharmaceutical properties. It has been revealed that supramolecular assemblies of antimicrobial peptides have the potential to increase antimicrobial efficacy[187, 192, 261-263], decrease haemolytic response and enhance stability towards serum proteins[187, 192, 262-266]. Beter *et al.* showed that when comparing self-assembled nanofibers (C_{12}-VVAGKKKGRW-NH_2 and KKKGRW-NH_2) with their corresponding soluble peptide molecules, the activity was increased substantially in the nanofibers.[267] The same trend was shown for self-assembled cylindrical nanostructures made from C_{16}-V_4K_4 functionalised with an (AKKARK)$_2$ heparin binding Cardin-motif by Chang *et al*.[268] The authors suggested that self-assembly of these compounds promotes bacterial cytoplasmic leakage, causing blisters on disorganised membranes of gram-negative bacteria, as these features were only observed above the critical aggregation concentration (CAC) of the peptides[268]. Chu-Kung *et al.* on the other hand found for YGAAKKAAKAAKKAAKAA (AKK) peptides, conjugated to fatty acids of varying length, the antimicrobial activity was lost when the minimal active concentration is higher than CAC.[269].

Beyond the self-assembly effect on antimicrobial activity and selectivity, it may also affect the pharmaceutical properties of the molecules. It has been proposed that self-assembled antimicrobial peptides may act as a vehicle-free self-controlled delivery system without having to add pharmaceutical excipient. From these "nanoscopic depots" the peptide would be gradually released to their target sites.[186, 263, 270-272]

In the next chapter we will discuss the activity, toxicity and mechanism of a group of multidomain peptides (MDPs) known to self-assemble into nanofibers, which is the origin of the work presented in **Paper VI**.

1.4.3 Antimicrobial drug potential of peptides that self-assemble into nanofibers

A series of self-assembling MDPs introduced by Dong and co-workers[273] have been thoroughly characterised with regards to antimicrobial efficacy and cytotoxicity. Based on these studies it has been shown that the self-assembly properties of these peptides are essential for their antimicrobial activity as well as their selectivity towards microbes.[187] The MDPs are based on an ABA motif where the B group consist of a β-sheet motif of alternating hydrophilic glutamine (Q) and hydrophobic leucine (L) groups, while the A groups consist of positively charged lysine (K) residues, with the general formula $K_x(QL)_yK_z$. The self-assembly of the peptides is driven by intermolecular hydrophobic interactions and hydrogen bonding between the subunits leading to a supramolecular fibrous structure (as illustrated in **Figure 22**).[186] In addition to increased activity, the $K_x(QL)_yK_z$ MDPs have been shown to be more stable against protease degradation due to their self-assembling nature.

To further increase the *in vivo* stability, MDPs with polyethylene glycol (PEG) groups attached to the N-terminus of the peptides have been tested. PEGylation is a well-known modification of both low molecular weight drug molecules and biomacromolecules for enhancing their pharmaceutical properties.[274-276] For $K_x(QL)_yK_z$ it has been shown that PEGylation minimises non-specific interactions with various cells, proteins and lipids in a biological environment and thereby improves the hemocompatibility of the peptides.[264] However, it has been shown that PEGylation of peptides might also lower the antibacterial activity depending on the length of the PEG group. Singh *et al.* have showed that attachment of PEG groups of increasing molecular weight to KYE28 reduced the peptide binding to lipid membranes and therefore lowered the antimicrobial effect.[277] This indicates that, with regards to PEG chain length, a balance between the reduced hemolysis and activity is essential in the design of the peptide .
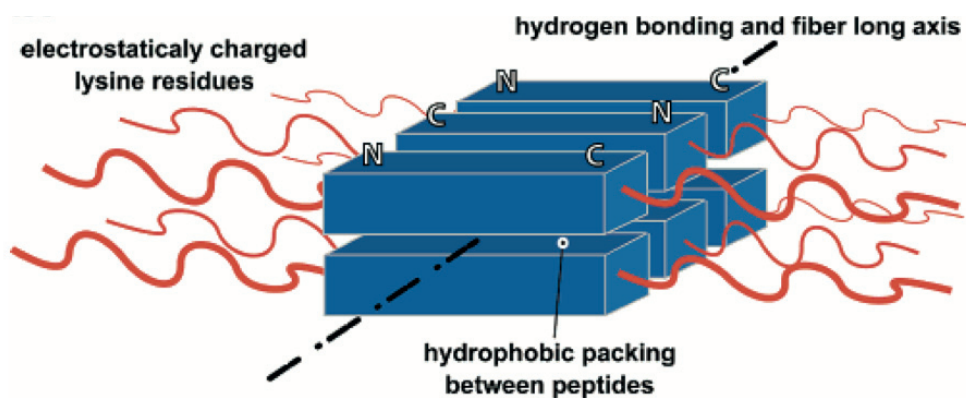
Figure 22. *Proposed model of nanofiber self-assembly of Kx(QL)yKz peptides. The illustration indicates hydrophobic packing region, axis of hydrogen bonding, and repulsive positive charges. Reprinted with permission from Dong et al. (2007). Copyright (2007) American Chemical Society.*

As discussed in the chapter above, self-assembly of AMPs may be utilised as drug delivery "nanoscopic depot" systems. However, this requires a high physical stability of the peptides in order to control the drug release rate. We recently showed in König, Nielsen *et al.* (publication not included in the thesis) that MDPs composed of $K_x(QL)_yK_z$ are extremely stable at physiological relevant conditions. TR-SANS measurements on these PEGylated peptides revealed that no significant exchange of peptide chains in-between nanofibers over a timeframe of 2-3 days at 37 °C could be observed.[189] A MDP analogue used by Xu *et al.* was also shown to remain stable in the presence of phospholipids, although they presented bacterial lytic abilities.[278] However, full comprehension of how lipid membrane interaction affects the physical stability and the biological activity of these peptides is yet to be unfolded. This motivated the work included in the last part of this thesis (**Paper VI**).

2. Aims of the thesis

As described in the introduction to this thesis, there is no general consensus on the mode of action of AMPs. The topic has therefore been extensively studied using a number of different techniques. The overall aim of the presented thesis was to examine whether X-rays and neutrons can be used to further understand the molecular mechanism and mode of action of AMPs, focusing specifically on how they affect lipid membranes. Small Angle Scattering techniques have previously to some extent been used to study the peptide-membrane interaction, however, most of these studies look at a more limited number of AMPs. We also aimed to further develop the method for extracting detailed information on peptide-membrane interactions from SAS data as previous studies in the field have often not properly taken into account variation of scattering contrasts upon peptide insertion into the membrane. We aimed to resolve whether this potentially led to misleading interpretations of in particular SAXS data to how peptides affect the membrane structure. Beyond the development of the methodology in the first part of the project, our goal was to conduct a more systematic study comparing effects on lipid dynamics with membrane structure using the same peptides, model systems and measuring conditions because such a study was lacking in literature.

Specific aims were as following:
- Develop a protocol to extract detailed information on peptide-membrane interactions using SAS data and model analysis (**Paper I**)
- Compare results from SAS data with results from surface sensitive methods including NR, QCM-D and AFM. (**Paper II**)
- By using the protocol developed in the first part of the project we aimed to study the peptide-membrane interaction of a range of natural AMPs varying in size and secondary structure, and investigate the effect of altering the lipid composition of the model membrane system. (**Paper III-IV**)
- Establish the effect of AMP on lipid dynamics through time-resolved SANS, and compare directly with structural data from static SAS and NR. (**Paper III-V**)
- Expand the work to more complex peptide systems known to self-assemble into larger nanostructures using SAS and NR. (**Paper VI**)

3. Summary of Papers

This thesis contains six papers two of which have been published in peer-reviewed journals, and four are manuscripts that have been submitted for peer-review. For a thematic overview of the papers, see **Figure 23.** This Chapter includes a short summary of each paper included in the thesis, as well as a contribution statement.
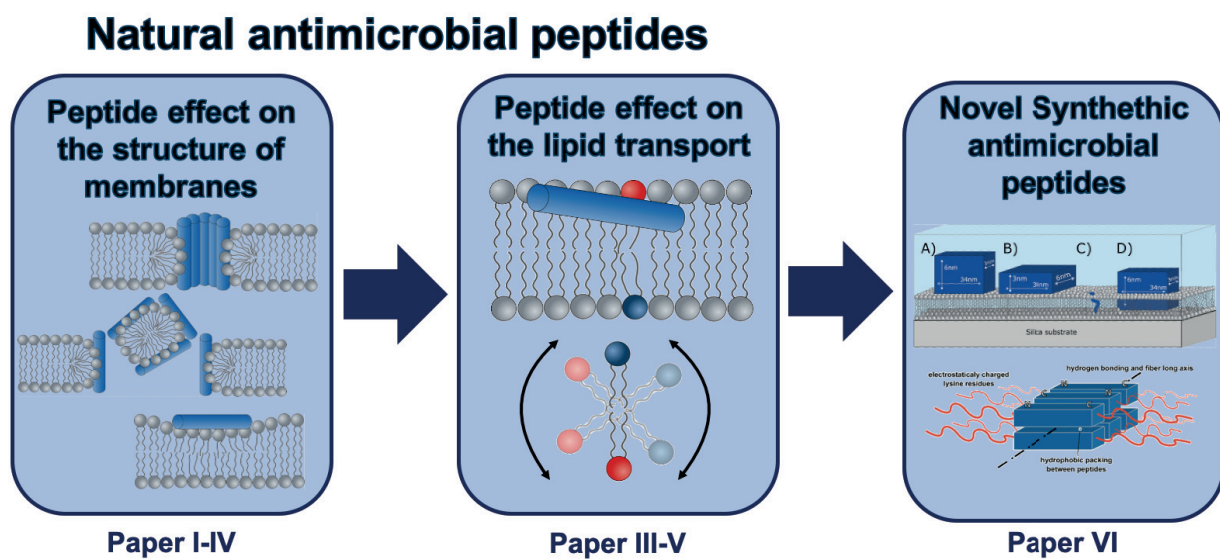
Figure 23. Overview of the papers included in this thesis divided by topic.

Paper I:

Summary: In **Paper I** we focused on developing a detailed scattering model to characterise the scattering data from liposome-peptide mixtures. We used indolicidin as a model peptide to develop the methodology because it is well characterised and has a random structure in solution. We modelled the contribution from the peptide as a pseudo-parsing group across the bilayer (in comparison to parsing of the lipids into four groups as discussed in Chapter 1.3.6), and the volume probability of the peptide as an additional Gaussian function. This modification entailed two extra fitting parameters: the position of the peptide in the bilayer (z_p) and the distribution of the peptide (σ_p). To correctly account for the changes in contrast through different parts of the bilayer upon peptide insertion, the contrast was weighed with the fraction of peptide in the tail region, f_{p_tail} (for details on how this was calculated, see **Paper I**).

Beyond the bound peptide, we allowed for a fraction of free chains not bound to the vesicles, expressed by the Debye formula described in Chapter 1.3.5.

In this work we found that the vesicle system had to be stabilised against aggregation to be probed in the presence of cationic peptides. Therefore, we included 2.5 % PEGylated DMPE lipids to the lipid mixtures. The scattering contribution from the PEG-chains tethered to the vesicle surface was also included in the scattering model.

Based on detailed analysis of the SAXS/SANS results from lipid vesicles with increasing amount of negatively charged lipids (DMPG), mixed with indolicidin in different ratios (from 1:100 to 1:5) we were able to determine that indolicidin inserted into the outer leaflet of the membrane. The peptide insertion caused a significant change in the electron density of the tail region, identified by a shift in the first minima of the SAXS scattering curve.

Further, we used contrast variation SANS to probe eventual segregation of anionic lipids in the membrane caused by addition of the cationic peptide. However, these results revealed that no such domain formation could be observed even at high peptide concentrations. The scattering results presented in **Paper I** for indolicidin supported the interfacial activity model described in Chapter 1.2.4 rather than a defined pore formation in the membrane or peptide-induced lipid segregation.

Contribution: Josefine Eilsø Nielsen (JEN), Victoria Ariel Bjørnestad (VAB) and Reidar Lund (RL) designed the experiments, and developed the scattering models. JEN and VAB prepared all the samples (including making the lipid vesicles). JEN and VAB performed the SAXS experiments, while JEN and RL collected SANS data. JEN and VAB analysed SAXS data, under guidance of RL. JEN analysed SANS data under guidance of RL. Bente A. Breiby (Department of Pharmacy, University of Oslo) did the DSC measurements which JEN analysed. PEGylation of lipid vesicles was the focus of the master project of VAB, under guidance of JEN and RL. JEN prepared all figures and wrote the first draft of the manuscript, under guidance of RL. The manuscript was finalised by all authors, and all authors took responsibility for the revisions after peer review.

Paper II:

Summary: In **Paper II** we presented QCM-D, NR and AFM data on supported lipid bilayers exposed to different concentrations of indolicidin. From the data we were able to extend our knowledge on the membrane effects of indolicidin and compare with SAXS/SANS data presented in **Paper I**. The results revealed that the membrane effect of indolicidin was highly concentration dependent, with extensive lipid removal at high concentrations, leading to formation of lipid patches on the surface of the bilayer. At the lower concentration of 0.8 μM, similar to a 1:10 peptide-lipid ratio used for SAXS, the position of the peptide seemed to be in the outer leaflet similar to SAXS data. Plotting the SLD profile (profile from SAXS was converted from X-rays to neutron for direct comparison with NR data) from both experiments revealed that the structure of the pristine bilayers is directly comparable while the SLD curve for the bilayers exposed to indolicidin showed a localised effect in the outer leaflet from both methods. However, analysis of NR data reported a deeper penetration of the peptide over the whole tail region, while SAXS determined only a localised peptide effect in the outer part. In the paper we discussed that these differences might be due to lack of sensitivity of the NR method, where the results were analysed using the traditional slab model that does not allow to extract the exact position of the peptide. An asymmetric model allowing the peptide to position in exact the same position as determined from SAXS was used to show that the NR data does not contradict the SAXS data; however, because this model does not lead to an overall increase in the fit quality, but rather over-parameterisation, the symmetric model was included in the main paper.

Contribution: Josefine Eilsø Nielsen (JEN), Marité Cárdenas (MC) and Reidar Lund (RL) designed the experiments. JEN prepared samples, including lipid films used to form supported lipid bilayers. JEN and MC performed the NR experiments with technical support from local contact Yuri Gerelli (YG). JEN did the analysis of NR data under guidance of Tania Kjellerup Lind (TKL) and MC. JEN did the QCM-D experiments under guidance of TKL and MC. JEN and MC did the AFM experiments. Håvard Jenssen (HJ) suggested the choice of peptide, while Abdullah Lone (AL) did the synthesis and purification of indolicidin under guidance of Paul Robert Hansen (PRH) and HJ. JEN and

RL did the comparative analysis with SAXS data. JEN prepared all figures and wrote the first draft of the manuscript, under guidance of MC and RL. AL, HJ and PRH wrote the synthesis chapter. The manuscript was finalised by all authors. JEN and RL took responsibility for the revisions after peer review.

Paper III:

Summary: Paper III continued the work from **Paper I** by expanding the analysis of SAXS data on lipid-peptide mixtures to a wide range of different antimicrobial peptides, LL-37, aurein 1.2, magainin II, cecropin A and colistin. The results from these SAXS experiments revealed how membrane effects and insertion of these peptides varied significantly. Through detailed SAXS modelling the peptide position and distribution in the bilayer for each specific peptide could be extracted. For example, while aurein 1.2 inserted transmembrane, magainin II on the other hand positioned in the outer leaflet. LL-37 had the most pronounced membrane effect of the probed peptide, with a concentration dependent effect, where the peptide at higher ratios actually solubilised the vesicles.

Beyond the structural data probed by SAXS, **Paper III** also contains a comprehensive TR-SANS study on how all the mentioned peptides plus indolicidin affected the transport of lipids (method explained in detail in Chapter 1.3.8). From these results we established that all the included peptides accelerate both the intra-vesicular lipid flip-flop and intervesicular lipid exchange in DMPC-DMPG-DMPE-PEG vesicles. The only exception was colistin, which is known to rather interact with LPS on the outer membrane of gram-negative bacteria. Comparing the effect of the different peptides, the magnitude of peptide-induced acceleration in flip-flop and exchange rates were similar, except for LL-37 which had a significantly larger effect than the others. The effect of indolicidin and LL-37 was further studied by varying the temperatures in order to extract the Arrhenius parameters for the transport processes. From the resulting Arrhenius plots, we could see that LL-37 had a pronounced effect on the activation energy of exchange, while indolicidin on the other hand seemed to significantly lower the activation energy of flip-flop. This difference was explained by the observed

difference in peptide insertion as seen by SAXS: while indolicidin lowers the activation energy for lipid flip-flop due to insertion in the outer leaflet of the lipid bilayer, LL-37 has a more significant impact on exchange explained by the peptide acting partially as a solubilising agent at higher concentrations.

Contribution: Josefine Eilsø Nielsen (JEN), Victoria Ariel Bjørnestad (VAB), Håvard Jenssen (HJ) and Reidar Lund (RL) designed the experiments. JEN and VAB prepared all samples. JEN and VAB conducted the SAXS experiments. JEN, VAB, HJ and RL perfomed the TR-SANS experiments with technical support from local contact Vitaliy Pipich (VP). JEN analysed the SAXS data with support from VAB and RL. JEN, VAB and RL analysed TR-SANS data. HJ contributed with the peptides. Bente A. Breiby (Department of Pharmacy, University of Oslo) did the DSC measurements which JEN analysed. JEN did CD experiments and analysed the data, under guidance of Dr. Per Eugen Kristiansen (Department of Biosciences, University of Oslo). JEN prepared all figures and wrote the first draft of the manuscript, under guidance of RL and HJ. The manuscript was finalised by all authors.

Paper IV:

Summary: While we in **Papers I-III** focused on lipid model systems composed of DMPC-DMPG-2.5%DMPE-PEG (referred to as PC-vesicles), in **Paper IV we** focused on model systems closer mimicking the actual lipid composition of bacteria. In these experiments we used DMPE-DMPG lipids (referred to as PE-vesicles) as these are naturally found in *E. coli* membranes. SAXS data revealed that this model system was significantly less stable than the PC-vesicles, and the amount of PEGylated lipids incorporated was therefore increased to 5%.

Both SAXS and TR-SANS data on PE vesicles in the presence of aurein 1.2, indolicidin, LL-37, colistin and lacticin Q was presented in this paper. The results revealed that the peptide insertion and membrane effect was significantly more challenging to analyse based on the scattering data. At higher concentration several of the peptides either partly solubilised the membrane or induced formation of multilamellar structures. However, the peptide insertion at lower concentration could be determined from the

SAXS data and revealed to be comparable with the results in PC-lipids as presented in **Papers I** and **III**. In the same as in PC-vesicles, all the added peptides caused an acceleration in lipid transport as determined by the KZAC TR-SANS method, except for colistin. Overall the data presented in this paper showed that using PE-vesicles closer mimicking real bacterial membranes introduced several experimental challenges, while the results on peptide effects indicated that the trends prior found in PC-vesicles is comparable to PE-vesicles when probed using the same methodology

Contribution: Josefine Eilsø Nielsen (JEN), Håvard Jenssen (HJ) and Reidar Lund (RL) designed the experiments. JEN prepared all the samples, including lipid vesicles, with help from Victoria Ariel Bjørnestad (Department of Chemistry, UiO). JEN collected SAXS data and analysed the data with guidance from RL. JEN, HJ and RL collected TR-SANS data with technical support from local contact Sylvain François Prévost (SFP). JEN and RL analysed TR-SANS data. JEN prepared all figures and wrote the first draft of the manuscript, under guidance of RL. The manuscript was finalised by all authors.

Paper V:

Summary: In this paper we study different approaches to extract information on lipid flip-flop and exchange from KZAC TR-SANS data. In the past, KZAC TR-SANS data liposomes have been analysed by extracting the rates indirectly from the decay in the net integral intensity over time. However, here we use a time-dependent scattering model to analyse the full Q-range scattering curves as a more direct approach. Using the scattering model, we gain information on the exchange and flip-flop rate as well as information on changes in size, or morphology of the vesicles. In this work we analysed lipid vesicles with and without addition of indolicidin. The results reveal that the lipid transport rates calculated using the two different approaches is comparable. We also show how peptide addition leads to an initial increase in the size of the liposomes, which was not detected by the traditional approach of only analysing the integral intensity over time.

Contribution: JEN and RL designed the experiments, collected the TR-SANS data, developed the model and analysed the SANS data. JEN prepared all the samples. JEN did the DLS measurements and analysis. JEN prepared all figures. JEN and RL wrote the manuscript together.

Paper VI:

Summary: In **Paper VI** we examined the membrane interaction of synthetic nanofiber forming peptides using SANS, SAXS and NR. Because these peptides form larger structures, the analysis of data was more complex than in the case of the natural peptides studied **Papers I-V**. The work presented in this paper exposes the benefit with using the surface sensitive NR method because it does not have the same issues related to 3D orientation averaging as SAXS/SANS. Based on the data we discussed both how the structure of the peptide and the membrane were affected by the peptide-lipid interactions. In this work we compared self-assembled peptides with monomeric peptides, that are not able to undergo assembly due to shorter chain length, at different concentrations. We found that the nanofibers interact more strongly with the membrane, both inserting into the core of the membrane as well as being absorbed as intact fibres on the surface. This supported the claim that self-assembled peptides have a higher antimicrobial activity.

Beyond the effect of self-assembly, we also studied the effect of PEGylation of peptide drug molecules. The results revealed that addition of PEG groups seems to decrease the peptide-membrane interaction when comparing with non-PEGylated peptides. This observation does not support the retained antimicrobial activity previously seen, indicating that the mechanism of the PEGylated peptide might not be based only on membrane interaction. However, reduced membrane interaction would explain why the hemolytic behaviour is lower for the PEGylated peptides.

Contribution: Josefine Eilsø Nielsen (JEN), Nico König (NK), Marité Cardenas (MC) and Reidar Lund (RL) designed the experiments. JEN, NK and MC collected NR data with technical support from local contacts, Maximilian WA Skoda (MWAS) (ISIS data) and Armando Maestro (AM) (ILL data). JEN analysed all NR data with input from NK, MWAS,

MC and RL. He Dong (HD) and Su Yang (SY) did synthesis and purification of peptides. JEN prepared lipid films for supported lipid bilayer. JEN prepared matched out lipid vesicles for SANS/SAXS experiments, while NK collected the SANS/SAXS data. NK analysed SANS/SAXS data on peptide, JEN analysed SAXS data on liposomes. JEN wrote a first draft of the manuscript, but HD and SY wrote the synthesis paragraph, and NK wrote the SANS and SAXS methods sections. The manuscript was further developed by JEN, NK, HD, MC and RL, and the manuscript was finalised by all authors.

4. Discussion of results and future perspective

In this chapter we will first discuss the strength and limitations of the methodology used in this project before we move into the biological relevancy and impact of the presented results.

4.1. Using SAXS, SANS and NR to determine peptide effect on the membrane structure and extracting the peptide position in a lipid bilayer.

4.1.1 Sensitivity of the SAXS/SANS method

As presented in Chapter 1.3.6, SAXS/SANS has previously been used to study peptide-membrane interactions. Several studies have been presented where the scattering from the peptide-liposome mixtures was either analysed only qualitatively, or with an unmodified SDP model, and therefore did not take into account the significant changes in contrast as the peptide inserts into the membrane. This approach has in some cases led to the conclusion that peptide insertion causes changes in the membrane thickness due to shifts in the measured scattering curves.[72] In the work presented in **Paper I** we investigated whether including the peptide scattering in the model allow us to extract more information about the peptide effect on the membrane structure as well as the peptide position in the bilayer from the scattering data.

In this work, we used a combination of SAXS and SANS to characterise liposomes with and without peptide. Through a joint fit analysis, we found that combining SANS and SAXS data gives a higher accuracy in the fit parameters, especially with regards to the thickness of the components in the bilayer. This can be explained by differences in contrast. In the case of X-rays, the electron density (determining the SLD) of the hydrophilic part is higher than the electron density of the aqueous solvent, while the electron density of the hydrophobic core is slightly below that of the solvent. For neutrons, when proteated liposomes are prepared in a deuterated buffer, this provides

a large contrast for the hydrophobic tail, while the head group is almost only slightly visible. The difference in the electron density profile and neutron SLD profile is presented in **Figure 24A-B**. Due to these differences in contrast, the scattering signal, proportional to the square of the contrast, are very different. X-rays are much more sensitive to the lipid head-groups, whereas neutrons provide more information on the hydrophobic core composed of the lipid tails
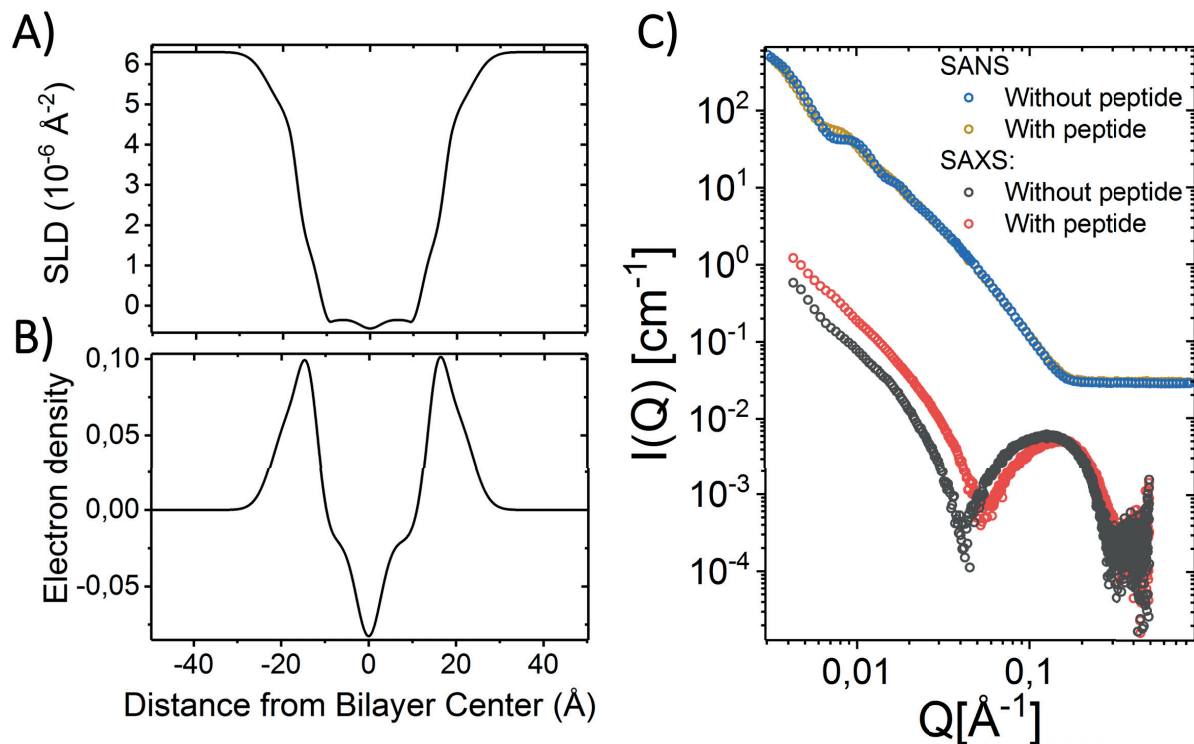
Figure 24. *Neutron SLD profile (A) and electron density profile (B) for liposomes illustrating the differences in contrast over the bilayer when using neutrons and X-rays. C) SANS and SAXS results of DMPC-DMPG(25%)-DMPE-PEG(2.5%) liposomes with and without 1:10 indolicidin (data from* ***Paper I****).[141]*

As shown in **Figure 24C,** the changes in the scattering curve upon peptide addition is significantly larger for SAXS than for SANS. While the SANS curves of the liposomes before and after peptide addition overlap (with only a small change in low Q due to a slight increase in size and polydispersity), the corresponding SAXS curves reveal an obvious overall shift towards higher Q values (especially with regards to the first minima).[141] Because of these results, we concluded that SANS experiments would not be sufficient to resolve the peptide insertion in the bilayer. However, SANS still give us valuable information on the peptide interaction because, as described above,

scattering patterns are highly sensitive to the thickness of the hydrophobic core. This is important because thickening or thinning of the bilayer are one of the suggested mechanisms for AMPs. As seen from the SANS data presented in **Figure 24C,** indolicidin does not seem to change the thickness of the bilayer, which was further confirmed by fit analysis.

The shift in the first minima of the SAXS curve can upon qualitative observation be interpreted as a change in the thickness of the bilayer. However, upon modifying the SDP scattering model to take into account the changes in contrast as the peptide inserts into the bilayer (especially taking care to calculate the fraction of peptide in the hydrocarbon tail region) we revealed that the changes in contrast is due to peptide insertion. This gives the same shift in the calculated scattering curve as we observed in the data (for mathematical description of the model see **Paper I**). The peptide has a substantially larger electron density compared to that of the lipid tails, which significantly alters the contrast and importantly the scattering cross-terms.

Because the shift in the minima of the scattering curve is very sensitive to the contrast changes across the bilayer, we hypothesised that the position and distribution of the peptide could be extracted from analysing the changes in the curves. The simulated curved presented in **Figure 25** reveal how the position and the depth of the minimum is indeed highly sensitive to the position and distribution of the peptide in the bilayer. A deeper minimum corresponds to a more symmetric bilayer, evident of the simulated SAXS curves for a symmetric transmembrane distribution. The same trend is seen for distribution of the peptide both in the inner and outer layer, modelled as symmetric double Gaussians. However, if the peptide only inserts in the outer leaflet because it is not able to transport across the bilayer, the scattering curve exhibits a shallower minimum due to the asymmetry. In **Paper III** we showed how these differences enable us to for example separate the insertion of aurein 1.2 which gives a deeper minimum and a significant shift towards higher Q, characteristic for a transmembrane distribution, while magainin II gives a shallower minimum characteristic for an asymmetric peptide distribution. As seen from the results presented in **Paper I** and **III,** using the modified SDP fit model, we were able to fully characterise the shift in the scattering curves of a series of different peptides by only varying the peptide position and distribution, without changing the structural parameters of the bilayer. One exception was LL-37, which was found to partly solubilise the membrane.
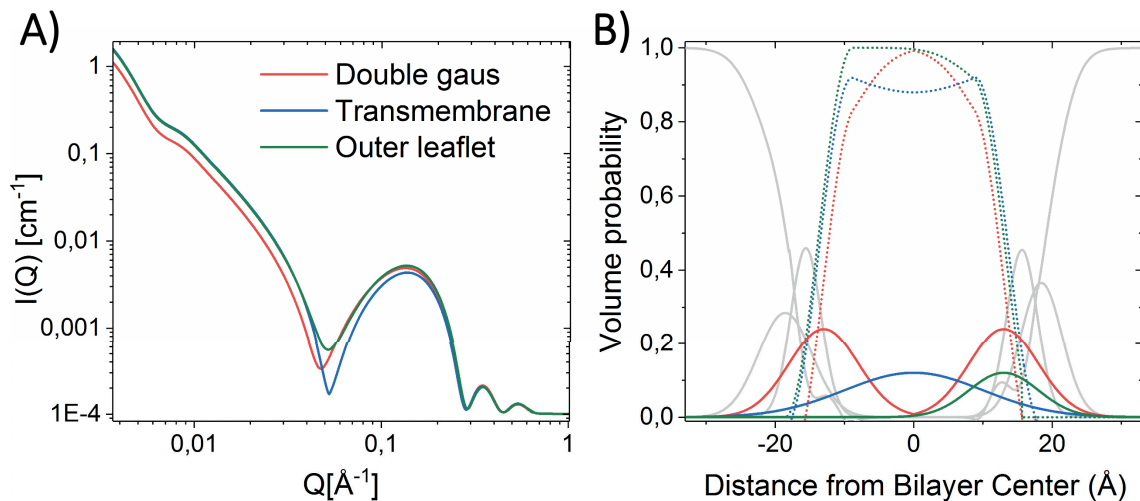
Figure 25. Simulated SAXS patterns (A) and resulting volume probability plot (B) showing the difference between peptide distribution as a single Gaussian in the outer leaflet, symmetric double Gaussian with peptide in outer and inner leaflet, and transmembrane distribution, using the SAXS model presented in **Paper I**.[141] *Figure taken from* **Paper III**.[83]

Contrary to the results we present here, Pan *et al.* have previously suggested that scattering data in itself does not allow for extraction of detailed information on peptide insertion in a bilayer. In their paper they instead use a combination of scattering data and MD simulations to determine these parameters.[137] Similar methodology was recently presented in Pachler *et al.* (published after our **Paper I** and **II**), where they use a combination of SAXS, SANS (using 4 contrasts) and MD simulations to determine the positions of two peptides in model membranes. In this work, they use a modified SDP model, similar to that in this work, with a single additional Gaussian in their volume probability plots representing the peptide.[145] While the Gaussians are allowed to vary freely across the bilayer in our analysis, they base the position and distribution of the peptides directly on MD simulations. Their argument against X-ray scattering data being an adequate basis for analysis of peptide-membrane interactions without accompanying computational data is justifiable. However, one of the main differences in the results we present in **Papers I**, **III** and **IV** and their results is the Q range of the SAXS data. While they probe a range from 0.0098 to 0.9 Å⁻¹, we present data from 0.0047 to 0.5 Å⁻¹ This allows us to also elucidate the size and polydispersity of the whole particle as well as this first minima, which we argue is essential in the analysis of the

contrast change across the bilayer and therefore the peptide position. It should be noted that the fit analysis of the scattering from the pure liposome solution describing all the feature over the whole Q range was initially problematic resulting in un-physical results with negative water probability curves. However, upon adding a series of physical constraints to the position (z) and distribution (σ) of the head and tail groups (further described in **Paper I**) we obtain stabile fits allowing for the detailed analysis presented in this work.

To further verify the peptide-liposome scattering model presented in **Paper I** we did NR experiments using the same membrane composition (minus 2.5 % DMPE-PEG) and measuring conditions. As presented in **Paper II,** the results of 1:10 peptide:lipid ratio showed the same trends as earlier seen from SAXS, with preferential interaction of the peptide indolicidin with the outer leaflet.

In conclusion the modified SDP model we propose in **Paper I** allows us to study the membrane effect of a series of different AMPs at different concentrations. In **Paper III** we show how we can distinguish between the different membrane effects of different AMPs which potentially gives valuable information on their mechanism of action. Another strength is the ability to also vary the lipid composition of the probed model membrane, like for example in **Paper I** where we study the impact of increasing amounts of negatively charged lipids. The approach we suggest is not limited to examining AMP-membrane interaction, but could also be used to investigate membrane interaction of other peptides/proteins like for example cancer peptides/drugs, or Amyloids relevant in Alzheimer's disease pathogenesis.

Overall this approach to studying peptide-membrane interactions provides beneficial flexibility in the experimental setup, however, there also some important limitations to the method as we will discuss in the following chapter.

4.1.2 Limitations of the SAXS/SANS protocol

Our intention with the work presented in **Paper I** was to develop a protocol for studying AMPs that potentially could be used in the development and screening of new drug candidates. For example, in Lone *et al.* we were able to separate the membrane effect of three compounds and correlate the differences in membrane bound peptide with

the antibacterial efficacy.[188] However, this protocol has some limitations that should be considered.

The first major limitation is related to the model membranes used to mimic bacterial membranes for these studies. SAS only gives an orientational and ensemble average of all the particles in the sample, and therefore ideally the sample needs to be uniform and consist of as few components as possible to be able to extract detailed information through modelling. The model systems used in this thesis are therefore significantly less complex than the real bacterial cell membrane.

In all experiments included in **Papers I-III** and **V-VI** we use model systems based on DMPC:DMPG mixtures (for the lipid vesicles we also incorporate 2.5 % DMPE-PEG for stabilisation). As previously discussed in Chapter 1.3.1, lipids with a PC head group are widely used in model systems even though these are not a natural part of bacterial membranes. Specifically, the saturated 14-carbon tail lipid DMPC, used in these experiments, is not found in any natural lipid membranes. However, the bacterial membrane does contain zwitterionic lipids, including PE-lipids, and PC is often used as a substitute for them because it is cheaper and easier to work with. The difference in the chemical structure of the PC and PE headgroup is three methyl groups on the nitrogen forming a choline group in PC, which is exchanged for hydrogens in PE. While PC lipids have an ideal packing parameter (truncated cone) for formation of lipid vesicles, PE has a smaller headgroup area and therefore a higher packing parameter (see **Figure 12**). Dependent on its saturation degree, PE has a cylinder or inverted truncated cone geometrical shape.[158] As a result, PE lipids prefer a slightly negative curvature which may result in deformed membranes and formation of multilamellar structures. PE lipids also have a much higher phase transition temperature than PC lipids, even when they have the same tail composition, such as 14:0 PC (DMPC) and 14:0 PE (DMPE). While DMPC exhibit a phase transition temperature of 24 °C, DMPE lipid shows transition at 50 °C.[279] This drastic change in the phase transition temperature may be explained by the PE headgroups ability to form hydrogen bonds in-between lipid in the membrane resulting in a more stable structure.

After developing the experimental protocols presented in **Papers I-III**, we were interested in modifying the model system to closer mimic bacterial membrane. In

Paper IV we therefore explore using PE as an alternative to PC. In this work we found that the 2.5 % PEGylated lipids we previously had used to stabilise PC-vesicles was not sufficient to stabilise the PE-vesicles. The amount of PEGylated lipids in this work was therefore increased to 5 %. The PEGylated lipids are necessary to prevent the aggregation of vesicles and eventual phase separation upon addition of cationic substrates like AMPs. The effect of peptide addition to non-PEGylated vesicles can be seen in **Figure 26A,** where the destabilisation is seen immediately as an increase in turbidity followed by formation of two distinct phases.[280] This effect can be explained by a number of factors, including depletion of the electrostatic repulsion which is important for the stability of liposomes.

To increase the stability of the vesicles we turned to a well-known strategy from pharmaceutical science; PEGylation. PEGylation of liposomes is known to improve the circulation time of vesicle-encapsulated drugs, and it has been reported that PEG-modified liposomes have about 5-fold prolonged circulation time in blood compared to conventional liposomes used in drug encapsulation.[281] The traditional explanation of why PEG on the surface of a liposomal drug carrier extends the circulation lifetime is that the polymer reduces or prevents protein adsorption. However, an alternative explanation is the ability PEG has in preventing self-aggregation of liposomes[282] as the polymer chains creates a steric barrier for aggregation (see **Figure 26B**). It is this mechanism we have utilised in our PEG modified lipid model systems for studying AMPs.
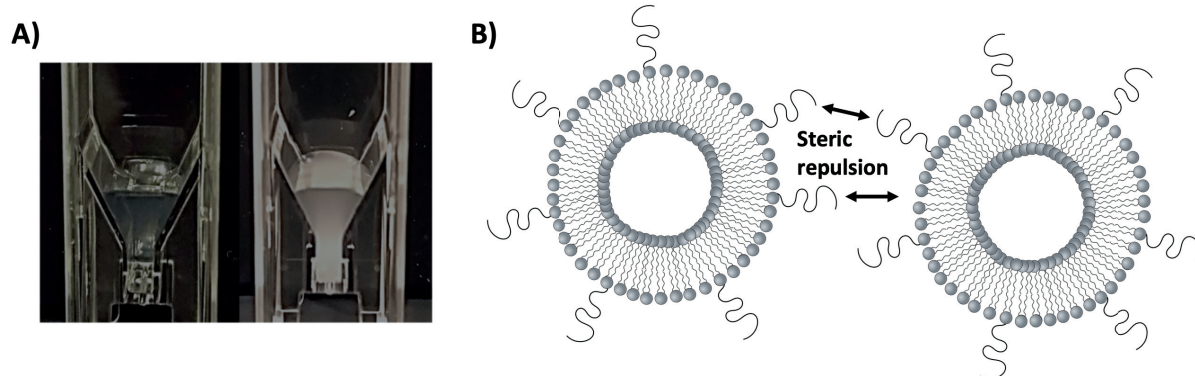
Figure 26. A) *The effect of adding a cationic substrate to PEGylated and non-PEGylated liposomes.* *B)* *Illustration of liposomes sterically stabilised by PEGylation. Adapted figure reprinted with permission from Bjørnestad (2018).*[280]

The steric stabilisation of liposomes due to PEG-modification has been explained by both an entropic and an enthalpic effect. The entropic effect is attributed to volume restrictions; when individual liposomes approach each other the available volume for the polymer chains linked to the surface is reduced. This result in a decreased number of available confirmations for the polymer chains, and hence a reduction in the entropy of the system. The enthalpic effect is explained by interpenetration effects; individual liposomes approaching each other leads to loss of bound solvent from the PEG chains, hence a positive change in enthalpy.[280, 283, 284]

Based on theoretical calculations it is generally assumed that at low surface coverage the PEG chains are in a so-called '*mushroom confirmation*', where the chains are in a Gaussian random coil-like state. At high surface coverages the close packing of the PEG chains compresses them into more extended structures referred to as a '*brush conformation*'.[285-287] Arleth and Vermehren has presented an analytical model that can be used to solve detailed structures of PEG-modified liposomes from SAS data. The R_g of the PEG chains (this parameter is directly related to the conformation of the chains) and distribution of PEG on the outer and inner surface of the bilayer are the important fit parameters in this model.[288] In the work presented in this thesis we have used these expressions in our modified SDP model to properly take into account the scattering contribution for the PEG chains (see **Paper I** for details). Through fit analysis of the SAXS data we found that the bilayer structure seems independent on the incorporation of only 2.5% PEGylated lipids when comparing with non-PEGylated liposomes.[280]

Even though DMPE-PEG incorporated in the vesicles in this concentration range does not seem to influence the bilayer structure in itself, it is still interesting to look at how the PEG may affect the peptide interaction. In the case of the structural SAXS data we argue that the amount of PEG and the PEG chain length (PEG MW = 2000 g/mol) chosen results in a neglectable interference due to peptide-polymer interactions. Based on results from amongst others Mineart *et al.,* PEG modified liposomes prepared in the co-extrusion manner (incorporating the PEGylated lipids in the initial lipid film) as used in all the experiments presented in this thesis result in a distribution of PEG chains on the inner and outer surface. Therefore, the actual amount of polymer chains on the surface of the vesicles is substantially lower than the amount added.[289] The PEG chains

situated in the inner leaflet are not available for initial interaction with the peptides. It is, however, difficult to compare peptide insertion in PEGylated and non-PEGylated vesicles directly as the latter system is not stabile enough for experiments. However, in **Paper II,** we compare the membrane effect of indolicidin as seen by NR experiments on non-PEGylated SLBs, with data from SAXS experiments on PEGylated vesicles. These results reveal that the interaction is comparable, pointing towards the addition of PEG having a low impact on the membrane interaction.

Even at the higher amount of PEG we still had problems with the colloidal stability for the DMPE vesicles upon AMP addition. The results presented in **Paper IV** is collected at 37 °C when the membrane is in the gel phase (confirmed by DSC measurements) due to the higher phase transition temperature of DMPE. We also tried to do experiments at temperatures above the phase transition; however, in these cases the vesicles immediately formed multilamellar structures, which prevented us from doing as accurate analysis as it obscures the scattering pattern and adds new parameters. The difference in the fluidic phase between the PC vesicles in **Papers I-III** and the PE vesicles in **Paper IV** is potentially problematic for the comparability of these results (as discussed in **Paper IV**). Even at 37 °C we observed solubilisation of the membrane and formation of micellar/disc-like structures, in addition to the formation of multilamellar structures, at high AMPs concentrations. Even with this destabilisation effect seen at high peptide:lipid ratios, we were still able to extract the peptide position in the bilayer at lower ratios. These results show the same trends as we saw in **Paper I-II** for indolicidin and **Paper III** for aurein 1.2, colistin and LL-37, and we argue that the results point towards the molecular peptide interaction on PE-vesicles being comparable with to PC-vesicles.

Although varying the lipids headgroups to match real bacterial membranes makes the system more biologically relevant, also the tail region of the lipids will be of importance. The real membrane consists of a mixture of saturated and unsaturated phospholipids with different tail lengths. However, using such a complex mixture in model systems for SAXS would complicate the analysis of the results. In the fit analyses, we based the parameters describing the basic structure of the membrane on reported values from MD simulations,[154, 203, 290] with regards to thickness, area per lipid and volume. This allows us to confine fit parameters in order to obtain more accurate results when adding a peptide. Using a mixture of lipids with different volumes, area

per lipid and thickness, would leave us with an increased number of unknown parameters in the fit analysis resulting in a higher uncertainty in the results. Beyond the simplification in the phospholipid composition, our model membranes lack incorporation of for example cardiolipins and membrane proteins, which may influence the peptide interaction when comparing directly with real bacterial cells.

Beyond the limitations related to the model systems, there are limitations related to the probed peptide system that needs to be considered. As discussed in Chapter 1.2.5 the relevant AMP concentration range for mode of action studies has been much debated in the literature. In the SAS experiments presented in **Papers I** and **III** experiments we have used a peptide:lipid molar ratio ranging from 1:100 to 1:5. It is clear that higher peptide amounts inserting into the bilayers leads to a more significant shift in the minimum of the SAXS curve, which enables us to do a more accurate analysis with the theoretical models. We therefore included higher peptide:lipid ratios in our experimental designs, even though these may not be biological relevant depending on which literature references one bases the arguments on. The higher ratios were found to be important in order to obtain a higher accuracy in the analysis. As well as fitting every curve (from each ratio) separately, we also tried to fit the whole concentration series simultaneously using the same structural parameters. As seen from **Papers I** and **III** this worked well for peptides like indolicidin, aurein 1.2 and magainin, where the position and distribution seem to be very stable upon changes in the peptide concentration, while LL-37 has a very concentration dependent action on the membrane. Therefore, using such a global fit in the latter case would not provide a good explanation of the data. We initially also did SAXS experiments on lower ratio like 1:200 and 1:500, however, at these ratios no significant changes in the scattering pattern could be detected, indicating that SAS does not provide the needed resolution to resolve peptide effects at low peptide:lipid ratios.

Despite the presented argument that SAXS data allows for analysis of peptide-membrane interactions, the validity of this claim is dependent on the nature of the peptide probed. In the case of self-assembling peptides, the data may be too complex to analyse using the modified SDP scattering model presented in **Paper I**. An example is presented in **Paper VI**, where we investigate the membrane interaction of AMPs that

self-assemble into defined nanofibers. Due to the complexity of this system SAXS data in this case only gave us qualitative information on a peptide-membrane interaction by comparing the calculated average (average scattering from peptide and lipids measured separately) and the measured mixture.

It has previously been shown that SANS together with contrast variations can be used to probe complex structures in lipid membranes.[291-294] Maric *et al.* developed a protocol for preparing stealth carrier nanodiscs in order to study the structure of membrane proteins. These discs consist of specifically deuterated lipids in order to make them invisible for neutrons in 100% D_2O. In this way the structure of membrane proteins can be probed in their native environment by SANS, while circumventing the intrinsic complexity of the carrier system.[291] We used the same principle in **Paper VI** to probe the structure of peptide nanofibers in the presence of liposomes that practically matched the solvent. To analyse these data, we were able to use the same scattering model as previously used to analyse the scattering for the pure peptide nanofibers in König *et al.*, due to the vesicles being invisible for the neutrons. The same principle could for example be used to study both pore-formation structures in membranes in a more detailed manner than the modified SDP model presented in this thesis.

Traditionally, research on antibiotics rely on assays like MIC to separate between effective and ineffective molecules in their drug development research. The methods presented here may be a supplementary approach to these traditional methods. The SAXS method is sensitive to small changes happening very quickly and may therefore be better for quickly finding differences between compounds than MIC, which looks for larger drastic changes over longer times. With the use of the bioSAXS setup at for example BM29, ESRF or P12, DESY (both beamlines used for the experiments presented in this thesis) one is able to screen a larger number of compounds in one experiment. However, the analysis of the data is not as efficient, and using the modified SDP model requires significant knowledge of lipid systems and scattering. It is especially easy to over-interpret the impact of the results if not aware of the limitation of the method. Taking this into account, we still argue that using this approach may be an interesting option in both screening and in-depth studies of new molecules, including peptide-mimetics.

4.1.3 Neutron Reflectometry as an alternative to SAS

The issues related to stability of the model system and complexity related to the 3D orientational averaging can be avoided by using NR which bases itself on SLBs rather than free floating vesicles. We utilise these differences in the study of the membrane interaction of peptide nanofibers as presented in **Paper VI**. From the NR data we were in this case able to resolve both how the peptide inserts in the membrane as well as the absorption of peptide fibres on the surface of the membrane. Using knowledge of the structure of the nanofiber themselves (characterised by SAXS in König *et al.*[189]), we hypothesise how the fibres orient on the membrane surface from the NR data. In this work we also studied a PEGylated version of the peptides. These are known to self-assemble into fibres with similar dimensions as the non-PEGylated version, but have an additional surrounding PEG layer.[189] By comparing NR data on PEGylated peptides with deuterated and proteated PEG groups we were able to describe how the PEG layer in close proximity to the bilayer compresses when comparing with the outer PEG layer, indicating an interaction between the PEG and the lipid headgroups. Based on this work it is apparent that NR does have some advantages when it comes to more complex peptide systems that should be considered in the choice of technique.

However, also this technique has some limitations. NR is a lot more time consuming than SAXS experiments and requires access to a neutron beamline. With SAXS one can study a larger series of peptides at different concentrations in one experiment (as seen in **Paper III**), while a NR experiment traditionally looks at only a few peptides at a couple of different concentrations. This was one of the main motivations for the work presented in **Paper II,** where we show that SAXS data can provide the comparable information to NR data in the case of "simple" peptides.

Similarly to SAXS, NR involves the use of simplified model membranes. SLBs used for NR, are in close contact with the solid surface. As compared to free-standing lipid bilayers they lack significant reservoirs of solution on both sides of the membrane, and the proximity of the substrate may affect the diffusion of lipids and peptides.[117] To be able to precisely determine the peptide position in the bilayer we use tail-deuterated lipids to increase the contrast between the peptide and the lipids. This partly constrains the selection of lipids in the bilayer composition both due to limited availability and high costs of deuterated lipids. Apart from the low availability and cost limitations, not

all lipids are suited to form high coverage SLBs, which together with low roughness are necessary factors to obtain high resolution NR data.

In the experiments presented in **Papers II** and **VI** we use SLBs containing 90% DMPC and 10% DMPG. These are relatively easy to form using the vesicle fusion protocol, but, as discussed above, are not the ideal mimic for the real bacterial membrane. We therefore tried to follow the protocol recently published by Lind *et al.*[134] to form supported lipid bilayers for NR studies. In their protocol they use unsaturated POPE-POPG lipid mixtures. However, because these lipids are not easily available in their deuterated form and deuteration is necessary for contrast with the substrate, we followed the same protocol only increasing the temperature with DMPE-DMPG lipids. Unfortunately, we were not able to achieve a sufficiently high coverage using this lipid composition (<80 % coverage), and these data were therefore not included in the final manuscript.

While the lack of the complexity of the 3D orientational averaging is beneficial with regards to analysis of the data, this also imposes limitations with regards to the information that can be extracted from NR data. Specular NR results gives information on the structure of the bilayer in the direction normal to the interface, and does therefore not allow for investigation of in-plane structures, like domain formation or height fluctuations (this can however be probed by off-specular scattering).

Overall, NR is a relevant technique that can be used to determine the membrane interaction of AMPs, including peptides that self-assemble into very complex structures as we show in **Paper VI**, but also this technique has its limitations that should be taken into account.

4.2 Using the KZAC TR-SANS method to determine peptide effect on lipid transport

4.2.1 Accuracy of the KZAC TR-SANS method

As previously discussed in Chapter 1.3.8, several methods can be used to probe the transport of lipids in a lipid membrane. In this work we chose to use the KZAC TR-SANS method because it enables us to study lipid transport without addition of large labels like for example fluorophores that potentially perturb the membrane and affect the transport rates. The method is well established and has been extensively used to study micelles and liposomes in the past. However, one relevant question is whether the decay in scattering intensity actually comes from single chain exchange and flip-flop rather than fusion of particles. In **Paper III** we therefore compared the decay rate for the same system at two different concentrations in order to hopefully answer this question. If the decay in scattering intensity observed is mainly due to fusion of liposomes one would expect it to be a concentration dependent process. However, as seen from **Figure 27,** both with and without addition of indolicidin the observed curves overlap at 2.5 and 5 mg/mL. We therefore argue that the increase in rates we observe with peptide addition is actually a result of acceleration of lipid flip-flop and exchange processes rather than increased occurrence of fusion/fission. This is also corroborated by similar trends of peptide accelerated lipid transport being observed in the past.[78-82]

In the case of the PE- vesicles studied in **Paper IV,** the same concentration dependent test for fusion was not performed. As described above, the SAXS curves at higher peptide ratios showed partial solubilisation and appearance of multilamellar structures when adding peptides to these liposomes. We were therefore not able to extract specific information on the rates of the transport processes based on the TR-SANS data in the same way as for the DMPC-DMPG liposomes in **Papers III** and **V.**
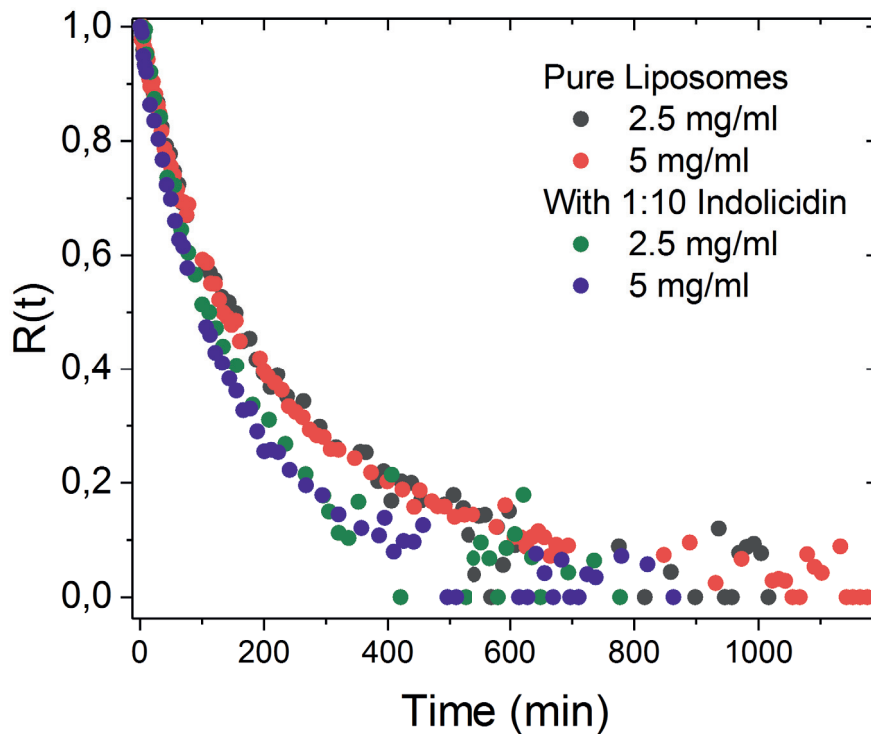
Figure 27. *R(t) curve for DMPC(75%)-DMPG(22.5%)-DMPE-PEG(2.5%) liposomes with and without indolicidin comparing liposome concentrations of 2.5 mg/mL and 5 mg/mL. The results reveal no concentration dependency in this range indicating that the loss of intensity is due to single chain exchange of lipids, not fusion of vesicles. Figure taken from **Paper III**.[83]*

The KZAC TR-SANS method allows us to simultaneously measure intervesicular exchange and intra-vesicular flip-flop. Other neutron based methods used in the past, like the asymmetric bilayer TR-SANS method used by Nguyen *et al.*, only shows lipid flip-flop motion.[82] However, the sensitivity to both exchange and flip-flop may also be seen as a disadvantage with the KZAC TR-SANS method because it calls for a more complex analysis of the data to extract the individual rates. This may introduce a higher error in the resulting parameters. As first shown by Nakano and co-workers, the rate constants can be derived by a kinetic analysis of the net change of the integral intensity over time, as discussed in Chapter 1.3.8. We used this approach to extract the peptide effect on exchange and flip-flop rates in **Paper III.** However, this is an indirect method of extracting the rates and does not take full advantage of the intrinsic spatial resolution of the SANS technique. Potential parallel kinetic processes, such as vesicle growth or morphological transitions cannot be deciphered, which may be important factors in fully understanding the impact an added peptide. This inspired us to do the work presented in **Paper V**, where we instead analyse SANS curves by applying a detailed time-dependent scattering function which allows us to extract the rates

directly from the full Q-range SANS data (see illustration **Figure 28A)**. In this work we used a simpler concentric shell model rather than the SDP model used for analysis of SAXS data in prior work. Because the liposomes we used either have a deuterated or proteated tail, while the headgroup is always proteated, we only had to consider the changes in contrast of the tail region and how this parameter evolved over time. For further details on the mathematics of the model see **Paper V**.

By modelling the full Q-range TR-SANS data for liposomes with and without indolicidin we found that the size of the vesicles changed over time upon addition of the peptide, with an initial steep growth that stabilise over time. This trend was also supported by DLS measurements on the same system. As we had already excluded fusion of liposomes and aggregation as a driver of the increase in size, we hypothesised that the growth behaviour rather can be explained by peptide effects on the molecular level. Addition of indolicidin to the vesicles leads to an inhomogeneous partial dissolution of lipids which initially increases the solubility of the lipids. This again leads to redistribution of lipids that become available. Once the lipids have been redistributed and the lipids /peptides have been homogenously distributed, the vesicles stabilize into the new size distribution (an Ostwald ripening like behaviour). This additional information shows the importance of considering the full Q-range SANS data in analysing the molecular exchange kinetics.

When comparing the results of the direct and indirect method of determining the rate constants from the same data set, we found that the two methods were comparable, as seen in **Figure 28B**. However, analysing the *R(t)* curve directly does give slightly faster rates than extracted from modelling the full Q-range data, and we do see an additional delay-time in the flip-flop rate extracted from the latter method. This additional delay-time is thought to be an unphysical artefact of the methodology that we are yet to fully understand. We speculate that an important contribution is the lack of sensitivity to lipid flip-flop in the first stage of the experiments because of insufficient contrast between the outer and inner leaflet of the vesicles. Over time, when enough lipids have exchanged between H- and D-vesicles (exchange only affects the outer leaflet) we obtain the necessary contrast to also see lipid flip-flop motions.

The accuracy of the alternative full Q model analysis approach highly depends on the quality of the experimental data, while the indirect approach used in the past by amongst other Nakano and co-workers, and by us in **Paper III** is less dependent on the quality of the SANS data. The factor is beneficial with regards to experimental design because the measuring time of each curve can be shortened. This gives us more time points as well as the ability to change in-between more samples over the same time period without losing larger time spans for each sample. However, we still argue that a combination of the direct and indirect method as we have done in **Paper V** increases the reliability of the results. This approach will also detect parallel kinetic processes, as for example solubilisation mechanisms, induced vesicle fusion, morphological changes and so on, which may be important when investigating the effect of a substrate like AMPs with unknown membrane effects. This would be especially interesting in a system that has not been previously characterised by SAXS (or alternative methods) as we have done in **Papers III-IV**.
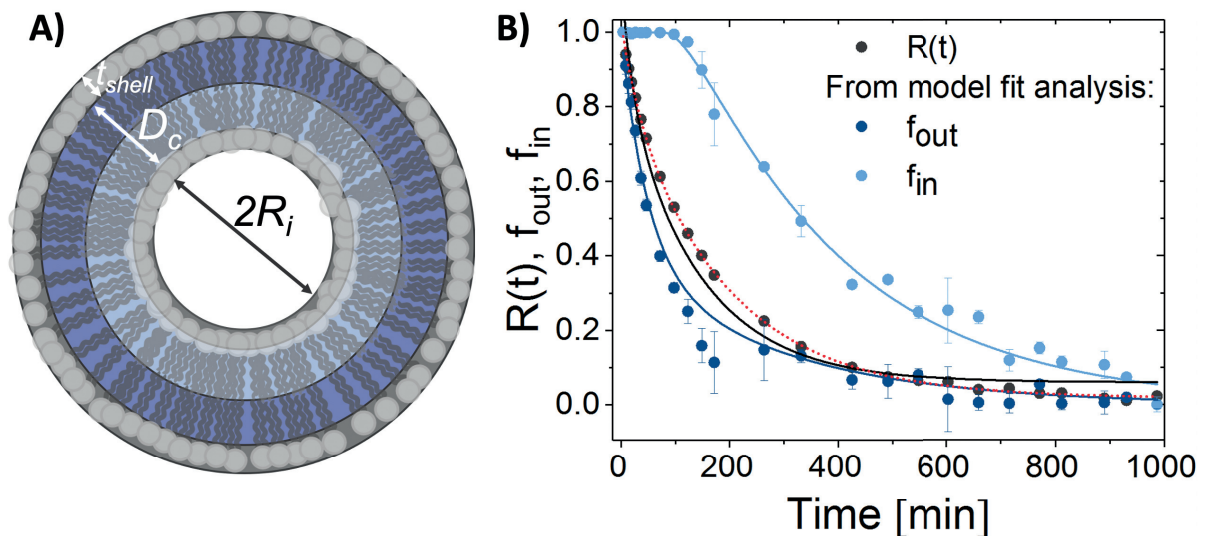
Figure 28. A) Illustration of the concentric shell model used to analyse TR-SANS data in **Paper V.** B) Results on lipid transport in liposomes as seen by the KZAC TR-SANS method. R(t) curve calculated from the net change of the integral intensity from TR-SANS, compared with the exchange, f_{out} and flip-flop, f_{in} fractions extracted directly from the full Q range scattering data through fit model analysis. The solid black line is a result of a joint fit of all curves extracting information on the exchange (k_{ex}) and flip-flop (k_{flip}) rates, while the red dotted line represents a separate fit to only the R(t) curve. Figures taken from **Paper V**.

4.2.2 Limitations of the KZAC TR-SANS methodology

In the same manner as for the SAXS/SANS protocol discussed above, also the KZAC TR-SANS entail limitations with regards to the model membrane system. The need for well-defined uniform liposomes is highly important in order to extract thermodynamic parameters, including the exchange and flip-flop rates, from the data. The use of deuterated (or partly deuterated) lipids imposes further limitations, as the types of deuterated lipids commercially available is limited, and the material very expensive. The use of deuterium labelling may potentially introduce isotope effects, as changes in hydrophobicity and noncovalent interactions between molecules including hydrogen bonding.[295] This should be considered in the interpretation of the data with relevance to biological systems. However, the impact of isotope effects is still considered less significant than labelling molecules by using larger fluorophores,[168] which have previously been used to monitor lipid movement in membranes.[50]

In **Paper III** and **V** we use the same PC-PG-vesicles as used for the SAXS data in **Papers I-III** because of their stability and uniformity. However, due to the same argument as presented above, this system does not really mimic the bacterial membrane with regards to lipid composition. In **Paper IV** we present TR-SANS data on PE-PG vesicles. The experiments revealed how all the added peptides, except for colistin, increase the rate of contrast decay also in these vesicles. The results are therefore comparable to the results for PC-PG vesicles presented in **Paper III**. However, due to the confounding factor of membrane solubilisation and formation of multilamellar structures as determined by SAXS, we were not able to extract accurate rates for flip-flop and exchange from these data in the same way as was done in **Papers III** and **V**. We still hypothesise that peptide insertion in the PE-PG membrane would cause the same deformation in the packing of the lipid tails as observed in PC-PG-vesicles. In PE-PG-vesicles, peptide insertion may also cause breakage of H-bonds between the headgroups further destabilising the close packing. This, together with the observation of a highly increased rate of decay in the case of 1:50 lacticin Q, which was not found to solubilise the membrane at this concentration from SAXS, points towards a peptide-induced increase in lipid transport motions also in the case of PE-PG lipids.

Beyond the potential influence of the lipid head group on the lipid transport, the tail group of the lipids are potentially even more important. Homan and Pownall showed

90

by fluorescence measurements that both lipid exchange and flip-flop significantly accelerates with decreasing chain length of the acyl tail groups.[50] Nakano *et al.* have compared the exchange and flip-flop rates of fully saturated DMPC and unsaturated POPC vesicles revealing that the flip-flop rates for DMPC was significantly faster than for POPC, where the rate of the latter could not even be detected in the TR-SANS experiment. Using a mixture of lipid tail groups with regards to length and degree of saturation as can be found in the real membrane, would therefore probably highly influence the lipid transport, and the lipid mixture would result in observation of a variety of different rates for both flip-flop and exchange. This is supported by recently published data from König *et al.* on exchange processes in polymer micelles rather than lipid vesicles, consisting of mixtures of polymers with different hydrophobic tail lengths (C_{22}-PEO5 and C_{28}-PEO5). From the TR-SANS data they were able to extract two distinct exchange rates, indicating that the exchange is decoupled even though different alkyl blocks mix inside the micelle core and crystallise cooperatively (as seen by DSC).[296] In these micellar systems, separating two decoupled rates for the two different chain lengths is easier than it would be in a vesicle sample, since the latter already has two distinct rates, the intra- and the inter-vesicular motion of lipids respectively. A mixture of two types of lipids with different tails would give room for four rates, mixtures of three giving six rates and so on. Accurately extracting all this information from the contrast decay rates would be very challenging and methods that only show lipid flip-flop (as discussed in Chapter 1.3.8) would probably be more useful in studying lipid transport in these kinds of lipid mixture systems.

As seen from the fusion experiments presented above, we succeed in stabilising the PC-PG vesicles and are therefore able to extract exchange and flip-flop rates from the data. In the same way as for the structural SAXS/SANS experiments, we use PEG to stabilise the liposomes. However, data presented by De Cuyper *et al.* has suggested that PEGylation of lipids may increase their inter-vesicular exchange rate. However, in their study they use a larger amount of DMPE-PEG (10%) than we used for our experiments (2.5-5%). We therefore tested the influence of PEG on the TR-SANS data both with and without peptide, by doing the same experiment using liposomes with 2.5 and 5% DMPE-PEG, as presented in **Figure 29**. These experiments interestingly revealed that increasing the PEG concentration did not affect the lipid transport in either case, with or without indolicidin.
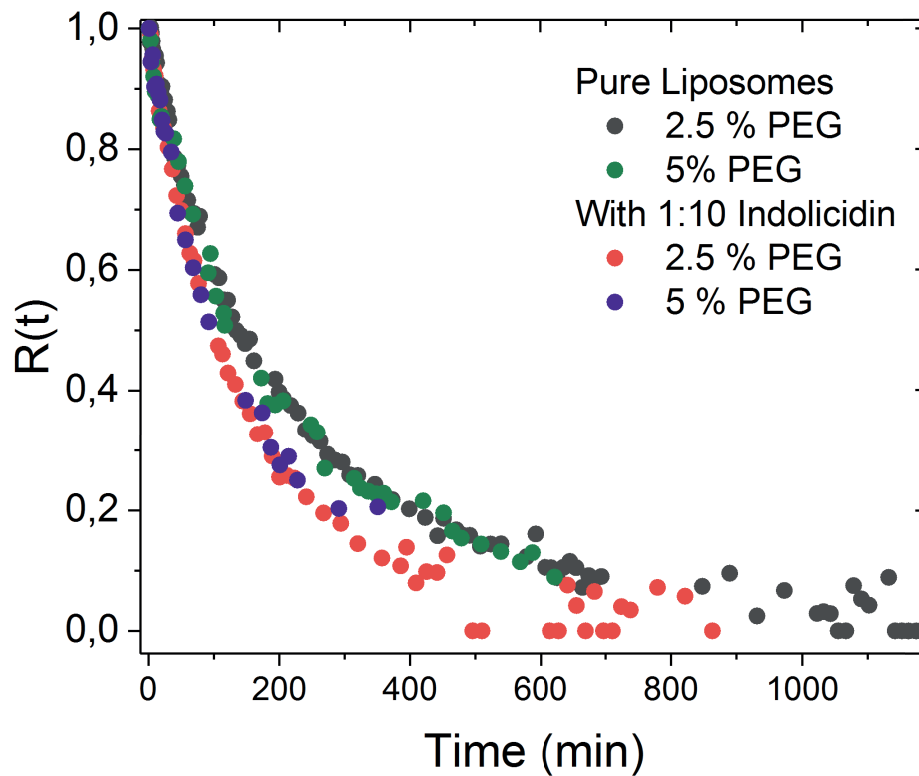
Figure 29. *R(t) curve for lipid vesicles with different PEG amounts, 5 and 2.5 % DMPE-PEG, with and without peptide, showing that PEGylation in this range does not seem to significantly affect the dynamics. Figure taken from* **Paper III**.[83]

Apart from issues related to the model system requirements, the KZAC TR-SANS method is highly time consuming and relies on access to neutron facilities over a longer period. For example, the data presented in **Papers III** and **V** is based on two separate five days experiments at MLZ, Garching, Germany. This is especially true if the aim of the experiment is to obtain information on activation energy, which entails experiments done at several different temperatures. The number of samples that can be probed using this method is therefore more limited than the structural studies done by SAXS. Therefore, only two peptides, indolicidin and LL-37, were chosen for further studies into the concentration and temperature dependency in the work presented in **Paper III**, while the rest of the peptides were only studied at one ratio and one temperature.

4.3. Impact of main findings and future perspective

As described in the introduction to this thesis, there is no general consensus on the mode of action of AMPs. The topic has therefore been extensively studied using a number of different techniques. In this project we aimed to shed a new light onto the question by systematically studying a variety of different molecules using X-ray and neutron-based techniques.

One of the major outputs from the research is the systematic comparison between structural effects seen by SAXS/SANS and NR, and peptide effects on lipid transport seen by TR-SANS. We initially hoped that through studying a series of different peptides in the same model system we would be able to formulate a general law relating the structure of the peptide with the membrane effect. This could also be very beneficial in the design of new antimicrobial compounds. Due to the restricted TR-SANS beamtime available for this project, the number of AMPs we could include in the study was limited. We therefor decided to focus on including natural AMPs varying in length as well as secondary structure. As well as the unstructured and α-helical peptides we did study, we initially also planned to including peptides with β-sheet motifs. However, unfortunately the supplier did not manage to synthesise these peptides in the quantity needed for these studies. Because the peptides included in the study are natural known AMPs these have all been previously studied to varying degree, which was beneficial for comparison and confirmation of the validity of our methods and results.

Upon analysing the data from **Papers I** and **III,** our initial hypothesis was that the amount of peptide incorporated in the tail region of the membrane (estimated from SAXS) would be correlated with the effect on lipid transport as estimated by TR-SANS. This hypothesis was formulated based on theories presented by amongst other Conboy and co-workers, stating that peptides can facilitate increased flip-flop through defect-driven lipid translocation or increased entropy of the transition state resulting in a lower barrier for flip-flop.[81, 215] However, no such correlation could be detected from our results. We therefore looked for correlations based on the number of charges, number of hydrophobic groups of the molecules and so on, without any clear trends being detected. This indicates that the peptide-membrane interaction is highly

complex and dependent on a variety of parameters. Even though no general law for the peptide effect could be formulated based on these results, we still conclude on a coherent scenario where all AMPs that insert into the membrane also accelerate the lipid transport to some extent. We further suggest, based on these data, that peptides acting in a concentration dependent detergent like manner, like LL-37, also have a more concentration dependent effect on the lipid transport. Even at concentrations below the threshold for solubilisation, LL-37 influenced the lipid transport more drastically than the other peptides.

An alternative design of the study which potentially could give more direct information regarding structure-activity relationships, would be to rather focus on one peptide structure and do point-mutations. This could for example include destabilisation of secondary structures, variation in length and the number and position of hydrophobic and charged amino acids. However, we estimate that in order to gain sufficient information from this type of study the number of sequences that needs to be included is rather extensive, especially if one wants to make variations of several of these natural AMPs, and this would therefor require access to a longer time period of TR-SANS. However, based on the results from our studies were LL-37 was recognised to have the most dramatic effect on the structure and dynamics we hope in the future to conduct an experiment using point mutations of the sequence in order to isolate the important features and motifs promoting the observed membrane effects.

We found it highly interesting that even AMPs that opposed to LL-37, do not significantly affect the membrane structure still was found to accelerates the lipid transport by lowering the activation energy. We therefore argue that acceleration of lipid transport may be an important factor in understanding the membrane effects of peptides that are not found to solubilise lipid membranes or form distinct membrane pores. If the rate of flip-flop increases in an uncontrolled manner due to additives such as AMPs, the lipid composition may become scrambled, potentially destabilising the membrane. Importantly, anionic lipids such as PG or CL present in bacterial cells, are also efficient ionophores.[297] By carrying small cations such as such as H^+, Na^+ or Ca^{2+}, the flip-flop process facilitates ion transport across the membrane. Information on these more subtle mechanisms where local destabilisation of bacterial membrane and

increased ion-transport might be sufficient for antimicrobial effect of these peptides without being followed by dramatic effects as immediate lysis of bacteria or large effects on membrane structure may be important information for future AMPs research and development. Especially considering that a lot of the methodology traditionally used by peptide scientist to study antimicrobial effect specifically look for more of these dramatic rather than subtle effects that are not visible on a microscopic scale. However, we do recognise that further work expanding the number of compounds tested is needed, and confirmation on the transferability of our results to more realistic biological systems, ultimately real bacteria, is still unconcluded.

Beyond the scope of this thesis are we currently collaborating with computational chemists (Assoc. Prof. Michele Cascella, University of Oslo and Prof. Thereza A. Soares, University of São Paulo) in simulating how the observed effect on lipid transport affects ion transport. So far, results from MD simulations have revealed that lipid flip-flop upon addition of a single LL-37 molecule and resulting changes in ion transport through the membrane can be detected within the simulation time scale. The simulations have revealed a preferential increase in ion transport for cations rather than anions indicating that the ions are transported due to accelerated flip-flop motions of anionic lipids rather than due to the transmembrane cationic peptide insertion in itself. In addition to the theoretical simulations, we also want to experimentally probe the peptide effect on ion transport across lipid vesicle membranes identical to the ones used in the SAXS/TR-SANS experiments. As a part of the thesis work, we have tried to use a fluorescence-based assay developed by W. Paxton *et al.* where they indirectly are able to measure the transport of KOH over membranes by fluorometrically monitoring the internal pH of the vesicles using 8-Hydroxypyrene-1,3,6-trisulfonic acid (HPTS) (for details on the experimental assay see the supplementary information of ref. [298]). However, our experiments so far have revealed that the ion transport (observed as an increase in internal pH) is immediate, even without addition of peptides. We plan to redo these experiments in the near future using a stopped-flow apparatus and a slightly modified protocol.

Apart from further investigating the influence of changes in the membrane structure and lipid transport, refinement of the model system and measuring conditions to improve the biological relevance is proposed as a future action in the project. Taking into account the limitations of the different methods as presented in Chapter 3.1 and

3.2, it would be interesting to study the AMP interaction on vesicles with varying lipid composition, especially with regards to the lipid tail group. It would also be interesting to develop a stabile model system using a stabiliser that is biologically more relevant than PEG. Incorporation of LPS on the vesicle surface has been suggested as a potentially interesting alternative in this regard. This would also enable us to study the peptide interaction with models mimicking the outer membrane of gram-negative bacteria, which is especially relevant for colistin.

Beyond phospholipids, real bacterial cells also consist of other lipids like cardiolipin. By calcein leakage experiments in model vesicles with and without cardiolipin Hernández-Villa *et al.* showed that cardiolipin may play a crucial role in regulation of the membrane lytic effect of AMPs.[299] Hung and Lee, on the other hand, found by using lamellar X-ray diffraction and oriented circular dichroism on *E. coli* mimicking model membranes with and without cardiolipin, that cardiolipin is the key component that enhances melittin insertion in the membrane.[300] Some peptides, like sapecin extracted from flesh flies (*Sarcophaga peregrina*), have been reported to have specific affinity towards cardiolipin.[124] These, and several other studies not featured here, points towards cardiolipin potentially playing an essential role in the AMP membrane interaction, but the clear mechanism is not fully elucidated and requires further experiments. Based on our prior results, it is of especial interest to us whether cardiolipin influence lipid flip-flop and how this is affected by AMP addition. Could even cardiolipin in itself be flipped across the membrane via the defects imposed by AMP addition? We hope to answer these questions in future NR experiments (experiment scheduled for March 2020 but currently postponed due to the corona pandemic) in collaboration with Dr. Luke Clifton at ISIS neutron facility using his protocol for tethered asymmetric bilayers. Preliminary experiments have revealed that we are able to deposit high coverage floating asymmetric bilayers with deuterated DPPC in the outer leaflet and 8:2 (mol/mol) deuterated DPPC:proteated cardiolipin in the inner leaflet (full asymmetry yet not obtained). In the future we hope to use this system to both study the peptide-membrane interaction in the presence of cardiolipins and follow flip-flop rates in this system over time upon peptide exposure.

Throughout **Papers I-VI** all experiments are done with the same buffer system. The chosen buffer is Tris-base/Tris-HCl with pH 7.4 at 37 °C. This buffer system lacks the inclusion of a physiological relevant salt concentration. Salt is expected to affect the electrostatic interactions, and studies have shown a significant effect of salt on the electrostatic binding of cationic AMPs to the lipid head group.[301] However inclusion of salt effects also further complicates the analysis of the system, and we therefore chose to not include salt in the stage of developing the methodology. Redoing some of the SAXS and TR-SANS in the presence of salt would be an interesting further experiment.

It should also be noted that the methodology presented in this thesis can not only be used to study the mechanism of action of AMPs on bacterial cell membrane, but also be used to study the selectivity of these peptide by adding them to membranes with lipid compositions mimicking mammalian cells. As discussed in Chapter 1.2.6, the presence of cholesterol in the eukaryote cell membrane has been suggested to be essential in the selectivity of AMPs. We have therefore used SAXS and NR to compare the effect of adding indolicidin and LL-37 to POPC and DMPC lipid vesicles with increasing amount of cholesterol (publication in preparation and therefore not included in the thesis). From the SAXS experiments we found that cholesterol concentrations above 30 mol % inhibits the peptide interaction both for indolicidin and LL-37 completely, resulting in a direct overlap between the scattering from the measured mixture and the calculated average (the peptide and the lipid vesicles measured separately and the scattering averaged).[104] From NR we observe that the peptide interaction is significantly reduced when comparing with membranes without cholesterol, but it is not completely inhibited. We are currently working on comparing our SAXS and NR results on model systems with toxicity results from real mammalian cells with altered amounts of cholesterol.

5. Concluding remarks

The overall goal of the presented thesis was to gain understanding of the molecular mode of action of antimicrobial peptides using neutron and X-ray scattering techniques. In the first phase of this work, we focused on developing stable model systems that mimic real bacterial cell membranes. In this work both PC-PG and PE-PG vesicles were used with addition of 2.5-5 % PEGylated lipids for increased stability. The next stage involved adding indolicidin to the model systems to study the interaction using both SANS, SAXS and NR. Through this work we showed how the peptide-interaction can be extracted from X-ray scattering data by using a modified SDP model. We also showed how indolicidin do not seem to affect the thickness of the membrane or be able to transport through the membrane.

The next phase of the project involved using the methodology developed in the first stages to probe the membrane-interaction of a broad range of different AMPs, LL-37, magainin II, aurein 1.2, Lacticin Q, cecropin A and colistin. The membrane insertion observed for each AMP is illustrated in Figure 30 (except colistin because this peptide does not interact with lipid vesicles based on our results)
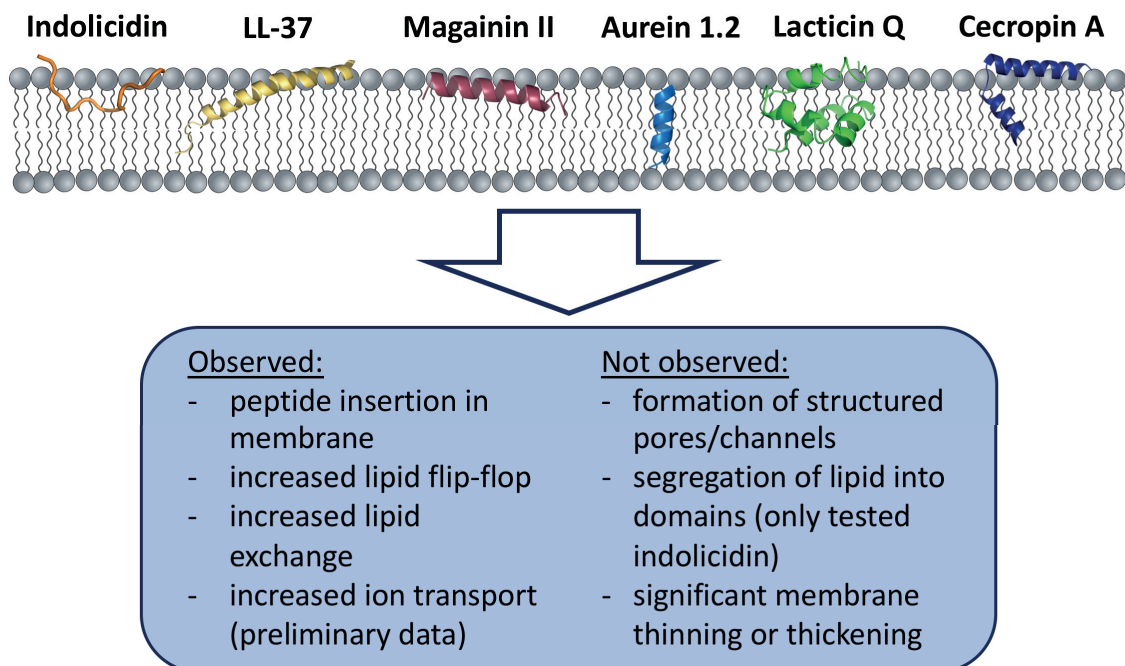
Figure 30. Schematic summary of AMP-membrane interaction based on results from a combination of SAXS, SANS and NR measurements.

Beyond characterising the structural membrane effect of each AMP, we also examined their effect on lipid transport using the KZAC TR-SANS methodology. These data revealed that all the AMPs probed in the study, except colistin, significantly accelerates both the inter-vesicular lipid exchange and intra-vesicular lipid flip-flop. By comparing the structural data from SAXS with TR-SANS data, we were able to conclude that the effect on lipid transport cannot be directly linked to the inserted amount of peptide or the peptide position in the bilayer. However, we did see that peptides known to solubilise the membrane at high concentrations, like LL-37, causes a more dramatic effect on lipid transport even at concentrations below the threshold for membrane solubilisation.

We hope that the work presented in this part of the thesis can further enhance the understanding of the mechanism of AMPs, by linking the accelerated lipid transport to other effect as increased ion transport and lipid scrambling. The knowledge that peptide induced changes in lipid flip-flop, even without formation of more complex pore-structures, can be sufficient to disturb transport of ions over the bacterial membrane may be important information for guiding the design of new "minimalistic" AMP based drug molecules.

In the final stage of the thesis work we studied the membrane interaction of self-assembling $K_x(QL)_yK_z$ peptides, which showed to be significantly more complicated than the natural AMPs discussed above. In this work using contrast variation together with SANS and NR proved very valuable to gain information about the peptide nanofiber insertion in the bilayer, and the resulting effects on both membrane and peptide structure. The results from this work point toward the membrane interaction being stronger for the peptide nanofibers, than for the equivalent shorter monomeric peptides, in support of the claim that self-assembly affects the antimicrobial activity of peptides. While addition of PEG groups to the peptide molecules on the other hand seemed to decrease the peptide-membrane interaction. The work presented here increases the understanding of how self-assembly and PEGylation, which have become frequently used strategies to increase the drugability of AMP based drugs, affect the peptide-membrane interaction of these compounds.

References

1. Tan, S. Y.; Tatsumura, Y., Alexander Fleming (1881–1955): discoverer of penicillin. *Singapore Med. J.* **2015,** *56* (7), 366.
2. Drider, D.; Rebuffat, S., *Prokaryotic antimicrobial peptides: from genes to applications*. Springer Science & Business Media: **2011.**
3. Phoenix, D. A.; Dennison, S. R.; Harris, F., *Antimicrobial peptides*. John Wiley & Sons: **2012.**
4. Nakatsuji, T.; Gallo, R. L., Antimicrobial peptides: old molecules with new ideas. *J. Investig. Dermatol.* **2012,** *132* (3), 887-895.
5. Pasupuleti, M.; Schmidtchen, A.; Malmsten, M., Antimicrobial peptides: key components of the innate immune system. *Crit. Rev. Biotechnol.* **2012,** *32* (2), 143-171.
6. Lee, M.; Shi, X.; Barron, A. E.; McGeer, E.; McGeer, P. L., Human antimicrobial peptide LL-37 induces glial-mediated neuroinflammation. *Biochem. Pharmacol.* **2015,** *94* (2), 130-141.
7. De Lorenzi, E.; Chiari, M.; Colombo, R.; Cretich, M.; Sola, L.; Vanna, R.; Gagni, P.; Bisceglia, F.; Morasso, C.; Lin, J. S.; Lee, M.; McGeer, P. L.; Barron, A. E., Evidence that the human innate immune peptide LL-37 may be a binding partner of amyloid-β and inhibitor of fibril assembly. *J. Alzheimers Dis.* **2017,** *59* (4), 1213.
8. Armiento, V.; Hille, K.; Naltsas, D.; Lin, J. S.; Barron, A. E.; Kapurniotu, A., The human cathelicidin LL-37 is a nanomolar inhibitor of amyloid self-assembly of islet amyloid polypeptide (IAPP). *Angew. Chem.* **2020.**
9. Haug, B. E.; Stensen, W.; Kalaaji, M.; Rekdal, Ø.; Svendsen, J. S., Synthetic antimicrobial peptidomimetics with therapeutic potential. *J. Med. Chem.* **2008,** *51* (14), 4306-4314.
10. Acedo, J. Z.; van Belkum, M. J.; Lohans, C. T.; Towle, K. M.; Miskolzie, M.; Vederas, J. C., Nuclear magnetic resonance solution structures of lacticin Q and aureocin A53 reveal a structural motif conserved among leaderless bacteriocins with broad-spectrum activity. *Biochemistry* **2016,** *55* (4), 733-742.
11. Wang, G., Structures of human host defense cathelicidin LL-37 and its smallest antimicrobial peptide KR-12 in lipid micelles. *J. Biol. Chem.* **2008,** *283* (47), 32637-32643.
12. Gesell, J.; Zasloff, M.; Opella, S. J., Two-dimensional 1H NMR experiments show that the 23-residue magainin antibiotic peptide is an α-helix in dodecylphosphocholine micelles, sodium dodecylsulfate micelles, and trifluoroethanol/water solution. *J. Biomol. NMR* **1997,** *9* (2), 127-135.
13. Wang, G.; Li, Y.; Li, X., Correlation of three-dimensional structures with the antibacterial activity of a group of peptides designed based on a nontoxic bacterial membrane anchor. *J. Biol. Chem.* **2005,** *280* (7), 5803-5811.
14. Rozek, A.; Friedrich, C. L.; Hancock, R. E., Structure of the bovine antimicrobial peptide indolicidin bound to dodecylphosphocholine and sodium dodecyl sulfate micelles. *Biochemistry* **2000,** *39* (51), 15765-15774.
15. Alberts, B.; Bray, D.; Hopkin, K.; Johnson, A. D.; Lewis, J.; Raff, M.; Roberts, K.; Walter, P., *Essential cell biology*. Garland Science: **2009.**
16. Madigan, M. T.; Martinko, J. M.; Dunlap, P. V.; Clark, D. P., *Brock biology of microorganisms*. 12th ed.; Pearson Benjamin Cummings: **2009**; p 65-73.
17. Matias, V. R.; Beveridge, T. J., Cryo-electron microscopy reveals native polymeric cell wall structure in Bacillus subtilis 168 and the existence of a periplasmic space. *Mol. Microbiol.* **2005,** *56* (1), 240-251.
18. Matias, V. R.; Al-Amoudi, A.; Dubochet, J.; Beveridge, T. J., Cryo-transmission electron microscopy of frozen-hydrated sections of Escherichia coli and Pseudomonas aeruginosa. *J. Bacteriol.* **2003,** *185* (20), 6112-6118.

19. Disalvo, E. A., *Membrane hydration: the role of water in the structure and function of biological membranes*. Springer: London, **2015**; Vol. 71.

20. Simons, K.; Vaz, W. L., Model systems, lipid rafts, and cell membranes. *Annu. Rev. Biophys. Biomol. Struct.* **2004,** *33*, 269-295.

21. Gorter, E.; Grendel, F., On bimolecular layers of lipoids on the chromocytes of the blood. *J. Exp. Med.* **1925,** *41* (4), 439.

22. Bar, R. S.; Deamer, D. W.; Cornwell, D. G., Surface area of human erythrocyte lipids: reinvestigation of experiments on plasma membrane. *Science* **1966,** *153* (3739), 1010-1012.

23. Danielli, J. F.; Davson, H., A contribution to the theory of permeability of thin films. *J. Cell. Comp. Physiol.* **1935,** *5* (4), 495-508.

24. Robertson, J. D., New observations on the ultrastructure of the membranes of frog peripheral nerve fibers. *J. Biophys. Biochem. Cytol.* **1957,** *3* (6), 1043.

25. Benson, A., On the orientation of lipids in chloroplast and cell membranes. *J. Am. Oil Chem. Soc.* **1966,** *43* (5), 265-270.

26. Green, D. E.; Perdue, J. F., Membranes as expressions of repeating units. *Proc. Natl. Acad. Sci. U.S.A.* **1966,** *55* (5), 1295.

27. Stoeckenius, W.; Engelman, D. M., Current models for the structure of biological membranes. *J. Cell Biol.* **1969,** *42* (3), 613.

28. Bagatolli, L. A.; Ipsen, J. H.; Simonsen, A. C.; Mouritsen, O. G., An outlook on organization of lipids in membranes: searching for a realistic connection with the organization of biological membranes. *Prog. Lipid Res.* **2010,** *49* (4), 378-389.

29. Luckey, M., *Membrane structural biology: with biochemical and biophysical foundations*. Cambridge University Press: **2014**.

30. Singer, S. J.; Nicolson, G. L., The fluid mosaic model of the structure of cell membranes. *Science* **1972,** *175* (4023), 720-731.

31. Israelachvili, J. N., Refinement of the fluid-mosaic model of membrane structure. *Biochim. Biophys. Acta, Biomembr.* **1977,** *469* (2), 221-225.

32. Tien, H. T.; Ottova, A. L., The lipid bilayer concept and its experimental realization: from soap bubbles, kitchen sink, to bilayer lipid membranes. *J. Membr. Sci.* **2001,** *189* (1), 83-117.

33. Nicolson, G. L., Update of the 1972 Singer-Nicolson fluid-mosaic model of membrane structure. *Discoveries* **2013,** *1* (1), e3.

34. Goñi, F. M., The basic structure and dynamics of cell membranes: An update of the Singer–Nicolson model. *Biochim. Biophys. Acta, Biomembr.* **2014,** *1838* (6), 1467-1476.

35. Mouritsen, O. G.; Bloom, M., Mattress model of lipid-protein interactions in membranes. *Biophys. J.* **1984,** *46* (2), 141-153.

36. Quinn, P. J.; Chapman, D.; Keith, A. D., The Dynamics Of Membrane Structur. *Crit. Rev. Biochem.* **1980,** *8* (1), 1-117.

37. Heimburg, T., *Thermal biophysics of membranes*. John Wiley & Sons: **2008**.

38. Cronan, J. E., Bacterial membrane lipids: where do we stand? *Annu. Rev. Microbiol.* **2003,** *57* (1), 203-224.

39. Sohlenkamp, C.; Geiger, O., Bacterial membrane lipids: diversity in structures and pathways. *FEMS Microbiol. Rev.* **2016,** *40* (1), 133-159.

40. White, D. C.; Frerman, F. E., Extraction, characterization, and cellular localization of the lipids of Staphylococcus aureus. *J. Bacteriol* **1967,** *94* (6), 1854-1867.

41. Simons, K.; Ikonen, E., Functional rafts in cell membranes. *Nature* **1997,** *387* (6633), 569.

42. López, D.; Kolter, R., Functional microdomains in bacterial membranes. *Genes Dev.* **2010,** *24* (17), 1893-1902.

43. Bramkamp, M.; Lopez, D., Exploring the existence of lipid rafts in bacteria. *Microbiol. Mol. Biol. Rev.* **2015,** *79* (1), 81-100.

44. Nickels, J. D.; Chatterjee, S.; Stanley, C. B.; Qian, S.; Cheng, X.; Myles, D. A.; Standaert, R. F.; Elkins, J. G.; Katsaras, J., The in vivo structure of biological membranes and evidence for lipid domains. *PLoS Biol.* **2017,** *15* (5), e2002214.

45. Mileykovskaya, E.; Dowhan, W., Visualization of phospholipid domains in Escherichia coli by using the cardiolipin-specific fluorescent dye 10-N-nonyl acridine orange. *J. Bacteriol.* **2000,** *182* (4), 1172-1175.

46. Kawai, F.; Shoda, M.; Harashima, R.; Sadaie, Y.; Hara, H.; Matsumoto, K., Cardiolipin domains in Bacillus subtilis marburg membranes. *J. Bacteriol.* **2004,** *186* (5), 1475-1483.

47. Oliver, P. M.; Crooks, J. A.; Leidl, M.; Yoon, E. J.; Saghatelian, A.; Weibel, D. B., Localization of anionic phospholipids in Escherichia coli cells. *J. Bacteriol.* **2014,** *196* (19), 3386-3398.

48. Raff, M.; Alberts, B.; Lewis, J.; Johnson, A.; Roberts, K., Molecular Biology of the Cell. . 4th ed.; National Center for Biotechnology Information's Bookshelf: **2002**.

49. Contreras, F.-X.; Sánchez-Magraner, L.; Alonso, A.; Goñi, F. M., Transbilayer (flip-flop) lipid motion and lipid scrambling in membranes. *FEBS Lett.* **2010,** *584* (9), 1779-1786.

50. Homan, R.; Pownall, H. J., Transbilayer diffusion of phospholipids: dependence on headgroup structure and acyl chain length. *Biochim. Biophys. Acta, Biomembr.* **1988,** *938* (2), 155-166.

51. Fadeel, B.; Xue, D., The ins and outs of phospholipid asymmetry in the plasma membrane: roles in health and disease. *Crit. Rev. Biochem. Mol. Biol.* **2009,** *44* (5), 264-277.

52. Gurtovenko, A. A.; Vattulainen, I., Molecular mechanism for lipid flip-flops. *J. Phys. Chem. B* **2007,** *111* (48), 13554-13559.

53. Sender, R.; Fuchs, S.; Milo, R., Revised estimates for the number of human and bacteria cells in the body. *PLoS Biol.* **2016,** *14* (8), e1002533.

54. Hooper, L. V.; Midtvedt, T.; Gordon, J. I., How host-microbial interactions shape the nutrient environment of the mammalian intestine. *Annu. Rev. Nutr.* **2002,** *22* (1), 283-307.

55. Bäckhed, F.; Ley, R. E.; Sonnenburg, J. L.; Peterson, D. A.; Gordon, J. I., Host-bacterial mutualism in the human intestine. *Science* **2005,** *307* (5717), 1915-1920.

56. Wilson, B. A.; Salyers, A. A.; Whitt, D. D.; Winkler, M. E., *Bacterial pathogenesis: a molecular approach*. American Society for Microbiology (ASM): **2011**.

57. Otto, M., Staphylococcal biofilms. *Gram-Positive Pathogens* **2019**, 699-711.

58. Lyczak, J. B.; Cannon, C. L.; Pier, G. B., Establishment of Pseudomonas aeruginosa infection: lessons from a versatile opportunist. *Microb. Infect.* **2000,** *2* (9), 1051-1060.

59. Strömstedt, A. A.; Ringstad, L.; Schmidtchen, A.; Malmsten, M., Interaction between amphiphilic peptides and phospholipid membranes. *Curr. Opin. Colloid Interface Sci.* **2010,** *15* (6), 467-478.

60. Baumann, G.; Mueller, P., A molecular model of membrane excitability. *J. Supramol. Struct.* **1974,** *2* (5-6), 538-557.

61. Sato, H.; Feix, J. B., Peptide–membrane interactions and mechanisms of membrane destruction by amphipathic α-helical antimicrobial peptides. *Biochim. Biophys. Acta, Biomembr.* **2006,** *1758* (9), 1245-1256.

62. Sani, M.-A.; Separovic, F., How membrane-active peptides get into lipid membranes. *Acc. Chem. Res.* **2016,** *49* (6), 1130-1138.

63. Yeaman, M. R.; Yount, N. Y., Mechanisms of antimicrobial peptide action and resistance. *Pharmacol. Rev.* **2003,** *55* (1), 27-55.

64. Wimley, W. C., Describing the mechanism of antimicrobial peptide action with the interfacial activity model. *ACS Chem. Biol.* **2010,** *5* (10), 905-917.

65. Nguyen, L. T.; Haney, E. F.; Vogel, H. J., The expanding scope of antimicrobial peptide structures and their modes of action. *Trends. Biotechnol.* **2011,** *29* (9), 464-472.

66. Shai, Y., Mechanism of the binding, insertion and destabilization of phospholipid bilayer membranes by α-helical antimicrobial and cell non-selective membrane-lytic peptides. *Biochim. Biophys. Acta, Biomembr.* **1999,** *1462* (1-2), 55-70.

67. Shai, Y.; Oren, Z., From "carpet" mechanism to de-novo designed diastereomeric cell-selective antimicrobial peptides. *Peptides* **2001,** *22* (10), 1629-1641.

68. Sevcsik, E.; Pabst, G.; Jilek, A.; Lohner, K., How lipids influence the mode of action of membrane-active peptides. *Biochim. Biophys. Acta, Biomembr.* **2007,** *1768* (10), 2586-2595.

69. Sevcsik, E.; Pabst, G.; Richter, W.; Danner, S.; Amenitsch, H.; Lohner, K., Interaction of LL-37 with model membrane systems of different complexity: influence of the lipid matrix. *Biophys. J.* **2008,** *94* (12), 4688-4699.

70. Chen, F.-Y.; Lee, M.-T.; Huang, H. W., Evidence for membrane thinning effect as the mechanism for peptide-induced pore formation. *Biophys. J.* **2003,** *84* (6), 3751-3758.

71. Huang, H. W., Molecular mechanism of antimicrobial peptides: the origin of cooperativity. *Biochim. Biophys. Acta, Biomembr.* **2006,** *1758* (9), 1292-1302.

72. Pabst, G.; Grage, S. L.; Danner-Pongratz, S.; Jing, W.; Ulrich, A. S.; Watts, A.; Lohner, K.; Hickel, A., Membrane thickening by the antimicrobial peptide PGLa. *Biophys. J.* **2008,** *95* (12), 5779-5788.

73. Teixeira, V.; Feio, M. J.; Bastos, M., Role of lipids in the interaction of antimicrobial peptides with membranes. *Prog. Lipid Res.* **2012,** *51* (2), 149-177.

74. Epand, R. M.; Epand, R. F., Calorimetric detection of curvature strain in phospholipid bilayers. *Biophys. J.* **1994,** *66* (5), 1450.

75. Epand, R. F.; Mowery, B. P.; Lee, S. E.; Stahl, S. S.; Lehrer, R. I.; Gellman, S. H.; Epand, R. M., Dual mechanism of bacterial lethality for a cationic sequence-random copolymer that mimics host-defense antimicrobial peptides. *J. Mol. Biol.* **2008,** *379* (1), 38-50.

76. Epand, R. M.; Epand, R. F., Lipid domains in bacterial membranes and the action of antimicrobial agents. *Biochim. Biophys. Acta, Biomembr.* **2009,** *1788* (1), 289-294.

77. Jean-François, F.; Castano, S.; Desbat, B.; Odaert, B.; Roux, M.; Metz-Boutigue, M.-H. l. n.; Dufourc, E. J., Aggregation of cateslytin β-sheets on negatively charged lipids promotes rigid membrane domains. A new mode of action for antimicrobial peptides? *Biochemistry* **2008,** *47* (24), 6394-6402.

78. Matsuzaki, K.; Murase, O.; Fujii, N.; Miyajima, K., An antimicrobial peptide, magainin 2, induced rapid flip-flop of phospholipids coupled with pore formation and peptide translocation. *Biochemistry* **1996,** *35* (35), 11361-11368.

79. Wimley, W. C.; White, S. H., Determining the membrane topology of peptides by fluorescence quenching. *Biochemistry* **2000,** *39* (1), 161-170.

80. Zhang, L.; Rozek, A.; Hancock, R. E., Interaction of cationic antimicrobial peptides with model membranes. *J. Biol. Chem.* **2001,** *276* (38), 35714-35722.

81. Anglin, T. C.; Brown, K. L.; Conboy, J. C., Phospholipid flip-flop modulated by transmembrane peptides WALP and melittin. *J. Struct. Biol.* **2009,** *168* (1), 37-52.

82. Nguyen, M. H.; DiPasquale, M.; Rickeard, B. W.; Doktorova, M.; Heberle, F. A.; Scott, H. L.; Barrera, F. N.; Taylor, G.; Collier, C. P.; Stanley, C. B.; Katsaras, J.; Marquardt, D., Peptide-Induced Lipid Flip-Flop in Asymmetric Liposomes Measured by Small Angle Neutron Scattering. *Langmuir* **2019,** *35* (36), 11735-11744.

83. Nielsen, J. E.; Bjørnestad, V. A.; Pipich, V.; Jenssen, H.; Lund, R., Beyond Structural Models for the Mode of Action: How Natural Antimicrobial Peptides Disrupts Lipid Membranes. *J. Colloid Interface Sci.* **2021,** *582*, 793-802.

84. Hugo, W. B.; Russell, A. D., *Pharmaceutical microbiology*. 8th. ed.; Wiley-Blackwell **2011**.

85. Chongsiriwatana, N. P.; Patch, J. A.; Czyzewski, A. M.; Dohm, M. T.; Ivankin, A.; Gidalevitz, D.; Zuckermann, R. N.; Barron, A. E., Peptoids that mimic the structure, function, and mechanism of helical antimicrobial peptides. *Proc. Natl. Acad. Sci. U.S.A.* **2008,** *105* (8), 2794-2799.

86. Brogden, K. A., Antimicrobial peptides: pore formers or metabolic inhibitors in bacteria? *Nat. Rev. Microbiol.* **2005,** *3* (3), 238-250.

87. Jenssen, H.; Hamill, P.; Hancock, R. E., Peptide antimicrobial agents. *Clin. Microbiol. Rev.* **2006,** *19* (3), 491-511.

88. Chongsiriwatana, N. P.; Lin, J. S.; Kapoor, R.; Wetzler, M.; Rea, J. A.; Didwania, M. K.; Contag, C. H.; Barron, A. E., Intracellular biomass flocculation as a key mechanism of rapid bacterial killing by cationic, amphipathic antimicrobial peptides and peptoids. *Sci. Rep.* **2017,** *7* (1), 1-15.

89. Hancock, R. E.; Sahl, H.-G., Antimicrobial and host-defense peptides as new anti-infective therapeutic strategies. *Nat. Biotechnol.* **2006,** *24* (12), 1551-1557.

90. Melo, M. N.; Castanho, M. A., Omiganan interaction with bacterial membranes and cell wall models. Assigning a biological role to saturation. *Biochim. Biophys. Acta, Biomembr.* **2007,** *1768* (5), 1277-1290.

91. Pistolesi, S.; Pogni, R.; Feix, J. B., Membrane insertion and bilayer perturbation by antimicrobial peptide CM15. *Biophys. J.* **2007,** *93* (5), 1651-1660.

92. Melo, M. N.; Ferre, R.; Castanho, M. A., Antimicrobial peptides: linking partition, activity and high membrane-bound concentrations. *Nat. Rev. Microbiol.* **2009,** *7* (3), 245-250.

93. Roversi, D.; Luca, V.; Aureli, S.; Park, Y.; Mangoni, M. L.; Stella, L., How many antimicrobial peptide molecules kill a bacterium? The case of PMAP-23. *ACS Chem. Biol.* **2014,** *9* (9), 2003-2007.

94. Melo, M. N.; Castanho, M. A., The mechanism of action of antimicrobial peptides: lipid vesicles vs. bacteria. *Front. Immunol.* **2012,** *3*, 236.

95. Prats, R.; De Pedro, M., Normal growth and division of Escherichia coli with a reduced amount of murein. *J. Bacteriol.* **1989,** *171* (7), 3740-3745.

96. Wiegand, I.; Hilpert, K.; Hancock, R. E., Agar and broth dilution methods to determine the minimal inhibitory concentration (MIC) of antimicrobial substances. *Nat. Protoc.* **2008,** *3* (2), 163.

97. Edgerton, M.; Koshlukova, S. E.; Lo, T. E.; Chrzan, B. G.; Straubinger, R. M.; Raj, P. A., Candidacidal activity of salivary histatins identification of a histatin 5-binding protein on Candida albicans. *J. Biol. Chem.* **1998,** *273* (32), 20438-20447.

98. Matsuzaki, K.; Sugishita, K.; Fujii, N.; Miyajima, K., Molecular basis for membrane selectivity of an antimicrobial peptide, magainin 2. *Biochemistry* **1995,** *34* (10), 3423-3429.

99. Raghuraman, H.; Chattopadhyay, A., Interaction of melittin with membrane cholesterol: a fluorescence approach. *Biophys. J.* **2004,** *87* (4), 2419-2432.

100. Verly, R. M.; Rodrigues, M. A.; Daghastanli, K. R. P.; Denadai, A. M. L.; Cuccovia, I. M.; Bloch Jr, C.; Frézard, F.; Santoro, M. M.; Piló-Veloso, D.; Bemquerer, M. P., Effect of cholesterol on the interaction of the amphibian antimicrobial peptide DD K with liposomes. *Peptides* **2008,** *29* (1), 15-24.

101. Brender, J. R.; McHenry, A. J.; Ramamoorthy, A., Does cholesterol play a role in the bacterial selectivity of antimicrobial peptides? *Front. Immunol.* **2012,** *3*, 195.

102. McHenry, A. J.; Sciacca, M. F.; Brender, J. R.; Ramamoorthy, A., Does cholesterol suppress the antimicrobial peptide induced disruption of lipid raft containing membranes? *Biochim. Biophys. Acta, Biomembr.* **2012,** *1818* (12), 3019-3024.

103. Sharma, V. K.; Mamontov, E.; Anunciado, D. B.; O'Neill, H.; Urban, V. S., Effect of antimicrobial peptide on the dynamics of phosphocholine membrane: role of cholesterol and physical state of bilayer. *Soft matter* **2015,** *11* (34), 6755-6767.

104. Nielsen, J. E.; Waldie, S.; Gerelli, Y.; Pichler, H.; Strohmeier, G. A.; Forsyth, T. V.; Haertlein, M.; Cárdenas, M.; Jenssen, H.; Lund, R., The role cholesterol plays in protecting mammalian cell towards antimicrobial peptide destruction (in preparation). **2020.**

105. Wessman, P.; Strömstedt, A. A.; Malmsten, M.; Edwards, K., Melittin-lipid bilayer interactions and the role of cholesterol. *Biophys. J.* **2008,** *95* (9), 4324-4336.

106. Peschel, A.; Sahl, H.-G., The co-evolution of host cationic antimicrobial peptides and microbial resistance. *Nat. Rev. Microbiol.* **2006,** *4* (7), 529.

107. Frick, I.-M.; Nordin, S. L.; Baumgarten, M.; Mörgelin, M.; Sørensen, O. E.; Olin, A. I.; Egesten, A., Constitutive and inflammation-dependent antimicrobial peptides produced by epithelium are differentially processed and inactivated by the commensal Finegoldia magna and the pathogen Streptococcus pyogenes. *J. Immunol.* **2011,** *187* (8), 4300-4309.

108. Jin, T.; Bokarewa, M.; Foster, T.; Mitchell, J.; Higgins, J.; Tarkowski, A., Staphylococcus aureus resists human defensins by production of staphylokinase, a novel bacterial evasion mechanism. *J. Immunol.* **2004,** *172* (2), 1169-1176.

109. Peschel, A.; Otto, M.; Jack, R. W.; Kalbacher, H.; Jung, G.; Götz, F., Inactivation of the dlt Operon inStaphylococcus aureus Confers Sensitivity to Defensins, Protegrins, and Other Antimicrobial Peptides. *J. Biol. Chem.* **1999,** *274* (13), 8405-8410.

110. Vuong, C.; Kocianova, S.; Voyich, J. M.; Yao, Y.; Fischer, E. R.; DeLeo, F. R.; Otto, M., A crucial role for exopolysaccharide modification in bacterial biofilm formation, immune evasion, and virulence. *J. Biol. Chem.* **2004,** *279* (52), 54881-54886.

111. Joo, H.-S.; Fu, C.-I.; Otto, M., Bacterial strategies of resistance to antimicrobial peptides. *Philos. Trans. R. Soc. Lond., B, Biol. Sci.* **2016,** *371* (1695), 20150292.

112. Andersson, D. I.; Hughes, D.; Kubicek-Sutherland, J. Z., Mechanisms and consequences of bacterial resistance to antimicrobial peptides. *Drug Resist. Updat.* **2016,** *26*, 43-57.

113. Park, C. B.; Yi, K.-S.; Matsuzaki, K.; Kim, M. S.; Kim, S. C., Structure–activity analysis of buforin II, a histone H2A-derived antimicrobial peptide: the proline hinge is responsible for the cell-penetrating ability of buforin II. *Proc. Natl. Acad. Sci. U.S.A.* **2000,** *97* (15), 8245-8250.

114. Shaw, J. E.; Alattia, J.-R.; Verity, J. E.; Privé, G. G.; Yip, C. M., Mechanisms of antimicrobial peptide action: studies of indolicidin assembly at model membrane interfaces by in situ atomic force microscopy. *J. Struct. Biol.* **2006,** *154* (1), 42-58.

115. Askou, H. J.; Jakobsen, R. N.; Fojan, P., An atomic force microscopy study of the interactions between indolicidin and supported planar bilayers. *J. Nanosci. Nanotechnol.* **2008,** *8* (9), 4360-4369.

116. Lind, T. K.; Zielinska, P.; Wacklin, H. P.; Urbanczyk-Lipkowska, Z.; Cárdenas, M., Continuous flow atomic force microscopy imaging reveals fluidity and time-dependent interactions of antimicrobial dendrimer with model lipid membranes. *ACS nano* **2013,** *8* (1), 396-408.

117. Clifton, L. A.; Campbell, R. A.; Sebastiani, F.; Campos-Terán, J.; Gonzalez-Martinez, J. F.; Björklund, S.; Sotres, J.; Cárdenas, M., Design and use of model biomembranes to study biomolecular interactions using complementary surface-sensitive techniques. *Adv. Colloid Interface Sci.* **2020**, 102118.

118. Fantner, G. E.; Barbero, R. J.; Gray, D. S.; Belcher, A. M., Kinetics of antimicrobial peptide activity measured on individual bacterial cells using high-speed atomic force microscopy. *Nat. Nanotechnol.* **2010,** *5* (4), 280-285.

119. Wang, K. F.; Nagarajan, R.; Camesano, T. A., Differentiating antimicrobial peptides interacting with lipid bilayer: Molecular signatures derived from quartz crystal microbalance with dissipation monitoring. *Biophys. Chem.* **2015,** *196*, 53-67.

120. Pate, M.; Blazyk, J., Methods for assessing the structure and function of cationic antimicrobial peptides. In *New Antibiotic Targets*, Springer: **2008**; pp 155-173.

121. Christensen, B.; Fink, J.; Merrifield, R.; Mauzerall, D., Channel-forming properties of cecropins and related model compounds incorporated into planar lipid membranes. *Proc. Natl. Acad. Sci. U.S.A.* **1988,** *85* (14), 5072-5076.

122. Guidelli, R.; Becucci, L., Mechanism of voltage-gated channel formation in lipid membranes. *Biochim. Biophys. Acta, Biomembr.* **2016,** *1858* (4), 748-755.

123. Woody, R. W., Circular dichroism of peptides. In *Conformation in Biology and Drug Design*, Elsevier: **1985**; pp 15-114.

124. Lohner, K.; Prenner, E. J., Differential scanning calorimetry and X-ray diffraction studies of the specificity of the interaction of antimicrobial peptides with membrane-mimetic systems. *Biochim. Biophys. Acta, Biomembr.* **1999,** *1462* (1), 141-156.

125. Strandberg, E.; Ulrich, A. S., NMR methods for studying membrane-active antimicrobial peptides. *Concept. Magn. Reson. A* **2004,** *23* (2), 89-120.

126. Hinds, M. G.; Norton, R. S., NMR spectroscopy of peptides and proteins. *Mol. Biotechnol.* **1997,** *7* (3), 315-331.

127. Porcelli, F.; Ramamoorthy, A.; Barany, G.; Veglia, G., On the role of NMR spectroscopy for characterization of antimicrobial peptides. In *Membr. Protein.*, Springer: **2013**; pp 159-180.

128. Bennett, W. D.; Sapay, N.; Tieleman, D. P., Atomistic simulations of pore formation and closure in lipid bilayers. *Biophys. J.* **2014,** *106* (1), 210-219.

129. Mihajlovic, M.; Lazaridis, T., Antimicrobial peptides in toroidal and cylindrical pores. *Biochim. Biophys. Acta, Biomembr.* **2010,** *1798* (8), 1485-1493.

130. Fernandez, D. I.; Le Brun, A. P.; Whitwell, T. C.; Sani, M.-A.; James, M.; Separovic, F., The antimicrobial peptide aurein 1.2 disrupts model membranes via the carpet mechanism. *Phys. Chem. Chem. Phys.* **2012,** *14* (45), 15739-15751.

131. Fernandez, D. I.; Le Brun, A. P.; Lee, T.-H.; Bansal, P.; Aguilar, M.-I.; James, M.; Separovic, F., Structural effects of the antimicrobial peptide maculatin 1.1 on supported lipid bilayers. *Eur. Biophys. J.* **2013,** *42* (1), 47-59.

132. Lind, T. K.; Darre, L.; Domene, C.; Urbanczyk-Lipkowska, Z.; Cárdenas, M.; Wacklin, H., Antimicrobial peptide dendrimer interacts with phosphocholine membranes in a fluidity dependent manner: A neutron reflection study combined with molecular dynamics simulations. *Biochim. Biophys. Acta, Biomembr.* **2015,** *1848* (10), 2075-2084.

133. Clifton, L. A.; Holt, S. A.; Hughes, A. V.; Daulton, E. L.; Arunmanee, W.; Heinrich, F.; Khalid, S.; Jefferies, D.; Charlton, T. R.; Webster, J. R., An accurate in vitro model of the E. coli envelope. *Angew. Chem. Int. Ed.* **2015,** *54* (41), 11952-11955.

134. Lind, T. K.; Skoda, M. W.; Cárdenas, M., Formation and characterization of supported lipid bilayers composed of phosphatidylethanolamine and phosphatidylglycerol by vesicle fusion, a simple but relevant model for bacterial membranes. *ACS omega* **2019,** *4* (6), 10687-10694.

135. Nielsen, J. E.; Lind, T. K.; Lone, A.; Gerelli, Y.; Hansen, P. R.; Jenssen, H.; Cárdenas, M.; Lund, R., A biophysical study of the interactions between the antimicrobial peptide indolicidin and lipid model systems. *Biochim. Biophys. Acta, Biomembr.* **2019,** *1861* (7), 1355-1364.

136. Hall, K.; Lee, T.-H.; Mechler, A. I.; Swann, M. J.; Aguilar, M.-I., Real-time measurement of membrane conformational states induced by antimicrobial peptides: balance between recovery and lysis. *Sci. Rep.* **2014,** *4*, 5479.

137. Pan, J.; Tieleman, D. P.; Nagle, J. F.; Kučerka, N.; Tristram-Nagle, S., Alamethicin in lipid bilayers: combined use of X-ray scattering and MD simulations. *Biochim. Biophys. Acta, Biomembr.* **2009,** *1788* (6), 1387-1397.

138. Dupuy, F. G.; Pagano, I.; Andenoro, K.; Peralta, M. F.; Elhady, Y.; Heinrich, F.; Tristram-Nagle, S., Selective Interaction of Colistin with Lipid Model Membranes. *Biophys. J.* **2018,** *114* (4), 919-928.

139. Zhu, S.; Sani, M. A.; Separovic, F., Interaction of cationic antimicrobial peptides from Australian frogs with lipid membranes. *Peptide Science* **2018,** *110* (3), e24061.

140. Qian, S.; Heller, W. T., Peptide-induced asymmetric distribution of charged lipids in a vesicle bilayer revealed by small-angle neutron scattering. *J. Phys. Chem. B* **2011,** *115* (32), 9831-9837.

141. Nielsen, J. E.; Bjørnestad, V. A.; Lund, R., Resolving the Structural Interactions between Antimicrobial Peptides and Lipid Membranes using Small-angle Scattering Methods: the case of Indolicidin. *Soft Matter* **2018,** *14* (43), 8750-8763.

142. Castelletto, V.; Barnes, R. H.; Karatzas, K.-A.; Edwards-Gayle, C. J.; Greco, F.; Hamley, I. W.; Rambo, R.; Seitsonen, J.; Ruokolainen, J., Arginine-Containing Surfactant-Like Peptides: Interaction with Lipid Membranes and Antimicrobial Activity. *Biomacromolecules* **2018**.

143. Castelletto, V.; Barnes, R. H.; Karatzas, K.-A.; Edwards-Gayle, C. J.; Greco, F.; Hamley, I. W.; Seitsonen, J.; Ruokolainen, J., Restructuring of Lipid Membranes by an Arginine-Capped Peptide Bolaamphiphile. *Langmuir* **2018**.

144. Doktorova, M.; Heberle, F. A.; Marquardt, D.; Rusinova, R.; Sanford, R. L.; Peyear, T. A.; Katsaras, J.; Feigenson, G. W.; Weinstein, H.; Andersen, O. S., Gramicidin increases lipid flip-flop in symmetric and asymmetric lipid vesicles. *Biophys. J.* **2019,** *116* (5), 860-873.

REFERENCES

145. Pachler, M.; Kabelka, I.; Appavou, M.-S.; Lohner, K.; Vácha, R.; Pabst, G., Magainin 2 and PGLa in Bacterial Membrane Mimics I: Peptide-Peptide and Lipid-Peptide Interactions. *Biophys. J.* **2019,** *117* (10), 1858-1869.

146. Semeraro, E. F.; Marx, L.; Frewein, M. P.; Pabst, G., Increasing complexity in small-angle X-ray and neutron scattering experiments: from biological membrane mimics to live cells. *Soft Matter* **2020.**

147. Kabelka, I.; Pachler, M.; Prévost, S.; Letofsky-Papst, I.; Lohner, K.; Pabst, G.; Vácha, R., Magainin 2 and PGLa in Bacterial Membrane Mimics II: Membrane Fusion and Sponge Phase Formation. *Biophys. J.* **2020,** *118* (3), 612-623.

148. Blondelle, S. E.; Lohner, K.; Aguilar, M.-I., Lipid-induced conformation and lipid-binding properties of cytolytic and antimicrobial peptides: determination and biological specificity. *Biochim. Biophys. Acta, Biomembr.* **1999,** *1462* (1-2), 89-108.

149. Buck, A. K.; Elmore, D. E.; Darling, L. E., Using fluorescence microscopy to shed light on the mechanisms of antimicrobial peptides. *Future Med. Chem.* **2019,** *11* (18), 2447-2460.

150. Venturoli, M.; Sperotto, M. M.; Kranenburg, M.; Smit, B., Mesoscopic models of biological membranes. *Phys. Rep.* **2006,** *437* (1-2), 1-54.

151. Lyatskaya, Y.; Liu, Y.; Tristram-Nagle, S.; Katsaras, J.; Nagle, J. F., Method for obtaining structure and interactions from oriented lipid bilayers. *Phys. Rev. E* **2000,** *63* (1), 011907.

152. Kucerka, N.; Pencer, J.; Sachs, J. N.; Nagle, J. F.; Katsaras, J., Curvature effect on the structure of phospholipid bilayers. *Langmuir* **2007,** *23* (3), 1292-1299.

153. Heberle, F. A.; Petruzielo, R. S.; Pan, J.; Drazba, P.; Kučerka, N.; Standaert, R. F.; Feigenson, G. W.; Katsaras, J., Bilayer thickness mismatch controls domain size in model membranes. *J. Am. Chem. Soc.* **2013,** *135* (18), 6853-6859.

154. Kučerka, N.; van Oosten, B.; Pan, J.; Heberle, F. A.; Harroun, T. A.; Katsaras, J., Molecular structures of fluid phosphatidylethanolamine bilayers obtained from simulation-to-experiment comparisons and experimental scattering density profiles. *J. Phys. Chem. B* **2014,** *119* (5), 1947-1956.

155. Xia, Y.; Li, M.; Charubin, K.; Liu, Y.; Heberle, F. A.; Katsaras, J.; Jing, B.; Zhu, Y.; Nieh, M.-P., Effects of nanoparticle morphology and acyl chain length on spontaneous lipid transfer rates. *Langmuir* **2015,** *31* (47), 12920-12928.

156. Doktorova, M.; Heberle, F. A.; Eicher, B.; Standaert, R. F.; Katsaras, J.; London, E.; Pabst, G.; Marquardt, D., Preparation of asymmetric phospholipid vesicles for use as cell membrane models. *Nat. Protoc.* **2018,** *13* (9), 2086-2101.

157. Israelachvili, J. N.; Mitchell, D. J., A model for the packing of lipids in bilayer membranes. *Biochim. Biophys. Acta, Biomembr.* **1975,** *389* (1), 13-19.

158. Israelachvili, J. N., Intermolecular and surface forces. 3rd. ed.; Academic press: **2011**; pp 535-576.

159. Lind, T. K.; Cárdenas, M., Understanding the formation of supported lipid bilayers via vesicle fusion—A case that exemplifies the need for the complementary method approach. *Biointerphases* **2016,** *11* (2), 020801.

160. Clifton, L. A.; Skoda, M. W.; Daulton, E. L.; Hughes, A. V.; Le Brun, A. P.; Lakey, J. H.; Holt, S. A., Asymmetric phospholipid: lipopolysaccharide bilayers; a Gram-negative bacterial outer membrane mimic. *J. R. Soc. Interface* **2013,** *10* (89), 20130810.

161. Seantier, B.; Breffa, C.; Felix, O.; Decher, G., Dissipation-enhanced quartz crystal microbalance studies on the experimental parameters controlling the formation of supported lipid bilayers. *J. Phys. Chem. B* **2005,** *109* (46), 21755-21765.

162. Hristova, K.; Wimley, W. C.; Mishra, V. K.; Anantharamiah, G.; Segrest, J. P.; White, S. H., An amphipathic α-helix at a membrane interface: a structural study using a novel X-ray diffraction method. *J. Mol. Biol.* **1999,** *290* (1), 99-117.

163. Münster, C.; Lu, J.; Bechinger, B.; Salditt, T., Grazing incidence X-ray diffraction of highly aligned phospholipid membranes containing the antimicrobial peptide magainin 2. *Eur. Biophys. J.* **2000,** *28* (8), 683-688.

164. Münster, C.; Spaar, A.; Bechinger, B.; Salditt, T., Magainin 2 in phospholipid bilayers: peptide orientation and lipid chain ordering studied by x-ray diffraction. *Biochim. Biophys. Acta, Biomembr.* **2002,** *1562* (1), 37-44.

165. Shen, H.-H.; Thomas, R. K.; Penfold, J.; Fragneto, G., Destruction and solubilization of supported phospholipid bilayers on silica by the biosurfactant surfactin. *Langmuir* **2010,** *26* (10), 7334-7342.

166. Åkesson, A.; Lind, T. K.; Barker, R.; Hughes, A.; Cárdenas, M., Unraveling dendrimer translocation across cell membrane mimics. *Langmuir* **2012,** *28* (36), 13025-13033.

167. Buck, Z.; Torres, J.; Miskowiec, A.; Mamontov, E.; Kaiser, H.; Hansen, F.; Taub, H.; Tyagi, M.; Collins, L.; Herwig, K., Effect of melittin on water diffusion and membrane structure in DMPC lipid bilayers. *EPL* **2018,** *123* (1), 18002.

168. Hedegaard, S. F.; Derbas, M. S.; Lind, T. K.; Kasimova, M. R.; Christensen, M. V.; Michaelsen, M. H.; Campbell, R. A.; Jorgensen, L.; Franzyk, H.; Cárdenas, M., Fluorophore labeling of a cell-penetrating peptide significantly alters the mode and degree of biomembrane interaction. *Sci. Rep.* **2018,** *8* (1), 1-14.

169. Waldie, S.; Lind, T. K.; Browning, K.; Moulin, M.; Haertlein, M.; Forsyth, V. T.; Luchini, A.; Strohmeier, G. A.; Pichler, H.; Maric, S., Localization of cholesterol within supported lipid bilayers made of a natural extract of tailor-deuterated phosphatidylcholine. *Langmuir* **2018,** *34* (1), 472-479.

170. Lindner, P.; Zemb, T., *Neutrons, X-rays, and light: scattering methods applied to soft condensed matter*. Elsevier Amsterdam: **2002;** Vol. 5.

171. König, B. W.; Krueger, S.; Orts, W.; Majkrzak, C. F.; Berk, N. F.; Silverton, J.; Gawrisch, K., Neutron reflectivity and atomic force microscopy studies of a lipid bilayer in water adsorbed to the surface of a silicon single crystal. *Langmuir* **1996,** *12* (5), 1343-1350.

172. Wacklin, H. P., Neutron reflection from supported lipid membranes. *Curr. Opin. Colloid Interface Sci.* **2010,** *15* (6), 445-454.

173. Åkesson, A.; Lind, T.; Ehrlich, N.; Stamou, D.; Wacklin, H.; Cárdenas, M., Composition and structure of mixed phospholipid supported bilayers formed by POPC and DPPC. *Soft Matter* **2012,** *8* (20), 5658-5665.

174. Gerelli, Y.; Porcar, L.; Fragneto, G., Lipid rearrangement in DSPC/DMPC bilayers: A neutron reflectometry study. *Langmuir* **2012,** *28* (45), 15922-15928.

175. Bobone, S.; Gerelli, Y.; De Zotti, M.; Bocchinfuso, G.; Farrotti, A.; Orioni, B.; Sebastiani, F.; Latter, E.; Penfold, J.; Senesi, R., Membrane thickness and the mechanism of action of the short peptaibol trichogin GA IV. *Biochim. Biophys. Acta, Biomembr.* **2013,** *1828* (3), 1013-1024.

176. Martel, A.; Antony, L.; Gerelli, Y.; Porcar, L.; Fluitt, A.; Hoffmann, K.; Kiesel, I.; Vivaudou, M.; Fragneto, G.; De Pablo, J. J., Membrane permeation versus amyloidogenicity: a multitechnique study of islet amyloid polypeptide interaction with model membranes. *J. Am. Chem. Soc.* **2016,** *139* (1), 137-148.

177. Clifton, L. A.; Ciesielski, F.; Skoda, M. W.; Paracini, N.; Holt, S. A.; Lakey, J. H., The effect of lipopolysaccharide core oligosaccharide size on the electrostatic binding of antimicrobial proteins to models of the gram negative bacterial outer membrane. *Langmuir* **2016,** *32* (14), 3485-3494.

178. Nordström, R.; Browning, K. L.; Parra-Ortiz, E.; Damgaard, L. S. E.; Häffner, S. M.; Maestro, A.; Campbell, R. A.; Cooper, J. F.; Malmsten, M., Membrane interactions of antimicrobial peptide-loaded microgels. *J. Colloid Interface Sci.* **2020,** *562*, 322-332.

179. Paracini, N.; Clifton, L. A.; Skoda, M. W.; Lakey, J. H., Liquid crystalline bacterial outer membranes are critical for antibiotic susceptibility. *Proc. Natl. Acad. Sci. U.S.A.* **2018,** *115* (32), E7587-E7594.

180. Born, M., Quantenmechanik der stoßvorgänge. *Zeitschrift für Physik* **1926,** *38* (11-12), 803-827.

181. Pedersen, J. S., Analysis of small-angle scattering data from colloids and polymer solutions: modeling and least-squares fitting. *Adv. Colloid Interface Sci.* **1997,** *70*, 171-210.

182. Mertens, H. D.; Svergun, D. I., Combining NMR and small angle X-ray scattering for the study of biomolecular structure and dynamics. *Arch. Biochem. Biophys.* **2017,** *628*, 33-41.

183. Debye, P., Molecular-weight determination by light scattering. *J. Phys. Chem.* **1947,** *51* (1), 18-32.

184. Lund, R.; Shu, J.; Xu, T., A small-angle x-ray scattering study of α-helical bundle-forming peptide–polymer conjugates in solution: chain conformations. *Macromolecules* **2013,** *46* (4), 1625-1632.

185. Dube, N.; Seo, J. W.; Dong, H.; Shu, J. Y.; Lund, R.; Mahakian, L. M.; Ferrara, K. W.; Xu, T., Effect of alkyl length of peptide–polymer amphiphile on cargo encapsulation stability and pharmacokinetics of 3-helix micelles. *Biomacromolecules* **2014,** *15* (8), 2963-2970.

186. Yang, M.; Xu, D.; Jiang, L.; Zhang, L.; Dustin, D.; Lund, R.; Liu, L.; Dong, H., Filamentous supramolecular peptide–drug conjugates as highly efficient drug delivery vehicles. *Chem. Commun.* **2014,** *50* (37), 4827-4830.

187. Xu, D.; Jiang, L.; Singh, A.; Dustin, D.; Yang, M.; Liu, L.; Lund, R.; Sellati, T. J.; Dong, H., Designed supramolecular filamentous peptides: balance of nanostructure, cytotoxicity and antimicrobial activity. *Chem. Commun.* **2015,** *51* (7), 1289-1292.

188. Lone, A.; Thomsen, T. T.; Nielsen, J. E.; Thulstrup, P. W.; Klitgaard, R. N.; Løbner-Olesen, A.; Lund, R.; Jenssen, H.; Hansen, P. R., Structure-Activity Study of an All-d Antimicrobial Octapeptide D2D. *Molecules* **2019,** *24* (24), 4571.

189. König, N.; Nielsen, J. E.; Willner, L.; Radulescu, A.; Mahmoudi, N.; Dong, H.; Lund, R., *Extraordinary physical stability of beta-sheet nanofibers formed by self-assembly of a de novo antimicrobial peptide confirmed by small-angle scattering techniques (submitted)* **2020.**

190. Molchanova, N.; Nielsen, J. E.; Sørensen, K. B.; Prabhala, B. K.; Hansen, P. R.; Lund, R.; Barron, A. E.; Jenssen, H., Halogenation as a tool to improve antimicrobial activity of peptoids. *Sci. rep.* **2020,** *10* (1), 14805.

191. Sun, J.; Jiang, X.; Lund, R.; Downing, K. H.; Balsara, N. P.; Zuckermann, R. N., Self-assembly of crystalline nanotubes from monodisperse amphiphilic diblock copolypeptoid tiles. *Proc. Natl. Acad. Sci. U.S.A.* **2016,** *113* (15), 3954-3959.

192. Häffner, S. M.; Malmsten, M., Influence of self-assembly on the performance of antimicrobial peptides. *Curr. Opin. Colloid Interface Sci.* **2018.**

193. Semeraro, E. F.; Devos, J. M.; Porcar, L.; Forsyth, V. T.; Narayanan, T., In vivo analysis of the Escherichia coli ultrastructure by small-angle scattering. *IUCrJ* **2017,** *4* (6), 751-757.

194. Nagle, J. F.; Tristram-Nagle, S., Structure of lipid bilayers. *Biochim. Biophys. Acta, Rev. Biomembr.* **2000,** *1469* (3), 159-195.

195. Pabst, G.; Rappolt, M.; Amenitsch, H.; Laggner, P., Structural information from multilamellar liposomes at full hydration: full q-range fitting with high quality x-ray data. *Phys. Rev. E* **2000,** *62* (3), 4000.

196. Riske, K. A.; Amaral, L. Q.; Lamy-Freund, M. T., Thermal transitions of DMPG bilayers in aqueous solution: SAXS structural studies. *Biochim. Biophys. Acta, Biomembr.* **2001,** *1511* (2), 297-308.

197. Brzustowicz, M. R.; Brunger, A. T., X-ray scattering from unilamellar lipid vesicles. *J. Appl. Crystallogr.* **2005,** *38* (1), 126-131.

198. Pencer, J.; Krueger, S.; Adams, C. P.; Katsaras, J., Method of separated form factors for polydisperse vesicles. *J. Appl. Crystallogr.* **2006,** *39* (3), 293-303.

199. Kučerka, N.; Nagle, J. F.; Sachs, J. N.; Feller, S. E.; Pencer, J.; Jackson, A.; Katsaras, J., Lipid bilayer structure determined by the simultaneous analysis of neutron and X-ray scattering data. *Biophys. J.* **2008,** *95* (5), 2356-2367.

200. Heberle, F. A.; Pan, J.; Standaert, R. F.; Drazba, P.; Kučerka, N.; Katsaras, J., Model-based approaches for the determination of lipid bilayer structure from small-angle neutron and X-ray scattering data. *Eur. Biophys. J.* **2012,** *41* (10), 875-890.

201. Eicher, B.; Heberle, F. A.; Marquardt, D.; Rechberger, G. N.; Katsaras, J.; Pabst, G., Joint small-angle X-ray and neutron scattering data analysis of asymmetric lipid vesicles. *J. Appl. Crystallogr.* **2017,** *50* (2).

202. Kiselev, M.; Lesieur, P.; Kisselev, A.; Lombardo, D.; Aksenov, V., Model of separated form factors for unilamellar vesicles. *Appl. Phys. A* **2002,** *74* (1), s1654-s1656.

203. Kučerka, N.; Nieh, M.-P.; Katsaras, J., Fluid phase lipid areas and bilayer thicknesses of commonly used phosphatidylcholines as a function of temperature. *Biochim. Biophys. Acta, Biomembr.* **2011,** *1808* (11), 2761-2771.

204. Klauda, J. B.; Kučerka, N.; Brooks, B. R.; Pastor, R. W.; Nagle, J. F., Simulation-based methods for interpreting x-ray data from lipid bilayers. *Biophys. J.* **2006,** *90* (8), 2796-2807.

205. Castelletto, V.; Cheng, G.; Stain, C.; Connon, C.; Hamley, I., Self-assembly of a peptide amphiphile containing L-carnosine and its mixtures with a multilamellar vesicle forming lipid. *Langmuir* **2012,** *28* (31), 11599-11608.

206. Dehsorkhi, A.; Castelletto, V.; Hamley, I. W.; Seitsonen, J.; Ruokolainen, J., Interaction between a cationic surfactant-like peptide and lipid vesicles and its relationship to antimicrobial activity. *Langmuir* **2013,** *29* (46), 14246-14253.

207. Narayanan, T.; Weerakkody, D.; Karabadzhak, A. G.; Anderson, M.; Andreev, O. A.; Reshetnyak, Y. K., pHLIP peptide interaction with a membrane monitored by SAXS. *J. Phys. Chem. B* **2016,** *120* (44), 11484-11491.

208. Heftberger, P.; Kollmitzer, B.; Heberle, F. A.; Pan, J.; Rappolt, M.; Amenitsch, H.; Kučerka, N.; Katsaras, J.; Pabst, G., Global small-angle X-ray scattering data analysis for multilamellar vesicles: the evolution of the scattering density profile model. *J. Appl. Crystallogr.* **2014,** *47* (1), 173-180.

209. Qian, S.; Wang, W.; Yang, L.; Huang, H. W., Structure of the alamethicin pore reconstructed by x-ray diffraction analysis. *Biophys. J.* **2008,** *94* (9), 3512-3522.

210. Lee, C.-C.; Sun, Y.; Qian, S.; Huang, H. W., Transmembrane pores formed by human antimicrobial peptide LL-37. *Biophys. J.* **2011,** *100* (7), 1688-1696.

211. Pencer, J.; Mills, T.; Anghel, V.; Krueger, S.; Epand, R. M.; Katsaras, J., Detection of submicron-sized raft-like domains in membranes by small-angle neutron scattering. *EUR. PHYS. J. E* **2005,** *18* (4), 447-458.

212. Marquardt, D.; Heberle, F. A.; Nickels, J. D.; Pabst, G.; Katsaras, J., On scattered waves and lipid domains: detecting membrane rafts with X-rays and neutrons. *Soft Matter* **2015,** *11* (47), 9055-9072.

213. Rai, D. K.; Qian, S., Interaction of the Antimicrobial Peptide Aurein 1.2 and Charged Lipid Bilayer. *Sci. Rep.* **2017,** *7* (1), 3719.

214. Liu, J.; Conboy, J. C., Direct measurement of the transbilayer movement of phospholipids by sum-frequency vibrational spectroscopy. *J. Am. Chem. Soc.* **2004,** *126* (27), 8376-8377.

215. Allhusen, J. S.; Conboy, J. C., The ins and outs of lipid flip-flop. *Acc. Chem. Res.* **2016,** *50* (1), 58-65.

216. Gerelli, Y.; Porcar, L.; Lombardi, L.; Fragneto, G., Lipid exchange and flip-flop in solid supported bilayers. *Langmuir* **2013,** *29* (41), 12762-12769.

217. Porcar, L.; Gerelli, Y., On the lipid flip-flop and phase transition coupling. *Soft Matter* **2020**.

218. Wah, B.; Breidigan, J. M.; Adams, J.; Horbal, P.; Garg, S.; Porcar, L.; Perez-Salas, U., Reconciling differences between lipid transfer in free-standing and solid supported membranes: a time-resolved small-angle neutron scattering study. *Langmuir* **2017,** *33* (14), 3384-3394.

219. Willner, L.; Poppe, A.; Allgaier, J.; Monkenbusch, M.; Richter, D., Time-resolved SANS for the determination of unimer exchange kinetics in block copolymer micelles. *EPL* **2001,** *55* (5), 667.

220. Lund, R.; Willner, L.; Richter, D.; Dormidontova, E. E., Equilibrium chain exchange kinetics of diblock copolymer micelles: Tuning and logarithmic relaxation. *Macromolecules* **2006,** *39* (13), 4566-4575.

221. Lund, R.; Willner, L.; Stellbrink, J.; Lindner, P.; Richter, D., Logarithmic chain-exchange kinetics of diblock copolymer micelles. *Phys. Rev. Lett.* **2006,** *96* (6), 068302.

222. Lund, R.; Willner, L.; Richter, D., Kinetics of block copolymer micelles studied by small-angle scattering methods. In *Controlled Polymerization and Polymeric Structures*, Springer: **2013**; pp 51-158.

223. Nakano, M.; Fukuda, M.; Kudo, T.; Endo, H.; Handa, T., Determination of interbilayer and transbilayer lipid transfers by time-resolved small-angle neutron scattering. *Phys. Rev. Lett.* **2007,** *98* (23), 238101.

224. Nakano, M.; Fukuda, M.; Kudo, T.; Matsuzaki, N.; Azuma, T.; Sekine, K.; Endo, H.; Handa, T., Flip-flop of phospholipids in vesicles: kinetic analysis with time-resolved small-angle neutron scattering. *J. Phys. Chem. B* **2009,** *113* (19), 6745-6748.

225. Garg, S.; Porcar, L.; Woodka, A.; Butler, P.; Perez-Salas, U., Noninvasive neutron scattering measurements reveal slower cholesterol transport in model lipid membranes. *Biophys. J.* **2011,** *101* (2), 370-377.

226. Kaihara, M.; Nakao, H.; Yokoyama, H.; Endo, H.; Ishihama, Y.; Handa, T.; Nakano, M., Control of phospholipid flip-flop by transmembrane peptides. *Chem. Phys.* **2013,** *419*, 78-83.

227. Matsuzaki, N.; Handa, T.; Nakano, M., Kinetic and thermodynamic analysis of cholesterol transfer between phospholipid vesicles and nanodiscs. *J. Phys. Chem. B* **2015,** *119* (30), 9764-9771.

228. Xia, Y.; Charubin, K.; Marquardt, D.; Heberle, F. A.; Katsaras, J.; Tian, J.; Cheng, X.; Liu, Y.; Nieh, M.-P., Morphology-induced defects enhance lipid transfer rates. *Langmuir* **2016,** *32* (38), 9757-9764.

229. Nakano, M., Evaluation of Interbilayer and Transbilayer Transfer Dynamics of Phospholipids Using Time-Resolved Small-Angle Neutron Scattering. *Chem. Pharm. Bull.* **2019,** *67* (4), 316-320.

230. Sugiura, T.; Takahashi, C.; Chuma, Y.; Fukuda, M.; Yamada, M.; Yoshida, U.; Nakao, H.; Ikeda, K.; Khan, D.; Nile, A. H.; Bankaitis, V.; Nakano, M., Biophysical parameters of the Sec14 phospholipid exchange cycle. *Biophys. J.* **2019,** *116* (1), 92-103.

231. Arenas, R. C.; Danielczak, B.; Martel, A.; Porcar, L.; Breyton, C.; Ebel, C.; Keller, S., Fast collisional lipid transfer among polymer-bounded nanodiscs. *Sci. Rep.* **2017,** *7*, 45875.

232. Zinn, T.; Willner, L.; Pipich, V.; Richter, D.; Lund, R., Effect of core crystallization and conformational entropy on the molecular exchange kinetics of polymeric micelles. *ACS Macro Lett.* **2015,** *4* (6), 651-655.

233. Kobayashi, S.; Takeshima, K.; Park, C. B.; Kim, S. C.; Matsuzaki, K., Interactions of the novel antimicrobial peptide buforin 2 with lipid bilayers: proline as a translocation promoting factor. *Biochemistry* **2000,** *39* (29), 8648-8654.

234. Zhang, L.; Rozek, A.; Hancock, R. E., Interaction of cationic antimicrobial peptides with model membranes. *Journal of Biological Chemistry* **2001,** *276* (38), 35714-35722.

235. Nakao, H.; Hayashi, C.; Ikeda, K.; Saito, H.; Nagao, H.; Nakano, M., Effects of Hydrophilic Residues and Hydrophobic Length on Flip-Flop Promotion by Transmembrane Peptides. *J. Phys. Chem. B* **2018,** *122* (15), 4318-4324.

236. Ulmschneider, J. P., Charged antimicrobial peptides can translocate across membranes without forming channel-like pores. *Biophys. J.* **2017,** *113* (1), 73-81.

237. Omar, R.; Sharma, S.; Yadav, V. K.; Yadav, A., Peptides as pharmaceutical leads: A mechanistic based exploration through molecular modeling and docking studies. **2017**.

238. Ramos, R.; Silva, J. P.; Rodrigues, A. C.; Costa, R.; Guardão, L.; Schmitt, F.; Soares, R.; Vilanova, M.; Domingues, L.; Gama, M., Wound healing activity of the human antimicrobial peptide LL37. *Peptides* **2011,** *32* (7), 1469-1476.

239. O'Driscoll, N. H.; Labovitiadi, O.; Cushnie, T. T.; Matthews, K. H.; Mercer, D. K.; Lamb, A. J., Production and evaluation of an antimicrobial peptide-containing wafer formulation for topical application. *Curr. Microbiol.* **2013,** *66* (3), 271-278.

240. Duplantier, A. J.; van Hoek, M. L., The human cathelicidin antimicrobial peptide LL-37 as a potential treatment for polymicrobial infected wounds. *Front. Immunol.* **2013,** *4*, 143.

241. Saporito, P.; Vang Mouritzen, M.; Løbner-Olesen, A.; Jenssen, H., LL-37 fragments have antimicrobial activity against Staphylococcus epidermidis biofilms and wound healing potential in HaCaT cell line. *J. Pept. Sci.* **2018,** *24* (7), e3080.

242. Boge, L.; Hallstensson, K.; Ringstad, L.; Johansson, J.; Andersson, T.; Davoudi, M.; Larsson, P. T.; Mahlapuu, M.; Håkansson, J.; Andersson, M., Cubosomes for topical delivery of the antimicrobial peptide LL-37. *Eur. J. Pharm. Biopharm.* **2019,** *134*, 60-67.

243. Mouritzen, M. V.; Andrea, A.; Qvist, K.; Poulsen, S. S.; Jenssen, H., Immunomodulatory potential of Nisin A with application in wound healing. *Wound Repair Regen.* **2019,** *27* (6), 650-660.

244. Hancock, R. E.; Lehrer, R., Cationic peptides: a new source of antibiotics. *Trends Biotechnol.* **1998,** *16* (2), 82-88.

245. Bommarius, B.; Jenssen, H.; Elliott, M.; Kindrachuk, J.; Pasupuleti, M.; Gieren, H.; Jaeger, K.-E.; Hancock, R.; Kalman, D., Cost-effective expression and purification of antimicrobial and host defense peptides in Escherichia coli. *Peptides* **2010,** *31* (11), 1957-1965.

246. Agyei, D.; Danquah, M. K., Industrial-scale manufacturing of pharmaceutical-grade bioactive peptides. *Biotechnol. Adv.* **2011,** *29* (3), 272-277.

247. Hilpert, K.; Volkmer-Engert, R.; Walter, T.; Hancock, R. E., High-throughput generation of small antibacterial peptides with improved activity. *Nat. Biotechnol.* **2005,** *23* (8), 1008-1012.

248. Strøm, M. B.; Rekdal, Ø.; Svendsen, J. S., Antimicrobial activity of short arginine-and tryptophan-rich peptides. *J. Pept. Sci.* **2002,** *8* (8), 431-437.

249. Hilpert, K.; Elliott, M. R.; Volkmer-Engert, R.; Henklein, P.; Donini, O.; Zhou, Q.; Winkler, D. F.; Hancock, R. E., Sequence requirements and an optimization strategy for short antimicrobial peptides. *Chem. Biol.* **2006,** *13* (10), 1101-1107.

250. Chongsiriwatana, N. P.; Miller, T. M.; Wetzler, M.; Vakulenko, S.; Karlsson, A. J.; Palecek, S. P.; Mobashery, S.; Barron, A. E., Short alkylated peptoid mimics of antimicrobial lipopeptides. *Antimicrob. Agents Chemother.* **2011,** *55* (1), 417-420.

251. Kim, H.; Jang, J. H.; Kim, S. C.; Cho, J. H., De novo generation of short antimicrobial peptides with enhanced stability and cell specificity. *J. Antimicrob. Chemother.* **2014,** *69* (1), 121-132.

252. Mojsoska, B.; Jenssen, H., Peptides and peptidomimetics for antimicrobial drug design. *Pharmaceuticals* **2015,** *8* (3), 366-415.

253. Wu, C. W.; Sanborn, T. J.; Huang, K.; Zuckermann, R. N.; Barron, A. E., Peptoid oligomers with α-chiral, aromatic side chains: sequence requirements for the formation of stable peptoid helices. *J. Am. Chem. Soc.* **2001,** *123* (28), 6778-6784.

254. Patch, J. A.; Barron, A. E., Helical peptoid mimics of magainin-2 amide. *J. Am. Chem. Soc.* **2003,** *125* (40), 12092-12093.

255. Kapoor, R.; Eimerman, P. R.; Hardy, J. W.; Cirillo, J. D.; Contag, C. H.; Barron, A. E., Efficacy of antimicrobial peptoids against Mycobacterium tuberculosis. *Antimicrob. Agents Chemother.* **2011,** *55* (6), 3058-3062.

256. Kapoor, R.; Wadman, M. W.; Dohm, M. T.; Czyzewski, A. M.; Spormann, A. M.; Barron, A. E., Antimicrobial peptoids are effective against Pseudomonas aeruginosa biofilms. *Antimicrob. Agents Chemother.* **2011,** *55* (6), 3054-3057.

257. Rosales, A. M.; Segalman, R. A.; Zuckermann, R. N., Polypeptoids: a model system to study the effect of monomer sequence on polymer properties and self-assembly. *Soft Matter* **2013,** *9* (35), 8400-8414.

258. Mojsoska, B.; Zuckermann, R. N.; Jenssen, H., Structure-activity relationship study of novel peptoids that mimic the structure of antimicrobial peptides. *Antimicrob. Agents Chemother.* **2015**, AAC. 00237-15.

259. Czyzewski, A. M.; Jenssen, H.; Fjell, C. D.; Waldbrook, M.; Chongsiriwatana, N. P.; Yuen, E.; Hancock, R. E.; Barron, A. E., In vivo, in vitro, and in silico characterization of peptoids as antimicrobial agents. *PloS one* **2016,** *11* (2).

260. Mojsoska, B.; Carretero, G.; Larsen, S.; Mateiu, R. V.; Jenssen, H., Peptoids successfully inhibit the growth of gram negative E. coli causing substantial membrane damage. *Sci. Rep.* **2017,** *7*, 42332.

261. Tencza, S. B.; Creighton, D. J.; Yuan, T.; Vogel, H. J.; Montelaro, R. C.; Mietzner, T. A., Lentivirus-derived antimicrobial peptides: increased potency by sequence engineering and dimerization. *J. Antimicrob. Chemother.* **1999,** *44* (1), 33-41.

262. Dempsey, C. E.; Ueno, S.; Avison, M. B., Enhanced membrane permeabilization and antibacterial activity of a disulfide-dimerized magainin analogue. *Biochemistry* **2003,** *42* (2), 402-409.

263. Chen, L.; Liang, J. F., Peptide fibrils with altered stability, activity, and cell selectivity. *Biomacromolecules* **2013,** *14* (7), 2326-2331.

264. Xu, D.; Ran, Q.; Xiang, Y.; Jiang, L.; Smith, B. M.; Bou-Abdallah, F.; Lund, R.; Li, Z.; Dong, H., Toward hemocompatible self-assembling antimicrobial nanofibers: understanding the synergistic effect of supramolecular structure and PEGylation on hemocompatibility. *RSC Adv.* **2016,** *6* (19), 15911-15919.

265. Panteleev, P. V.; Myshkin, M. Y.; Shenkarev, Z. O.; Ovchinnikova, T. V., Dimerization of the antimicrobial peptide arenicin plays a key role in the cytotoxicity but not in the antibacterial activity. *Biochem. Biophys. Res. Commun.* **2017,** *482* (4), 1320-1326.

266. Chen, W.; Yang, S.; Li, S.; Lang, J. C.; Mao, C.; Kroll, P.; Tang, L.; Dong, H., Self-Assembled Peptide Nanofibers Display Natural Antimicrobial Peptides to Selectively Kill Bacteria without Compromising Cytocompatibility. *ACS Appl. Mater. Interfaces* **2019,** *11* (32), 28681-28689.

267. Beter, M.; Kara, H. K.; Topal, A. E.; Dana, A.; Tekinay, A. B.; Guler, M. O., Multivalent presentation of cationic peptides on supramolecular nanofibers for antimicrobial activity. *Mol. Pharm.* **2017,** *14* (11), 3660-3668.

268. Chang, R.; Subramanian, K.; Wang, M.; Webster, T. J., Enhanced antibacterial properties of self-assembling peptide amphiphiles functionalized with heparin-binding cardin-motifs. *ACS Appl. Mater. Interfaces* **2017,** *9* (27), 22350-22360.

269. Chu-Kung, A. F.; Nguyen, R.; Bozzelli, K. N.; Tirrell, M., Chain length dependence of antimicrobial peptide–fatty acid conjugate activity. *J. Colloid Interface Sci.* **2010,** *345* (2), 160-167.

270. Kokkoli, E.; Mardilovich, A.; Wedekind, A.; Rexeisen, E. L.; Garg, A.; Craig, J. A., Self-assembly and applications of biomimetic and bioactive peptide-amphiphiles. *Soft Matter* **2006,** *2* (12), 1015-1024.

271. Tian, X.; Sun, F.; Zhou, X. R.; Luo, S. Z.; Chen, L., Role of peptide self-assembly in antimicrobial peptides. *J. Pept. Sci.* **2015,** *21* (7), 530-539.

272. Lombardi, L.; Falanga, A.; Del Genio, V.; Galdiero, S., A new hope: self-assembling peptides with antimicrobial activity. *Pharmaceutics* **2019,** *11* (4), 166.

273. Dong, H.; Paramonov, S. E.; Aulisa, L.; Bakota, E. L.; Hartgerink, J. D., Self-assembly of multidomain peptides: balancing molecular frustration controls conformation and nanostructure. *J. Am. Chem. Soc.* **2007,** *129* (41), 12468-12472.

274. Roberts, M.; Bentley, M.; Harris, J., Chemistry for peptide and protein PEGylation. *Adv. Drug Deliv. Rev.* **2002,** *54* (4), 459-476.

275. Turecek, P. L.; Bossard, M. J.; Schoetens, F.; Ivens, I. A., PEGylation of biopharmaceuticals: a review of chemistry and nonclinical safety information of approved drugs. *J. Pharm. Sci.* **2016,** *105* (2), 460-475.

276. AlQahtani, A. D.; O'Connor, D.; Domling, A.; Goda, S. K., Strategies for the production of long-acting therapeutics and efficient drug delivery for cancer treatment. *Biomed. Pharmacother.* **2019,** *113*, 108750.

277. Singh, S.; Papareddy, P.; Mörgelin, M.; Schmidtchen, A.; Malmsten, M., Effects of PEGylation on membrane and lipopolysaccharide interactions of host defense peptides. *Biomacromolecules* **2014,** *15* (4), 1337-1345.

278. Xu, D.; Chen, W.; Tobin-Miyaji, Y. J.; Sturge, C. R.; Yang, S.; Elmore, B.; Singh, A.; Pybus, C.; Greenberg, D. E.; Sellati, T. J., Fabrication and Microscopic and Spectroscopic Characterization of Cytocompatible Self-Assembling Antimicrobial Nanofibers. *ACS Infect. Dis.* **2018,** *4* (9), 1327-1335.

279. Silvius, J. R., Thermotropic phase transitions of pure lipids in model membranes and their modifications by membrane proteins. *Lipid-protein interactions* **1982,** *2*, 239-281.

280. Bjørnestad, V. A. Liposomes as a model system for the study of surface active peptides. Master thesis, University of Oslo, Oslo, **2018**.

281. Papahadjopoulos, D.; Allen, T.; Gabizon, A.; Mayhew, E.; Matthay, K.; Huang, S.; Lee, K.; Woodle, M.; Lasic, D.; Redemann, C., Sterically stabilized liposomes: improvements in pharmacokinetics and antitumor therapeutic efficacy. *Proc. Natl. Acad. Sci. U.S.A.* **1991,** *88* (24), 11460-11464.

114

282. Allen, C.; Dos Santos, N.; Gallagher, R.; Chiu, G.; Shu, Y.; Li, W.; Johnstone, S.; Janoff, A.; Mayer, L.; Webb, M., Controlling the physical behavior and biological performance of liposome formulations through use of surface grafted poly (ethylene glycol). *Biosci. Rep.* **2002,** *22* (2), 225-250.

283. Evans, R.; Napper, D., Steric stabilization I. *Colloid Polym. Sci.* **1973,** *251* (6), 409-414.

284. Evans, R.; Napper, D.-H., Steric stabilization II. *Colloid Polym. Sci.* **1973,** *251* (5), 329-336.

285. Alexander, S., Adsorption of chain molecules with a polar head a scaling description. *J. Phys. France* **1977,** *38* (8), 983-987.

286. de Gennes, P., Conformations of polymers attached to an interface. *Macromolecules* **1980,** *13* (5), 1069-1075.

287. Hristova, K.; Needham, D., Phase behavior of a lipid/polymer-lipid mixture in aqueous medium. *Macromolecules* **1995,** *28* (4), 991-1002.

288. Arleth, L.; Vermehren, C., An analytical model for the small-angle scattering of polyethylene glycol-modified liposomes. *J. Appl. Crystallogr.* **2010,** *43* (5), 1084-1091.

289. Mineart, K. P.; Kelley, E. G.; Nagao, M.; Prabhu, V. M., Processing–structure relationships of poly (ethylene glycol)-modified liposomes. *Soft Matter* **2017,** *13* (31), 5228-5232.

290. Pan, J.; Heberle, F. A.; Tristram-Nagle, S.; Szymanski, M.; Koepfinger, M.; Katsaras, J.; Kučerka, N., Molecular structures of fluid phase phosphatidylglycerol bilayers as determined by small angle neutron and X-ray scattering. *Biochim. Biophys. Acta, Biomembr.* **2012,** *1818* (9), 2135-2148.

291. Maric, S.; Skar-Gislinge, N.; Midtgaard, S.; Thygesen, M. B.; Schiller, J.; Frielinghaus, H.; Moulin, M.; Haertlein, M.; Forsyth, V. T.; Pomorski, T. G., Stealth carriers for low-resolution structure determination of membrane proteins in solution. *Acta Crystallogr. D Biol. Crystallogr.* **2014,** *70* (2), 317-328.

292. Kynde, S. A.; Skar-Gislinge, N.; Pedersen, M. C.; Midtgaard, S. R.; Simonsen, J. B.; Schweins, R.; Mortensen, K.; Arleth, L., Small-angle scattering gives direct structural information about a membrane protein inside a lipid environment. *Acta Crystallogr. D Biol. Crystallogr.* **2014,** *70* (2), 371-383.

293. Midtgaard, S. R.; Darwish, T. A.; Pedersen, M. C.; Huda, P.; Larsen, A. H.; Jensen, G. V.; Kynde, S. A. R.; Skar-Gislinge, N.; Nielsen, A. J. Z.; Olesen, C., Invisible detergents for structure determination of membrane proteins by small-angle neutron scattering. *FEBS J.* **2018,** *285* (2), 357-371.

294. Luchini, A.; Tidemand, F. G.; Johansen, N. T.; Campana, M.; Sotres, J.; Ploug, M.; Cárdenas, M.; Arleth, L., Peptide disc mediated control of membrane protein orientation in supported lipid bilayers for surface-sensitive investigations. *Anal. Chem.* **2019,** *92* (1), 1081-1088.

295. Wade, D., Deuterium isotope effects on noncovalent interactions between molecules. *Chem. Biol. Interact.* **1999,** *117* (3), 191-217.

296. König, N.; Willner, L.; Pipich, V.; Zinn, T.; Lund, R., Cooperativity during melting and molecular exchange in micelles with crystalline cores. *Phys. Rev. Lett.* **2019,** *122* (7), 078001.

297. Abramson, J. J.; Shamoo, A. E., Anionic detergents as divalent cation ionophores across black lipid membranes. *J Membrane Biol* **1979,** *50* (3-4), 241-255.

298. Paxton, W. F.; Price, D.; Richardson, N. J., Hydroxide ion flux and pH-gradient driven ester hydrolysis in polymer vesicle reactors. *Soft Matter* **2013,** *9* (47), 11295-11302.

299. Hernández-Villa, L.; Manrique-Moreno, M.; Leidy, C.; Jemioła-Rzemińska, M.; Ortíz, C.; Strzałka, K., Biophysical evaluation of cardiolipin content as a regulator of the membrane lytic effect of antimicrobial peptides. *Biophys. Chem.* **2018,** *238*, 8-15.

300. Hung, W.-C.; Lee, M.-T., The interaction of melittin with E. coli membrane: The role of cardiolipin. *Chinese Journal of Physics* **2006,** *44* (2), 137-149.

301. Aoki, W.; Ueda, M., Characterization of antimicrobial peptides toward the development of novel antibiotics. *Pharmaceuticals* **2013,** *6* (8), 1055-1081.

Scientific papers

Paper I

Resolving the Structural Interactions between Antimicrobial Peptides and Lipid Membranes using Small-angle Scattering Methods: the case of Indolicidin

Josefine Eilsø Nielsen, Victoria Ariel Bjørnestad and Reidar Lund

Check for updates

Resolving the structural interactions between antimicrobial peptides and lipid membranes using small-angle scattering methods: the case of indolicidin†

Josefine Eilsø Nielsen, [ID] Victoria Ariel Bjørnestad and Reidar Lund [ID] *

Using small angle X-ray and neutron scattering (SAXS/SANS) and detailed theoretical modelling we have elucidated the structure of the antimicrobial peptide, indolicidin, and the interaction with model lipid membranes of different anionic lipid compositions mimicking typical charge densities found in the cytoplasmic membrane of bacteria. First, we show that indolicidin displays a predominantly disordered, random chain conformation in solution with a small fraction ($\approx$1%) of fiber-like nanostructures that are not dissolved at higher temperatures. The peptide is shown to strongly interact with the membranes at all charge densities without significantly perturbing the lipid bilayer structure. Instead, the results show that indolicidin inserts into the outer leaflet of the lipid vesicles causing a reduced local order of the lipid packing. This result is supported by an observed change in the melting point of the lipids upon addition of the peptide, as seen by differential scanning calorimetry experiments. The peptide does not to our observation affect the thickness of the membrane or form distinct structural pores in the membrane at physiologically relevant concentrations as has been previously suggested as an important mode of action. Finally, using sophisticated contrast variation SANS, we show that the peptide does not affect the random lateral distribution of anionic lipids in the membrane. Together, these results demonstrate that the structural aspects of the mode of action of antimicrobial peptides can be elucidated in detail using SAS techniques with liposomes as model systems.

1. Introduction

Antibiotic resistance is one of the biggest threats to global health according to the World Health Organisation.[1] Antimicrobial peptides (AMPs) are a group of surface active molecules which constitute a natural part of the innate immune system across all domains of life. They are potent antimicrobial agents shown to have effect against a broad spectrum of pathogens, including both Gram-positive and Gram-negative bacteria.[2] AMPs seem to be able to evade much of the bacterial resistance mechanisms and are therefore promising candidates for future antibiotics. Instead of blocking specific biochemical pathways as is the mode of action of most commercially available antibiotic agents, AMPs act physically on the cytoplasmic membrane itself. The exact microscopic mechanism for the disturbance of the membrane has not been fully demonstrated. The main consensus is that the AMPs cause a disruption of the structural integrity of

the bacterial membrane, for example by inducing formation of pores or transient channels in the membrane.[3–5]

Indolicidin is a relatively small cationic peptide with only 13 amino acid residues and is believed to be completely disordered, *i.e.* without any secondary and higher-order structure.[6] It belongs to the cathelicidin family of antimicrobial peptides and has a high content of tryptophan and proline. The peptide exhibits significant antimicrobial effect against both Gram-positive and Gram-negative bacteria,[7] as well as having anti-fungal properties.[8] It is generally believed that the main mechanism of this activity is related to the formation of small pores, which cause leakage across the lipid bacterial membrane, that are formed despite its intrinsic disordered structure in solution. Circular dichroism spectroscopy (CD) measurements suggest that indolicidin adopts a disordered extended structure and either stacks in the membrane or extends across the membrane as an aggregate.[6] Other possible modes of actions have also been suggested, including inhibition of the DNA synthesis[9] and inhibition of nucleic acid and protein synthesis in the bacteria cells.[10]

The interaction between antimicrobial peptides and supported model lipid membranes has been investigated using molecular

Department of Chemistry, University of Oslo, 0315 Oslo, Norway.
E-mail: reidar.lund@kjemi.uio.no

† Electronic supplementary information (ESI) available. See DOI: 10.1039/c8sm01888j

dynamics (MD) simulations[11,12] as well as various experimental techniques including NMR and fluorescence techniques. From simulation studies, it has been reported that indolicidin induces local thinning of membranes consisting of unsaturated lipids[12] and that incorporation of indolicidin in the membrane interface results in a decrease of the lipid order parameter for the outer tail region.[11] This is also supported experimentally by NMR and fluorescence measurements[13] on micellar systems consisting of dodecylphosphocholine (DPC) and sodium dodecyl sulphate (SDS); these systems do, however, lack the characteristic bilayer structure of a bacterial inner membrane. Fluorescence spectroscopy measurements have shown that indolicidin increases the permeability of membrane containing anionic lipids.[14] By using techniques like neutron reflectivity (NR),[15] quartz crystal microbalance with dissipation monitoring (QCM-D) and atomic force microscopy (AFM),[16] it is possible to investigate the detailed surface interactions between AMPs and supported lipid bilayers that have a closer resemblance to the prokaryote membrane. Using these methods, one has been able to obtain an indication of how some AMPs insert into the membrane and cause pore formation. The proximity between the solid substrate and the lipid bilayer in methods involving supported bilayers may, however, affect the membrane in terms of e.g. the mobility and dielectric properties of the bilayer.[17] This problem can be avoided by using free-floating lipid bilayers such as lipid vesicles.

Lipid vesicles are well-established model systems that can mimic either eukaryotic or prokaryotic plasma membranes depending on the phospholipids used. The plasma membrane of prokaryotic cells contains mainly a combination of anionic and zwitterionic phospholipids, while eukaryotic cells have zwitterionic phospholipids as well as cholesterol in their membranes. The inclusion of anionic lipids in model lipid membranes used to probe interaction with AMPs is considered to be important since the negative charge is expected to play a significant role in the bacterial selectivity of the positively charged AMPs. It has further been suggested by amongst other Epand and Epand[18] that the mode of action for AMPs is connected to a clustering of negatively charged phospholipids around the peptides as it intercalates into the membrane, resulting in the formation of lipid domains. Interestingly, the development of an asymmetric distribution of charged lipids in model membranes caused by a peptide has been observed for the alpha helical peptides aurein 1.2, melittin and alamethicin. Although domains are not observed directly in the experiment, the modelling of the SANS data indicates domain formation.[19,20] Lipid domain formations can be studied directly using SANS on liposomes with partly deuterated lipids and contrast matched solvent.[21]

Using small-angle X-ray/neutron scattering (SAXS/SANS) techniques, it is possible to probe the interaction between lipid vesicles and peptides in situ in solution on a nanometre scale without perturbing the system. However, because of the many components in the system, the technique demands significant effort in theoretical modelling to extract detailed structural data. The use of lipid vesicles as model systems for probing the interactions with antimicrobial peptides is furthermore

complicated by the fact that vesicles may phase separate in the presence of peptides. Here, we circumvent this problem by introducing poly(ethylene glycol) (PEG) as a protective layer on the surface, using "PEGylated lipids", i.e. lipids conjugated with polyethylene glycol (PEG).[22] Only a small fraction of PEG covalently bound to the surface of the vesicles provides a steric (entropic) stabilisation of the lipid vesicles which inhibits aggregation. Using SAXS combined with detailed modelling, the density profiles of the bilayer as well as the overall vesicular size can be extracted, giving us real-space information of the lipid membrane systems.[23] From analysis of the obtained data we can procure information of the position of the head- and tailgroups of the phospholipids in the bilayer membrane, the thickness of the membrane, and the surface area per lipid. It is possible to clearly resolve these features using X-ray scattering because of the substantial difference in the electron density of the lipid headgroups, the tails and the surrounding water. Nevertheless, there are few studies employing SAXS to probe the interaction between various AMPs and liposomes. In the study of two alpha helical peptides, LL-37 and PLGa, mixed with unilamellar lipid vesicles (ULV) a shift in the bilayer scattering at high q was observed. This was interpreted as originating from membrane thickening in the case of LL-37,[24,25] and membrane thinning in the case of PLGa,[26] due to formations of transient pores. In another SAXS study, surfactant-like peptides were found to induce a transition from multilamellar (MLV) to unilamellar lipid vesicles (ULV) due to electrostatic repulsions.[27–29] One study where MD simulations and experimental SAXS data were compared, it was found that alpha helical alamethicin peptides inserts into the bilayer tail region rather that in the surface of the outer headgroup, with a resultant thinning of the membrane.[30]

In this work we have systematically studied the interaction between model lipid vesicles and indolicidin, an archetypical unstructured antimicrobial peptide, using SAXS and applied a detailed model to extract accurate structural information. The data provides deep insight into the distribution of the peptide within the bilayer as well as the structural integrity of the lipid membranes itself. From the result we gain important insight into the structural mechanism of the peptide where we show that the insertion of the indolicidin does not seem to significantly affect the thickness of the membrane or the lateral distribution of the anionic lipids. Instead, the peptide causes a disordering of the tail packing in the membrane, which is also reflected in a shift of the melting point of the liposomes as seen by differential scanning calorimetry.

2. Experimental section

2.1. Sample preparation

Synthetic DMPC (1,2-dimyristoyl-sn-glycero-3-phosphocholine), DMPG (1,2-dimyristoyl-sn-glycero-3-phospho-(1′-rac-glycerol)), and DMPE-PEG (1,2-dimyristoyl-sn-glycero-3-phosphoethanolamine-N-[methoxy(polyethylene glycol)-2000]) was purchased from Avanti Polar Lipids and used as received without further

purification. The lipids, in the correct proportions (varying the DMPG to DMPC ratio), were dissolved in a 1:3 methanol : chloroform solution to give the same concentration as would be in the final vesicle solution. The organic solvents were removed completely under vacuum using a Heidolph rotary evaporator with a Vacuubrand vacuum pump. The resulting lipid film was hydrated with 50 mM Tris buffer, pH 7.4, for at least one hour at a temperature of ~ 10 °C above the melting temperature of the lipid mixture. After sonication for 10 minutes, the lipid dispersions were extruded through a 100 nm pore diameter polycarbonate filter (>21 times) using an Avanti mini-extruder fitted with two 1 mL airtight syringes.

For the SANS experiments, performed at Oak Ridge National lab, a combination of lipids with protonated and deuterated tails and Tris–D$_2$O and Tris–H$_2$O were used to match the Scattering Length Density (SLD) of the both headgroup and average lipid tail. This was achieved by mixing 34% d-DMPC (1,2-dimyristoyl-d$_{54}$-sn-glycero-3-phosphocholine), 31% h-DMPC, 32.5% h-DMPG and 2.5% DMPE-PEG in 38% Tris–D$_2$O and 62% Tris–H$_2$O. Provided that the lipids are randomly distributed, vesicles with this composition will essentially be contrast matched and exhibit very low scattering intensity. In the event of any nanoscopic domain formation (clustering of DMPG lipids) an excess scattering signal will be visible due to the residual contrast between protonated DMPG and partly deuterated DMPC tails. As a reference, a sample with fully protonated lipid vesicles in 100% Tris–D$_2$O was prepared.

Indolicidin, purchased from Isca Biochemicals Limited, was dissolved in 50 mM Tris buffer, pH 7.4, to the desired concentration. The peptide solution was gently heated to 45 °C for 7 minutes while shaking to ensure full dissolution of the peptide.

2.3. Differential scanning calorimetry

Thermal analysis was performed using a differential scanning calorimeter (DSC) for solutions, the TA Instruments "nano-DSC" instrument, which allows detection of heat flows on a μJ s^{-1} scale. The heating rate was 2 °C min^{-1} and samples were scanned from 5 to 60 °C. The thermogram was recorded during both heating and cooling and each sample was measured for 3–5 scans to look for hysteresis effects. The Tris buffer was measured separately using the same settings and the buffer curve was subtracted from the thermograms using the Origin Lab Software. The measured power was converted to specific heat capacity C_p in J mol^{-1} K^{-1}. The enthalpy values were obtained by direct integration of the area under the baseline subtracted peaks.

2.4. Small angle X-ray scattering

SAXS experiments on mixtures of peptide and liposomes were performed at the automated BM29 bioSAXS beamline[31] at the European Synchrotron Radiation Facility (ESRF) in Grenoble, France. The data was obtained using an energy of 12.5 keV and a detector distance of 2.87 m, covering a q range ($q = 4\pi \sin(\theta/2)/\lambda$), where θ is the scattering angle and λ is the X-ray wavelength) of about 0.0047 Å^{-1} to 0.5 Å^{-1}. The data set was calibrated to an

absolute intensity scale using water as a primary standard. 40 μL samples were run through a capillary using the flow mode of the automated sample changer.[32] SAXS data were collected in ten successive frames of 0.5 s each to monitor radiation damage and the data reduction was done using the standard tool at BM29.[33]

The SAXS experiments to determine the concentration dependence of the peptide structure were performed at the ID02 beamline at ESRF. The X-ray wavelength was 0.995 Å and the sample-detector distance was set to 3 m, covering a q range of about 0.005 to 0.5 Å^{-1}. The data were calibrated to absolute scale using water as a primary standard.

2.5. Small angle neutron scattering

SANS measurements were carried out at the Bio-SANS beamline[34] at the High Flux Isotope Reactor (HFIR) at Oak Ridge National Laboratory, USA. By using a combination of a main and a wing detector, one single instrument configuration was able to cover a q range of 0.003 to 0.8 Å^{-1}. Scattered neutrons were collected with a 1 × 1 m two-dimensional (2D) position-sensitive detector having 192 × 192 pixels (ORDELA, Inc., Oak Ridge, TN). A neutron wavelength of 5 Å and detector distance of 15.5 m were used in all measurements. The 2D data set was corrected for detector dark current, pixel sensitivity, and scattering from backgrounds (Tris–D$_2$O, Tris–H$_2$O and quartz cell). The scattering intensity profiles $I(q)$ were obtained by azimuthally averaging the processed 2D images, which were normalized using water as a secondary standard.

3. Theoretical section

3.1. Free peptide in solution: random polymer-like chains with fiber-like clusters

In order to extract accurate and detailed structural information, the SAXS data for the pure peptide chains were analysed using a combination of free chains and rectangular fibres characterized by dimensions $a < b < c$.

$$I(q) = \phi \cdot V_p \cdot \Delta\rho^2 \cdot (P_{chain}(q) \cdot f_{chain} + N_p \cdot P_{sheet}(q)(1 - f_{chain})) \quad (1)$$

where ϕ is the volume fraction of the polymer, V_p is the volume of the polymer, $\Delta\rho$ is the excess scattering length density and f_{chain} is the fraction of free chains. N_p, the average number of peptides in each sheet, is defined as $N_p = \dfrac{abc}{V_p}$. $P_{chain}(q)$ is the form factor of the free peptide chains given by the Debye expression for Gaussian chains:

$$P_{chain}(q) = \frac{2 \cdot \exp\left[-(qR_g)^2\right] - 1 + (qR_g)^2}{(qR_g)^4} \quad (2)$$

where R_g is the radius gyration of the peptide chains.

Under the assumption that the lengths of the peptide sheets are much greater than the lateral dimension, i.e. $c \gg a, b$, the form factor $P_{sheet}(q)$ is given by

$$P_{sheet}(q) = F_c(q)\frac{1}{2\pi}\int_0^{2\pi} A_{sheet}(q, \alpha)^2 d\alpha \quad (3)$$

where the amplitude is given by

$$A_{\text{sheet}}(q, \alpha) = \frac{\sin(qb\cos(\alpha)/2)}{qb\cos(\alpha)/2} \cdot \frac{\sin(qa\sin(\alpha)/2)}{qa\sin(\alpha)/2} \quad (4)$$

and

$$F_c(q) = (2\text{Si}(qc)/(qc) - 4\sin^2(qc/2)/(qc)^2 \quad (5)$$

where $\text{Si}(x) = \int_0^x t^{-1}\sin t\, \mathrm{d}t$.

3.2. SAXS and SANS model for asymmetric unilamellar lipid vesicles

From a joint fit of synchrotron X-ray scattering data and neutron scattering data we can extract detailed information on the structure of the membrane of the vesicles as earlier described by amongst others Eicher *et al.*[35] The high-resolution and the peculiar difference in electron density between the head- and tail-groups of the lipid and water provides a significant sensitivity to changes in the contrast in X-ray scattering. We therefore chose a scattering model that provides detailed information on the structure of the bilayer.

The scattering density profile model (SPD), as developed by Nagle, Kučerka and co-workers,[36,37] and later modified to account for asymmetry in the bilayer,[35,38] describes the bilayer structure in terms of volume probability profiles of quasi-molecular fragments. The one-dimensional volume probability profiles for each segment is scaled by the number of electrons in the case of X-ray scattering and by the neutron scattering length density (SLD) in the case of neutron scattering. It has previously been shown[39,40] that the coherent scattering from large unilamellar vesicles (LUV), where the size of the vesicles and the thickness of the bilayer are well separated, can be described by the separated form factor (SFF) approximation:

$$I_{\text{lip}}(q) = n \cdot S(q)|P_{\text{TS}}(q)|^2 |P_{\text{FB}}(q)|^2 \quad (6)$$

where n is the number of scatterers, defined as

$$n = \frac{\phi}{V_{\text{lipid}} \cdot P_{\text{agg}}} \quad (7)$$

with ϕ being the volume fraction and V_{lipid} the total volume of a phospholipid given by $V_{\text{lipid}} = M_{\text{lipid}}/(N_A \cdot d_{\text{lipid}})$. N_A is Avogrados number, M_{lipid} is the molecular weight and d_{lipid} is the density. P_{agg} is the number of phospholipids in each lipid vesicle, *i.e.* the aggregation number of the vesicle, given by

$$P_{\text{agg}} = \frac{4\pi(R_{\text{shell}})^3 - 4\pi(R_{\text{shell}} - t_{\text{shell}})^3}{3V_{\text{tail}}} \quad (8)$$

where R_{shell} is the outer radius of the vesicles, t_{shell} is the thickness of the bilayer and V_{tail} is the volume occupied by each double tail of the phospholipid.

$S(q)$ is the structure factor accounting for interaction between particles ($S(q) = 1$ in our case because all samples are sufficiently diluted), P_{TS} is the form factor of an infinitely thin spherical shell (containing information on the radius of the lipid vesicles and the polydispersity), and $P_{\text{FB}}(q)$ is the form factor of a flat bilayer sheet (containing information on the bilayer thickness and the distribution of the phospholipids segments across the bilayer).

The flat bilayer form factor can be expressed[41] as

$$|P_{\text{FB}}(q)| = \int_{-D_i}^{D_o} \Delta\rho(z)e^{iqz}\mathrm{d}z = \sqrt{(F_{\cos}^2 + F_{\sin}^2)} \quad (9)$$

where $\Delta\rho$ is the difference in the SLDs of the membrane and the solvent, and $F_{\cos}^2$ and $F_{\sin}^2$ are the real and the imaginary parts of F_{FB} (*cf.* eqn (S1) and (S2) in the ESI†). The integral extends over the full bilayer thickness from the inner distance D_i to the outer distance D_o.

Following Kučerka and co-workers,[38] we parse the phospholipids into the following segments, as seen in Fig. 1: hydrocarbon terminal methyl (CH_3), hydrocarbon methylene (CH_2),
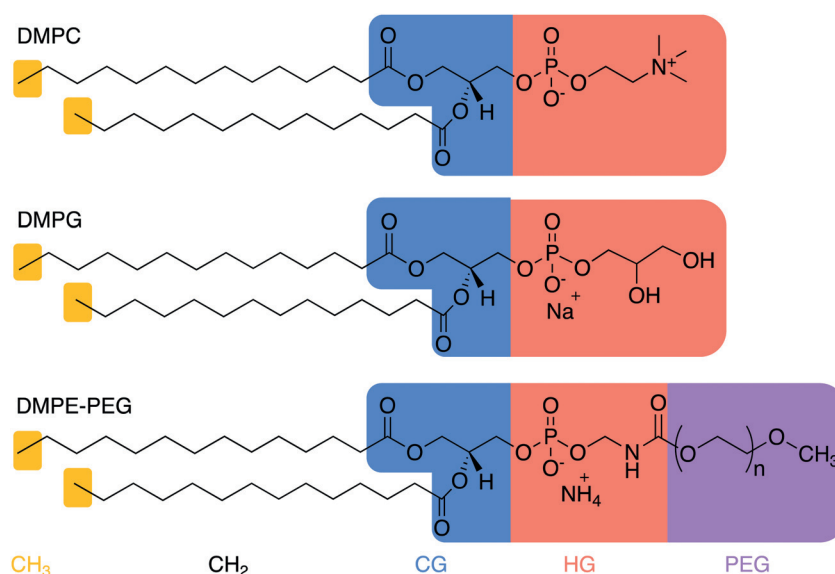

Fig. 1 Illustration of the bilayer parsing for DMPC, DMPG and DMPE-PEG (from top to bottom).

carbonyl + glycerol (CG) (common for all three phospholipid) and outer part of head group (HG). The HG-group is different for the three phospholipids and an average dependent on the mole fraction of each component in the specific mix is therefore used in the calculations.

The volume probability distributions of the components are described by Gaussian functions[37]

$$P_n(z) = \frac{c_n}{\sqrt{2\pi}} \left(\exp\left[-\frac{(z + z_n)^2}{2\sigma_n^2} \right] + \exp\left[-\frac{(z - z_n)^2}{2\sigma_n^2} \right] \right) \quad (10)$$

where σ_n and z_n are the width and position of the distribution, respectively, and $c_n = V_n/(A_L \sigma_n)$. V_n is the volume of the group n and A_L is the area per lipid, which is equal to the integrated area under the curve.

The hydrocarbon groups (HC representing the tails) are modelled using a half period squared sine/cosine function to account for the asymmetry in the bilayer, $e.g.$ potential differences in the segmental distribution of the inner and the outer HC group[35]

$$P_{HC}(z) =$$

$$\begin{cases} \sin\left(\frac{z - z_{MN_i} + \sigma_{MN_i}}{2\sigma_{MN_i}} \frac{\pi}{2} \right)^2 & \text{for } z_{MN_i} - \sigma_{MN_i} \leq z < z_{MN_i} + \sigma_{MN_i} \\ 1 & \text{for } z_{MN_i} + \sigma_{MN_i} \leq z < z_{MN_o} - \sigma_{MN_o} \\ \cos\left(\frac{z - z_{MN_o} + \sigma_{MN_o}}{2\sigma_{MN_o}} \frac{\pi}{2} \right)^2 & \text{for } z_{MN_o} - \sigma_{MN_o} \leq z < z_{MN_o} + \sigma_{MN_o} \end{cases}$$

$$(11)$$

where $z_{MN_{i,o}}$ is the 0.5-probability value for the HC group and $2\sigma_{MN_{i,o}}$ is the width of the squared sine/cosine function. The volume probability distribution of the methylene groups (CH_2) can be expressed separately as

$$P_{CH_2}(z) = P_{HC}(z) - P_{CH_3}(z) \quad (12)$$

These expressions for the distributions of the lipid tails comply with spatial conservation consideration[35,37] as the height of the expression for $P_{HC}(z)$ is equal to one in the central hydrocarbon region as there is no water present in this region of the membrane.

The volume probability distribution of the water is chosen to be the last group and the spatial conservation requirement is applied to give

$$P_w(z) = 1 - \sum_n P_n(z) \quad (13)$$

where $n = CH_3^{i,o}$, $CH_2^{i,o}$, $CG^{i,o}$, $HG^{i,o}$.

A number of constrains has been introduced to avoid nonphysical results. The position of the terminal methyl groups was fixed to zero (at the centre of the bilayer) and the width of the methyl group was fixed to the reference value 2.3 Å found by Kucerka $et~al.$[42] for similar systems (the fit is not very sensitive to σ_M and this was therefore not varied from the reference value). To prevent negative probability values for the water distribution curve, constraints on the z values and the sigma

values for the tail group and the headgroups were incorporated in the fitting regime. The positions of the CH_2 tails are limited based on the width of the CH_3 Gaussian function ($z_{CH_2} \geq \sigma_{CH_3} + 2\sigma_{CH_2}$) to yield physical possible values for the distribution of the groups in the tail region. Further, the positions and distributions of the two headgroup parsings in the inner and outer leaflet are limited by the positions and widths of the half period squared sine/cosine functions representing the tails in such a way that the sum of these functions will be equal to or less than one.

The total volumes of the head group and hydrocarbon chain, as well as the area per lipid, were constrained according to values from reported MD simulation of DMPC,[42] DMPG[43] and DMPE[44] phospholipids in a bilayer at different temperatures (an averaged value adjusted according to mole fraction of each lipid was used). To increase the reliability of the fit parameters, a joint fit of SAXS and SANS data was performed. The smearing due the experimental resolution effects was taken into account using standard procedures.[45] With varying ratios of DMCP to DMPG lipids, the changes in fit parameters were mainly limited to the changes in volume (and resulting scattering length density) of the outer lipid headgroup, as well as batch to batch differences in the polydispersity and radius of the vesicles.

3.3. Analytical model for PEGylated liposomes

Because a small amount of PEGylated DMPE lipids was used to stabilize the lipid vesicles against aggregation, the scattering from the PEG chains was included in the fit model for SAXS/SANS data. The PEG chains on the inner and outer leaflet of the lipid bilayer have a Gaussian random coil confirmation and can therefore be described by the following analytical model[46,47]

$$I_{PEG\text{-}liposomes}(q) = I_{lip}(q) + I_{chain}(q) + I_{c_i c_i}(q) + I_{c_i c_o}(q)$$
$$+ I_{c_o c_o}(q) + I_{sc_i}(q) + I_{sc_o}(q) \quad (14)$$

where $I_{lip}(q)$ is the scattering from the lipid vesicles themselves (eqn (6)) and $I_{chain}(q)$ is the scattering from the PEG-chains alone given by

$$I_{chain}(q) = n\Delta\rho_{PEG}^2 V_{PEG}^2 N_{PEG}$$

$$\cdot 2\frac{\exp\left[-(qR_g)^2 \right] - 1 + (qR_g)^2}{(qR_g)^4} \quad (15)$$

In this expression, n is the number of scatterers as defined in eqn (7), $\Delta\rho$ is the excess scattering length density, V_{PEG} is the partial specific molecular volume of a single PEG chains, R_g is the radius of gyration of the chains and N_{PEG} is defined as the number of PEG chains per liposomes given by

$$N_{PEG} = f_{PEG} \cdot P_{agg} \quad (16)$$

f_{PEG} is the fraction of PEG-modified lipids in the liposomes and P_{agg} is the aggregation number of the liposomes (eqn (8)).

The next terms, $I_{c_i c_i}(q)$ and $I_{c_o c_o}(q)$, are the interference terms between PEG chains attached to the inner surface of the vesicles and between the PEG chains on the outer surface,

respectively, while $I_{c_ic_o}(q)$ is the inter-interference between the inner and outer PEG chains:

$$I_{c_ic_i}(q) = n\Delta\rho_{PEG}{}^2 V_{PEG}{}^2 N_{PEG}f_{inner} \cdot (N_{PEG}f_{inner} - 1)$$

$$\cdot \left[\frac{1 - \exp\left[-(qR_g)^2\right]}{(qR_g)^2}\right]^2 \cdot \left[\frac{\sin(q(R_{inner} - R_g))}{q(R_{inner} - R_g)}\right]^2 \quad (17)$$

$$I_{c_oc_o}(q) = n\Delta\rho_{PEG}{}^2 V_{PEG}{}^2 N_{PEG}(1 - f_{inner}) \cdot (N_{PEG}(1 - f_{inner}) - 1)$$

$$\cdot \left[\frac{1 - \exp\left[-(qR_g)^2\right]}{(qR_g)^2}\right]^2 \cdot \left[\frac{\sin(q(R_{outer} - R_g))}{q(R_{outer} - R_g)}\right]^2 \quad (18)$$

$$I_{c_ic_o}(q) = n\Delta\rho_{PEG}{}^2 V_{PEG}{}^2 2N_{PEG}f_{inner} \cdot (1 - f_{inner})$$

$$\cdot \left[\frac{1 - \exp\left[-(qR_g)^2\right]}{(qR_g)^2}\right]^2 \cdot \left[\frac{\sin(q(R_{inner} - R_g))}{q(R_{inner} - R_g)}\right]^2$$

$$\cdot \left[\frac{\sin(q(R_{outer} - R_g))}{q(R_{outer} - R_g)}\right]^2 \quad (19)$$

Here, f_{inner} is the fraction of PEG in the inner leaflet, while R_{inner} and R_{outer} are the inner and outer radius of the liposomes, respectively, defined as

$$R_{inner} = R + z_{HG_i} - d_{disp} \quad (20)$$

$$R_{outer} = R + z_{HG_o} + d_{disp} \quad (21)$$

where d_{disp} is a displacement factor for the centre of mass of the PEG polymer chains. This was incorporated to account for the partial mixing of the polymer and the bilayer at the interface, since close packing of polymers has been reported for PEGylated lipid micellar systems in the past.[48]

The last remaining terms $I_{sc_i}(q)$ and $I_{sc_o}(q)$ are the interference cross-terms of the outer and inner chains with the bilayer:

$$I_{sc_i}(q) = nA_bA_s \cdot \Delta\rho_{PEG}V_{PEG}2N_{PEG}(1 - f_{inner})$$

$$\cdot (N_{PEG}(1 - f_{inner}) - 1)$$

$$\cdot \left[\frac{1 - \exp\left[-(qR_g)^2\right]}{(qR_g)^2}\right] \cdot \left[\frac{\sin(q(R_{inner} - R_g))}{q(R_{inner} - R_g)}\right] \quad (22)$$

$$I_{sc_o}(q) = nA_bA_s \cdot \Delta\rho_{PEG}V_{PEG}2N_{PEG}f_{inner} \cdot (N_{PEG}f_{inner} - 1)$$

$$\cdot \left[\frac{1 - \exp\left[-(qR_g)^2\right]}{(qR_g)^2}\right] \cdot \left[\frac{\sin(q(R_{outer} - R_g))}{q(R_{outer} - R_g)}\right] \quad (23)$$

where A_{TS} and A_{FB} are the scattering amplitudes corresponding to scattering form factors $F_{TS}(q)$ and $F_{FB}(q)$ respectively.

3.4. Incorporation of the peptide contribution to the bilayer scattering

To be able to use the analytical scattering models to quantitatively describe the interaction between antimicrobial peptides and lipid vesicles, the described model for the liposomes was modified to account for the scattering of the peptide, either inserted in the membrane or as free chains. It was decided to introduce the peptide as an additional pseudo-parsing group across the bilayer (in comparison to parsing of the lipids into four groups as shown in Fig. 1) and model the volume probability of the peptide as an additional Gaussian function (eqn (10)). The integral under the curve was scaled by the total volume fraction of added peptides and the fraction of peptide bound to the liposomes, f_{bp}, in the following way

$$c_{pep} = \frac{V_p \cdot f_p \cdot f_{bp}}{A_L \cdot \sigma_p} \quad (24)$$

Further, to account for the changes in contrast as a result of the peptide potentially integrating into either the head-region, tail-region of the phospholipids or somewhere in the interface between the two areas of the bilayer, the difference in contrast is weighed by a fraction, f_{p_tail}, which gives the fraction of peptide in the tail region

$$\Delta\rho_p(z) = f_{p\_tail} \cdot (\rho_p - \rho_{CH_2}) + (1 - f_{p\_tail}) \cdot (\rho_p - \rho_w) \quad (25)$$

where $\rho(p)$, $\rho(CH_2)$ and $\rho(w)$ are the SLDs of the peptide, methylene groups, and water, respectively.

The f_{p_tail} is expressed as the integral of the overlap of the peptide Gaussian function with the half period squared sine/cosine function expressing the volume probability of the HC groups in the following way

$$f_{p_{tail}} = \frac{\int_{z_{inter}}^{z_{CH2} + \sigma_{CH2}} P_{HC}dz + \int_{Z_p - 5\sigma_p}^{z_{inter}} P_p dz}{\int P_p dz} \quad (26)$$

where z_{inter} is the intersect between the two overlapping curves found numerically by the Brent–Dekker method[49] and P_{HC} is the function described in eqn (11). P_p is the Gaussian function expressing the volume distribution of the peptide (details are given in ESI†).

The form factor for the flat bilayer including the peptides is

$$\left|P_{FB_{pep}}(q)\right|$$

$$= \int_{-D_i}^{D_o} \Delta\rho(z)e^{iqz}dz \quad (27)$$

$$= \sqrt{\left(\left(F_{cos,lipid} + F_{cos,peptid}\right)^2 + \left(F_{sin,lipid} + F_{sin,peptid}\right)^2\right)}$$

where

$$F_{cos,peptide} = \left|c_{pep}\sigma_p\Delta\rho_p\cos(qz_p) \cdot \exp\left[\frac{(q\sigma_p)^2}{2}\right]\right| \quad (28)$$

and

$$F_{sin,peptide} = \left|c_{pep}\sigma_p\Delta\rho_p\sin(qz_p) \cdot \exp\left[\frac{(q\sigma_p)^2}{2}\right]\right| \quad (29)$$

To account for potential free peptide chains that are not bound to vesicles, an additional term was added to the model

$$I_{fp}(q) = \varphi \cdot (1 - f_{bp}) \cdot \Delta\rho_p{}^2 \cdot V_p \cdot P_{chain}(q) \quad (30)$$

where φ is the total volume fraction and $P(q)_{chain}$ is the form factor of a Gaussian chain expressed by the Debye formula[50] given in eqn (2).

The full expression for the intensity, including peptide in the bilayer, the PEGylation, and the free peptide chains is then

$$I = n((P_{TS}(q))^2 (P_{FB_{pep}}(q))^2 + I_{chain}(q) + I_{c_i c_i}(q)$$
$$+ I_{c_i c_o}(q) + I_{c_o c_o}(q) + I_{sc_i}(q) + I_{sc_o}(q)) + I_{fp}(q) \qquad (31)$$

In the fit analysis, we allowed the concentration to vary slightly due to uncertainties in the determination of the exact value during the sample preparation.

4. Results and discussion

Structure and conformation of indolicidin in solution

The chemical structure of the antimicrobial peptide indolicidin is displayed in Fig. 2(A) together with the amino acid sequence. Fig. 2(B) shows the obtained SAXS scattering data from indolicidin in Tris buffer at 37 °C at different concentrations together with the fits of the model described in Section 3.1. At intermediate to high q we observe the typical polymer-like scattering which can be accurately described with the Debye function for random Gaussian chains (eqn (2)). At all concentrations we see an upturn at low q that can be described by a power-law, q^{-x}, with $x \approx 2$. This indicates formation of some large extended or plate-like structures. Interestingly, these structures are still present for the whole concentration range of 5–0.65 mg mL^{-1}. In addition, as shown in the inset, the larger structures are not broken up at higher temperatures, persisting at temperatures up to 45 °C.

More quantitatively, the data can be described using scattering expressions for single polymer-like chains with a contribution from aggregated peptide filaments as described in Section 3.1. The result from the fit analysis indicates that the peptides predominantly form disordered polymer-like structures, but that there is also a small amount (about 1 percent) of filament sheet peptide structures.

Although it is difficult to extract accurate structural information on the presumably heterogeneous and large structures, we obtain an apparent width of around 450–1500 Å depending on the concentration, and a thickness of about 90–100 Å. The length is about 700 Å at the lowest concentration, increasing to a value above the visible size in the measured q range (less than 4000 Å) for the other concentrations. For the free peptide chains, we obtain a radius of gyration of about 12 Å.

Based on circular dichroism (CD) experiments,[6] indolicidin was found to adopt a random coil conformation without any secondary structure. Our data confirm the existence of 99 percent largely disordered peptide chains but also show that a small amount of the peptide assembles into filament sheet structures. This structure has been also observed for synthetic antimicrobial peptides in the past.[51]

Structural SAXS characterization of vesicles with varying charge densities

In order to investigate the detailed nanostructure of the membrane system, including the segmental distribution in the bilayer, we proceed to a detailed joint SAXS and SANS analysis of the vesicles. The SAXS and SANS data on liposomes of the same composition used for a joint fit analysis are shown in Fig. 3A. In order to increase the accuracy of the fits, the SANS and SAXS data were simultaneously analysed using the previously described fit model yielding excellent agreement. SAXS data for the liposomes with increasing amount of negatively charged lipids (DMPG) are presented in Fig. 3B together with the corresponding fits, as well as the SANS data obtained with "full contrast" of hydrogenated lipids in D$_2$O. The data resemble the typical scattering for vesicles, with strong scattering at low q where the overall size of the liposomes and the polydispersity can be extracted. For the SAXS data, a rather pronounced minimum is visible at intermediate q; this minimum is highly sensitive to the negative contrast, *i.e.* lower electron density than water, of the lipid tails and positive contrast (higher electron density) of the headgroups. The minimum is rather shallow, indicating an asymmetry in the bilayer which is confirmed through the fit
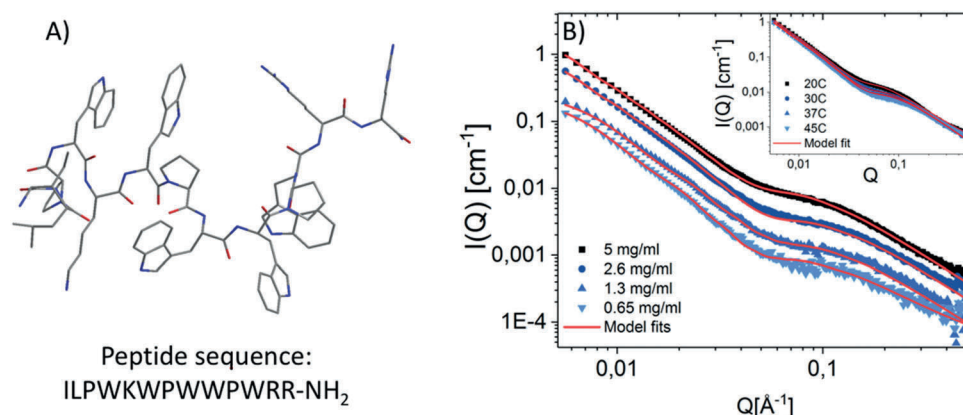

Fig. 2 (A) Chemical structure of indolicidin, cationic antimicrobial peptide from bovine, with the amino acid sequence below. (B) Scattering data of indolicidin with altering concentration and model fit. Results indicate predominantly free unstructured peptide chains with a small fraction of sheet like filaments. Inset graph shows how the enlarged structures cannot be broken up with increasing temperature to 45 °C (concentration shown is 5 mg mL^{-1}).
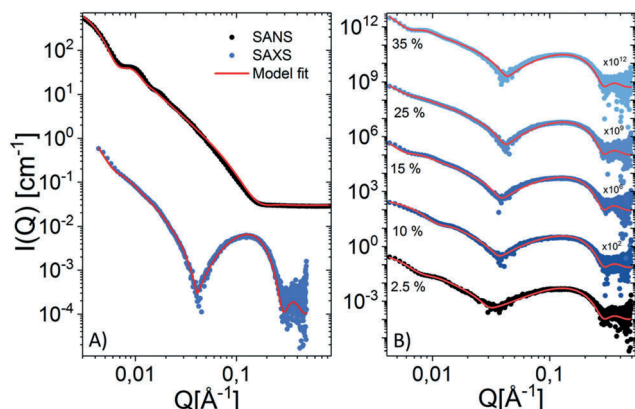
Fig. 3 (A) SANS and SAXS data for 25% DMPG liposomes and the result of a simultaneous model fit analysis of the data (different batches of liposomes but same composition and preparation). (B) Scaled SAXS data for DMPC–DMPG–(DMPE-PEG) liposomes with altering amounts of negative charge (DMPG) along with fit model (red line).

analysis; this analysis did not provide accurate fits using symmetrical bilayers (see Fig. S1 in the ESI†). This slight asymmetry is displayed in the calculated volume probability plot presented in Fig. 4A. It shows that the CG and HG groups on the outer leaflet have a slightly longer distance from the hydrocarbon chain than they have on the inner leaflet. The asymmetry can be explained by an interplay between the electrostatic interactions and curvature[38] caused by the charged phospholipids as well as changes caused by the PEG chains connected to the surface of the outer and inner leaflet of the bilayer. At higher q, we see a pronounced maximum which provides the detailed bilayer structure. From the joint fits we obtain both the volume probability functions, depicted in Fig. 4A, as well as the corresponding electron density profiles across the bilayer, depicted in Fig. 4B.

As seen in Table S1 in the ESI,† although the size and polydispersity vary slightly from batch to batch, the structure of the bilayer itself is not affected by increasing the amount of negatively charged lipids, most likely because DMPC and DMPG are of similar sizes. This is clearly visible from the electron density plot presented in Fig. 4A, where the curve overlaps. As seen from

the table, the major change with increasing amount of DMPG compared to DMPC in the liposomes is the systematic decrease in the average volume of the HG group. This is in good agreement with previously reported MD simulations of the headgroup volume which show that the volume of DMPG is lower than for DMPC.

The structural fit parameters are generally in very good agreement with previously reported data for the same lipids, but the σ_{HG} is slightly higher than reported for DMPC liposomes in the past.[52] This could be explained by the introduction of the covalently bound PEG group to the outer headgroup of some of these lipids. The fit for the bilayer is shown to be reliable by its ability to fit all five systems with the same structural parameters, providing us a solid starting point for quantitative analysis of the bilayer's interaction with peptides.

Interaction between indolicidin and model membranes

Differential scanning calorimetry (DSC). The interactions between indolicidin and model lipid membranes were first probed using differential scanning calorimetry (DSC). Fig. 5 shows the effect of indolicidin on the thermal behaviour of liposomes with the typical lipid mixture of 90 mol% DMPC, 7.5% DMPG and 2.5% DMPE-PEG. As seen in the figure, the addition of the peptide has a significant effect on the heat capacity, C_p, which displays a significant shift and broadening of the peak as compared to the neat lipid vesicles, where the melting peak is relatively sharp corresponding to a $T_m = 24.2\ °C$. The melting temperature is progressively decreasing with the amount of peptide added with a concomitant increase in the width of the melting transition. The shift in the peak indicates an intercalation of the peptide in the membrane tail region or displacement of the lipid head groups, which affects the packing of the phospholipid tails in the bilayer. The latter was also found in reference[53] where indolicidin was directly incorporated into DMPC and DMPG lipids in organic solvents during the sample preparation. In contrast, we chose to mix the extruded lipid vesicles and peptide in the buffer directly before conducting the experiment to mimic the biological situation where antimicrobial peptides are introduced to bacteria.
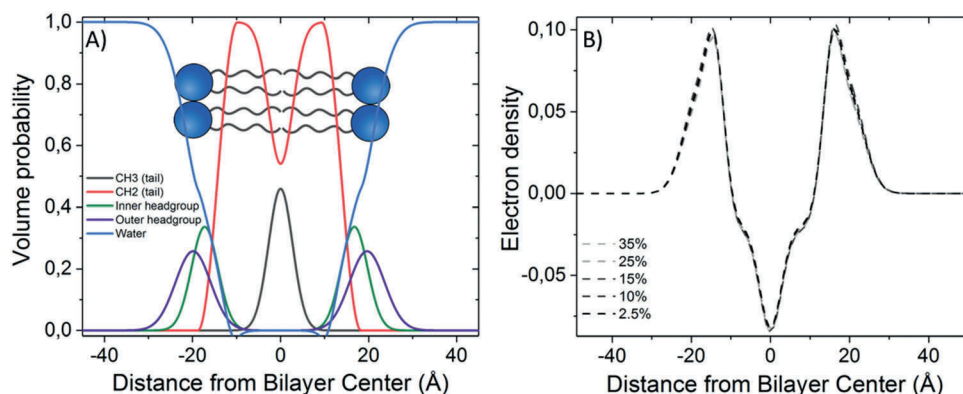

Fig. 4 (A) Illustration of the volume probability distribution for an asymmetric bilayer, 25 mol% negatively charged liposomes as an example. (B) Electron density distribution profile for liposomes with altering amount of negatively charged phospholipids showing that they overlap.
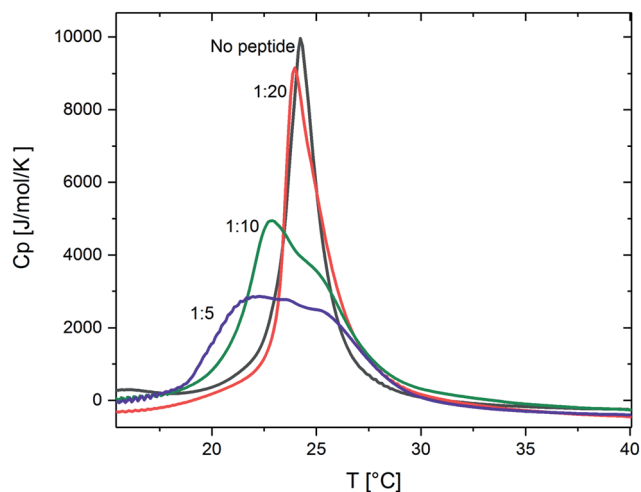
Fig. 5 DSC heating scans illustrating the effect of indolicidin on the thermal phase behaviour of DMPC–DCPG–DMPE-PEG lipid vesicles. The peptide : lipid ratios are indicated and the measurement of the pure lipids is included for reference.

Table 1 The estimated melting temperature (T_m) and the enthalpy of the transition (ΔH) for each peak. For the 1 : 10 and 1 : 5 ratios a range from the first to the last maximum of the overlapping peaks is provided

Sample	T_m (°C)	ΔH (kJ mol^{-1})
No peptide	24.2	33.5
1 : 20	23.9	34.2
1 : 10	23–25	34.6
1 : 5	22–25	31.8

The values for the melting temperatures (T_m) and the enthalpies (ΔH) are listed in Table 1.

Structural SAXS and SANS results: peptide–lipid interactions

The effect of adding indolicidin to the lipid membranes is qualitatively illustrated in Fig. 6 where the scattering curves of peptide–lipid mixtures is compared to the calculated average expected in the absence of interactions. The latter is obtained by averaging the scattered intensity of the individual unmixed solutions.

An interaction between the peptide and the lipid vesicles is clearly present since the scattering curves are different, in particular at low and intermediate q. Notably, the minimum in the intermediate q range is shifted. In order to determine these structural effects, the data were analysed using the detailed model described in Section 3.4.

The results from the fit analysis of X-ray scattering data from liposomes mixed with increasing amounts of indolicidin are shown in Fig. 7. From Fig. 7A we see that the joint fit analysis gives good agreement between the fitted model and the experimental SAXS and SANS data. As seen from the SANS data in Fig. 7, where the curves overlap at intermediate and high q (when not scaled), the insertion of the peptide in the bilayer cannot be resolved using SANS alone. The SAXS curves in Fig. 7(B and C), however, we clearly see that increasing amounts of peptide addition result in systematic shifts of the minima, showing the strength of using SAXS to describe the insertion of a substance into the bilayer.

The resultant fit parameters presented in Table 2 show that the insertion of the peptides changes the overall size and polydispersity of the vesicles; this is seen as a shift and smearing of the slight oscillations at low q in all the SAXS and SANS curves in Fig. 7. More interestingly, the fit analysis showed that the bilayer structure remains mostly intact upon exposure of moderate amounts of the peptide (up to 1 : 10 peptide–lipid ratios) leading to moderate changes in the volume probability curves shown in Fig. 7(A and B). For the peptide : lipid ratios of 1 : 10 and less, the shift in the experimental scattering curves could be accounted for by simply implementing the scattering contribution for the peptide. This is due to substantially larger electron density of the peptide compared to that of the lipid tails which thereby alters the contrast within the bilayer and the surrounding solvent. The change in electron density with increasing amount of indolicidin is visually illustrated by the electron density (ED) plots obtained from the fits in Fig. 8(C and D).

By quantitatively considering the change in the contrast, the detailed model fit analyses reveal that the structure of the bilayer remains essentially unaltered for moderate peptide additions. By increasing the peptide concentration up to a 1 : 5
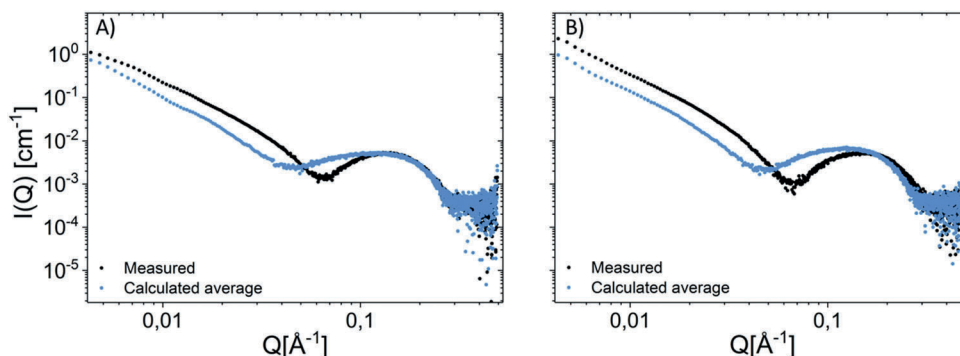

Fig. 6 Qualitative comparison of the measured data of 10 (A) and 25 (B) mol% negatively charged lipid vesicles mixed with indolicidin to the calculated average where the scattering from the liposomes and the peptide have been measured separately and summed together. The measured curves show clear shifts in the minimum at intermediate q indicating a significant interaction between the peptide and the liposomes.
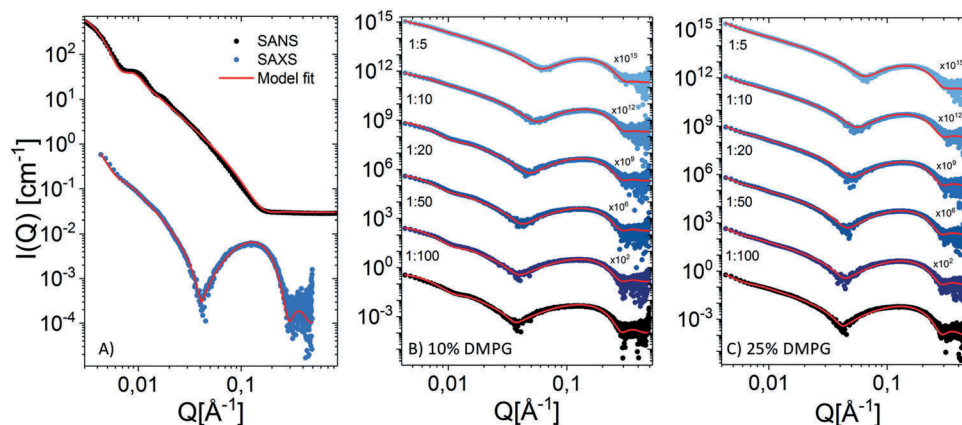
Fig. 7 (A) Simultaneous fit of SANS and SAXS data of 1:10 peptide addition (different batches of liposomes but with the same composition and preparation). (B and C) Scaled SAXS and SANS data for DMPC–DMPG–(DMPE-PEG) liposomes of differing amounts of negatively charged phospholipids with added peptide in an increasing peptide:lipid mol-ratios from 1:100 up to 1:5 along with fit model (red line). Liposomes in (B) have 10 mol% DMPG while liposomes in (C) have 25 mol% DMPG (latter matches amount of negative charge in *E. coli* bacteria).

Table 2 Important fit parameters from the analysis of liposomes with added indolicidin. Values outside of the experimental q-range noted with (−), and joint SAXS/SANS fits noted with §. The error of the fits is found to be less than 5%

	Liposomes with 10 mol% PG/PE					Liposomes with 25 mol% PG/PE				
Fraction peptide	1:100	1:50	1:20	1:10	1:5	1:100	1:50	1:20	1:10§	1:5
ULV radius [Å]	261	265	267	—	—	430	—	—	—	—
Bilayer thickness [Å]	38.8 ± 0.5	38.8 ± 0.5	38.8 ± 0.5	38.8 ± 0.5	37.9 ± 0.5	38.8 ± 0.5	38.8 ± 0.5	38.8 ± 0.5	38.8 ± 0.5	35.7 ± 0.5
$Z_{peptide}$ [Å]	12	9.2	9.2	9.7	9.7	14	13.7	12	12	9.6
$\sigma_{peptide}$ [Å]	3	3	3	3	3	3	3	3	3	3
f_{fp}	0	0	0	0	0.25	0	0	0	0	0.18
σ_{SD}	0.29	0.32	0.31	0.35	0.45	0.4	0.4	0.45	0.45	0.45

ratio, however, we observe that completely satisfactorily fits can no longer be obtained without a slight modification of the bilayer structure: reducing the thickness of hydrocarbon layer in the outer leaflet by 0.7 Å. Interestingly, this becomes more pronounced with increasing DMPG content, where we find a 3 Å reduction in the thickness. We should, however, keep in mind that these concentrations correspond to physiologically irrelevant values of about 100× the MIC (minimal inhibitory concentration).[6] Some degree of change in the thickness of the bilayer caused by the introduction of AMPs has also been found in other SAXS studies at higher peptide–lipid ratios.[24,26] Although membrane thinning has been proposed as an important mechanism of action for AMPs,[54] our data do not seem to support a significant detectable effect at the lowest concentrations, which are at more physiological relevant conditions. Nevertheless, the peptide interaction can be clearly detected at these low concentrations using SAXS.

From the volume probability plots in Fig. 8A and B we see that indolicidin seems to be located at the interface between the tail and head region of the outer leaflet of the membrane. While the quality of the fits is highly sensitive to the peak position of the peptide, indicating a strong preference to the lipid tail/head interface, it is less sensitive to the width of the peptide distribution. Nevertheless, with increasing amounts the peptide seems to be able to insert slightly deeper into the tail region of the bilayer, causing the shift of the Gaussian function representing the peptide group in the volume

probability plot as well as the ED curve towards lower z values. The insertion partly into the lipid tail region of the bilayer is supported by the thermal analysis presented above (Fig. 5), where the peptide was shown to lower the melting point and broaden the melting peak of the lipids, indicating significant alteration of the packing of the tails.

Contrast variation SANS: peptide-induced lateral segregation of lipids?

In order to further investigate the structure of the liposomes after peptide addition, SANS experiments with contrast variation were used to detect potential lateral segregation of lipids induced by the peptide. This experiment, complementary to SAXS which provides the radial distribution, tests the hypothesis that AMPs induce local clustering of anionic lipids due to the electrostatic charge neutralization, an effect which may play a role in their mode of action.[18] To this end, we designed the experiment based on the work by Heberle *et al.*[21] where DMPC lipids with perdeuterated tails were mixed with regular proteated DMPG lipids so that the average contrast of fully mixed tails matches that of the headgroup (SLD 2.01×10^{10} cm^{-2}). By placing these liposomes in a H_2O/D_2O buffer mixture which matches both the tails and head groups, a very low scattering signal is expected as the residual scattering only origins from the contrast between individual lipids as well as the PEG chains. If the anionic lipids would cluster together with the peptide and form
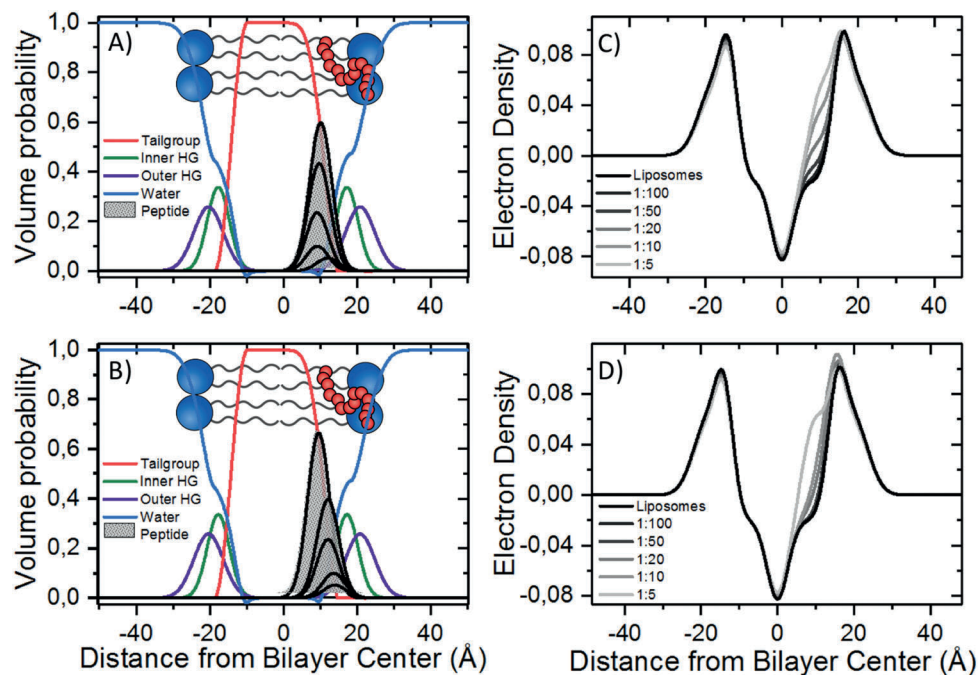
Fig. 8 Volume probability distribution for lipid membranes of (A) 10% and (B) 25% negatively charged lipids with increasing amount of indolicidin. The area of the Gaussian function of the peptide (grey coloured peaks) increases with increasing amounts of indolicidin added to the sample. Electron density profiles for the volume probabilities in (A) and (B) can be seen (C) and (D), respectively, showing that the addition of peptide increases the electron density in the outer bilayer leaflet.
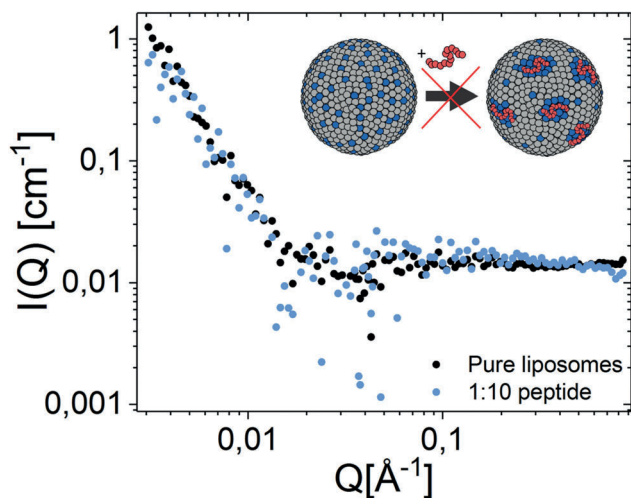

Fig. 9 Neutron scattering results for lipid vesicles with peptide at 37 °C. Contrast matched liposomes in D_2O/H_2O solvent show no lateral segregation of anionic lipids upon addition of the cationic peptide.

microdomains, a significant signal is expected at intermediate to high q. As seen in Fig. 9, however, the scattered signal remains very low upon addition of indolicidin. Similar results were obtained for various charge densities, temperatures and even upon replacing the anionic lipid with a shorter DLPG. From these limited data we conclude that both the peptides and the lipids are homogenously distributed in the vesicles and that indolicidin does not seem to promote any lateral segregation of the lipids in these model membranes. This agrees with the earlier observed tendency that

a substrate that changes the crystallinity of the membrane locally (for example cholesterol) has to be introduced to observe the formation of lipid domains.[21]

Structural insight into the mode of action of indolicidin

From the analysis of the data presented above, the structural interaction between indolicidin and the model lipid bilayers gives insight into a possible mode of action of the peptide. Although SAXS measurements of the pure peptide revealed some degree of clustering, indolicidin is predominantly disordered with a random coil formation. Hence, it seem likely that insertion of the peptide into the bilayer occurs without any higher order structures as implied in the barrel-stave or toroidal pore models.[54] This is consistent with our SAXS results of the peptide lipid mixtures, which do not provide evidence for any folding or significant structuring within the lipid bilayer, but rather an insertion primarily of the outer leaflet and a perturbation of the lipids in the outer region. Indolicidin remaining a random coil structure in the presence of membranes has also been seen from CD measurements *e.g.* by Falla T. J. *et al.*[6] The high tryptophan content of indolicidin and the presence of the partially charged and bulky indole side group provides a possible explanation of the preferred positioning in the outer leaflet, in close proximity to the lipid–water interface.[55] Our experimental data are consistent with the MD simulation study where indolicidin was found to be located in the outer leaflet resulting in a decrease in the ordering of the lipids.[11] In this study some degree of membrane thinning (at the most $\sim$4.1 Å) was observed, consistent with our results

at high peptide–lipid ratios. Interestingly, we observed the strongest effect in DMPG rich lipids, where the fraction of bound peptides is high (82% bound peptide compared to 75% for the lipids with less PG). This indicates that the positively charged indolicidin has a higher affinity for membranes with more negative charge. This is consistent with the MD simulations where the same effect was observed when comparing pure PC membranes with pure PG membranes.

The present work thus points towards a scenario where the lipids are disordered rather than forming a distinct "pore" or "channel" as is suggested in *e.g.* the "barrel-stave" model. Instead, our data support the "interfacial activity" picture presented by Wimley.[56] Here, it was suggested that the insertion of the peptide into the bilayer results in a change in the packing of the tails which leads to a disruption of the permeability barrier imposed by the hydrocarbon core in the membrane. This may cause leakage of polar solutes across the membrane resulting in lysis and death of bacteria cells. This is compatible with the present SAXS study, where the peptide partitions into the interfacial region between the head- and tail-groups in the outer leaflet, also reflected in the significant shift in the melting temperature from the DSC measurements. A simple illustration for the structure and distribution of indolicidin causing disordering of the packing of the lipids in the membrane within the bilayer of the ULV is given in Fig. 10.

The incorporation of 2.5 mol% PEGylated lipids in the preparation of the vesicles used in this study prevents peptide-induced fusion and aggregation of the vesicles and the formation of multi-lamellar vesicles observed in other studies.[28,29] This enables us to maintain the integrity of the vesicle which facilitates the study of single membrane bilayers and the interaction of the peptide in great detail using scattering methods. Although the joint fit analysis of SAXS and SANS data shows that the structure of the bilayer is largely unaffected by the introduction of indolicidin, the overall size of the lipid vesicles and the polydispersity is increased systematically with increasing peptide concentration without the observation of aggregation. This may be explained by an accelerated lipid exchange that leads to an Ostwald-type ripening process with an overall growth into larger vesicles that are energetically more favourable, as well as an accompanying increase in the overall size distribution (σ_{SD}). An increase in the lipid dynamics might be related to the mode of action of the peptide as this could affect the transport of ions over the membrane[14] but further studies are needed in order to make any concluding statement.

5. Conclusion and outlook

In this work, we have developed a methodology using SAXS and SANS to investigate the structural interaction between antimicrobial peptides and lipid model membranes in detail. Our data suggest that indolicidin, a natural occurring antimicrobial peptide, forms predominantly random coil structures in solution, although a slight tendency (about 1%) to form larger plate-like structures was found. By using a minor fraction of PEGylated DMPE lipids we show that we can form unilamellar DMPC/DMPG vesicles that are stable towards aggregation upon interactions with the peptide for a large tuneable range of anionic charge densities. This allows us to carefully *in situ* characterize the structural aspects of the peptide–lipid interactions in model membranes that mimic cytoplasmic bacterial cells *in situ* in dilute solutions without resorting to any bilayer support that may perturb the membrane. Moreover, by modifying a theoretical model to take into account the scattering contribution from both the peptide and lipid membrane components, we are able to determine both the bilayer structure as well as the location and distribution of the peptide within the lipid bilayer. By using these techniques, we have shown how indolicidin inserts in the outer leaflet of lipid vesicles, positioning at the interface between the lipid headgroups and the lipid tail region. The insertion of indolicidin into this region of the bilayer affects the packing of the lipid tails in the membrane, resulting in a change in the melting temperature as seen from DSC measurements and increased lipid exchange seen as a growth in size from SANS and SAXS. Interestingly, we only observe significant changes in the bilayer structure above physiologically relevant concentrations corresponding to 100× MIC (1 : 5 peptide–lipid ratio). The results support the "interfacial activity" scenario presented by Wimley[56] over other frequently presented mechanisms involving pore formation in the membrane caused by distinct channels of highly structured peptides. Additionally, by using SANS we have shown that the anionic lipids are homogenously distributed among the zwitterionic lipids without any detectable clustering around the cationic peptide as it inserts into the membrane.

In summary, we have developed a convenient approach to accurately determine the structural interaction between peptide, or other surface-active molecules, and lipid vesicles. This may provide valuable insight into the structural aspects related to the mode of action of peptides complementary to other methods based on *e.g.* NMR, fluorescence and AFM, where the relevant structural length scales are missing. Furthermore, the methodology presented is versatile and is not limited to antimicrobial peptides but can also easily be applied to other lipids, as well as other peptide or surface-active (bio)molecules.
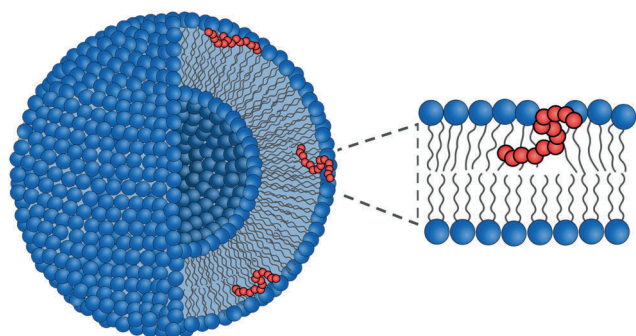

Fig. 10 Illustration of the structure of indolicidin as it inserts into the outer leaflet of the membrane, locally changing the packing of the lipid tails.

Conflicts of interest

There are no conflicts to declare.

Acknowledgements

References

1 World Health Organization, Antibiotic resistance, accessed 21 Sep, 2017.

2 C. D. Fjell, J. A. Hiss, R. E. W. Hancock and G. Schneider, *Nat. Rev. Drug Discovery*, 2011, **11**, 37–51.

3 M. Zasloff, *Nature*, 2002, **415**, 389–395.

4 Y. Shai and Z. Oren, *J. Biol. Chem.*, 1996, **271**, 7305–7308.

5 R. E. W. Hancock and G. Diamond, *Trends Microbiol.*, 2000, **8**, 402–410.

6 T. J. Falla, D. N. Karunaratne and R. E. Hancock, *J. Biol. Chem.*, 1996, **271**, 19298–19303.

7 M. E. Selsted, M. J. Novotny, W. L. Morris, Y.-Q. Tang, W. Smith and J. S. Cullor, *J. Biol. Chem.*, 1992, **267**, 4292–4295.

8 I. Ahmad, W. R. Perkins, D. M. Lupan, M. E. Selsted and A. S. Janoff, *Biochim. Biophys. Acta, Biomembr.*, 1995, **1237**, 109–114.

9 A. Rozek, C. L. Friedrich and R. E. Hancock, *Biochemistry*, 2000, **39**, 15765–15774.

10 K. A. Brogden, *Nat. Rev. Microbiol.*, 2005, **3**, 238–250.

11 J. C. Hsu and C. M. Yip, *Biophys. J.*, 2007, **92**, L100–L102.

12 C. Neale, J. C. Hsu, C. M. Yip and R. Pomes, *Biophys. J.*, 2014, **106**, L29–L31.

13 H. Khandelia and Y. N. Kaznessis, *J. Phys. Chem. B*, 2007, **111**, 242–250.

14 T. I. Rokitskaya, N. I. Kolodkin, E. A. Kotova and Y. N. Antonenko, *Biochim. Biophys. Acta, Biomembr.*, 2011, **1808**, 91–97.

15 T. K. Lind, L. Darre, C. Domene, Z. Urbanczyk-Lipkowska, M. Cárdenas and H. Wacklin, *Biochim. Biophys. Acta, Biomembr.*, 2015, **1848**, 2075–2084.

16 T. K. Lind, P. Zielinska, H. P. Wacklin, Z. Urbanczyk-Lipkowska and M. Cárdenas, *ACS Nano*, 2013, **8**, 396–408.

17 M. Eeman and M. Deleu, *Biotechnol., Agron., Soc. Environ.*, 2010, **14**, 719.

18 R. M. Epand and R. F. Epand, *Biochim. Biophys. Acta, Biomembr.*, 2009, **1788**, 289–294.

19 S. Qian and W. T. Heller, *J. Phys. Chem. B*, 2011, **115**, 9831–9837.

20 D. K. Rai and S. Qian, *Sci. Rep.*, 2017, **7**, 3719.

21 F. A. Heberle, R. S. Petruzielo, J. Pan, P. Drazba, N. Kučerka, R. F. Standaert, G. W. Feigenson and J. Katsaras, *J. Am. Chem. Soc.*, 2013, **135**, 6853–6859.

22 M. C. Woodle and D. D. Lasic, *Biochim. Biophys. Acta, Rev. Biomembr.*, 1992, **1113**, 171–199.

23 F. A. Heberle, J. Pan, R. F. Standaert, P. Drazba, N. Kučerka and J. Katsaras, *Eur. Biophys. J.*, 2012, **41**, 875–890.

24 E. Sevcsik, G. Pabst, W. Richter, S. Danner, H. Amenitsch and K. Lohner, *Biophys. J.*, 2008, **94**, 4688–4699.

25 E. Sevcsik, G. Pabst, A. Jilek and K. Lohner, *Biochim. Biophys. Acta, Biomembr.*, 2007, **1768**, 2586–2595.

26 G. Pabst, S. L. Grage, S. Danner-Pongratz, W. Jing, A. S. Ulrich, A. Watts, K. Lohner and A. Hickel, *Biophys. J.*, 2008, **95**, 5779–5788.

27 A. Dehsorkhi, V. Castelletto, I. W. Hamley, J. Seitsonen and J. Ruokolainen, *Langmuir*, 2013, **29**, 14246–14253.

28 V. Castelletto, R. H. Barnes, K.-A. Karatzas, C. J. Edwards-Gayle, F. Greco, I. W. Hamley, R. Rambo, J. Seitsonen and J. Ruokolainen, *Biomacromolecules*, 2018, **19**, 2782–2794.

29 V. Castelletto, R. H. Barnes, K.-A. Karatzas, C. J. Edwards-Gayle, F. Greco, I. W. Hamley, J. Seitsonen and J. Ruokolainen, *Langmuir*, 2018, DOI: 10.1021/acs.langmuir.8b01014.

30 J. Pan, D. P. Tieleman, J. F. Nagle, N. Kučerka and S. Tristram-Nagle, *Biochim. Biophys. Acta, Biomembr.*, 2009, **1788**, 1387–1397.

31 P. Pernot, A. Round, R. Barrett, A. De Maria Antolinos, A. Gobbo, E. Gordon, J. Huet, J. Kieffer, M. Lentini and M. Mattenet, *J. Synchrotron Rad.*, 2013, **20**, 660–664.

32 A. Round, F. Felisaz, L. Fodinger, A. Gobbo, J. Huet, C. Villard, C. E. Blanchet, P. Pernot, S. McSweeney and M. Roessle, *Acta Crystallogr., Sect. D: Biol. Crystallogr.*, 2015, **71**, 67–75.

33 A. De Maria Antolinos, P. Pernot, M. E. Brennich, J. Kieffer, M. W. Bowler, S. Delageniere, S. Ohlsson, S. Malbet Monaco, A. Ashton and D. Franke, *Acta Crystallogr., Sect. D: Biol. Crystallogr.*, 2015, **71**, 76–85.

34 G. W. Lynn, W. Heller, V. Urban, G. Wignall, K. Weiss and D. A. Myles, *Physica B*, 2006, **385**, 880–882.

35 B. Eicher, F. A. Heberle, D. Marquardt, G. N. Rechberger, J. Katsaras and G. Pabst, *J. Appl. Crystallogr.*, 2017, **50**, 419–429.

36 J. B. Klauda, N. Kučerka, B. R. Brooks, R. W. Pastor and J. F. Nagle, *Biophys. J.*, 2006, **90**, 2796–2807.

37 N. Kučerka, J. F. Nagle, J. N. Sachs, S. E. Feller, J. Pencer, A. Jackson and J. Katsaras, *Biophys. J.*, 2008, **95**, 2356–2367.

38 N. Kucerka, J. Pencer, J. N. Sachs, J. F. Nagle and J. Katsaras, *Langmuir*, 2007, **23**, 1292–1299.

39 J. Pencer, S. Krueger, C. P. Adams and J. Katsaras, *J. Appl. Crystallogr.*, 2006, **39**, 293–303.

40 M. Kiselev, P. Lesieur, A. Kisselev, D. Lombardo and V. Aksenov, *Appl. Phys. A: Mater. Sci. Process.*, 2002, **74**, s1654–s1656.

41 M. R. Brzustowicz and A. T. Brunger, *J. Appl. Crystallogr.*, 2005, **38**, 126–131.

42 N. Kučerka, M.-P. Nieh and J. Katsaras, *Biochim. Biophys. Acta, Biomembr.*, 2011, **1808**, 2761–2771.

43 J. Pan, F. A. Heberle, S. Tristram-Nagle, M. Szymanski, M. Koepfinger, J. Katsaras and N. Kučerka, *Biochim. Biophys. Acta, Biomembr.*, 2012, **1818**, 2135–2148.

44 N. Kučerka, B. van Oosten, J. Pan, F. A. Heberle, T. A. Harroun and J. Katsaras, *J. Phys. Chem. B*, 2014, **119**, 1947–1956.

45 J. S. Pedersen, D. Posselt and K. Mortensen, *J. Appl. Crystallogr.*, 1990, **23**, 321–333.

46 L. Arleth and C. Vermehren, *J. Appl. Crystallogr.*, 2010, **43**, 1084–1091.

47 J. S. Pedersen and M. C. Gerstenberg, *Macromolecules*, 1996, **29**, 1363–1365.

48 L. Arleth, B. Ashok, H. Onyuksel, P. Thiyagarajan, J. Jacob and R. P. Hjelm, *Langmuir*, 2005, **21**, 3279–3290.

49 R. P. Brent, *Comput. J.*, 1971, **14**, 422–425.

50 P. Debye, *J. Chem. Phys.*, 1946, **14**, 636–639.

51 D. Xu, L. Jiang, A. Singh, D. Dustin, M. Yang, L. Liu, R. Lund, T. J. Sellati and H. Dong, *Chem. Commun.*, 2015, **51**, 1289–1292.

52 N. Kučerka, Y. Liu, N. Chu, H. I. Petrache, S. Tristram-Nagle and J. F. Nagle, *Biophys. J.*, 2005, **88**, 2626–2637.

53 V. V. Andrushchenko, H. J. Vogel and E. J. Prenner, *Biochim. Biophys. Acta, Biomembr.*, 2007, **1768**, 2447–2458.

54 L. T. Nguyen, E. F. Haney and H. J. Vogel, *Trends Biotechnol.*, 2011, **29**, 464–472.

55 W.-M. Yau, W. C. Wimley, K. Gawrisch and S. H. White, *Biochemistry*, 1998, **37**, 14713–14718.

56 W. C. Wimley, *ACS Chem. Biol.*, 2010, **5**, 905–917.

Resolving the Structural Interactions between Antimicrobial Peptides and Lipid Membranes using Small-angle Scattering Methods: the case of Indolicidin

Josefine Eilsø Nielsen[1], Victoria Ariel Bjørnestad[1] and Reidar Lund*[1]

[1]Department of Chemistry, University of Oslo, 0315 Oslo, Norway

Corresponding author: reidar.lund@kjemi.uio.no

1. Form Factor of asymmetric flat lipid bilayer:

The form factor for asymmetric flat lipid bilayers is given by

$$
\begin{aligned}
F_{cos}(q) = \Delta\rho_{HG} &\left(c_{HG_i}\sigma_{HG_i}\cos(qz_{HG_i}) \cdot exp\left[-\frac{(q\sigma_{HG_i})^2}{2}\right] \right. \\
&\left. + c_{HG_o}\sigma_{HG_o}\cos(qz_{HG_o}) \cdot exp\left[-\frac{(q\sigma_{HG_o})^2}{2}\right] \right) \\
+ \Delta\rho_{CG} &\left(c_{CG_i}\sigma_{CG_i}\cos(qz_{CG_i}) \cdot exp\left[-\frac{(q\sigma_{CG_i})^2}{2}\right] \right. \\
&\left. + c_{CG_o}\sigma_{CG_o}\cos(qz_{CG_o}) \cdot exp\left[-\frac{(q\sigma_{CG_o})^2}{2}\right] \right) \\
+ &\frac{\pi^2\Delta\rho_{MN}\cos(q\sigma_{MN_i})\sin(qz_{MN_i})}{-\pi^2 q + 4q^3\sigma_{MN_i}^2} \\
+ (-1)&\frac{\pi^2\Delta\rho_{MN}\cos(q\sigma_{MN_o})\sin(qz_{MN_o})}{-\pi^2 q + 4q^3\sigma_{MN_o}^2} + 2\Delta\rho_M c_M \sigma_M \cos(qz_M) \\
\cdot &exp\left[-\frac{(q\sigma_M)^2}{2}\right] - 2\Delta\rho_{MN}c_M\sigma_M\cos(qz_M) \cdot exp\left[-\frac{(q\sigma_M)^2}{2}\right]
\end{aligned}
\tag{S1}
$$

$$F_{sin}(q) = \Delta\rho_{HG}\left(c_{HG_i}\sigma_{HG_i}\sin(qz_{HG_i})\cdot exp\left[-\frac{(q\sigma_{HG_i})^2}{2}\right]\right.$$

$$\left.+\ c_{HG_o}\sigma_{HG_o}\sin(qz_{HG_o})\cdot exp\left[-\frac{(q\sigma_{HG_o})^2}{2}\right]\right)$$

$$+\ \Delta\rho_{CG}\left(c_{CG_i}\sigma_{CG_i}\sin(qz_{CG_i})\cdot exp\left[-\frac{(q\sigma_{CG_i})^2}{2}\right]\right.$$

$$\left.+\ c_{CG_o}\sigma_{CG_o}\sin(qz_{CG_o})\cdot exp\left[-\frac{(q\sigma_{CG_o})^2}{2}\right]\right)+q^{-1}\Delta\rho_{MN}\left[1\right.$$

$$\left.-\ \frac{\pi^2\cos(q\sigma_{MN_i})\cos(qz_{MN_i})}{-\pi^2-4q^3\sigma_{MN_i}^2}\right]$$

$$+\ (-1)q^{-1}\Delta\rho_{MN}\left[1-\frac{\pi^2\cos(q\sigma_{MN_o})\cos(qz_{MN_o})}{-\pi^2-4q^3\sigma_{MN_o}^2}\right] \tag{S2}$$

where σ_n and z_n are the width and position of the distribution respectively and $c_n = V_n/(A_L\sigma_n)$. V_n is the volume of the group n and A_L is the area per lipid, which is equal to the integrated area under the curve (n = HG (inner and outer), CG (inner and outer) , MN (inner and outer) and M).

2. Calculation of fraction of peptides in hydrocarbon tail region:

The integrals in equation 30 used to find the area of the overlap of the peptide Gaussian function and the hydrocarbon Gaussian function were derived to be the following:

$$\int_{z_p-5\sigma_p}^{z_{inter}}P_p = -\frac{c_p}{2}\sigma_p\,\text{erf}\left(\frac{z_p-z_{inter}}{\sqrt{2}\sigma_p}\right)+\frac{c_p}{2}\sigma_p\,\text{erf}\left(\frac{5\sigma_p}{\sqrt{2}\sigma_p}\right) \tag{S3}$$

$$\int_{z_{inter}}^{z_{MN_o}+\sigma_{MN_o}}P_{HC}$$

$$=\frac{2\big(K_1(z_{MN_o}+\sigma_{MN_o})+K_2\big)+\sin\big(2\big(K_1(z_{MN_o}+\sigma_{MN_o})+K_2\big)\big)}{4K_1}$$

$$-\frac{2(K_1z_{inter}+K_2)+\sin\big(2(K_1z_{inter}+K_2)\big)}{4K_1} \tag{S4}$$

where the two constants are defined as

$$K_1 = \pi/4\sigma_{MN_o} \tag{S5}$$

and

$$K_2 = \pi(-z_{MN_o}+\sigma_{MN_o})/(4\sigma_{MN_o}) \tag{S6}$$

3. Fit parameters for neat liposomes with altering charge density:

Amount of negative lipids	2.5%	10%	15%	25%[§]	35%
Radius	*350*	*262*	*455*	*450*	*470*
Area	*60.4**				
z_{CH3}	*0**				
z_{CH2o}	*14.1 $\pm$ 0.2***				
z_{CH2i}	*-13.8 $\pm$ 0.2***				
z_{CGo}	*16.1 $\pm$ 0.4***				
z_{CGi}	*-15.7 $\pm$ 0.4***				
z_{HGo}	*19.5 $\pm$ 0.2***				
z_{HGi}	*-19.3 $\pm$ 0.2***				
σ_{CH3}	*2.3**				
σ_{CH2}	*4.9 $\pm$ 0.3*				
σ_{CG}	*2 $\pm$ 0.2*				
σ_{HG}	*4.1 $\pm$ 0.5*				
DB	*38.8*				
DC	*11.7*				
VL	*1123*	*1106*	*1105*	*1099*	*1098*
V_{CH2}	*24.5*	*24.4*	*24.6*	*24.4*	*24.4*
V_{CG}	*153**				
V_{HG}	*176*	*165*	*158*	*157*	*155*
Rg PEG	*15**				
dcorr	*-10*	*-12*	*-8.2*	*-8.6*	*-11*
σ_{SD}	0.3	0.3	0.33	0.35	0.24

Table S1 Fit parameters for liposomes with altering amount of negatively charged liposomes as indicated in the table. Hard constrained parameters are designated by * and soft constrained by limits in fitting regime indicated by **. The units for all numbers carry the appropriate power of Å. §For this sample a joint fit analysis of SAXS and SANS data was performed.
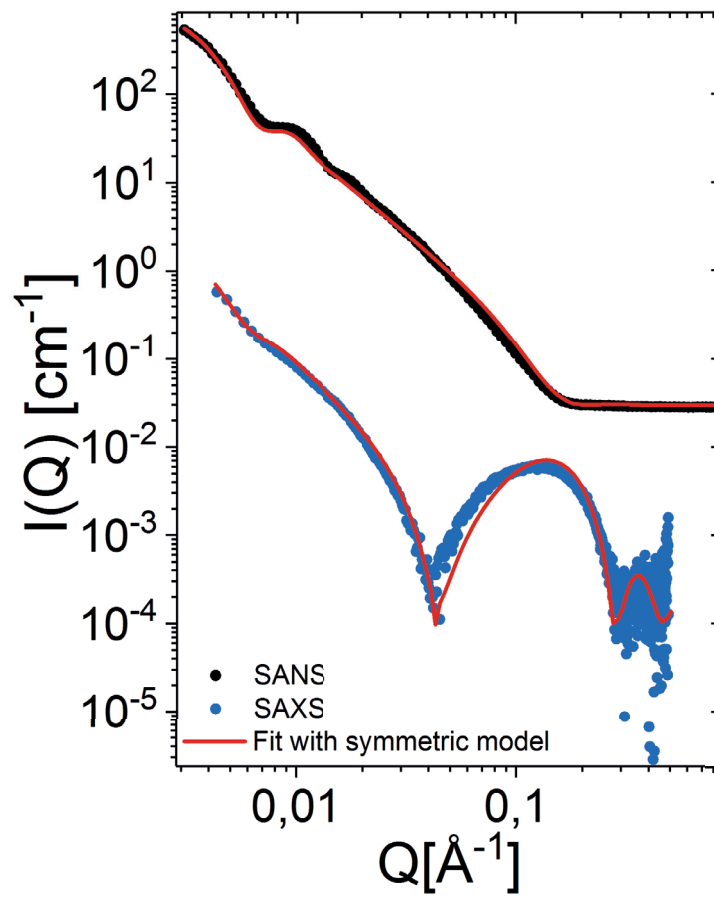
4. Fit with symmetric model:

Figure S2 Neutron and x-ray scattering plot for DMPC-DMPG 25 % liposomes and the joint fit using a symmetric bilayer model. As seen from the figure the symmetric bilayer model has a deeper minimum at intermediate q than the experimental data, therefor slight asymmetry was introduced.
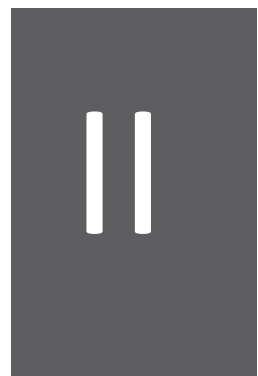
Paper II

A biophysical study of the interactions between the antimicrobial peptide indolicidin and lipid model systems

Josefine Eilsø Nielsen, Tania Kjellerup Lind, Abdullah Lone, Yuri Gerelli, Paul Robert Hansen, Håvard Jenssen, Marité Cárdenas and Reidar Lund

A biophysical study of the interactions between the antimicrobial peptide indolicidin and lipid model systems

Josefine Eilsø Nielsen[a], Tania Kjellerup Lind[b], Abdullah Lone[c], Yuri Gerelli[d],
Paul Robert Hansen[e], Håvard Jenssen[c], Marité Cárdenas[b], Reidar Lund[a,*]

[a] *Department of Chemistry, University of Oslo, 0315 Oslo, Norway*
[b] *Biofilms Research Center for Biointerfaces, Department of Biomedical Science, Health and Society, Malmö University, 20506 Malmö, Sweden*
[c] *Department of Science and Environment, Roskilde University, 4000 Roskilde, Denmark*
[d] *Institut Laue - Langevin, 38000 Grenoble, France*
[e] *Department of Drug Design and Pharmacology, University of Copenhagen, 2100 Copenhagen, Denmark*

A B S T R A C T

The naturally occurring peptide indolicidin from bovine neutrophils exhibits strong biological activity against a broad spectrum of microorganisms. This is believed to arise from selective interactions with the negatively charged cytoplasmic lipid membrane found in bacteria. We have investigated the peptide interaction with supported lipid model membranes using a combination of complementary surface sensitive techniques: neutron reflectometry (NR), atomic force microscopy (AFM), and quartz crystal microbalance with dissipation monitoring (QCM-D). The data are compared with small-angle X-ray scattering (SAXS) results obtained with lipid vesicle/peptide solutions. The peptide membrane interaction is shown to be significantly concentration dependent. At low concentrations, the peptide inserts at the outer leaflet in the interface between the headgroup and tail core. Insertion of the peptide results in a slight decrease in the lipid packing order of the bilayer, although not sufficient to cause membrane thinning. By increasing the indolicidin concentration well above the physiologically relevant conditions, a deeper penetration of the peptide into the bilayer and subsequent lipid removal take place, resulting in a slight membrane thinning. The results suggest that indolicidin induces lipid removal and that mixed indolicidin-lipid patches form on top of the supported lipid bilayers. Based on the work presented using model membranes, indolicidin seems to act through the interfacial activity model rather than through the formation of stable pores.

1. Introduction

Antimicrobial peptides (AMPs) show promising potential as future antibiotics with potent activity against a broad spectrum of pathogens. AMPs are part of the innate immune response found in all classes of life, including humans, animals, fungi, and bacteria. A wide range of AMPs extracted from different species found in nature have so far been studied for their potential as future antibiotics. The mode of action of antimicrobial peptides has extensively researched creating a consensus that membrane binding and membrane destabilization is a key function in the AMPs ability to kill bacteria [1–4]. Overcoming non-specific membrane destabilization would require a more profound redesign of the bacteria which is difficult to achieve through mutation and therefore AMPs have a significantly lower risk of developing resistance. Despite a great number of scientific studies, the precise molecular mechanism for the membrane interaction is not yet fully unveiled. This is mainly due to the experimental challenges in detecting the peptide insertion and associated small structural alterations within the membrane, in particular at physiologically relevant concentrations.

Scattering and imaging techniques, as small-angle X-ray/neutron scattering (SAXS/SANS) for solutions [5–24], neutron reflectometry (NR) for surfaces [25–32] and atomic force microscopy (AFM) [33,34] have been extensively used to study the structure of model lipid membranes. Moreover, the internal structure of living bacteria (including the cytoplasmic membrane) has been resolved using a combination of small and wide angle X-ray scattering [35]. With these methods, the interaction between peptides and model membrane can be investigated with high resolution in situ at low peptide concentrations. Lipid bilayers are often used as models of cellular membranes either in the form of free floating bilayers in solution or as supported lipid bilayers (SLBs) on solid surfaces. SLBs in combination with a set of surface sensitive techniques enable morphological, overall binding and detailed structural investigation of peptide interaction with model cellular membranes [32,36]. On the other hand, free floating lipid bilayers such as unilamellar lipid vesicles (ULVs) give complementary insight into the interaction between model membranes and AMPs that lack the unavoidable influence of the supporting substrate [5,6,23,24,37,38]. Despite its simplicity, the scattering signal from the bulk solution approach gives the orientational average structures. This complex system thus demands significant effort in theoretical modelling in real space to

extract detailed structural data from the experimental results. Here, we combine bulk scattering and surface scattering techniques to overcome the limitations of these techniques and exploit their complementarities.

Ideally to fully mimic the cell membrane of bacteria the lipid composition of the model membranes should include the natural lipids found in bacteria membranes, for example a lipid extract with mainly phosphatidylethanolamine (PE), phosphatidylglycerol (PG) lipids and cardiolipin in the case of the gram-negative bacteria *Escherichia coli*. However, simpler membrane mimics including pure lipids with known molecular volumes and chemical structure are necessary in order to extract detailed structural information from the scattering data. Conventionally, either pure phosphatidylcholine (PC) lipids or a combination of PC and PG lipids have been used as a substitute in formation of supported lipid bilayers as model membrane systems [25,27,29,33,39–44]. Recently, it was shown that stable SLBs can be formed with a combination of PE and PC lipids [45], although a preparation of model supported bilayers with both PE and negative charged PG lipids is to the authors' knowledge yet to be reported in literature. Therefore, in this study we use PC-PG lipids as a simple model bacterial membrane.

Most conventional AMPs are α-helical peptides, and these have been vastly studied using various scattering techniques and model membranes resulting in the proposal of several possible molecular modes of actions. The literature is quite extensive in this respect so we will briefly describe a few examples: Maculatin 1.1 (21 residues, net charge +3) was found to cause a slight thickening of the membrane and the peptide translocated through passive diffusion as measured by neutron reflectometry [46]. The shorter aurein 1.2 (13 residues, net charge +2), on the other hand, led to a slight degree of membrane thinning with the peptide being integrated into the lipid tail region rather than translocating across the membrane [25]. This led to the conclusion that aurein 1.2 acts via the carpet model. In the carpet model, the peptide initially binds to the lipid surface and covers the membrane as a carpet, which over time and upon increased peptide surface concentration results in disintegration of the membrane in a detergent like manner [1,25]. A study using grazing incidence diffraction (GID) on multilamellar lipid membranes on solid supports, demonstrates that magainin 2 (23 residues, net charge +5) adsorb to the bilayer at low peptide-lipid ratio, while translocation of the peptide occurred at higher amounts of peptide [39,47]. The peptide was also found to promote significant disordering in the lamellar stacking of the lipids in the membrane [42]. However interestingly, no experimental evidence for pore formation was found in this study [39] contrary to what has been reported in the past using neutron off-specular scattering [48]. A similar concentration dependency was also seen for alamethicin (20 residues, net charge −1) [49], which perturbs the membrane by causing non-lamellar lipid structures as observed by X-ray diffraction [50]. A combination of diffuse X-ray scattering at small and wide angles in stacked multi-layered membrane samples and NR of single lipid bilayers showed that the cyclic peptide colistin (11 residues, net charge +5) partitions deeper towards the hydrocarbon middle region of membranes mimicking the outer membrane of Gram negative bacteria [7]. As seen from the literature the proposed mechanism of AMPs does not only vary according to the conformational shape of the peptides, but can also be linked to the size of the peptide. Comparing synthetic peptides with varying size has indicated that smaller peptides are able to penetrate into the bilayer affecting the lipid phase and ordering [25,29], while larger sized peptides situated on the surface of the membrane [27]. The effect of peptide size, conformational shape and hydrophobicity needs to be further studied to get a better understanding of the impact on the mechanism of action.

Here, we systematically study the structural interaction between AMP, indolicidin (13 residues, net charge +4) extracted from bovine neutrophils, and model lipid membranes made of PC and PG lipids. Contrary to the peptides used in the studies mentioned above, indolicidin has been found to be largely unstructured in solution

[6,51,52] and retains a Gaussian chain structure with ~1% fibers as seen by SAXS [6]. Earlier studies suggest that addition of indolicidin results in local membrane thinning and solubilisation as determined by AFM [34], while partial insertion into the bilayer and removal of lipids at higher concentrations (≥5 μM) was suggested by quartz crystal microbalance with dissipation monitoring (QCM-D) [40]. However a recent SAXS study revealed that at physiologically relevant low peptide to lipid ratios, no significant perturbation of the lipid bilayer was detected [6]. In this work we will investigate these interactions in more detail using a multitude of experimental techniques with different structural resolution using the same model lipid membrane. This is achieved by comparing high resolution neutron and X-ray scattering techniques; NR and SAXS with AFM and QCM-D. Apart from comparing the methods and investigating the structural interactions of flat versus curved bilayers, this allows us to gain detailed insights into the lipid interaction of indolicidin. Indolicidin was chosen for this study because of its simple structure and small size enabling us to more straightforwardly model and deduce its interaction with membranes. Furthermore, indolicidin is one of the most studied natural AMPs. However, its lipid interaction has not previously been studied using neutron reflectometry. The data reveal that the peptide perturbs the lipid membrane without any clear pore formation as previously suggested [51], without causing significant thinning of the bilayers as observed for other small peptides [29,53].

2. Experimental section

2.1. Materials and sample preparation

Synthetic DMPC (1,2-dimyristoyl-sn-glycero-3-phosphocholine), DMPG (1,2-dimyristoyl-sn-glycero-3-phospho-(1′-rac-glycerol)), and DMPE-PEG(1,2-dimyristoyl-sn-glycero-3-phosphoethanolamine-N-[methoxy(polyethylene glycol)-2000]) were purchased from Avanti Polar Lipids and used as received without further purification. Lipid stocks were prepared in volume ratios of 1:3 methanol:chloroform and mixed in the correct proportions to give the same mass as the aimed final vesicle solution.

The SLBs for the NR, QCM-D and AFM experiments were created through fusion of tip sonicated vesicles as previously described [54]. In short, the lipid were dissolved in chloroform/methanol and mixed according to the desired molar ratio. The solvent was then removed under a stream of nitrogen, and the vials left in vacuum for at least 1 h. Lipid films were then kept at −20 °C until use. Immediately prior to the experiments, the lipid films were hydrated with MilliQ water to a concentration of 0.2 mg/ml and incubated for 1 h at 35 °C. The solution was then sonicated using a tip sonicator for 10 min on a 50% duty cycle (5 s on/off). The solution was mixed 1:1 with a 4 mM CaCl$_2$ solution immediately prior to formation of lipid bilayers. The lipid suspension in CaCl$_2$ was injected into the cell and left for approximately 10 min to equilibrate prior to extensive rinsing with buffer. In all the experiments, both the clean surface and the pristine lipid bilayer were fully characterized prior to peptide injection.

For preparation of 100 nm unilamellar liposomes for SAXS experiments, 2.5 mol% of DMPE-PEG was added in addition to DMPC and DMPG to sterically stabilize the liposomes against phase separation upon peptide addition. In the preparation, the organic solvent was removed completely under vacuum using a Heidolph rotary evaporator with a Vacuubrand vacuum pump. The resulting lipid film was hydrated with 50 mM tris(hydroxymethyl) aminomethane buffer (tris-buffer), pH 7.4, for at least 1 h at ~10 °C above the melting temperature of the lipid mixture (35 °C). After sonication for 10 min, the lipid dispersions were extruded through a 100 nm pore diameter polycarbonate filter (> 21 times) using an Avanti mini-extruder fitted with two 1 ml airtight syringes.

Indolicidin (ILPWKWPWWPWRR-CONH$_2$) was synthesized using standard 9-fluorenylmethyloxycarbonyl protecting group (Fmoc)

chemistry with 2-(1H-benzotriazol-1-yl)-1,1,3,3-tetramethyluronium hexafluorophosphate (HBTU) and *N*-Methylmorpholine (NMM) as coupling reagents on an automated peptide synthesizer (ResPep SL; Intavis Bioanalytical Instruments AG) in a 15 μmol scale in microcolumns using a 4-Methylbenzhydrylamine hydrochloride (MBHA) resin (0.65 mmol/g). After completion of the peptide chain, the peptide were cleaved from the resin using TFA:H$_2$O:TIS (95:2.5:2.5) for 2 × 1 h. Crude peptide was purified by preparative reverse-phase HPLC system consisting of Waters™ 600 Pump, In-line Degasser, 600 Controller and 2996 Photodiode Array Detector, the column used was a Waters™ XSelect® Peptide CSH C18 OBD™, 5 μm, 19 × 250 mm on an acetonitrile-water gradient. The peptide purity was determined by analytical reverse-phase High-performance liquid chromatography (HPLC) system consisting of Waters™ 717 plus Autosampler, In-line Degasser AF, 600 Controller and 2996 Photodiode Array Detector, the column used was a Waters™ Symmetry™ C18, 5 μm, 4.6 × 250 mm on an acetonitrile-water gradient. The peptide mass was determined using a Bruker Microflex™ (MALDI-TOF-Mass Spectrometry) (see Supplementary material).

2.2. Quartz crystal microbalance with dissipation monitoring

QCM-D experiments were performed using a Q-SENSE E4 system (Qsense, Biolin Scientific, Stockholm, Sweden) with 50 nm Qsense Silicon Oxide sensors. The fundamental frequency and six overtones (3rd, 5th, 7th, 9th, 11th and 13th) were recorded during the experiment. The instrument was set to equilibrate at 37 °C before performing any measurements. The lipids were prepared using the method described above in MilliQ water and injected using a peristaltic pump (Ismatec IPC-N 4) at a flow rate of 100 μL/min. After following the SLB formation (upon reaching a frequency of −24 Hz and dissipation close to 0), the remaining lipids in the cells were rinsed off with MilliQ. Upon stabilization of the baseline, the solvent was exchanged to tris-buffer and again left to stabilize under flow. The peptide was injected in the desired concentration dissolved in tris-buffer. The experiments were performed in duplicates to validate the results.

2.3. Neutron reflectometry

Neutron reflection (NR) measurements were performed using flow-through cells and 80 × 50 × 15 mm Silica crystals from SIL'TRONIX Silicon Technologies. The reflectometer FIGARO [55] at Institut Laue-Langevin (Grenoble, France) was used to record the time-of-flight reflectivity at two angles of incidence (0.8 and 3.2°) to cover the Q-range ($Q = 4\pi \sin(\theta/2)/\lambda$ where θ is the scattering angle and λ is the neutron wavelength). The instrumental resolution was set to $\frac{\Delta\lambda}{\lambda} = 7\%$. Flow through solid-liquid cells were provided by the neutron facility. They were composed by a plastic water reservoir in close contact with the polished surface of the silicon substrates. The water reservoir was equipped with inlet and outlet connections to exchange the aqueous solution. Substrate and reservoir were sandwiched between two aluminium plates connected to a water bath for temperature regulation. The temperature, measured by a thermocouple in close contact with the silicon substrate, was maintained at 37 °C. Prior to the experiment, the crystals were fully characterized in D$_2$O and H$_2$O to determine the structural parameters of the silicon oxide layer present on the surface. After injection, the lipids were equilibrated in the cell for ~20 min before rinsing with tris-buffer, and the bilayers were characterized in three contrasts (D-tris, H-tris and 50:50H/D-tris hereafter referred to as CM3). Then, 10 ml of the peptide solution (in D-tris, CM3 and H-tris sequentially) in the desired concentration were injected into the cell at a flow rate of ~2 ml/min using a syringe pump, and the resulting system was fully characterized in all three contrasts. Finally, the membranes were measured again after rinsing with H-tris and D-tris. The use of different contrast conditions is known as the contrast variation method and it allows for simultaneous fitting of multiple

reflectivity data sets, leading to an unambiguous solution and a more precise structural determination [56].

All NR profiles were analysed using an optical matrix method where the surface is modelled as sequential layers representing the substrate and lipid bilayer (three layers: one for the lipid tail and two for the hydrated head groups) as well as peptide and solvent which were allowed to penetrate the different layers freely. The fit analysis was done using the Motofit package taking into account the experimental resolution [57]. The NR data analysis provides information on the internal structure of thin films at an interface [58]. In particular, for SLBs, it allows to determine thickness, composition and surface coverage not only of the entire bilayer but of the different regions composing it, such as headgroups and hydrophobic tails. For this reason, the lipid bilayer before and after interaction with 0.8 μM indolicidin and rinsing were fitted using a 5 layer model (distinguishing silicon oxide – water – head– tail – head), while the 10 μM indolicidin bilayer after rinsing was fitted using an 8 layer model in which the 3 extra layers account for indolicidin/lipids patches forming on top of the bilayer (as single or double layers). During the fitting analysis, a model dividing the tail region into two layers to simulate asymmetric bilayers was considered. As discussed in the Supplementary material, this did not improve the quality of the fit significantly and therefore a symmetric model for the bilayer composition was chosen.

The error of the fit parameters for the thickness and solvent amount was determined by the Monte Carlo error analysis fitting algorithm included in the Motofit package [57] and reflects the quality of the fit. The area per molecule is calculated based on the fit parameters as

$$A_{mol} = \frac{V}{\varphi \cdot t}$$

where V is the volume of the lipid head/tail group (see table S1), φ is the lipid volume fraction (1-solvent [%]) and t is the thickness of the layer. The error in the area per molecule, δA_{mol}, was calculated as

$$\delta A_{mol} = \sqrt{\left(\frac{\delta\varphi}{\varphi}\right)^2 + \left(\frac{\delta t}{t}\right)^2} \cdot A_{mol}$$

2.4. Atomic force microscopy

Measurements were carried out on a Nanoscope IV multimode AFM (Veeco Instruments Inc.). Images were generated in the PeakForce Quantitative Mechanical Property Mapping® (QNM) mode with a silicon oxide tip (Olympus micro cantilever OTR8 PS-W) having a spring constant of 0.15 N/m and a radius of curvature of < 20 nm. Peak Force Tapping™ mode is different from contact and traditional tapping mode since it allows for precisely controlling the imaging force in order to keep indentations small, thus enabling non-destructive and high-resolution imaging. This mode is ideal for imaging of soft matter in liquid environments at high resolution. A liquid flow cell (glass probe holder, MTFML, Bruker Corporation) was used to scan the surfaces in a liquid environment and to exchange solution in situ. The setup was optimized for real-time continuous flow imaging where the solution constantly exchanges via a slow gravity feed [33].

First, a freshly cleaved mica surface was imaged in ultrapure water in order to ensure a clean and smooth surface (RMS: < 500 pm) prior to bilayer measurements. Small unilamellar vesicles were introduced into the AFM liquid flow cell and vesicle attachment and bilayer formation were imaged. The lipids were incubated in the AFM for at least 30 min and imaged to secure high coverage before rinsing the membrane with water. Before introducing the peptide, the membranes were rinsed in excess tris-buffer. The peptide solution was introduced to the membrane and the flow was maintained while imaging for at least 90 min. In this way, new peptides were continuously brought to the interface during scanning. Then, the membrane was rinsed with tris-buffer while imaging. All images were recorded at a resolution of 256 × 256 pixels

with a scan rate of 1 Hz. The z-setpoint and differential gains were manually optimized during each scan. Images were analysed and processed in the Gwyddion 2.22 software. The experiment was performed in duplicates to validate the results.

2.5. Small angle X-ray scattering

SAXS experiments of mixtures of peptide and liposomes were performed at the automated BM29 bioSAXS beamline [59] at the European Synchrotron Radiation Facility (ESRF) in Grenoble, France. The data was obtained using an energy of 12.5 keV and a detector distance of 2.87 m, covering a Q range of 0.0047 Å^{-1} to 0.5 Å^{-1}. The data set was calibrated to an absolute intensity scale using water as a primary standard. 45 μL samples were run through a capillary using the flow mode of the automated sample changer [60]. SAXS data was collected in ten successive frames of 0.5 s each to monitor radiation damage and the data reduction was done using the standard tool at BM29 [61]. The SAXS results were analysed using the theoretical model described in detail in Ref. [6]. In short, the model provides a detailed description of the membrane by dividing into probability functions for each component (lipid sub-units/peptide) across the bilayer.

3. Results and discussion

3.1. Concentration dependent interaction between indolicidin and SLB

QCM-D constitutes a useful technique to screen different experimental conditions for biomolecular interaction with model membranes. The simultaneous measurement of both changes in frequency and dissipation allows us to extract information on the viscoelastic properties of the membrane due to the direct relationship between the frequency and the mass adsorbed to the surface, while the dissipation is dependent on the rigidity of the layer. For example, the typical QCM-D signal observed from an adsorption process of a rigid film is a decrease in frequency due to the addition of mass on the surface without any significant changes in the dissipation due to the rigidity. For a soft and heterogeneous film (containing water), however, an increase in the dissipation will follow the adsorption due to the dampening of the oscillations of the QCM-D sensor. Upon desorption of material from the surface, for example removal of lipids due to solubilisation, the frequency increases as a result of mass removal, while the changes in dissipation depend on the hydration and rigidity of the remaining material.

Fig. 1A–C shows the QCM-D signals upon increasing concentrations of indolicidin (1, 5 and 10 μM) added to an SLB made of DMPC-DMPG. Immediately after peptide injection, there was a significant decrease in the frequency and an increase in the dissipation for all the samples, indicating peptide adsorption to the membrane. However, the point at which the QCM-D signals reached steady state was concentration dependent. At 1 μM, the dissipation reached an inflection point and then flattened at values higher than for the original SLB. For 5 μM, on the other hand, both frequency and dissipation reached an inflection point that was followed by a slow increase in the frequency. For the highest concentration of 10 μM, the frequency and dissipation displayed different steps where a peak in frequency (and the dissipation) was followed by equilibration at values slightly higher in frequency (and lower in dissipation) than before peptide addition. These signals are typical indicators of significant lipid removal from the membrane.

Plots of Δd versus Δf with the 7th harmonic were constructed and shown in Fig. 1D to better visualise the different d/f regimes related to various steps in the indolicidin interaction with the lipid membrane. For the lower concentrations of 1 μM and 2 μM, two regimes were observed: in regime 1) there was a large increase in the dissipation that was accompanied by a large decrease in the frequency, and in regime 2) there was a region where the dissipation decreased without any significant change in the frequency that stabilized around −8 to −10 Hz.

The former indicates penetration of the peptide into the bilayer while the latter signal indicates the formation of a stiffer absorbed layer. For 2 μM, the slope of the first regime was less steep than in the case of 1 μM, with a smaller increase in the dissipation over the same decrease in frequency. This behaviour might indicate a deeper insertion into the bilayer at the higher concentration, while at lower peptide concentrations the peptide occupies a more superficial location on the membrane which is reflected in an apparent less rigid structure. Similar behaviour was seen for PAMAM dendrimers at higher concentrations (up to 8 μM) [27].

For the higher indolicidin concentrations (5 and 10 μM) close to the reported minimum inhibitory concentration (MIC) value of indolicidin (8–16 μM dependent on the type of bacteria) [62], the slope for regime 1 was similar to the one observed for the lower concentrations (Fig. 1D), although the rate of the initial binding was significantly higher than the lower concentrations (Fig. 1A–C). The initial rapid binding at higher concentrations agreed with reported data for zwitterionic PC membranes and indolicidin [40]. However, regime 2 differed from the one observed for the lower concentrations giving an increase in frequency which was accompanied by a small dissipation. The inflection points between regime 1 and 2 occurred at −6 Hz and −8 Hz for 5 and 10 μM, respectively. Finally, for 10 μM indolicidin steady state was achieved at a higher frequency than the original bilayer. Regime 2 for the highest peptide concentrations indicated a loss of wet mass at the surface, pointing towards peptide-induced solubilisation of the phospholipid membrane. Similar results were previously obtained for higher indolicidin concentrations on pure PC membranes [40]. The difference in the behaviour of the dissipation between 5 and 10 μM might be a result of the peptide penetrating deeper into the bilayer resulting in more rigid membranes. Aurein 1.2, that resembles indolicidin in size, was shown to cause similar behaviour by QCM-D where addition of high concentrations (20 μM) resulted in a steady state frequency higher than the initial baseline [25].

Although the QCM-D measurements point towards different steps in the molecular mechanism of action between indolicidin and lipid membranes as a function of peptide concentration, they could not provide any structural information on the changes induced in the lipid membrane. Therefore, experiments were carried out using NR on the same system to provide higher resolution information of the structural interaction of the AMP. Fig. 2A, B and C show the reflectivity profiles, best fits and SLD profiles for DMPC/DMPG (90/10) bilayers before and after exposure to either 0.8 (1:10 peptide-lipid ratio) or 10 μM (~1:1 peptide lipid ratio) indolicidin in two solvent contrasts (H$_2$O and D$_2$O). The structural parameters for the pristine SLBs were similar and thus only one of the SLB reflectivity curves are shown in Fig. 2 (Table 1 gives the parameters used to fit the data). The full data sets for the two SLBs are given in the Supplementary material Fig. S2.

From the fit analysis of the pristine SLBs NR data, we obtained a thickness and area per lipid that was comparable with literature values based on MD simulations and SAXS data on DMPC/DMPG phospholipids [9,13,63]. Moreover, the SLDs obtained were in agreement with the theoretical SLD values for the lipid mixture as shown in Table S1. Moreover, the total bilayer thickness seemed unaffected by exposure to 0.8 μM peptide, while a slight decrease from 38 to 36 Å was seen for the bilayers exposed to 10 μM indolicidin. This slight thinning is, however, within the error of the fit analysis. Furthermore, peptide addition caused a change in the fitted SLD values for both lipid headgroup and core as compared to that for pure lipid bilayers. For 10 μM indolicidin, peptide addition resulted in changes of the SLD profile throughout the whole bilayer, while 0.8 μM mainly affected the SLD profile for the outer headgroup and the tail region. The observed changes in SLD are explained by the peptide having a different SLD than the lipids thus resulting in a change in the average SLDs of the modelled layers upon insertion of the peptide (see Table S1).

The NR fit analysis of the 0.8 μM indolicidin data (1:10 peptide to lipid ratio) indicates that the peptide inserted into the outer headgroup
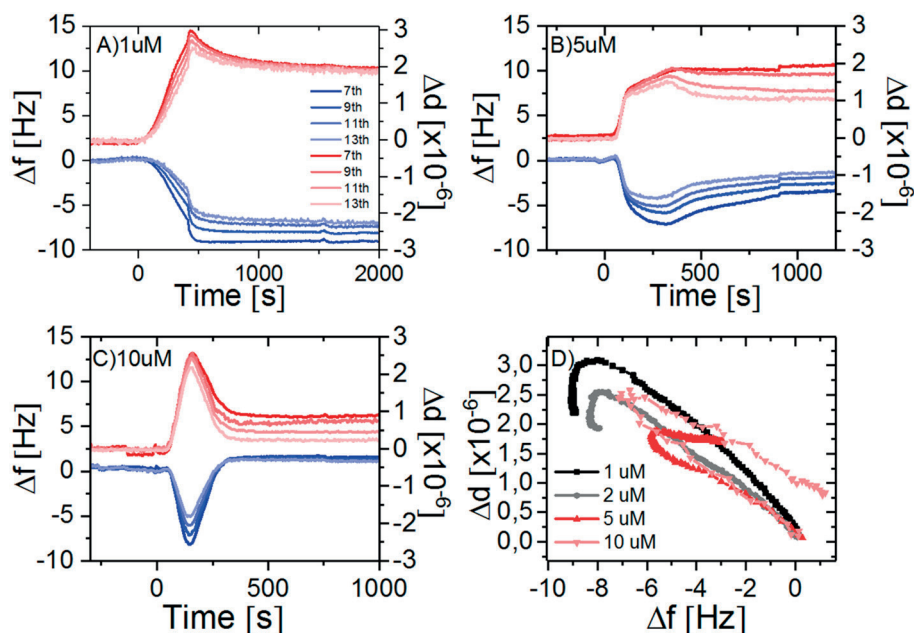
Fig. 1. QCM-D results showing addition of indolicidin to supported lipid bilayers composed of DMPC and DMPG in a molar ratio of 9:1. Three concentrations of indolicidin 1 μM (A), 5 μM (B) and 10 μM (C) were added to the bilayers at $t = 0$ s in a continuous flow. Changes in frequency are shown in blue and dissipation in red. For clarity, four overtones are plotted (see legend in panel A). Both the frequency and dissipation at all the harmonics are normalized to zero before addition of the peptide. The supported lipid bilayer formation is not shown in the plot (see the Supplementary material Fig. S1 for an example of typical SLB formation). (D) Change in dissipation against change in frequency with increasing concentration (1 μM, 2 μM, 5 μM and 10 μM). For clarity, only the 7th harmonic is shown, and the frequency and dissipation are offset to 0 before addition of the peptide. (For interpretation of the references to color in this figure legend, the reader is referred to the web version of this article.)

and tail region of the bilayer and did not affect the inner headgroup. For 10 μM (approximately 1:1 ratio) indolicidin, the peptide penetrated deeper into the bilayer which could be observed as a change in the average SLD of the inner headgroup region in Fig. 2B. The amount of peptide inserted in the head region of the membrane could readily be calculated from the SLD values and it increased significantly from 0 to 60% in the inner head group and 13 to 36% in the outer headgroup when increasing the concentration of the peptide from 0.8 to 10 μM. On the other hand, the amount of peptide incorporated in the tail region did not seem to be affected by the peptide concentration and remained at 17%. This points towards a clear affinity of the peptide for the head-tail interface also upon penetration to the inner leaflet.

3.2. Lipid removal caused by peptide insertion

Table 1 shows that the bilayer coverage decreased significantly for 10 μM indolicidin, implying that more lipids were removed from the membrane as the peptide (surface) concentration increased. Lipid removal is in agreement with our QCM-D experiments (Fig. 1), where injection of 10 μM indolicidin led to a decrease in mass on the sensor explained as removal of phospholipids from the bilayer. The changes in

the thickness and solvent fraction of the tail region indicated that the peptide significantly disturbed the ordering of the tails, which is also corroborated by DSC experiments published in a recent work by Nielsen et al. [6].

In Fig. 3, the NR and SLD profile of the bilayer exposed to 0.8 μM is shown before and after extensive rinsing with tris-buffer using three contrasts (D-tris, H-tris and cm3-tris). Note that this is different from Fig. 2 where we only compare the samples in the presence of peptide and prior to rinsing with buffer. The corresponding fit parameters for the SLB in the presence of indolicidin and extensive rinse are shown in Table 1, while those fit parameters for the data of 0.8 μM showing the bilayer before rinsing is given in Table S1 in the Supplementary material. The inset in Fig. 3 shows the reduced reflectivity, RQ[4], plotted against Q to highlight the appearance of a distinct peak at the Q range of 0.10–0.13 Å^{-1} upon incubation with indolicidin (marked with an arrow in Fig. 3A). This peak was clear for the H-tris data due to the high contrast towards the deuterated lipids. This contribution was modelled by addition of two mixed lipid/peptide layers (it was seen that two extra layers were needed to fully explain the data), separated by a thin water layer (6 Å). The coverage of the middle lipid/peptide layer (in direct contact with the SLB) was 27% for 0.8 μM, while the outer lipid/
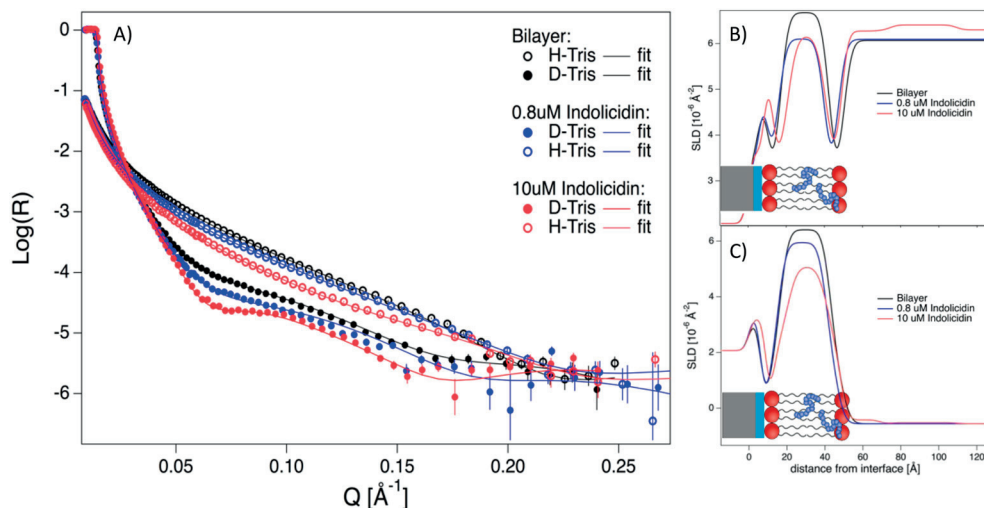

Fig. 2. NR measurements of DMPC-DMPG SLBs before and after addition of 0.8 and 10 μM indolicidin. (A) Reflectivity profiles together with the best fits (lines) to the described models. SLD profiles obtained from the fit analysis against distance from the interface for an SLB before and after being exposed to indolicidin in the indicated concentration of D-contrast (B) and H-contrast (C). In this case, 10 ml of the peptide was flushed into the cell and rinsed off with buffer prior to the NR measurements (the experiments with the two concentrations were performed in separate cells). The slight difference in the SLD of the bulk is due to incomplete exchange of the solution when changing contrast (and typically accounts by for example 3% H2O presence in the D2O contrast).

Table 1
Fitted parameters for tail-deuterated DMPC/DMPG membranes prior to and after exposure to 0.8 µM and 10 µM indolicidin and extensive rinse with buffer. A_{mol} is the molecular area per lipid component including solvent. The amount of indolicidin incorporated in the different layers is estimated based on the change in SLD observed after exposure to the peptide. As seen from the table, increasing the concentration of indolicidin from 0.8 to 10 µM results in deeper penetration of the peptide into the bilayer causing higher lipid removal.

| Layer	d [Å]	Solvent [%]	SLD [10^{-6} Å^{-2}]	Indolicidin %	d [Å]	Solvent [%]	SLD [10^{-6} Å^{-2}]	Indolicidin %
Pristine SLB								
Water	3	100	–	–	4 ± 1	100	–	–
Head (inner)	6 ± 1	18 ± 3	1.83	–	6 ± 1	13 ± 3	1.83	–
Tail	25 ± 1	4 ± 1	6.7	–	26 ± 1	1 ± 1	6.7	–
Head (upper)	6 ± 1	18 ± 3	1.83	–	6 ± 1	13 ± 3	1.83	–
Total thickness (Å)	37 ± 2	A_{mol} 64 ± 2 Å^2			38 ± 2	A_{mol} 60 ± 1 Å^2		
SLB after addition of	0.8 µM indolicidin				10 µM indolicidin			
Water	3	100	–	–	4 ± 1	100	–	–
Head (inner)	6 ± 1	19 ± 3	1.83	–	8 ± 1	13 ± 3	2.6	60 ± 3
Tail/indolicidin	25 ± 1	6 ± 1	6.1	17 ± 1	21 ± 1	15 ± 2	6.1	17 ± 1
Head/indolicidin	6 ± 1	10 ± 4	2	13 ± 2	7 ± 1	13 ± 3	2.3	36 ± 2
Total thickness (Å)	37 ± 2	A_{mol} N/A			36 ± 2	A_{mol} N/A		
Indolicidin/lipid	–	–	–	–	27 ± 5	98 ± 1	5.2 ± 0.4	10 ±
Water	–	–	–	–	6 ± 1	100	–	
Indolicidin/lipid	–	–	–	–	34 ± 1	98 ± 1	6.0 ± 0.4	0

peptide layer had a low coverage of only 2%. The SLD for both of these layers were found to be 5.6 10^{-6} Å^2 indicating that these patches mainly are composed of phospholipids, with only around 4% peptide.

Rinsing with buffer induced major changes in the reflectivity profile with disappearance of the peak at intermediate Q. Therefore, these patches seem to be relatively loosely attached structures. The thickness of the patches was similar to the thickness of one bilayer i.e. 37 Å. These patches might originate from peptide/lipids complexes (for example mixed micelles) as suggested from the SLD values obtained from the analysis. Their low surface coverage is compatible with the amount of lipids removed from the bilayer by the insertion of the peptide (17%). Indeed, we observed a change in the composition of the lipid core layer allowing to include the inserted peptide as described above. This mechanism is illustrated in Scheme 1. Lipid removal can be explained by the decrease in the energy barrier against solubilisation of individual lipids in the outer leaflet of the bilayer upon peptide integration in the bilayer. This is a typical behaviour for the interaction of biosurfactants with lipid membranes including surfactin, which is a natural lipopeptide surfactant with antibiotic properties. In this case, progressive lipid removal takes place upon reaching a threshold biosurfactant concentration [43]. The removal of lipids due to peptide insertion is characteristic for the detergent-like interaction mechanism that has been reported for a series of linear amphipathic cationic peptides resulting in gradual membrane disintegration [64].

No evidence of distinct pores or channels in the membrane was observed at 0.8 µM indolicidin, a concentration that can be considered as physiologically relevant. Under this condition, the peptide did not seem to affect the inner headgroup and the bilayer coverage remained stable even as lipids were exchanged by peptides. These results on

simple model membranes might suggest that the mechanism of indolicidin is linked to disordering of the lipids in the bilayer upon peptide insertion rather than defined pore formation. A possible explanation of why pore-formation could not be seen in the case of indolicidin may be linked to the lack of a secondary structure in solution. Both melittin [44] and magainin [48] are examples of peptides with an alpha-helical secondary structure that have shown to form pores by quasi elastic neutron scattering (QENS) together with AFM and off-specular neutron reflectometry. The alpha-helical secondary structure may be essential for the clustering of the peptides in the membrane resulting in the formation of barrel-stave or toroidal pores. Peptide induced lipid disordering, as we observe for indolicidin, was suggested by Wimley, among others, to cause lysis of bacteria and eventually, cell death [2].

The formation of lipid/peptide patches upon addition of indolicidin could visually be followed by time resolved AFM imaging, and analysis of the corresponding height profiles (Fig. 4). In Fig. 4A and B, the pre-formed SLB is shown as evidenced by the presence of a few defects of ~4 nm in depth, which is in agreement with the fit parameters from NR on the same type of SLBs as shown in Table 1 and typical for a DMPC/DMPG bilayer [9,13,63]. The bilayer defects disappeared immediately after a continuous flow of 0.8 µM indolicidin solution was flushed over the bilayer, and new patches were formed on top of the bilayer (seen as light dots in Fig. 4C). This suggests that indolicidin readily integrated and filled the defects present in the SLB. From the height profile in Fig. 4D, the height of these patches could be determined to be 3.5–4 nm and 7–8 nm and thus correspond to a single or double peptide-lipid bilayer in perfect agreement with the results from the fit analysis of the NR data. The formation of these patches happened on the time scale of
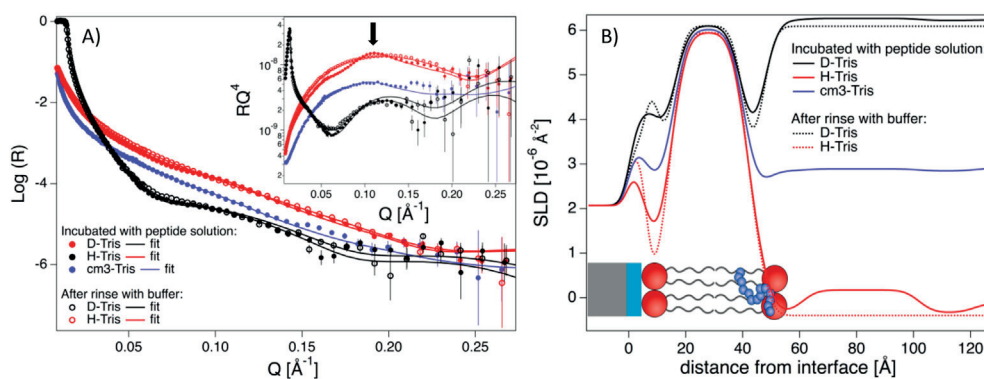
Fig. 3. NR measurements of a DMPC-DMPG SLB after being exposed to 0.8 µM indolicidin and after rinsing with buffer. A) Reflectivity profiles for the measurements together with the best fit. Inset shows the same curves plotted in a RQ^4 against Q to increase the visibility of the change in high Q after rinsing. B) SLD profiles resulting from the fit analysis against distance from the interface for an SLB before and after rinsing with buffer. Inset illustrates the proposed position of the peptide in the membrane resulting from the fit. The arrow marks the peak that arises from the repetition of peptide/lipid patches on top of the SLB.
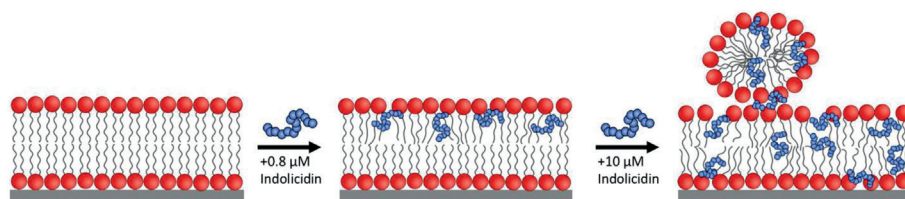
Scheme 1. Illustration of concentration dependent interaction of indolicidin with lipid bilayers based on fit analysis of SAXS and NR results.

minutes in the AFM experiment and did not change appearance with incubation with the peptide over a time period of approximately 2 h. When the membrane was subsequently rinsed with tris-buffer, however, most of the mixed lipid/peptide structures were removed as seen in Fig. 4E and F, also in agreement with our NR results. In contrast to the NR experiment, not all the single bilayer patches were removed as seen from the AFM image and the corresponding height profile. An explanation to this discrepancy could be that the flow rate in the AFM experiment was significantly lower than for NR. A very low flow rate (~50 μL/min) in AFM is necessary in order to enable imaging under flow. This might lead to less efficient removal of the lipid/peptide patches.

3.3. Comparing reflectivity results for supported lipid bilayers with SAXS data of unilamellar lipid vesicles

In order to compare the SLB results with unilamellar lipid vesicles, we performed SAXS experiments on peptide-vesicle samples with similar lipid: peptide ratios. The SAXS results for DMPC-DMPG-DMPE-PEG liposomes with and without added indolicidin (1:10) are shown in Fig. 5A. DMPE-PEG was added in the vesicle formulation to prevent aggregation of vesicles upon peptide addition, but that should not affect the interaction with peptides due to the low molar ratio of 2.5%. The data was fitted using the asymmetric scattering density profile model (SDP), as developed by Nagle, Kučerka and co-workers [8,10,11,15] modified to account for the peptide scattering as described by Nielsen et al. [6]. Fit analysis of the scattering curves for the liposomes gave a membrane thickness of 37.4 Å and an area per lipid of 60 Å^2, in agreement with the results found in the NR data analysis (Table 1). In

Fig. 5, the SLD profiles calculated from the fit parameters from both SAXS and NR are shown for comparison. The curves representing the peptide-free membrane (red) found from the two methods virtually overlap except for the oscillation in neutron SLD at the inner leaflet for NR representing the silicon surface below the bilayer. The latter is not relevant in the case of SAXS where free floating unilamellar vesicles (ULVs) are used.

Upon addition of indolicidin, a shift in the X-ray scattering curve at intermediate Q took place as shown in Fig. 5A. For SAXS data of lipid bilayers the minimum in the scattering curve at intermediate Q is highly sensitive to the negative contrast, i.e. lower electron density than water of the lipid tails and positive contrast (higher electron density) of the headgroups. Through theoretical modelling, it was found that this shift in the minima upon peptide addition was caused by a change in the scattering contrast as the peptide inserted into the bilayer. The insertion is clearly visible due to the peptide having a higher electron density than the lipids (as seen in Table S1 of the Supplementary material). The SAXS data analysis suggests that the peptide inserted at the interface between the head and tail region on the outer leaflet of the membrane as a random coil. This is illustrated in the volume probability curve showing the membrane structure with the additional Gaussian peak representing the peptide inserting in the membrane (Fig. 5B).

To facilitate the comparison between the SAXS and NR results, the electron density profile from our SAXS measurements was converted to a neutron SLD profile in H$_2$O and plotted together with the SLD profile obtained from NR analysis (for 0.8 μM as the lipid: peptide ratio in these two cases were similar) and plotted in Fig. 5C. Both NR and SAXS data did not show major changes in the bilayer structure, as the overall
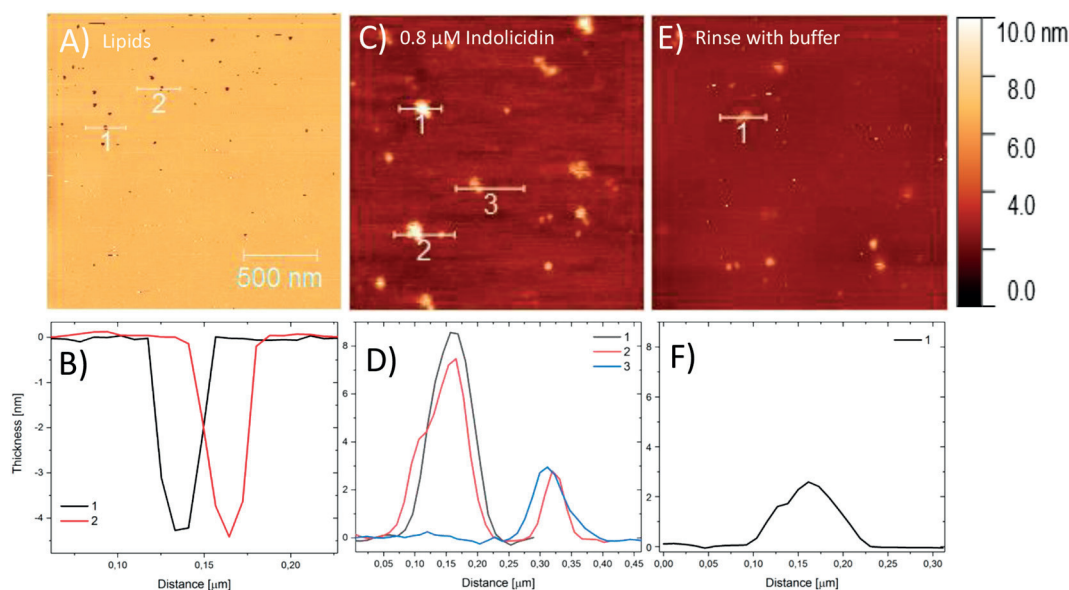
Fig. 4. Time-lapse series of AFM images of a lipid bilayer made of DMPC and DMPG captured under continuous flow of the indicated solution. The scale bar in A applies to all images. A) SLB formed on a Mica surface with good coverage but some remaining holes allowing for measurements of the thickness of the bilayer from the height profile of two indicated pores as seen in B). C) 0.8 μM indolicidin flowed over the surface resulting in disappearance of the visible holes in the bilayer and formation of bilayer patches with height profiles shown in graph D). E) SLB after rinsing with buffer resulting in removal of most of the patches and a decrease in the height of the patches shown in graph F.
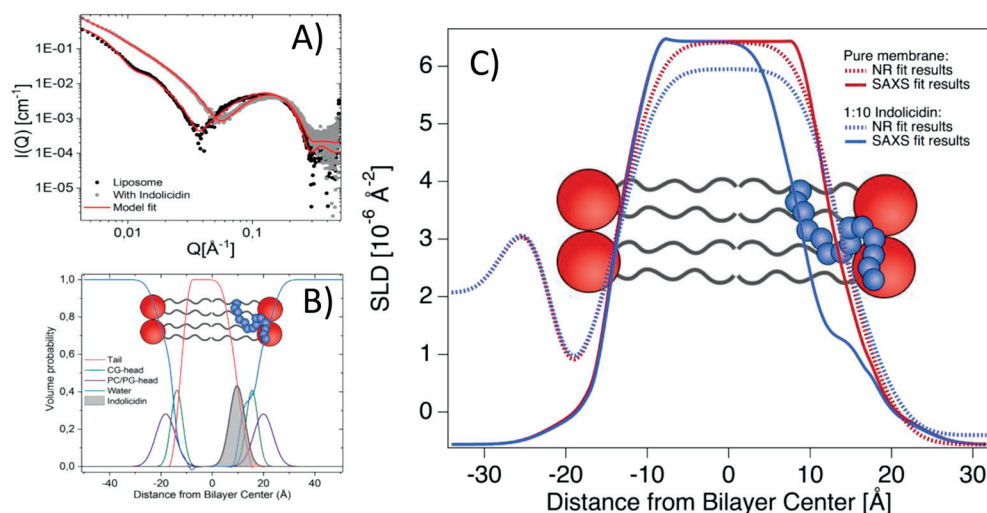
Fig. 5. Comparison with previously reported small angle X-ray scattering results for liposomes exposed to indolicidin [6]. A) Scattering curves and model fits for liposomes with and without peptide. B) Illustration of the volume probability distribution for the bilayer with the peptide positioned in the interface between the headgroups and the tail region on the outer leaflet of the membrane. C) Comparison of the neutron SLD profile derived from the NR experiment (- - -) and SAXS experiment (—) (the latter is converted from X-ray to neutron SLD to directly compare the two methods). The distance z = 0 marks the centre of the bilayer.

thickness of the bilayer remained constant. However, in SAXS experiments, peptide to lipid ratios above 1:10 showed a ~3 Å thinning of the bilayer [6], which is also supported by molecular dynamics simulations for this peptide [53,65].

The model used to analyse the NR data is the traditional slab model that does not allow to extract the exact position of the peptide. Instead each layer is averaged with a common SLD. Further division of the lipid core layer into two layers to model peptide asymmetry did not lead to an improved fit quality but rather over-parametrization. This might be due to the lack of contrast, in particular between the peptide and lipid head (see the SLD values given in Table S1). Therefore, we used the symmetric profile to analyse the data to prevent over-interpretation of the data and to minimise the number of fitting parameters. However, a fit to a model allowing for an asymmetric peptide position in the bilayer (see details of the model in Fig. S3) is included in the Supplementary material to show that the NR data does not contradict the SAXS modelling of an asymmetric distribution (Fig. S4).

In Fig. 5C, a comparison of the peptide effect on the bilayer as seen for both NR and SAXS is presented by the corresponding SLD profiles for the 1:10 peptide-lipid samples. The SLD profile from the NR results showed a decreased plateau of the SLD in the middle of the bilayer representing the tail region when compared to the pure bilayer. This is due to the peptide having a lower SLD than the deuterated tail. The effect that the peptide insertion had on the outer headgroups of the lipid bilayer was not easily detected using NR, as mentioned above. For SAXS, the sensitivity to changes in electron density as the peptide incorporates in the bilayer allowed us to determine the specific peptide location [6]. When comparing the SLD profile from NR with the one from SAXS we could see that the effect indolicidin had on the SLD profile was localised in the outer leaflet (interface between head and tail). The deeper penetration of the peptide seen from the NR SLD profile, might be due to lack of sensitivity of the method as described above. However, the deeper penetration might also additionally be explained by the use of SLBs formed on negatively charged silicon oxide surfaces that could attract the positively charged peptide deeper into the bilayer. Although the NR fit allowed only up to 4 ± 1 vol% solvent in the tail region prior to peptide interaction, small pre-existing defects (holes) in the SLB (as seen visually by AFM in Fig. 4) could facilitate deeper peptide penetration into the membrane. However, as indolicidin has some polar sidechains, as well as hydrophobic aromatic groups, it is likely from a physical chemical perspective that the peptide will insert in the interface between the head group that is partly hydrated and the lipid tail region. It is less likely that indolicidin will position only in the non-hydrated tail region.

4. Conclusion

The combination of NR, QCM-D, AFM and SAXS allowed us to establish the structural interaction of indolicidin, a naturally occurring antimicrobial peptide, with a model lipid bilayer. Our data suggest that the insertion of indolicidin in the bilayer is strongly dependent on the concentration. From QCM-D and NR, we conclude that indolicidin interacts mainly with the outer headgroup and tail region at lower concentrations (≤2 μM) while the peptide penetrates deeper into the bilayer diffusing also into the inner headgroup at higher concentrations (≥5 μM). Interestingly, the resulting effect on the bilayer thickness is also concentration dependent. Low concentrations of indolicidin cause no changes to the thickness or overall structure of the bilayer, while higher concentrations result in a disordering of the bilayer and a slight thinning of the bilayer. Similar trends were observed for lipid vesicles probed by SAXS. Combination of the information of the peptide insertion from these methods provides good evidence in support of the "interfacial activity" scenario presented by Wimley [2] where the peptide causes a disordering of the lipids in the bilayer by inserting in the interface between the lipid head and tail region. This is believed to result in lysis of bacteria and eventual cell death, however, further studies using lipid compositions closer mimicking bacteria membrane needs to be studied to fully elucidate the mode of action. Further, indolicidin seems to dissolve lipids in the membrane resulting in the formation of lipid/peptide patches on the supported lipid bilayer as seen by AFM and NR and in an increase in the size of the vesicles as seen by SAXS.

In this work we show how detailed analysis of scattering techniques on supported lipid bilayers as well as unilamellar lipid vesicles, together with QCM-D and AFM imaging, are high resolution biophysical techniques for the study of peptide interactions with model lipid membranes.

Transparency document

The Transparency document associated with this article can be found, in online version.

Acknowledgements

also grateful to the ESRF for SAXS beamtime at BM29, and the PSCM lab for support during both the NR and SAXS experiment. We acknowledge use of the Norwegian national infrastructure for X-ray diffraction and scattering (RECX). We would also like to thank Victoria Ariel Bjørnestad for her contribution to the SAXS experiments and the modelling of SAXS data.

Appendix A. Supplementary data

Supplementary data to this article can be found online at https://doi.org/10.1016/j.dummy.2019.01.002.

References

[1] L.T. Nguyen, E.F. Haney, H.J. Vogel, The expanding scope of antimicrobial peptide structures and their modes of action, Trends Biotechnol. 29 (2011) 464–472, https://doi.org/10.1016/j.tibtech.2011.05.001.

[2] W.C. Wimley, Describing the mechanism of antimicrobial peptide action with the interfacial activity model, ACS Chem. Biol. 5 (2010) 905–917, https://doi.org/10.1021/cb1001558.

[3] R.E. Hancock, A. Rozek, Role of membranes in the activities of antimicrobial cationic peptides, FEMS Microbiol. Lett. 206 (2002) 143–149, https://doi.org/10.1111/j.1574-6968.2002.tb11000.x.

[4] H. Jenssen, P. Hamill, R.E. Hancock, Peptide antimicrobial agents, Clin. Microbiol. Rev. 19 (2006) 491–511, https://doi.org/10.1128/CMR.00056-05.

[5] T. Narayanan, D. Weerakkody, A.G. Karabadzhak, M. Anderson, O.A. Andreev, Y.K. Reshetnyak, pHLIP peptide interaction with a membrane monitored by SAXS, J. Phys. Chem. B 120 (2016) 11484–11491, https://doi.org/10.1021/acs.jpcb.6b06643.

[6] J.E. Nielsen, V.A. Bjørnestad, R. Lund, Resolving the structural interactions between antimicrobial peptides and lipid membranes using small-angle scattering methods: the case of indolicidin, Soft Matter 14 (2018) 8750–8763, https://doi.org/10.1039/C8SM01888J.

[7] F.G. Dupuy, I. Pagano, K. Andenoro, M.F. Peralta, Y. Elhady, F. Heinrich, S. Tristram-Nagle, Selective interaction of colistin with lipid model membranes, Biophys. J. 114 (2018) 919–928, https://doi.org/10.1016/j.bpj.2017.12.027.

[8] J.B. Klauda, N. Kučerka, B.R. Brooks, R.W. Pastor, J.F. Nagle, Simulation-based methods for interpreting X-ray data from lipid bilayers, Biophys. J. 90 (2006) 2796–2807, https://doi.org/10.1529/biophysj.105.075697.

[9] N. Kučerka, Y. Liu, N. Chu, H.I. Petrache, S. Tristram-Nagle, J.F. Nagle, Structure of fully hydrated fluid phase DMPC and DLPC lipid bilayers using X-ray scattering from oriented multilamellar arrays and from unilamellar vesicles, Biophys. J. 88 (2005) 2626–2637, https://doi.org/10.1529/biophysj.104.056606.

[10] N. Kučerka, J.F. Nagle, J.N. Sachs, S.E. Feller, J. Pencer, A. Jackson, J. Katsaras, Lipid bilayer structure determined by the simultaneous analysis of neutron and X-ray scattering data, Biophys. J. 95 (2008) 2356–2367, https://doi.org/10.1529/biophysj.108.132662.

[11] N. Kucerka, J. Pencer, J.N. Sachs, J.F. Nagle, J. Katsaras, Curvature effect on the structure of phospholipid bilayers, Langmuir 23 (2007) 1292–1299, https://doi.org/10.1021/la062455t.

[12] J. Nagle, M. Wiener, Relations for lipid bilayers. Connection of electron density profiles to other structural quantities, Biophys. J. 55 (1989) 309–313, https://doi.org/10.1016/S0006-3495(89)82806-1.

[13] J. Pan, F.A. Heberle, S. Tristram-Nagle, M. Szymanski, M. Koepfinger, J. Katsaras, N. Kučerka, Molecular structures of fluid phase phosphatidylglycerol bilayers as determined by small angle neutron and X-ray scattering, Biochim. Biophys. Acta Biomembr. 1818 (2012) 2135–2148, https://doi.org/10.1016/j.bbamem.2012.05.007.

[14] J. Pan, D.P. Tieleman, J.F. Nagle, N. Kučerka, S. Tristram-Nagle, Alamethicin in lipid bilayers: combined use of X-ray scattering and MD simulations, Biochim. Biophys. Acta Biomembr. 1788 (2009) 1387–1397, https://doi.org/10.1016/j.bbamem.2009.02.013.

[15] B. Eicher, F.A. Heberle, D. Marquardt, G.N. Rechberger, J. Katsaras, G. Pabst, Joint small-angle X-ray and neutron scattering data analysis of asymmetric lipid vesicles, J. Appl. Crystallogr. 50 (2017), https://doi.org/10.1107/S1600576717000656.

[16] F.A. Heberle, J. Pan, R.F. Standaert, P. Drazba, N. Kučerka, J. Katsaras, Model-based approaches for the determination of lipid bilayer structure from small-angle neutron and X-ray scattering data, Eur. Biophys. J. 41 (2012) 875–890, https://doi.org/10.1007/s00249-012-0817-5.

[17] F.A. Heberle, R.S. Petruzielo, J. Pan, P. Drazba, N. Kučerka, R.F. Standaert, G.W. Feigenson, J. Katsaras, Bilayer thickness mismatch controls domain size in model membranes, J. Am. Chem. Soc. 135 (2013) 6853–6859, https://doi.org/10.1021/ja3113615.

[18] J.D. Nickels, S. Chatterjee, C.B. Stanley, S. Qian, X. Cheng, D.A. Myles, R.F. Standaert, J.G. Elkins, J. Katsaras, The in vivo structure of biological membranes and evidence for lipid domains, PLoS Biol. 15 (2017) e2002214, , https://doi.org/10.1371/journal.pbio.2002214.

[19] D.K. Rai, S. Qian, Interaction of the antimicrobial peptide aurein 1.2 and charged lipid bilayer, Sci. Rep. 7 (2017) 3719, , https://doi.org/10.1038/s41598-017-03795-6.

[20] S. Qian, W.T. Heller, Peptide-induced asymmetric distribution of charged lipids in a

[21] vesicle bilayer revealed by small-angle neutron scattering, J. Phys. Chem. B 115 (2011) 9831–9837, https://doi.org/10.1021/jp204045t.

[21] C.-C. Lee, Y. Sun, S. Qian, H.W. Huang, Transmembrane pores formed by human antimicrobial peptide LL-37, Biophys. J. 100 (2011) 1688–1696, https://doi.org/10.1016/j.bpj.2011.02.018.

[22] S. Qian, W. Wang, L. Yang, H.W. Huang, Structure of the alamethicin pore reconstructed by X-ray diffraction analysis, Biophys. J. 94 (2008) 3512–3522, https://doi.org/10.1529/biophysj.107.126474.

[23] V. Castelletto, R.H. Barnes, K.-A. Karatzas, C.J. Edwards-Gayle, F. Greco, I.W. Hamley, R. Rambo, J. Seitsonen, J. Ruokolainen, Arginine-containing surfactant-like peptides: interaction with lipid membranes and antimicrobial activity, Biomacromolecules (2018), https://doi.org/10.1021/acs.biomac.8b00391.

[24] V. Castelletto, R.H. Barnes, K.-A. Karatzas, C.J. Edwards-Gayle, F. Greco, I.W. Hamley, J. Seitsonen, J. Ruokolainen, Restructuring of lipid membranes by an arginine-capped peptide bolaamphiphile, Langmuir (2018), https://doi.org/10.1021/acs.langmuir.8b01014.

[25] D.I. Fernandez, A.P. Le Brun, T.C. Whitwell, M.-A. Sani, M. James, F. Separovic, The antimicrobial peptide aurein 1.2 disrupts model membranes via the carpet mechanism, Phys. Chem. Chem. Phys. 14 (2012) 15739–15751, https://doi.org/10.1039/C2CP43099A.

[26] A. Åkesson, T. Lind, N. Ehrlich, D. Stamou, H. Wacklin, M. Cárdenas, Composition and structure of mixed phospholipid supported bilayers formed by POPC and DPPC, Soft Matter 8 (2012) 5658–5665, https://doi.org/10.1039/C2SM00013J.

[27] A. Åkesson, T.K. Lind, R. Barker, A. Hughes, M. Cárdenas, Unraveling dendrimer translocation across cell membrane mimics, Langmuir 28 (2012) 13025–13033, https://doi.org/10.1021/la3027144.

[28] T.K. Lind, Understanding peptide dendrimer interactions with model cell membrane mimics, in, Department of Chemistry, Faculty of Science, University of Copenhagen, 2014.

[29] T.K. Lind, L. Darre, C. Domene, Z. Urbanczyk-Lipkowska, M. Cárdenas, H. Wacklin, Antimicrobial peptide dendrimer interacts with phosphocholine membranes in a fluidity dependent manner: a neutron reflection study combined with molecular dynamics simulations, Biochim. Biophys. Acta, Biomembr. 1848 (2015) 2075–2084, https://doi.org/10.1016/j.bbamem.2015.05.015.

[30] Y. Gerelli, L. Porcar, G. Fragneto, Lipid rearrangement in DSPC/DMPC bilayers: a neutron reflectometry study, Langmuir 28 (2012) 15922–15928, https://doi.org/10.1021/la303662e.

[31] Y. Gerelli, L. Porcar, L. Lombardi, G. Fragneto, Lipid exchange and flip-flop in solid supported bilayers, Langmuir 29 (2013) 12762–12769, https://doi.org/10.1021/la402708u.

[32] A. Martel, L. Antony, Y. Gerelli, L. Porcar, A. Fluitt, K. Hoffmann, I. Kiesel, M. Vivaudou, G. Fragneto, J.J. De Pablo, Membrane permeation versus amyloidogenicity: a multitechnique study of islet amyloid polypeptide interaction with model membranes, J. Am. Chem. Soc. 139 (2016) 137–148, https://doi.org/10.1021/jacs.6b06985.

[33] T.K. Lind, P. Zielinska, H.P. Wacklin, Z. Urbanczyk-Lipkowska, M. Cárdenas, Continuous flow atomic force microscopy imaging reveals fluidity and time-dependent interactions of antimicrobial dendrimer with model lipid membranes, ACS Nano 8 (2013) 396–408, https://doi.org/10.1021/nn404530z.

[34] J.E. Shaw, J.-R. Alattia, J.E. Verity, G.G. Privé, C.M. Yip, Mechanisms of antimicrobial peptide action: studies of indolicidin assembly at model membrane interfaces by in situ atomic force microscopy, J. Struct. Biol. 154 (2006) 42–58, https://doi.org/10.1016/j.jsb.2005.11.016.

[35] E.F. Semeraro, J.M. Devos, L. Porcar, V.T. Forsyth, T. Narayanan, In vivo analysis of the Escherichia coli ultrastructure by small-angle scattering, IUCrJ 4 (2017) 751–757, https://doi.org/10.1107/S2052252517013008.

[36] S. Bobone, Y. Gerelli, M. De Zotti, G. Bocchinfuso, A. Farrotti, B. Orioni, F. Sebastiani, E. Latter, J. Penfold, R. Senesi, Membrane thickness and the mechanism of action of the short peptaibol trichogin GA IV, Biochim. Biophys. Acta Biomembr. 1828 (2013) 1013–1024, https://doi.org/10.1016/j.bbamem.2012.11.033.

[37] G. Pabst, S.L. Grage, S. Danner-Pongratz, W. Jing, A.S. Ulrich, A. Watts, K. Lohner, A. Hickel, Membrane thickening by the antimicrobial peptide PGLa, Biophys. J. 95 (2008) 5779–5788, https://doi.org/10.1529/biophysj.108.141630.

[38] E. Sevcsik, G. Pabst, W. Richter, S. Danner, H. Amenitsch, K. Lohner, Interaction of LL-37 with model membrane systems of different complexity: influence of the lipid matrix, Biophys. J. 94 (2008) 4688–4699, https://doi.org/10.1529/biophysj.107.123620.

[39] C. Münster, A. Spaar, B. Bechinger, T. Salditt, Magainin 2 in phospholipid bilayers: peptide orientation and lipid chain ordering studied by x-ray diffraction, Biochim. Biophys. Acta Biomembr. 1562 (2002) 37–44, https://doi.org/10.1016/S0005-2736(02)00357-7.

[40] K.F. Wang, R. Nagarajan, T.A. Camesano, Differentiating antimicrobial peptides interacting with lipid bilayer: molecular signatures derived from quartz crystal microbalance with dissipation monitoring, Biophys. Chem. 196 (2015) 53–67, https://doi.org/10.1016/j.bpc.2014.09.003.

[41] K. Hristova, W.C. Wimley, V.K. Mishra, G. Anantharamiah, J.P. Segrest, S.H. White, An amphipathic α-helix at a membrane interface: a structural study using a novel X-ray diffraction method, J. Mol. Biol. 290 (1999) 99–117, https://doi.org/10.1006/jmbi.1999.2840.

[42] C. Münster, J. Lu, B. Bechinger, T. Salditt, Grazing incidence X-ray diffraction of highly aligned phospholipid membranes containing the antimicrobial peptide magainin 2, Eur. Biophys. J. 28 (2000) 683–688, https://doi.org/10.1007/s002490050008.

[43] H.-H. Shen, R.K. Thomas, J. Penfold, G. Fragneto, Destruction and solubilization of supported phospholipid bilayers on silica by the biosurfactant surfactin, Langmuir

26 (2010) 7334–7342, https://doi.org/10.1021/la904212x.

[44] Z. Buck, J. Torres, A. Miskowiec, E. Mamontov, H. Kaiser, F. Hansen, H. Taub, M. Tyagi, L. Collins, K. Herwig, Effect of melittin on water diffusion and membrane structure in DMPC lipid bilayers, EPL 123 (2018) 18002, , https://doi.org/10.1209/0295-5075/123/18002.

[45] A.M. Sendecki, M.F. Poyton, A.J. Baxter, T. Yang, P.S. Cremer, Supported lipid bilayers with phosphatidylethanolamine as the major component, Langmuir 33 (2017) 13423–13429, https://doi.org/10.1021/acs.langmuir.7b02323.

[46] D.I. Fernandez, A.P. Le Brun, T.-H. Lee, P. Bansal, M.-I. Aguilar, M. James, F. Separovic, Structural effects of the antimicrobial peptide maculatin 1.1 on supported lipid bilayers, Eur. Biophys. J. 42 (2013) 47–59, https://doi.org/10.1007/s00249-012-0796-6.

[47] T. Salditt, Lipid–peptide interaction in oriented bilayers probed by interface-sensitive scattering methods, Curr. Opin. Struct. Biol. 13 (2003) 467–478, https://doi.org/10.1016/S0959-440X(03)00113-1.

[48] S.J. Ludtke, K. He, W.T. Heller, T.A. Harroun, L. Yang, H.W. Huang, Membrane pores induced by magainin, Biochemistry 35 (1996) 13723–13728, https://doi.org/10.1021/bi9620621.

[49] H.W. Huang, Y. Wu, Lipid-alamethicin interactions influence alamethicin orientation, Biophys. J. 60 (1991) 1079–1087, https://doi.org/10.1016/S0006-3495(91)82144-0.

[50] K. Lohner, E.J. Prenner, Differential scanning calorimetry and X-ray diffraction studies of the specificity of the interaction of antimicrobial peptides with membrane-mimetic systems, Biochim. Biophys. Acta Biomembr. 1462 (1999) 141–156, https://doi.org/10.1016/S0005-2736(99)00204-7.

[51] T.J. Falla, D.N. Karunaratne, R.E. Hancock, Mode of action of the antimicrobial peptide indolicidin, J. Biol. Chem. 271 (1996) 19298–19303, https://doi.org/10.1074/jbc.271.32.19298.

[52] A. Rozek, C.L. Friedrich, R.E. Hancock, Structure of the bovine antimicrobial peptide indolicidin bound to dodecylphosphocholine and sodium dodecyl sulfate micelles, Biochemistry 39 (2000) 15765–15774, https://doi.org/10.1021/bi000714m.

[53] C. Neale, J.C. Hsu, C.M. Yip, R. Pomes, Indolicidin binding induces thinning of a lipid bilayer, Biophys. J. 106 (2014) L29–L31, https://doi.org/10.1016/j.bpj.2014.02.031.

[54] B.W. König, S. Krueger, W. Orts, C.F. Majkrzak, N.F. Berk, J. Silverton, K. Gawrisch, Neutron reflectivity and atomic force microscopy studies of a lipid bilayer in water adsorbed to the surface of a silicon single crystal, Langmuir 12 (1996) 1343–1350, https://doi.org/10.1021/la950580r.

[55] R. Campbell, H. Wacklin, I. Sutton, R. Cubitt, G. Fragneto, FIGARO: the new

[56] horizontal neutron reflectometer at the ILL, Eur. Phys. J. Plus 126 (2011) 107, , https://doi.org/10.1140/epjp/i2011-11107-8.

[56] T. Crowley, E. Lee, E. Simister, R. Thomas, The use of contrast variation in the specular reflection of neutrons from interfaces, Phys. B Condens. Matter 173 (1991) 143–156, https://doi.org/10.1016/0921-4526(91)90044-F.

[57] A. Nelson, Co-refinement of multiple-contrast neutron/X-ray reflectivity data using MOTOFIT, J. Appl. Crystallogr. 39 (2006) 273–276, https://doi.org/10.1107/S0021889806005073.

[58] J. Penfold, R. Thomas, The application of the specular reflection of neutrons to the study of surfaces and interfaces, J. Phys. Condens. Matter 2 (1990) 1369, https://doi.org/10.1088/0953-8984/2/6/001.

[59] P. Pernot, A. Round, R. Barrett, A. De Maria Antolinos, A. Gobbo, E. Gordon, J. Huet, J. Kieffer, M. Lentini, M. Mattenet, Upgraded ESRF BM29 beamline for SAXS on macromolecules in solution, J. Synchrotron Rad. 20 (2013) 660–664, https://doi.org/10.1107/S0909049513010431.

[60] A. Round, F. Felisaz, L. Fodinger, A. Gobbo, J. Huet, C. Villard, C.E. Blanchet, P. Pernot, S. McSweeney, M. Roessle, BioSAXS sample changer: a robotic sample changer for rapid and reliable high-throughput X-ray solution scattering experiments, Acta Crystallogr. Sect. D: Biol. Crystallogr. 71 (2015) 67–75, https://doi.org/10.1107/S1399004714026959.

[61] A. De Maria Antolinos, P. Pernot, M.E. Brennich, J. Kieffer, M.W. Bowler, S. Delageniere, S. Ohlsson, S. Malbet Monaco, A. Ashton, D. Franke, ISPyB for BioSAXS, the gateway to user autonomy in solution scattering experiments, Acta Crystallogr. Sect. D: Biol. Crystallogr. 71 (2015) 76–85, https://doi.org/10.1107/S1399004714019609.

[62] H.M. Jindal, C.F. Le, M.Y. Mohd Yusof, R.D. Velayuthan, V.S. Lee, S.M. Zain, D.M. Isa, S.D. Sekaran, Antimicrobial activity of novel synthetic peptides derived from indolicidin and ranalexin against Streptococcus pneumoniae, PLoS One 10 (2015) e0128532-e0128532, , https://doi.org/10.1371/journal.pone.0128532.

[63] N. Kučerka, M.-P. Nieh, J. Katsaras, Fluid phase lipid areas and bilayer thicknesses of commonly used phosphatidylcholines as a function of temperature, Biochim. Biophys. Acta Biomembr. 1808 (2011) 2761–2771, https://doi.org/10.1016/j.bbamem.2011.07.022.

[64] B. Bechinger, K. Lohner, Detergent-like actions of linear amphipathic cationic antimicrobial peptides, Biochim. Biophys. Acta Biomembr. 1758 (2006) 1529–1539, https://doi.org/10.1016/j.bbamem.2006.07.001.

[65] J.C. Hsu, C.M. Yip, Molecular dynamics simulations of indolicidin association with model lipid bilayers, Biophys. J. 92 (2007) L100–L102, https://doi.org/10.1529/biophysj.107.108050.

SUPPLEMENTARY MATERIAL

A Biophysical Study of the Interactions between the Antimicrobial Peptide Indolicidin and Lipid Model Systems

Josefine Eilsø Nielsen[1], Tania Kjellerup Lind[2], Abdullah Lone[3], Yuri Gerelli[4], Paul Robert Hansen[5], Håvard Jenssen[3], Marité Cárdenas[2] and Reidar Lund*[1]

[1]Department of Chemistry, University of Oslo, 0315 Oslo, Norway
[2]Biofilms Research Center for Biointerfaces and Department of Biomedical Science, Health and Society, Malmö University, 20506 Malmö, Sweden.
[3]Department of Science and Environment, Roskilde University, 4000 Roskilde, Denmark
[4]The Institut Laue Langevin, 38042 Grenoble, France
[5]Department of Drug Design and Pharmacology, University of Copenhagen, 2100 Copenhagen, Denmark
*Corresponding author: reidar.lund@kjemi.uio.no

Typical QCM-D results for formation of DMPC90-DMPG10 bilayers before peptide exposure:
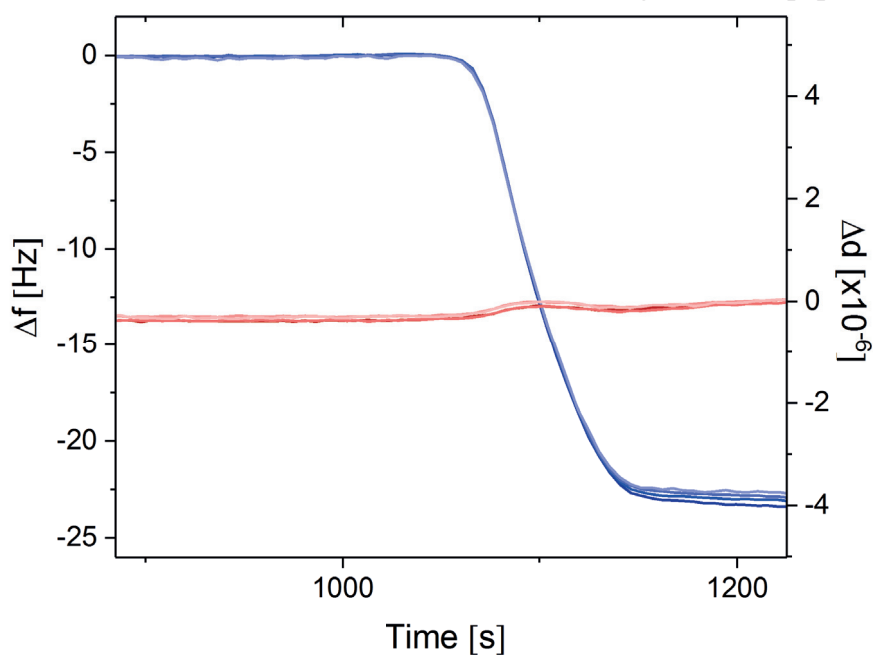
Figure S1. QCM-D results showing formation supported lipid bilayers composed of DMPC and DMPG in a molar ratio of 9:1. Changes in frequency are shown in blue and dissipation in red. For clarity, both the frequency and dissipation at all the harmonics are normalized to zero before addition of the peptide.

|	Neutron SLD [10^{-6} Å^{-2}][a]	X-ray SLD [10^{-6} Å^{-2}][a]
d54DMPC		
Head	1.84	14.0
Tail	6.7	7.71
d54DMPG		
Head	2.46	15.1
Tail	6.7	7.71
d54DMPC:d54DMPG 9:1		
Head	1.83	14.11
Tail	6.7	7.71
indolicidin	2.09[b]/3.12[c]	12.2

Table S1. Theoretical SLDs for the lipids and peptide used in this study.
[a]Calculated from the molecular component volume (based on MD simulations(13, 60)) and neutron scattering lengths.
[b]Calculated from the peptide molecular volume and the neutron scattering length.
[c]Calculated assuming exchange of all labile hydrogen atoms to deuterium in D_2O.

Neutron Reflectometry results for bilayer 1 and 2 before peptide exposure:
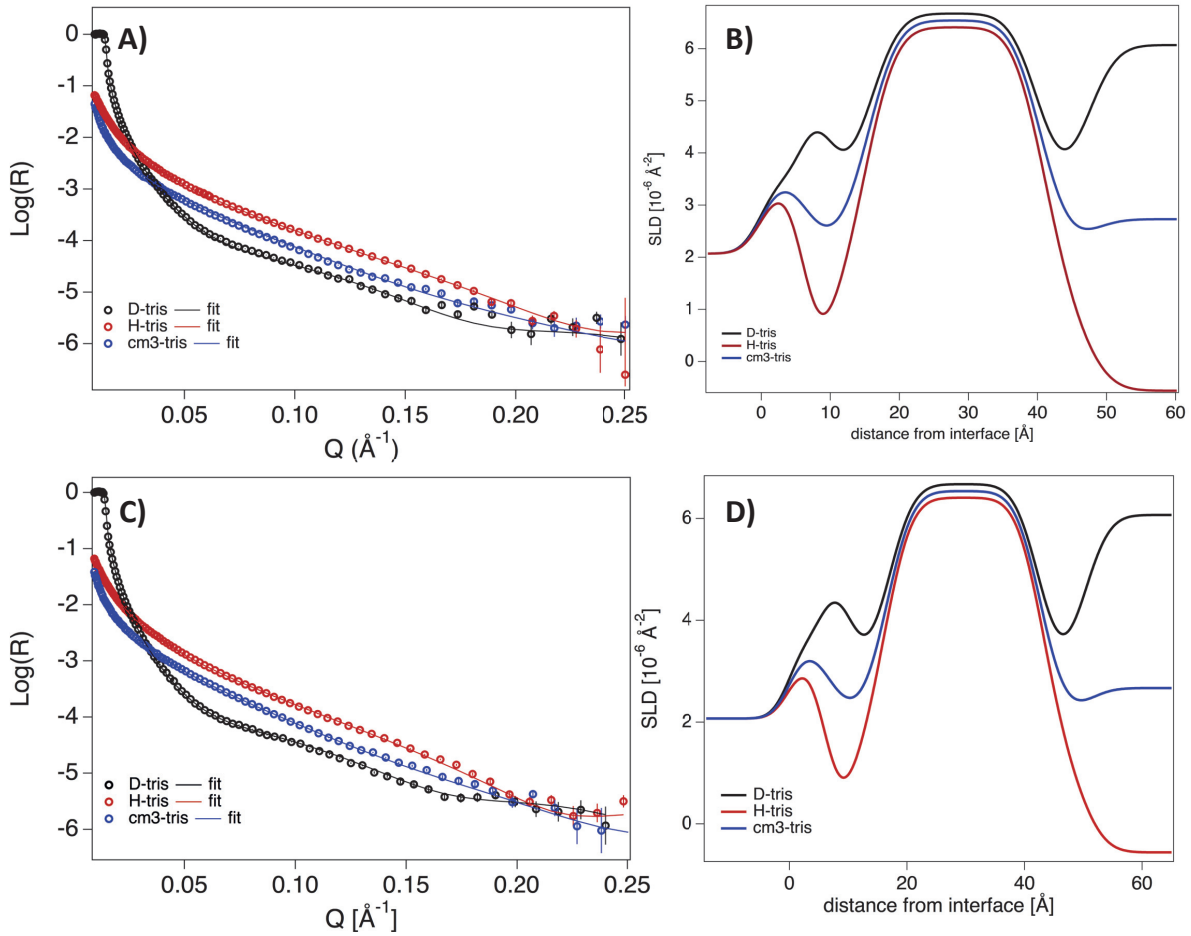

Figure S2. NR measurements of SLB before addition Indolicidin. Reflectivity profiles for the measurements together with best fit for bilayer 1(A) and bilayer 2(B). SLD profiles obtained from the fit analysis against distance from the interface for bilayer 1 (B) and bilayer 2 (D).

Fit parameters for SLBs exposed to 0.8 µM indolicidin without rinsing with buffer:

| Layer	d [Å]	Solvent [%]	SLD [10^{-6} Å^{-2}]	Indolicidin %
Before rinse 0.8 µM indolicidin				
Water	3	100	-	-
Head (inner)	6 ± 1	19 ± 3	1.83	-
Tail	25 ± 1	6 ± 1	6.1	-
Head (upper)	6 ± 1	10 ± 3	2	17 ± 2
Lipid/Indolicidin	42 ± 5	73 ± 1	6.4	13 ± 1
Water	17 ± 1	100	-	-
Lipid patch	40 ± 6	98 ±1	6.4	

Table S2. Fitted parameters for tail-deuterated DMPC/DMPG membranes after incubation with 0.8µM Indolicidin prior to rinse with buffer showing bilayer patches that are removed with rinsing. A_{mol} is the molecular area per lipid component including solvent.

**Fit model for Neutron reflectometry results with and without extra peptide layer:**
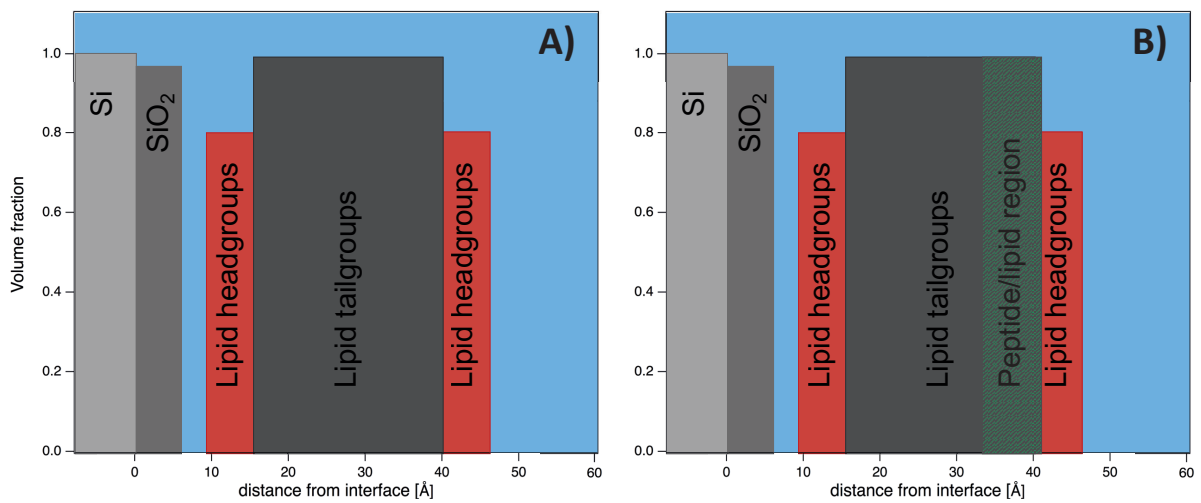
Figure S3. Illustration of model used to fit the neutron reflectometry data. A) symmetric bilayer model. B) Asymmetric model corresponding to the SAXS model with peptide insertion in the outer leaflet used to fit the data in Figure S3. Both the composition and size of the peptide block is varied.
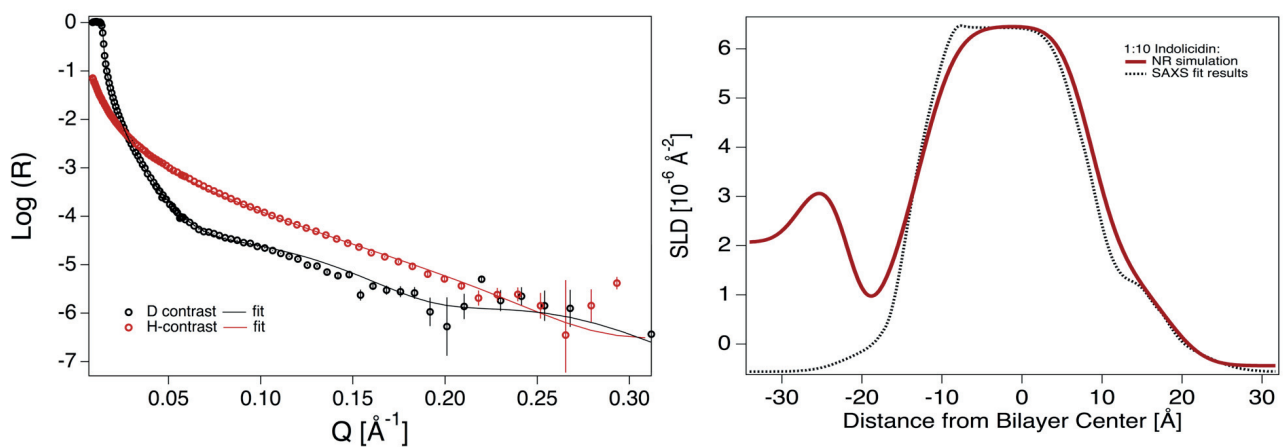

Figure S4. Fit analysis of NR data with an additional box of the peptide as illustrated in Figure S2B varied in size and composition (amount of peptide). The result show that the NR does not contradict the SAXS modelling, but the resolution in the NR data are not high enough to conclude on this fit model based on NR alone.

Analytical results of the purified indolicidin:
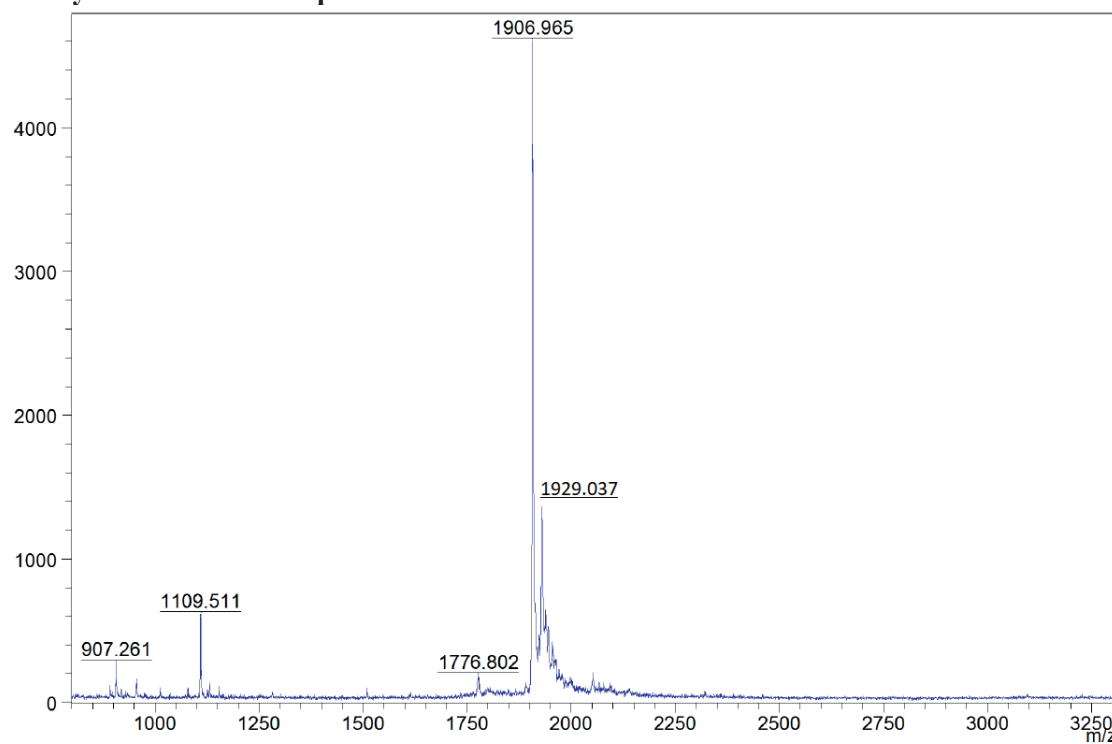
Figure S5. MALDI-TOF-MS results of the purified peptide: [MH$^+$]: 1906.965 and [MNa$^+$]: 1929.037 (1906.33 g/mol calculated)
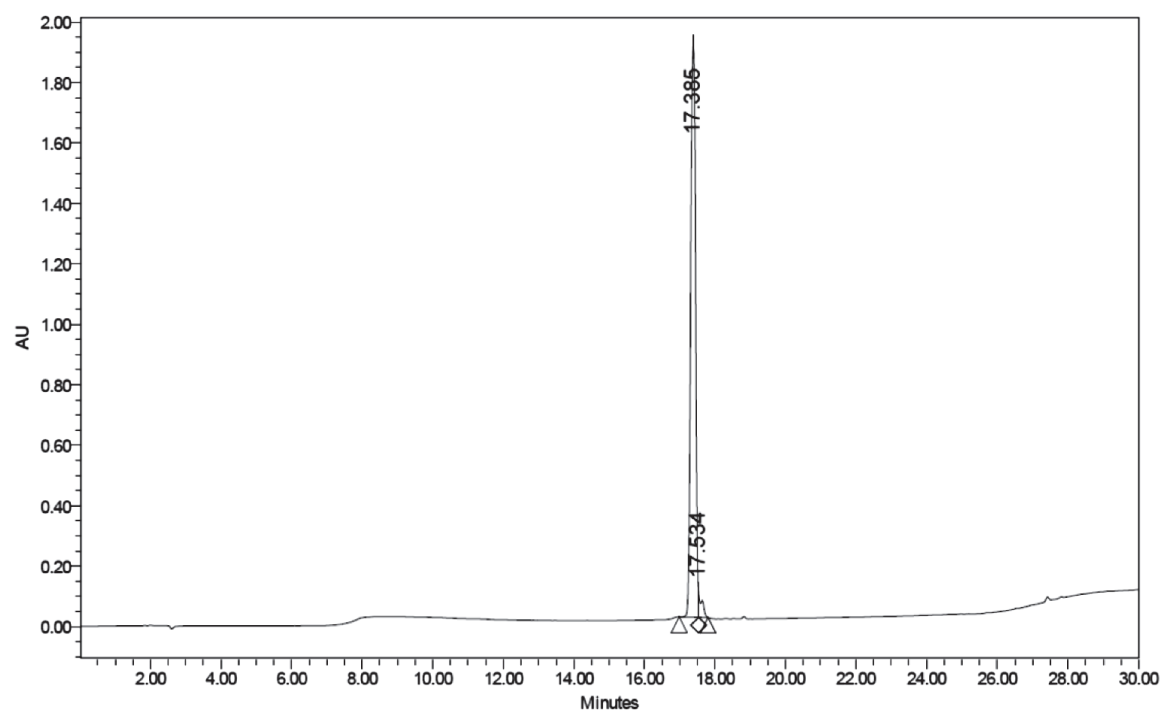
Figure S6. Analytical HPLC results of the purified peptide showing a purity of 97.1 % (retention time 17.385).
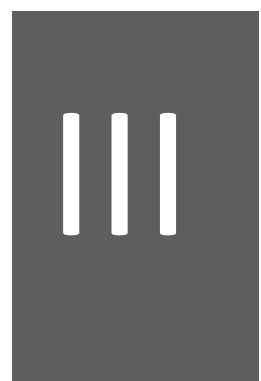
Paper III

Beyond Structural Models for the Mode of Action: How Natural Antimicrobial Peptides Disrupts Lipid Membranes

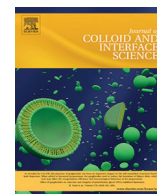Josefine Eilsø Nielsen, Victoria Ariel Bjørnestad, Vitaliy Pipich, Håvard Jenssen and Reidar Lund

III

# Beyond structural models for the mode of action: How natural antimicrobial peptides affect lipid transport

Josefine Eilsø Nielsen [a], Victoria Ariel Bjørnestad [a], Vitaliy Pipich [b], Håvard Jenssen [c], Reidar Lund [a,*]

[a] Department of Chemistry, University of Oslo, Postboks 1033 Blindern, 0315 Oslo, Norway
[b] Jülich Centre for Neutron Science (JCNS) at Heinz Maier-Leibnitz Zentrum (MLZ), Forschungszentrum Jülich GmbH, 85747 Garching, Germany
[c] Department of Science and Environment, Roskilde University, Universitetsvej 1, Roskilde 4000, Denmark

GRAPHICAL ABSTRACT
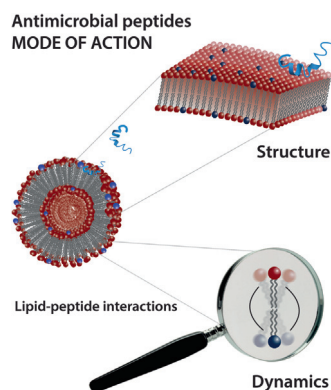
ARTICLE INFO

ABSTRACT

Hypothesis: Most textbook models for antimicrobial peptides (AMP) mode of action are focused on structural effects and pore formation in lipid membranes, while these deformations have been shown to require high concentrations of peptide bound to the membrane. Even insertion of low amounts of peptides in the membrane is hypothesized to affect the transmembrane transport of lipids, which may play a key role in the peptide effect on membranes.

Experiments: Here we combine state-of-the-art small angle X-ray/neutron scattering (SAXS/SANS) techniques to systematically study the effect of a broad selection of natural AMPs on lipid membranes. Our approach enables us to relate the structural interactions, effects on lipid exchange processes, and thermodynamic parameters, directly in the same model system.

Findings: The studied peptides, indolicidin, aurein 1.2, magainin II, cecropin A and LL-37 all cause a general acceleration of essential lipid transport processes, without necessarily altering the overall structure of the lipid membranes or creating organized pore-like structures. We observe rapid scrambling of the lipid composition associated with enhanced lipid transport which may trigger lethal signaling processes and enhance ion transport. The reported membrane effects provide a plausible canonical mechanism of AMP-membrane interaction and can reconcile many of the previously observed effects of AMPs on bacterial membranes.

© 2020 The Author(s). Published by Elsevier Inc. This is an open access article under the CC BY license (http://creativecommons.org/licenses/by/4.0/).

1. Introduction

Antimicrobial peptides [1–6] show significant broad-spectrum antibacterial activity. Several bacterial resistance mechanisms e.g. extracellular proteases, [7] sequestration, [8] cell surface modifications [9,10] and increased efflux activity, [11] have been described. However, it is apparent that the microbes rarely develop resistance traits similar to what render many conventional antibiotics ineffective [12]. Contrary it is evident that antimicrobial peptides and bacterial resistance mechanisms have evolved in symphony to stabilize a host-pathogen balance [13]. It is believed that the peptides target multiple hydrophobic sites, and have a combined immunomodulatory activity making resistance development more difficult [14]. It is suggested that the peptides owe their antimicrobial properties to the disruptions of the cytoplasmic membrane, [2,15,16], although a few peptides also are described to have intracellular targets [15,17]. Chongsiriwatana and co-workers recently suggested a combination of membrane permeabilization with flocculation effect on internal ribosomes, RNA and DNA causing the bactericidal effects in a study of a wide range of natural and synthetic peptidomimetics [18]. Two physical characteristics are regarded as fundamental for most AMPs: their cationic charge and hydrophobic amino acids. The amphiphilic nature provides surface affinity towards lipid membranes and the basis of selectivity is likely to be related to electrostatic attraction between positively charged AMPs and the residual negative charge of microbial cell surfaces [19]. These properties combined with their small sizes promote easy translocation of the peptides through the outer membrane of Gram-negative and the cell wall of Gram-positive bacteria [20,21].

Although their membrane interactions are believed to be an important component of their antimicrobial activity, the mechanism is not yet fully understood. In the classical view, peptides are thought to permeabilise the membrane, causing essential molecules to leak through the cytoplasmic membrane through distinct channels [2,6,22]. Several suggested mechanisms involve various degrees of pore formation or deformations of the membrane. Many of these have been criticized [4,23] for their high peptide-lipid (P:L) ratios because these would be unrealistic under physiological conditions [24]. Experimental data indicating clearly defined pore structures at low concentrations are very limited [4]. Most evidence comes indirectly from membrane permeability studies where AMPs generally cause a release of dyes in liposomes [25]. Screening experiments have also failed to show any clear relationship between the AMP-induced membrane permeability and the antimicrobial activity of the AMP, [18,26] questioning the existence of nanometre pores. Similar confusion is observed in biological assays, where a wide spectrum of fluorescent probes is available for determination of membrane damage [27,28]. The conclusions drawn from these studies often contradict the classical growth experiments. This suggests that very subtle membrane changes might be enough to prevent bacterial growth [29] or that the effect on the membrane is the first step in a mechanism that involves intracellular targets [18]. These observations have also been confirmed with electron microscopy, where clear membrane damage is observed only as subsets of the exposed bacterial cells at concentrations well above the minimal bactericidal concentration [30,31].

While most textbook examples emphasize the importance of the peptide structure formation in pore formation, [1] the nanoscopic nature of these pores is not clear. Recently, Wimley and co-workers suggest an "interfacial model" where the peptide rather perturbs the lipid bilayer, creating pores of a transient nature that would still allow some transport through the membrane [4,15]. Within this picture well-defined structural peptide folds are not necessary. Beyond the structural defects imposed by the

peptides several studies have reported that the peptides may also affect the motion of the membrane lipids [23,32–37]. Hereunder, lipid flip-flop, transport of single lipids between leaflets, which without influence of peptides or proteins is known to be extremely slow [38].

In this work we have used advanced X-ray and neutron scattering techniques to study the effect of peptides on the basic properties of the cell membrane mimics. We have used unilamellar lipid vesicles that have been shown to be a simplified yet relevant model for studying antimicrobial peptide-membrane interactions [39]. Contrary to previous studies, we have focused both on changes in the structure and the dynamics of the lipid membrane upon interaction with the antimicrobial peptides as illustrated in Fig. 1. Using a wide range of natural antimicrobial peptides, varying in size, charge, degree of helicity and origin, we show how the peptides have a profound impact on the exchange processes of the phospholipids constituting the membrane. Except *colistin* (*polymyxin E*), which is known to mainly target the lipopolysaccharides (LPS) on the outer membrane of Gram-negative bacteria [40], all of the investigated peptides significantly accelerates both the flip-flop motion and the molecular transport of phospholipids without changing the overall structure of the membrane in any significant way. We speculate that this is a general feature of a broad range of antimicrobial peptides and that it is important for their mode of action. Alteration of the lipid exchange processes would have a significant impact on many fundamental properties of the lipid membrane such as the lipid composition and distribution in the inner and outer leaflets and transport processes, including ion transfer. The results we present may offer an explanation as to why leakage across the membrane has been seen in experiments without clear evidence of pore-formation.

2. Materials and methods

2.1. Vesicle preparation

Unilamellar lipid vesicles were prepared by making a lipid film of *DMPC* (75%), *DMPG* (22.5%) and DMPE-PEG (2.5%) by dissolving the lipids in methanol:choloform and removing the solvent by vacuum using a Heidolph rotary evaporator with a Vacuubrand vacuum pump. The lipid film was hydrated in a 50 mM Tris buffer of pH 7.4, then sonicated for 15 min and the resulting lipid dispersion was extruded through a through a 100 nm pore diameter polycarbonate filter (>21 times) using an Avanti mini-extruder fitted with two 1 mL airtight syringes.

2.2. Small angle X-ray scattering

SAXS experiments were performed at the bio-SAXS BM29 beamline at European Synchrotron Radiation Facility (ESRF) in Grenoble in France, with a detector distance of 2.87 m and energy of 12.5 keV, covering a Q range of 0.0047 Å^{-1} to 0.5 Å^{-1} at 37 °C.

The SAXS results on the pure lipid vesicles were analysed using *t*-he scattering density profile (SDP) model presented by Kučerka and co-worker, which allow the bilayer structure to be described in terms of one-dimensional volume probability profiles of quasi-molecular lipid fragments [41–43]. Each leaflet of the membrane is parsed into the hydro- carbon terminal methyl (CH_3), hydrocarbon methylene (CH_2), carbonyl + glycerol (CG) (common for all three phospholipid) and outer part of head group (PC/G head), and the volume probability distributions of the components are described by Gaussian functions (equation 6 in the supplementary information). However, based on prior work from Eicher et al. the volume probability of the hydrocarbon methylene (CH_2) group (calculated by subtracting the volume probability of the CH_3 from
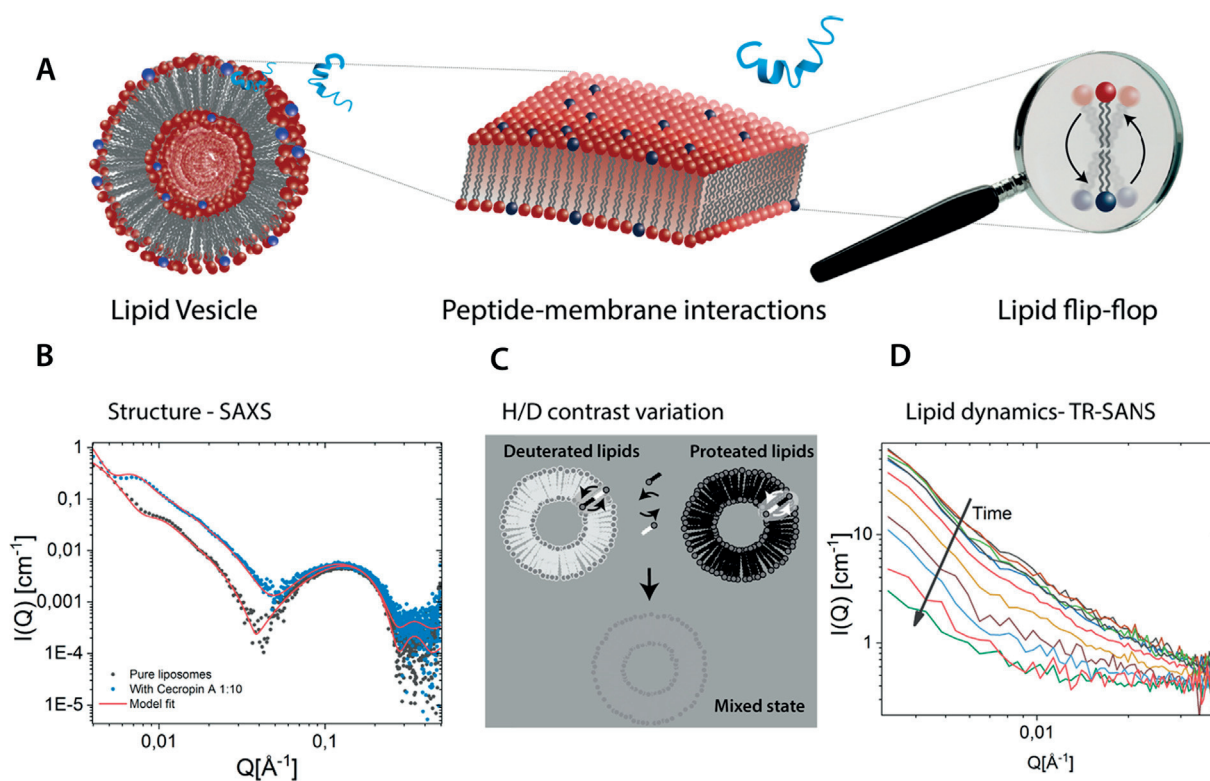
Fig. 1. Methodology used to study peptide-membrane interactions on both a structural and dynamical level. A) Illustration of lipid vesicles used as model systems for bacteria membrane. B) Example of SAXS data used to determine structural peptide-membrane interaction. C) Illustration of the TR-SANS method where deuterated and proteated liposomes are re-suspended at time zero and then the gradual mixing of lipids through exchange and flip-flop are tracked over time through detection of increased scattering intensity. D) Example of TR-SANS data for DMPC/DMPG at 37 °C.

the hydrocarbon groups (HC representing the tails)) is modelled using a half period squared sine/cosine function to account for eventual asymmetry in the bilayer [44]. To analyse the lipid-peptide mixtures the contribution from the peptide was added in the model as a pseudo-parsing group across the bilayer, and the volume probability of the peptide as an additional Gaussian function [45]. For a detailed mathematical description of the theoretical scattering model used to analyse the SAXS data, see the supplementary information.

2.3. Time resolved small angle neutron scattering

TR-SANS experiments were performed on the KWS-2 beamline at the Heinz Maier-Leibnitz (FRM II) center, MLZ in Garching, Germany using detector distance of 20 m and a wave length of 5 Å, covering a Q range of 0.0032 $Å^{-1}$ to 0.039 $Å^{-1}$.

3. Results and discussion

3.1. Most natural antimicrobial peptides do not change the overall structure of lipid membranes

To study the membrane interaction of different AMPs we did SAXS experiments on peptide-lipid mixtures which allows us to precisely investigate structural changes in the lipid bilayer as well as the overall effect on the vesicle morphology. As shown in a previous study [45,46] the SAXS patterns of lipid vesicles are extremely sensitive to the insertion of antimicrobial peptides due to the significant contrast in electron density between the tail region in the core of the lipid membrane and the peptide. Of the wide range of AMPs found in nature we chose to study four well known

α-helical AMPs: *LL-37* [47], a human peptide, *cecropin A* [48] found in moths, and *magainin II* [49] and *aurein 1.2* [50] found in frogs. In addition, we have previously performed an in-depth study of the unstructured peptide *indolicidin* of bovine origin [45,46]. The chemical structures of the AMPs are shown in the supplementary information Figure S1 and the helicity of the peptides in the presence of our lipid model system has been confirmed with circular dichroism spectroscopy as seen in Figure S2 and Table S1. The effect on the scattering pattern depends on the peptide concentration as seen in Fig. 2, with an increasing shift in the first minima (dotted line) to higher Q with increasing peptide to lipid ratio. The shifts in the scattering pattern is due to the peptide penetrating into the bilayer, but the exact position of the peptide cannot be deduced from mere visual inspection. To extract detailed structural information from the SAXS data we have therefore used an analytical scattering model which is described mathematically in the supplementary information [45]. Parameters related to the lipid bilayer have been constrained within the previously found values (see supplementary information for details). From these analysis, we may deduce the volume probability profiles which show the distribution of the different chemical groups, including the peptide, across the bilayer. The main fitting parameters used to describe the changes in the scattering pattern upon peptide addition are the position $Z_{peptide}$ and distribution $\sigma_{peptide}$ of the peptide, which describes the insertion in the membrane.

The fit analysis of the scattering patterns reveals important differences in the peptide-lipid interactions of the four peptides. This can be seen from the volume probability distribution plot in Fig. 3 and key fit parameters in Table 1. The larger peptide *cecropin A* with 37 residues does not penetrate into the bilayer and is distributed mainly on the surface of the vesicles, while the smaller *magainin II* with 23 residues penetrates into the interface between
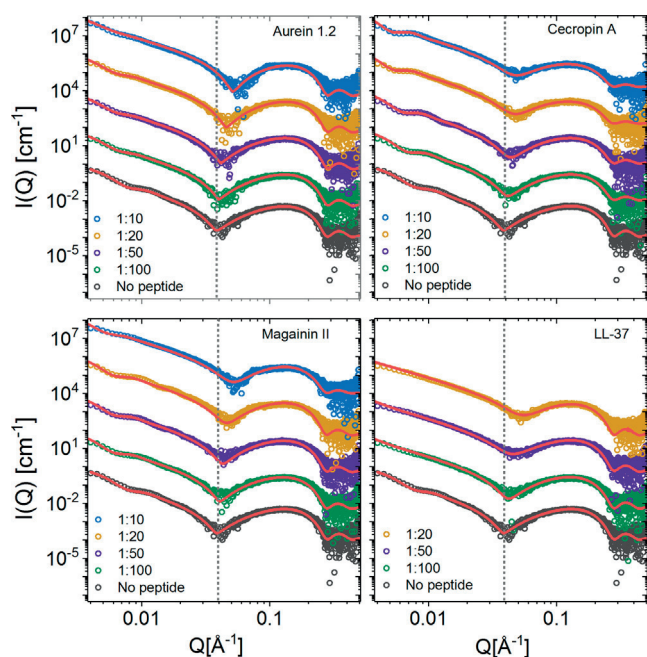
Fig. 2. Small angle X-ray scattering data with model fits (–––) for peptide-lipid mixtures at ratios 1:100, 1:50, 1:20 and 1:10. Peptide insertion result in a change in the bilayer contrast (scattering length density of the bilayer compared to the buffer) seen as a shift in the minima at intermediate Q-values. A line has been added at the minima to visualize the shift.

the tail and head region of the outer leaflet. The latter shows high similarity to *indolicidin* [51], a natural, unstructured AMP with 13 residues that has previously been studied in detail using the same

SAXS technique [45] as well as with Neutron Reflectometry [46]. *Aurein 1.2* with 13 residues penetrates deeper into the bilayer, with a symmetric distribution of peptides spanning across the entire bilayer. In the scattering patterns in Fig. 2 these changes can be seen as subtle difference in the position and depth of the minima. A symmetric distribution of peptides within the membrane results in a depth of minimum that is more similar to that of the unperturbed bilayer structure while the asymmetrical distribution of the other peptides results in shallower minima. A comparison of the simulated scattering curves from different peptide distributions has been included in the supplementary information, Figure S3. Here we considered i) a single Gaussian in the outer leaflet, ii) symmetric double gaussian with peptide in outer and inner leaflet, and, iii); a broad transmembrane distribution pf the peptide. Although the distribution of *aurein 1.2* spans over the core of the bilayer, the short peptide is not long enough to form distinct pores, [52] an observation which is in agreement with earlier studies using neutron in-plane scattering [53]. Nano-DSC experiments included in supplementary information Figure S4 and S5 confirms that all peptides disturbs the packing of the lipids resulting in a lowered melting temperature (T_m), the same behaviour has previously been seen for peptides known to insert into the hydrophobic region of the lipid membrane [45].

At the lower peptide ratios depicted in Fig. 2, the scattering pattern does not reveal any notable effect of *LL-37* with 37 residues on the overall structure of the membrane. The insertion of the peptide in the bilayer at this concentration range seems highly concentration dependent, where increased concentration leads to a deeper insertion as illustrated in the volume probability plot in Fig. 3. The scattering pattern of the higher concentrations of *LL-37*, however, is remarkably different than the effect of the other peptides (supplementary information Figure S6). Here the entire shape of the scattering curve is altered, and the slope at low Q follows a
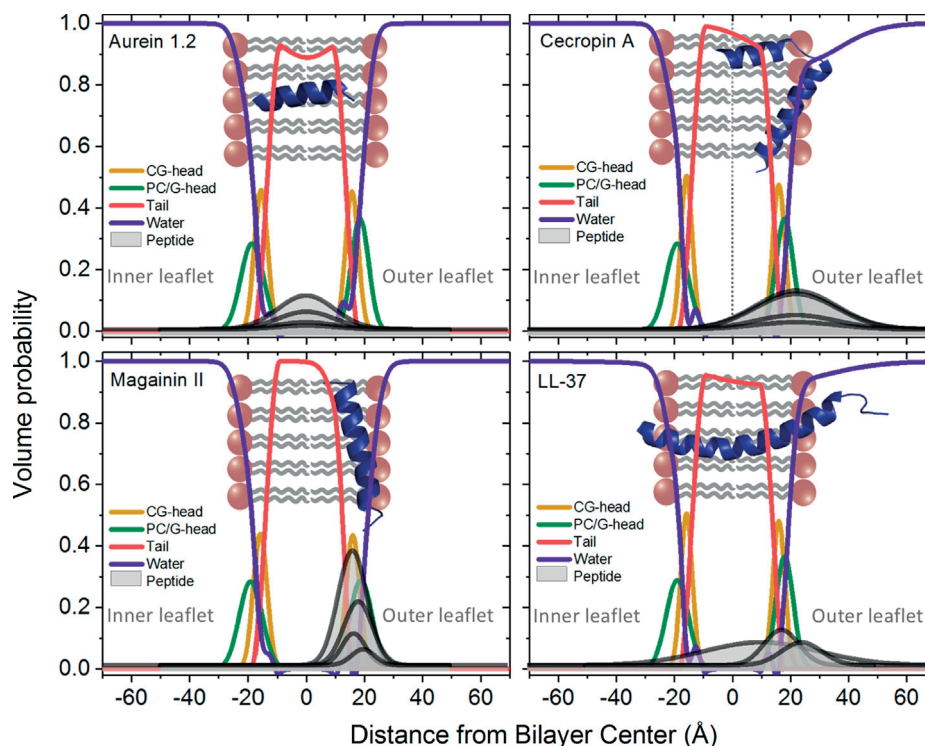
Fig. 3. Volume probability distributions for the lipid membranes with various amounts of peptide (aurein 1.2, cecropin A, magainin II and LL-37). The area of the Gaussian function of the peptide (grey coloured peaks) increases with increasing amounts of peptide added to the sample. Inset drawing illustrates the proposed position of the peptides (PDB ID): Aurein 1.2: 1VM5, Magainin II: 2MAG, Cecropin A: 2LA2 (the PDB structure of a close Cecropin analog used as an illustration as the PDB of Cecropin A from 1988 [56] is not available in the PDB database), LL-37: 2K6O [57–60] in the membranes resulting from the fit (peptide is not in scale to lipids in drawing).

Table 1
Overview of the key fitting parameters from SAXS data on liposome-peptide mixtures (for detailed list see supplementary information Table S2).

| Fraction peptide	Aurein 1.2				Cecropin A				Magainin II				LL-37		
	1:100	1:50	1:20	1:10	1:100	1:50	1:20	1:10	1:100	1:50	1:20	1:10	1:100	1:50	1:20
Bilayer thickness[Å]	38.6 ± 0.5	38.6 ± 0.5	38.6 ± 0.5	38.6 ± 0.5	38.6 ± 0.5	38.6 ± 0.5	38.4 ± 0.5	38.4 ± 0.5	38.6 ± 0.5	38.7 ± 0.5	38.8 ± 0.5	38.8 ± 0.5	38.6 ± 0.5	38.6 ± 0.5	38.6 ± 0.5
$Z_{peptide}$[Å]	0.3	0.3	0.3	0.3	22.8	22.9	23	23	19.6	17.1	18.3	16.3	25	18	11
$\sigma_{peptide}$[Å]	10	9.7	9.8	10	13.9	14.1	14.2	14	4.1	4.2	5.1	5	7	6	20
$f_{micelles}$	-	-	-	-	-	-	-	-	-	-	-	-	0	0.01	0.03
Ratio P/L in micelles	-	-	-	-	-	-	-	-	-	-	-	-	-	0.08	0.1
f_{free}	0	0	0	0	0	0	0.1	0.4	0	0	0	0	-	-	-
σ_{SD}	0.3	0.3	0.3	0.45	0.23	0.23	0.23	0.22	0.25	0.25	0.25	0.3	0.29	0.6	0.6

power law of Q^{-1} compared to the steeper slope of the scattering curves for the other peptides. This indicates that the peptides partially solubilize the membrane and causes the formation of mixed micelles of peptide and lipids. The same behaviour has previously been reported by Sevcsik and co-workers based on SAXS where the resulting structures were reported to have a disc-like shape [54,55]. At peptide-lipid ratios of 1:100, 1:50 and 1:20 analysis of the scattering curves indicates only a 0–0.03 fraction of mixed micelles (see Table S2).

3.2. The phospholipid transport in bacterial membranes are accelerated by natural AMPs.

Studies of the lipid exchange processes in the model membranes by time resolved SANS contrast variation technique (Fig. 1 C/D) provide evidence that both the intra-vesicular flip-flop and inter-vesicular exchange of lipids is greatly affected by the addition of various AMPs. This technique exploits the fact that neutrons are scattered differently by hydrogen and deuterium, so that mixing identical, but differently labelled vesicles with H-lipids and D-lipids in H_2O/D_2O buffer mixtures that match the average scattering length density of the liposome mix after full exchange (zero average contrast) result in decreased scattering intensity over time (see Fig. 1E) due to the exchange of lipids between the vesicles [61–68]. In other words, the liposomes gradually become matched to the background, and therefore progressively become "invisible" for neutrons with time. The experimental method and analysis of the data is described in detail in the supplementary information. Previously, it has been shown that the exchange and flip-flop rates are directly dependent on the acyl chain length due to changes in solubility and fluidity [69,70]. All the experiments presented are done at temperatures above the melting temperature of the lipids (above 24°) as the membrane is then in the fluid liquid crystalline phase.

Comparing the rate of intensity decay, R(t) presented in Fig. 4A reveal a clear impact of addition of various peptides at 37 °C. Fit analyses of the R(t) curves by the model described in the supplementary information reveal two independent processes: a fast exchange process and a slower flip-flop process. Rates for both of these processes can be extracted from the fit analysis. The rate of exchange being higher than the flip-flop rate has also been reported previously for the same lipids [61,70,71]. As a positive control we used *colistin* [72], a commercially available peptide antibiotic that is known to have another target than the cytoplasmic membrane [40], contrary to what is suggested for a range of other AMPs as described in the introduction. The absence of any membrane interaction with *colistin* in the used concentration range was confirmed using SAXS (see Figure S7) and DSC (see Figure S5B). Contrary to what we see with our model system, Dupuy and co-workers have observed some colistin interaction with model membranes mimicking Gram-positive and Gram-negative bacteria, [73] however the model system and more importantly, the methodology in this study differs from ours. There the peptide was mixed in the organic lipid solution before preparation of lipid films for hydration, while in our case the peptide was mixed with the lipid vesicles directly prior to the measurement.

As can be seen from the decay curves, R(t), shown in Fig. 4. All the peptides tested except colistin significantly accelerate the lipid transport in our model membranes. The model liposomes used for the experiments also include a small amount of PEGylated lipids to prevent fusion and aggregation of vesicles upon peptide addition. To validate this, vesicles with 2.5 and 5% PEGylated DMPE with and without 1:10 indolicidin were measured. The results show no difference in lipid exchange processes between the two systems (Fig. 5A). Furthermore, in order to provide further evidence that the evolution of the intensity over time is due to single chain exchange
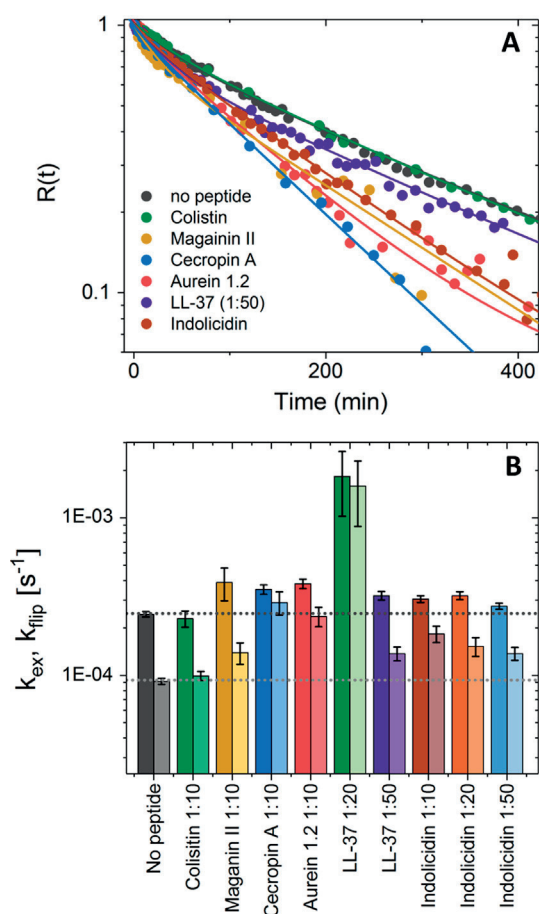
Fig. 4. Results from TR-SANS studies on the effect of natural antimicrobial peptides on the lipid dynamics in membrane model systems at 37 °C. A) Rate of contrast decay, R(t), of lipid vesicles after mixing D- and H-labelled vesicles with addition of indicated peptides in the ratio 1:10. LL-37, as indicated in the legend, is shown at a mixing ratio 1:50. Solid curves are fitted curves according to equation 36 in supplementary information. B) Rate constants for exchange (dark colours) and flip-flop (light colours) based on the curve fitting of R(t) data for various natural peptides. The inset dotted lines indicate the k values for exchange (k_{ex}) and flip-flop (k_{flip}) of pure lipid vesicles for comparison.

and flip-flop, and not fusion of vesicles or other collision induced mechanisms, identical samples with different overall concentrations were tested at the same temperature. The curves overlap
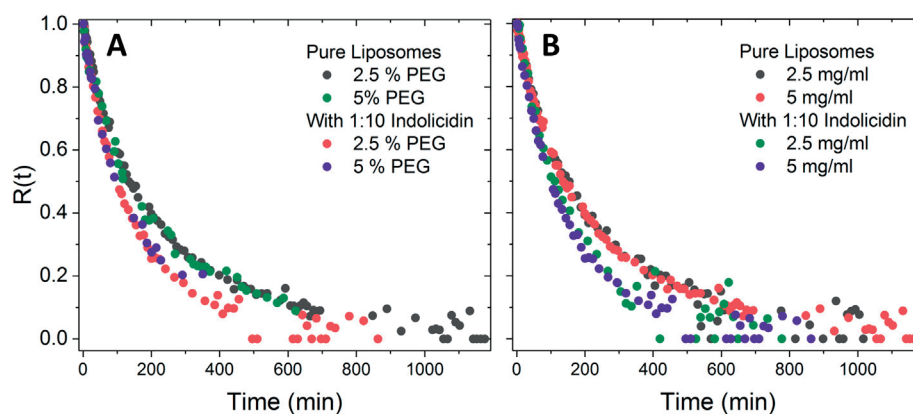
perfectly and we can conclude that there is no effect of fusion in the investigated concentration range (Fig. 5B).

Indolicidin, aurein 1.2, maganin II, cecropin A and low ratios of LL-37 (1:50 peptide:lipid ratio) are seen to significantly accelerate the lipid exchange process in the same order while the effect on the lipid flip-flop varies considerably amongst the peptides. Given the very different nature of the peptides in terms of molecular weight, secondary structure, flexibility, and surface characteristics, it may appear that lipid exchange is the outcome of an early initial electrostatic interaction between the peptides and the lipid membrane. A firmer anchoring of the peptide in the membrane on the other hand assists lipid flip-flop, and the architectural differences amongst the peptides mirror the diverse flip-flop rates we report. Furthermore, we do not, find a direct correlation between the fraction of peptide localized in the head or tail region of the membrane, or the size of the peptides, and the effect they infer on the lipid flip-flop. Nguyen and co-workers found that peptides that tend to localize at the surface of the membranes accelerated the flip-flop to a higher degree than peptides that insert into the bilayer [35]. This supports our observation of a significant acceleration of the flip-flop process by cecropin A, magainin II and indolicidin which all were found to localize on the membrane surface in the analysis of the SAXS data. They seem to accelerate the lipid transport to the same degree, corresponding well with insertion into the interface of the head and tail region of the outer leaflet However, although aurein 1.2 inserts deep into the core of the membrane, the peptide also gives a dramatic effect on the flip-flop rate. Fernandez and co-workers have previously suggested that aurein 1.2 acts in a detergent like manner by neutron reflectometry and nuclear magnetic resonance experiments [74]. Here we do not, in contrast to *LL-37*, observe membrane dissolution and micelle formation in our SAXS experiments. However, the significant amphiphilic nature of *aurein 1.2* would explain the strong observed effect on lipid transport. Although the localization within the bilayer vary with the peptide, the overall effect on the dynamics is similar. This demonstrates that although the peptide interacts in varying manner with the membrane structurally and displays different interaction strength and concentration dependence, the overall effect on the lipid dynamics is similar. Combined this point towards a canonical effect of the peptides that likely constitutes an important part of their antibacterial mode of action.

It is interesting to compare the results for *LL-37* and *indolicidin* in more detail. For *LL-37* we find a strong concentration dependence on both the structure and lipid dynamics. At a 1:10 peptide:lipid ratio, when the vesicles still persist, *LL-37* causes a dramatic acceleration of both lipid exchange and flip-flop from

Fig. 5. A) R(t) curve for different PEG amounts, 5 and 2.5% DMPE-PEG, with and without peptide showing that PEGylation in this range does not seem to significantly affect the dynamics.B) R(t) curve for liposomes with and without peptide, with liposome concentration of 2.5 mg/mL and 5 mg/mL. The results reveal no concentration dependency in this range indicating that the loss of intensity is due to single chain exchange of lipids, not fusion of vesicles.

hours to a few minutes that is faster that the time resolution of the measurement. When the peptide concentration is lowered to 1:20, a profound acceleration is still observed. Here the end state is reached within 20 min, thereby giving fewer data points and therefore large error bars in the calculated exchange and flip-flop rates. For *indolicidin* we do not see the same clear concentration dependency, but only a slight decrease in the rate of flip-flop with decreasing concentration of peptide. As seen from SAXS [45] *indolicidin* only inserts into the bilayers outer leaflet without any notably change in the overall structure of the bilayer at all tested concentrations. Although all peptides, except *colistin* have similar levels of this effect, it is challenging to correlate the structural and dynamic effects quantitatively. A very weak concentration dependence of the flip-flop rate is seen from *indolicidin*, without a corresponding marked concentration dependent effect on the exchange rate.

3.3. The acceleration of the lipid exchange processes can be explained by a reduction of the activation energy or effectively reduced friction

The difference we see in the structural interaction of *LL-37* and indolicidin provides an explanation of the variance observed in their impact on the lipid transport. A deeper look into the thermodynamic parameters extracted from measurements at different temperatures might provide a more thorough understanding on the phenomenon.

From TR-SANS experimental data on identical samples at different temperatures we can extract the activation temperatures (E_a) and an attempt time (τ_0) through the Arrhenius equation:

$$k = \frac{1}{\tau_0} \exp\left(-\frac{E_a}{RT}\right)$$

From the fitted data depicted in Fig. 6, we find for LL-37, a large decrease in the activation energy of the exchange kinetics from

103 kJ/mol without peptide to 77 kJ/mol after peptide addition. For the flip-flop process, however, the activation barrier is constant about 75 kJ/mol with and without peptide while at the same time the characteristic diffusion time, τ_0, is reduced by 5% The latter points towards a reduction of the effective friction coefficient or entropic effect experienced when the peptide transverses the bilayer. *Indolicidin* on the other hand, affects the activation energy of the flip-flop which decreases from 74 kJ/mol to 64–66 kJ/mol after peptide addition without a significant effect on the activation energy of the lipid exchange. With this we can conclude that the increases in the rates of flip-flop for *LL-37* and exchange for *indolicidin* are not due to a change in the activation energy of the processes but rather in the pre-exponential factor. This effect can be explained by a reduction in the effective friction factor as the lipid passes the bilayer, e.g. through defects, or, possibly a lower entropic barrier upon peptide interaction. Applying an Eyring approach (see supplementary information for details and Table S4), we do find a small increase in the $T\Delta S$, for flip-flop with addition of the peptides. This possibly indicates complexation between the lipid and peptide. It has previously been hypothesized by, amongst other Conboy and co-workers, that peptides can facilitate increased flip-flop through defect-driven lipid translocation or increased entropy of the transition state resulting in a lower barrier for flip-flop [34,75]. Further it has been hypothesised in the past that AMPs may cause formation of lipid domains consisting of anionic lipids in the outer leaflet of the membrane due to their cationic charge [76]. One could imagine that the increased transmembrane transport of lipids observed in this study was linked to this process where insertion of peptides in the surface of the outer layer induces an asymmetric distribution of anionic lipids between leaflets, a lipid scrambling process. However, we have earlier showed that domains of anionic lipid could not be observed in similar model vesicles upon addition of *indolicidin*, using a contrast variation and SANS [45].
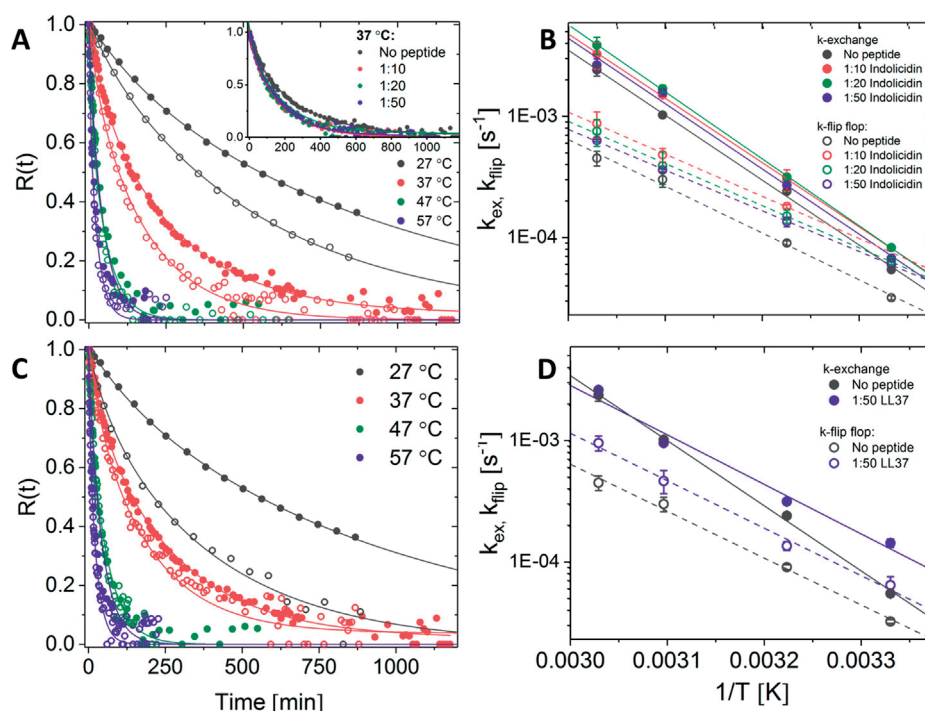
Fig. 6. Results from TR-SANS experiments on the effect of natural antimicrobial peptides on lipid dynamics in membrane model systems at four different temperatures. A) Rate of contrast decay, R(t), of lipid vesicles after mixing D- and H-vesicles with addition of 1:50 indolicidin (A) (inset graph shows concentration effect of indolicidin at 37 °C) and 1:50 LL-37 (C). Solid points represent the data for pure lipid vesicles, while open dots represent the vesicle samples upon peptide addition. Solid curves are fitting curves according to equation 36 in supplementary information. B) Arrhenius plots of the rates of exchange (k_{ex}) and flip-flop (k_{flip}) for samples with indolicidin 1:10, 1:20 and 1:50 (B) and LL-37 (1:50) (D).

For *LL-37* on the other hand both the SAXS and TR-SANS data already reveal more pronounced effects and concentration dependence. *LL-37* inserts deeper into the core dependent on concentration of peptide to lipid. The effect on the dynamics is also highly concentration dependent. When the peptide inserts into the core of the membranes the local polarity of the hydrocarbon region might be increased due to the hydrophilic charged sidechains of *LL-37*. This results in a reduced energy barrier for the lipid headgroups to pass through the hydrocarbon region resulting in increased flip-flop [77]. Furthermore, *LL-37* is seen to partly solubilise the lipid bilayers resulting in a dramatic increase in lipid exchange, this can be associated with introduction of defects in the membrane supporting translocation of lipids over the membrane.

4. Conclusion

In this work we employed multiple techniques to investigate the effects of various representative natural antimicrobial peptides on membrane model systems. With a combination of structural and topological information obtained from SAXS measurements and comparison of kinetic parameters describing the lipid transport as measured by time-resolved SANS experiments we are able to compare the effects of the peptide on the membrane structure with the effects on lipid exchange and flip-flop directly. To our knowledge this study is the first of its kind, systematically using both static and time resolved techniques to look at the effect of antimicrobial peptides with a single model system allowing for direct comparison of the effects. These results give significant insight into how the membrane effect of antimicrobial peptides is rather complex and cannot be correlated directly to molecular size, structure or charge independently. Instead, it is related to the structural interactions that cannot easily be predicted from the isolated chemical characteristics. While the presented results show that acceleration of the lipid transport is a general feature of these peptides, the level of effect on lipid flip-flop and exchange varies between peptides. A direct comparison of the activation energies of lipid exchange and lipid flip-flop in membranes interacting with *LL-37* and *indolicidin* reveal how the overall general increase in transport seen for both peptides have different origins. While *indolicidin* lowers the activation energy for lipid flip-flop due to insertion in the outer leaflet of the lipid bilayer, *LL-37* has a more significant impact on the intervesicular lipid exchange which can be explained by the peptide acting partially as a solubilising agent at higher, non-biologically relevant, concentrations. The latter also questions the detergent model often proposed as an AMP mechanism although it shows that peptides that act like potent amphiphiles also have profound, most likely stronger, impact on the lipid membrane exchange processes.

Beyond the results presented here we confirm that the same trend of a general peptide induced acceleration of lipid transport also can be observed in model systems closer mimicking the membrane of a real bacteria cell, consisting solely of PE-PG lipids [78]. The comprehensive results reported here, together with previous independent studies on structure and lipid exchange processes, support a coherent scenario in which acceleration of lipid flip-flop is an important part of the membrane destabilization without the combined observation of significant structural changes in the membrane. Bacterial death due to an increase in lipid dynamics might both be linked to scrambling of lipid composition within (flip-flop) and between (exchange) neighbouring membrane, increased transport of ions and other solutes across the membrane and solubilisation and permeability of the membrane as has all been observed in literature [32,79]. Moreover, the effects seen here may be the first step of a more complex mechanism where

increased lipid flip-flops allows the peptide to enter the bacteria cells to target intracellular RNA, DNA or ribosomes as previously suggested [18]. In order to fully understand their biological function, more in depth studies using complex membranes consisting of more realistic lipid mixtures and addition of membrane proteins are needed. Nevertheless, given the general effect of AMPs and their profound canonical acceleration of the lipid dynamics give valuable insight into the microscopic mechanisms and reconcile many of the previously observed effects of AMP on bacterial membranes.

CRediT authorship contribution statement

Josefine E. Nielsen: Conceptualization, Methodology, Investigation, Visualization, Writing - original draft. **Victoria A. Bjørnestad:** Methodology, Investigation, Writing - review & editing. **Vitaliy Pipich:** Investigation, Writing - review & editing. **Håvard Jenssen:** Conceptualization, Resources, Investigation, Supervision, Writing - review & editing. **Reidar Lund:** Conceptualization, Investigation, Methodology, Supervision, Writing - original draft.

Declaration of Competing Interest

The authors declared that there is no conflict of interest.

Appendix A. Supplementary material

Supplementary data to this article can be found online at https://doi.org/10.1016/j.jcis.2020.08.094.

References

[1] H. Jenssen, P. Hamill, R.E. Hancock, Peptide antimicrobial agents, Clin. Microbiol. Rev. 19 (3) (2006) 491–511.

[2] M. Zasloff, Antimicrobial peptides of multicellular organisms, Nature 415 (6870) (2002) 389.

[3] R.M. Epand, H.J. Vogel, Diversity of antimicrobial peptides and their mechanisms of action, Biochim. Biophys. Acta, Biomembr. 1462 (1–2) (1999) 11–28.

[4] W.C. Wimley, Describing the mechanism of antimicrobial peptide action with the interfacial activity model, ACS Chem. Biol. 5 (10) (2010) 905–917.

[5] L.T. Nguyen, E.F. Haney, H.J. Vogel, The expanding scope of antimicrobial peptide structures and their modes of action, Trends Biotechnol. 29 (9) (2011) 464–472.

[6] T. Rončević, J. Puizina, A. Tossi, Antimicrobial Peptides as Anti-Infective Agents in Pre-Post-Antibiotic Era?, Int. J. Mol. Sci. 20 (22) (2019) 5713.

[7] I.-M. Frick, S.L. Nordin, M. Baumgarten, M. Mörgelin, O.E. Sørensen, A.I. Olin, A. Egesten, Constitutive and inflammation-dependent antimicrobial peptides

produced by epithelium are differentially processed and inactivated by the commensal Finegoldia magna and the pathogen Streptococcus pyogenes, J. Immunol. 187 (8) (2011) 4300–4309.

[8] T. Jin, M. Bokarewa, T. Foster, J. Mitchell, J. Higgins, A. Tarkowski, Staphylococcus aureus resists human defensins by production of staphylokinase, a novel bacterial evasion mechanism, J. Immunol. 172 (2) (2004) 1169–1176.

[9] A. Peschel, M. Otto, R.W. Jack, H. Kalbacher, G. Jung, F. Götz, Inactivation of the dlt Operon inStaphylococcus aureus Confers Sensitivity to Defensins, Protegrins, and Other Antimicrobial Peptides, J. Biol. Chem. 274 (13) (1999) 8405–8410.

[10] C. Vuong, S. Kocianova, J.M. Voyich, Y. Yao, E.R. Fischer, F.R. DeLeo, M. Otto, A crucial role for exopolysaccharide modification in bacterial biofilm formation, immune evasion, and virulence, J. Biol. Chem. 279 (52) (2004) 54881–54886.

[11] H.-S. Joo, C.-I. Fu, M. Otto, Bacterial strategies of resistance to antimicrobial peptides, Philos. Trans. R. Soc. Lond., B, Biol. Sci. 371(1695) (2016) 20150292.

[12] D.I. Andersson, D. Hughes, J.Z. Kubicek-Sutherland, Mechanisms and consequences of bacterial resistance to antimicrobial peptides, Drug Resist. Updat. 26 (2016) 43–57.

[13] A. Peschel, H.-G. Sahl, The co-evolution of host cationic antimicrobial peptides and microbial resistance, Nat. Rev. Microbiol. 4 (7) (2006) 529.

[14] C.D. Fjell, J.A. Hiss, R.E.W. Hancock, G. Schneider, Designing antimicrobial peptides: form follows function, Nat Rev Drug Discov 11 (1) (2011) 37–51.

[15] R.E. Hancock, A. Rozek, Role of membranes in the activities of antimicrobial cationic peptides, FEMS Microbiol. Lett. 206 (2) (2002) 143–149.

[16] S. Omardien, J.W. Drijfhout, F.M. Vaz, M. Wenzel, L.W. Hamoen, S.A. Zaat, S. Brul, Bactericidal activity of amphipathic cationic antimicrobial peptides involves altering the membrane fluidity when interacting with the phospholipid bilayer, Biochim. Biophys. Acta, Biomembr. 1860 (11) (2018) 2404–2415.

[17] C.-F. Le, C.-M. Fang, S.D. Sekaran, Intracellular targeting mechanisms by antimicrobial peptides, Antimicrob. Agents Chemother. 61 (4) (2017) e02340–e02416.

[18] N.P. Chongsiriwatana, J.S. Lin, R. Kapoor, M. Wetzler, J.A. Rea, M.K. Didwania, C. H. Contag, A.E. Barron, Intracellular biomass flocculation as a key mechanism of rapid bacterial killing by cationic, amphipathic antimicrobial peptides and peptoids, Sci. Rep. 7 (1) (2017) 1–15.

[19] B.M. Peters, M.E. Shirtliff, M.A. Jabra-Rizk, Antimicrobial peptides: primeval molecules or future drugs?, PLoS Pathog. (2010).

[20] W. Vollmer, D. Blanot, M.A. De Pedro, Peptidoglycan structure and architecture, FEMS Microbiol. Rev. 32 (2) (2008) 149–167.

[21] T. Ikeda, H. Hirayama, H. Yamaguchi, S. Tazuke, M. Watanabe, Polycationic biocides with pendant active groups: molecular weight dependence of antibacterial activity, Antimicrob. Agents Chemother. 30 (1) (1986) 132–136.

[22] Y. Shai, Z. Oren, Diastereomers of cytolysins, a novel class of potent antibacterial peptides, J. Biol. Chem. 271 (13) (1996) 7305–7308.

[23] L. Zhang, A. Rozek, R.E. Hancock, Interaction of cationic antimicrobial peptides with model membranes, J. Biol. Chem. 276 (38) (2001) 35714–35722.

[24] M.N. Melo, R. Ferre, M. Castanho, Antimicrobial peptides: linking partition, activity and high membrane-bound concentrations, Nat Rev Micro 7 (3) (2009) 245–250.

[25] W. Wang, D.K. Smith, K. Moulding, H.M. Chen, The dependence of membrane permeability by the antibacterial peptide cecropin B and its analogs, CB-1 and CB-3, on liposomes of different composition, J. Biol. Chem. 273 (42) (1998) 27438–27448.

[26] J. He, A.J. Krauson, W.C. Wimley, Toward the de novo design of antimicrobial peptides: Lack of correlation between peptide permeabilization of lipid vesicles and antimicrobial, cytolytic, or cytotoxic activity in living cells, Biopolymers 102 (1) (2014) 1–6.

[27] S.F. Hedegaard, M.S. Derbas, T.K. Lind, M.R. Kasimova, M.V. Christensen, M.H. Michaelsen, R.A. Campbell, L. Jorgensen, H. Franzyk, M. Cárdenas, Fluorophore labeling of a cell-penetrating peptide significantly alters the mode and degree of biomembrane interaction, Sci. Rep. 8 (1) (2018) 1–14.

[28] B.-H. Gan, T.N. Siriwardena, S. Javor, T. Darbre, J.-L. Reymond, Fluorescence imaging of bacterial killing by antimicrobial peptide dendrimer G3KL, ACS Infect. Dis. 5 (12) (2019) 2164–2173.

[29] L. Netuschil, T.M. Auschill, A. Sculean, N.B. Arweiler, Confusion over live/dead stainings for the detection of vital microorganisms in oral biofilms-which stain is suitable?, BMC Oral Health 14 (1) (2014) 2.

[30] N.R. de Almeida, J. Catazaro, M. Krishnaiah, Y.S. Chhonker, D.J. Murry, R. Powers, M. Conda-Sheridan, Understanding interactions of Citropin 1.1 analogues with model membranes and their influence on biological activity, Peptides 119 (2019) 170119.

[31] B. Mojsoska, G. Carretero, S. Larsen, R.V. Mateiu, H. Jenssen, Peptoids successfully inhibit the growth of gram negative E. coli causing substantial membrane damage, Sci. Rep. 7 (2017) 42332.

[32] K. Matsuzaki, O. Murase, N. Fujii, K. Miyajima, An antimicrobial peptide, magainin 2, induced rapid flip-flop of phospholipids coupled with pore formation and peptide translocation, Biochemistry 35 (35) (1996) 11361–11368.

[33] W.C. Wimley, S.H. White, Determining the membrane topology of peptides by fluorescence quenching, Biochemistry 39 (1) (2000) 161–170.

[34] T.C. Anglin, K.L. Brown, J.C. Conboy, Phospholipid flip-flop modulated by transmembrane peptides WALP and melittin, J. Struct. Biol. 168 (1) (2009) 37–52.

[35] M.H. Nguyen, M. DiPasquale, B.W. Rickeard, M. Doktorova, F.A. Heberle, H.L. Scott, F.N. Barrera, G. Taylor, C.P. Collier, C.B. Stanley, J. Katsaras, D. Marquardt, Peptide-Induced Lipid Flip-Flop in Asymmetric Liposomes Measured by Small Angle Neutron Scattering, Langmuir 35 (36) (2019) 11735–11744.

[36] J. LeBarron, E. London, Effect of lipid composition and amino acid sequence upon transmembrane peptide-accelerated lipid transleaflet diffusion (flip-flop), Biochim. Biophys. Acta, Biomembr. 1858 (8) (2016) 1812–1820.

[37] M.A. Kol, A.N. van Laak, D.T. Rijkers, J.A. Killian, A.I. de Kroon, B. de Kruijff, Phospholipid flop induced by transmembrane peptides in model membranes is modulated by lipid composition, Biochemistry 42 (1) (2003) 231–237.

[38] M. Raff, B. Alberts, J. Lewis, A. Johnson, K. Roberts, Molecular Biology of the Cell, National Center for Biotechnology Information's Bookshelf (2002).

[39] D. Roversi, V. Luca, S. Aureli, Y. Park, M.L. Mangoni, L. Stella, How many antimicrobial peptide molecules kill a bacterium? The case of PMAP-23, ACS Chem. Biol. 9 (9) (2014) 2003–2007.

[40] J. Li, R.L. Nation, R.W. Milne, J.D. Turnidge, K. Coulthard, Evaluation of colistin as an agent against multi-resistant Gram-negative bacteria, Int. J. Antimicrob. Agents 25 (1) (2005) 11–25.

[41] J.B. Klauda, N. Kučerka, B.R. Brooks, R.W. Pastor, J.F. Nagle, Simulation-based methods for interpreting x-ray data from lipid bilayers, Biophys. J. 90 (8) (2006) 2796–2807.

[42] N. Kucerka, J. Pencer, J.N. Sachs, J.F. Nagle, J. Katsaras, Curvature effect on the structure of phospholipid bilayers, Langmuir 23 (3) (2007) 1292–1299.

[43] N. Kučerka, J.F. Nagle, J.N. Sachs, S.E. Feller, J. Pencer, A. Jackson, J. Katsaras, Lipid bilayer structure determined by the simultaneous analysis of neutron and X-ray scattering data, Biophys. J. 95 (5) (2008) 2356–2367.

[44] B. Eicher, F.A. Heberle, D. Marquardt, G.N. Rechberger, J. Katsaras, G. Pabst, Joint small-angle X-ray and neutron scattering data analysis of asymmetric lipid vesicles, J. Appl. Crystallogr. 50 (2) (2017).

[45] J.E. Nielsen, V.A. Bjørnestad, R. Lund, Resolving the Structural Interactions between Antimicrobial Peptides and Lipid Membranes using Small-angle Scattering Methods: the case of Indolicidin, Soft Matter 14 (2018) 8750–8763.

[46] J.E. Nielsen, T.K. Lind, A. Lone, Y. Gerelli, P.R. Hansen, H. Jenssen, M. Cárdenas, R. Lund, A biophysical study of the interactions between the antimicrobial peptide indolicidin and lipid model systems, Biochim. Biophys. Acta, Biomembr. 1861 (7) (2019) 1355–1364.

[47] J. Johansson, G.H. Gudmundsson, M.n.E. Rottenberg, K.D. Berndt, B. Agerberth, Conformation-dependent antibacterial activity of the naturally occurring human peptide LL-37, J. Biol. Chem. 273 (6) (1998) 3718–3724.

[48] H. Steiner, D. Hultmark, Å. Engström, H. Bennich, H. Boman, Sequence and specificity of two antibacterial proteins involved in insect immunity, Nature 292 (5820) (1981) 246.

[49] M. Zasloff, Magainins, a class of antimicrobial peptides from Xenopus skin: isolation, characterization of two active forms, and partial cDNA sequence of a precursor, PNAS 84 (15) (1987) 5449–5453.

[50] T. Rozek, K.L. Wegener, J.H. Bowie, I.N. Olver, J.A. Carver, J.C. Wallace, M.J. Tyler, The antibiotic and anticancer active aurein peptides from the Australian bell frogs Litoria aurea and Litoria raniformis: the solution structure of aurein 1.2, Eur. J. Biochem. 267 (17) (2000) 5330–5341.

[51] M.E. Selsted, M.J. Novotny, W.L. Morris, Y.-Q. Tang, W. Smith, J.S. Cullor, Indolicidin, a novel bactericidal tridecapeptide amide from neutrophils, J. Biol. Chem. 267 (7) (1992) 4292–4295.

[52] M.-A. Sani, F. Separovic, How membrane-active peptides get into lipid membranes, Acc. Chem. Res. 49 (6) (2016) 1130–1138.

[53] D.K. Rai, S. Qian, Interaction of the Antimicrobial Peptide Aurein 1.2 and Charged Lipid Bilayer, Sci. Rep. 7 (1) (2017) 3719.

[54] E. Sevcsik, G. Pabst, A. Jilek, K. Lohner, How lipids influence the mode of action of membrane-active peptides, Biochim. Biophys. Acta, Biomembr. 1768 (10) (2007) 2586–2595.

[55] E. Sevcsik, G. Pabst, W. Richter, S. Danner, H. Amenitsch, K. Lohner, Interaction of LL-37 with model membrane systems of different complexity: influence of the lipid matrix, Biophys. J. 94 (12) (2008) 4688–4699.

[56] T.A. Holak, A. Engstroem, P.J. Kraulis, G. Lindeberg, H. Bennich, T.A. Jones, A.M. Gronenborn, G.M. Clore, The solution conformation of the antibacterial peptide cecropin A: a nuclear magnetic resonance and dynamical simulated annealing study, Biochemistry 27 (20) (1988) 7620–7629.

[57] G. Wang, Structures of human host defense cathelicidin LL-37 and its smallest antimicrobial peptide KR-12 in lipid micelles, J. Biol. Chem. 283 (47) (2008) 32637–32643.

[58] G. Wang, Y. Li, X. Li, Correlation of three-dimensional structures with the antibacterial activity of a group of peptides designed based on a nontoxic bacterial membrane anchor, J. Biol. Chem. 280 (7) (2005) 5803–5811.

[59] J. Gesell, M. Zasloff, S.J. Opella, Two-dimensional 1H NMR experiments show that the 23-residue magainin antibiotic peptide is an α-helix in dodecylphosphocholine micelles, sodium dodecylsulfate micelles, and trifluoroethanol/water solution, J. Biomol. NMR 9 (2) (1997) 127–135.

[60] J.-K. Kim, E. Lee, S. Shin, K.-W. Jeong, J.-Y. Lee, S.-Y. Bae, S.-H. Kim, J. Lee, S.R. Kim, D.G. Lee, Structure and function of papiliocin with antimicrobial and anti-inflammatory activities isolated from the swallowtail butterfly, Papilio xuthus, J. Biol. Chem. 286 (48) (2011) 41296–41311.

[61] M. Nakano, M. Fukuda, T. Kudo, H. Endo, T. Handa, Determination of interbilayer and transbilayer lipid transfers by time-resolved small-angle neutron scattering, Phys. Rev. Lett. 98 (23) (2007) 238101.

[62] N. Matsuzaki, T. Handa, M. Nakano, Kinetic and thermodynamic analysis of cholesterol transfer between phospholipid vesicles and nanodiscs, J. Phys. Chem. B 119 (30) (2015) 9764–9771.

[63] S. Garg, L. Porcar, A. Woodka, P. Butler, U. Perez-Salas, Noninvasive neutron scattering measurements reveal slower cholesterol transport in model lipid membranes, Biophys. J. 101 (2) (2011) 370–377.

[64] M. Nakano, M. Fukuda, T. Kudo, N. Matsuzaki, T. Azuma, K. Sekine, H. Endo, T. Handa, Flip-flop of phospholipids in vesicles: kinetic analysis with time-resolved small-angle neutron scattering, J. Phys. Chem. B 113 (19) (2009) 6745–6748.

[65] Y. Xia, K. Charubin, D. Marquardt, F.A. Heberle, J. Katsaras, J. Tian, X. Cheng, Y. Liu, M.-P. Nieh, Morphology-induced defects enhance lipid transfer rates, Langmuir 32 (38) (2016) 9757–9764.

[66] M. Kaihara, H. Nakao, H. Yokoyama, H. Endo, Y. Ishihama, T. Handa, M. Nakano, Control of phospholipid flip-flop by transmembrane peptides, Chem. Phys. 419 (2013) 78–83.

[67] M. Nakano, Evaluation of interbilayer and transbilayer transfer dynamics of phospholipids using time-resolved small-angle neutron scattering, Chem. Pharm. Bull. 67 (4) (2019) 316–320.

[68] T. Sugiura, C. Takahashi, Y. Chuma, M. Fukuda, M. Yamada, U. Yoshida, H. Nakao, K. Ikeda, D. Khan, A.H. Nile, V. Bankaitis, M. Nakano, Biophysical parameters of the Sec14 phospholipid exchange cycle, Biophys. J. 116 (1) (2019) 92–103.

[69] Y. Xia, M. Li, K. Charubin, Y. Liu, F.A. Heberle, J. Katsaras, B. Jing, Y. Zhu, M.-P. Nieh, Effects of nanoparticle morphology and acyl chain length on spontaneous lipid transfer rates, Langmuir 31 (47) (2015) 12920–12928.

[70] R. Homan, H.J. Pownall, Transbilayer diffusion of phospholipids: dependence on headgroup structure and acyl chain length, Biochim. Biophys. Acta, Biomembr. 938 (2) (1988) 155–166.

[71] Y. Gerelli, L. Porcar, L. Lombardi, G. Fragneto, Lipid exchange and flip-flop in solid supported bilayers, Langmuir 29 (41) (2013) 12762–12769.

[72] Y. Koyama, A new antibiotic'colistin'produced by spore-forming soil bacteria, J. Antibiot. 3 (1950) 457–458.

[73] F.G. Dupuy, I. Pagano, K. Andenoro, M.F. Peralta, Y. Elhady, F. Heinrich, S. Tristram-Nagle, Selective Interaction of Colistin with Lipid Model Membranes, Biophys. J. 114 (4) (2018) 919–928.

[74] D.I. Fernandez, A.P. Le Brun, T.C. Whitwell, M.-A. Sani, M. James, F. Separovic, The antimicrobial peptide aurein 1.2 disrupts model membranes via the carpet mechanism, PCCP 14 (45) (2012) 15739–15751.

[75] J.S. Allhusen, J.C. Conboy, The ins and outs of lipid flip-flop, Acc. Chem. Res. 50 (1) (2016) 58–65.

[76] R.M. Epand, R.F. Epand, Lipid domains in bacterial membranes and the action of antimicrobial agents, Biochim. Biophys. Acta, Biomembr. 1788 (1) (2009) 289–294.

[77] H. Nakao, C. Hayashi, K. Ikeda, H. Saito, H. Nagao, M. Nakano, Effects of Hydrophilic Residues and Hydrophobic Length on Flip-Flop Promotion by Transmembrane Peptides, J. Phys. Chem. B 122 (15) (2018) 4318–4324.

[78] J.E. Nielsen, S.F. Prévost, H. Jenssen, R. Lund, Impact of Antimicrobial Peptides on E. coli-mimicking Lipid Model Membranes: correlating structural and dynamic effects using scattering methods (submitted) (2020).

[79] T.I. Rokitskaya, N.I. Kolodkin, E.A. Kotova, Y.N. Antonenko, Indolicidin action on membrane permeability: carrier mechanism versus pore formation, Biochim. Biophys. Acta, Biomembr. 1808 (1) (2011) 91–97.

SUPPLEMENTARY INFORMATION

Authors: *Josefine Eilsø Nielsen[1], Victoria Ariel Bjørnestad[1], Vitaliy Pipich[2], Håvard Jenssen[3] and Reidar Lund[1] **

Affiliations: *[1]Department of Chemistry, University of Oslo, Postboks 1033 Blindern, 0315 Oslo, Norway.*
[2]Jülich Centre for Neutron Science (JCNS) at Heinz Maier-Leibnitz Zentrum (MLZ), Forschungszentrum Jülich GmbH, 85747 Garching, Germany
[3]Department of Science and Environment, Roskilde University, Universitetsvej 1, Roskilde 4000, Denmark

*Correspondence to: Reidar.lund@kjemi.uio.no

Materials and methods:

Materials:

Synthetic DMPC (1,2-dimyristoyl-sn-glycero-3-phosphocholine), d-DMPC (1,2-dimyristoyl-d54-sn-glycero-3-phosphocholine), DMPG (1,2-dimyristoyl-sn-glycero-3-phospho-(1'-rac-glycerol)), d-DMPG (1,2-dimyristoyl-d54-sn-glycero-3-phospho-(1'-rac-glycerol)) and DMPE-PEG (1,2-dimyristoyl-sn-glycero-3-phosphoethanolamine-N-[methoxy(polyethylene glycol)-2000]) were purchased from Avanti Polar Lipids. The peptides *indolicidin*, *aurein* 1.2, *magainin II*, *LL-37* and *cecropin A* were purchased from Schafen-N ApS, Copenhagen. The 50 mM tris buffer was prepared by mixing Tris-base with Tris-HCl (Sigma Aldrich) in the correct ratio to achieve a pH of 7.4 in 50 % D_2O (Sigma-Aldrich) and 50 % H_2O (MiliQ).

Sample preparation:

The lipids in a ratio of 75 mol % DMPC, 22.5 mol % DMPG and 2.5 mol % DMPE-PEG were dissolved in a 1:3 methanol:chloroform solution. The organic solvents were removed under vacuum using a Heidolph rotary evaporator with a Vacuubrand vacuum pump. The resulting lipid film was hydrated with Tris buffer for at least one hour at a temperature of 34 °C. After sonication for 15 minutes, the lipid dispersions were extruded through a 100 nm pore diameter polycarbonate filter (>21 times) using an Avanti mini-extruder fitted with two 1 mL airtight syringes.

The peptides were dissolved in Tris buffer to the desired concentration.

Circular dichroism measurements:

Circular dichroism spectra were recorded using a Jasco J-810 spectropolarimeter (Jasco International Co). All measurements were taken using a quartz cuvette (Starna) with 1 mm path length. Samples were scanned at 50 nm/min with a bandwidth of 1 nm and a response time of 1 s over the wavelength range 190–250 nm. The samples were scanned 5 times and the data averaged. A sample-free control was measured and subtracted from the samples. Spectra were

recorded both for pure peptide and lipid samples as well as mixes of different lipid to peptide ratios. All measurements were done at 37 °C. The α-helicity content in % (f_H) of the peptides were estimated from the single-point method, from the mean residue ellipticity at 222 nm ($[\Theta]_{222}$) and the following equation, where f_H and n represent the α-helical content and the number of peptide bonds, respectively:[1]

$$f_H = 100\% \cdot [\Theta]_{222}/(40000 \cdot (1 - 2.5/n)) \qquad (1)$$

Where n is the number of residues.

DSC measurements:
Thermal analysis was performed using a differential scanning calorimeter (DSC) TA Instruments "nano-DSC" instrument for solutions, which allows detection of heat flows on the μJ/s scale. The heating rate was 2°C/min and samples were scanned from 5 to 45 °C. The thermograms were recorded during both heating and cooling for each sample to look for hysteresis effects. The Tris buffer was measured separately using the same settings. The background subtraction, peak integration and peak modelling were performed using the NanoAnalyze Software. The measured power was converted to molar heat capacity in kJ/mol/K.

SAXS data collection:
SAXS experiments were performed at the automated BM29 bioSAXS beamline[2] at the European Synchrotron Radiation Facility (ESRF) in Grenoble, France. The data was obtained using a detector distance of 2.87 meter and energy of 12.5 keV, covering a Q range of 0.0047 Å^{-1} to 0.5 Å^{-1}. The data set was calibrated to an absolute intensity scale using water as a primary standard. 45 μL samples were run through a capillary using the flow mode of the automated sample changer.[3] SAXS data were collected in twenty successive frames of 1 s each to monitor radiation damage and the data reduction was done using the standard tool at BM29.[4]

SAXS data analysis:
From a joint fit of synchrotron X-ray scattering data we can extract detailed information on the structure of the membrane.[5-8] The high-resolution and the peculiar difference in electron density between the head- and tail-groups of the lipid and water provides a significant sensitivity to changes in the contrast in X-ray scattering. It has previously been shown[9, 10] that the coherent scattering from large unilamellar vesicles (LUV), where the size of the vesicles and the thickness of the bilayer are well separated, can be described by the separated form factor (SFF) approximation:

$$I_{lip}(\;\;) = n \cdot S(Q)|P_{TS}(Q)|^2|P_{FB}(Q)|^2 \qquad (2)$$

where n is the number of scatterers, defined as

$$n = \frac{\phi}{V_{lipid} \cdot P_{agg}} \qquad (3)$$

with ϕ being the volume fraction and V_{lipid} the total volume of a phospholipid given by $V_{lipid} = M_{lipid}/(N_A \cdot d_{lipid})$. N_A is Avogadro's number, M_{lipid} is the molecular weight and d_{lipid} is the density. P_{agg} is the number of phospholipids in each lipid vesicle, i.e. the aggregation number of the vesicle given by

$$P_{agg} = \frac{4\pi(R_{shell})^3 - 4\pi(R_{shell} - t_{shell})^3}{3V_{tail}} \qquad (4)$$

where R_{shell} is the outer radius of the vesicles, t_{shell} is the thickness of the bilayer and V_{tail} is the volume occupied by each double tail of the phospholipid.

$S(Q)$ is the structure factor accounting for interaction between particles ($S(Q) = 1$ in our case because all samples are sufficiently diluted), $P_{TS}(Q)$ is the form factor of an infinitely thin spherical shell (containing information on the radius of the lipid vesicles and the polydispersity), and $P_{FB}(Q)$ is the form factor of a flat bilayer sheet (containing information on the bilayer thickness and the distribution of the phospholipids segments across the bilayer).

The flat bilayer form factor can be expressed[11] as

$$|P_{FB}(Q)| = \left| \int_{-D_i}^{D_0} \Delta\rho(z)e^{iQz}dz \right| = \sqrt{(F_{cos}^2 + F_{sin}^2)} \qquad (5)$$

where $\Delta\rho$ is the difference in the SLDs of the membrane and the solvent, and F_{cos}^2 and F_{sin}^2 are the real and the imaginary parts of $P_{FB}(Q)$.[8] The integral extends over the full bilayer thickness from the inner distance D_i to the outer distance D_o.

Following Kučerka and co-workers[8], we parse the phospholipids into the following segments: hydrocarbon tail group, carbonyl+ glycerol (CG) (common for all three phospholipid) and outer part of head group (PC/G).

The volume probability distributions of the components are described by Gaussian functions[7]

$$P_n(z) = \frac{c_{n_{outer}}}{\sqrt{2\pi}} exp\left[-\frac{(z + z_{n_{outer}})^2}{2\sigma_{n_{outer}}^2} \right] + \frac{c_{n_{inner}}}{\sqrt{2\pi}} exp\left[-\frac{(z - z_{n_{inner}})^2}{2\sigma_{n_{inner}}^2} \right] \qquad (6)$$

where $\sigma_{n_{outer}}/\sigma_{n_{inner}}$ and $z_{n_{outer}}/z_{n_{inner}}$ are the width and position of the distribution of the outer/inner group n, respectively, and $c_n = V_n/(A_L\sigma_n)$. V_n is the volume of the group n and A_L is the area per lipid, which is equal to the integrated area under the curve.

The hydrocarbon groups (HC representing the tails) are modelled using a half period squared sine/cosine function to account for the asymmetry in the bilayer, e.g. potential differences in the segmental distribution of the inner and the outer HC group [5]

$$P_{HC}(z) = \begin{cases} sin\left(\dfrac{z - z_{MN_i} + \sigma_{MN_i}}{2\sigma_{MN_i}}\dfrac{\pi}{2}\right)^2 \\ for\ z_{MN_i} - \sigma_{MN_i} \leq z < z_{MN_i} + \sigma_{MN_i} \\ \\ 1\ for\ z_{MN_i} + \sigma_{MN_i} \leq z < z_{MN_o} - \sigma_{MN_o} \\ \\ cos\left(\dfrac{z - z_{MN_o} + \sigma_{MN_o}}{2\sigma_{MN_o}}\dfrac{\pi}{2}\right)^2 \\ for\ z_{MN_o} - \sigma_{MN_o} \leq z < z_{MN_o} + \sigma_{MN_o} \end{cases} \qquad (7)$$

where $z_{MN_{i,o}}$ is the 0.5-probability value for the HC group and $2\sigma_{MN_{i,o}}$ is the width of the squared sine/cosine functions. The volume probability distribution of the methylene groups (CH$_2$) can be expressed separately as

$$P_{CH_2}(z) = P_{HC}(z) - P_{CH_3}(z) \qquad (8)$$

These expressions for the distributions of the lipid tails comply with spatial conservation consideration[5, 7] as the height of the expression for $P_{HC}(z)$ is equal to one in the central hydrocarbon region as there is no water present in this region of the membrane.

The volume probability distribution of the water is chosen to be the last group and the spatial conservation requirement is applied to give

$$P_w(z) = 1 - \sum_n P_n(z) \qquad (9)$$

where $n = CH_3^{i,o}, CH_2^{i,o},\ CG^{i,o}, HG^{i,o}$.

The total volumes of the head group and hydrocarbon chain, as well as the area per lipid, were constrained according to values from reported MD simulation of DMPC[12], DMPG[13] and DMPE[14] phospholipids.

Because a small amount of PEGylated DMPE lipids was used to stabilize the lipid vesicles against aggregation, the scattering from the PEG chains was included in the fit model for SAXS/SANS data. The PEG chains on the inner and outer leaflet of the lipid bilayer have a Gaussian random coil confirmation and can therefore be described by the following analytical model:[15, 16]

$$I_{PEG-liposomes}(Q) \qquad (10)$$
$$= I_{lip}(Q) + I_{chain}(Q) + I_{c_i c_i}(Q) + I_{c_i c_o}(Q) + I_{c_o c_o}(Q) + I_{sc_i}(Q)$$
$$+ I_{sc_o}(Q)$$

where $I_{lip}(Q)$ is the scattering from the lipid vesicles themselves (eq. 6) and $I_{chain}(Q)$ is the scattering from the PEG-chains alone given by

$$I_{chain}(Q) = n\Delta\rho_{PEG}^2 V_{PEG}^2 N_{PEG} \cdot 2 \frac{exp[-(QR_g)^2] - 1 + (QR_g)^2}{(QR_g)^4} \qquad (11)$$

In this expression, n is the number of scatterers as defined in Eq. 3, $\Delta\rho$ is the excess scattering length density, V_{PEG} is the partial specific molecular volume of a single PEG chains, R_g is the radius of gyration of the chains and N_{PEG} is defined as the number of PEG chains per liposomes given by

$$N_{PEG} = f_{PEG} \cdot P_{agg} \qquad (12)$$

f_{PEG} is the fraction of PEG-modified lipids in the liposomes and P_{agg} is the aggregation number of the liposomes (Eq.4).

The next terms, $I_{c_i c_i}(Q)$ and $I_{c_o c_o}(Q)$, are the interference terms between PEG chains attached to the inner surface of the vesicles and between the PEG chains on the outer surface, respectively, while $I_{c_i c_o}(Q)$ is the inter-interference between the inner and outer PEG chains:

$$I_{c_i c_i}(Q) = n\Delta\rho_{PEG}^2 V_{PEG}^2 N_{PEG} f_{inner} \cdot (N_{PEG} f_{inner} - 1) \cdot \left[\frac{1 - exp\left[-(QR_g)^2\right]}{(QR_g)^2} \right]^2$$
$$\cdot \left[\frac{sin\left(Q(R_{inner} - R_g)\right)}{Q(R_{inner} - R_g)} \right]^2 \qquad (13)$$

$$I_{c_o c_o}(Q) = n\Delta\rho_{PEG}^2 V_{PEG}^2 N_{PEG}(1 - f_{inner}) \cdot (N_{PEG}(1 - f_{inner}) - 1)$$
$$\cdot \left[\frac{1 - exp\left[-(QR_g)^2\right]}{(QR_g)^2} \right]^2 \cdot \left[\frac{sin\left(Q(R_{outer} - R_g)\right)}{Q(R_{outer} - R_g)} \right]^2 \qquad (14)$$

$$I_{c_i c_o}(Q) = n \Delta \rho_{PEG}^2 V_{PEG}^2 2 N_{PEG}^2 f_{inner} \cdot (1 - f_{inner}) \cdot \left[\frac{1 - exp\left[-(QR_g)^2 \right]}{(QR_g)^2} \right]^2$$

$$\cdot \left[\frac{sin\left(Q(R_{inner} - R_g) \right)}{Q(R_{inner} - R_g)} \right]^2 \cdot \left[\frac{sin\left(Q(R_{outer} - R_g) \right)}{Q(R_{outer} - R_g)} \right]^2 \qquad (15)$$

Here, f_{inner} is the fraction of PEG in the inner leaflet, while R_{inner} and R_{outer} are the inner and outer radius of the liposomes, respectively, defined as

$$R_{inner} = R + z_{HGi} - d_{disp} \qquad (16)$$

$$R_{outer} = R + z_{HGo} + d_{disp} \qquad (17)$$

where d_{disp} is a displacement factor for the centre of mass of the PEG polymer chains. This was incorporated to account for the partial mixing of the polymer and the bilayer at the interface, since close packing of polymers has been reported for PEGylated lipid micellar systems in the past.[17]

The last remaining terms $I_{sc_i}(Q)$ and $I_{sc_o}(Q)$ are the interference cross-terms of the outer and inner chains with the bilayer:

$$I_{sc_i}(Q) = n A_b A_s \cdot \Delta \rho_{PEG} V_{PEG} 2 N_{PEG} (1 - f_{inner}) \cdot (N_{PEG}(1 - f_{inner}) - 1)$$

$$\cdot \left[\frac{1 - exp\left[-(QR_g)^2 \right]}{(QR_g)^2} \right] \cdot \left[\frac{sin\left(Q(R_{inner} - R_g) \right)}{Q(R_{inner} - R_g)} \right] \qquad (18)$$

$$I_{sc_o}(Q) = n A_b A_s \cdot \Delta \rho_{PEG} V_{PEG} 2 N_{PEG} f_{inner} \cdot (N_{PEG} f_{inner} - 1)$$

$$\cdot \left[\frac{1 - exp\left[-(QR_g)^2 \right]}{(QR_g)^2} \right] \cdot \left[\frac{sin\left(Q(R_{outer} - R_g) \right)}{Q(R_{outer} - R_g)} \right] \qquad (19)$$

where A_{TS} and A_{FB} are the scattering amplitudes corresponding to scattering form factors $F_{TS}(Q)$ and $F_{FB}(Q)$ respectively.

To be able to use the analytical scattering models to quantitatively describe the interaction between antimicrobial peptides and lipid vesicles, the peptide was introduced as an additional pseudo-parsing group across the bilayer and modelled as an additional Gaussian function in the volume probability (eq. 6) as formerly published by Nielsen and co-workers.[18, 19] The integral under the curve was scaled by the total volume fraction of added peptides and the fraction of peptide bound to the liposomes, f_{bp}, in the following way

$$c_{pep} = \frac{V_p \cdot f_p \cdot f_{bp}}{A_L \cdot \sigma_p} \qquad (20)$$

Further, to account for the changes in contrast as a result of the peptide potentially integrating into either the head-region, tail-region of the phospholipids or somewhere in the interface between the two areas of the bilayer, the difference in contrast is weighed by a fraction, f_{p_tail}, which gives the fraction of peptide in the tail region

$$\Delta\rho_p(z) = f_{p\_tail} \cdot (\rho_p - \rho_{CH_2}) + (1 - f_{p_{tail}}) \cdot (\rho_p - \rho_w) \qquad (21)$$

where $\rho(p)$, $\rho(CH_2)$ and $\rho(w)$ are the SLDs of the peptide, methylene groups, and water, respectively.

The f_{p_tail} is expressed as the integral of the overlap of the peptide Gaussian function with the half period squared sine/cosine function expressing the volume probability of the HC groups in the following way

$$f_{p\_tail} = \frac{\int_{z_{inter}}^{z_{CH_2}+\sigma_{CH_2}} P_{HC}dz + \int_{Z_p-5\sigma_p}^{z_{inter}} P_p dz}{\int P_p \, dz} \qquad (22)$$

where z_{inter} is the intersect between the two overlapping curves found numerically by the Brent-Dekker method[20] and P_{HC} is the function described in eq. 7. P_p is the Gaussian function expressing the volume distribution of the peptide (details in reference[19])

The form factor for the flat bilayer including the peptides is

$$\left|P_{FB_{pep}}(Q)\right| = \left|\int_{-D_i}^{D_0} \Delta\rho(z)e^{iQz}dz\right| \qquad (23)$$

$$= \sqrt{\left(\left(F_{cos,lipid} + F_{cos,peptid}\right)^2 + \left(F_{sin,lipid} + F_{sin,peptid}\right)^2\right)}$$

where

$$F_{cos,peptide} = \left|c_{pep}\sigma_p\Delta\rho_p \cos(Qz_p) \cdot exp\left[\frac{(qQ_p)^2}{2}\right]\right| \qquad (24)$$

and

$$F_{sin,peptide} = \left|c_{pep}\sigma_p\Delta\rho_p \sin(Qz_p) \cdot exp\left[\frac{(qQ_p)^2}{2}\right]\right| \qquad (25)$$

To account for potential free peptide chains not bound to the lipid vesicles, an additional term was added to the model

$$I_{fp}(Q) = \varphi \cdot (1 - f_{bp}) \cdot \Delta\rho_p^2 \cdot V_p \cdot P_{chain}(Q) \tag{26}$$

Where φ is the total volume fraction and $P(q)_{chain}$ is the form factor of a Gaussian chain expressed by the Debye formula[21] given in Eq. 2.

The full expression for the intensity, including peptide in the bilayer, the PEGylation, and the free peptide chains is then

$$I = n\left(\left(\mathrm{P_{TS}}(Q)\right)^2 \left(\mathrm{P_{FB_{pep}}}(Q)\right)^2 + I_{chain}(Q) + I_{c_ic_i}(Q) + I_{c_ic_o}(Q) + I_{c_oc_o}(Q) \right. \tag{27}$$
$$\left. + I_{sc_i}(Q) + I_{sc_o}(Q)\right) + I_{fp}(Q)$$

In the fit analysis, we allowed the concentration to vary slightly due to uncertainties in the determination of the exact value during the sample preparation.

To account for formation of mixed peptide-lipid micelles due to solubilisation of the vesicles upon peptide addition the model was modified to include a fraction of micelle scattering.

$$I_{micelle}(Q) = \frac{n_{micelle}}{P_{agg\_micelle}} P_{micelle}(Q) \tag{28}$$

where $n_{micelle}$ is defined as

$$n_{micelle} = (Mconc_{lipid} \cdot f_{L_{micelle}} + Mconc_{peptide} \cdot f_{P_{micelle}})/V_{micelle} \tag{29}$$

Where $Mconc_{lipid}$ and $Mconc_{peptide}$ is the total molar concentration of lipids and peptides respectively, and $f_{L_{micelle}}$ and $f_{P_{micelle}}$ is the fraction of the lipids and peptides incorporated in the micelles respectively, and $V_{micelle} = \frac{4}{3}\pi(r_{micelle} + D)^3$ where $r_{micelle}$ is the core radius and D is the thickness of the shell..

$P_{agg_{micelle}} = V_{core}/ (f_{PL}f_{core}V_p + V_{tail} \cdot (1 - f_{PL}))$ is the aggregation number per micelle scaled by f_{PL} which is the ratio of peptide to lipid in the micelles, and f_{core} is the fraction of peptide chain incorporated in the core, where $V_{core} = \frac{4}{3}\pi(r_{micelle})^3$ and $P_{micelle}(Q)$ is the form factor for spherical core-shell micelle with defined as:

$$P_{micelle}(Q) = \int_0^{\pi/2} \left[\Delta\rho_{shell} V_{micelle} A_{sphere}(Q r_{micelle}) \right.$$
$$\left. + (\Delta\rho_{core} - \Delta\rho_{shell}) V_{core} A_{sphere}(Q r_{core}) \right]^2 \sin\alpha \, d\alpha \qquad (30)$$

where $\Delta\rho_{shell}$ is the difference in the SLDs of the shell and the solvent, and $\Delta\rho_{core}$ is the difference in the SLDs of the core and the solvent, $A_{sphere}(x) = 3[\sin(x) - x\cos(x)]/x^3$. $\Delta\rho_{shell}$ and $\Delta\rho_{core}$ were determined from a weighted average of the peptide and lipids using a fitting parameter describing the fraction of the peptide in the core, f_{core}, as such:

$$\Delta\rho_{shell} = \frac{Z_{lipidhead} + Z_{peptide} \cdot (1 - f_{core})}{f_{PL} \cdot (1 - f_{core}) \cdot V_p + V_{head} \cdot (1 - f_{PL})} \qquad (31)$$

$$\Delta\rho_{core} = \frac{Z_{lipidtail} + Z_{peptide} \cdot f_{core}}{f_{PL} \cdot f_{core} \cdot V_p + V_{tail} \cdot (1 - f_{PL})} \qquad (32)$$

where Z_i is the number of electrons in the group i.

The full expression for the intensity, including peptide in the bilayer, the PEGylation, the free peptide chains and mixed micelles is then

$$I = n\left(\left(P_{TS}(Q)\right)^2 \left(P_{FB_{pep}}(Q)\right)^2 + I_{chain}(Q) + I_{c_i c_i}(Q) + I_{c_i c_o}(Q) + I_{c_o c_o}(Q) \right.$$
$$\left. + I_{sc_i}(Q) + I_{sc_o}(Q) \right) + I_{fp}(Q) + I_{micelle}(Q) \qquad (33)$$

TR-SANS data collection:

TR-SANS experiments were performed on the KWS-2 beamline at the Heinz Maier-Leibnitz (FRM II) center, MLZ in Garching, Germany using detector distance of 20 meters and a wave length of 5 Å, covering a Q range of 0.0032 Å^{-1} to 0.039 Å^{-1}. D-liposomes were mixed into H-liposomes (1:1) directly before the first measurement using a Finntip micropipette and mixed with either pure buffer (to make sure concentration of the non-peptide samples compare to the peptide samples) or peptide solution 1:1. The samples were filled into round Hellma quarts banjo-cells with a path length of 1 mm and kept in a temperature-controlled rack during the full experiment. The samples were measured with shorter measurement times and intervals in the beginning but increasing measurement times and longer intervals over time due to the descending contrast.

TR-SANS data analysis:

The TR-SANS data were evaluated by determining the relaxation function $R(t)$ according to

$$R(t) = \sqrt{\frac{I(t) - I_\infty}{I(0) - I_\infty}} \quad (34)$$

where $I(t) = \int I(Q,t)dQ$ is the integral intensity at a given time, I_∞ is the intensity of the premixed blend representing the final state and $I(0)$ is the averaged intensity of the H-vesicles and D-vesicles measured separately representing the initial state before exchange and flip-flop has taken place.

The exchange mechanism can be explained by the following differential equations with rate constants of exchange (k_{ex}) and flip-flop (k_{flip}) by[22]

$$-\frac{d|\Delta\rho_{out}|}{dt} = k_{ex}(|\Delta\rho_{out}| - 0) + k_{flip}(|\Delta\rho_{out}| - |\Delta\rho_{in}|),$$
$$-\frac{d|\Delta\rho_{in}|}{dt} = -k_{flip}(|\Delta\rho_{out}| - |\Delta\rho_{in}|) \quad (35)$$

where $\Delta\rho_{out}$ and $\Delta\rho_{in}$ are the contrast of the inner and outer leaflets of the vesicles with the solvent. As we have used a zero-average contrast solvent the H and D-vesicles can be assumed to have identical absolute values of contrast where one is positive and the other negative.

With the initial condition that $\Delta\rho_{out}(0) = \Delta\rho_{in}(0) = 1$ and taking an average of $|\Delta\rho_{out}|$ and $|\Delta\rho_{in}|$ the $R(t)$, normalized contrast has been explained by a double-exponential decay function[22]

$$R(t) = \left(\frac{1}{2} - \frac{k_{flip}}{X}\right) \exp\left(\frac{-k_{ex} + 2k_{flip} + X}{2}t\right)$$
$$+ \left(\frac{1}{2} + \frac{k_{flip}}{X}\right) \exp(\frac{k_{ex} + 2k_{flip} - X}{2}t) \quad (36)$$

Where $X = \sqrt{4k_{flip}^2 + k_{ex}^2}$.

To extract thermodynamically parameters, $\ln k_{ex}$ and k_{flip} can be plotted against the inverse temperature in Kelvin, $1/T$ for samples measured at different temperatures giving an Arrhenius relationship. From this analysis we obtain the activation energy, E_a and the fundamental time constant, τ_0 according to
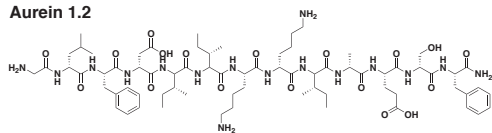
$$\tau = \tau_0 \exp\left(\frac{E_a}{RT}\right) \quad (37)$$

where $\tau = 1/k$, R is the universal gas constant and τ_0 is a system specific constant and is related to the time between each time the molecule "attempts" to overcome the energetic barrier.[23]
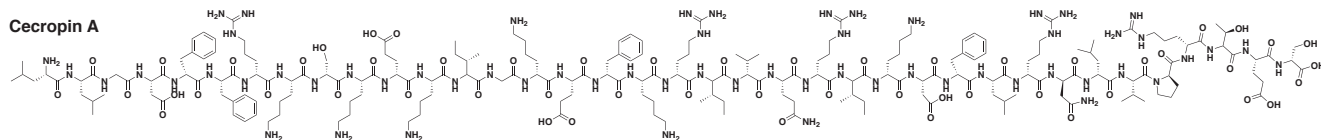
$$\tau = \tau_{00} \exp(-\Delta S/R) exp\, (\Delta H/RT) \qquad\qquad (38)$$

Where ΔS is the entropy change, ΔH is the enthalpy change and τ_{00} is the estimated fundamental time constant.
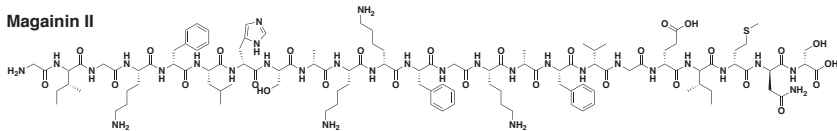
Aurein 1.2

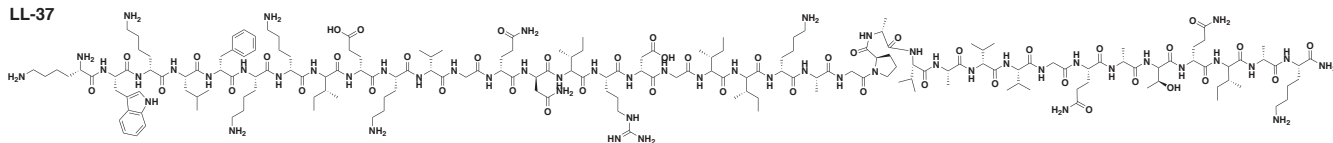**Cecropin A**

Magainin II

LL-37

Figure S1. Chemical structure of *aurein 1.2*, *cecropin A, magainin II* and *LL37*.
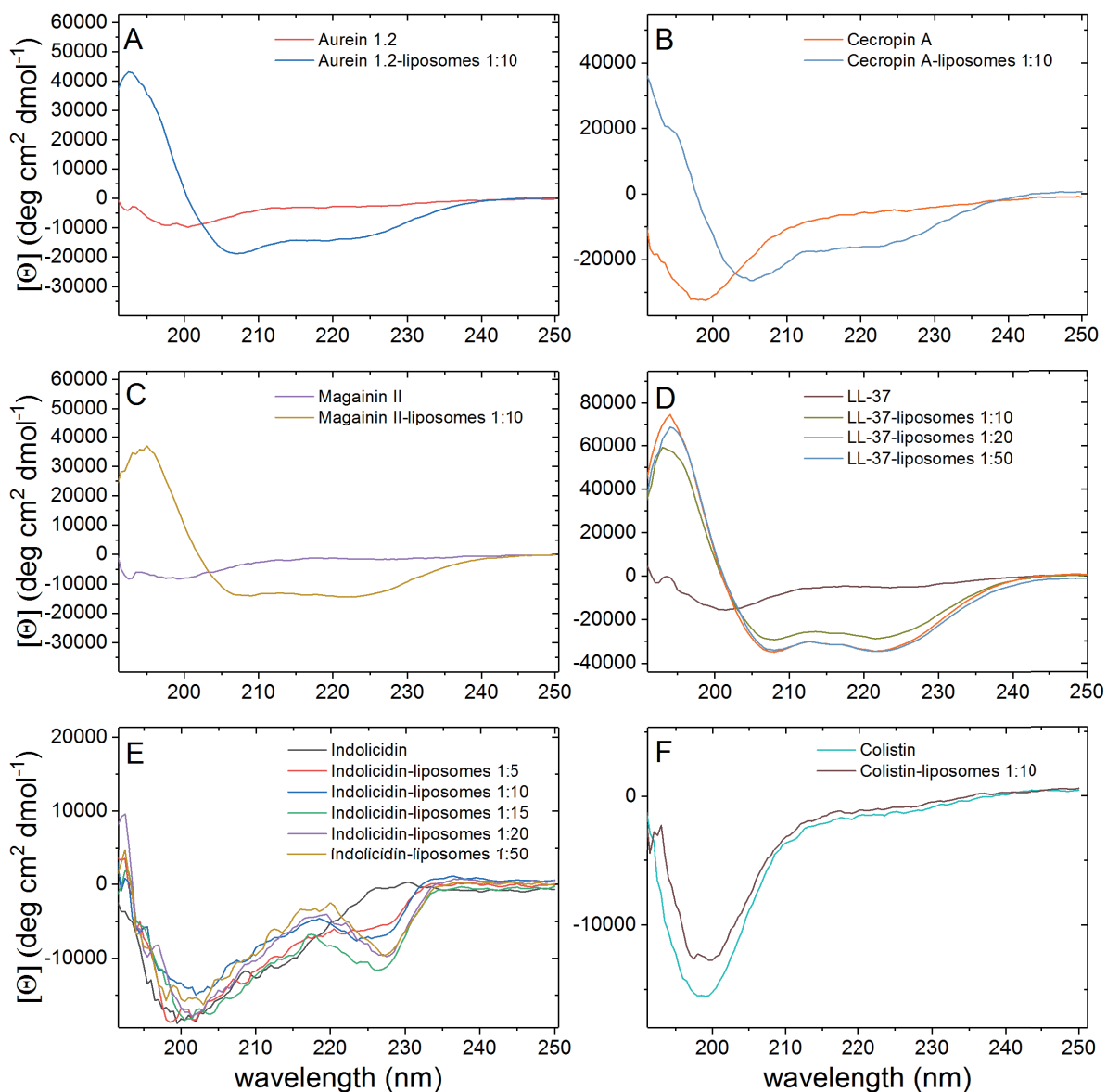
Figure S2. Circular dichroism spectra of peptides with and without mixing with DMPC-DMPG-DMPE-PEG liposomes. From the spectra it can be seen that aurein 1.2 (A) *cecropin A* (B), *aurein* 1.2 (B), *magainin II* (C) and *LL-37* (D) all fold into an α-helical structure in the presence of liposomes (the α-helical content has been calculated by the single-point method and is reported in table S1. *Indolicidin* (E) disordered extended structure as has also been reported in the past by Falla and co-workers.[24] It was suggested that these circular dichroism results indicate that the peptide either stacks in the membrane or extends across the membrane as an aggregate, the first theory is in support of our SAXS results.[18, 19], while *colistin* (F) shows an unstructured peptide mostly unaffected by liposome addition.

Table S1. α-helicity of the peptides as studied by CD-spectrometry.

Peptide	Peptide:lipid ratio	α--helical content (%)*
indolicidin	1:0	-
	1:10	-
	1:15	-
--	1:20	-
--	1:50	-
colistin	1:0	-
	1:10	-
Aurein 1.2	1:0	8
	1:10	43
cecropin A	1:0	15
	1:10	43
magainin II	1:0	4
	1:10	41
LL-37	1:0	13
	1:10	77
	1:20	92
	1:50	92

Alpha helical content calculated from the single point method according to equation 1 for the peptides with apha helical motifs.

	Liposomes	Aurein 1.2				Cecropin A				Magainin II				LL-37		
		1:100	1:50	1:20	1:10	1:100	1:50	1:20	1:10	1:100	1:50	1:20	1:10	1:100	1:50	1:20
Radius	375	400	420	430	450	400	375	375	560	420	485	485	530	375	390	550
Area	60.4*															
z_{CH3}	0*															
z_{CH2o}	14.1±0.2**	13.9±0.2	13.8±0.2	13.7±0.2	13.7±0.2	14.1±0.2	14.1±0.2	14.1±0.2	14.1±0.2	14.1±0.2	14.1±0.2	14.1±0.2	14.1±0.2	14.1±0.2	14.1±0.2	14.1±0.2
z_{CH2i}	-14.0±0.2**	-13.9±0.2	-13.8±0.2	-13.8±0.2	-13.8±0.2	-14.1±0.2	-14.1±0.2	-14.1±0.2	-14.1±0.2	-14.1±0.2	-14.1±0.2	-14.1±0.2	-14.1±0.2	-14.1±0.2	-14.1±0.2	-14.1±0.2
z_{CGo}	15.9±0.4**	15.9±0.4	15.9±0.4	15.9±0.4	15.9±0.4	15.9±0.4	15.9±0.4	15.9±0.4	15.9±0.4	15.9±0.4	15.9±0.4	15.9±0.4	15.9±0.4	15.9±0.4	15.9±0.4	15.9±0.4
z_{CGi}	-15.9±0.4**	-15.9±0.4	-15.9±0.4	-15.9±0.4	-15.9±0.4	-15.9±0.4	-15.9±0.4	-15.9±0.4	-15.9±0.4	-15.9±0.4	-15.9±0.4	-15.9±0.4	-15.9±0.4	-15.9±0.4	-15.9±0.4	-15.9±0.4
$z_{PC/Go}$	18.9±0.4**	19.2±0.4	19.2±0.4	19.2±0.4	19.2±0.4	19.2±0.4	19.2±0.4	19.2±0.4	19.2±0.4	19.2±0.4	19.3±0.4	19.4±0.4	19.4±0.4	19.2±0.4	19.2±0.4	19.2±0.4
$z_{PC/Gi}$	-19.3±0.2**	-19.4±0.2	-19.4±0.2	-19.4±0.2	-19.4±0.2	-19.4±0.2	-19.4±0.2	-19.2±0.2	-19.2±0.2	-19.4±0.2	-19.4±0.2	-19.4±0.2	-19.4±0.2	-19.4±0.2	-19.4±0.2	-19.4±0.2
σ_{CH3}	2.3*															
σ_{CH2}	4.9±0.3	4.9±0.3	4.9±0.3	4.9±0.3	4.9±0.3	4.9±0.3	4.9±0.3	4.9±0.3	4.9±0.3	4.9±0.3	4.9±0.3	4.9±0.3	4.9±0.3	4.9±0.3	4.9±0.3	4.9±0.3
σ_{CG}	2.1±0.2	2.1±0.2	2.1±0.2	2.1±0.2	2.1±0.2	2.1±0.2	2.1±0.2	2.1±0.2	2.1±0.2	2.1±0.2	2.3±0.2	2.3±0.2	2.1±0.2	2.1±0.2	2.1±0.2	2.1±0.2
$\sigma_{PC/G}$	3.8±0.5	3.8±0.5	3.8±0.5	3.8±0.5	3.8±0.5	3.8±0.5	3.8±0.5	3.8±0.5	3.8±0.5	3.9±0.5	3.9±0.5	3.8±0.5	3.8±0.5	3.8±0.5	3.8±0.5	3.8±0.5
V_{HL}	319**															
V_{CH2}	25.3	25.4	25.4	25.4	25.4	25.4	25.4	25.4	25.4	25.4	25.4	25.4	25.3	25.4	25.4	25.4
f_{PEG}	0.025*															
R_g PEG	15*															
d_{disp}	-6															
f_{inner}	0.5															
$Z_{peptide}$	-	0.3	0.3	0.3	0.3	22.8	22.9	23	23	19.6	17.1	18.3	16.3	25	18	11
$\sigma_{peptide}$	-	10	9.7	9.8	10	13.9	14.1	14.2	14	4.1	4.2	5.1	5	7	6	20
$f_{micelles}$	-	-	-	-	-	-	-	-	-	-	-	-	-	0	0.01	0.03
Ratio P/L in micelles	-	-	-	-	-	-	-	-	-	-	-	-	-	-	0.08	0.1
free	-	0	0	0	0	0	0	0.1	0.4	0	0	0	0	-	-	-
σ_{SD}	0.27	0.3	0.3	0.3	0.45	0.23	0.23	0.23	0.22	0.25	0.25	0.25	0.3	0.29	0.6	0.6

Table S2. Fit parameters from the analysis of scattering data of liposomes with added peptide. The error of the fits is found to be less than 5 %. Hard constrained parameters are designated by * and soft constrained by limits in fitting regime indicated by **. The units for all numbers carry the appropriate power of Å

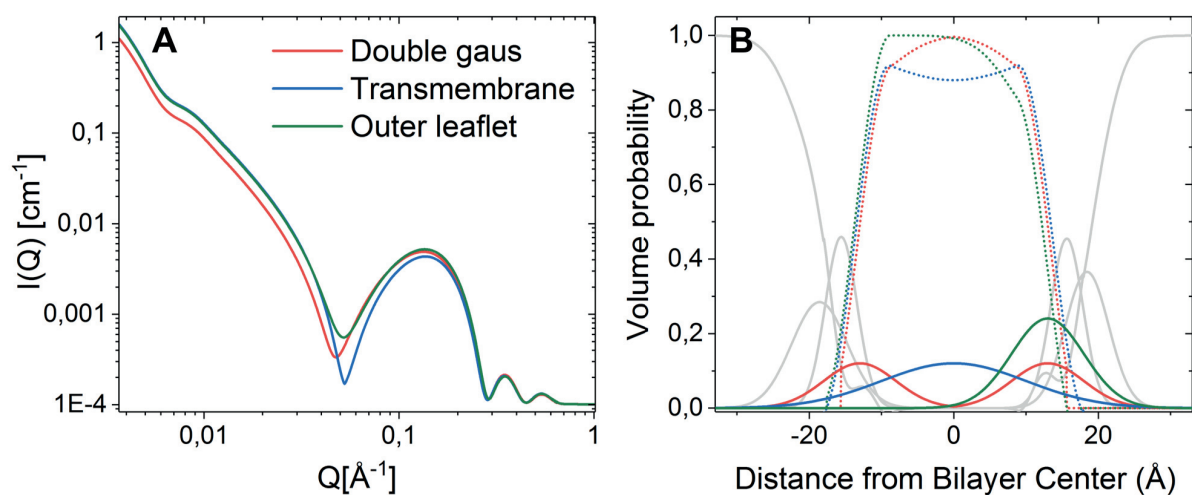| Fraction peptide	Aurein 1.2				Cecropin A				Magainin II				LL-37		
	1:100	1:50	1:20	1:10	1:100	1:50	1:20	1:10	1:100	1:50	1:20	1:10	1:100	1:50	1:20
Bilayer thickness[Å]	38.6±0.5	38.6±0.5	38.6±0.5	38.6±0.5	38.6±0.5	38.6±0.5	38.4±0.5	38.4±0.5	38.6±0.5	38.7±0.5	38.8±0.5	38.8±0.5	38.6±0.5	38.6±0.5	38.6±0.5
$Z_{peptide}$[Å]	0.3	0.3	0.3	0.3	22.8	22.9	23	23	19.6	17.1	18.3	16.3	25	18	11
$\sigma_{peptide}$[Å]	10	9.7	9.8	10	13.9	14.1	14.2	14	4.1	4.2	5.1	5	7	6	20
$f_{micelles}$	-	-	-	-	-	-	-	-	-	-	-	-	0	0.01	0.03
Ratio P/L in micelles	-	-	-	-	-	-	-	-	-	-	-	-	-	0.08	0.1
f_{free}	0	0	0	0	0	0	0.1	0.4	0	0	0	0	-	-	-
σ_{SD}	0.3	0.3	0.3	0.45	0.23	0.23	0.23	0.22	0.25	0.25	0.25	0.3	0.29	0.6	0.6

Figure S3. Simulated SAXS patterns (A) and resulting volume probability plot (B) showing the difference between peptide distribution as a single gaussian in the outer leaflet, symmetric double gaussian with peptide in outer and inner leaflet, and transmembrane distribution, using the SAXS model described in detail above.
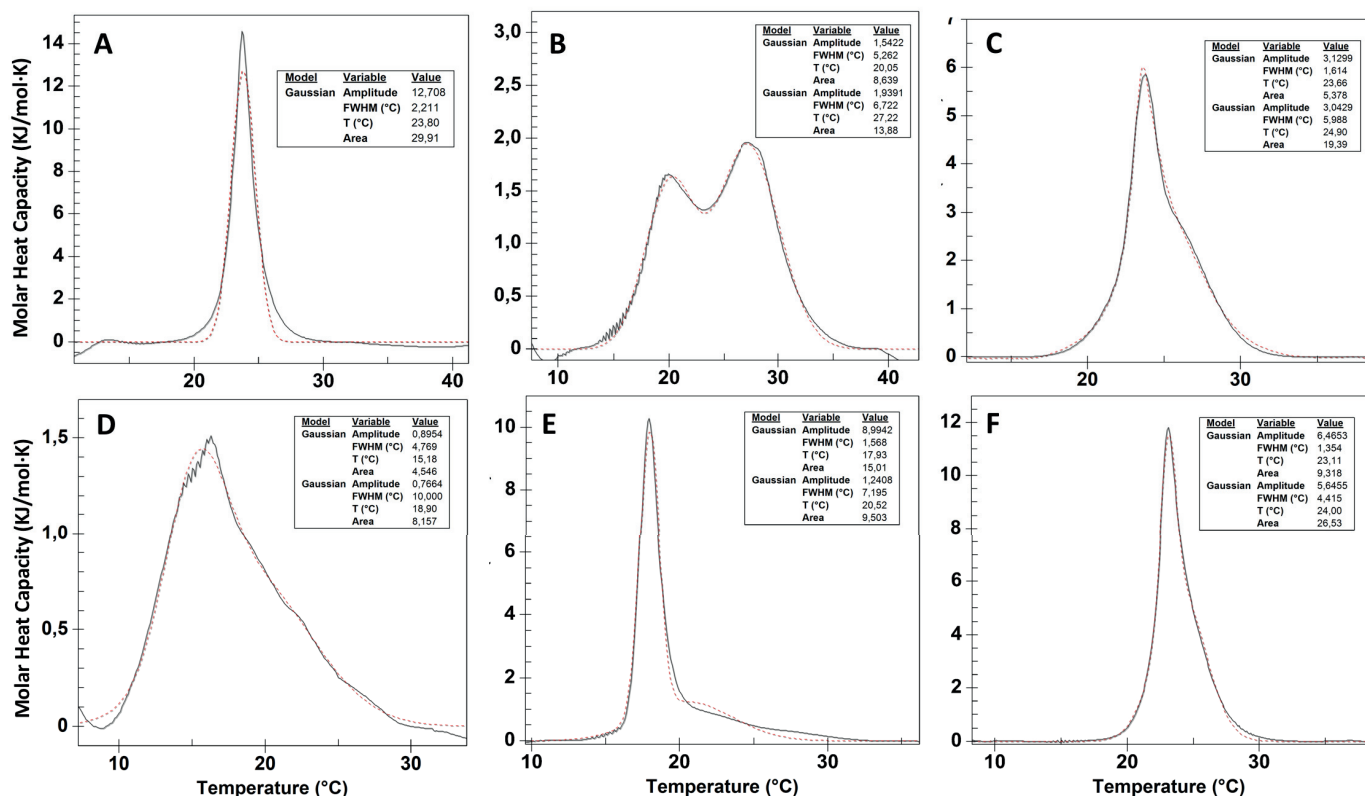
Figure S4. DSC heating scans illustrating the effect of peptides on the thermal phase behaviour of DMPC–DMPG–DMPE-PEG lipid vesicles. The black solid line is the measurement and the red dotted line is a Gaussian fit analysis (results of fit are inset). Comparing the results from pure lipid vesicles (A) with the addition of *LL-37* 1:20 (B) and 1:50 (C) show how the peptide insertion in the membrane causes formation of additional peaks at higher melting temperatures indicating an increased ordering of the lipids. This might be explained by the slight solubilisation of lipids and formation of mixed micellar structures. Addition of another peptide *indolicidin* 1:10 (D) 1:20 (E) and 1:50 (F) also result in formation of several additional melting peaks the shift here is to lower temperatures. Similar results were reported by Nielsen and co-workers in the past with the same lipids but with slightly less anionic lipids 10% compared to 25 % as studied here.[19]

Table S3. Thermodynamic parameters extracted from DSC data.

	Delta H	Tm [°C]	Delta S [$J/mol/K$]	Delta S T^a[kJ/mol]
Liposomes	29.9	23.8	1007.2	31.2
LL-37 1:20	8.6	20.0	294.6	9.1
	13.9	27.2	462.1	14.3
LL-37 1:50	5.4	23.7	181.2	5.6
	19.4	24.9	650.6	20.2
Indolicidin 1:10	4.5	15.2	157.7	4.9

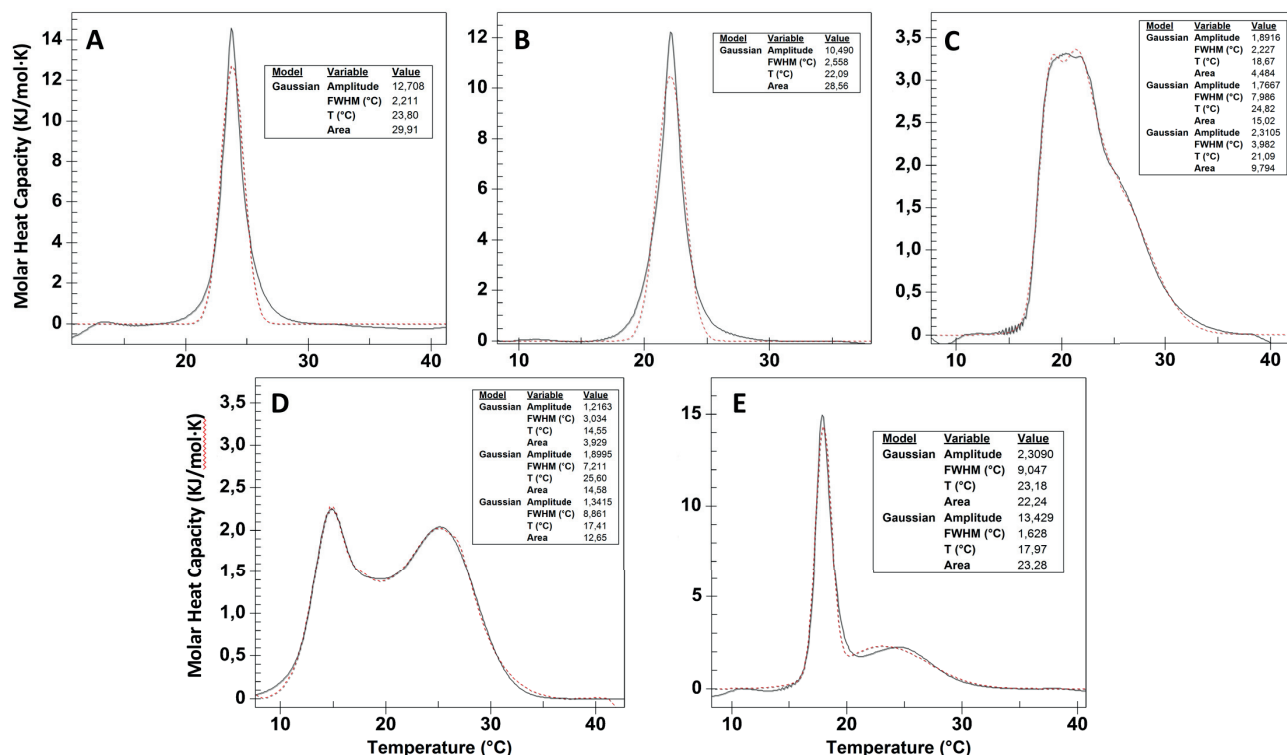|	8.2	18.2	0.0279982	8.7
Indolicidin 1:20	15.0	17.9	0.0515666	16.0
	9.5	20.5	0.0323595	10.0
Indolicidin 1:50	9.3	23.1	0.0314521	9.8
	26.5	24.0	0.0892815	27.7

[a] 37 °C.

Figure S5. DSC heating scans illustrating the effect of peptides on the thermal behaviour of DMPC–DCPG–DMPE-PEG lipid vesicles. The black solid line is the measurement and the red dotted line is a Gaussian fit analysis (results of fit are inset). When comparing the results of the pure lipid vesicles (A) (same figure as shown in figure S7) with the lipid mix with *colistin* 1:10 (B) only a very slight shift is seen in the observed melting temperature (~1 °C) without any broadening of the peak. This supports the SAXS and TR-SANS results showing that colistin has no significant effect on the structure or dynamics of lipid vesicles. While *cecropin A* 1:10 (C), *magainin II* 1:10 (D) and *aurein 1.2* 1:10 (E) addition all result in a significant broadening of the peak with shift in the melting temperatures to lower temperatures, similar to the results seen from indolicidin in figure S7.
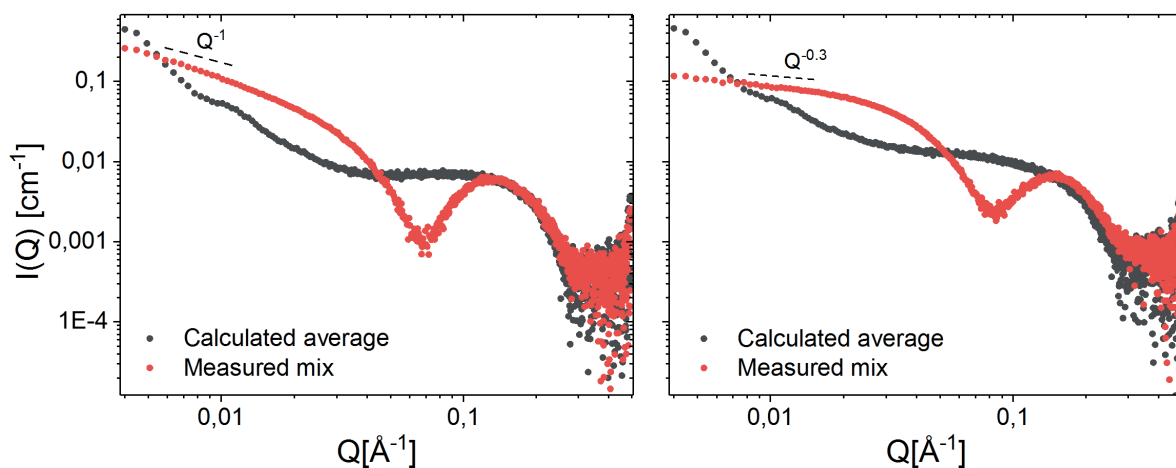
Figure S6. Qualitative comparison of the measured data of liposomes mixed with *LL-37* 1:10 ratio (A) and 1:5 ratio (B) to the calculated average where the scattering from the liposomes and the peptide have been measured separately and summed together. The measured curve shows a clear change in morphology indicating significant solubilisation of the lipid vesicles and formation of mixed micelles.
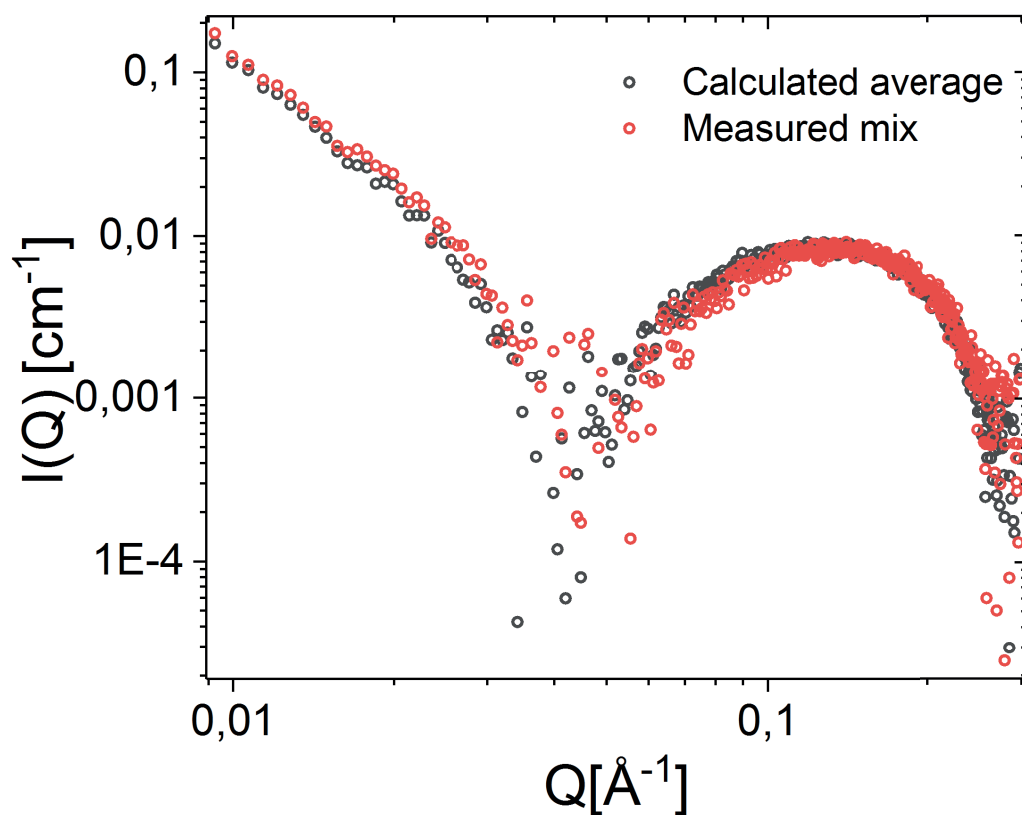

Figure S7. Qualitative comparison of the measured SAXS data of liposomes mixed SAXS *colistin* 1:10 revealing a lack of peptide lipid interaction compliant with no acceleration in lipid

dynamics as seen by TR-SANS presented in figure 4. The SAXS data was collected using a Bruker NANOSTAR equipped with a microfocus X-ray source (IµS Cu, InCoatec, Germany) and a VÅNTEC-2000 detector.

Table S4. Thermodynamic parameters of lipid exchange and flip-flop with and without *indolicidin* and *LL-37*.

	Lipid exchange				Lipid flip-flop			
	E_a [kJ/mol]	ΔH [kJ/mol]	$T\Delta S^a$ [kJ/mol]	ΔG [kJ/mol]	E_a [kJ/mol]	ΔH [kJ/mol]	$T\Delta S^a$ [kJ/mol]	ΔG [kJ/mol]
Liposomes	103	100	2.6	98	75	71	-28.6	100
Indolicidin 1:10	103	99	2.2	97	64	62	-36.9	99
Indolicidin 1:20	102	101	4.2	97	67	64.2	-34	98
Indolicidin 1:50	103	101	3.6	97	67	64.0	-34	98
LL-37 1:50	77	74	-22.7	97	76	73	-30.7	104

[a] Thermodynamic parameters were calculated using the Eyring approach directly.[22, 25]

References:

[1] H. Jenssen, J.H. Andersen, D. Mantzilas, T.J. Gutteberg, A wide range of medium-sized, highly cationic, α-helical peptides show antiviral activity against herpes simplex virus, Antiviral Res. 64(2) (2004) 119-126.

[2] P. Pernot, A. Round, R. Barrett, A. De Maria Antolinos, A. Gobbo, E. Gordon, J. Huet, J. Kieffer, M. Lentini, M. Mattenet, Upgraded ESRF BM29 beamline for SAXS on macromolecules in solution, J. Synchrotron Rad. 20(4) (2013) 660-664.

[3] A. Round, F. Felisaz, L. Fodinger, A. Gobbo, J. Huet, C. Villard, C.E. Blanchet, P. Pernot, S. McSweeney, M. Roessle, BioSAXS Sample Changer: a robotic sample changer for rapid and reliable high-throughput X-ray solution scattering experiments, Acta Crystallogr., Sect D: Biol. Crystallogr. 71(1) (2015) 67-75.

[4] A. De Maria Antolinos, P. Pernot, M.E. Brennich, J. Kieffer, M.W. Bowler, S. Delageniere, S. Ohlsson, S. Malbet Monaco, A. Ashton, D. Franke, ISPyB for BioSAXS, the gateway to user autonomy in solution scattering experiments, Acta Crystallogr., Sect D: Biol. Crystallogr. 71(1) (2015) 76-85.

[5] B. Eicher, F.A. Heberle, D. Marquardt, G.N. Rechberger, J. Katsaras, G. Pabst, Joint small-angle X-ray and neutron scattering data analysis of asymmetric lipid vesicles, J. Appl. Crystallogr. 50(2) (2017).

[6] J.B. Klauda, N. Kučerka, B.R. Brooks, R.W. Pastor, J.F. Nagle, Simulation-based methods for interpreting x-ray data from lipid bilayers, Biophys. J. 90(8) (2006) 2796-2807.

[7] N. Kučerka, J.F. Nagle, J.N. Sachs, S.E. Feller, J. Pencer, A. Jackson, J. Katsaras, Lipid bilayer structure determined by the simultaneous analysis of neutron and X-ray scattering data, Biophys. J. 95(5) (2008) 2356-2367.

[8] N. Kucerka, J. Pencer, J.N. Sachs, J.F. Nagle, J. Katsaras, Curvature effect on the structure of phospholipid bilayers, Langmuir 23(3) (2007) 1292-1299.

[9] J. Pencer, S. Krueger, C.P. Adams, J. Katsaras, Method of separated form factors for polydisperse vesicles, J. Appl. Crystallogr. 39(3) (2006) 293-303.

[10] M. Kiselev, P. Lesieur, A. Kisselev, D. Lombardo, V. Aksenov, Model of separated form factors for unilamellar vesicles, Appl. Phys. A 74(1) (2002) s1654-s1656.

[11] M.R. Brzustowicz, A.T. Brunger, X-ray scattering from unilamellar lipid vesicles, J. Appl. Crystallogr. 38(1) (2005) 126-131.

[12] N. Kučerka, M.-P. Nieh, J. Katsaras, Fluid phase lipid areas and bilayer thicknesses of commonly used phosphatidylcholines as a function of temperature, Biochim. Biophys. Acta, Biomembr. 1808(11) (2011) 2761-2771.

[13] J. Pan, F.A. Heberle, S. Tristram-Nagle, M. Szymanski, M. Koepfinger, J. Katsaras, N. Kučerka, Molecular structures of fluid phase phosphatidylglycerol bilayers as determined by small angle neutron and X-ray scattering, Biochim. Biophys. Acta, Biomembr. 1818(9) (2012) 2135-2148.

[14] N. Kučerka, B. van Oosten, J. Pan, F.A. Heberle, T.A. Harroun, J. Katsaras, Molecular structures of fluid phosphatidylethanolamine bilayers obtained from simulation-to-experiment comparisons and experimental scattering density profiles, J. Phys. Chem. B 119(5) (2014) 1947-1956.

[15] L. Arleth, C. Vermehren, An analytical model for the small-angle scattering of polyethylene glycol-modified liposomes, J. Appl. Crystallogr. 43(5) (2010) 1084-1091.

[16] J.S. Pedersen, M.C. Gerstenberg, Scattering form factor of block copolymer micelles, Macromolecules 29(4) (1996) 1363-1365.

[17] L. Arleth, B. Ashok, H. Onyuksel, P. Thiyagarajan, J. Jacob, R.P. Hjelm, Detailed structure of hairy mixed micelles formed by phosphatidylcholine and PEGylated phospholipids in aqueous media, Langmuir 21(8) (2005) 3279-3290.

[18] J.E. Nielsen, T.K. Lind, A. Lone, Y. Gerelli, P.R. Hansen, H. Jenssen, M. Cárdenas, R. Lund, A biophysical study of the interactions between the antimicrobial peptide indolicidin and lipid model systems, Biochim. Biophys. Acta, Biomembr. 1861(7) (2019) 1355-1364.

[19] J.E. Nielsen, V.A. Bjørnestad, R. Lund, Resolving the Structural Interactions between Antimicrobial Peptides and Lipid Membranes using Small-angle Scattering Methods: the case of Indolicidin, Soft Matter 14 (2018) 8750-8763.

[20] R.P. Brent, An algorithm with guaranteed convergence for finding a zero of a function, Comput. J. 14(4) (1971) 422-425.

[21] P. Debye, The intrinsic viscosity of polymer solutions, J. Chem. Phys. 14(10) (1946) 636-639.

[22] M. Nakano, M. Fukuda, T. Kudo, H. Endo, T. Handa, Determination of interbilayer and transbilayer lipid transfers by time-resolved small-angle neutron scattering, Phys. Rev. Lett. 98(23) (2007) 238101.

[23] T. Zinn, L. Willner, V. Pipich, D. Richter, R. Lund, Effect of core crystallization and conformational entropy on the molecular exchange kinetics of polymeric micelles, ACS Macro Letters 4(6) (2015) 651-655.

[24] T.J. Falla, D.N. Karunaratne, R.E. Hancock, Mode of action of the antimicrobial peptide indolicidin, J. Biol. Chem. 271(32) (1996) 19298-19303.

[25] R. Homan, H.J. Pownall, Transbilayer diffusion of phospholipids: dependence on headgroup structure and acyl chain length, Biochim. Biophys. Acta, Biomembr. 938(2) (1988) 155-166.

Paper IV

Impact of Antimicrobial Peptides on *E. coli*-mimicking Lipid Model Membranes: correlating structural and dynamic effects using scattering methods

Josefine Eilsø Nielsen, Sylvain François Prévost, Håvard Jenssen and Reidar Lund

IV

ARTICLE

Impact of Antimicrobial Peptides on *E. coli*-mimicking Lipid Model Membranes: correlating structural and dynamic effects using scattering methods

Josefine Eilsø Nielsen,[a] Sylvain François Prévost,[b] Håvard Jenssen[c] and Reidar Lund*[a]

The mechanism of action of antimicrobial peptides (AMPs) has been debated over many years, and various models have been proposed. In this work we combine small angle X-ray/neutron scattering (SAXS/SANS) techniques to systematically study the effect of AMPs on the cytoplasmic membrane of *Escherichia coli* bacteria using a simplified model system of 4:1 DMPE:DMPG ([1,2-dimyristoyl-sn-glycero-3-phosphoethanolamine]:[1,2-dimyristoyl-sn-glycero-3-phospho-(10-rac-glycerol)]) phospholipid unilamellar vesicles. The studied antimicrobial peptides aurein 1.2, indolicidin, LL-37, lacticin Q and colistin vary in size, charge, degree of helicity and origin. The peptides insert into the bilayer to various degrees, and are found to accelerate the dynamics of phospholipids significantly as seen by time resolved SANS (TR-SANS) measurements, with the exception of colistin that is suggested to rather interact with lipopolysaccharides (LPS) on the outer membrane of *E. coli*. We compare these results with earlier published data on model systems based on PC-lipids (phosphatidylcholines), showing comparable effect with regards to peptide insertion and effect on dynamis. However, model systems based on PE-lipids (phosphatidylethanolamine) are more prone to destabilisation upon addition of peptides, with formation of multilamellar structures and morphological changes. These properties of PE-vesicles lead to less conclusive results regarding peptide effect on structure and dynamics of the membrane.

Introduction

Antimicrobial peptides (AMPs) are important agents in the first line defence to kill pathogenic microorganisms in humans, animals, insects and are even secreted by some bacteria. They defend the host against foreign infectious organisms including Gram-positive and Gram-negative bacteria, fungi, protozoa and viruses[1-3], through host immune modulation and/or direct targeting of the infectious organisms. Their direct antimicrobial properties have been known for decades, yet the mode of action of AMPs are found to be quite complex, and many different theories have been presented. However, there is a general consensus that most AMPs in some way or another mainly target the cytoplasmic membrane of the microorganism.[4] Their ability to only attack foreign organisms and not their host is amongst other explained by the difference in lipid composition of the cytoplasmic membrane of eukaryote and prokaryote cells. Eukaryote cell membranes mostly consist of neutrally charged lipids (zwitterionic) and cholesterol,[5] while prokaryote membranes include a substantial amount of negative charged lipids in combination with zwitterionic lipids and cardiolipins.[6] Even though AMPs vary vastly in structure, the common feature of most of the peptide is their overall cationic (positive) charge. This enables electrostatic interactions with anionic (negative) lipids in the bacteria membrane, thus potentially playing a regulatory role in the target cell selectivity.[7]

To study peptide-lipid interaction in detail using biophysical and biochemical methodologies, the use of model membrane systems to mimic the cytoplasmic membrane of bacteria is essential.[8] Real bacteria cells contain much more than the cytoplasmic membrane such as an outer membrane and intracellular ribosomes, a chromosome, and plasmids. Even the inner membrane itself is intricate with a diverse group of membrane proteins as well as different phospholipids as described above. The complexity will for many of these techniques obscure the results, complicating the interpretation with regards to the specific membrane-peptide
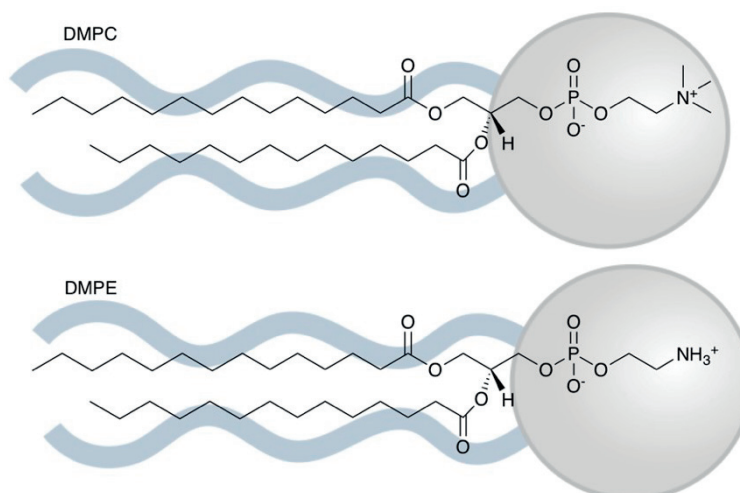
[a.] Department of Chemistry, University of Oslo, 0315 Oslo, Norway.
E-mail: reidar.lund@kjemi.uio.no
[b.] Institut Laue - Langevin, 38000 Grenoble, France
[c.] Department of Science and Environment, Roskilde University, 4000 Roskilde, Denmark

Figure 1. Chemical structure of DMPC and DMPE phospholipids showing the difference in the head group from a choline group in DMPC to an amine in DMPE.

interaction. Therefore, the model systems most frequently used are phospholipid membranes either as flat supported bilayers, tethered lipid bilayers, free-floating lipid micelles, or vesicles. The flat model membranes are used for surface sensitive techniques like neutron reflectometry (NR),[9-15] atomic force microscopy (AFM),[16-19] Dual Polarisation Interferometry (DPI)[19] and Surface Plasmon Resonance spectroscopy.[19, 20] While the free-floating lipid micelles or vesicles can be studied by techniques like nuclear magnetic resonance (NMR),[11, 21-23] small angle X-ray or neutron scattering (SAXS/SANS),[13, 24-35] and fluorescence spectroscopy.[20, 36] Recent efforts have gone into developing model systems more closely related to the real bacteria membrane. Clifton and co-workers recently presented a full NR characterization of a floating lipid membrane closely mimicking the inner and outer membrane of *E. coli* including the LPS layer.[10] Even some reports of nanoscale structural determinations of live bacterial cells have been reported recently. While Semeraro et al. have determined the ultrastructure of live *E. coli* using ultra-SAXS and detailed modelling,[37] Nickels and co-workers have used SANS and contrast variation to characterise the membrane heterogeneities of live *Bacillus subtilis*.[38] Although these findings reveal that it is possible to determine structural parameters of live cells they still justify the need for simplified model systems due to the high complexity in differentiating the specific effects of an added substrate.

The composition of the model systems can be adjusted depending on the specific cell type that one wishes to mimic. The most common composition of lipids used to mimic bacteria membranes is the combination of zwitterionic phospholipid with a phosphatidylcholine (PC) headgroup and negatively charged phospholipids with for example phosphatidylglycerol (PG) headgroups. These lipids are often chosen both because of commercial availability and because they are known to form relatively stable uniform lipid vesicles, and supported lipid bilayers with high coverage on for example mica or silica surfaces.[39] However, the use of PC to mimic the overall neutral part of the membrane, which in reality should be phosphatidylethanolamine (PE) in the case of most bacteria has been debated in the literature.[40] The difference in the chemical structure of the PC and PE headgroup is the three methyl groups on the nitrogen forming a choline group in PC, which is exchanged for hydrogens in PE (Figure 1). This seemingly small difference in the chemical structure result in a major increase in the phase transition temperature where the lipids in the membrane changes from the gel phase to the liquid crystalline phase. While 14:0 PC (DMPC) exhibit a phase transition temperature of 24°C, the equivalent 14:0 PE (DMPE) lipid shows transition at 50°C.[41] This drastic increase may be explained by the PE headgroups ability to form hydrogen bonds in-between lipid in the membrane resulting in a more stable structure.

Table 1. Overview of antimicrobial peptides.

Peptide	Sequence	MW (g/mol)	Net charge at pH 7.0	Ratio of hydrophilic residues / total number of residues
Aurein 1.2	GLFDIIKKIAESF-CONH$_2$	1480	1+	38 %
Indolicidin	ILPWKWPWWPWRR-CONH$_2$	1906	4+	23 %
LL-37	LLGDFFRKSKEKIGKEFKRIVQRIKDFLRNLVPRTES	4493	6+	54 %
Lacticin Q	MAGFLKVVQLLAKYGSKAVQWAWANKGKILDWLNAGQAIDWVVSKIKQILGIK	5898	6+	34 %

In this work, we have compared the structure of lipid bilayers consisting of 4:1 DMPC/DMPG or 4:1 DMPE/DMPG respectively, and their interaction with the natural antimicrobial peptide, indolicidin.[42] Furthermore we present additional data for the lipid-peptide interaction with PE lipids for a wide range of natural AMPs; aurein 1.2,[43] LL-37,[44] lacticin Q[45] (details given in Table 1) and colistin[46,][47] (negative control because of expected lack of interaction with cytoplasmic membranes) showing the effect of the peptides on the membrane structure using SAXS, and membrane dynamics using time resolved SANS.

Experimental

Materials and methods

Synthetic DMPE (1,2-dimyristoyl-sn-glycero-3-phosphoethanolamine, $C_{33}H_{66}NO_8P$), d54-DMPE (fully deuterated tail ($C_{13}D_{27}$)$_2$, hydrogenated polar headgroup $C_7H_{12}NO_8P$), DMPG (1,2-dimyristoyl-sn-glycero-3-phospho-(10-rac-glycerol) (sodium salt), $C_{34}H_{66}O_{10}P$), d54-DMPG (fully deuterated tail ($C_{13}D_{27}$)$_2$, hydrogenated polar headgroup $C_8H_{12}O_{10}P$) and DMPE-PEG (1,2-dimyristoyl-sn-glycero-3-phosphoethanolamine-N-[methoxy(polyethylene glycol)-2000], with M_w(PEG)=2000 g/mol, ca. 45 CH_2CH_2O units) was purchased from Avanti Polar Lipids. The peptides indolicidin, aurein 1.2, LL-37 and lacticin Q were purchased from Schafen-N ApS, Copenhagen, while Colistin was purchased from Sigma-Aldrich. The 50 mM Tris buffer was prepared by mixing Tris-base with Tris-HCl (Sigma Aldrich) to achieve a pH of 7.4 in either pure H_2O (MilliQ) for SAXS measurements or in 50% D_2O (Sigma-Aldrich) and 50% H_2O for TR-SANS measurements.

For DMPE/DMPG lipid vesicle preparation 75 mol% DMPE, 22.5 mol% DMPG and 2.5 mol% DMPE-PEG were dissolved in a 1:3 methanol:chloroform solution. The organic solvents were removed completely under vacuum using a Heidolph rotary evaporator with a Vacuubrand vacuum pump to prepare a thin lipid film. Then the film was hydrated with 50 mM Tris buffer, pH 7.4, for at least one hour at a temperature of 55°C. After sonication using a ultrasonic bath for 10 minutes, the lipid dispersions were extruded through a 100 nm pore diameter Avanti polycarbonate filter (≥21 times) using an Avanti mini-extruder fitted with two 1 mL airtight syringes.

The antimicrobial peptides were dissolved in 50 mM Tris buffer, pH 7.4, to the desired concentration directly before the experiments.

Small angle X-ray scattering (SAXS)

The synchrotron SAXS data was collected at beamline P12 operated by EMBL Hamburg at the PETRA III storage ring (DESY, Hamburg, Germany).[48] The data was obtained using a radiation wavelength of 1.24 Å and a detector distance of 3.0 m, covering a Q range of 0.0032 Å^{-1} to 0.73 Å^{-1}, where Q is the magnitude of the scattering vector: $Q = \frac{4\pi}{\lambda}\sin\frac{\Theta}{2}$, with θ the scattering angle. Data reduction was done automatically with the software available at the beam line and the 1D data were brought to absolute intensity scale using water as a primary standard. The SAXS results were analysed using the theoretical model described in the electronic supplementary information.[29,30] In short, the model provides a comprehensive description of the membrane by dividing it into probability functions for each component (lipid sub-units/peptide) across the bilayer. Error of scattering analysis is estimated to be ≤4%.

Time resolved small angle neutron scattering (TR-SANS)

TR-SANS experiments were performed on the D11 beamline at The Institut Laue–Langevin (ILL) facilities, Grenoble, France using detector distance of 20.5 m and a wave length of 6 Å (fwhm 9%), covering a Q range of 0.002 Å^{-1} to 0.034 Å^{-1}. D-liposomes (vesicles consisting of lipids with deuterated tails) were mixed with H-liposomes (vesicles consisting of lipids with proteated tails) 1:1 directly before the first measurement using a Finntip micropipette and mixed with either pure buffer (to make sure concentration of the non-peptide samples compare to the peptide samples) or peptide solution 1:1. The samples were filled into Hellma quartz banjo-cells with a path length of 1 mm and kept in a temperature-controlled rack during the full experiment. The samples were measured with shorter measurement times and intervals in the beginning but increasing measurement times and longer intervals over time due to the descending contrast.

The TR-SANS data were evaluated by determining the relaxation function $R(t)$ according to:

$$R(t) = \sqrt{\frac{I(t)-I_\infty}{I(0)-I_\infty}} \qquad (1)$$

where $I(t) = \int I(Q,t)dQ$ is the integral intensity at a given time, I_∞ is the intensity of the premixed blend representing the final state and $I(0)$ is the averaged intensity of the H-vesicles and D-vesicles measured separately representing the initial state before exchange and flip-flop has taken place.

Results and discussion

Comparing PE and PC lipids in model systems

The SAXS results together with calculated electron density profiles of model membranes consisting of DMPE/DMPG (PE-vesicles) and DMPC/DMPG (PC-vesicles) (as previously published by Nielsen and co-workers[30]) at 37°C are displayed in Figure 2. From these data we can compare the structure of the pure lipid membrane as well as how the membrane is affected by adding an antimicrobial peptide. As seen from the scattering curves plotted in Figure 2A comparing the scattering of the pure lipid vesicles, the shape of the scattering curve from the PE-vesicles differs from that of the PC-vesicles. This difference can be explained mainly by PE-vesicles having a thicker membrane than PC-vesicles at this temperature, as well as a contrast difference due to the smaller volume of the PE headgroup and incorporation of a slightly higher amount of PEGylated lipids to stabilise the system (5% DMPE-PEG in the case of PE vesicles contrary to only 2.5% DMPE-PEG in the case of PC-vesicles). To confirm that the increased amount of PEG does not affect the structure of the lipid bilayers pure PE-vesicles with both 2.5 and 5% of PEGylated lipids have been analysed (see ESI Figure S1).

The estimated overall thickness of the DMPE/DMPG membrane based on model fits was found to be 45 Å (see Table S1 of the ESI). Lee and co-workers have reported a membrane thickness for a bilayer with the same DMPE/DMPG mixture of 44 Å calculated from DPI measurements, but in these measurements the temperature was 28°C[49] potentially explaining the slight difference. The increased thickness of the membrane of PE-vesicle when compare to the PC vesicles is obvious in the electron density profile in Figure 2B and can be explained by the difference in the phase transition temperature. As the lipids in the PE-vesicles are in the gel phase the membrane is more ordered resulting in tighter packing in the lateral direction, however upon melting to the liquid crystalline phase the lipids are more disordered resulting in a thinning of the membrane. Similar behaviour have been reported previously for PC lipids in studies where the thickness has been measured as a function of temperature.[50]

Overall the PE-vesicles were found to be less stable than the PC-vesicles upon addition of any positively charged substrates, with rapid fusion of vesicles and formation of multilamellar structures observed at higher concentrations. The difference in the molecular geometry of PE lipids in comparison to PC lipids provides an explanation of this behaviour. PE lipids prefer a slightly negative curvature resulting in a deformed membrane and formation of multilamellar structure.[40, 51] Due to the incorporation of 5% PEGylated lipids (DMPE-PEG) in the membrane the unilamellar vesicles are more stable against fusion due to steric hindrance.[30] This allows us to quantitatively study the peptide-membrane interaction by analysing the individual bilayer structure using SAXS.
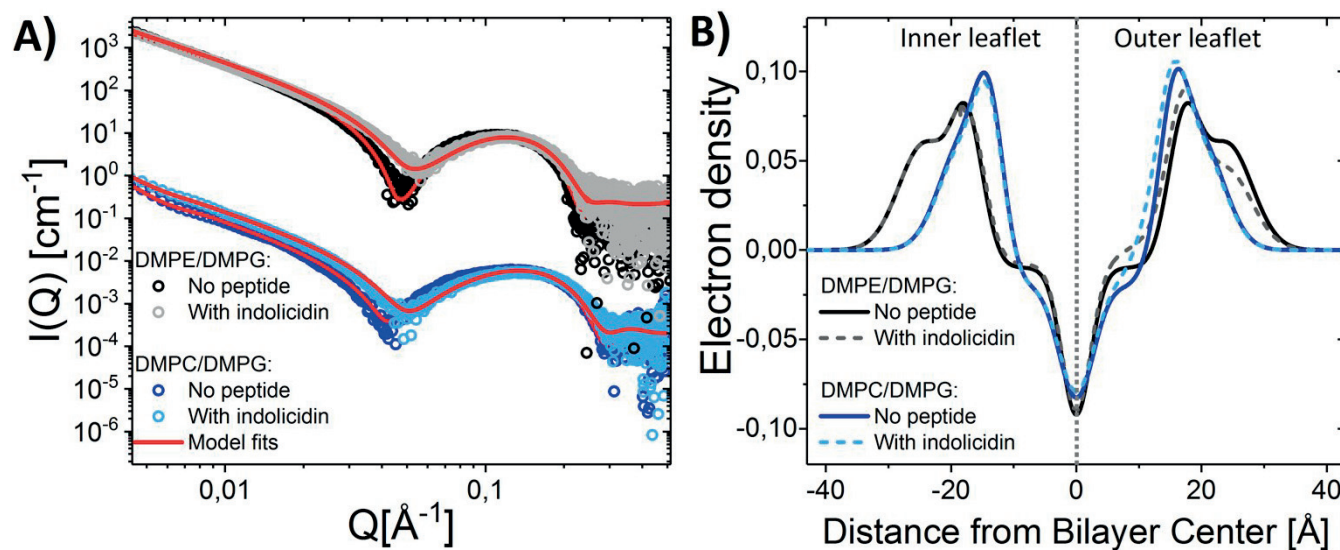

Figure 2. A) SAXS data comparing DMPE/DMPG and DMPC/DMPG[30] liposomes with and without addition of indolicidin (in a ratio of 1:20) at 37°C plotted together with model fits. The data of DMPE/DMPG liposomes have been offset with a factor of 1000 to better display the data. B) Electron density profiles calculated from the fit parameters of SAXS data shown in A) (detailed fit parameters included in ESI Table S1 for DMPE/DMPG vesicles and in ref [30] for DMPC/DMPG vesicles).

Journal Name

ARTICLE

As seen, the scattering data for both lipid model systems (Figure 2A) clearly show how addition of indolicidin in a lipid:peptide mol ratio of 20:1 result in a slight shift in the first minima to higher Q. This effect has previously been explained by Nielsen et al. as a change in the electron density of the membrane core upon insertion of the peptide in the bilayer.[13, 29, 30] Indolicidin is reported to insert in the outer leaflet of the membrane in the interface between the head and tail region of DMPC/DMPG membranes as seen by SAXS, SANS and NR,[13, 30] an observation supported by molecular dynamics simulations.[52] As is evident from the electron density profile in Figure 2B the same behaviour can be seen in the PE-vesicles where you see an increase in the electron density in the outer part of the tail region, close to the interface with the outer head group. However, contrary to the results reported for PC-vesicles[13, 30] the volume of the head group is increased upon peptide addition. This is seen in the electron density as a change in the contrast of the outer headgroup. This change can be explained by the peptide disrupting the packing more for lipids in the gel phase, as well as potential destabilisation due to breakage of hydrogen bonds caused by the peptide insertion. Furthermore, the scattering profile from peptide-lipid mixtures in the case of PE-vesicles could not be explained solely by the insertion of peptide in the membrane as the case is for PC-vesicles. A slight solubilisation of the membrane was also observed with an estimate of 4% mixed peptide-lipid micelles present in the system after peptide addition. This may, as mentioned above, be related with the negative curvature strain on the membrane that favour destabilization and micelle formation.

Comparing data on a wide range of natural AMPs

To broaden the knowledge of the lipid interaction of AMPs in general a range of natural peptides from various sources was mixed with the PE-vesicles mimicking the composition of *E. coli* membrane. The full results for varying amounts of peptide addition in range from 1:20 to 1:100 peptide:lipid ration is shown in Figure 3 (fits for lacticin Q 1:20 is not shown as addition of this amount of peptide lead to formation of multilamellar structures preventing an accurate fit analysis with the model described in ref.[30]). As seen from the scattering curves in Figures 3A-3D all four peptides cause a similar slight shift in the first minima at intermediate Q, with increasing effects as a function of increasing concentration. This can as described above be explained by the shift in electron density of the hydrocarbon core region of the membrane upon insertion of peptide, due to the large contrast between the aliphatic tails and the peptides. In Figure 3E-H the volume probability plots calculated from the fit parameters of the SAXS data (parameters are included in Table S1 of the ESI) is displayed. From these plots, the spatial distribution of the peptide within and at the membrane can be extracted.
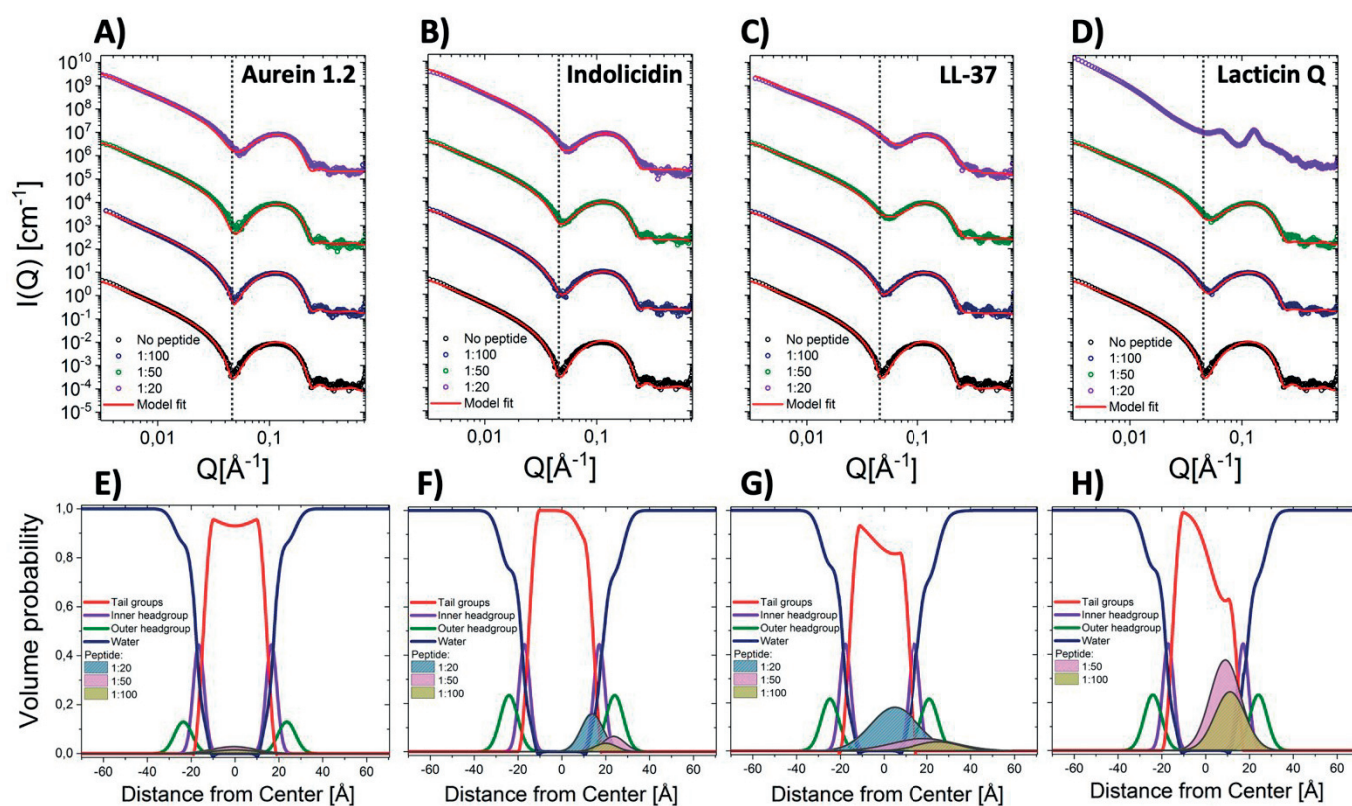

Figure 3. A) SAXS data of peptide-lipid interaction of a wide range of natural AMPs: aurein 1.2 (A), indolicidin (B), LL-37 (C) and lacticin Q (D) mixed with *E. coli* mimicking lipid vesicles (DMPE/DMPG), together with model fits. The lipid:peptide ratio is indicated in the plot, and a line has been added at the minimum of the pure liposomes in order to visualise the shift upon peptide addition. Volume probability distribution for lipid membranes of with addition of aurein 1.2 (E), indolicidin (F), LL-37 (G) and lacticin Q (H) showing the position of the peptide in the membrane.

ARTICLE   Journal Name

Aurein 1.2 is the smallest α-helical peptide in this study with only 13 residues and the lowest overall cationic charge of +1 at pH 7. It is found to insert into the core of the hydrocarbon region of the membrane as seen in Figure 3E. In addition to the deep insertion the peptide was found to have a pronounced detergent effect on the bilayer at the highest concentration (1:20) resulting in formation of around 48% mixed peptide-lipid micelles. Indications of a similar detergent effect of this peptide was reported by Fernandez and co-workers based on NMR and NR studies.[11] However, at lower concentrations at 1:50 and 1:100 ratios, only 5% and 0% mixed micelles were detected. This leaves room for a discussion on whether the solubilisation effects observed at the high peptide concentration provides a relevant explanation for the antimicrobial activity at physiological conditions which likely involve lower concentrations.

Indolicidin, is also a 13 residues peptide, but compared to aurein 1.2 it adopts an extended random coil structure in solution and a net charge of +4. As described in the section above the indolicidin addition lead to a very slight solubilisation at the highest lipid:peptide ratio of 1:20. However, at all concentrations most of the peptide seems to insert into the membrane without any significant changes in the thickness or overall structure of the membrane. The position of the peptide in the membrane seem quite stable in the outer with only a slight deeper penetration with increasing concentration as seen in Figure 3F. The differences in the penetration depth between the similarly sized aurein 1.2 and indolicidin can be explained by a variation in the number of charged and aromatic amino acids. Because of the high tryptophan content of indolicidin and the presence of the partially charged and bulky indole side group this peptide is more likely to position in the outer leaflet, in close proximity to the lipid–water interface.[53] For LL-37, a much bigger α-helical peptide with 37 residues a concentration dependent insertion is visible, with increasing penetration as a function of higher peptide:lipid ratio (Figure 3G). Also, for this peptide a solubilisation effect was observed, with 1-5% formation of mixed micelles dependent on the concentration of peptide. The same effect has been reported in the past with PC-vesicles by both Sevcsik and co-workers[26, 54] and Nielsen and co-workers[29] with almost full solubilisation of the membrane at high peptide concentrations.

Lacticin Q with 53 residues is the largest α-helical peptide and is according to reported literature much less studied than the other peptides included in the study. As seen in the volume probability plot in Figure 3H, the peptide exhibits a similar insertion in the outer leaflet of the bilayer as the much smaller peptide indolicidin. However, the size of the peptide is much bigger resulting in a larger portion of the Gaussian distribution even at low peptide:lipid ratios. Interestingly even though the highest peptide ratio of 1:20 resulted in destabilisation of the lipids and eventually phase separation, the lower ratios shown here (1:50 and 1:100) did not lead to solubilisation of the membrane, and the changes in the scattering pattern can solely be explained by peptide insertion. As seen from the sequence presented in Table 1, Lacticin Q has in the same way as indolicidin several aromatic tryptophans and tyrosines, as well as charged groups which support the similar peptide positioning in the outer head-tail interface as observed for indolicidin. The difference in the ability to solubilise the membrane between LL-37 and Lacticin Q may be explained by LL-37 having fewer bulky aromatic groups and more charged amino acids (even though the net charge is the same) increasing the membrane solubilisation abilities.
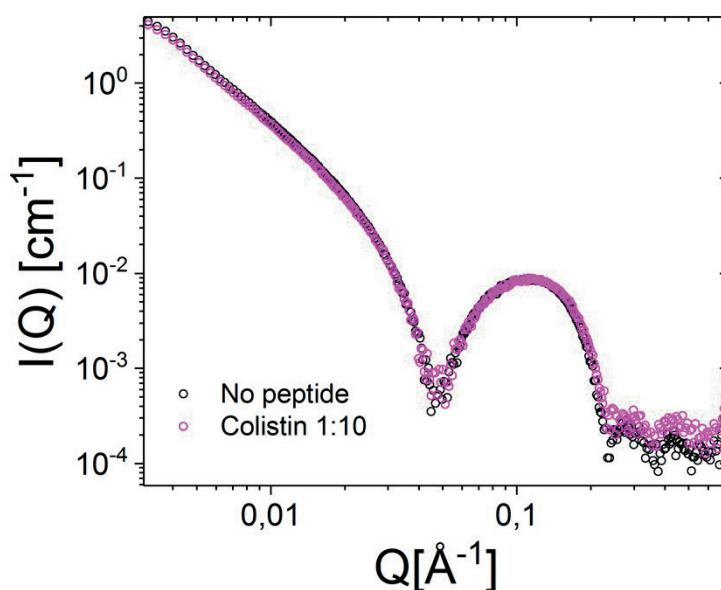

Figure 4. Qualitative comparison of the measured data of DMPE/DMPG-vesicles mixed 10:1 with colistin to the calculated average where the scattering from the liposomes and the peptide have been measured separately and summed together.

As a negative control we used the natural cyclic peptide colistin, a commercially available peptide antibiotic that is known to have other targets than the cytoplasmic membrane, contrary to what is suggested for the other AMPs included in the study. Colistin is reported to rather affect the outer membrane through displacement of divalent cations and interaction with lipopolysaccharides (LPS), explaining its selectivity towards Gram-negative bacteria.[47, 55, 56] Alternatively, intracellular targets like peptide binding to ribosomes indicating passage through the outer and inner membrane has been presented.[57] However, although some scenarios have been presented where colistin was suggested to also target the inner membrane itself[58] although our current results does not support this. The absence of any membrane interaction with colistin in the in the range of 1:10 to 1:100 was confirmed using SAXS. This can be seen by a perfect overlap of the measured peptide lipid vesicle mixture and the calculated average in Figure 4. These results confirm that our methodology is able to differentiate between the effect or lack thereof different cationic peptides.

The effect on exchange and flip-flop of phospholipids upon addition of peptides

In order to study the effect of the peptides on lipid dynamics, contrast variation TR-SANS measurements were performed. The method is illustrated in Figure 5A and described in detail in Ref.[29] As seen in Figure 5B the reduced intensity, $R(t)$, proportional to the excess contrast (Eq 1.), decrease as a function of time for DMPE/DMPG lipid vesicles with and without addition of AMPs (see ESI Figure S2 for raw SANS curves over time). The decrease in scattering intensity can be directly correlated to intervesicular exchange and intravesicular flip-flop of phospholipids.[29, 59-61] The activation energy of lipid flip-flop of PE is estimated to be lower than for PC when both lipids are in the liquid crystalline phase due to a smaller lipid head group volume and a smaller hydration shell for PE lipids.[62] However, in our experiment the membrane is in the gel phase as the experiment is done at 37 C and the phase transition temperature for the 4:1 DMPE/DMPG was estimated by DSC to be 44.7°C (se ESI Figure S3). Trial experiments at 47°C, above the phase transition temperature, was attempted but resulted in destabilization of the vesicles with formation of multilamellar structures over time both with and without addition of peptide. Nakano and co-workers have previously shown that the exchange and flip-flop rate constants can be extracted from TR-SANS data on pure PC-liposomes by fitting a double exponential decay function to the data.[60] However, this model was not able to explain the R(t) of the DMPE/DMPG liposomes indicating that in this system there is more than two rates due to the mixture of the lipids.
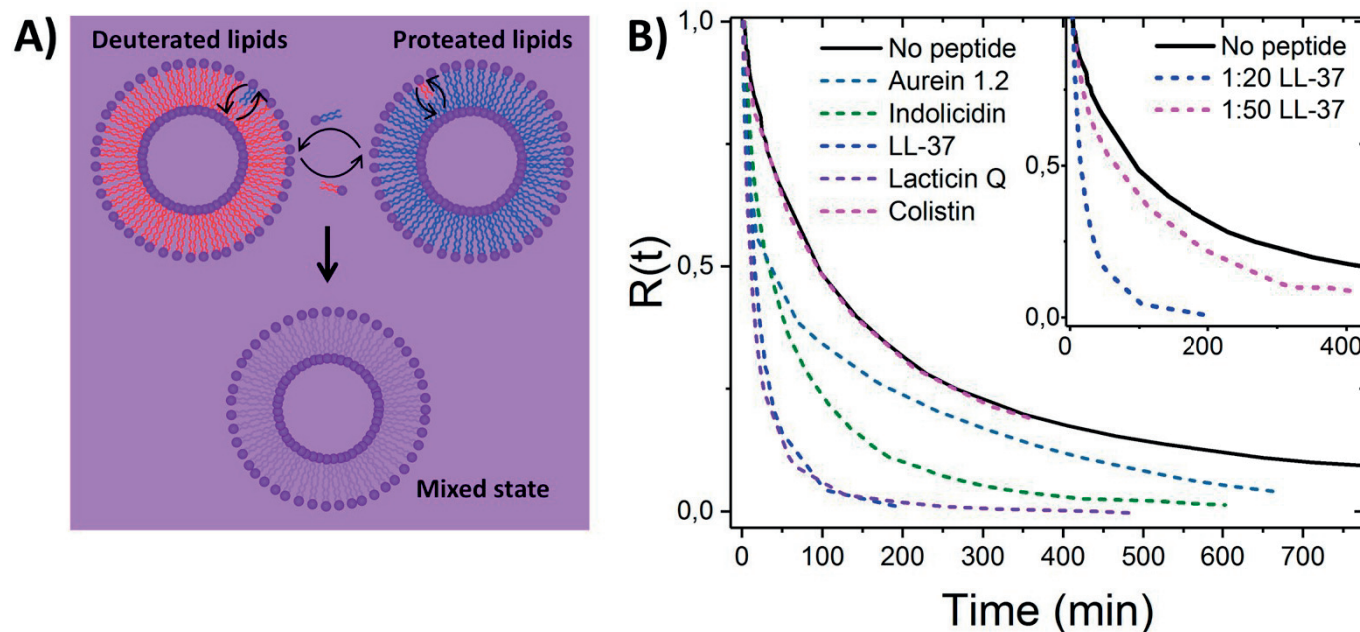

Figure 5. A) Illustration of H/D contrast variation technique used to study intravesicular lipid flip-flop and intervesicular lipid exchange by mixing deuterated and hydrogenated lipids in a zero-average contrast Tris buffer (mix of H_2O and D_2O to match the average contrast of the mixed liposomes). B) Rate of contrast decay, $R(t)$, of pure DMPE/DMPG liposomes (solid line) and liposomes with added aurein 1.2 (1:50), indolicidin (1:20), LL-37 (1:20), lacticin Q (1:50) and colistin (1:10) (dotted line) based on TR-SANS measurements (lipid:peptide ratios chosen based on the stability of liposome system). Inserted graph highlight the concentration dependent effect of LL-37. All samples were measured at 37°C.

As qualitatively seen from the $R(t)$ functions in Figure 5B, all peptides except colistin were found to accelerate the lipid dynamics significantly. The same trend of lipid dynamics acceleration upon introduction to AMPs has previously been seen using PC based membranes.[28, 29, 63, 64,27] Nielsen and co-workers previously reported lowering of the activation energy for lipid flip-flop upon addition of indolicidin after measuring 4:1 DMPC/DMPG lipid vesicles mixed with indolicidin 1:20 at four different temperature.[29] For the DMPE/DMPG lipid vesicles, a combination of a lowering in the activation energy as well as partly solubilisation of the membrane as seen by SAXS provide an explanation of the observed effects. A potential peptide induced breakage of hydrogen bonding between PE lipids may play a significant role lowering the effective activation barrier.

As seen from Figure 5B the largest peptides in the study, lacticin Q seem to have the most pronounced acceleration of the peptides reaching the end state after only around 2 hours, even at the low peptide lipid ratio of 1:50. While LL-37 shows the same degree of acceleration at 1:20, at 1:50 the effect on the dynamics is lower. A significant concentration dependence for LL-37 on the lipid dynamics was also observed for in PC-vesicles by Nielsen and co-workers[29], and was related to the observed structural effect. The penetration of the peptide in the bilayer seems to increase progressively with increasing concentrations where the peptide at localized at the interface at low peptide addition whereas it assumes a more trans-membrane conformation at higher concentrations. Aurein 1.2 causes a dramatic acceleration of the lipid dynamics at higher concentrations than 1:50, reaching end-state outside the resolution of our experimental setup. This can be explained by partial solubilisation of the membrane as seen by SAXS. However, at 1:50 the effect is on the level of LL-37 at the same ratio showing a significant acceleration as compared to pure lipid vesicles. The same is seen for indolicidin, while colistin overlaps with the $R(t)$ curve of the pure membrane indicating no effect on the dynamics. When correlating these results with the absence of structural effects as seen by SAXS it is not surprising that colistin did not have any observed effect on the membrane dynamics. While all the peptides that were found to insert into the membrane by SAXS seem to also affect the lipid dynamics. Nguyen et al. found in their study on asymmetric lipid vesicles that peptides localized towards the surface of the membrane has a more pronounced effect on the dynamics than peptides that penetrate deeper into the membrane.[28] This supports the pronounced effect we see for lacticin Q and indolicidin, both found to position on the outer leaflet. However, this does not explain the dramatic effects seen for LL-37 and aurein 1.2 that seem to be able to penetrate deeper into the bilayer according to SAXS. Though, in the latter case the detergent effects observe specifically for PE-lipids may provide parts of the explanation. Due to these effects observed by SAXS, and the destabilisation effect seen upon increase in temperature, it becomes difficult to extract quantitative rates for exchange and flip-flop, and activation energy in the same way as done previously for PC-lipid systems using the same technique.[29, 59-61] Thus, we can conclude by qualitative comparison that the same general trend of acceleration of lipid dynamics upon peptide addition can be observed also for lipid model membranes consisting of DMPE/DMPG lipids.

Conclusions

We have demonstrated how the effect of a range of different natural antimicrobial peptides on lipid membranes can be studied in detail using small angle scattering techniques. By using complex model systems, we can mimic the lipid composition of the cytoplasmic membrane of bacteria. However, SAXS/SANS results show how these systems with PE lipids are less stable upon peptide addition when comparing to frequently used model systems where the PE lipids are exchanged for PC lipids. Even though PC and PE both are zwitterionic and have a comparable structure, they vary considerably in phase transition temperature due to PE lipids ability to form inter molecular hydrogen bonds. This result in PE vesicles being more prone to undergo morphological transitions and formation of multilamellar structures. As seen using SAXS, addition of PEGylated PE lipids in the vesicles prevent the formation of multilamellar structures upon peptide addition, and in our case 5% of PEGylated PE enabled detailed studies of structure and dynamics of vesicles mixed with five different AMPs.

Based on modelling of SAXS data we were able to compare the insertion of aurein 1.2, indolicidin, LL-37, lacticin Q and colistin in the lipid membrane, and estimate the amount of solubilisation of the vesicles in the studied concentration range. The results show that four of the peptides insert into the membrane with a deeper insertion of aurein 1.2 and LL-37 (the latter also in a concentration dependent manner) than for indolicidin and lacticin Q. A fifth one, colistin, was not found to interact with the lipid vesicles. By using H/D contrast variation and TR-SANS we see that four out of five peptides have significant effect on the dynamics of the phospholipids, with a clear acceleration when comparing to the pure lipid system at 37°C. This is not surprising as colistin is known to interact with the LPS outer membrane of Gram-negative bacteria. The data presented indicate that the larger peptides LL-37 and Lacticin Q seems to have a more pronounced effect on the transport than the smaller peptides. However, the peptide membrane interaction is very complex, and the effect on dynamics cannot easily be predicted from the structural interaction of the peptide or the peptide sequence independently, in support with previous data from Nielsen et al. on DMPC/DMPG lipids. The data do reveal that AMPs generally have profound impact on lipid dynamics that may have important consequences in the spatial distribution of lipids on cytosolic and outer membrane side. In addition, the ion transport may be influenced by the enhanced lipid transport. These factors may in turn lead to lipid scrambling, signalling events or loss of net electrical potential which eventually lead to cell death.

Conflicts of interest

There are no conflicts to declare.

Acknowledgements

Notes and references

1.   Y. Lai and R. L. Gallo, *Mod Trends Immunol*, 2009, **30**, 131-141.
2.   M. Zasloff, *Nature*, 2002, **415**, 389.
3.   H. Jenssen, P. Hamill and R. E. Hancock, *Clin. Microbiol. Rev.*, 2006, **19**, 491-511.
4.   M. R. Yeaman and N. Y. Yount, *Pharmacol. Rev.*, 2003, **55**, 27-55.
5.   A. A. Spector and M. A. Yorek, *J. Lipid Res.*, 1985, **26**, 1015-1035.
6.   N. Shaw, *Adv. Appl. Microbiol*, 1974, **17**, 63-108.
7.   H. W. Huang, *Biochemistry*, 2000, **39**, 8347-8352.
8.   D. Roversi, V. Luca, S. Aureli, Y. Park, M. L. Mangoni and L. Stella, *ACS Chem. Biol.*, 2014, **9**, 2003-2007.
9.   L. A. Clifton, R. A. Campbell, F. Sebastiani, J. Campos-Terán, J. F. Gonzalez-Martinez, S. Björklund, J. Sotres and M. Cárdenas, *Adv. Colloid Interface Sci.*, 2020, 102118.
10. L. A. Clifton, S. A. Holt, A. V. Hughes, E. L. Daulton, W. Arunmanee, F. Heinrich, S. Khalid, D. Jefferies, T. R. Charlton and J. R. Webster, *Angew. Chem. Int. Ed.*, 2015, **54**, 11952-11955.
11. D. I. Fernandez, A. P. Le Brun, T. C. Whitwell, M.-A. Sani, M. James and F. Separovic, *Phys. Chem. Chem. Phys.*, 2012, **14**, 15739-15751.
12. D. I. Fernandez, A. P. Le Brun, T.-H. Lee, P. Bansal, M.-I. Aguilar, M. James and F. Separovic, *Eur. Biophys. J.*, 2013, **42**, 47-59.
13. J. E. Nielsen, T. K. Lind, A. Lone, Y. Gerelli, P. R. Hansen, H. Jenssen, M. Cárdenas and R. Lund, *Biochim. Biophys. Acta, Biomembr.*, 2019, **1861**, 1355-1364.
14. T. K. Lind, L. Darre, C. Domene, Z. Urbanczyk-Lipkowska, M. Cárdenas and H. Wacklin, *Biochim. Biophys. Acta, Biomembr.*, 2015, **1848**, 2075-2084.
15. T. K. Lind, M. W. Skoda and M. Cárdenas, *ACS omega*, 2019, **4**, 10687-10694.
16. T. K. Lind, P. Zielinska, H. P. Wacklin, Z. Urbanczyk-Lipkowska and M. Cárdenas, *ACS nano*, 2013, **8**, 396-408.
17. H. J. Askou, R. N. Jakobsen and P. Fojan, *J. Nanosci. Nanotechnol.*, 2008, **8**, 4360-4369.
18. J. E. Shaw, J.-R. Alattia, J. E. Verity, G. G. Privé and C. M. Yip, *J. Struct. Biol.*, 2006, **154**, 42-58.
19. K. Hall, T.-H. Lee, A. I. Mechler, M. J. Swann and M.-I. Aguilar, *Sci. Rep.*, 2014, **4**, 5479.
20. S. E. Blondelle, K. Lohner and M.-I. Aguilar, *Biochim. Biophys. Acta, Biomembr.*, 1999, **1462**, 89-108.
21. M.-A. Sani and F. Separovic, *Acc. Chem. Res.*, 2016, **49**, 1130-1138.
22. S. Zhu, M. A. Sani and F. Separovic, *Peptide Science*, 2018, **110**, e24061.
23. F. Porcelli, A. Ramamoorthy, G. Barany and G. Veglia, in *Membr. Protein.*, Springer, 2013, pp. 159-180.
24. G. Pabst, S. L. Grage, S. Danner-Pongratz, W. Jing, A. S. Ulrich, A. Watts, K. Lohner and A. Hickel, *Biophys. J.*, 2008, **95**, 5779-5788.
25. E. F. Semeraro, L. Marx, M. P. Frewein and G. Pabst, *Soft Matter*, 2020.
26. E. Sevcsik, G. Pabst, W. Richter, S. Danner, H. Amenitsch and K. Lohner, *Biophys. J.*, 2008, **94**, 4688-4699.
27. M. Doktorova, F. A. Heberle, D. Marquardt, R. Rusinova, R. L. Sanford, T. A. Peyear, J. Katsaras, G. W. Feigenson, H. Weinstein and O. S. Andersen, *Biophys. J.*, 2019, **116**, 860-873.
28. M. H. Nguyen, M. DiPasquale, B. W. Rickeard, M. Doktorova, F. A. Heberle, H. L. Scott, F. N. Barrera, G. Taylor, C. P. Collier, C. B. Stanley, J. Katsaras and D. Marquardt, *Langmuir*, 2019, **35**, 11735-11744.
29. J. E. Nielsen, V. A. Bjørnestad, V. Pipich, H. Jenssen and R. Lund, *J. Colloid Interface Sci.*, 2021, **582**, 793-802.
30. J. E. Nielsen, V. A. Bjørnestad and R. Lund, *Soft Matter*, 2018, **14**, 8750-8763.
31. V. Castelletto, R. H. Barnes, K.-A. Karatzas, C. J. Edwards-Gayle, F. Greco, I. W. Hamley, R. Rambo, J. Seitsonen and J. Ruokolainen, *Biomacromolecules*, 2018.
32. V. Castelletto, R. H. Barnes, K.-A. Karatzas, C. J. Edwards-Gayle, F. Greco, I. W. Hamley, J. Seitsonen and J. Ruokolainen, *Langmuir*, 2018.
33. S. Qian and W. T. Heller, *J. Phys. Chem. B*, 2011, **115**, 9831-9837.
34. M. Pachler, I. Kabelka, M.-S. Appavou, K. Lohner, R. Vácha and G. Pabst, *Biophys. J.*, 2019, **117**, 1858-1869.

35. I. Kabelka, M. Pachler, S. Prévost, I. Letofsky-Papst, K. Lohner, G. Pabst and R. Vácha, *Biophys. J.*, 2020, **118**, 612-623.
36. A. K. Buck, D. E. Elmore and L. E. Darling, *Future Med. Chem.*, 2019, **11**, 2447-2460.
37. E. F. Semeraro, J. M. Devos, L. Porcar, V. T. Forsyth and T. Narayanan, *IUCrJ*, 2017, **4**, 751-757.
38. J. D. Nickels, S. Chatterjee, C. B. Stanley, S. Qian, X. Cheng, D. A. Myles, R. F. Standaert, J. G. Elkins and J. Katsaras, *PLoS Biol.*, 2017, **15**, e2002214.
39. A. Åkesson, T. Lind, N. Ehrlich, D. Stamou, H. Wacklin and M. Cárdenas, *Soft Matter*, 2012, **8**, 5658-5665.
40. K. Lohner and E. J. Prenner, *Biochim. Biophys. Acta, Biomembr.*, 1999, **1462**, 141-156.
41. J. R. Silvius, *Lipid-protein interactions*, 1982, **2**, 239-281.
42. M. E. Selsted, M. J. Novotny, W. L. Morris, Y.-Q. Tang, W. Smith and J. S. Cullor, *J. Biol. Chem.*, 1992, **267**, 4292-4295.
43. T. Rozek, K. L. Wegener, J. H. Bowie, I. N. Olver, J. A. Carver, J. C. Wallace and M. J. Tyler, *Eur. J. Biochem.*, 2000, **267**, 5330-5341.
44. J. Johansson, G. H. Gudmundsson, M. n. E. Rottenberg, K. D. Berndt and B. Agerberth, *J. Biol. Chem.*, 1998, **273**, 3718-3724.
45. K. Fujita, S. Ichimasa, T. Zendo, S. Koga, F. Yoneyama, J. Nakayama and K. Sonomoto, *Appl. Environ. Microbiol.*, 2007, **73**, 2871-2877.
46. P. Stansly and G. Brownlee, *Nature*, 1949, **163**, 611-611.
47. J. Li, R. L. Nation, R. W. Milne, J. D. Turnidge and K. Coulthard, *Int. J. Antimicrob. Agents*, 2005, **25**, 11-25.
48. C. E. Blanchet, A. Spilotros, F. Schwemmer, M. A. Graewert, A. Kikhney, C. M. Jeffries, D. Franke, D. Mark, R. Zengerle and F. Cipriani, *J. Appl. Crystallogr.*, 2015, **48**, 431-443.
49. T.-H. Lee, C. Heng, M. J. Swann, J. D. Gehman, F. Separovic and M.-I. Aguilar, *Biochim. Biophys. Acta, Biomembr.*, 2010, **1798**, 1977-1986.
50. N. Kučerka, M.-P. Nieh and J. Katsaras, *Biochim. Biophys. Acta, Biomembr.*, 2011, **1808**, 2761-2771.
51. R. M. Epand and R. F. Epand, *Biophys. J.*, 1994, **66**, 1450.
52. J. C. Hsu and C. M. Yip, *Biophys. J.*, 2007, **92**, L100-L102.
53. W.-M. Yau, W. C. Wimley, K. Gawrisch and S. H. White, *Biochemistry*, 1998, **37**, 14713-14718.
54. E. Sevcsik, G. Pabst, A. Jilek and K. Lohner, *Biochim. Biophys. Acta, Biomembr.*, 2007, **1768**, 2586-2595.
55. N. Paracini, L. A. Clifton, M. W. Skoda and J. H. Lakey, *Proc. Natl. Acad. Sci. U.S.A.*, 2018, **115**, E7587-E7594.
56. D. E. Santos, L. r. Pol-Fachin, R. D. Lins and T. A. Soares, *J. Chem. Inf. Model.*, 2017, **57**, 2181-2193.
57. M. J. Trimble, P. Mlynárčik, M. Kolář and R. E. Hancock, *Cold Spring Harb Perspect Med*, 2016, **6**, a025288.
58. F. G. Dupuy, I. Pagano, K. Andenoro, M. F. Peralta, Y. Elhady, F. Heinrich and S. Tristram-Nagle, *Biophys. J.*, 2018, **114**, 919-928.
59. M. Nakano, *Chem. Pharm. Bull.*, 2019, **67**, 316-320.
60. M. Nakano, M. Fukuda, T. Kudo, H. Endo and T. Handa, *Phys. Rev. Lett.*, 2007, **98**, 238101.
61. M. Nakano, M. Fukuda, T. Kudo, N. Matsuzaki, T. Azuma, K. Sekine, H. Endo and T. Handa, *J. Phys. Chem. B*, 2009, **113**, 6745-6748.
62. R. Homan and H. J. Pownall, *Biochim. Biophys. Acta, Biomembr.*, 1988, **938**, 155-166.
63. M. Kaihara, H. Nakao, H. Yokoyama, H. Endo, Y. Ishihama, T. Handa and M. Nakano, *Chem. Phys.*, 2013, **419**, 78-83.
64. T. C. Anglin, K. L. Brown and J. C. Conboy, *J. Struct. Biol.*, 2009, **168**, 37-52.

Electronic Supplementary Information

Impact of Antimicrobial Peptides on *E. coli*-mimicking Lipid Model Membranes: correlating structural and dynamic effects using scattering methods

Josefine Eilsø Nielsen,[a] Sylvain François Prévost,[b] Håvard Jenssen[c] and Reidar Lund*[a]

[a] Department of Chemistry, University of Oslo, 0315 Oslo, Norway, [b] Institut Laue - Langevin, 38000 Grenoble, France, [c] Department of Science and Environment, Roskilde University, 4000 Roskilde, Denmark

Experimental section:

Differential Scanning Calorimetry (DSC)
Thermal analysis was performed using the TA Instruments "nano-DSC" instrument for solutions, which allows detection of heat flows on a µJ/s scale. The heating rate was 2°C/min and samples were scanned from 10 to 70°C. The Tris buffer was measured separately using the same settings and the buffer curve was subtracted from the thermograms using the NanoAnalyze software. The measured power was converted to specific heat capacity C_p in kJ/mol/K. The enthalpy values were obtained by integration of the area under the phase transition peak.

Scattering model used to analyse small angle X-ray scattering (SAXS) data:
From fit analysis of SAXS data we can extract detailed information on the structure of the membrane in large unilamellar vesicles (LUVs).[1-4] The significant difference in electron density (ED) between the head- and tail-groups of the lipid and water provides a significant sensitivity to changes in the contrast in X-ray scattering. It has previously been shown[5,6] that the coherent scattering from LUVs, where the size of the vesicles and the thickness of the bilayer are well separated, can be described by the separated form factor (SFF) approximation:

$$I_{lip}(Q) = n \cdot S(Q)|F_{TS}(Q)|^2|F_{FB}(Q)|^2 \qquad (1)$$

where n is the number of scatterers, defined as

$$n = \frac{\phi}{V_{lipid} \cdot P_{agg}} \qquad (2)$$

with ϕ being the volume fraction and V_{lipid} the total volume of a phospholipid given by $V_{lipid} = M_{lipid}/(N_A \cdot d_{lipid})$. N_A is Avogadro's number, M_{lipid} is the molecular weight and d_{lipid} is the density. P_{agg} is the number of phospholipids in each lipid vesicle, i.e. the aggregation number of the vesicle given by

$$P_{agg} = \frac{4\pi(R_{shell})^3 - 4\pi(R_{shell} - t_{shell})^3}{3V_{tail}} \qquad (3)$$

where R_{shell} is the outer radius of the vesicles, t_{shell} is the thickness of the bilayer and V_{tail} is the volume occupied by each double tail of the phospholipid.

$S(Q)$ is the structure factor accounting for interaction between particles (in our case $S(Q) = 1$ because all liposome samples are sufficiently diluted), $F_{TS}(Q)$ is the form factor of an infinitely thin spherical shell (containing information on the radius of the lipid vesicles and the polydispersity), and $F_{FB}(Q)$ is the form factor of a flat bilayer sheet (containing information on the bilayer thickness and the distribution of the phospholipids segments across the bilayer).

The flat bilayer form factor can be expressed[7] as

$$|F_{FB}(Q)| = \int_{-D_i}^{D_0} \Delta\rho(z)e^{iQz}dz = \sqrt{(F_{cos}^2 + F_{sin}^2)} \tag{4}$$

where $\Delta\rho$ is the difference in the scattering length densities (SLDs) of the membrane and the solvent, and F_{cos}^2 and F_{sin}^2 are the real and the imaginary parts of $F_{FB}(Q)$.[4] The integral extends over the full bilayer thickness from the inner distance D_i to the outer distance D_o.

Following Kučerka and co-workers[4], we parse the phospholipids into the following segments: hydrocarbon tail group (HC), carbonyl+ glycerol (CG) (common for all three phospholipid) and outer part of head group (PC/G).

The volume probability distributions of the components are described by Gaussian functions[3]

$$P_n(z) = \frac{c_n}{\sqrt{2\pi}}\left(exp\left[-\frac{(z+z_n)^2}{2\sigma_n^2}\right] + exp\left[-\frac{(z-z_n)^2}{2\sigma_n^2}\right]\right) \tag{5}$$

where σ_n and z_n are the width and position of the distribution, respectively, and $c_n = V_n/(A_L\sigma_n)$. V_n is the volume of the group n and A_L is the area per lipid, which is equal to the integrated area under the curve.

The hydrocarbon groups (HC) are modelled using a half period squared sine/cosine function to account for the asymmetry in the bilayer, e.g. potential differences in the segmental distribution of the inner and the outer HC group [1]

$$P_{HC}(z) = \begin{cases} sin\left(\frac{z - z_{MN_i} + \sigma_{MN_i}}{2\sigma_{MN_i}}\frac{\pi}{2}\right)^2 \\ for\ z_{MN_i} - \sigma_{MN_i} \leq z < z_{MN_i} + \sigma_{MN_i} \\ 1\ for\ z_{MN_i} + \sigma_{MN_i} \leq z < z_{MN_o} - \sigma_{MN_o} \\ cos\left(\frac{z - z_{MN_o} + \sigma_{MN_o}}{2\sigma_{MN_o}}\frac{\pi}{2}\right)^2 \\ for\ z_{MN_o} - \sigma_{MN_o} \leq z < z_{MN_o} + \sigma_{MN_o} \end{cases} \tag{6}$$

where $z_{MN_{i,o}}$ is the 0.5-probability value for the HC group and $2\sigma_{MN_{i,o}}$ is the width of the squared sine/cosine functions. The volume probability distribution of the methylene groups (CH₂) can be expressed separately as

$$P_{CH_2}(z) = P_{HC}(z) - P_{CH_3}(z) \tag{7}$$

These expressions for the distributions of the lipid tails comply with spatial conservation consideration[1, 3] as the height of the expression for $P_{HC}(z)$ is equal to one in the central hydrocarbon region as there is no water present in this region of the membrane.

The volume probability distribution of the water is chosen to be the last group and the spatial conservation requirement is applied to give

$$P_w(z) = 1 - \sum_n P_n(z) \tag{8}$$

where $n = CH_3^{i,o}, CH_2^{i,o}, CG^{i,o}, HG^{i,o}$.

The total volumes of the head group and hydrocarbon chain, as well as the area per lipid, were constrained according to values from reported molecular dynamics simulation of DMPC[8], DMPG[9] and DMPE[10] phospholipids.

Because a small amount of PEGylated DMPE lipids was used to stabilize the lipid vesicles against aggregation, the scattering from the PEG chains was included in the fit model for SAXS/SANS data. The PEG chains on the inner and outer leaflet of the lipid bilayer have a Gaussian random coil confirmation and can therefore be described by the analytical model, previously described by Arleth et al.[11] See Nielsen et al. for details on how the PEG contribution, $I_{PEG}(Q)$ is included to the SDP model.[12]

To be able to use the analytical scattering models to quantitatively describe the interaction between antimicrobial peptides and lipid vesicles, the peptide was introduced as an additional pseudo-parsing group across the bilayer and modelled as an additional Gaussian function in the volume probability (Eq. 5) as formerly published by Nielsen et al.[12, 13] The integral under the curve was scaled by the total volume fraction of added peptides and the fraction of peptide bound to the liposomes, f_{bp}, in the following way

$$c_{pep} = \frac{V_p \cdot f_p \cdot f_{bp}}{A_L \cdot \sigma_{peptide}} \tag{9}$$

Further, to account for the changes in contrast as a result of the peptide potentially integrating into either the head-region, tail-region of the phospholipids or somewhere in the interface between the two areas of the bilayer, the difference in contrast is weighed by a fraction, f_{p_tail}, which gives the fraction of peptide in the tail region

$$\Delta \rho_p(z) = f_{p\_tail} \cdot \left(\rho_p - \rho_{CH_2}\right) + (1 - f_{p_{tail}}) \cdot \left(\rho_p - \rho_w\right) \tag{10}$$

where $\rho(p)$, $\rho(CH_2)$ and $\rho(w)$ are the SLDs of the peptide, methylene groups, and water, respectively.

The f_{p_tail} is expressed as the integral of the overlap of the peptide Gaussian function with the half period squared sine/cosine function expressing the volume probability of the HC groups in the following way

$$f_{p\_tail} = \frac{\int_{z_{inter}}^{z_{CH_2}+\sigma_{CH_2}} P_{HC} dz + \int_{Z_p - 5\sigma_{pepetide}}^{z_{inter}} P_p dz}{\int P_p \, dz} \tag{11}$$

where z_{inter} is the intersect between the two overlapping curves found numerically by the Brent-Dekker method[14] and P_{HC} is the function described in Eq. 6. P_p is the Gaussian function expressing the volume distribution of the peptide (details in reference[12])

The form factor for the flat bilayer including the peptides is

$$\left|F_{FB_{pep}}(Q)\right| = \int_{-D_i}^{D_0} \Delta\rho(z)e^{iQz}dz \qquad (12)$$

$$= \sqrt{\left(\left(F_{cos,lipid} + F_{cos,peptid}\right)^2 + \left(F_{sin,lipid} + F_{sin,peptid}\right)^2\right)}$$

where

$$F_{cos,peptide} = \left|c_{pep}\sigma_{peptide}\Delta\rho_p \cos\left(Qz_{peptide}\right) \cdot exp\left[\frac{\left(Q\sigma_{ppeptide}\right)^2}{2}\right]\right| \qquad (13)$$

and

$$F_{sin,peptide} = \left|c_{pep}\sigma_{peptide}\Delta\rho_p \sin\left(Qz_{ppeptide}\right) \cdot exp\left[\frac{\left(Q\sigma_{peptide}\right)^2}{2}\right]\right| \qquad (14)$$

To account for potential free peptide chains not bound to the lipid vesicles, an additional term was added to the model

$$I_{fp}(Q) = \varphi \cdot (1 - f_{bp}) \cdot \Delta\rho_p^2 \cdot V_p \cdot F_{chain}(Q) \qquad (15)$$

Where φ is the total volume fraction and $F(q)_{chain}$ is the form factor of a Gaussian chain expressed by the Debye formula.[15]

To account for formation of mixed peptide-lipid micelles due to solubilisation of the vesicles upon peptide addition the model was modified to include a fraction of micelle scattering.[13]

$$I_{micelle}(Q) = \frac{n_{micelle}}{P_{agg\_micelle}} F_{micelle}(Q) \qquad (16)$$

where n_{micelle} is defined as

$$n_{micelle} = (Mconc_{lipid} \cdot f_{micelle} + Mconc_{peptide} \cdot f_{P_{micelle}})/V_{micelle} \qquad (17)$$

Where $Mconc_{lipid}$ and $Mconc_{peptide}$ is the total molar concentration of lipids and peptides respectively, and f_{micelle} and $f_{P_{micelle}}$ is the fraction of the lipids and peptides incorporated in the micelles respectively, and $V_{micelle} = \frac{4}{3}\pi(r_{micelle} + D)^3$ where $r_{micelle}$ is the core radius and D is the thickness of the shell..

$P_{agg_{micelle}} = V_{core}/(f_{PL}f_{core}V_p + V_{tail} \cdot (1 - f_{PL})$ is the aggregation number per micelle scaled by f_{PL} which is the ratio of peptide to lipid in the micelles, and f_{core} is the fraction of peptide chain incorporated in the core, where $V_{core} = \frac{4}{3}\pi(r_{micelle})^3$ and $F_{micelle}(Q)$ is the form factor for spherical core-shell micelle with defined as:

$$P_{micelle}(Q) = \int_0^{\pi/2} \left[\Delta\rho_{shell}V_{micelle}A_{sphere}(Qr_{micelle}) \right.$$
$$\left. + (\Delta\rho_{core} - \Delta\rho_{shell})V_{core}A_{sphere}(Qr_{core})\right]^2 \sin\alpha\, d\alpha \qquad (18)$$

where $\Delta\rho_{shell}$ is the difference in the SLDs of the shell and the solvent, and $\Delta\rho_{core}$ is the difference in the SLDs of the core and the solvent, $A_{sphere}(x) = 3[\sin(x) - x\cos(x)]/x^3$. $\Delta\rho_{shell}$ and $\Delta\rho_{core}$ were determined from a weighted average of the peptide and lipids using a fitting parameter describing the fraction of the peptide in the core, f_{core}, as such:

$$\Delta\rho_{shell} = \frac{Z_{lipidhead} + Z_{peptide}\cdot(1 - f_{core})}{f_{PL}\cdot(1 - f_{core})\cdot V_p + V_{head}\cdot(1 - f_{PL})} \qquad (19)$$

$$\Delta\rho_{core} = \frac{Z_{lipidtail} + Z_{peptide}\cdot f_{core}}{f_{PL}\cdot f_{core}\cdot V_p + V_{tail}\cdot(1 - f_{PL})} \qquad (20)$$

where Z_i is the number of electrons in the group i.

The full expression for the intensity, including peptide in the bilayer, the PEGylation, the free peptide chains and mixed micelles is then

$$I = n\left(F_{TS}(Q)^2 F_{FB_{pep}}(Q)^2 + I_{PEG}(Q)\right) + I_{fp}(Q) + I_{micelle}(Q) \qquad (21)$$

In the fit analysis, we allowed the concentration to vary slightly due to uncertainties in the determination of the exact value during the sample preparation.

Results:

Table S1. Fit results from SAXS data on DMPE (75%), DMPG (22.5%), DMPE-PEG (2.5%) liposomes with and without addition of indicated peptide at different ratios. All data measured at 37°C.

|	Fraction of peptide	Bilayer thickness [Å]	Volume headgroup	Volume CH_2	$Z_{peptide}$ [Å]	$\sigma_{peptide}$ [Å]	$f_{micelles}$	Ratio P/L in micelles	f_{bp}	σ_{SD}
Liposomes	-	45	256	24.6	-	-	-	-	1	0.36
Aurein 1.2	1:20	44	255	25.0	0	10	0.48	0.05	1	0.38
	1:50	44	257	24.7	-1	10	0.05	0.01	1	0.36
	1:100	46	258	24.6	0	10	-	-	1	0.36
Indolicidin	1:20	45	281	24.5	14	5	0.04	0.05	1	0.36
	1:50	45	273	24.6	24	6	0.02	0.02	1	0.36
	1:100	45	266	24.6	23	6	-	-	1	0.36
LL-37	1:20	47	272	25.3	5	11	0.09	0.05	1	0.43
	1:50	46	262	25.0	18	13	0.04	0.02	1	0.38
	1:100	46	260	24.8	25	10	0.01	0.01	1	0.38
Lacticin Q	1:20	-	-	-	-	-	-	-	1	-
	1:50	45	280	25.2	9	7	-	-	1	0.36
	1:100	45	272	25.0	11	7	-	-	1	0.36
Colistin	1:10	45	256	24.6	-	-	-	-	0	0.36
	1:20	45	256	24.6	-	-	-	-	0	0.36
	1:50	45	256	24.6	-	-	-	-	0	0.36
	1:100	45	256	24.6	-	-	-	-	0	0.36
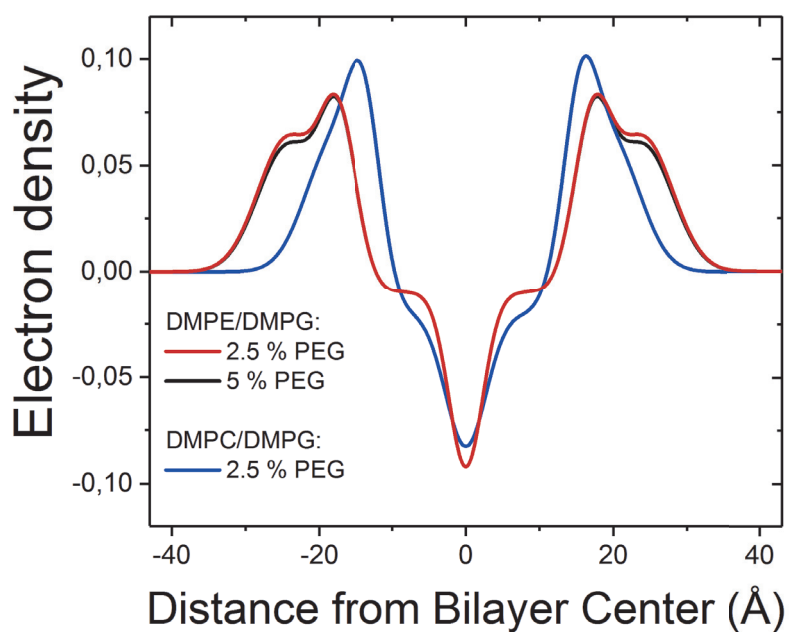
Figure S1. Electron density profiles calculated from the fit parameters of SAXS data on DMPE/DMPG lipid vesicles with 2.5 and 5% PEG and DMPC/DMPG vesicles with 2.5% PEG.
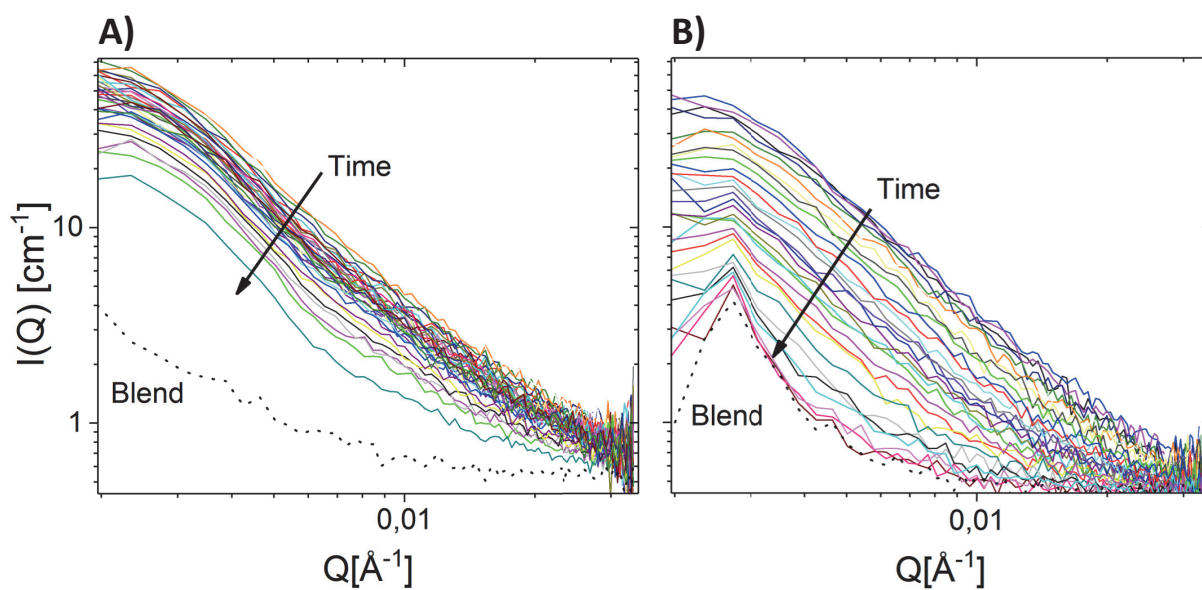

Figure S2. TR-SANS data on pure DMPE/DMPG liposomes (A) and DMPE/DMPG liposomes with Indolicidin (B) showing the decrease in scattering intensity over time due to lipid exchange and flip-flop.
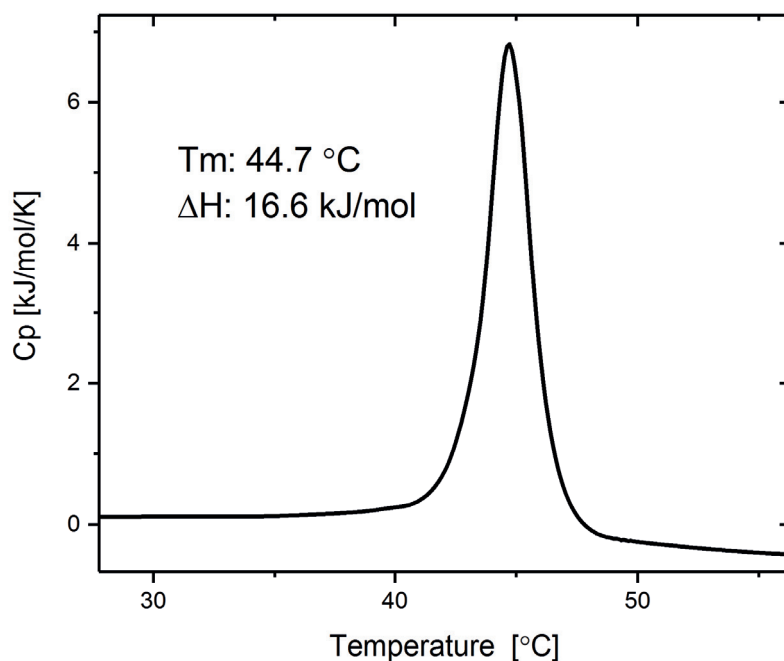
Figure S3. Nano-DSC data on DMPE (75%), DMPG (22.5%), DMPE-PEG (2.5%) liposomes showing the phase transition of the lipid bilayer.

References:

1.   B. Eicher, F. A. Heberle, D. Marquardt, G. N. Rechberger, J. Katsaras and G. Pabst, *J. Appl. Crystallogr.*, 2017, **50**.

2.   J. B. Klauda, N. Kučerka, B. R. Brooks, R. W. Pastor and J. F. Nagle, *Biophys. J.*, 2006, **90**, 2796-2807.

3.   N. Kučerka, J. F. Nagle, J. N. Sachs, S. E. Feller, J. Pencer, A. Jackson and J. Katsaras, *Biophys. J.*, 2008, **95**, 2356-2367.

4.   N. Kucerka, J. Pencer, J. N. Sachs, J. F. Nagle and J. Katsaras, *Langmuir*, 2007, **23**, 1292-1299.

5.   J. Pencer, S. Krueger, C. P. Adams and J. Katsaras, *J. Appl. Crystallogr.*, 2006, **39**, 293-303.

6.   M. Kiselev, P. Lesieur, A. Kisselev, D. Lombardo and V. Aksenov, *Appl. Phys. A*, 2002, **74**, s1654-s1656.

7.   M. R. Brzustowicz and A. T. Brunger, *J. Appl. Crystallogr.*, 2005, **38**, 126-131.

8.   N. Kučerka, M.-P. Nieh and J. Katsaras, *Biochim. Biophys. Acta, Biomembr.*, 2011, **1808**, 2761-2771.

9.   J. Pan, F. A. Heberle, S. Tristram-Nagle, M. Szymanski, M. Koepfinger, J. Katsaras and N. Kučerka, *Biochim. Biophys. Acta, Biomembr.*, 2012, **1818**, 2135-2148.

10. N. Kučerka, B. van Oosten, J. Pan, F. A. Heberle, T. A. Harroun and J. Katsaras, *J. Phys. Chem. B*, 2014, **119**, 1947-1956.

11. L. Arleth and C. Vermehren, *J. Appl. Crystallogr.*, 2010, **43**, 1084-1091.

12. J. E. Nielsen, V. A. Bjørnestad and R. Lund, *Soft Matter*, 2018, **14**, 8750-8763.

13. J. E. Nielsen, V. A. Bjørnestad, V. Pipich, H. Jenssen and R. Lund, *J. Colloid Interface Sci.*, 2021, **582**, 793-802.

14.   R. P. Brent, *Comput. J.*, 1971, **14**, 422-425.
15.   P. Debye, *J. Chem. Phys.*, 1946, **14**, 636-639.

Kinetics of Lipid Exchange and Flip-flop in Lipid Bilayers with added Peptides: Extracting the Leaflet Compositions using Time-resolved Small-angle Neutron Scattering

Josefine Eilsø Nielsen and Reidar Lund

Manuscript

V

Kinetics of Lipid Exchange and Flip-flop in Lipid Bilayers with added Peptides:

Extracting the Leaflet Compositions using Time-resolved Small-angle Neutron Scattering

Authors: Josefine Eilsø Nielsen and Reidar Lund[1] [*]

Affiliations: [1]Department of Chemistry, University of Oslo, Postboks 1033 Blindern, 0315 Oslo, Norway.
*Correspondence to: reidar.lund@kjemi.uio.no

Keywords: Lipid exchange, lipid flip-flop, antimicrobial peptides, time-resolved small-angle neutron Scattering, dynamic light scattering

ABSTRACT: It is well-known that lipids constituting the cytoplasmic membrane undergo continuous reorganization to maintain the exact composition important for the integrity of the cell. The transport of lipids is controlled by mainly membrane proteins, but also spontaneous lipid transport between leaflets, lipid "flip-flop", occurs. It has previously been shown that spontaneous intravesicular lipid "flip-flop" and intervesicular lipid exchange can be deduced indirectly from contrast variation time resolved small angle neutron scattering (TR-SANS) data, by monitoring the loss of SANS intensity over time. In this work we present a new more direct approach to extracting the rates for lipid intravesicular flip-flop and intervesicular lipid exchange from TR-SANS data by modelling the full Q-range data, and in this way making use of both the structural and temporal resolution of SANS. Using this approach, we have analysed data on liposomes with and without a substrate known to accelerate the lipid transport processes, the antimicrobial peptide indolicidin. The rate constants extracted from the methods are comparable, and the activation energies calculated from the rates are consistent. However, we found that addition of indolicidin did not only lead to an acceleration of lipid transport but also an increase in the size of the liposomes, which would not have been detected by the traditional approach of only monitoring the net SANS intensity. We conclude that both methods provide comparable results with regards to thermodynamical relevant parameters, but modelling of full Q-range TR-SANS data is a very useful upon investigating the effect of for example an added peptide or protein because it also yields additional information on changes in size and morphology of the vesicles.

INTRODUCTION

The cell membrane relies on controlled transport through the membrane in order to maintain its integrity, because an exact composition in terms of lipid and ions (protons, sodium, calcium etc.) is required for healthy cell function. The balance is mainly kept by transmembrane proteins, which accurately regulate the composition of lipids and the balance of ions.(1) The cytoplasmic membrane of eukaryotic and prokaryotic cells requires maintaining an asymmetric lipid composition on both the inner and outer leaflet to function. In contrast to *in plane* diffusion, it has long been known that lipid "flip-flop" is relatively slow (min-hours-days-months) in absence of transmembrane proteins ("flippases" and "floppases"),(2) which have been found to significantly accelerate the process (seconds).(1, 3, 4) Flippases and floppases are adenosine triphosphate (ATP) dependent membrane proteins which move lipids to the inner monolayer and outer monolayer respectively,(5) and in that manner carefully maintain the lipid composition and rejuvenate the outer leaflet as lipids are synthesized within the cytoplasm. In the absence of flippases, the lipid composition is thus rather constant and if spontaneous "flip-flop" occurs in an uncontrolled manner, the lipid composition may be altered leading to destabilization of the membrane. Lipid scrambling and malfunction of flippases and floppases have recently been linked to human diseases including cancer, highlighting the importance of lipid dynamics.(1) Destabilisation of the bacterial membrane through accelerated lipid flip-flop has further been suggested as an essential step in the mode of action of antimicrobial peptides (AMPs). (6-13)

In order to probe lipid dynamics, it is essential to avoid perturbations from equilibrium, and it is desirable to monitor the nanostructure and potential changes simultaneously. In this respect, time-resolved small-angle X-ray/neutron scattering (TR-SAXS/SANS) techniques have recently emerged as increasingly powerful tools to study nanostructures in the 1-100 nm range, with temporal resolution starting from a few milliseconds. In particular, over the last decade a novel hydrogen/deuterium (H/D) contrast variation technique based on TR-SANS as a "label-free" method has emerged to study molecular exchange processes.(14-16) Contrary to other methods such as EPR, fluorescence and temperature-jump experiments, the kinetic zero-average contrast (KZAC) TR-SANS method does not require chemical labelling or perturbation that disturbs equilibrium other than simple H/D exchange which do not considerably affect the physico-chemical properties of the system. The idea was originally developed to investigate the dynamics of block copolymer micelles,(14, 15) which was shown to be dominated by activated diffusion of single chains, a process that strongly depends on surface tension between the solvent and the hydrophobic part, chain-length and temperature.(14, 15, 17, 18) The TR-SANS method has later been adapted to study lipid exchange in unilamellar vesicles (ULVs), i.e. liposomes.(19-21) As first shown by Nakano and co-workers, both lipid "flip-flop" and inter-membrane exchange can be deduced by monitoring the loss of SANS intensity over time.(19) However, in order to derive the rate constants for lipid flip-flop and inter-bilayer exchange, a kinetic analysis was developed to resolve

2

the net change of the integral intensity over time and not by analysing the (time-dependent) scattering curves. Thus, this experiment and similar later approaches,(13, 21, 22) did not take full advantage of the intrinsic spatial resolution of the SANS technique and the determination of the flip-flop rate can only be deduced indirectly by analysing the decay of the overall scattered intensity. Moreover, by analysing only the net intensity, potential parallel kinetic processes, such as vesicle growth or morphological transitions cannot easily be deciphered. Perez-Salas and co-workers have later introduced an alternative approach where they extract the exchange and flip-flop rates from fit analysing the full Q range scattering curves using a model with a time-independent prefactor containing the form factor of the lipid particles multiplied with a time-dependent function containing the exchange and flip rates which are dependent on changes in the contrast of the inner and outer leaflet of the vesicles.(23, 24)

The kinetics of lipid flip-flop can be determined more directly by using asymmetric bilayer where one leaflet is labelled. Conboy and co-workers used Sum-Frequency Vibrational Spectroscopy that requires deposition of a deuterated leaflet on a solid substrate (supported bilayer). Upon flip-flop, the composition of the inner and outer leaflet is mixed, which can be followed by monitoring the amount of $-CH_3$ (as opposed to $-CD_3$) groups on the surface. The same idea has also been used in neutron reflectometry by Gerelli and co-workers who deposited a H/D labelled bilayer on silica. However, here it was found that inter-bilayer exchange was rate limiting and lipid flip-flop was too fast within experimental time window. Flip-flop can also be detected by TR-SANS using asymmetric vesicles where one leaflet contains a deuterated lipid. Similar to the KZAC TR-SANS technique, flip-flop can be detected upon loss in the overall intensity. Using this approach, the authors investigate the effect of peptide insertion finding that the rate for flip-flop is accelerated although molecular exchange between vesicles could not be observed using this technique. Several other studies have indicated that antimicrobial peptides (AMPs) induce changes in lipid dynamics, more specifically by accelerating flip-flop motion (25-27). At least in model systems, peptides can accelerate lipid flip-flop motions in a manner proportional to the amount of peptide inserted into the membrane.(28, 29) In one study AMPs were found to induce "flip-flop" at concentrations much lower than those needed to cause leakage of calcein.(8) Hence, although there is significant evidence that AMPs may accelerate flip-flop, the molecular mechanism and its implications are not clear. Moreover, other mechanisms for peptide-induced lipid transport and redistribution needs to be considered. In this context, inter-bilayer exchange may play an important role as this leads to redistribution of the lipid composition, first at the outer leaflet leading to a scrambling of the composition in the presence of other lipid sources.

In this work, we investigate the lipid exchange and "flip-flop" motion using the KZAC TR-SANS method using the full Q-range to make use of both the structural and temporal resolution of SANS. The approach we present is similar to what has been previously presented by Perez-Salas and co-worker, however, because we

add an antimicrobial peptide to our vesicle system we take into account a time-dependent change in the form factor of the vesicles caused by the peptide interaction, as well as the changes in contrast resulting from lipid dynamics. Our results reveal that upon addition of AMP, the lipid dynamics, both the inter-bilayer and intra-bilayer flip-flop motions, is considerably accelerated. For the flip-flop, the effect can primarily be attributed to a reduction of the activation energy of about 15%. This likely results from mediation of head-group - tail interaction by the peptides. The analysis also show that the acceleration of the lipid dynamics is accompanied by a growth and consequently, broader distribution of the vesicles likely caused by Ostwald-like ripening process. We also speculate that the change in dynamics in may cause effects such as lipid scrambling and enhanced transport of solutes over the membrane that are detrimental to living bacteria. This thus may constitute an important mode of action for AMP activity.

MATERIALS AND METHOD:

Materials:

Synthetic DMPC (1,2-dimyristoyl-sn-glycero-3-phosphocholine), d-DMPC (1,2-dimyristoyl-d54-sn-glycero-3-phosphocholine), DMPG (1,2-dimyristoyl-sn-glycero-3-phospho-(1'-rac-glycerol)), d-DMPG (1,2-dimyristoyl-d54-sn-glycero-3-phospho-(1'-rac-glycerol)) and DMPE-PEG (1,2-dimyristoyl-sn-glycero-3-phosphoethanolamine-N-[methoxy(polyethylene glycol)-2000]) was purchased from Avanti Polar Lipids. The peptide indolicidin was purchased from Isca Biochemicals Limited. The tris buffer was prepared by mixing 50mM Tris-base with Tris-HCl (Sigma Aldrich) in the correct ratio to achieve a pH of 7.4 in 50% D_2O (Sigma-Aldrich) and 50% H_2O (MiliQ).

Sample preparation:

The lipids in a ratio of 75 mol % DMPC, 22.5 mol% DMPC and 2.5 % DMPE-PEG were dissolved in a 1:3 Methanol: Chloroform solution. The organic solvents were removed completely under vacuum using a Heidolph rotary evaporator with a Vacuubrand vacuum pump. The resulting lipid film was hydrated with Tris buffer for at least one hour at a temperature of 34°C. After sonication for 15 minutes, the lipid dispersions were extruded through a 100 nm pore diameter polycarbonate filter (>21 times) using an Avanti mini-extruder fitted with two 1 mL airtight syringes. Indolicidin, was dissolved in Tris buffer to the desired concentration.

4

TR-SANS data collection:

SANS data were collected at the KWS1 SANS beamline, at the Heinz Maier-Leibnitz (FRM II) center, MLZ in Garching, Germany. D-liposomes where mixed with H-liposomes (1:1) directly before the first measurement using a Finntip micropipette and mixed with either pure buffer (to make sure concentration of the non-peptide samples compare to the peptide samples) or peptide solution 1:1. The samples where filled in round Hellma quarts banjo-cells with a path length of 1 mm, and kept in a temperature controlled rack during the experiment.

Extraction of relaxation function:

The TR-SANS data can be evaluated by determining the relaxation function $R(t)$ according to

$$R(t) = \sqrt{\frac{I(t) - I_\infty}{I(0) - I_\infty}} \qquad (1)$$

where $I(t) = \int I(Q,t)dQ$ is the integral intensity at a given time, I_∞ is the intensity of the premixed blend representing the final state and $I(0)$ is the averaged intensity of the H-vesicles and D-vesicles measured separately representing the initial state before exchange and flip-flop has taken place.
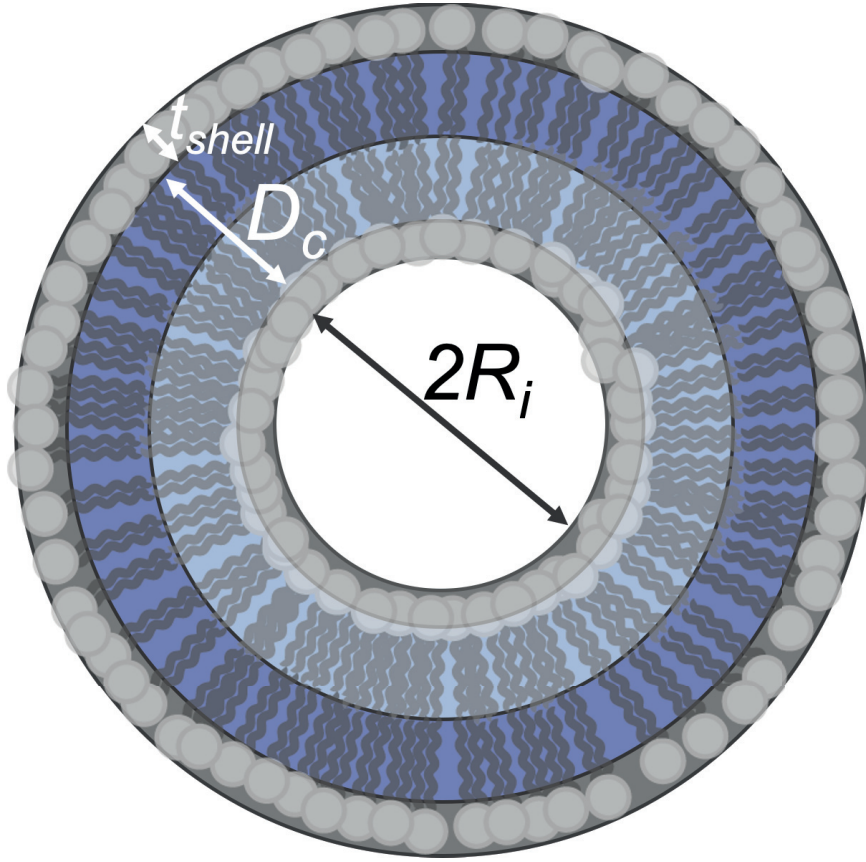
Data modelling of TR-SANS data

Figure 1: Schematic illustration of the concentric shell model.

For analysis of the TR-SANS data a model of concentric shells of finite thicknesses was chosen (see Figure 1). In this model the bilayer was divided into four concentric shells; one inner solvated shell consisting of headgroups and water with amplitude $A(q)_{h,i}$, two middle shell of the tail groups with amplitude $A(q)_{t,i}$ and $A(q)_{t,o}$ and one outer shell of headgroups and water with amplitude $A(q)_{h,o}$. In our experimental design, we have used a $\approx 50\%$ mixture of lipids with deuterated and proteated tails respectively, however the head groups are the same in all cases. We therefore have to consider that the contrast for the tail region of inner and outer leaflet, $\Delta\rho(t)_{t,i}$ and $\Delta\rho(t)_{t,o}$ depends on time. The total form factor of the can thereby be expressed as the following

6

$$A_{H/D}(Q) = \Delta\rho_{h,i}A_{h,i}(Q)V_{h,i} + \Delta\rho_{t,i}(t)A_{t,i}(Q)V_{t,i} + \Delta\rho_{t,o}(t)A_{t,o}(Q)V_{t,o}$$
$$+ \Delta\rho_{h,o}A_{h,o}(Q)V_{h,o}$$

$$(2)$$

where $V_{h,i}, V_{t,i}, V_{t,o}, V_{h,o}$ are the volumes of the inner head- and tail group, and outer tail- and head group shells respectively. The volume of each shell is defined as:

$$V_{h,i} = 4\pi \frac{(R_i + t_{shell})^3 - (R_i)^3}{3} \tag{3}$$

$$V_{t,i} = 4\pi \frac{(R_i + t_{shell} + D_c/2)^3 - (R_i + t_{shell})^3}{3} \tag{4}$$

$$V_{t,o} = 4\pi \frac{(R_i + t_{shell} + D_c)^3 - (R_i + t_{shell} + D_c/2)^3}{3} \tag{5}$$

$$V_{h,o} = 4\pi \frac{(R_i + t_{shell} + D_c + t_{shell})^3 - (R_i + t_{shell} + D_c)^3}{3} \tag{6}$$

$$A_{h,i}(Q) = \frac{(R_i + t_{shell})^3 A(Q, R_i + t_{shell}) - (R_i)^3 A(Q, R_i)}{(R_i + t_{shell})^3 - R_i^3} \tag{7}$$

$$A_{t,i} = \frac{(R_i + t_{shell} + D_c/2)^3 A(q, R_i + t_{shell} + D_c/2) - (R_i + t_{shell})^3 A(q, R_i + t_{shell})}{(R_i + t_{shell} + D_c/2)^3 - (R_i + t_{shell})^3} \tag{8}$$

$$A_{t,o} = 4\pi \frac{(R_i + t_{shell} + D_c)^3 - (R_i + t_{shell} + D_c/2)^3}{3} \tag{9}$$

$$A_{t,o} = \frac{(R_i + t_{shell} + D_c)^3 A(q, R_i + t_{shell} + D_c) - (R_i + t_{shell})^3 A(q, R_i + t_{shell} + D_c/2)}{(R_i + t_{shell} + D_c)^3 - (R_i + t_{shell} + D_c/2)^3} \tag{10}$$

$$A_{h,o}(Q)$$
$$= \frac{(R_i + 2t_{shell} + D_c)^3 A(Q, R_i + 2t_{shell} + D_c) - (R_i + t_{shell} + D_c)^3 A(Q, R_i + t_{shell} + D_c)}{(R_i + 2t_{shell} + D_c)^3 - (R_i + t_{shell} + D_c)^3} \tag{11}$$

where R_i is the inner radius of the vesicle, D_c is the total thickness of the hydrocarbon region, t_{shell} is the thickness of each head group shell. The scattering contrast towards the lipid tails at the inner and outer leaflets depend on time and can be written as:

$$\Delta\rho_{t,i}^{D}(t) = (1 - f_{in}(t)) \cdot \rho_{tail,D} + f_{in}(t) \cdot \rho_{tail,H} - \rho_0 \qquad (12)$$

$$\Delta\rho_{t,o}^{D}(t) = (1 - f_{out}(t)) \cdot \rho_{tail,D} + f_{out}(t) \cdot \rho_{tail,H} - \rho_0 \qquad (13)$$

$$\Delta\rho_{t,i}^{H}(t) = f_{in}(t) \cdot \rho_{tail,D} + (1 - f_{in}(t)) \cdot \rho_{tail,H} - \rho_0 \qquad (14)$$

$$\Delta\rho_{t,o}^{H}(t) = f_{out}(t) \cdot \rho_{tail,D} + (1 - f_{out}(t)) \cdot \rho_{tail,H} - \rho_0 \qquad (15)$$

Here $f_{in}(t)$ and $f_{out}(t)$ is excess fraction of either H- and D-lipid in the inner and outer leaflet respectively.

To consider the hydration of the inner and outer shell, $\Delta\rho_{h,i}$ and $\Delta\rho_{h,o}$ is calculated as follows

$$\Delta\rho_{h,i} = (1 - f_{wi}) \cdot \rho_{headgroup} + f_{wi} \cdot \rho_0 - \rho_0 \qquad (16)$$

$$\Delta\rho_{h,o} = (1 - f_{w,o}) \cdot \rho_{headgroup} + f_{w,o} \cdot \rho_0 - \rho_0 \qquad (17)$$

where i=inner or o=outer headgroup, $\rho_{headgroup}$ is the scattering length density of the lipid headgroup, ρ_0 is the scattering length density of the water. The fraction of water in the inner and outer shell(30), f_w, is given by

$$f_{w,i} = 1 - \frac{V_{head}P_i}{((R_i + t_{shell})^3 - R_i^3)} \qquad (18)$$

$$f_{w,o} = 1 - \frac{V_{head}P_o}{(R_i + 2t_{shell} + D_c)^3 - (R_i + t_{shell} + D_c)^3} \qquad (19)$$

where P_i and P_o are the number of phospholipids of the inner and the outer leaflet of the vesicle respectively.

$$P_i = 4\pi \frac{(R_i + t_{shell} + D_c/2)^3 - (R_i + t_{shell})^3}{3V_{tail}} \qquad (20)$$

$$P_o = 4\pi \frac{(R_i + t_{shell} + D_c)^3 - (R_i + t_{shell} + D_c/2)^3}{3V_{tail}} \qquad (21)$$

where V_{tail} is the volume occupied by the hydrophobic tails of the phospholipid.

8

The scattering from the PEG chains was included in the fit model for SANS data. (31, 32) The PEG chains on the inner and outer leaflet of the lipid bilayer have a Gaussian random coil confirmation and can therefore be described by the following analytical model(31, 32)

$$
\begin{aligned}
I_{PEG-liposomes}(Q) \\
= n \\
\cdot \left(f_{mix} \cdot I_{lipH}(Q) + (1 - f_{mix}) \cdot I_{lipD}(Q) + I_{chain}(Q) + I_{c_i c_i}(Q) \right. \\
\left. + I_{c_i c_o}(Q) + I_{c_o c_o}(Q) \right)
\end{aligned}
\tag{22}
$$

Where n is defined as

$$
n = \frac{\phi}{V_{lipid} \cdot (\langle P_o \rangle + \langle P_i \rangle)}
\tag{23}
$$

where ϕ is the volume fraction and V_{lipid} is the total volume of the phospholipid taken as the average between weighted DMPC and DMPG. The average aggregation number and intensities were calculated assuming a Gaussian distribution, $g(R_{in})$, of the inner radius of the vesicles.

$$
I(Q) = \int_0^\infty g(R_{in}) \, I(Q, R_{in}) dR_{in}
\tag{24}
$$

and $I_{lipH/D}(Q)$ is the scattering intensity for the H and D-liposomes calculated as

$$
I_{lipH}(Q) = A_H(Q)^2 + I_{sc_i}(Q) + I_{sc_o}(Q)
\tag{25}
$$

$$
I_{lipD}(Q) = A_D(Q)^2 + I_{sc_i}(Q) + I_{sc_o}(Q)
\tag{26}
$$

Where $A(Q)$ is calculated according to eq. 2 with the only difference in the H- and D-type liposomes is given by the contrast to the tails (Eqs. 12-15), $I_{sc_i}(Q)$ and $I_{sc_o}(Q)$ are the interference cross-terms of the outer and inner chains with the bilayer of the H-liposomes and D-liposomes (dependent on the A(Q)):

9

$$I_{sc_i}^{H/D}(Q) = A_{H/D}(Q) \cdot \Delta\rho_{PEG} V_{PEG} 2 N_{PEG}(1 - f_{inner}) \cdot (N_{PEG}(1 - f_{inner}) - 1)$$

$$\cdot \left[\frac{1 - exp\left[-\left(QR_g\right)^2\right]}{\left(QR_g\right)^2} \right] \cdot \left[\frac{sin\left(Q(R_i - R_g)\right)}{Q(R_i - R_g)} \right] \qquad (27)$$

$$I_{sc_o}^{H/D}(Q) = A(Q) \cdot \Delta\rho_{PEG} V_{PEG} 2 N_{PEG} f_{inner} \cdot (N_{PEG} f_{inner} - 1) \cdot \left[\frac{1 - exp\left[-\left(QR_g\right)^2\right]}{\left(QR_g\right)^2} \right]$$

$$\cdot \left[\frac{sin\left(Q(R_i + 2t_{shell} + D_c - R_g)\right)}{Q(R_i + 2t_{shell} + D_c - R_g)} \right] \qquad (28)$$

In this expression, $\Delta\rho_{PEG}$ is the excess scattering length density, V_{PEG} is the partial specific molecular volume of a single PEG chains, R_g is the radius of gyration of the chains, f_{inner} is the fraction of PEG in the inner leaflet and N_{PEG} is defined as the number of PEG chains per liposomes given by

$$N_{PEG} = f_{PEG} \cdot P_{agg} \qquad (29)$$

f_{PEG} is the fraction of PEG-modified lipids in the liposomes and $P_{agg} = P_i + P_o$, is the aggregation number of the liposomes.

$I_{chain}(Q)$ is the scattering from the PEG-chains alone given by

$$I_{chain}(Q) = n\Delta\rho_{PEG}^2 V_{PEG}^2 N_{PEG} \cdot 2 \frac{exp[-\left(QR_g\right)^2] - 1 + \left(QR_g\right)^2}{\left(QR_g\right)^4} \qquad (30)$$

The last terms, $I_{c_i c_i}(q)$ and $I_{c_o c_o}(q)$, are the interference terms between PEG chains attached to the inner surface of the vesicles and between the PEG chains on the outer surface, respectively, while $I_{c_i c_o}(q)$ is the inter-interference between the inner and outer PEG chains:

10

$$I_{c_i c_i}(Q) = n\Delta\rho_{PEG}^2 V_{PEG}^2 N_{PEG} f_{inner} \cdot (N_{PEG} f_{inner} - 1) \cdot \left[\frac{1 - exp\left[-(QR_g)^2\right]}{(QR_g)^2}\right]^2$$

$$\cdot \left[\frac{sin\left(Q(R_i - R_g)\right)}{Q(R_i - R_g)}\right]^2 \tag{31}$$

$$I_{c_o c_o}(Q) = n\Delta\rho_{PEG}^2 V_{PEG}^2 N_{PEG} (1 - f_{inner}) \cdot (N_{PEG}(1 - f_{inner}) - 1)$$

$$\cdot \left[\frac{1 - exp\left[-(QR_g)^2\right]}{(QR_g)^2}\right]^2 \cdot \left[\frac{sin\left(Q(R_i + 2t_{shell} + D_c - R_g)\right)}{Q(R_i + 2t_{shell} + D_c - R_g)}\right]^2 \tag{32}$$

$$I_{c_i c_o}(Q) = n\Delta\rho_{PEG}^2 V_{PEG}^2 2N_{PEG}^2 f_{inner} \cdot (1 - f_{inner}) \cdot \left[\frac{1 - exp\left[-(QR_g)^2\right]}{(QR_g)^2}\right]^2$$

$$\cdot \left[\frac{sin\left(Q(R_i - R_g)\right)}{Q(R_i - R_g)}\right]^2 \cdot \left[\frac{sin\left(Q(R_i + 2t_{shell} + D_c - R_g)\right)}{Q(R_i + 2t_{shell} + D_c - R_g)}\right]^2 \tag{33}$$

Calculation of thermodynamical parameters from TR-SANS data

Following Nakano et al, the lipid transport processes can be described by the following differential equations with rate constants of exchange (k_{ex}) and flip-flop (k_{flip}) by(19)

$$-\frac{d|\Delta\rho_{out}|}{dt} = k_{ex}(|\Delta\rho_{out}| - 0) + k_{flip}(|\Delta\rho_{out}| - |\Delta\rho_{in}|),$$

$$-\frac{d|\Delta\rho_{in}|}{dt} = -k_{flip}(|\Delta\rho_{out}| - |\Delta\rho_{in}|) \tag{34}$$

where $\Delta\rho_{out}$ and $\Delta\rho_{in}$ are the contrast of the inner and outer leaflets of the vesicles with the solvent. As we have used a zero-average contrast solvent the H and D-vesicles can be assumed to have identical absolute values of contrast where one is positive and the other negative.

With the initial condition that $\Delta\rho_{out}(0) = \Delta\rho_{in}(0) = 1$ and taking an average of $|\Delta\rho_{out}|$ and $|\Delta\rho_{in}|$ the $R(t)$, normalized contrast has been explained by a double-exponential decay function(19)

$$R(t) = \left(\frac{1}{2} - \frac{k_{flip}}{X}\right)\exp(Yt) + \left(\frac{1}{2} + \frac{k_{flip}}{X}\right)\exp(Zt) \tag{35}$$

Where $X = \sqrt{4k_{flip}^2 + k_{ex}^2}$, $Y = \frac{-k_{ex}+2k_{flip}+X}{2}$ and $Z = \frac{k_{ex}+2k_{flip}-X}{2}$.

Similarly, the excess fraction of either H- and D-lipid in the inner and outer and leaflet as a function of time can be expressed by:

$$f_{out}(t) = \left(\frac{k_{ex}-Z}{Y-Z}\right)\exp(-Y(t-d)) + \left(\frac{Y-k_{ex}}{Y-Z}\right)\exp(-Z(t-d)) \tag{36}$$

$$\begin{aligned} f_{in}(t) = &\left(\frac{k_{ex}-Z}{Y-Z}\right)\cdot\frac{k_{flip}+k_{ex}-Y}{k_{flip}}\exp(-Y(t-d)) \\ &+ \left(\frac{Y-k_{ex}}{Y-Z}\right)\cdot\frac{k_{flip}+k_{ex}-Z}{k_{flip}}\exp(-Z(t-d)) \end{aligned} \tag{37}$$

where d is a delay time.

To extract further thermodynamical parameters, $\ln k_{ex}$ and k_{flip} can be plotted against the inverse temperature in Kelvin, $1/T$ for samples measured at different temperatures giving an Arrhenius type relationship. From this analysis we obtain the activation energy, E_a and the fundamental time constant, τ_0 according to

$$\tau = \tau_0 \exp\left(\frac{E_a}{RT}\right) \tag{38}$$

where $\tau = 1/k$, R is the universal gas constant and τ_0 is a system specific constant and is related to the time between each time the molecule "attempts" to overcome the energetic barrier.(33)

$$\tau = \tau_{00} \exp(-\Delta S/R)exp(\Delta H/RT) \tag{39}$$

Where ΔS is the entropy change, ΔH is the enthalpy change and τ_{00} is the estimated fundamental time constant.

DLS experiments:

Dynamic light scattering experiments were performed at 37°C on an ALV/CGS-8F multi-detector version compact goniometer system, with 8 fiber optical detection units, from ALV-GmbH., Langen, Germany. The intensity correlation function was measured at 8 scattering angles simultaneously in the range 22-141°. The measurement was performed using a beam of vertically polarized light with an incident wavelength of 632.8 nm. The sample solutions were filtered in an atmosphere of filtered air through 5μm filters (Millipore) directly into precleaned 2mm NMR tubes. The concentration of liposomes was lowered to 0.5 mg/ml to avoid multiple scattering.

The correlation functions were analysed using a single stretched exponential:

$$g(t) = exp\left[-\left(\frac{t}{\tau_{fe}}\right)^{\beta}\right]$$
(40)

where τ_{fe} is the effective relaxation time and β ($0 < \beta \leq 1$) is a measure of the width of the distribution of relaxation times. Further the mean relaxation time is given by:

$$\tau = \frac{\tau_{fe}}{\beta} \; \Gamma\left(\frac{1}{\beta}\right)$$
(41)

where $\Gamma\left(\frac{1}{\beta}\right)$ is the gamma function of β^{-1}. In the present work, the relaxation mode was observed to be diffusive in all cases (q^2 dependent).

In the analysis of the correlation function data, a non-linear fitting algorithm (a modified Levenberg–Marquardt method) was used to obtain best-fit values of the parameters τ_{fe} and β in Eq. 40.

The hydrodynamic radius (R_h) can be calculated through the Stokes-Einstein relationship from the relaxation time because the relaxation mode is diffusive:

$$R_h = \frac{k_b T}{6\pi\eta D}$$

<div align="right">(42)</div>

where T is the temperature, η is the viscosity of the medium, D is he mutual diffusion coefficient ($D = 1/\tau q^2$) and k_b is the Boltzmann constant.
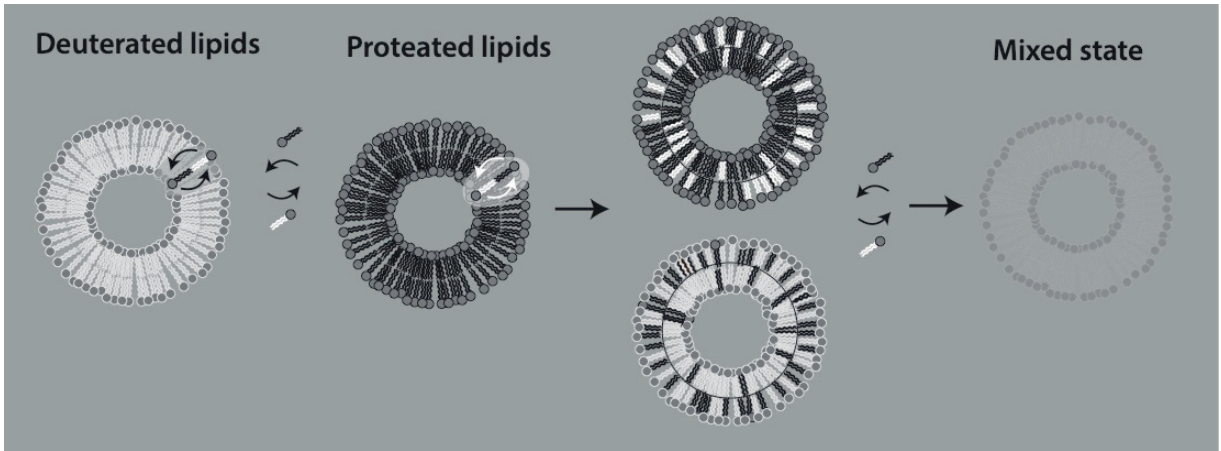
RESULTS AND DISCUSSIONS

Figure 2: Schematic illustration of the TR-SANS technique designed to resolve the lipid dynamics, intra-vesicular flip-flop and intervesicular exchange processes. The method, first developed for micelles,(34) is based on mixing perdeuterated vesicles with proteated vesicles in a solvent that consist of about 50% H/D matching the average scattering length density. As the molecules rearrange, contrast is lost and the neutron scattering intensity gradually decreases.

The TR-SANS method illustrated in Figure 2, is based on mixing proteated, H- (black) and perdeuterated, D-labelled (white) vesicles, and observing the decay in the scattering intensity over time. As the molecules mix and the average contrast decrease towards the mean solvent background (50% H/D solvent), the intensity decreases. An example of results obtained using the method is given for liposomes at 37 °C in Figure 3 where the scattered intensity as a function of the Q-vector is plotted at different times after mixing the solutions. The results reveal that, as expected, the intensity decreases gradually with time as the contrast is lost. However, the intensity is related to a change in contrast of both the inner and outer leaflet which are not necessarily following the same time dependence. Thus in order to extract accurate information about the kinetic process, the data were analysed using a multi-shell model for vesicles where the time-dependent contrast for the inner

and outer leaflet is taken into account and determined independently. The fit results are shown as solid lines demonstrating an excellent description of the data. As can be observed at low Q, the data exhibit an upturn, i.e. residual intensity even at the near contrast matched conditions. This effect, which also is naturally described by our model, comes from the finite scattering contribution of the small amount of fully proteated PEG chains that still contributes coherently to the scattered intensity.
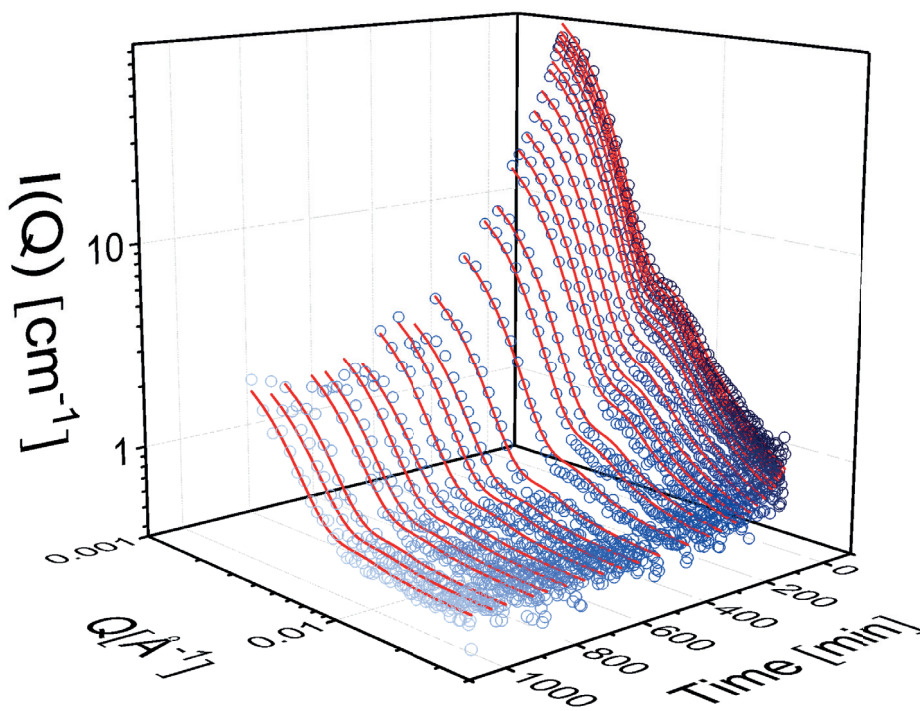

Figure 3: Scattered intensity plotted as a function of q and the time obtained for 2.5 mg/ml DMPC/DMPG lipid vesicles in 25 mM Tris buffer at 37 C, together with best fit.

In order to evaluate the kinetic process more in detail we proceeded to perform experiments at various temperatures, 27, 37, 47 and 57 °C. The data are shown in Figure 4. As seen from the plots the scattering model is able to explain the data of the pristine liposomes at the three lowest temperatures by only varying the contrast of the inner and outer layer. While at 57 °C the resolution of the data is not high enough to use the described fit model because the measuring times had to be lowered in order to follow the fast kinetics observed at this temperature. The structural fit parameters giving information on the particle size and membrane thickness are presented in Table 1. The results from the fit analysis are consistent with prior published SAXS and SANS data on liposomes consisting of the same lipid mixtures.(35)
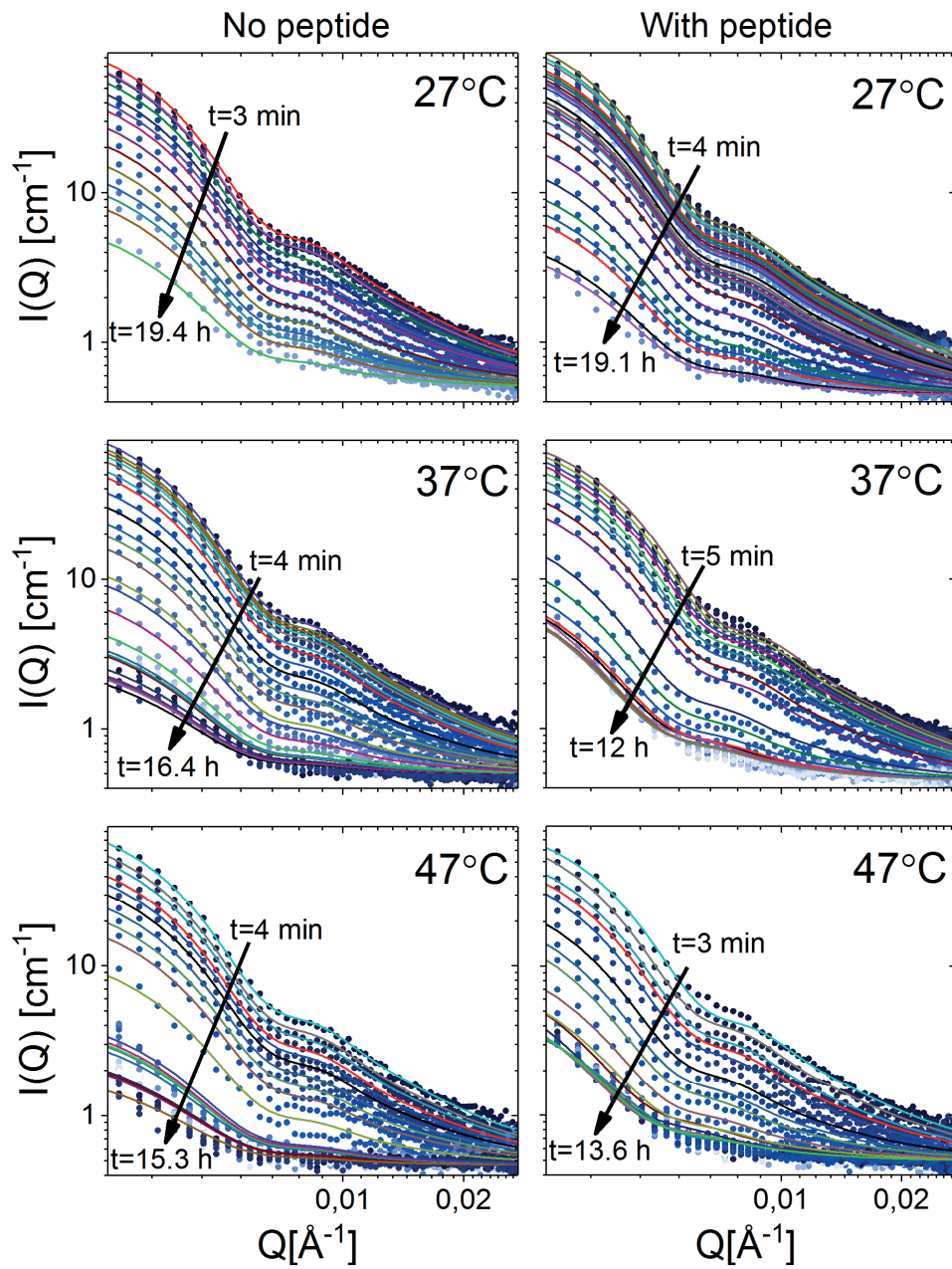
Figure 4: TR-SANS data including fits of DMPC/DMPG/DMPE-PEG vesicles with and without added peptides (1:20 indolicidin) at different temperatures. The start and end times are indicated.

Table 1: Structural fit parameter of liposomes with and without indolicidin (1:20) at different temperatures, as based on SANS data.

	27 °C		37 °C		47 °C	
	No peptide	With peptide	No peptide	With peptide	No peptide	With peptide
R_i [nm]	40	38.5-44[d]	40	39-54[d]	40	41.7-62[d]
V_{head}[Å³][a]	330	330	332	332	334	334
V_{tail}[Å³][a]	770	770	775	775	785	785
t_{shell} [Å][b]	6	6	6	6	6	6
D_c [Å][b]	26	26	25	25	24	24
f_{PEG}[c]	0.025	0.04	0.025	0.06	0.025	0.05
Rg_{PEG} [Å][b]	15	15	15	15	15	15

[a]*Hard constrained parameters(36, 37).* [b]*Soft constrained by limits.* [c]*Allowed to vary slightly in liposome samples with peptide to account for the extra proteated peptide material (the value is based on a fit of the end state curve).* [d]*Parameter dependent on time, see Figure 4.*

In Nature, the rate of lipid flip-flop is highly regulated by membrane proteins, and it is known that addition of drugs like for example AMPs may also affect the lipid motions. In these cases, it is especially interesting to use a methodology that is both able to determine the exchange and flip-flop rate, as well as any other kinetic processes such as changes in the morphology or size of the vesicles as this may be an important factor in fully understanding how addition of peptides or proteins affect lipid membranes. In order to study whether these effects can be characterized using the described direct scattering model approach, we added a peptide, indolicidin, that is already known to insert into the outer leaflet of the membrane(35) resulting in acceleration of lipid transport motions.(13) The TR-SANS results on liposomes with 1:20 indolicidin at 27, 37 and 47 °C are shown together with best fit in Figure 4. As seen from the plots the model is able to fully explain the scattering data over time at every temperature, but in the case of the lipid-peptide mixtures changing the contrast of the inner and outer leaflet is not sufficient to obtain well describing fit curves. In this case we therefore also varied the size of the liposomes (see Table 1), which as seen from the figure resulted in a good explanation of the data by the fit model. The thickness of the bilayer upon peptide addition was also set to vary in the fit analysis, however the results revealed that this parameter remained unchanged, which is

supported by previously published small angle X-ray scattering (SAXS) and neutron reflectometry (NR) data.(35, 38)
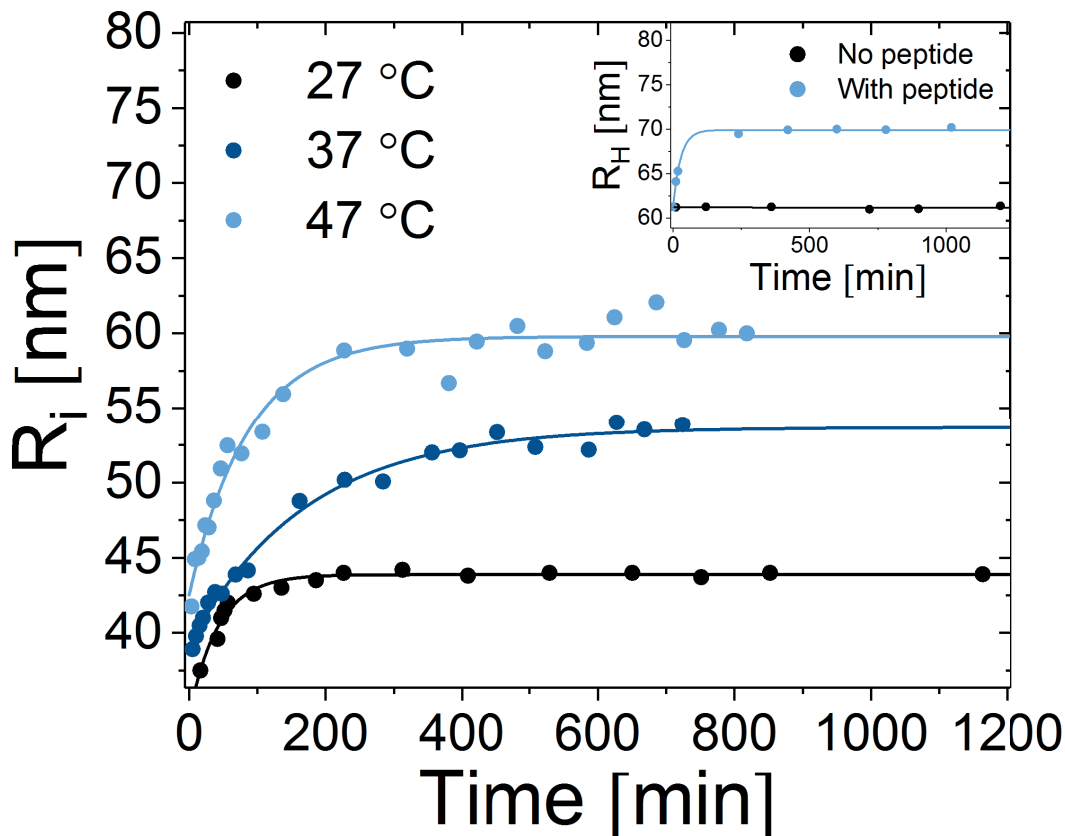

Figure 5: The inner radius of the liposomes with 1:20 indolicidin, as a function of time based on fit analysis of TR-SANS data. Inset shows a comparison of the radius of hydration of liposomes with and without 1:20 indolicidin at 37 °C based on DLS data.

The inner radii (R_i) of the liposomes as a function of time, at different temperatures have been plotted in Figure 5. As seen for the Figure the liposomes initially increase in size after peptide addition, but eventually reach a stable plateau. The growth of the particles was found to follow the exponential expression $R(t) = \Delta R * \left(1 - \exp\left(-\frac{t}{tau}\right)\right) + R_{start}$ where ΔR is the difference between the end and start size of the particles, tau is the time constant and R_{start} is the initial liposome size. When comparing the effect at different temperatures it is obvious that the effect is more pronounced with increasing temperatures. The same trend can be observed in the hydrodynamic radius (R_H) when comparing neat liposomes with liposomes-indolicidin mixtures using DLS at 37 °C (the sample for these experiments are not the exact same as the samples used for the TR-SANS experiments and therefore absolute values should not be compared directly, but the preparation

method and lipid content is the same). The results show how the liposomes without peptides are very stable over a long time, and we have previously tried to follow the structure over months without any observed changes in size or bilayer structure. The liposomes contain 2.5 % PEGylated DMPE-lipids in order to increase the stability of the vesicles against self-aggregation in the presence of a cationic substrate like indolicidin. The PEGylation together with inclusion of 25% negative charged (DMPG and DMPE-PEG are both anionic) lipid provides an explanation of the extreme physical stability observed in the DLS data for the pristine liposome system.

Upon peptide addition the physical stability of the PEGylated liposomes is disturbed causing a growth of the particles. Generally these type of changes can occur via different mechanisms: at the particle level the liposomes can change size due to aggregation, fusion, coacervation or precipitation, while at the molecular level, the mechanism can be Ostwald ripening, described as asymmetric molecular exchange where larger vesicles grow on the expense of the smaller ones.(39) As seen from previous SAXS and SANS data, incorporation of 2.5 % PEGylated DMPE is sufficient to stabilise the liposomes from aggregation and induction of multilamellar structures caused by addition of indolicidin.(35) Another possible explanation is peptide induced fusion of liposome particles. However, in Nielsen et al. we did TR-SANS experiments on the same system at different overall concentrations (2.5 and 5 mg/ml) revealing a perfect overlap of the intensity decay functions.(13) This indicates that vesicle fusion events does not frequently occur because these would be concentration dependent, and therefore give a steeper decay in the TR-SANS results at higher concentrations. It should also be noted that fusion would likely cause a larger increase in the size than observed in our SANS and DLS experiments.

These evidences therefore rather point toward a peptide effect on the molecular level being the cause of the observed growth behaviour. Previous, NR and atomic force microscopy (AFM) experiments has revealed that indolicidin addition to supported lipid membranes composed of DMPC and DMPG causes solubilisation and removal of lipids. We hypothesise that addition of indolicidin leads to an inhomogeneous partial dissolution of lipids and initially increases the solubility of the lipids including the PEGylated lipids. This leads to redistribution of lipids that become available. Once the lipids have been redistributed and the lipids /peptides have been homogenously distributed, the vesicles stabilize into the new size distribution.
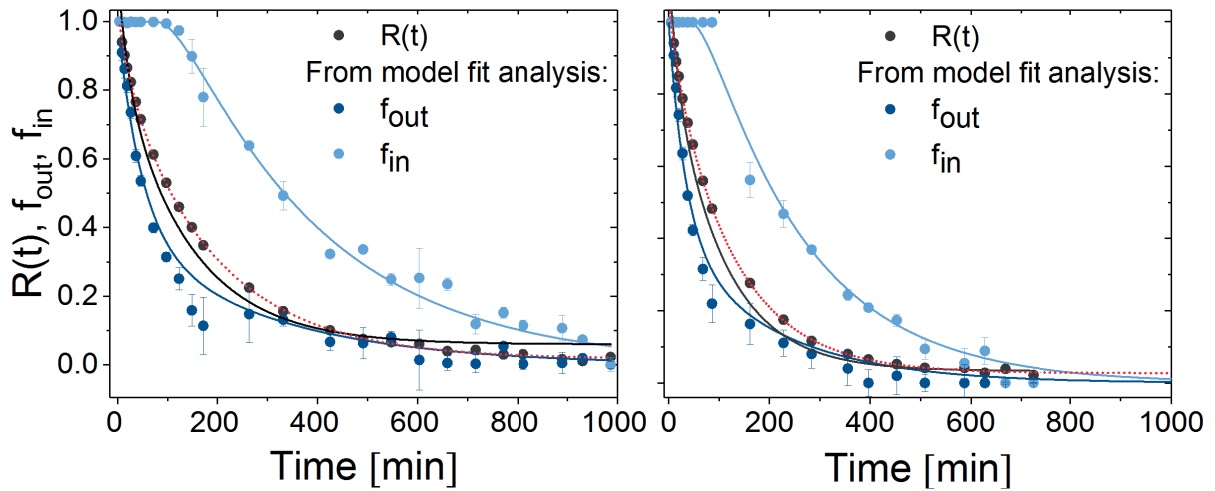
Figure 6: Results for exchange and flip-flop of liposomes without peptide (A) and with peptide (B). The plot shows the excess fraction of either H- and D-lipid in the inner and outer and leaflet ($f_{in}(t)$ and $f_{out}(t)$ respectively) based on direct modelling of full Q range TR-SANS data, and the R(t) curves extracted from the integral net loss of scattering intensity (Eq. 1). The solid black line is a result of a joint fit of all curves extracting information on the exchange (k_{ex}) and flip-flop (k_{flip}) rates, while the red dotted line represents a separate fit to only the R(t) curve.

Apart from the changes in particle size we extract information on the excess fraction of either H- and D-lipid in the inner and outer leaflet as plotted in Figure 5. In order to compare the results from the direct and indirect approaches to analysing TR-SANS data, the traditional R(t) curve (Eq. 1) has been plotted together with the $f_{in}(t)$ and $f_{out}(t)$ parameters in Figure 5, and the data has been analysed simultaneously using the expressions shown in Eq. 34-36, with the same exchange (k_{ex}) and flip-flop (k_{flip}) rates. As seen from the solid lines plotted in Figure 6 all the data is well explained by the models when using the same lipid transport rates. This indicates that the results we get from the two different approaches are comparable. However, as seen from Figure 5, the f_{in} curve (gives information on flip-flop motions of lipids) apparently displays an initial "delay time", which required a modification of the expected kinetic model. (see Eq. 35-36)

This delay time can be explained by a lack of sensitivity to lipid flip-flop in the first stage of the experiments because of insufficient contrast between the outer and inner leaflet of the vesicles. Over time, when enough lipids have exchanged between H- and D-vesicles, taking into account that lipid exchange only affects the outer leaflet, sufficient contrast is obtained to also see lipid flip-flop motions from the TR-SANS scattering curves. To compare the result from model analysis of the TR-SANS data directly, with the traditional extraction of the exchange and flip-flop rates from the R(t) curve, we have included analysis of the R(t) curve independently using the model described in Eq. 34 (red dotted line in Figure 6).

The exchange and flip-flop rates found by both approaches described above are shown in Arrhenius plots in Figure 7. The rates obtained using only the R(t) curve, as seen in the inset graph, are consistently higher than

the parameters extracted from the joint fit analysis. However, the linear fit curve is almost parallel, which explains why the activation energy (E_a) and change in enthalpy (ΔH) which are proportional to the slope of the curves, are rather consistent. The reason for the difference in absolute rates might be related to the (time-dependent) contrast between the inner and outer leaflet which affect the cross-terms of the scattering amplitudes which are not taken into account when using the integrated scattering method, R(t). See Table 2 for full list of thermodynamical parameters extracted from the Arrhenius plot. When comparing the parameters for the liposomes with and without peptides, we find the same overall trends as in Nielsen *et al.*(13) where indolicidin significantly lowers the activation energy of lipid flip-flop. While the exchange rates are highly affected by peptide addition the activation energy of this process is less affected.
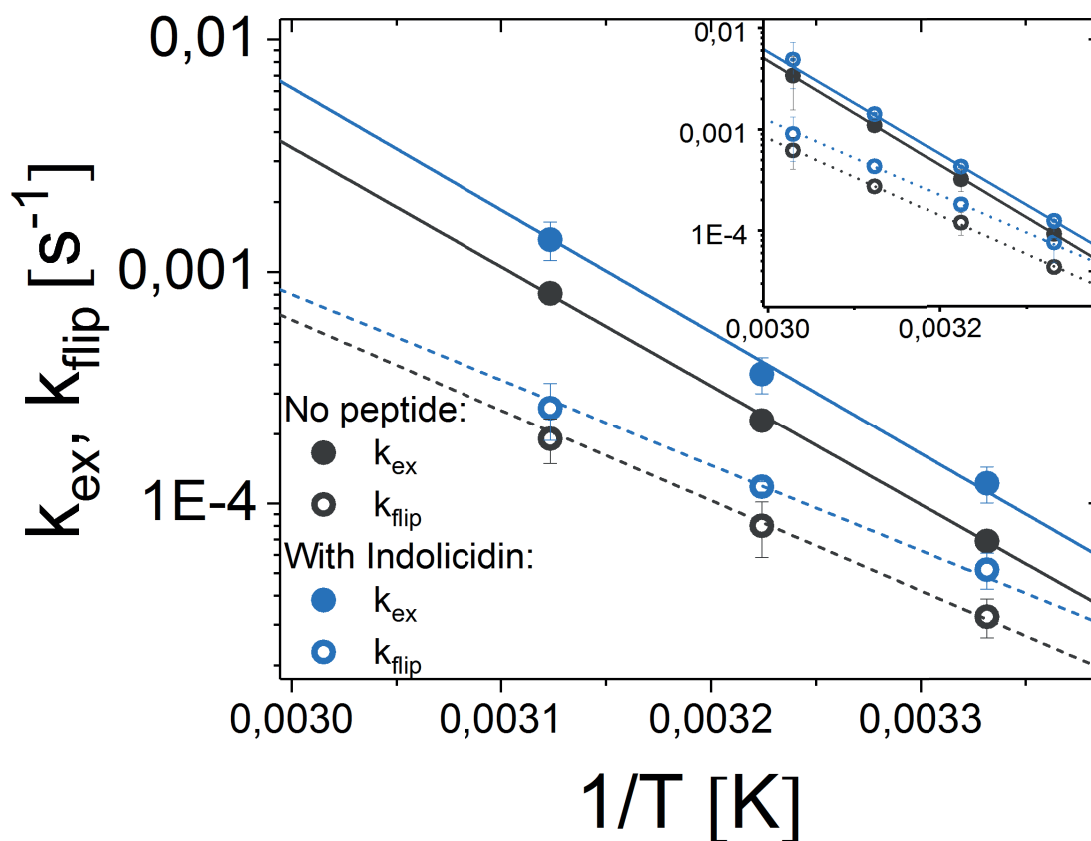

Figure 7: Arrhenius plot for liposomes with and without 1:20 indolicidin based on joint fit of f_{out}, f_{in} and R(t). Inset displays the same parameters calculated from an independent analysis of the R(t) curve.

Table 2: Thermodynamical parameters of liposomes with and without peptide.

	Lipid exchange					Lipid flip-flop				
	k_{ex}^{*} $[min^{-1}]$	E_a [kJ /mol]	ΔH[kJ /mol]	$T\Delta S$ [kJ /mol]	ΔG[kJ /mol]	k_{flip}^{*} $[min^{-1}]$	E_a [kJ /mol]	ΔH [kJ /mol]	$T\Delta S$ [kJ /mol]	ΔG [kJ /mol]
No peptide										
Joint fit	$1.4\cdot10^{-2}$	100	97	0	98	$4.8\cdot10^{-3}$	74	68	-29	100
R(t)	$1.9\cdot10^{-2}$	100	97	1	97	$7.1\cdot10^{-3}$	75	72	-27	99
With peptide										
Joint fit	$2.1\cdot10^{-2}$	96	93	3	96	$7.1\cdot10^{-3}$	64	62	-38	99
R(t)	$2.5\cdot10^{-2}$	98	95	4	96	$1.1\cdot10^{-2}$	66	63	-36	98

*The rate constants (k) of exchange and flip-flop are extrapolated to 37.0 °C from the Arrhenius data.

CONCLUSION

Lipid vesicles are frequently used as model system for understanding the biophysical behaviour of membrane systems. In this work, we have developed a scattering model that can be used to analyse full Q-range TR-SANS to investigate both lipid flip-flop and exchange rates in lipid vesicles directly, as well as other kinetic processes like morphological or particle size changes, simultaneously. We have demonstrated that the model is able to explain scattering data both for pure lipid vesicle systems as well as liposomes in the presence of accelerating substrates like peptides or proteins. Upon analysing TR-SANS data from liposomes with an added antimicrobial peptide, indolicidin we found that a change in the size of the particles was necessary to to fully explain the progression of the scattering curves over time. This peptide induced growth can be explained by a limited Ostwald-like ripening process due to the peptide increasing the solubilisation of the lipids. However, the process is transient and as the peptide is presumably uniformly distributed over the vesicles, the system settles to a new equilibrium. The change in the overall size would not have been described by only monitoring the loss of overall SANS intensity over time, which is the traditional approach to analysing TR-SANS data of liposomes as first presented by Nakano and co-workers.(19) However, both approaches give information on the exchange and flip-flop rates of the lipids. When comparing results from the analysing the same TR-SANS data using the two methods we found a trend where rates extracted from the R(t) curve representing the SANS intensity decay over time are consistently higher than the rates found by fit analysing

the full Q range curve. This however, did not affect the activation energy found from the Arrhenius plot resulting from each method. We therefore conclude that a direct modelling provides more information on the system, especially relevant upon addition of substrates because these might also influence other kinetic processes that will be hidden when only focusing on following the intensity over time. However, this approach requires high resolution data and is more time consuming than the indirect approach. This issue is reflected in the missing fit analysis results from the highest temperature (57 °C) because the kinetics at this temperature was too fast to obtain sufficient quality data needed for model analysis. In conclusion both methods provide comparable results with regards to thermodynamical relevant parameters.

Supplementary Materials:

References:

1.   2011. Transmembrane Dynamics of Lipids. John Wiley & Sons, Inc., New Jersey.
2.   Raff, M., B. Alberts, J. Lewis, A. Johnson, and K. Roberts. 2002. Molecular Biology of the Cell. . National Center for Biotechnology Information's Bookshelf.
3.   Langer, M., R. Sah, A. Veser, M. Gütlich, and D. Langosch. 2013. Structural Properties of Model Phosphatidylcholine Flippases. Chem Biol 20(1):63-72.
4.   Contreras, F. X., L. Sánchez-Magraner, A. Alonso, and F. M. Goñi. 2010. Transbilayer (flip-flop) lipid motion and lipid scrambling in membranes. FEBS Letters 584(9):1779-1786.
5.   Fadeel, B., and D. Xue. 2009. The ins and outs of phospholipid asymmetry in the plasma membrane: roles in health and disease. Crit. Rev. Biochem. Mol. Biol. 44(5):264-277.
6.   Matsuzaki, K., O. Murase, N. Fujii, and K. Miyajima. 1996. An antimicrobial peptide, magainin 2, induced rapid flip-flop of phospholipids coupled with pore formation and peptide translocation. Biochemistry 35(35):11361-11368.
7.   Wimley, W. C., and S. H. White. 2000. Determining the membrane topology of peptides by fluorescence quenching. Biochemistry 39(1):161-170.
8.   Zhang, L., A. Rozek, and R. E. Hancock. 2001. Interaction of cationic antimicrobial peptides with model membranes. J. Biol. Chem. 276(38):35714-35722.
9.   Anglin, T. C., K. L. Brown, and J. C. Conboy. 2009. Phospholipid flip-flop modulated by transmembrane peptides WALP and melittin. J. Struct. Biol. 168(1):37-52.

10.	Nguyen, M. H., M. DiPasquale, B. W. Rickeard, M. Doktorova, F. A. Heberle, H. L. Scott, F. N. Barrera, G. Taylor, C. P. Collier, C. B. Stanley, J. Katsaras, and D. Marquardt. 2019. Peptide-Induced Lipid Flip-Flop in Asymmetric Liposomes Measured by Small Angle Neutron Scattering. Langmuir 35(36):11735-11744.

11.	LeBarron, J., and E. London. 2016. Effect of lipid composition and amino acid sequence upon transmembrane peptide-accelerated lipid transleaflet diffusion (flip-flop). Biochim. Biophys. Acta, Biomembr. 1858(8):1812-1820.

12.	Kol, M. A., A. N. van Laak, D. T. Rijkers, J. A. Killian, A. I. de Kroon, and B. de Kruijff. 2003. Phospholipid flop induced by transmembrane peptides in model membranes is modulated by lipid composition. Biochemistry 42(1):231-237.

13.	Nielsen, J. E., V. A. Bjørnestad, V. Pipich, H. Jenssen, and R. Lund. 2021. Beyond Structural Models for the Mode of Action: How Natural Antimicrobial Peptides Disrupts Lipid Membranes. J. Colloid Interface Sci. 582:793-802.

14.	Lund, R., L. Willner, D. Richter, and E. E. Dormidontova. 2006. Equilibrium Chain Exchange Kinetics of Diblock Copolymer Micelles: Tuning and Logarithmic Relaxation. Macromolecules 39(13):4566-4575.

15.	Lund, R., L. Willner, J. Stellbrink, P. Lindner, and D. Richter. 2006. Logarithmic chain-exchange kinetics of diblock copolymer micelles. Phys. Rev. Lett. 96(6):068302.

16.	Lund, R., L. Willner, and D. Richter. 2013. Kinetics of Block Copolymer Micelles Studied by Small-Angle Scattering Methods. Adv Polym Sci 259:51-158.

17.	Choi, S. H., T. P. Lodge, and F. S. Bates. 2010. Mechanism of Molecular Exchange in Diblock Copolymer Micelles: Hypersensitivity to Core Chain Length. Physical Review Letters 104(4):47802.

18.	Lund, R., L. Willner, V. Pipich, I. Grillo, P. Lindner, J. Colmenero, and D. Richter. 2011. Equilibrium Chain Exchange Kinetics of Diblock Copolymer Micelles: Effect of Morphology. Macromolecules 44(15):6145-6154.

19.	Nakano, M., M. Fukuda, T. Kudo, H. Endo, and T. Handa. 2007. Determination of interbilayer and transbilayer lipid transfers by time-resolved small-angle neutron scattering. Phys. Rev. Lett. 98(23):238101.

20.	Nakano, M., M. Fukuda, T. Kudo, N. Matsuzaki, T. Azuma, K. Sekine, H. Endo, and T. Handa. 2009. Flip-Flop of Phospholipids in Vesicles: Kinetic Analysis with Time-Resolved Small-Angle Neutron Scattering. J. Phys. Chem. B 113(19):6745-6748.

21.	Garg, S., L. Porcar, A. Woodka, P. Butler, and U. Perez-Salas. 2011. Noninvasive neutron scattering measurements reveal slower cholesterol transport in model lipid membranes. Biophys. J. 101(2):370-377.

22.	Xia, Y., M. Li, K. Charubin, Y. Liu, F. A. Heberle, J. Katsaras, B. Jing, Y. Zhu, and M.-P. Nieh. 2015. Effects of nanoparticle morphology and acyl chain length on spontaneous lipid transfer rates. Langmuir 31(47):12920-12928.

23.	Wah, B., J. M. Breidigan, J. Adams, P. Horbal, S. Garg, L. Porcar, and U. Perez-Salas. 2017. Reconciling differences between lipid transfer in free-standing and solid supported membranes: a time-resolved small-angle neutron scattering study. Langmuir 33(14):3384-3394.

24.	Breidigan, J. M., N. Krzyzanowski, Y. Liu, L. Porcar, and U. Perez-Salas. 2017. Influence of the membrane environment on cholesterol transfer. J. Lipid Res. 58(12):2255-2263.

25.	Zhang, L., A. Rozek, and R. E. W. Hancock. 2001. Interaction of Cationic Antimicrobial Peptides with Model Membranes. Journal of Biological Chemistry 276(38):35714-35722.

26.	Wimley, W. C., and S. H. White. 2000. Determining the Membrane Topology of Peptides by Fluorescence Quenching †. Biochemistry-Us 39(1):161-170.

27. Kobayashi, S., K. Takeshima, C. B. Park, and S. C. Kim. 2000. Interactions of the novel antimicrobial peptide buforin 2 with lipid bilayers: proline as a translocation promoting factor. Biochemistry 39(29):8648-8654.

28. Kol, M. A., A. N. C. van Laak, D. T. S. Rijkers, J. A. Killian, A. I. P. M. de Kroon, and B. d. Kruijff. 2003. Phospholipid Flop Induced by Transmembrane Peptides in Model Membranes Is Modulated by Lipid Composition. Biochemistry 42(1):231-237.

29. Kol, M. A., A. de Kroon, D. Rijkers, and J. A. Killian. 2001. Membrane-spanning peptides induce phospholipid flop: a model for phospholipid translocation across the inner membrane of E. coli. Biochemistry.

30. Kiselev, M., P. Lesieur, A. Kisselev, D. Lombardo, and V. Aksenov. 2002. Model of separated form factors for unilamellar vesicles. Appl. Phys. A 74(1):s1654-s1656.

31. Arleth, L., and C. Vermehren. 2010. An analytical model for the small-angle scattering of polyethylene glycol-modified liposomes. J. Appl. Crystallogr. 43(5):1084-1091.

32. Pedersen, J. S., and M. C. Gerstenberg. 1996. Scattering form factor of block copolymer micelles. Macromolecules 29(4):1363-1365.

33. Zinn, T., L. Willner, V. Pipich, D. Richter, and R. Lund. 2015. Effect of core crystallization and conformational entropy on the molecular exchange kinetics of polymeric micelles. ACS Macro Lett. 4(6):651-655.

34. Lund, R., L. Willner, D. Richter, and E. E. Dormidontova. 2006. Equilibrium chain exchange kinetics of diblock copolymer micelles: Tuning and logarithmic relaxation. Macromolecules 39(13):4566-4575.

35. Nielsen, J. E., V. A. Bjørnestad, and R. Lund. 2018. Resolving the Structural Interactions between Antimicrobial Peptides and Lipid Membranes using Small-angle Scattering Methods: the case of Indolicidin. Soft Matter 14(43):8750-8763.

36. Kučerka, N., M.-P. Nieh, and J. Katsaras. 2011. Fluid phase lipid areas and bilayer thicknesses of commonly used phosphatidylcholines as a function of temperature. Biochim. Biophys. Acta, Biomembr. 1808(11):2761-2771.

37. Pan, J., F. A. Heberle, S. Tristram-Nagle, M. Szymanski, M. Koepfinger, J. Katsaras, and N. Kučerka. 2012. Molecular structures of fluid phase phosphatidylglycerol bilayers as determined by small angle neutron and X-ray scattering. Biochim. Biophys. Acta, Biomembr. 1818(9):2135-2148.

38. Nielsen, J. E., T. K. Lind, A. Lone, Y. Gerelli, P. R. Hansen, H. Jenssen, M. Cárdenas, and R. Lund. 2019. A biophysical study of the interactions between the antimicrobial peptide indolicidin and lipid model systems. Biochim. Biophys. Acta, Biomembr. 1861(7):1355-1364.

39. Casals, E., A. M. a. Galán, G. Escolar, M. Gallardo, and J. Estelrich. 2003. Physical stability of liposomes bearing hemostatic activity. Chem. Phys. Lipids 125(2):139-146.

Paper VI

Lipid Membrane Interactions of Self-assembling antimicrobial nanofibers: effect of PEGylation

Josefine Eilsø Nielsen, Nico König, Su Yang, Maximilian WA Skoda, Armando Maestro, He Dong, Marité Cardenas, and Reidar Lund

VI

PAPER

Lipid membrane interactions of self-assembling antimicrobial nanofibers: effect of PEGylation†

Josefine Eilsø Nielsen, [ID] [a] Nico König, [ID] [ab] Su Yang,[c] Maximilian W. A. Skoda, [ID] [d] Armando Maestro, [ID] [e] He Dong, [ID] [c] Marité Cárdenas[f] and Reidar Lund [ID] *[a]

Supramolecular assembly and PEGylation (attachment of a polyethylene glycol polymer chain) of peptides can be an effective strategy to develop antimicrobial peptides with increased stability, antimicrobial efficacy and hemocompatibility. However, how the self-assembly properties and PEGylation affect their lipid membrane interaction is still an unanswered question. In this work, we use state-of-the-art small angle X-ray and neutron scattering (SAXS/SANS) together with neutron reflectometry (NR) to study the membrane interaction of a series of multidomain peptides, with and without PEGylation, known to self-assemble into nanofibers. Our approach allows us to study both how the structure of the peptide and the membrane are affected by the peptide–lipid interactions. When comparing self-assembled peptides with monomeric peptides that are not able to undergo assembly due to shorter chain length, we found that the nanofibers interact more strongly with the membrane. They were found to insert into the core of the membrane as well as to absorb as intact fibres on the surface. Based on the presented results, PEGylation of the multidomain peptides leads to a slight net decrease in the membrane interaction, while the distribution of the peptide at the interface is similar to the non-PEGylated peptides. Based on the structural information, we showed that nanofibers were partially disrupted upon interaction with phospholipid membranes. This is in contrast with the considerable physical stability of the peptide in solution, which is desirable for an extended *in vivo* circulation time.

1. Introduction

The increase in bacterial resistance to low molecular weight antibiotics has encouraged research into the use of larger peptide or polymer-like molecules as therapeutics, which employ a different antimicrobial mechanism to overcome the existing antibiotic problem. Supramolecular assemblies of antimicrobial peptides (AMPs) have the potential to provide higher efficacy,[1–5] decreased hemolytic response and enhanced stability to serum proteins.[1–3,5–8] Increased activity has been reported by Beter *et al.* upon comparing self-assembled C_{12}-VVAGKKKGRW-NH$_2$ and KKKGRW-NH$_2$ nanofibers with their

corresponding soluble peptide molecules.[9] Similar results were reported by Chang *et al.* for self-assembled cylindrical nanostructures made from C_{16}–V$_4$K$_4$ functionalised with an (AKKARK)$_2$ heparin binding Cardin-motif, which displayed strongly enhanced activity against Gram-negative bacteria above the critical micellar concentration (CMC). In the latter case it was suggested that self-assembly promotes the bacterial cytoplasmic leakage, causing blisters on disorganized membranes of Gram-negative bacteria.[10] Contrary to the mentioned systems, Chu-Kung *et al.* found for YGAAKKAA-KAAKKAAKAA (AKK) peptides, conjugated to fatty acids of varying length, that the antimicrobial activity was lost when the minimal active concentration is higher than CMC. While the conjugation of AKK with a fatty acid was shown to increase its affinity to lipid membranes, at concentrations above the CMC the self-assembled structure inhibits binding of the peptide to cell membranes.[11] These inconsistencies indicate a required balance between hydrophobicity and assembly to optimise the antimicrobial activity, as was also reported by Molchanova and co-workers. These authors found that assembly in itself was not the cause of lowered activity for halogenated peptoids but was rather associated with increasing hydrophobicity.[12]

Cytoplasmic membrane interaction is an important feature of AMPs, either as a mechanism of action in itself, or as a step in the transmembrane transport to exert intracellular activity.[13,14]

[a]*Department of Chemistry, University of Oslo, 0315 Oslo, Norway. E-mail: reidar. lund@kjemi.uio.no*

[b]*Jülich Centre for Neutron Science (JCNS) and Institute for Complex Systems (ICS), Forschungszentrum Jülich GmbH, 52425 Jülich, Germany*

[c]*Department of Chemistry & Biochemistry, The University of Texas at Arlington, Arlington, Texas 76019, USA*

[d]*ISIS Pulsed Neutron and Muon Source, Science and Technology Facilities Council, Rutherford Appleton Laboratory, Harwell Science and Innovation Campus, Didco, Oxfordshire OX11 OQX, UK*

[e]*Institut Laue – Langevin, 38000 Grenoble, France*

[f]*Biofilms Research Center for Biointerfaces, Department of Biomedical Science, Health and Society, Malmö University, 20506 Malmö, Sweden*

† Electronic supplementary information (ESI) available. See DOI: 10.1039/d0ra07679a

In self-assembled peptides, the surface charge density and charge to surface area ratio differs from that of the single peptide molecules.[15] Indeed, self-assembly has been related to both the "detergent mechanism", where the peptides remove lipids from the membrane forming mixed micelles,[16,17] and membrane pore-formation.[18,19] However, the detailed effect of larger supramolecular assembly and how they structure in the presence of membranes is still an open question.

In this study we investigate the membrane interaction of a series of multidomain peptides (MDPs) previously introduced by Dong and co-workers,[20] which exhibit antimicrobial activity against are range of different bacteria.[1] For these MDPs the self-assembly properties have been found to directly relate to their efficacy and cytotoxicity.[1] The MDPs are based on an ABA motif where the B group consist of a β-sheet motif of alternating hydrophilic glutamine (Q) and hydrophobic leucine (L) groups, while the A groups consist of positively charged lysine (K) residues, with the general formula $K_x(QL)_yK_z$. MDP self-assembly is driven by intermolecular hydrophobic interactions and hydrogen bonding between the peptide subunits leading to a supramolecular fibrous structure.[21] A MDP analogue used by Xu *et al.* was shown to remain stable in the presence of phospholipids, although they presented bacterial lytic abilities.[22] Thus, it is likely that MDP membrane interaction is influenced by their self-assembly properties.

Further than affecting the antimicrobial activity and selectivity, self-assembly of AMPs affects the pharmaceutical properties of the molecules. Self-assembled antimicrobial peptides may act as a vehicle-free self-controlled delivery system, where the peptide is gradually released from the "nanoscopic depot".[5,15,21,23,24] This approach has the advantage of eliminating the physical encapsulation or covalent conjugation of pharmaceutical excipients in traditional formulations since it is no longer necessary to insert the active peptide in a delivery vehicle.[25] The self-assembly approach allows for the release of active molecules without having to overcome issues related to steric hindrance or diffusion barriers.[21] However, physical stability of the self-assembly structures under various conditions is a key parameter in the use of these systems as drug-delivery systems. König *et al.* recently showed using time resolved small angle neutron scattering (TR-SANS) that MDPs composed of $K_x(QL)_yK_z$ are extremely stable at physiological relevant conditions, without any significant exchange of peptide chains in-between nanofibers over a timeframe of 2–3 days at 37 °C.[26] This is a significant attribute for the development of long-circulation peptide-based biomaterials. However, it is yet to be determined whether the presence of a phospholipid membrane affects the physical stability of the peptides and their implication for the biological activity, which is the focus of current study.

The lack of *in vivo* stability, due to protease susceptibility, and hemocompatibility toward red blood cells remains one of the main challenges associated with using peptides in antibacterial treatment in the clinics. The $K_x(QL)_yK_z$ MDPs are designed to tackle these issues both through their self-assembling nature and also due to the additional attachment of polyethylene glycol (PEG) groups to the N-terminus of the peptides. PEG improves the hemocompatibility of these peptides because it minimizes non-specific interactions with various cells, proteins and lipids in a biological environment.[6] PEGylation has been also reported to lower the antibacterial activity in some instances depending on the length of the PEG group bound to the peptides. Singh *et al.* have shown that PEGylation of KYE28 reduces peptide binding to lipid membranes with increasing molecular weight of the PEG block, resulting in a lowered antimicrobial effect,[27] indicating a needed balance between the reduced hemolysis and activity in the design of the peptide with regards to PEG chain length. Beyond reduction in hemolysis, PEGylation is a well-known modification of both low molecular weight drug molecules and biomacromolecules to enhance their pharmaceutical properties.[28] For example, it's known to increase the *in vivo* half-life of parenteral drugs as well as reduce immunogenicity.[28–30]

In this work, we study the effects of MDPs with and without PEGylation on model lipid membranes using SAXS/SANS and specular neutron reflectometry (NR) at solid–liquid interfaces. NR is a powerful tool for studying peptide–membrane interactions due to the ability to resolve the detailed structure of membranes on length scales from a few Ångstrøms to tens of nanometres. NR also allows to simultaneously resolve potential lipid removal as well as peptide insertion into partly deuterated supported lipid bilayers (SLBs).[31–38] In an earlier work, we showed that NR results can be directly compared to results from detailed modelling of small angle X-ray scattering (SAXS) data on monomeric peptide lipid bilayer using SLBs or unilamellar vesicles respectively.[31] For supramolecular nanofibers in particular, NR has an advantage over bulk methods since it lacks 3D orientation averaging and enables precise structural determination of complex MDP–membrane structures. Here, MDPs made of $K_3W(QL)_6K_2$ with and without PEGylation are used in combination with SLB constituted of DMPC/DMPG and studied by contrast variation NR. The results are compared to a shorter, monomeric unstructured $K_3W(QL)_3K_2$ thereby allowing a direct comparison of the role of self-assembly on peptide–membrane interactions.

2. Experimental section

2.1 Materials and sample preparation

Peptide synthesis. 4-Methylbenzhydrylamine (MBHA) rink amide resin, Fmoc-protected amino acids, 2-(1*H*-benzotriazol-1-yl)-1,1,3,3-tetramethyluronium hexafluorophosphate (HBTU), piperidine, diisopropylethylamine (DIPEA) and PEG2000 were purchased from Sigma-Aldrich. Dimethylformamide (DMF), acetic anhydride, trifluoroacetic acid (TFA), triisopropylsilane (TIS) and acetonitrile (ACN) were purchased from Fisher Scientific and used as received. The synthetic procedure followed the standard Fmoc-solid phase peptide synthesis method on a Prelude® peptide synthesizer. In brief, all the syntheses were set up at a 50 μmol scale using MBHA rink amide resin. The Fmoc group was deprotected utilizing 20% (v/v) piperidine/DMF for 5 minutes and repeated once. The coupling reaction was carried out for 30 min by adding 4 equivalents of Fmoc-protected amino acid, 4 equivalents of HBTU and 8

equivalents of DIPEA with respect to Fmoc-protected amino acids. After the completion of the synthesis, the N-terminus of the peptides were acetylated using DIPEA and acetic anhydride in DMF for 1 h. The completion of the coupling reaction was confirmed by the Kaiser test. The acetylated peptide was cleaved in a mixture of TFA/TIS/H$_2$O (95/2.5/2.5 by volume). After 3 h, cleavage solution was filtered, and the filtrates were collected. The resins were washed three times with neat TFA and the TFA was combined with filtrate solutions and evaporated under airflow. The residual peptide solution was precipitated in cold diethyl ether, followed by centrifugation and cold diethyl ether washing for three times. The crude peptide was dried under vacuum overnight before HPLC purification. Peptides were purified using a preparative reverse phase C4 column with a linear gradient of H$_2$O/ACN (5% to 95% of acetonitrile in 30 min) containing 0.05% TFA and the elution was monitored at both 230 nm and 280 nm. The HPLC fraction was collected, combined and lyophilized for 2 days. PEGylated peptide was synthesized as follows. After the final deprotection of the Fmoc group, peptide resins were treated with 4 equivalents of carboxyl terminated PEG, 4 equivalents of HBTU and 8 equivalents of DIPEA in DMF. The reaction mixture was stirred overnight. Kaiser test was performed to confirm the completion of the PEGylation reaction. The cleavage and purification steps followed the same procedure as those for acetylated peptides.

Peptide	N-terminus	Peptide sequences	C-terminus
3W32	CH$_3$CO–	KKKWQLQLQLKK	–CONH$_2$
3W62	CH$_3$CO–	KKKWQLQLQLQLQLKK	–CONH$_2$
D–P–3W62	D–PEG2000–	KKKWQLQLQLQLQLKK	–CONH$_2$
H–P–3W62	H–PEG2000–	KKKWQLQLQLQLQLKK	–CONH$_2$

Preparation of lipid films. Synthetic DMPC (1,2-dimyristoyl-*sn-glycero*-3-phosphocholine), D54-DMPC (1,2-dimyristoyl-d54-*sn-glycero*-3-phosphocholine), DMPG (1,2-dimyristoyl-*sn-glycero*-3-phospho-(1′-*rac*-glycerol)), D54-DMPG (1,2-dimyristoyl-d54-*sn-glycero*-3-[phospho-*rac*-(1-glycerol)] (sodium salt)) and DMPE-PEG (1,2-dimyristoyl-*sn-glycero*-3-phosphoethanolamine-*N*-[methoxy(polyethylene glycol)-2000] (ammonium salt)) were purchased from Avanti Polar Lipids. Lipid films where prepared by dissolving the lipids in a methanol: chloroform solution to a 1 : 3 volume ratio, followed by solvent removal under a stream of nitrogen flow. The vials where then left under vacuum for at least one hour to ensure complete removal of organic solvents. Lipid films were then kept at −20 °C until use.

Matched out lipid vesicles. For the SANS and SAXS experiments the lipid films were first hydrated in a Tris buffer solution for at least one hour at 24 °C, followed by sonication in a sonication bath for 15 min, and extrusion using an Avanti mini extruder equipped with two 1 ml syringes and a 100 nm pore diameter polycarbonate filter. The lipid solution was pushed through the filter >21 times to make unilamellar lipid vesicles. For these experiments a combination of lipids with protonated and deuterated tails and D$_2$O (D-) or H$_2$O (H-) based 50 mM Tris buffer pH 7.4 (Sigma Aldrich) were used to match the Scattering Length Density (SLD) of both the headgroup and average lipid

tail (match out vesicles). This was achieved by mixing 32 mol% d-DMPC (1,2-dimyristoyl-d54-*sn-glycero*-3-phosphocholine), 53 mol% h-DMPC, 10 mol% h-DMPG and 5 mol% DMPE-PEG in 10 mg ml^{-1} 36% D–Tris and 64% H–Tris. Addition of 5% PEGylated DMPE lipids was necessary in order to stabilise the vesicles against aggregation upon peptide addition. Provided that the lipids are randomly distributed, vesicles with this composition will essentially be contrast matched for neutrons, and thus exhibit very low scattering intensity. This enables a direct comparison of the scattering from the partly deuterated peptide D–P–3W62 in the absence or presence of lipid vesicles to detect structural changes to the peptide.

Supported lipid bilayers. SLBs for the NR experiments were created through fusion of tip sonicated small unilamellar vesicles (SUVs) as previously described.[39] Prior to the experiments, the lipid films were hydrated with MilliQ water to a concentration of 0.2 mg ml^{-1} and incubated for one hour at 35 °C. The solution was then sonicated using a tip sonicator for 10 min on a 50% duty cycle (5 s on/off). The solution was mixed 1 : 1 with a 4 mM CaCl$_2$ solution immediately prior to formation of lipid bilayers. The lipid suspension in CaCl$_2$ was injected into the NR cell and left for approximately 10 minutes to equilibrate prior to extensive rinsing with buffer. In all the experiments, both the clean surface and the pristine lipid bilayer were fully characterized prior to peptide injection.

2.2 Small angle neutron scattering

SANS experiments were carried out at the time-of-flight instrument Sans2d located at the STFC ISIS Neutron and Muon Source in Didcot, United Kingdom. The sample solutions were filled into quartz cuvettes with a sample thickness of 1 mm and placed into a thermostatted sample holder rack at 37 °C. Using neutron wavelengths 2–14 Å and a detector distance of 4 m, a Q range of 0.004–1 Å^{-1} ($Q = 4\pi \sin(\theta)/\lambda$ where θ is the scattering angle and λ is the neutron wavelength) was covered, with a resolution of roughly $dQ/Q \approx$ 2–10%. The data were reduced according to instrument standard protocols and fitted with a geometrical scattering model outlined in the ESI.†

2.3 Small angle X-ray scattering

The synchrotron SAXS data was collected at beamline P12 operated by EMBL Hamburg at the PETRA III storage ring (DESY, Hamburg, Germany).[40] The data was obtained using a radiation wavelength of 1.24 Å and a detector distance of 3.0 m, covering a Q range of 0.0032 Å^{-1} to 0.73 Å^{-1}. Data reduction was done automatically with the software available at the beam line and the 1D data were brought to absolute intensity scale using water as a primary standard.

The data were fitted with geometrical scattering models outlined in the ESI.†

2.4 Neutron reflectometry

NR measurements were performed using custom-made solid/liquid flow-through cells and 80 × 60 × 15 mm silicon crystals that were cleaned for 15 minutes in Piranha (3 : 1 H$_2$SO$_4$/H$_2$O$_2$) solution at 80 °C prior to the experiment. NR experiments

were performed on FIGARO[41] at Institut Laue-Langevin (Grenoble, France) and INTER at ISIS neutron source (Didcot, United Kingdom). Both instruments were used to record the time-of-flight reflectivity at two angles of incidence (Figaro: 0.8 and 3.2 degrees and Inter: 0.7 and 2.3 degrees) to cover the Q-range ∼0.01–0.33 Å^{-1}. The instrumental resolution for Figaro was set to $\frac{\Delta Q}{Q} = 7\%$ and Inter $\frac{\Delta Q}{Q} = 3\%$. The temperature, controlled by a circulating water bath, was maintained at 37 °C.

First, the silicon crystals were fully characterized in D_2O and H_2O to determine the structural parameters of the silicon oxide layer present on the surface (see ESI Fig. S1†). Second, SUVs were added and equilibrated in the cell for ∼10 min before rinsing with H–Tris. The resulting SLBs were characterized in three contrasts (D–Tris, H–Tris and a H/D–Tris mixture that matches the SLD of silicon, 62 : 38 v/v H_2O : D_2O, hereafter referred to as CMSi). Third, 10 ml solution (in D–Tris, CMSi and H–Tris sequentially) at the desired peptide concentration were injected into the cell at a flow rate of 1 ml min^{-1} using a syringe pump, and the resulting system was fully characterized in all three contrasts previously described. Finally, the membranes were measured again after extensive rinsing with H–Tris, CMSi and D–Tris. The use of different isotopic contrast conditions is known as the contrast variation method and it allows for simultaneous fitting of multiple reflectivity data sets, leading to reduced ambiguity and a more precise structural determination:[42] the different contrasts highlight or suppress different parts of the system. For example, the deuterated lipid tails and deuterated PEG moieties are suppressed (or matched out) while the peptide and lipid headgroups are highlighted in D–Tris.

All reflectivity profiles were analysed using the Motofit package taking into account the experimental resolution.[43] The NR data analysis provides information on the internal structure of thin films at an interface[44] and, in for SLBs, this includes the composition, thickness and coverage of the different layers that compose the membrane: inner heads, lipid tails and outer heads. For fit analysis, the optical matrix method was used where the surface is modelled with three layers: one for the lipid tail and two for the hydrated head groups representing the membrane as well as solvent which were allowed to penetrate the different layers freely before peptide addition. The roughness was constrained to be the same for each interface across the whole bilayer. Upon MDP addition, the reflectivity profiles were fitted using one additional layer to account for peptide fibres absorbed on top of the bilayer (with different orientations, see sketch in Fig. 3). SLD values are calculated and fixed as given in Table S1 in the ESI.†

The error of the fit parameters for the thickness and solvent amount was determined by the Monte Carlo error analysis fitting algorithm included in the Motofit package[43] and reflects the uncertainty of the fit. The area per molecule is calculated based on the fit parameters as

$$A_{\text{mol}} = \frac{V}{\varphi \times t}$$

where V is the volume of the lipid head/tail group, φ is the lipid volume fraction (1-solvent [%]) and t is the thickness of the

layer. The error in the area per molecule, δA_{mol}, was calculated as

$$\delta A_{\text{mol}} = \sqrt{\left(\frac{\delta\varphi}{\varphi}\right)^2 + \left(\frac{\delta t}{t}\right)^2}\, A_{\text{mol}}$$

The amount of peptide inserted into the different layers of the membrane is calculated from the changes in the SLD by

$$\frac{\left(\rho_{\text{observed}} - \rho_{\text{lipid}}\right)}{\left(\rho_{\text{peptide}} - \rho_{\text{lipid}}\right)} \times 0.01 \times \varphi$$

where ρ_{observed} is the fitted SLD of the lipid/peptide layer, and ρ_{lipid} and ρ_{peptide} is the theoretical SLD of lipid and peptide respectively.

3. Results and discussion

3.1 SANS/SAXS data confirming peptide–lipid interaction

Given that earlier results suggested that there were minimal interactions between MDPs and lipids,[22] we performed a range of small-angle neutron and X-ray scattering (SANS/SAXS) studies. We aimed to qualitatively detect whether the MDPs interact with the membranes by comparing the calculated average scattering profiles for the individual components and the actual mixtures. Here, SANS enables us to focus on the peptide structure in the presence of lipids, since the lipid vesicles were matched out by the solvents and therefore do not contribute to the scattering curve (Fig. 1A). The scattering intensity for the vesicles measured by SANS alone was very low, confirming that the vesicles were properly matched out under these conditions (64% H–Tris 36% D–Tris). In contrast, the SAXS data shows a clear scattering pattern characteristic for large unilamellar vesicles, and has been fitted with an established theoretical scattering model as described in a previous publication.[45] The neutron and X-ray scattering curves for the peptide solutions are similar to other reported results[26] and were also fitted with a scattering model for core–shell sheet structures. The models are briefly outlined in the ESI† where the fit parameters are reported as well.

The fact that the lipid vesicles are practically matched out in the SANS experiments enables us to highlight the scattering from peptide molecules and gives an indication of how their supramolecular structure changes upon mixing with lipid vesicles. Fig. 1A demonstrates that there is a slight change in the scattering signal when comparing the peptide in the presence ("mix") and absence of lipid vesicles ("calculated average"). This indicates an interaction between the peptides and the membrane slightly affecting the overall structure of the peptide. This is confirmed by complementary SAXS data on the exact same samples, where the scattering from the calculated average and the actual mixture differs (Fig. 1B). However, the exact peptide–lipid structures are hard to extract due to the orientational average and many components and degrees of freedom of the system. A tentative fit of the SANS data for the mixed sample, where the vesicles are practically matched out, with the scattering model used for the pure peptide yields structural
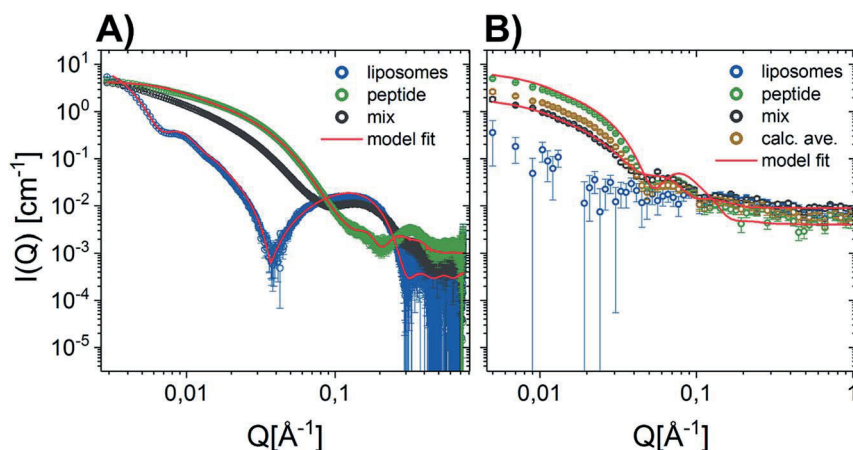
Fig. 1 Scattering data of D−P−3W62 mixed with match-out DMPC−DMPG lipid vesicles comparing the scattering from the pure vesicles, pure peptide, mix of peptide and vesicle 9 : 10 (weight ratio) and the calculated average (average scattering from peptide and lipids measured separately). Where possible, data have been fitted with geometrical scattering models (solid lines). (A) SANS results (B) SAXS results.
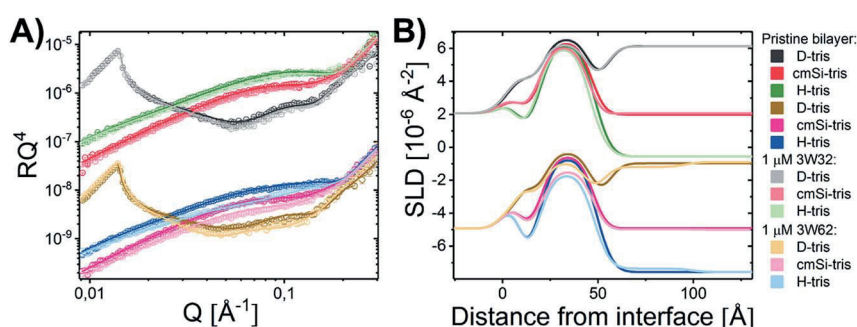

Fig. 2 (A) NR measurements of a DMPC−DMPG (all tail deuterated) SLB at a molar ratio of 9 : 1 before and after being exposed to 1 μM 3W32 and 3W62. Reflectivity profiles for the measurements plotted together with the best fit. (B) SLD profiles resulting from the fit analysis against distance from the interface for an SLB before and after exposure to peptide. The data has been shifted in y-axis for clarity.

parameters in good agreement with the pure peptide (compare Tables S3 in the ESI†) – with two exceptions: (1) while the free peptide in solution exhibits a uniform PEG shell of $d_a \sim d_b \sim 30$ Å thickness around the peptide fibre, the PEG distribution becomes asymmetric in the presence of lipid vesicles. The PEG layer on the longer side of the peptide core becomes compressed ($d_a \sim 13$ Å) while the PEG layer on the shorter fibre side is slightly extended ($d_b \sim 35$ Å). Assuming that the fibers adsorb on the surface of the vesicle, this result makes sense. (2) The apparent peptide concentration drops to ∼60% of the expected value, indicating that some peptide fibers disintegrate upon contact with the vesicles. While these findings are speculative given the structural complexity of the mixed vesicle/fibre sample, it provides additional information to the interactions. In order to investigate the membrane peptide structure, we therefore proceeded to NR.

3.2 Comparing the membrane interactions of shorter monomeric analogues with self-assembled peptide nanofibers

Quantitative details on the MDP−membrane interaction were instead obtained by NR. Here, we varied the peptide length,

presence of PEGylation and peptide concentration systematically. First, the peptide–membrane interaction of shorter monomeric peptides (3W32) and longer self-assembling peptides with the same basic motif as 3W32 (3W62) were used. Fig. 2 shows the reflectivity profile and best fits for DMPC/ DMPG bilayers at a 9 : 1 molar ratio before and after exposure to both of these peptides in H−Tris, cmSi and D−Tris contrast, together with the corresponding SLD profiles based on best fit analysis (Fig. 2B). The thickness and area per lipid calculated for the pristine bilayers (Table 1) are comparable with literature values based on MD simulations on DMPC/DMPG phospholipids[46–48] and previous NR results.[31]

Addition of the shorter 3W32 peptide had only a slight effect on the membrane structure (Fig. 2). The overall bilayer thickness was unaffected (when taking into account the fit error) by peptide addition. Some peptide insertion occurs as evidenced by the fact that the SLDs of the tail layer and the outer head layer in the SLBs changed upon peptide addition. Based on the changes in SLDs and the surface coverage, the amount of inserted peptide is calculated to be 5 vol% in the tail and 8 vol% in the outer head region (Table 1). These peptides exist as free chains in monomeric form in solution (as confirmed by SAXS

Table 1   Fitted parameters for tail-deuterated DMPC/DMPG membranes prior to and after exposure to 1 μM 3W32 and 3W62 peptide. The amount of peptide incorporated in the different layers is estimated based on the change in SLD observed after exposure to the peptide

| Layer	d [Å]	Coverage [%]	SLD [10^{-6} Å^{-2}]	Peptide vol%	d [Å]	Coverage [%]	SLD [10^{-6} Å^{-2}]	Peptide vol%
Pristine SLB								
Water	3	0	—	—	4 ± 1	0	—	—
Head (inner)	6 ± 1	85 ± 3	1.83	—	6 ± 1	83 ± 3	1.83	—
Tail	26 ± 1	95 ± 1	6.7	—	27 ± 1	94 ± 1	6.7	—
Head (upper)	6 ± 1	85 ± 3	1.83	—	6 ± 1	83 ± 3	1.83	—
Total membrane thickness (Å)	38 ± 2	$A_{mol} = 63 \pm 3$ Å^2			39 ± 2	$A_{mol} = 61 \pm 2$ Å^2		
SLB after addition of	**1 μM 3W32**				**1 μM 3W62**			
Water	3	0	—	—	4 ± 1	0	—	—
Head (inner)	6 ± 1	85 ± 3	1.83	—	6 ± 1	85 ± 3	1.83	—
Tail/peptide	26 ± 1	95 ± 1	6.25	5 ± 1	26 ± 1	90 ± 1	6.0	11 ± 1
Head/peptide	7 ± 1	75 ± 4	1.75	8 ± 2	6 ± 1	72 ± 4	1.78	13 ± 2
Total membrane thickness (Å)	39 ± 2		A_{mol} N/A		38 ± 2		A_{mol} N/A	
Peptide layer	—	—	—	—	46 ± 1	12 ± 1	$1.5/2.2/3.2 \pm 0.2^{a}$	100

[a] SLD of peptide taking into account D/H exchange, see ESI Table S1. Fixed parameters during fitting.

data presented in the ESI Fig. S3†) and probably they insert as single chains in the membrane similar to other AMPs having a random coil structure such as indolicidin.[31] However, when comparing to indolicidin, not only is the amount of inserted 3W32 in the hydrophobic lipid region significantly lower,[31] but 3W32 seems unable to penetrate into the inner head group of the bilayer at this concentration. This might suggest that the amount of hydrophobic leucine groups is too low to provide sufficient driving force for membrane penetration. This is also reflected in the lack of assembly observed in solution, where SAXS results show that 3W32 exist as random coils rather than nanosheets as the longer 3W62 peptides (see ESI† for more information).

Contrary to 3W32, the longer peptide 3W62 had a more pronounced effect on NR data and corresponding SLD profile of the membrane for the best fits as seen from Fig. 2. Peptide addition results in a slight shift in the reflectivity curve of the D–Tris curve to lower Q indicating a thickening of the peptide–lipid membrane. This thickening cannot be explained by a uniform increase in the lipid membrane thickness due to peptide penetration for 3W32. Rather, addition of an uneven adsorbed peptide layer on the membrane's surface is necessary: best fits are obtained when assuming a peptide layer absorbed on top of the SLB (comparative best fits for model with and without uneven adsorbed peptise layer are shown in ESI Fig. S4†). Indeed, the SLB thickness is unaffected by peptide addition although the SLB's SLD change reveal that there is about 11% and 14% peptide insertion in the tail region and the outer head group respectively. These amounts are comparable to the inserted amounts of the shorter peptide 3W32. The additional peptide layer is 46 ± 1 Å thick with a coverage of 12 vol%.

What is the origin of the extra layer on top of the SLB? As determined by SAXS, the dimensions of the peptide nanofibers are found to have an approximate cross-section of 26×58 Å^2 and a length of ≥500 Å with some dispersity (see Fig. S2 and
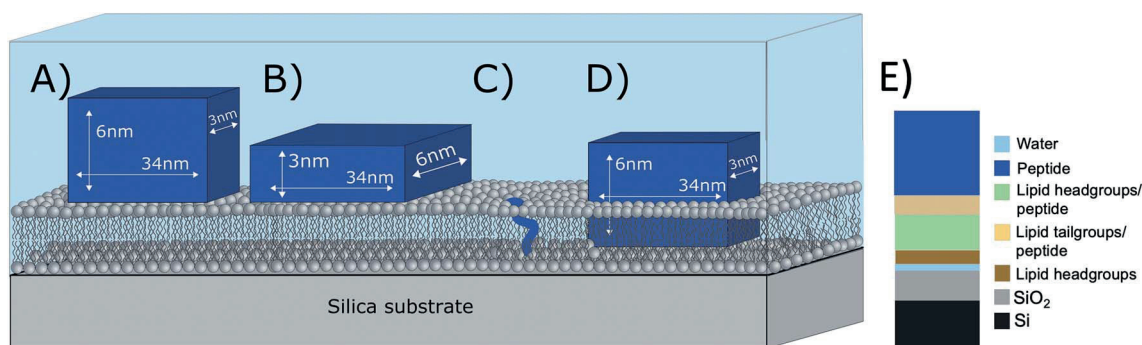
Fig. 3   Illustration of possible positioning of the peptide nanofibers on the SLBs based on NR fit results: (A) vertical orientation (B) horizontal orientation (C) monomeric insertion. (D) Embedded orientation. The peptide nanofibers were found to have the following cross-section 26×58 Å^2 with an estimated length ≥500 Å. For simplicity, the drawings are out-of-scale with respect to the long axis (peptide length). (E) Illustration on how the model used to analyse reflectivity data in Fig. 2B).

Table S3 of the ESI†). Thus, we can imagine the nanofiber as a thin and long cuboid. Taking into account the structure of the peptide[26] with the lysine residues located at the short end of the fibres, an orientation with the nanofiber cuboid standing on its thin side on the SLB should facilitate the favourable electrostatic interaction between the positively charged lysine and the negatively charged DMPG headgroups on the surface of the SLB (as illustrated in Fig. 3A and hereby renamed to "vertical orientation"). However, the thickness of the peptide layer determined by fit analysis of NR data was 46 ± 1 Å rather than ∼61 Å. One possible explanation is that the peptide sheets are randomly placed on both the "thin" (Fig. 3A), and "thick" face (Fig. 3B, hereby named to "horizontal orientation") or in a slightly tilted position. A more complex model dividing the layer into two distinct peptide layers allowing the density of each layer to vary freely is included in the ESI (Fig. S5 and Table S4†). These results give a combination of approximately 50 vol% of the adsorbed fibres positioning in the vertical orientation (∼60 Å thick layer) and 50 vol% in the horizontal orientation (∼30 Å thick layer) with the surface coverage of 15% and 7%, respectively. However, because the overall surface coverage of the absorbed bilayer is so low the resolution of the NR method used does not allow us to fully conclude on the orientation of the peptide at this low concentration. Monte Carlo error analysis (see ESI Fig. S6†) showed a significant level of correlation between the thickness of the two upper peptide layers using this model and therefor the simpler model of only one 46 ± 1 Å has been included in the manuscript.

The described peptide nanofiber adsorption on top of the SLB does not explain the changes observed in the SLD of the bilayer core and outer head layer. Rather this could be explained by a fraction of free peptides being able to penetrate into the bilayer either as smaller fragment of a fibre or as monomers (Fig. 3C). However, recent TR-SANS experiments on these nanofibers showed that no significant peptide release from the fibres occurred under similar experimental conditions[26] or by NMR in the presence of a lipid membrane.[22] For example, peptide exchange could take place directly between the absorbed peptide fibres on the surface and the lipid bilayer. In addition, the peptide fibres are formed due to intermolecular hydrogen bonds along the sheets and these bonds might be broken by competing hydrogen bonds with the phospholipid head groups.

An alternative scenario to explain the change in the SLB of the lipid bilayer is that some intact nanofibers penetrate into the SLB with its short axis facing down the membrane (Fig. 3D). This partly embedded position would explain the 46 ± 1 Å peptide layer observed on the surface of the membrane being thinner than the height of the peptide in the vertical orientation. In this scenario the peptide nanofibers are protruding 15 ± 5 Å from the SLB (with 7% surface coverage). The sum of the thickness of the membrane tail and outer head layer is approximately 33 Å, indicating that in the embedded position of the peptide the lysine residues on the bottom part of the peptide fibre positions in close proximity to the hydrated inner head region of the membrane but do not penetrate into them. This hypothesis concurs with results seen by negative stained TEM from a peptide with similar structure, where an intact peptide nanofibers was observed inserting into the outer membrane of *Escherichia coli* bacteria.[22] Additionally, this scenario concurs with the extreme physical stability of these peptides in the absence[26] and presence of a lipid.[22] Additional experiments such as Cryo-EM, SANS or fluorescence microscopy could be useful to further support whether peptide sheet penetration into the lipid membrane takes place or not. Beyond the static measurements to determine the structural peptide–lipid interaction, time-resolved NR measurements showed that the interaction happens quite fast, certainly in less than 5 minutes, after which the structure has reached equilibrium (see ESI Fig. S7†). In summary, the analysis of our NR data suggests that the self-assembled peptides have a stronger membrane interaction than the monomeric peptide, confirming the increased antibacterial activity for the former ones seen in the past by Xu and co-workers.[1]

3.3 The effect of PEGylation on the peptide–membrane interaction

Earlier results by Xu and co-workers showed that MDP PEGylation does not significantly affect the antimicrobial efficacy of the resulting nanofibers.[6] However, increased steric hindrance and solubility as well changes in hydrogen bonding in PEGylated MDPs might lead to changes in how these interact with
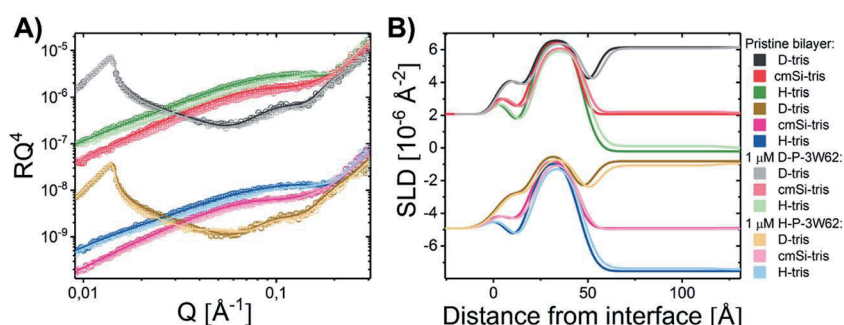

Fig. 4 (A) NR measurements of a DMPC–DMPG SLB before and after being exposed to 1 μM H−P−3W62 and D−P−3W62. Reflectivity profiles for the measurements plotted together with the best fit. (B) SLD profiles resulting from the fit analysis against distance from the interface for an SLB before and after exposure to peptide with buffer. The data has been shifted in y-axis for clarity.

Table 2 Fitted parameters for tail-deuterated DMPC/DMPG membranes prior to and after exposure to 1 μM H–P–3W62 and D–P–3W62 peptide. The amount of peptide incorporated in the different layers is estimated based on the change in SLD observed after exposure to the peptide

Layer	d [Å]	Coverage [%]	SLD [10^{-6} Å^{-2}]	Peptide [%]	d [Å]	Coverage [%]	SLD [10^{-6} Å^{-2}]	Peptide [%]
Pristine SLB								
Water	3	0	—	—	3 ± 1	0	—	—
Head (inner)	7 ± 1	82 ± 3	1.83	—	7 ± 1	84 ± 3	1.83	—
Tail	25 ± 1	94 ± 1	6.7	—	26 ± 1	98 ± 2	6.7	—
Head (upper)	7 ± 1	82 ± 3	1.83	—	7 ± 1	84 ± 3	1.83	—
Total membrane thickness (Å)	$\mathbf{39 \pm 2}$	$A_{mol} = \mathbf{62 \pm 3}$ Å^2			$\mathbf{40 \pm 2}$	$A_{mol} = \mathbf{60 \pm 3}$ Å^2		
SLB after addition of	**1 μM H–P–3W62**				**1 μM D–P–3W62**			
Water	4	100	—	—	4 ± 1	0	—	—
Head (inner)	7 ± 1	82 ± 3	1.83	—	6 ± 1	84 ± 3	1.83	—
Tail/peptide	25 ± 1	92 ± 1	6.39	6 ± 1	26 ± 1	92 ± 2	6.37	6 ± 1
Head/peptide	7 ± 1	70 ± 4	1.56	a	7 ± 1	68 ± 3	1.95	a
Total membrane thickness (Å)	$\mathbf{39 \pm 2}$		A_{mol} N/A		$\mathbf{39s \pm 2}$		A_{mol} N/A	
Peptide layer	64 ± 3	6 ± 1	$1.1/1.4/1.9 \pm 0.3$		64 ± 3	6 ± 1	$4.3/4.6/5.2 \pm 0.2$	
PEG layer	28 ± 4	2 ± 1	0.7 ± 0.3		28 ± 4	2 ± 1	7.2 ± 0.4	

a Cannot be determined with accuracy due to lack of contrast.

biological membranes. To explore such effects, a PEGylated version of 3W62 was synthesized in both hydrogenated or deuterated PEG versions and are hereby named as H–P–3W62 and D–P–3W62 respectively. These peptides (1 μM) were added to pre-formed DMPC–DMPG SLB and NR data were collected (Fig. 4). The use of deuterated and hydrogenated PEGylated peptides enables more precise determination of the positioning of PEG upon peptide–membrane interaction since it provides, otherwise non-existing, contrast between the peptide and the PEG group. During data analysis, co-refinement of both the H– and D–P–3W62 systems was not possible due to small differences in the initial underlying silica surfaces and pristine bilayer structure prior to peptide addition. Across the replicates,

the lipid membrane thickness of the pristine bilayers (compare Tables 1 and 2) was comparable although the surface coverage was slightly higher for one of the samples (B in Table 2 with 98% coverage while the other SLBs had 94–95% coverage).

For both H– and D–P–3W62, only relatively small changes in the reflectivity profiles were observed (Fig. 4). However, the same model applied for the non-PEGylated peptide allowed to obtain satisfactory fits for the PEGylated peptides (Fig. 4): there was peptide adsorption on the membrane's surface, peptide insertion into the membrane as well as a slight membrane thickening. However, the extent of adsorption was lower for PEGylated peptides: the additional peptide layer was ~64 Å thick and presented a SLD in between that of pure peptide and
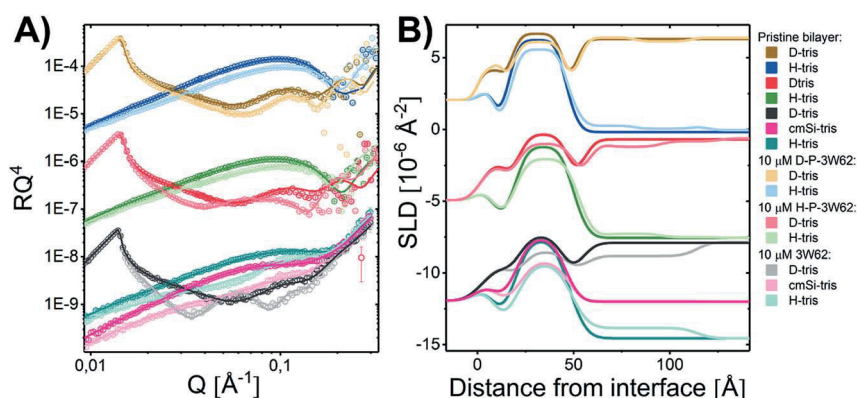
Fig. 5 (A) NR measurements of a DMPC–DMPG SLB before and after being exposed to 10 μM 3W62 (measured at Inter beamline, ISIS, UK), H–P–3W6 and D–P–3W62 (measured at Figaro beamline at ILL, France). Reflectivity profiles for the measurements plotted together with the best fit. The differences at high Q for the two upper curves arise from different background subtraction at Figaro beamline at ILL as compared to Inter. (B) SLD profiles resulting from the fit analysis against distance from the interface for an SLB before and after exposure to peptide with buffer. The data have been shifted in y-axis for clarity.

Table 3 Fitted parameters for tail-deuterated DMPC/DMPG membranes prior to and after exposure to 10 μM 3W62, D–P–3W62 and D–P–3W62 peptide. The amount of peptide incorporated in the different layers is estimated based on the change in SLD observed after exposure to the peptide

Layer	10 μM 3W62				10 μM H–P–3W62				10 μM D–P–3W62			
	d [Å]	Coverage [%]	SLD [10^{-6} Å^{-2}]	Peptide [%]	d [Å]	Coverage [%]	SLD [10^{-6} Å^{-2}]	Peptide [%]	d [Å]	Coverage [%]	SLD [10^{-6} Å^{-2}]	Peptide [%]
Pristine SLB												
Water	3	0	—	—	2 ± 1	0	—	—	3	0	—	—
Head (inner)	6 ± 1	87 ± 3	1.83	—	6 ± 1	80 ± 3	1.83	—	6 ± 1	82 ± 3	1.83	—
Tail	26 ± 1	96 ± 1	6.7	—	27 ± 1	92 ± 2	6.7	—	28 ± 1	96 ± 1	6.7	—
Head (upper)	6 ± 1	87 ± 3	1.83	—	6 ± 1	80 ± 3	1.83	—	6 ± 1	82 ± 3	1.83	—
Total membrane thickness (Å)	38 ± 2	A_{mol} = 61 ± 3 Å²			39 ± 2	A_{mol} = 60 ± 3 Å²			40 ± 2	A_{mol} = 60 ± 3 Å²		
SLB after addition of												
Water	3	0	—	—	3 ± 1	0	1.83	—	3	0	1.83	—
Head (inner)	7 ± 1	82 ± 3	1.8	—	6 ± 1	84 ± 3	1.83	—	6 ± 1	82 ± 3	1.81	—
Tail/peptide	26 ± 1	88 ± 1	5.9	9 ± 4	26 ± 1	87 ± 2	6.38	14 ± 1	28 ± 1	90 ± 1	6.37	5 ± 1
Head/peptide	7 ± 1	79 ± 4	1.7	14 ± 1	7 ± 1	68 ± 3	1.74	36 ± 2	7 ± 1	76 ± 4	2.3	6 ± 1
Total membrane thickness (Å)	41 ± 2	A_{mol} N/A			39 ± 2	A_{mol} N/A			40 ± 2	A_{mol} N/A		
First layer	60 ± 1	34 ± 1	1.5/2.2/3.2 ± 0.2		8 ± 2	5 ± 1	0.7 ± 0.4	5 ± 1	5 ± 3	5 ± 1	0.7 ± 0.5	7 ± 0.5
Second layer	—	—	—		29 ± 4	14 ± 1	2.1 ± 0.3		29 ± 4	10 ± 1	2.1 ± 0.4	
Third layer	—	—	—		27 ± 4	4 ± 1	0.7 ± 0.3		26 ± 4	2 ± 1	0.7 ± 0.5	

pure PEG. On top of this mixed peptide-PEG layer, there was an additional 28 Å layer with an SLD matching pure PEG. This suggests that the peptide nanosheets absorbed to the surface in the vertical orientation (Fig. 3A) with a highly hydrated PEG layer facing the bulk solution. The size of the PEG layer is in very good agreement with SAXS results for this peptide showing a thickness of ∼30 Å.[26] The peptide layer's surface coverage was significantly lower than for the non-PEGylated 3W62 (12%). This might be a consequence of the increased steric hindrance and the increased peptide solubility due PEGylation making the peptide nanofibers less prone to interact with the hydrophobic part of the membrane.

Interestingly, the SLD of both the lipid core and outer lipid headgroup changed upon peptide addition (Table 2). This decrease in SLD is likely due to peptide penetration since it is unlikely for the hydrophilic PEG groups to be fully immersed into the lipid membrane core and the change in SLD was similar for both H– and D–P–3W62 (6.39×10^{-6} Å^{-2} or 6.37×10^{-6} Å^{-2}, respectively). Assuming that only peptide integrates into the SLB's core, the estimated peptide insertion is 6%, and thus lower than for the non-PEGylated peptide of the same length (11%).

In contrast to the change in SLD of the SLB core region, the SLD of the outer lipid headgroup differed for H–P–3W62 (a decrease from to 1.56×10^{-6} Å^{-2}) and D–P–3W62 (an increase to 1.95×10^{-6} Å^{-2}). Thus, PEG inserted into the headgroup region leading to a net SLD decrease in this layer (H-PEG has a lower SLD), while the opposite is true for the deuterated PEG (with higher SLD). This suggest that the peptide inserts into the hydrophobic core of the membrane with the charged lysins positioned on the surface of the membrane partially embedded in the hydrated lipid head groups with PEG group sticking out. This suggests that the sheet nanostructures probably are destabilised and peptide insertion into the membrane probably occurs either as single chains or smaller fragments. Substantial interaction between PEG and lipid membranes with POPC and POPG lipids was reported earlier by Zhang W. and co-workers and suggested to arise from hydrogen bonding between the PEG polymer and the lipid headgroups.[49] In summary, some peptide insertion and adsorption onto lipid membranes occurs although to a lower extent that non-PEGylated peptides, even though peptide PEGylation was reported to have no effect on the antimicrobial activity of the peptides.[6]

3.4 The effect of concentration on the peptide–membrane interaction

To determine whether the membrane interaction for these peptides is cooperative or concentration dependent, separate experiments were performed at 10 μM. The reflectivity profiles for 3W62, H–P–3W62 and D–P–3W62 are shown in Fig. 5A. All pristine membranes were 38–40 Å thick with surface coverage ranging between 92 and 96%. The changes in the reflectivity profiles for the membranes before and after 10 μM peptide addition were substantially larger than for 1 μM. When comparing the PEGylated and non-PEGylated peptide it is obvious that the latter (Fig. 4A) induced a larger change in

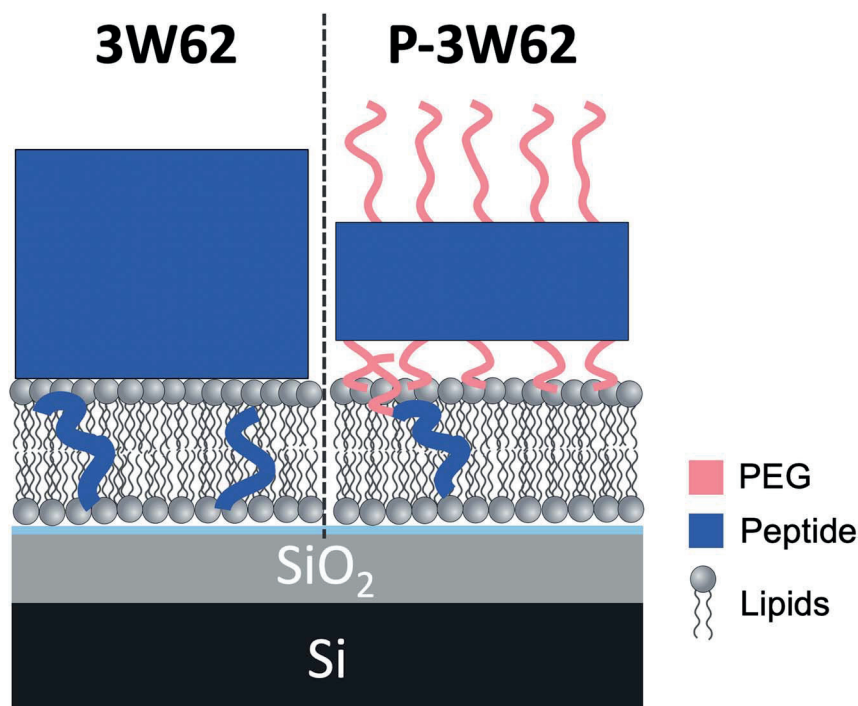Fig. 6   Illustration showing a comparison of the peptide position for 10 µM 3W62 and P−3W62 based on fit results of NR profiles shown in Fig. 5.

reflectivity for the D–Tris contrast. Based on fit analysis of the data for the non-PEGylated peptide 3W62, significant peptide adsorption on the membrane's surface occurred (as seen from the SLD profile in Fig. 5B): the peptide layer had a surface coverage of 34%. Moreover, substantial peptide insertion in the membrane occurred (9% in the inner headgroup leaflet, 12% in the core and 35% in the outer headgroup leaflet) with consequential lipid removal (the coverage of the tail region decreases from 96 to 88%). Similar concentration dependent effects were observed for other AMPs in the past.[31,33] The surface coverage of the additional nanosheet layer of the 3W62 peptide is significantly higher when comparing with the 1 µM sample of the same peptide (35% compared to 12%). The thickness of the peptide layer of 60 Å corresponds with the peptide sheet adsorbing in the vertical orientation (as illustrated in Fig. 3A). Comparing with the lower concentration, we see that the higher concentration affects the inner head group (see Table 3) which seems to be adsorbing deeper into the membrane either as intact sheets, as fragments or as monomers.

As for the data described in Section 3.3 on the PEGylated peptides, the change in the membrane core SLD seems to be mainly due to peptide insertion and not PEG (estimated to be 5 ± 1% for H–P–3W62 and 6 ± 1% for D–P–3W62 as seen in Table 3), while a combination of PEG and peptide positions in the head region of the outer leaflet. Interestingly, the estimated amount of inserted peptide for the PEGylated peptide seems to be independent of the concentration in this range. This is opposed to the non-PEGylated peptide which exhibited a much more concentration dependent insertion. This suggests a concentration threshold above which there is no further

nanosheet destabilization takes place possibly due to steric effects caused by the large PEG chain.

While the inserted peptide amount seems to be concentration independent, the adsorbed amount of peptide on top of the SLB increased with peptide concentration. Due to the increased amount of adsorbed nanosheets on the surface with increased peptide concentration, the independent positioning of PEG and peptide can be resolved in this case: there is a three-layer system comprised of a relative thin inner PEG layer (5–8 Å), followed by a peptide layer (29 Å) and a thicker outer PEG layer (26–27 Å) (see illustration in Fig. 6). Thus, at lower peptide concentration, similar mixed PEG/peptide layer structure should be found but cannot be resolved due to low surface concentration. This suggest a horizontal orientation positioning (as illustrated in Fig. 3B) which enables strong interaction between the PEG closest to the membrane and the lipid headgroups, leading to both partial insertion and lateral extension of PEG chains over the membrane surface. These results agree with the SANS data presented in Fig. 1 where a thinning of the PEG layer (a_p) was observed when comparing data from pure peptide with data on mixed peptide–liposomes samples. Moreover, the outer PEG layer is highly hydrated and extend for 26–27 Å regardless of concentration in agreement with the dimensions found for these peptides by SAXS (hydrated PEG layer of ∼30 Å).[6,26]

4.   Conclusions

Combining data from SANS, SAXS and NR enabled us to study the peptide–membrane interactions of MDPs, varying both the peptide's length and concentration as well as the effect of PEGylation. The results suggested that the peptide interaction is

stronger for the longer peptides that self-assemble into well-defined fiber as compared to the shorter monomeric peptides. This supports the claim that self-assembled peptides have a higher antimicrobial activity. For all self-assembling peptides regardless of concentration, additional peptide layers on the surface of the SLB had to be added to fully explain the reflectivity profiles. In addition, insertion of the peptides into the core of the membrane had to be taken into account into the modelling. Addition of PEG groups to the peptide molecules seemed to decrease the peptide–membrane interaction as compared to non-PEGylated peptide. This observation does not support the retained antimicrobial activity seen in the past, indicating that the mechanism of the PEGylated peptide might not be only based on the membrane interaction. However, decreased membrane interaction would explain why the hemolytic properties decrease for the PEGylated peptides. When increasing the peptide concentration, the changes in the reflectivity profiles was more pronounced. Due to the use of peptide conjugates with both deuterated and hydrogenated PEG the spatial distribution of each component could be determined specifically using contrast variation. The PEGylated peptide molecules inserted into the membrane with only the peptide part in the lipid tail region, while a combination of peptide and PEG chains was found in the hydrated lipid headgroup region. Together the data suggested that the formation of supramolecular peptide structure increase while PEGylation decrease lipid interactions. Our results indicate that the peptide fibre structure is partly destabilized when added to phospholipid membranes, contrary to the extraordinary physical stability of the assembled peptides in the absence of lipids as previously reported.[26] However, more specific peptide–lipid exchange studies would provide further insight into how different lipids affect the peptide structure.

Conflicts of interest

There are no conflicts to declare.

Acknowledgements

References

1 D. Xu, L. Jiang, A. Singh, D. Dustin, M. Yang, L. Liu, R. Lund, T. J. Sellati and H. Dong, *Chem. Commun.*, 2015, **51**, 1289–1292.

2 S. M. Häffner and M. Malmsten, *Curr. Opin. Colloid Interface Sci.*, 2018, **38**, 57–79.

3 C. E. Dempsey, S. Ueno and M. B. Avison, *Biochemistry*, 2003, **42**, 402–409.

4 S. B. Tencza, D. J. Creighton, T. Yuan, H. J. Vogel, R. C. Montelaro and T. A. Mietzner, *J. Antimicrob. Chemother.*, 1999, **44**, 33–41.

5 L. Chen and J. F. Liang, *Biomacromolecules*, 2013, **14**, 2326–2331.

6 D. Xu, Q. Ran, Y. Xiang, L. Jiang, B. M. Smith, F. Bou-Abdallah, R. Lund, Z. Li and H. Dong, *RSC Adv.*, 2016, **6**, 15911–15919.

7 P. V. Panteleev, M. Y. Myshkin, Z. O. Shenkarev and T. V. Ovchinnikova, *Biochem. Biophys. Res. Commun.*, 2017, **482**, 1320–1326.

8 W. Chen, S. Yang, S. Li, J. C. Lang, C. Mao, P. Kroll, L. Tang and H. Dong, *ACS Appl. Mater. Interfaces*, 2019, **11**, 28681–28689.

9 M. Beter, H. K. Kara, A. E. Topal, A. Dana, A. B. Tekinay and M. O. Guler, *Mol. Pharm.*, 2017, **14**, 3660–3668.

10 R. Chang, K. Subramanian, M. Wang and T. J. Webster, *ACS Appl. Mater. Interfaces*, 2017, **9**, 22350–22360.

11 A. F. Chu-Kung, R. Nguyen, K. N. Bozzelli and M. Tirrell, *J. Colloid Interface Sci.*, 2010, **345**, 160–167.

12 N. Molchanova, J. E. Nielsen, K. Sørensen, B. K. Prabhala, P. R. Hansen, R. Lund, A. Barron and H. Jenssen, *Sci. Rep.*, 2020, **10**, 14805.

13 R. E. Hancock and A. Rozek, *FEMS Microbiol. Lett.*, 2002, **206**, 143–149.

14 K. A. Brogden, *Nat. Rev. Microbiol.*, 2005, **3**, 238–250.

15 X. Tian, F. Sun, X. R. Zhou, S. Z. Luo and L. Chen, *J. Pept. Sci.*, 2015, **21**, 530–539.

16 B. Bechinger and K. Lohner, *Biochim. Biophys. Acta, Biomembr.*, 2006, **1758**, 1529–1539.

17 L. Chen, N. Patrone and J. F. Liang, *Biomacromolecules*, 2012, **13**, 3327–3333.

18 H. Sato and J. B. Feix, *Biochim. Biophys. Acta, Biomembr.*, 2006, **1758**, 1245–1256.

19 M.-A. Sani and F. Separovic, *Acc. Chem. Res.*, 2016, **49**, 1130–1138.

20 H. Dong, S. E. Paramonov, L. Aulisa, E. L. Bakota and J. D. Hartgerink, *J. Am. Chem. Soc.*, 2007, **129**, 12468–12472.

21 M. Yang, D. Xu, L. Jiang, L. Zhang, D. Dustin, R. Lund, L. Liu and H. Dong, *Chem. Commun.*, 2014, **50**, 4827–4830.

22 D. Xu, W. Chen, Y. J. Tobin-Miyaji, C. R. Sturge, S. Yang, B. Elmore, A. Singh, C. Pybus, D. E. Greenberg and T. J. Sellati, *ACS Infect. Dis.*, 2018, **4**, 1327–1335.

23 E. Kokkoli, A. Mardilovich, A. Wedekind, E. L. Rexeisen, A. Garg and J. A. Craig, *Soft Matter*, 2006, **2**, 1015–1024.

24 L. Lombardi, A. Falanga, V. Del Genio and S. Galdiero, *Pharmaceutics*, 2019, **11**, 166.

25 Z. L. Tyrrell, Y. Shen and M. Radosz, *Prog. Polym. Sci.*, 2010, **35**, 1128–1143.

26 N. König, J. E. Nielsen, L. Willner, A. Radulescu, N. Mahmoudi, H. Dong and R. Lund, Extraordinary physical stability of beta-sheet nanofibers formed by self-assembly of a de novo antimicrobial peptide confirmed by small-angle scattering techniques, 2020, submitted.

27 S. Singh, P. Papareddy, M. Mörgelin, A. Schmidtchen and M. Malmsten, *Biomacromolecules*, 2014, **15**, 1337–1345.

28 P. L. Turecek, M. J. Bossard, F. Schoetens and I. A. Ivens, *J. Pharm. Sci.*, 2016, **105**, 460–475.

29 A. D. AlQahtani, D. O'Connor, A. Domling and S. K. Goda, *Biomed. Pharmacother.*, 2019, **113**, 108750.

30 M. Roberts, M. Bentley and J. Harris, *Adv. Drug Delivery Rev.*, 2002, **54**, 459–476.

31 J. E. Nielsen, T. K. Lind, A. Lone, Y. Gerelli, P. R. Hansen, H. Jenssen, M. Cárdenas and R. Lund, *Biochim. Biophys. Acta, Biomembr.*, 2019, **1861**, 1355–1364.

32 T. K. Lind, L. Darre, C. Domene, Z. Urbanczyk-Lipkowska, M. Cárdenas and H. Wacklin, *Biochim. Biophys. Acta, Biomembr.*, 2015, **1848**, 2075–2084.

33 A. Åkesson, T. K. Lind, R. Barker, A. Hughes and M. Cárdenas, *Langmuir*, 2012, **28**, 13025–13033.

34 D. I. Fernandez, A. P. Le Brun, T. C. Whitwell, M.-A. Sani, M. James and F. Separovic, *Phys. Chem. Chem. Phys.*, 2012, **14**, 15739–15751.

35 A. Martel, L. Antony, Y. Gerelli, L. Porcar, A. Fluitt, K. Hoffmann, I. Kiesel, M. Vivaudou, G. Fragneto and J. J. De Pablo, *J. Am. Chem. Soc.*, 2016, **139**, 137–148.

36 D. I. Fernandez, A. P. Le Brun, T.-H. Lee, P. Bansal, M.-I. Aguilar, M. James and F. Separovic, *Eur. Biophys. J.*, 2013, **42**, 47–59.

37 R. Nordström, K. L. Browning, E. Parra-Ortiz, L. S. E. Damgaard, S. M. Häffner, A. Maestro, R. A. Campbell, J. F. Cooper and M. Malmsten, *J. Colloid Interface Sci.*, 2020, **562**, 322–332.

38 L. A. Clifton, R. A. Campbell, F. Sebastiani, J. Campos-Terán, J. F. Gonzalez-Martinez, S. Björklund, J. Sotres and M. Cárdenas, *Adv. Colloid Interface Sci.*, 2020, 102118.

39 B. W. König, S. Krueger, W. Orts, C. F. Majkrzak, N. F. Berk, J. Silverton and K. Gawrisch, *Langmuir*, 1996, **12**, 1343–1350.

40 C. E. Blanchet, A. Spilotros, F. Schwemmer, M. A. Graewert, A. Kikhney, C. M. Jeffries, D. Franke, D. Mark, R. Zengerle and F. Cipriani, *J. Appl. Crystallogr.*, 2015, **48**, 431–443.

41 R. Campbell, H. Wacklin, I. Sutton, R. Cubitt and G. Fragneto, *Eur. Phys. J. Plus*, 2011, **126**, 107.

42 T. Crowley, E. Lee, E. Simister and R. Thomas, *Phys. B*, 1991, **173**, 143–156.

43 A. Nelson, *J. Appl. Crystallogr.*, 2006, **39**, 273–276.

44 J. Penfold and R. Thomas, *J. Phys.: Condens. Matter*, 1990, **2**, 1369.

45 J. E. Nielsen, V. A. Bjørnestad and R. Lund, *Soft Matter*, 2018, **14**, 8750–8763.

46 N. Kučerka, Y. Liu, N. Chu, H. I. Petrache, S. Tristram-Nagle and J. F. Nagle, *Biophys. J.*, 2005, **88**, 2626–2637.

47 J. Pan, F. A. Heberle, S. Tristram-Nagle, M. Szymanski, M. Koepfinger, J. Katsaras and N. Kučerka, *Biochim. Biophys. Acta, Biomembr.*, 2012, **1818**, 2135–2148.

48 N. Kučerka, M.-P. Nieh and J. Katsaras, *Biochim. Biophys. Acta, Biomembr.*, 2011, **1808**, 2761–2771.

49 W. Zhang, J. M. Metzger, B. J. Hackel, F. S. Bates and T. P. Lodge, *J. Phys. Chem. B*, 2020, **124**(12), 2417–2424.

SUPPLEMENTARY INFORMATION

Lipid Membrane Interactions of Self-assembling antimicrobial nanofibers: effect of PEGylation

Josefine Eilsø Nielsen[1], Nico König[1,2], Su Yang[3], Maximilian WA Skoda[4], Armando Maestro[5], He Dong[3], Marité Cardenas[6], and Reidar Lund*[1]

[1]Department of Chemistry, University of Oslo, 0315 Oslo, Norway
[2] Jülich Centre for Neutron Science (JCNS) and Institute for Complex Systems (ICS), Forschungszentrum Jülich GmbH, 52425 Jülich, Germany
[3]Department of Chemistry & Biochemistry, The University of Texas at Arlington, Arlington, Texas 76019, United States
[4]ISIS-STFC, Rutherford Appleton Laboratory, Chilton, Oxon OX11 0QX, United Kingdom
[5]Institut Laue - Langevin, 38000 Grenoble, France
[6]Biofilms Research Center for Biointerfaces, Department of Biomedical Science, Health and Society, Malmö University, 20506 Malmö, Sweden

*Corresponding author: reidar.lund@kjemi.uio.no

Table S1. Theoretical SLDs for the lipids and peptide used in this study.

|	Neutron SLD $[10^{-6}\ \text{Å}^{-2}]$[a]
d54DMPC	
Head	1.84
Tail	6.7
d54DMPG	
Head	2.46
Tail	6.7
d54DMPC:d54DMPG 9:1	
Head	1.83
Tail	6.7
3W32	1.54[b]/2.15[c]/3.14[d]
3W62	1.54[b]/2.17[c]/3.26[d]

[a]*Calculated from the molecular component volume (based on MD simulations[1, 2]) and neutron scattering lengths.*
[b]*Calculated from the peptide molecular volume and the neutron scattering length.*
[c]*Calculated assuming exchange of 38% labile hydrogen atoms to deuterium in cmSi*
[d]*Calculated assuming exchange of all labile hydrogen atoms to deuterium in D_2O*

Neutron reflectivity data on pure silica crystals:
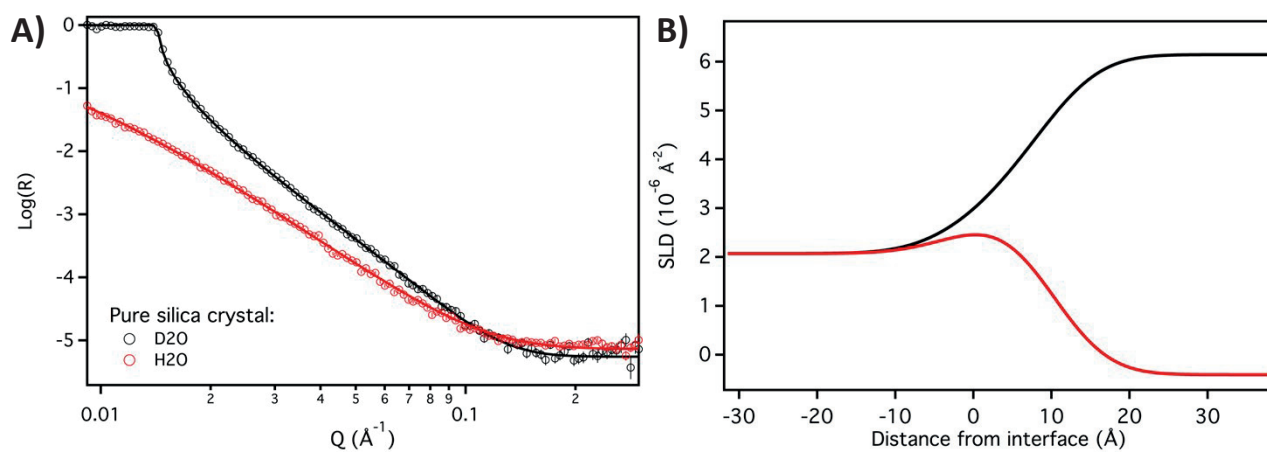
Figure S1. *A) Neutron reflectivity profiles on pure silica crystals in H_2O and D_2O plotted together with best fit. B) SLD profiles calculated from best fit of reflectivity profiles.*

Details on the small-angle scattering analysis

The SAXS data of the pure lipid vesicles shown in Figure 1A in the main manuscript were fitted with an elaborated model that is presented in detail in reference [3]. The fit parameters are given in Table S2. The SAXS and SANS data of the pure peptide solution (Figure 1 in the main manuscript) were fitted simultaneously with a core-shell-shell model that is sketched in Figure S2 and presented in detail in reference [4]. The model is an elongated prism with a rectangular cross-section. The hydrophobic tryptophan and leucine residues form the fiber core (grey) of dimensions a_i and b_i. It is surrounded by the hydrophilic peptide moieties, the backbone as well as the lysine and glutamine residues (blue), which have a thickness of a_o and b_o, respectively. Finally, PEG forms a polymer shell around the peptide fiber (pink), with thicknesses a_p and b_p, respectively. This model was also used to tentatively fit the SANS data of a peptide/vesicle mixture, where the vesicles were matched out so that the scattering originates from the peptide molecules alone. However, this model is a strong simplification and cannot account for all factors implied by the fiber-vesicle interaction, so the fit results can only serve as hints. All fit parameters are given in Table S3.

Table S2. Fit parameters of the pure vesicle SAXS data.

Parameter	Fit result
Radius	450
Area	60.4*
z_{CH3}	0*
z_{CH2o}	14.1 ±0.2**
z_{CH2i}	-14.0±0.2**
z_{CGo}	16.0±0.4**
z_{CGi}	-15.8±0.4**
Z_{HGo}	19.5±0.2**
Z_{HGi}	-19.3±0.2**
σ_{CH3}	2.3*
σ_{CH2}	4.7±0.3
σ_{CG}	2.1±0.2
σ_{HG}	4.1±0.5
VL	1123
V_{CH2}	24.8
V_{CG}	153*
V_{HG}	176
Rg PEG	15*
dcorr	-7
σ_{SD}	0.22

*Hard constrained parameters are designated by * and soft constrained by limits in fitting regime indicated by **. The units for all numbers carry the appropriate power of Å.*
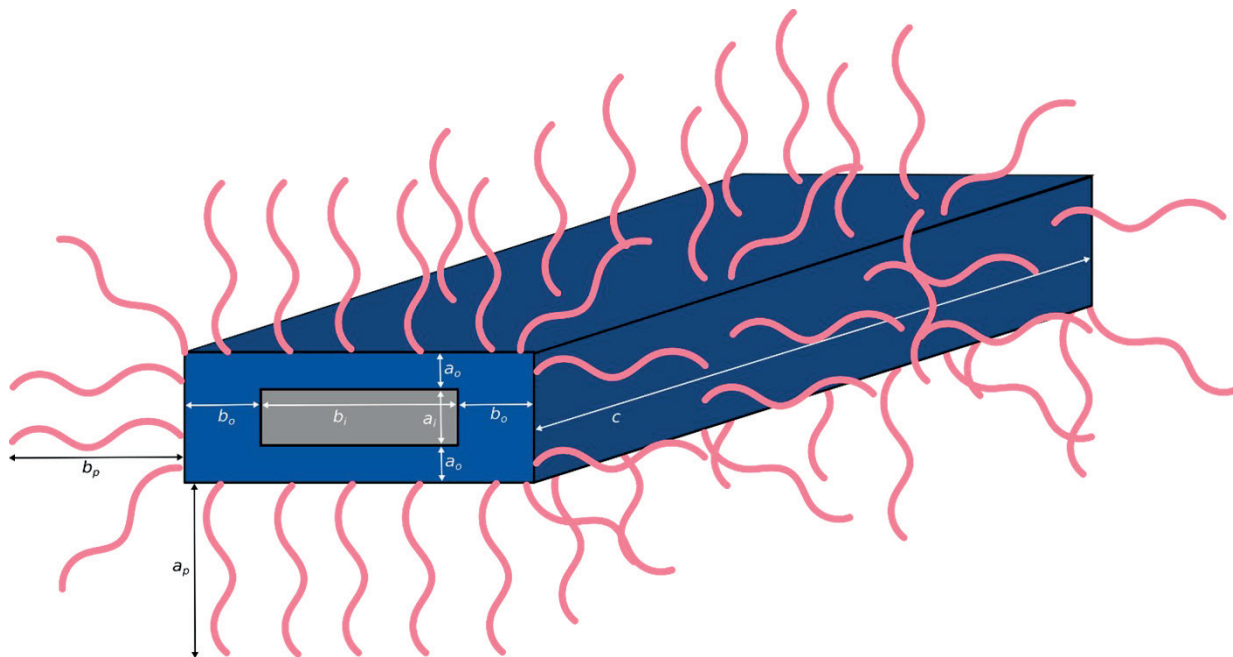
Figure S2. *Sketch of the geometrical scattering model for the peptide fibers.*

Table S3. Fit parameters of the peptide SAS data, using the model sketched in Figure S2.

|	Pure peptide (SAXS)[a]	Pure peptide (SANS)[a]	Peptide in mix (SANS)
ai (Å)	9.0	9.0	8.5
ao (Å)	8.4	8.4	10.0
bi (Å)	44.3	44.3	47.7
bo (Å)	6.6	6.6	10.0
ap (Å)	29.1	29.1	12.9
bp (Å)	31.4	31.4	35.9
c (Å)	500	500	490
concentration (mg/mL)	11.0	11.0	3.0
Mpep,i (Da)	473	473	473
Mpep,o (Da)	1851	1851	1851
Mpol (Da)	2400	2400	2400
dpep,i (g/mL)	0.95	0.95	0.95
dpep,o (g/mL)	1.36	1.36	1.36
dpol (g/mL)	1.30	1.30	1.30
bpep,i (cm)	7.52E-11	-3.13E-13	-3.13E-13
bpep,o (cm)	2.79E-10	4.42E-11	4.42E-11
bpol (cm)	3.38E-10	2.22E-10	2.22E-10

[a]*Fitted simultaneously.*

**Scattering data on 3W32 peptide showing a Gaussian free chain structure in solution up to concentration 10 mg/ml.**
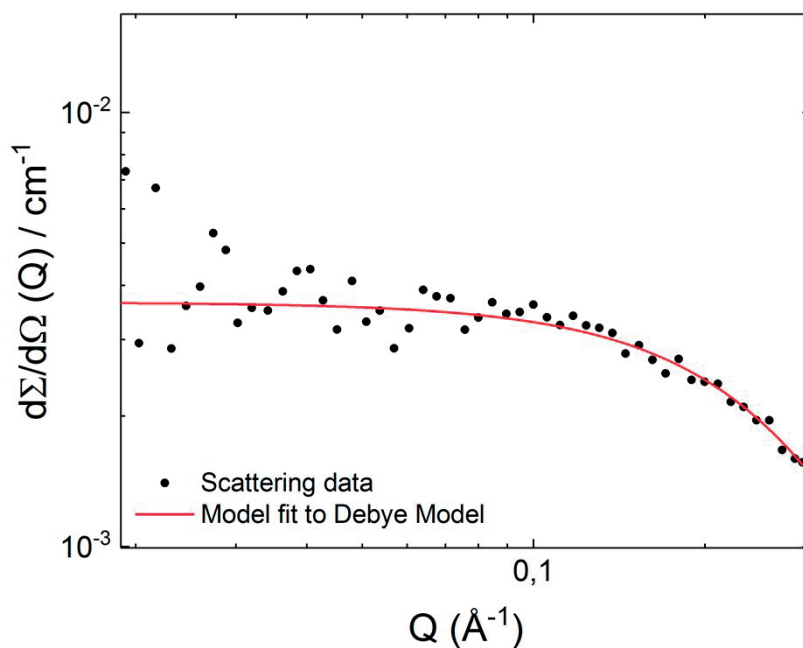
Figure S3. SAXS data on 3W32 in solution at 5 mg/ml measured at a Bruker Nanostar lab-SAXS. Model fit using a Debye scattering model shows a Rg of 5.6 Å.

Simulation of model with and without absorbed peptide layers on the surface of the membrane:
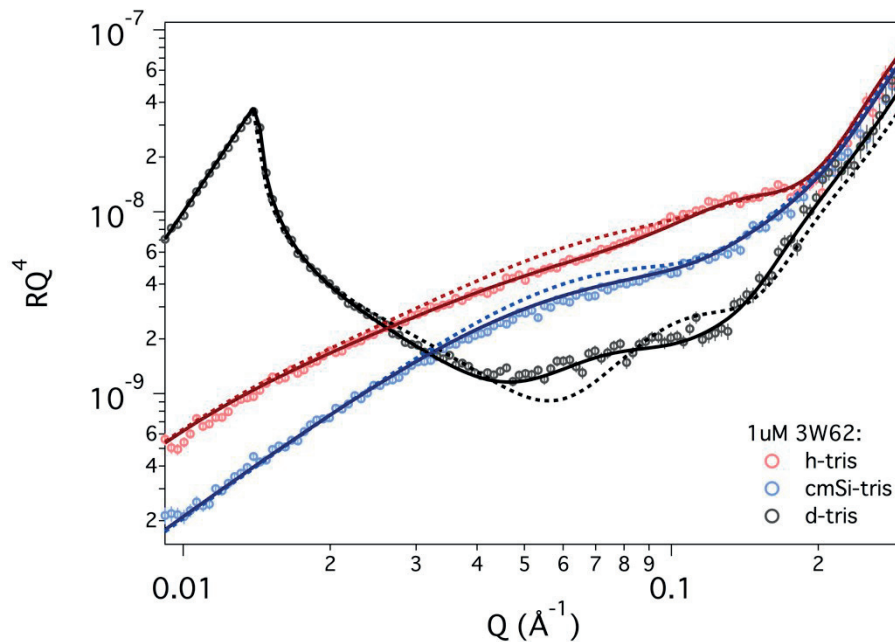
Figure S4. Reflectivity profile for DMPC-DMPG SLB at a molar ratio of 9:1 after being exposed to 1 μM 3W62. Dotted line represents best fit using a 3 layer model with incorporation of peptide in membrane while solid line represent best fit using a 4 layer model (illustrated in Figure 3) with an additional peptide layers on the surface om the membrane. The data has been plotted as RQ⁴ versus Q to better visualise the difference.

Comparisson of 4 and 5 layer model with absorbed peptide layers on the surface of the membrane:
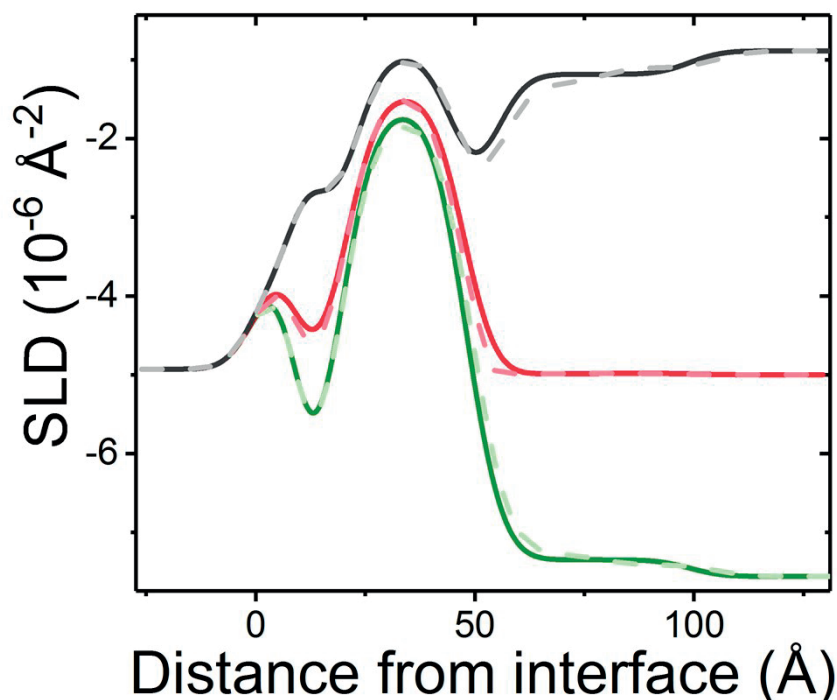
Figure S5. SLD profile for DMPC-DMPG SLB at a molar ratio of 9:1 after being exposed to 1 μM 3W62. Solid line represents best fit using a 4 layer model with one 46 Å peptide layer on the surface of the membrane while dotted line represent best fit using a 5 layer model with two additional peptide layers of 25 and 27 Å on the surface om the membrane.

Table S4. *Fitted parameters for tail-deuterated DMPC/DMPG membranes prior to and after exposure to 1 μM 3W62 peptide using the 5 layer model. The amount of peptide incorporated in the different layers is estimated based on the change in SLD observed after exposure to the peptide.*

Layer	d [Å]	Coverage [%]	SLD [10^{-6} Å^{-2}]	Peptide vol %
Pristine SLB				
Water	4 ± 1	0	-	-
Head (inner)	6 ± 1	83 ± 3	1.83	-
Tail	27 ± 1	94 ± 1	6.7	-
Head (upper)	6 ± 1	83 ± 3	1.83	-
Total membrane thickness (Å)	39 ± 2	$A_{mol} = 61 \pm 2$ Å^2		
SLB after addition of	**1 μM 3W62**			
Water	4 ± 1	0	-	-
Head (inner)	6 ± 1	85 ± 3	1.83	-
Tail/peptide	26 ± 1	85 ± 2	6.0	11 ± 1
Head/peptide	6 ± 1	79 ± 3	1.78	14 ± 2
Total membrane thickness (Å)	38 ± 2		A_{mol} N/A	
First peptide layer	25 ± 5	15 ± 1	1.5/2.2/3.2 ± 0.2*	100
Second peptide layer	27 ± 3	8 ± 2	1.5/2.2/3.2 ± 0.2*	100

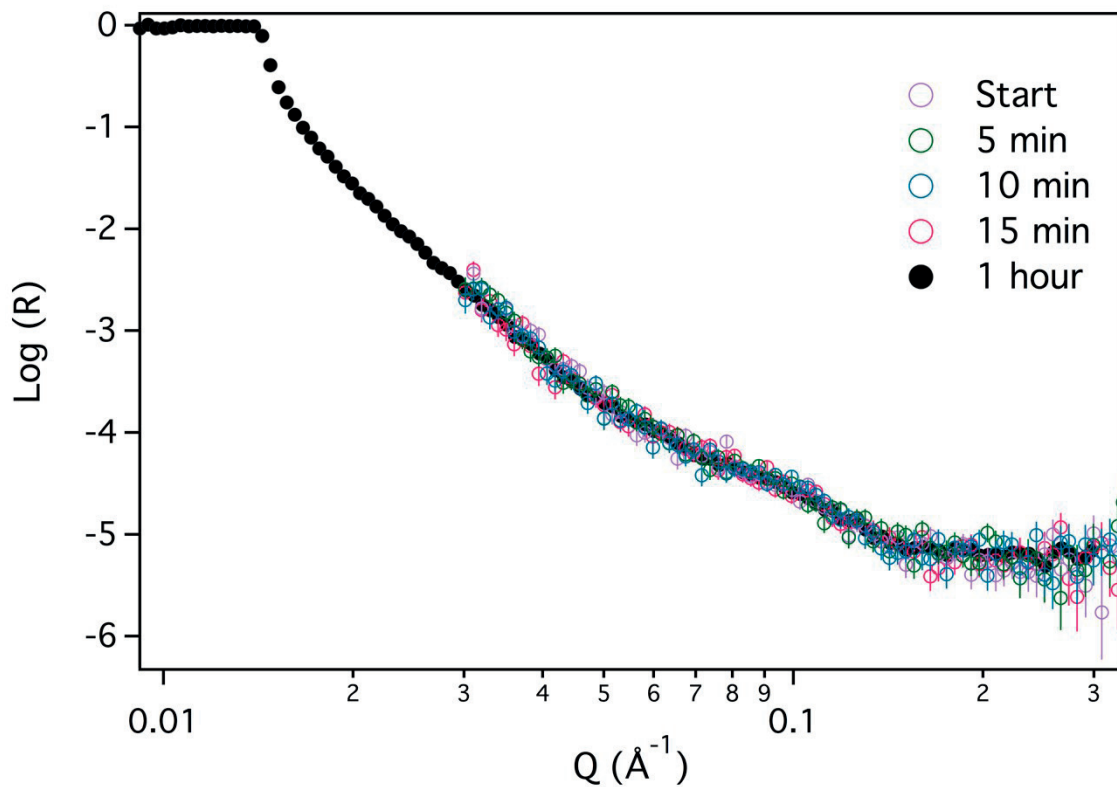## Monte Carlo error analysis on the 5 layer model for 1 µM 3W62:

Figure S6. Monte Carlo error analysis showing correlation between the thickness of the 4th and the 5th layer (indicated with a black circle).

Kinetic measurements of 1 μM peptide addition:

Figure S7. *Reflectivity profile for DMPC-DMPG SLB at a molar ratio of 9:1 after being exposed to 1 μM 3W62 recorded over time (only the second angle for the first 15 min). Results reveal that the peptide-lipid interaction is faster than 5 min as all the curves overlay.*

1.   N. Kučerka, M.-P. Nieh and J. Katsaras, *Biochim. Biophys. Acta, Biomembr.*, 2011, **1808**, 2761-2771.
2.   J. Pan, F. A. Heberle, S. Tristram-Nagle, M. Szymanski, M. Koepfinger, J. Katsaras and N. Kučerka, *Biochim. Biophys. Acta, Biomembr.*, 2012, **1818**, 2135-2148.
3.   J. E. Nielsen, V. A. Bjørnestad and R. Lund, *Soft Matter*, 2018, **14**, 8750-8763.
4.   N. König, J. E. Nielsen, L. Willner, A. Radulescu, N. Mahmoudi, H. Dong and R. Lund, *Extraordinary physical stability of beta-sheet nanofibers formed by self-assembly of a de novo antimicrobial peptide confirmed by small-angle scattering techniques (submitted)*, 2020.